INTERNATIONAL SCIENTIFIC CONFERENCE

INDUSTRY 4.0

13-16. DECEMBER 2017, BOROVETS, BULGARIA

ISSN (Print) - 2535-0153
ISSN (Online) - 2535-0161

VOLUME 1

DOMINANT TECHNOLOGIES IN "INDUSTRY 4.0"
TECHNOLOGICAL BASIS OF "INDUSTRY 4.0"

PROCEEDINGS

ORGANIZER
SCIENTIFIC-TECHNICAL UNION of MECHANICAL ENGINEERING "INDUSTRY 4.0"

INTERNATIONAL EDITORIAL BOARD

EDITORS IN CHIEF:	
Prof. D.Sc. Georgi Popov, DHC, Technical University of Sofia, BG	Prof. Dr. Dr. Jivka Ovtcharova, DHC, Karlsruhe Institute of Technology, GE

Members:		
Cor. member Alexey Beliy	National Academy of Sciences of Belarus	BY
Cor. member Svetozar Margenov	Bulgarian Academy of Science	BG
Prof. Alexander Afanasyev	Institute for Information Transmission Problems	RU
Prof. Alexander Guts	Omsk State University	RU
Prof. Andrzej Golabczak	Technical University of Lodz	PL
Prof. Andrey Firsov	Saint-Petersburg Polytechnic University	RU
Prof. Bobek Shuklev	Ss. Cyril and Methodius University of Skopje	MK
Prof. Boris Gordon	Tallinn University of Technology	EE
Prof. Branko Sirok	University of Ljubljana	SI
Prof. Claudio Melchiorri	University of Bologna	IT
Prof. Cveta Martinovska	Goce Delchev University, Stip	MK
Prof. Dale Dzemydiene	Mykolas Romeris University, Vilnius	LT
Prof. Dimitar Yonchev	Free Bulgarian University, Sofia	BG
Prof. Dimitrios Vlachos	Aristotle University of Thessaloniki	GR
Prof. Galina Nikolcheva	Technical University of Sofia	BG
Prof. Gerard Lyons	National University of Ireland, Galway	IE
Prof. Henrik Carlsen	Technical University of Denmark	DK
Prof. Idilia Bachkova	University of Chemical Technology and Metallurgy	BG
Prof. Idit Avrahami	Ariel Univerity	IL
Prof. Iurii Bazhal	National University of Kyiv-Mohyla Academy	UA
Prof. Jürgen Köbler	University of Offenburg	DE
Prof. Jiri Maryska	Technical University of Liberec	CZ
Prof. Lappalainen Kauko	University of Oulo	FI
Dr. Liviu Jalba	SEEC Manufuture Program	RO
Prof. Luigi del Re	Johannes Kepler University, Linz	AT
Prof. Majid Zamani	Technical University of Munich	DE
Prof. Martin Eigner	Technical University of Kaiserslautern	DE
Prof. Michael Valasek	Czech Technical University in Prague	CZ
Prof. Milija Suknovic	University of Belgrade	RS
Prof. Miodrag Dashic	University of Belgrade	RS
Prof. Mladen Velev	Technical University of Sofia	BG
Prof. Murat Alanyali	TOBB University of Economics and Technology	TR
Prof. Nina Bijedic	Dzemal Bijedic University of Mostar	BA
Prof. Olga Zaborovskaia	State Inst. of Econom., Finance, Law and Technologies	RU
Prof. Pavel Kovach	University of Novi Sad	RS
Prof. Petar Kolev	University of Transport Sofia	BG
Prof. Peter Korondi	Budapest University of Technology and Economics	HU
Prof. Peter Sincak	Technical University of Košice	SK
Prof. Petra Bittrich	Berlin University of Applied Sciences	GE
Prof. Radu Dogaru	University Politehnica of Bucharest	RO
Prof. Raicho Ilarionov	Technical University of Gabrovo	BG
Prof. Raul Turmanidze	Georgian Technical University	GE
Prof. René Beigang	Technical University of Kaiserslautern	DE
Prof. Rozeta Miho	Polytechnic University of Tirana	AL
Prof. Sasho Guergov	Technical University of Sofia	BG
Prof. Seniye Ümit Oktay Firat	Marmara University, Istambul	TR
Prof. Sreten Savicevic	University of Montenegro	ME
Prof. Stefan Stefanov	Technical University of Sofia	BG
Prof. Svetan Ratchev	University of Nottingham	UK
Prof. Sveto Svetkovski	St. Cyril and St. Methodius University of Skopje	MK
Prof. Tomislav Šarić	University of Osijek	HR
Prof. Vasile Cartofeanu	Technical University of Moldova	MD
Prof. Vidosav Majstorovic	Technical University of Belgrade	RS
Prof. Vjaceslavs Bobrovs	Riga Technical University	LV
Prof. Inocentiu Maniu	Politehnica University of Timisoara	RO
Dipl.-Kfm. Michael Grethler	Karlsruhe Institute of Technology	DE

II INTERNATIONAL SCIENTIFIC CONFERENCE
INDUSTRY 4.0
13-16.DECEMBER 2017, BOROVETS, BULGARIA
www.industry-4.eu

Year I Volume 1/1 DECEMBER 2017

ISSN (Print) - 2535-0153
ISSN (Online) - 2535-0161

THEMATIC FIELDS

TECHNOLOGICAL BASIS OF "INDUSTRY 4.0"
DOMINANT TECHNOLOGIES IN "INDUSTRY 4.0"

ORGANIZER

SCIENTIFIC-TECHNICAL UNION OF MECHANICAL ENGINEERING "INDUSTRY 4.0"

108 Rakovski str., 1000 Sofia
e-mail: office@industry-4.eu
www.industry-4.eu

C O N T E N T S

AUGMENTED INTELLIGENCE FOR TEACHING ROBOTS BY IMITATION

Prof. Lekova A. PhD [1], Prof. Pavlov V. PhD[2], Assoc. Prof. Chavdarov I. PhD [1], Assoc. Prof. Krastev A. PhD [1], Datchkinov P [2], Stoyanov I. [3]
Institute of Robotics, BAS [1]
Technical University. Sofia [2]
Professional High School of Computing and Technology Systems, Pravets [3]

alekova.iser@gmail.com

Abstract: *The process of augmenting intelligence in Human Robot Interaction has a complex character and can't be pre-programmed explicitly. Nowadays, teaching robots is a well established concept ranging from demonstration by variants of teleoperation to imitation by external observations. We illustrate an innovative approach for learning intelligence and gestures by imitations of robots by brain augmentation captured by Emotiv brain-listening headset and human poses tracked by Microsoft Kinect motion-sensing device. Thus, robots learn continuously by observations from human brain activities and motions and really become personal. By innovative algorithms, robot operations that satisfy the current physical, cognitive, emotional and social intelligence over time are calculated and transmitted to robot sensors, modules and controllers. The concept of added brain intelligence will also evolve into technology to increase brain capacity and will shape our experience and skills in the future. Summarizing, the paper proposes a new concept for human-robot personal communication by augmenting bio intelligence to robot and vice versa - machine intelligence to human.*

Keywords: TEACHING ROBOTS BY IMITATION, HUMANOID ROBOT NAO, KINECT-ENABLED APPLICATIONS, EMOTIV-ENABLED APPLICATIONS, AUGMENTED BIO INTELLIGENCE, TEACHERS FOR ROBOTS

1. Introduction

Recently, teaching robots has been popular as "programing by demonstration", used when kinematics or dynamic models are difficult to be described and programmed in advanced. The robot behaves like a 'puppet' that operator move and manipulate in real time or record its posture in a timeline-based program in offline mode. We propose another type of teaching - by augmenting brain and gesture intelligence. Robots of the future will coexist and cooperate with humans, therefore they have to achieve physical, cognitive, emotional and social intelligence. The Fourth Revolution began with the rapid development of ICT and AI in particular, allowing a new paradigm for communication: by augmenting bio intelligence to robot and vice versa - machine intelligence to human. An innovative approach for Human-robot interaction (HRI) by brain or motion augmentation that help to personalize the communication with humans are proposed and to some extent illustrated in this paper.

Training robots in complex tasks require humanistic intelligence or human-like movements, impossible to be preprogrammed and calibrated in advance since it is personally specific, difficult to obtain due to the dynamic environment in HRI and continuous need of new repertoire. That imposes human intelligence to be integrated into the digital devices and robots that surround us everywhere. But not digitally by pushing a button, clicking, dragging or speaking, but biologically and continuously through emotions, thoughts or intentions [1]. Thus, digital devices will connect to our physical, emotional and mental state and will be able to meet our needs and at the same time learn from us and really become personal [1]. Thus, we can add intelligence through continuous interaction and feedback between the person and the robot, which will be permanently linked to each other, and the intelligence of the robot will begin to coincide with our own. A symbiosis that puts individual human values at the center of future interfaces to digital devices obeying to the ethical and philosophical considerations. If the robot is connected to human biological essence (the part of us that is most related to our individuality is our brain) on the basis of signals from the brain activity the relevant information can be found about current cognitive and emotional states that play an important role in decision-making, adequate behavior and a healthy lifestyle. Nowadays, teaching robots (the learners) in movements is a well-established concept ranging from demonstration by variants of teleoperation, hand guiding and shadowing to imitation by sensors on a Human (the teacher) or by external observations [2]. Sensors used to record the movements are external to the teacher and may or may not be located on the robot learner. Teaching robots by brain augmentation is a new concept with remarkable development since a decade or two ago recording and decoding brain activity by portable devices was science fiction. Sensors used to record the brain activity are located on the teacher. The brain keeps our cognitive and emotional intelligence, it is a rich source of information and our experience, extremely adaptable and manages our actions [1]. However, what happens in our brains and how to measure it is a great challenge. The brain is hidden and protected, and if invasive approaches and expensive equipment have been used so far, portable, non-invasive and affordable EEG devices (based on encephalography) have emerged with a high-quality output signal. They measure the change in brain pulse voltage by means of sensors on the scalp. "EMOTIV" [3] and "NeuroSky"[4] are pioneers in the field, and the signals received are comparable to those of expensive medical EEGs.

Teaching robots by motion augmentation requires the use of human motion capturing systems for extracting the observed poses. Motion sensing devices and technologies like Microsoft Kinect [5] and Leap Motion [6] allow developers to create innovative applications and solutions that allow users to interact naturally with digital technologies. Leap Motion, the world's most powerful hand tracking, builds a more human reality, really immersive, where Virtual Reality might start with your or robot hands.

The concept of added brain intelligence will also evolve into technology to increase brain capacity and will change our experience and skills in the future by increasing our memory or even communicating with each other by thoughts faster and smarter. Machines learn from information while we learn from experience, so if the information is processed from the robot, we will overcome the massive masses of data avoiding to be overwhelmed by information. Robots will process data and give us the essential and "experience" and this will inevitably affect the health of future generations. Moreover, for people who have suffered from an accident or illness - such brain-machine interfaces will replace lost functionality using emotions, facial expression, and thoughts.

How to teach social or mechanical robots? According to Wikipedia - a social robot is an autonomous robot that interacts and communicates with humans by following social behaviors and rules attached to its role. So, a new profession should be established into near future – *teachers to teach robots.* Those teachers should be aware with social skills and roles. From technical point of view the

teachers should be aware with system architecture and system-level view, with the SDK for the technology, how to set up configuration options for the services and how to program the motion-sensing or brain-listening controllers, etc. From developing point of view they should be aware with software algorithms how to process the signals from the brain over time together with machine learning algorithms in order to find relevant information about current emotions, thoughts or intentions that have to be translated into commands for the robots sensors and teletype printing or speech generators. Software algorithms that analyze the Kinect skeleton stream data and identify the 3D positions of body limbs over time with inverse kinematics is an attempt a kinematic model of the robot to be recovered and to be an input for the kinematic modules of the robot.

Thus, we propose a new concept for human-robot personal communication by augmenting bio intelligence to robot and vice versa - machine intelligence to human. The proposed innovative approach for learning intelligence and gestures by imitations of robots by brain augmentation captured by Emotiv brain-listening headset and human poses tracked by Microsoft Kinect motion-sensing device are illustrated and partially implemented in projects METEMSS [7] and Robo-academy [8].

Emotiv Insight

Microsoft Kinect V2

Walking robot

Anthropomorphic Hands

Humanoid robot NAO

Fig.1 *Assistive technologies in METEMSS [7]*

2. Training robots by Imitation

Training humanoid NAO robot by body parts guiding and integration of the brain-waves and motion sensing systems to humanoid and non-humanoid robots are used as assistive to therapists tools (fig.1.) used for learning by imitation in the context of play for children with special needs in order to engage these children and motivate their social activity, expression of emotions and more body movements [7]. The calibration of used technologies, as well as their integration is for easy to set-up at homes or schools from people without engineer skills.

2.1. Augmented brain Intelligence

In this Section we demonstrate EEG-based system that by a Brain–Computer Interfaces (BCI) translate in real time the electrical activity of the brain to commands in order to control humanoid robot NAO. The research in BCI has started in 1973 [9]. BCIs are systems that can bypass conventional channels of communication (i.e., muscles) to provide direct communication and control between the human brain and physical devices by translating different patterns of brain activity into commands in real time [10]. With these commands a mobile robot can be controlled or can serve as an assistant of child or a therapist in a joyful skills-learning environment by imitation. Proposed, developed and tested by experiments is an innovative model for development of brain-robot game for learning skills by imitation to help the child to become more emotionally engaged with the social world. The brain activity under consideration is the blinking rate in time that provides a way to monitor the attention and social engagement by measuring blinking on NAO's eyes because children with autism avoid eye contact. The authors in [11] reviews the deployment of EGG based control in assistive robots, especially for those who in need and neurologically disabled. They describe the methods used for (i) EEG data acquisition and signal preprocessing, (ii) feature extraction and (iii) signal classification methods.

In the proposed system we use EMOTIV Insight Brain Activity Tracker with 5 electrodes and 2 referenced to record EEG signal. It is a 5 channel, wireless headset that records and translates human brainwaves into meaningful data you can understand. In the current project we use 1 of them on the forehead to construct a Brain-Computer Interface (BCI) to control the NAO eyes led sensors through wireless interface. First, EEG signals were filtered in order to extract the different brain rhythms (δ, θ, α, β), so that the different frequency bands were individually analyzed, as well as combined together. The existing EEG based biometric systems are classified to the employed acquisition protocols in terms of cognitive task, the number of electrodes and their spatial configuration, the feature extraction algorithms, the classification algorithms and their effectiveness in clustering the observations [11]. For example, Fig. 2. shows an examples of Delta, Theta, Alpha, Beta, and Gamma waves acquired through the channel O2 using a "rest state with closed eyes" protocol.

We considered different channel configurations to obtain the most reliable acquisition protocol using the AF4channel. Then, we extract the features for eye-blinking from EEG signals as the ratio between the power of Theta and Alpha rhythms. We map the changing of this peak to parameters of eye-LEDs that mimic NAO blinking in order to control NAO's eye-LEDs in ALLeds module on the robot side.

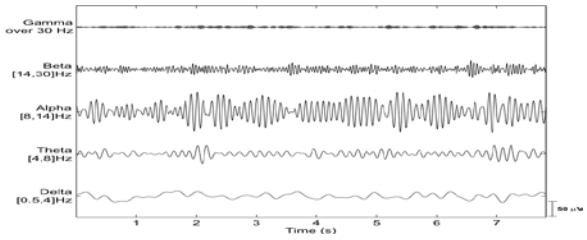

Fig. 2. *Taken from [11] - Delta, Theta, Alpha, Beta, and Gamma waves acquired through the channel O2 using a "rest state with closed eyes" protocol*

The proposed EMOTIV-NAO framework, combining the BCI with the APIs of the NAO robot, is enough general and could be used for different cognitive tasks or other EEG-based controlled mobile robots.

2.2. Training robots in human-like movements

Human-robot interaction by gestures personalizes the communication with humans in various contexts, from daily life to special educational needs. Human-like movements in gestures can't be pre-programmed explicitly since the localization and motion planning of humanoid robots relies on dynamic/kinematic models, which are not always available or difficult to obtain due to the dynamic environment in HRI. Since, the marker based motion captured systems for extracting 3D poses over time are expensive

and require careful calibration, a lot of work has been studied for imitation by external observations for extracting 3D poses from an image sequence. Sensors used to record the movements are external to the teacher and may or may not be located on the robot learner. We propose in [12, 13, 14] different innovative approaches for teaching robots to imitate gestures. In [12] we integrate Kinect motion-sensing device and controller with direct feedback from an originally developed angular displacement sensors mounted in an artificial anthropomorphic robot hand. The robot learns by external observations of the 3D teacher poses captured by Kinect. We analyze the Kinect skeleton stream data and identify the 3D positions of upper body limbs over time. Inverse kinematics algorithm for calculating the corresponding joint angles for each pose and decomposition into a per-frame algorithm and a method for optimal control of joint motors by position in a lack of a dynamic model is found. More details for the proposed, developed and tested by experiments models for teaching robots to imitate gestures can be found in [12] and [13], where two different prototype of artificial hands were designed and tested. Processing Kinect body data to solve Inverse Kinematics task for teleoperation of humanoid robot NAO is presented in more details in [14]. We analyze the Kinect depth and body stream data and identify the 3D positions of upper body limbs over time. The important joints for motion retargeting of upper limbs are left and right shoulder, elbow, wrist and hand (Fig.3.).

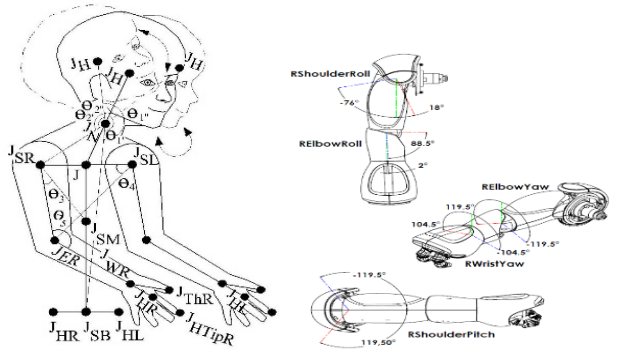

Fig.3. *Important joints for motion retargeting of upper limbs to 3D model of the Nao right upper limb*

3. Training robots by body parts guiding and shadowing labelled and tailored to bio signals

This section illustrates how to teach by animation programmable robots in complex movements by body part guiding and recording in timeline mode. The illustration of steps are for NAO robot with Choregraphe [15] - a multi-platform desktop application, allowing teachers to create animations, behaviors and dialogs, test them on a simulated robot, or directly on a real one, monitor and control NAO and enrich Choregraphe behaviors with own Python code.

In Choregraphe you can use an 'Animation Mode' for Training robots by body parts guiding and shadowing. In the 'Animation Mode' you create movements easily, in conjunction with the Timeline Editor. In this mode, *the robot behaves like a puppet* that you can manipulate, letting you record its posture in a Timeline. In this mode, tactile commands help you manipulate the robot. You can use tactile commands to manage the stiffness. A visual feedback let you know which limb is currently stiffened or not. Yellow means that the Stiffness is 'On'. Green means that the Stiffness is 'Off'. Use Stiffness-control tactile commands to manipulate its limbs one by one in order to make the robot take the posture you want to store. When you change the real NAO position, you can see that the virtual 3D NAO changes position too. To move joints of a simulated robot, using the Limb properties that allow you to check and modify the joint values (and then move the limbs) using the Limb properties. This panel enables you to modify the joint values of each limb and allows you to adjust the joint value. You can move it, as well as enter a value in the associated text box. The robot tries to reach the command value with its joint as soon as possible. At each steps you have to save the defined values in the currently opened Timeline box [15].

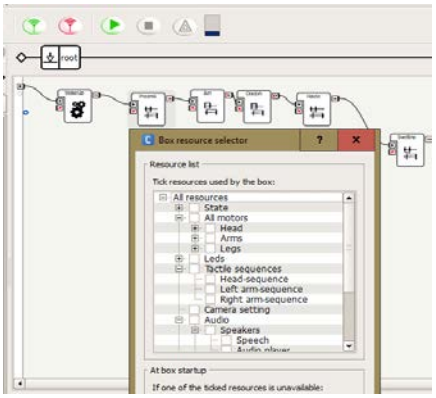

Fig. 4. *Resource list used in the Timeline box*

We propose during the animation to decompose the desired movement in order to use switch case over the single motions. For instance, you teach your robot in complex movements, however you would like to use script to switch them depending on daytime, accessibility, task to do, obstacles at home/office, brain activity, emotions and intensions. Thus, you need to run a Python script to access a Timeline object. In Python *load and unload* events methods automatically are called when the box is loaded or unloaded. Resource list used in the Choregraphe Timeline box (as shown in Fig.4) in Python method *"onResource"* is called when the resources of the box are set to Callback on demand and the resources are asked by another box. You need to define resource functions for it to be called.

The choreographies tailored to songs in the project METEMSS [7] are an example how to adapt to the *style of dance* that fits the target groups.

4. Training teachers to teach robots

The proposed from us new paradigm for augmenting bio intelligence to robot and machine intelligence to human requires a change in the way how robots to be trained. This imposes a new profession "teachers for robots" to be appeared in a near future. It is most natural for our community programmers to be assigns to do this by going through additional training. What additional skills are required and how to teach social or mechanical robots? Robot communicates with humans obeying to rules attached to its role. So, teachers should be aware with skills and roles. Since the robots will work at the same workplace and coexist with people and other robots, they need to socialize. Robots must comply with ethical and legal norms. Asimov's three laws for the behavior of robots are a good basis for the development of a modern legal normative base. They have to be "implemented" in the teaching process but not only. The perception of "good and bad" for people and robots is different. Additional training of teachers for generic guidelines for robot behavior is imposed by the greater ubiquity of robots.

Another point of view could be seen in [16], where authors make a concrete, operational proposal as to how the information-theoretic concept of empowerment can be used as a generic heuristic to quantify concepts, such as self- preservation, protection of the human partner, and responding to human actions. They focus less on how a robot can technically achieve a predefined goal and more on what a robot should do in the first place. They are interested how a heuristic should look like, which motivates the robot's behavior in interaction with humans. They present proof-of-principle scenarios demonstrating how empowerment interpreted in light of these perspectives allows one to specify core concepts with a similar aim as Asimov's Three Laws of Robotics in an operational way. Significantly, this way does not depend on having to establish

an explicit verbalized understanding of human language and conventions in the robots [16].

Robot teachers must have sufficient knowledge of the technical specifications and robot services. They need to apply appropriate syllabus and teaching through appropriate programming tools. Robot training methods today are at an early stage of development. One is the teaching by imitation, which is specifically and partly offered in the present work. It is illustrated in terms of imitation of some human movements that are reproduced by a particular robot. This approach will continue with respect to all movements and imitation of human behavior in different conditions.

Where the training should take place? Probably in specialized services and / or in "robot schools". The future development of robotics will impose not only new rules and legislations to be created but also engineering knowledge, practical manuals and training syllabuses.

5. Conclusions

The main contribution in the proposed paper is the innovative model how to augment to robots physical, cognitive, emotional and social intelligence and vice versa experience and memory to humans. We describe and demonstrate the potential of the EMOTIV-ROBOT and KINECT-ROBOT frameworks for providing a natural interface to teach robots by imitation to perform mechanical and social tasks that are impossible to be preprogramed and calibrated in advance. At the same time, the proposed from us new paradigm for augmenting bio intelligence to robot and machine intelligence to human requires transformations in the way how robots to be trained. The learning of people how to teach robots and appearance of new profession “teachers for robots" is inevitable. These teachers should take additional training in knowledge and heuristics concerning how to motivate the robot’s social behavior in interaction with humans and updating the Asimov’s Three Laws of Robotics.

Acknowledgments

This research is supported by the BAS grants DSD-2/05.04.2016.

References

[1]. Warp E., IFA+ Summit 2017: Brain Wearables, The Next Level of Intelligence. URL: https://www.emotiv.com/videos/ifa-summit-17-erica-warp-brain-wearables-4-sept-2017-next-level-intelligence/

[2]. Argall B, Chernova S, Veloso M, Browning B. A survey of robot learning from demonstration. Robotics and Autonomous Systems 2009; 57(5): pp. 469-483.

[3]. Emotiv Insight Brainware, URL: https://www.emotiv.com/

[4]. NeuroSky: EEG & ECG Biosensor Solutions. URL: http://neurosky.com/

[5]. MS Kinect for Windows. https://developer.microsoft.com/en-us/windows/kinect

[6]. Leap Motion. https://www.leapmotion.com/

[7]. Methodologies and technologies for enhancing the motor and social skills of children with developmental problems (METEMSS). URL: http://ir.bas.bg/metemss/en/final-relults.html

[8]. Robo-academy. URL: facebook.com/robo.academy.bg/

[9]. Vidal, J. "Toward direct brain-computer communication". Annual Review of Biophysics and Bioengineering. 1973. 2 (1): pp. 157–80.

[10]. Krishnan N. et al, Electroencephalography (EEG) Based Control in Assistive Mobile Robots: A Review, IOP Conference Series: Materials Science and Engineering, 2016 IOP Conf. Ser.: Mater. Sci. Eng. 121 01, 2017

[11].Campisi, P., La Rocca, D., 2014. Brain waves for automatic biometric-based user recognition. IEEE Trans. Inf. Forensics Secur. 9, pp. 782–800.

[12]. Botsova, R., Lekova, A., & Chavdarov, I. (2015). Imitation learning of robots by integrating Microsoft Kinect and PID controller with a sensor for angular displacement in a robot joint. In ACM Proceedings of the 16th International Conference on Computer Systems and Technologies, pp. 268-275

[13]. Lekova A, D. Ryan, R. Davidrajuh, Fingers and Gesture Recognition with Kinect v2 Sensor, Information Technologies and Control, DE GRUYTER OPEN , 3/2016 , pp.24-30

[14]. Lekova A, Krastev A, Chavdarov I. Wireless Kinect-Nao Framework Based on Takagi-Sugeno Fuzzy Inference System. AUTOMATICS AND INFORMATICS'2016, 2016, pp. 111-116

[15]. Aldebaran documentation - Choregraphe User Guide. URL: http://doc.aldebaran.com/2-1/software/choregraphe/index.html

[16]. Salge Ch, Daniel P. Empowerment as Replacement for the Three Laws of Robotics. Frontiers in Robotics and AI, VOL=4 , 2017, 25 pages

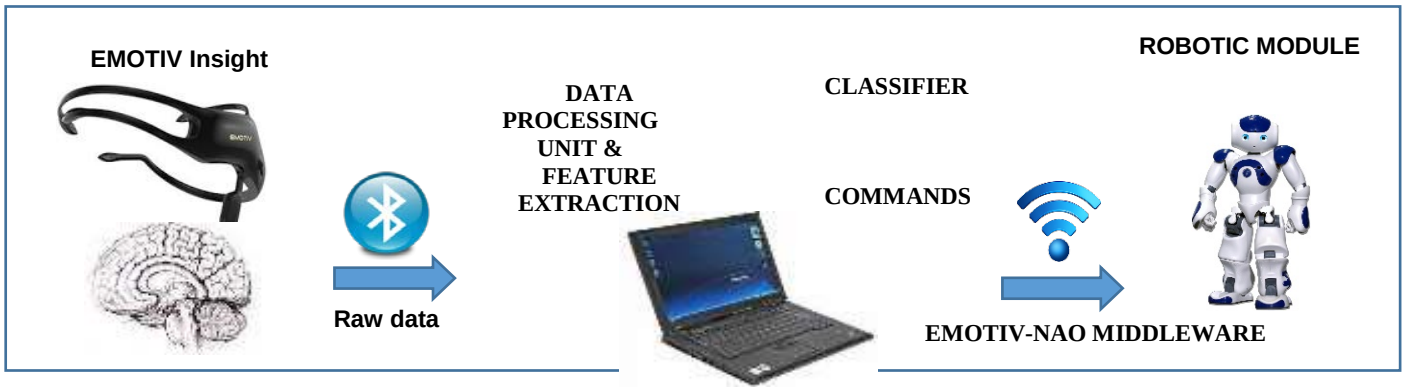

Fig. 3. *EMOTIV-NAO wireless framework for developing an EEG based brain-robot interface*

SIMULATION AND MOTION CONTROL OF INDUSTRIAL ROBOT

Yaser ALAIWI [1], Aşkın MUTLU [1]
Faculty of Engineering – Department of Mechanical Engineering, Istanbul University, Turkey[1]
yaser.alaiwi@istanbul.edu.tr, askin@istanbul.edu.tr

Abstract: *This research proposes a simulation of a Stäubli TX90 robot based on Simulink Toolbox of Matlab. The goal is to predict the position and trajectory of its end-effector, with high reliability. The simulator takes into consideration loading, deformations, calibrated kinematic parameters, and all eventual sources of disturbance. A comparison between real and simulated data reveals the reliability and the accuracy of the simulator.*

KEYWORDS*: SIMULATION, PID CONTROL, STÄUBLI TX90, INDUSTRIAL ROBOT*

1. Introduction

This robot has six degrees of freedom; all of them are rotational, driven by servo motors. The robot has the appearance that can be seen in Figure 1:

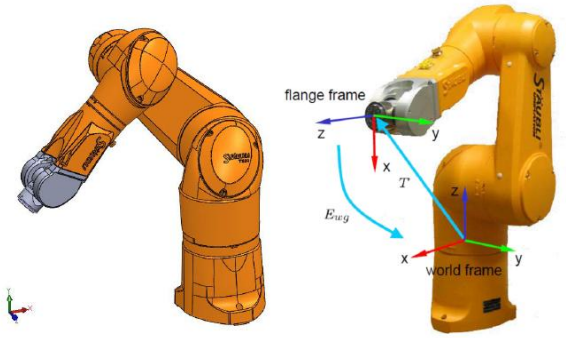

Figure 1: *Stäubli Robot TX90 Real view and SolidWorks Design*

The simulation should provide an accurate position of the robot's end-effector. The TX90 robot is a serial manipulator robot with six rotational joints. The link frames and the kinematic parameters of the TX90 robot, following the notations of the modified Denavit and Hartenberg method proposed by Khalil and Kleinfinger [1], are shown in Figure 2.

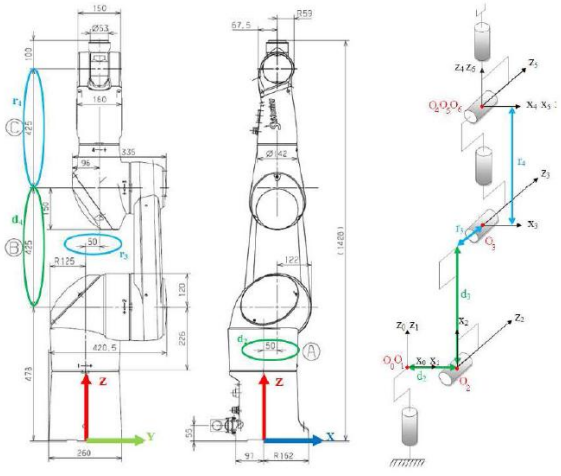

Figure 2: *Kinematic description of the Stäubli TX90 robot*

The kinematic parameters (αj, dj, θj, rj, βj [5]) were calibrated previously by using an autonomous calibration method [2, 3, 4] which aims to identify the difference between the nominal and the real values of the kinematic parameters and then to have a better knowledge of the position of the end- effector (rate of knowledge improvement is about 94 %). The nominal values of the kinematic parameters (in bold) D-H are shown in Table 1.

Table 1. *The Standard Kinematic model in Denavit-Hartenberg Convention*

j	**α_i**	**a**	**θ_i**	**d_i**
units	*[rad]*	*[mm]*	*[rad]*	*[mm]*
1	-1.5708	50	0	350
2	0	425	0	50
3	-1.5708	0	0	0
4	1.5708	0	0	425
5	-1.5708	0	0	0
6	0	0	0	100

Previously, identification of the dynamic parameters, and identification of the elastic parameters and the joint stiffness matrix were carried out on the TX90 robot [4]. These parameters are taken into consideration in the simulator for the nearest representation of the reality.

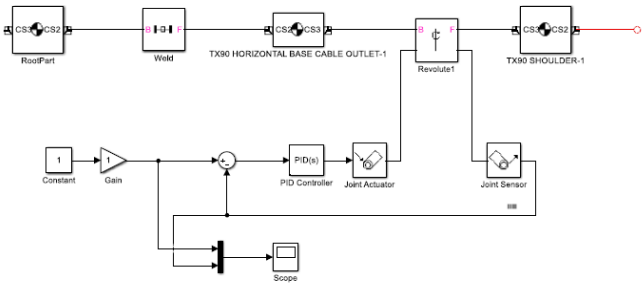

Figure 3: PID Controller diagram in Simulink

2. Description of the Simulation Tool

To model the dynamics and the control of the robot, the simulation tool must be coupled with Simulink blocks and use Matlab functions in order to compute for example: The inverse kinematic model, the trajectory generation and the control blocks.

The chosen tool to simulate the TX90 is SimMechanics [6,7,8] which is a sub-tool of Simulink®. Consequently, its models can be interfaced with ordinary Simulink block diagrams which speed up the simulation and integrate everything in the same environment. Moreover, it is simple to use and its block set consists of seven sub-libraries that represent the following: bodies, joints, sensors (joint sensors, body sensors), actuators (joint actuators, body actuators), gearboxes, constraints and drivers, and force elements.

SimMechanics tool allows to:

Model all the elements of a multi-body system (i.e. bodies, joints, connections, forces) in Simulink;

Import full models from CAD systems (i.e. Stäubli SolidWorks CAD [9]), with the properties of inertia, lengths, angles;

Generate a 3D animation to visualize system dynamics.

3. Trajectory Generation, Control and Simulation in SolidWorks

The approach used for the generation of trajectories in the case of the TX90 was not provided by the manufacturer for reasons of confidentiality. The study of the position and the velocity signals (given by the "Stäubli recorder") and the calculation of the accelerations (derivation of the velocity) show that the approach is applied in the joint space using the trapezoidal velocity law. This approach provides during movement: a continuous velocity (ensures a minimum time by saturating the velocity and acceleration at the same time) and a continuous acceleration (replaces the acceleration and braking phases by a law of the second degree and therefore the position is a law of the fourth degree) [10].

On the other hand, only the name of the controller used by Stäubli has been provided by the manufacturer through a confidential agreement and so it is not possible to present it in this paper. The controller and the trajectory generations blocks are designed under the environment of Simulink.

Figure 4: *Control Diagram of Staübli Robot Tx-90*

We can see the control sequence of Staübli Robot Tx-90 in Figure 4 and the Simulink Diagram with PID controllers in the following Figure 5.

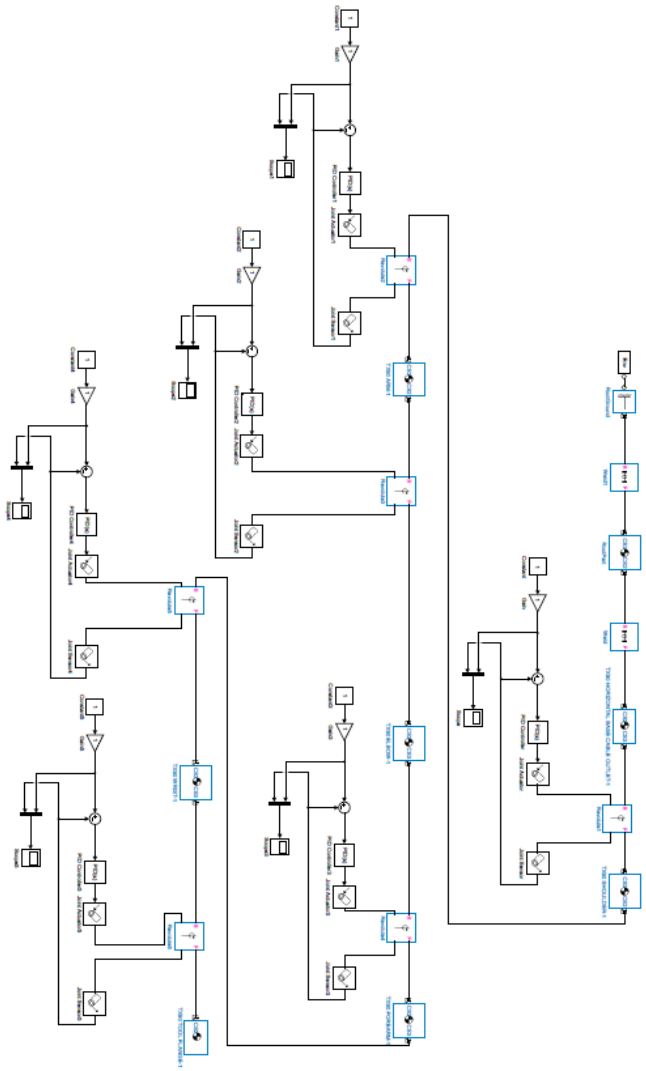

Figure 5: *Simulink Diagram with PID controllers*

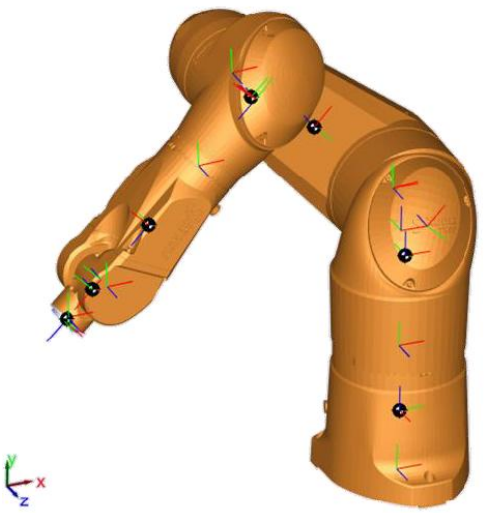

Figure 6: *Three-dimensional animation of the TX90 robot in Simulink*

We built three dimensional model from technical drawings for Stäubli Robot TX90 and after making the proper assembly mates we could make motion analysis. we can see the simulation results for tracking this arbitrary trajectory (3600 mm length) in a time of 6 seconds that means total velocity is 0.6 m/s Figure 7.

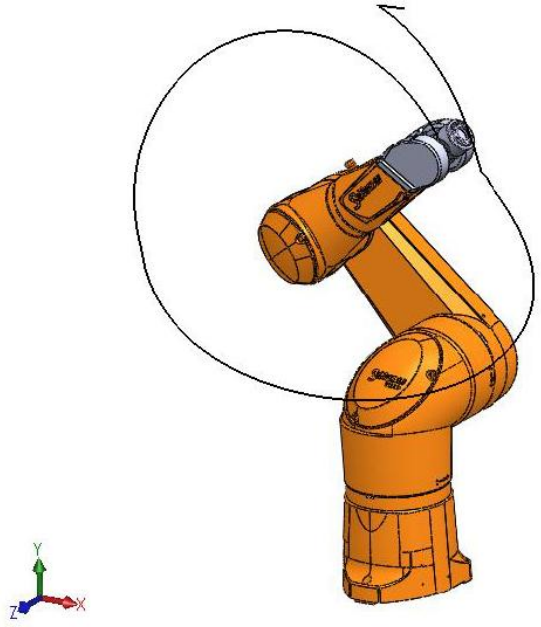

Figure 7: *SolidWorks Trajectory tracking and Motion Simulation*

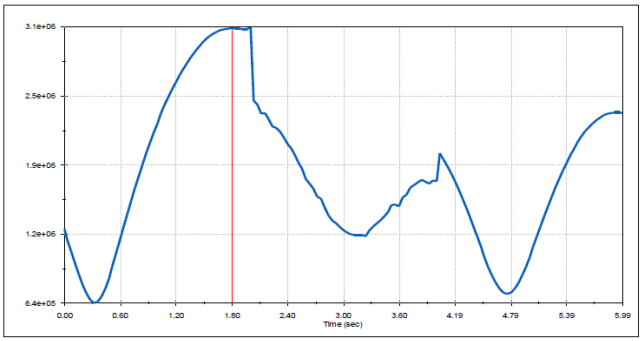

Figure 8: *Angular Momentum*

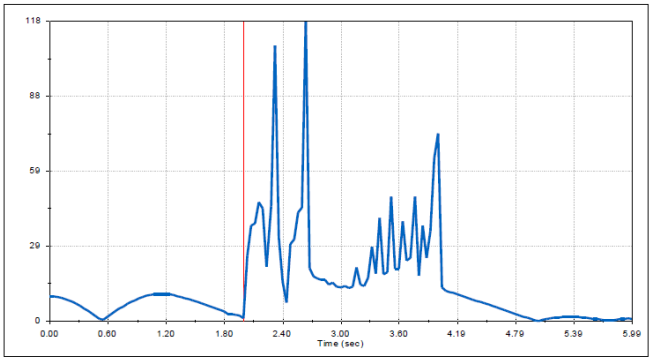

Figure 9: *Motor Torque*

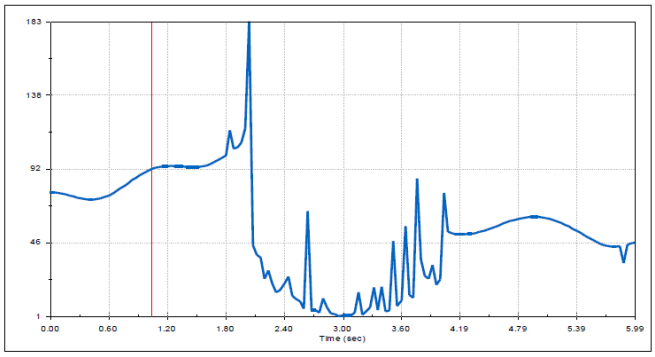

Figure 10: *Angular Acceleration*

4.Conclusion

This research has presented the implementation of the Stäubli TX90 simulator using Sol idWorks and SimMechanics which is an interactive three-dimensional modeling of mechanical systems in Simulink®. It allows building simulations and automatically generates 3D animations of multi-body systems such as robots. Blocks representing all external perturbations (deformations, cutting forces, flexibilities, loads) have been integrated into this simulator. This simulator is able to predict the position and trajectory of the end-effector according to the loading and deformation in order to represent reality with high reliability.

The simulation results indicate that SimMechanics can be used for modeling other robots with the same morphology as the TX90, (i.e. anthropomorphic, open, series). Block parameters defining for example the different bodies, joints, kinematic models (i.e. MGI, MGD) can be easily modified to be adapted to other robots. Moreover, the simulator can be used to validate the feasibility and to predict errors of other maintenance operations that need high precision such as welding.

5.References

[1] W. Khalil and J.F. Kleinfinger, A new geometric notation for open and closed loop robots, in International Conference on Robotics and Automation, San Francisco, CA, April, 1986, pp. 1174–1180.

[2] H. Hage, P. Bidaud, N. Jardin, Practical consideration on the identification of the kinematic parameters of the Stäubli TX90 robot. The 13th World Congress in Mechanism and Machine Science, Guanajuato, Mexico, 19-25 June, 2011.

[3] S. Besnard, Etalonnage géométrique des robots séries et parallèles, Doctoral dissertation, Nantes, France, September, 2000.

[4] H. Hage, Identification et simulation physique d'un robot Stäubli TX90 pour le fraisage à grande vitesse, doctoral dissertation, Paris, France, February, 2012.

[5] S. A. Hayati, Robot arm geometric link calibration, in proceedings IEEE International Conference on Decision and Control, San Antonio, December, 1988, pp. 1477_1483.

[6] Information on
http://www.mathworks.com/products/simmechanics/

[7] Y. Shaoqiang, L. Zhong, L. Xingshan, Modeling and simulation of robot based on Matlab/SimMechanics, in Proceeding of Control Conference 27th Chinese, 2008.

[8] L. Brezina, O. Andrs, T. Brezina, NI LabView—Matlab SimMechanics Stewart platform design, Applied and Computational Mechanics 2 (2008) 235–242.

[9] Information on http://www.staubli.com

[10] W. Khalil, E. Dombre, Modélisation, identification et commande des robots, second edition, Paris, 1999.

Digital Image Correlation Analysis of CFRP during compression test

C.Barile, C.Casavola, T.Mizzi, G.Pappalettera, C.Pappalettere

Politecnico di Bari,

Dipartimento di Meccanica, Matematica e Management, viale Japigia 182 -70126 Bari

Abstract

The present paper examines the mechanical behavior of composite laminate subjected to uniaxial compression by DIC (Digital Image Correlation) 3D technique, in particular by analyzing the stability of the buckling equilibrium.

The purpose is how to measure the off-plane displacements, typically founded in buckling, in any point of the ROI (region of interest) of the investigated structure, using a full-field and non-contact measurement technique.

The innovative aspect of this work is therefore to solve this problem through an experimental approach with DIC 3D technique.

1 Introduction

Structures in composite materials are obtained by joining at least two materials, with very different physical and mechanical characteristics. The purpose of this matching is to obtain a final material with better characteristics than those referable to the single initial materials. The composite is generally made up by reinforcement and matrix, giving rise to a solid and continuous material, able to transmit and redistribute internal stress. We can state that composites are non-homogeneous and non-isotropic materials, where the individual constituents are bonded to each other in an insoluble way in order to obtain a final product that combines the best properties of the components. The Fiber Reinforced Polymers (FRP) analyzed in this work are made up by a carbon fiber material (reinforcement) and by epoxy resin as a matrix.

The main carbon fiber properties [1] are: high mechanical strength, high elastic modulus, low density, low crack sensitivity, fatigue resistance and good ability to dampen vibrations. Moreover, the thermal expansion coefficients allow having structures with dimensional stability over a great range of temperature variation.

Epoxy resins [2] represent a group of thermosetting polymeric materials that do not create reaction products when they cure (reticulate) and therefore have a low reticulation retention. They also have good adhesion to other materials, good chemical and environmental resistance, good mechanical properties and good electrical insulation properties. All of these features, together with a remarkable weight reduction combined with high strength (high SWR: strength to weight ratio), make possibility of combining those two materials very appealing in the aeronautic field.

Composites are non-homogeneous and anisotropic materials, so they respond differently to a given load, depending on the direction considered; as a consequence, a proper approach to material characterization, should employ full-field measurement techniques as, for example, those based on Digital Image Correlation [3].

The three-dimensional DIC technique uses two cameras in order to look at the object from two different directions, obtaining a binocular view that allows to determine the three displacement coordinates (X, Y, Z) for each generic point of the analyzed area [4]. Measurement requires the application of a speckle random pattern on the specimen test.

The 3D DIC technique can also be applied to non-flat surfaces that are displaced off the plane, as in the case of buckling structures; in fact, it provides information about both the shape of the body and the three-dimensional strain field. For this purpose, several images are captured by the two cameras and the speckle pattern for each deformed configuration is analyzed with respect to a reference one.

2 Materials and Methods

2.1 Material description and preparation of the component for measurement

The material analyzed is a composite laminate made up of an epoxy resin mat with carbon fiber reinforcement.

The size of the component subjected to uniaxial compression is 150x100x5 (mm). The layout of the plies, according to the manufacturer's reference is as follows.

Type I layup: FF = 0T / 0F / 0T / 0T / 0F / 0T / 0T / 45F / 0T / SF where F = Fabric, T = Tape

The speckle pattern to be analyzed by DIC was introduced by spraying the specimen (Fig.1). To this scope a matt white spray and a black matt spray were used.

Four electrical strain gauges, two for each side of the pieces, were applied on each specimen [5], in order to evaluate the local strain

resulting from the application of compressive loads. in such a way it is possible to compare local behaviour obtainable by strain gages with overall behaviour obtained by DIC.

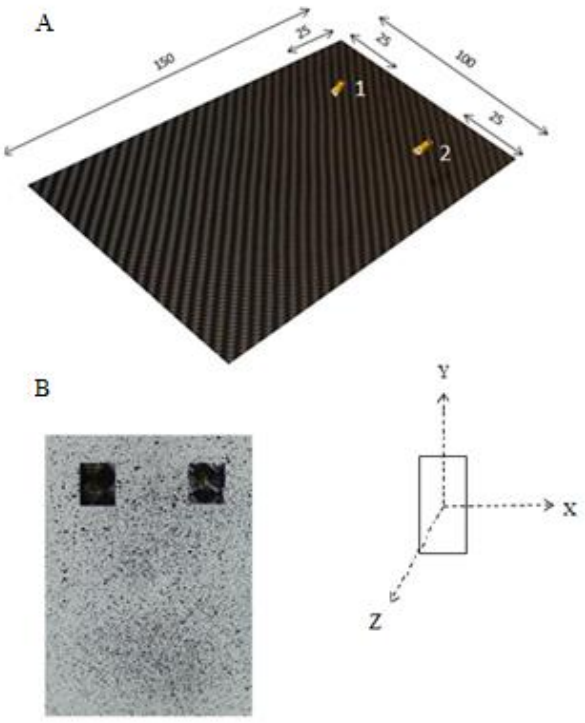

Figure 1. Composite laminate
a) Extensimeter application allowances
b) component prepared with speckle pattern

The strain gauges used are HBM LY1, with a measuring base l_0 = 3mm, gage factor k = 1.99.
The strain gauges adopted are able to evaluate deformations in one direction (uniaxial). Strain gages with a resistance of 350 Ω were used because the composites are bad conductors.

2.2 Description of the compression test machine

Compression test were performed by following the ASTM 7137 (Compression After Impact "CAI") standard defined for the composite. In particular this standard specifies the applied constrains and the ambient condition and the compression rate.
Test were performed on a SCHENCK servo-hydraulic machine. In this machine the lower clamp is movable while the upper crosshead is fixed and must be initially positioned with the highest precision in order to avoid torsional or flexural deformations that could introduce errors in the measurement process. The main setting for the test are listed as below:

- Static test, then monotonic test
- Load cell from 250 KN
- Axial channel (being uniaxial compression)
- Control in "displacement rate" (1.25 mm / min until breakage [5])
- Acquisition frequency of 10 HZ

2.3 Configuration of the measurement chain

For a greater accuracy of the tests and to measure the variables involved in the phenomenon of instability of the specimens, a measurement chain was required to complete the reading of displacements and deformations in a suitable manner.
In order to measure displacements and deformations of the whole surface of the specimens in the field three - dimensional, the Dynamics Q400 system with ISTRA 4D software was used.
It includes two Manta industrial cameras, with Ricoh 16mm lenses, fixed on the same support in order to avoid vibrations. System also includes a 4-channel data acquisition and synchronization unit and a light source.
Lighting is used to ensure that the speckle pattern on the specimen, once acquired, has a fairly wide grayscale span range; this means that the background is sufficiently clear (white) and dark (dark) without going into saturation in areas under DIC analysis , but also ensuring uniformity of luminance in these same areas.
It has been chosen to use an optic with a reduced focal length because the latter allow the capture of sufficiently large test specimens to monitor the whole component.
The cameras were coupled to a National Instruments® NIDAQ 9171 acquisition card which allows analog to digital conversion of the acquired signal.
To synchronize acquisition with the start of the test, a trigger signal exiting from the loading machine was sent to the acquisition system by a BNC cable.

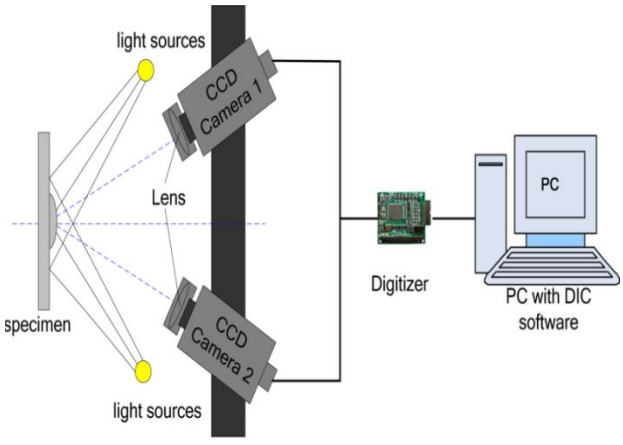

Figure 2. Schematic of a complete 3-D DIC system [6]

Settings for the DIC system are listed below:

- Distance between cameras l=40cm
- Distance between lens and piece d=50cm
- Inclination angle of the cameras =21.8°
- Diaphragm opening =f/8

Figure 3. Overview of experimental set-up

The adopted compressive test fixture is shown in Figure4.
It utilizes adjustable retention plates to support the specimen edges and inhibit buckling when the specimen is -loaded.
The fixture consists of one base plate, two base slide plates, two angles, four side plates, one top plate, and two top slide plates. The side supports are knife edges, which provide no restraint to local out-of-plane rotation.
The top and bottom supports provide no clamp-up, but provide some rotational restraint due to the fixture geometry (the slide plates have a squared geometry and overlap the specimen by 8 mm [0.30 in.]). The fixture is adjustable to accommodate small variations in specimen length, width and thickness. The top plate and slide plates, which are not directly attached to the lower portion of the fixture, slip over the top edge of the test specimen. The side plates are sufficiently short to ensure that a gap between the side rails and the top plate is maintained during the test.
The configuration of the panel edge-constraint structure can have a significant effect on test results. In the standard test fixture, the top and bottom supports provide no clamp-up, but provide some restraint to local out-of-plane rotation due to the fixture geometry. The side supports are knife edges, which provide no rotational restraint.

Edge supports must be co-planar. Results are affected by the geometry of the various slide plates local to the specimen.
Results are also affected by the presence of gaps between the slide plates and the specimen, which can reduce the effective edge support and can result in concentrated load introduction conditions at the top and bottom specimen surfaces.
Additionally, results may be affected by variations in torque applied to the slide plate fasteners; loose fasteners may also reduce the effective edge support.

Figure 4. Edge-constraint structure adopted in the experiment

3 Results and Discussion

In order to measure the displacements and deformations of the entire surface of the composite in the three-dimensional field, the mechanical uniaxial compression test was monitored using the 3D system, acquiring a series of images that represent the displacement off the plane(z-displacement), starting from the first non-deformed configuration of the component until it came to break, with acquisition frequency of 1Hz, for the entire duration of the test.
The analysis of these frames (Fig.5), at certain steps, allows to view the buckling in CFRP subjected to uniaxial compression.
The images are captured and correlated by setting a “high accuracy” mode that allows a correlation with a 3d residuum of less than 0.4 pix, a facet size of 19 pixels and an accuracy of 0.1 pixels that allows locating 1180 grid point in the region of interest (ROI) of composite laminate.

t=0s t=40s

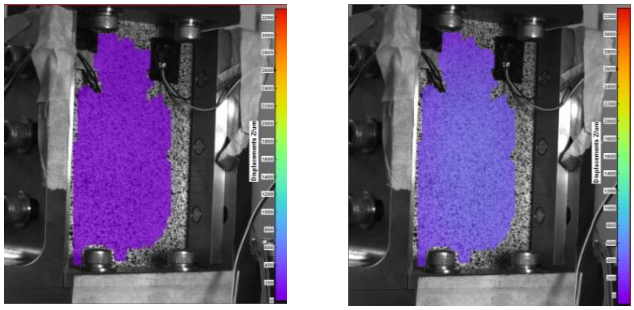

t=80s t=100s

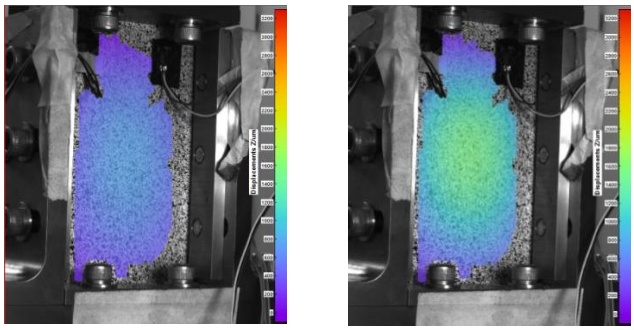

t=116s t=120s

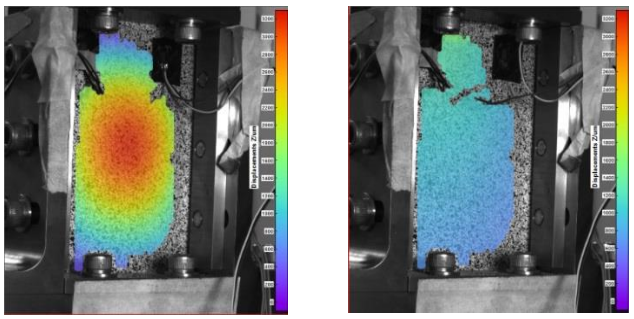

Figure 5. Frames of out of plane displacement of the composite taken by DIC at various steps

From the analysis of the images, the following considerations can be done: the component, due to the adopted fixtured and the low displacement rate implemented (1.25 mm / min) is subjected, in the first load steps to low out of plane displacement values (e.g. 400 μm at the center of the specimen at step t = 40s).

The component begins to buckle after 80 seconds from the beginning of the test when an out of plane displacement equal to 800 μm is recorded. After 116 s out of plane displacement becomes more evident and it reaches a value of 3200 μm while the specimen broke soon after, namely at 120 seconds.

Temporal load law is reported in Fig.6.

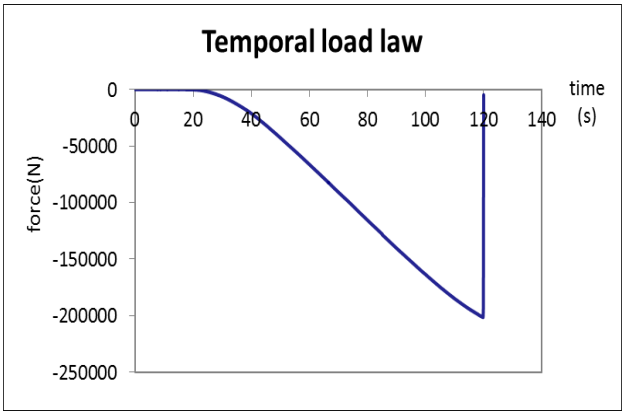

Figure 6. Temporal load law of the machine

There is a first hyperbolic trend in the first 40 s until reaching a load of about -21kN. At this point the first instability of the component is recorded because some out of plane displacement are observable at this point. Successively there is a linear behavior, which terminated at t= 80 seconds. From that point until 116 seconds a slight slope change occurs as a result of the buckling of the specimen as it is inferable by observing DIC images.

The abrupt cut of curve is caused by the breaking of the specimen with the consequent detachment of the supporting LVDTs immediately after reaching maximum load, recorded at the break of the sample at t = 120 s corresponding to F = -200 kN.

Using two additional electrical strain gauges at known locations [5] it has been possible a comparison between the ε_{yy} -t results obtained by ER and DIC; to verify the accuracy the deformation ε_{yy} value was read across the strain gauges 1 and 2 and it was compared to the corresponding DIC reading along a gauge of 3 mm corresponding to the measurement base l_0 of the strain gauges, located at the points where ER where applied (Fig.7)

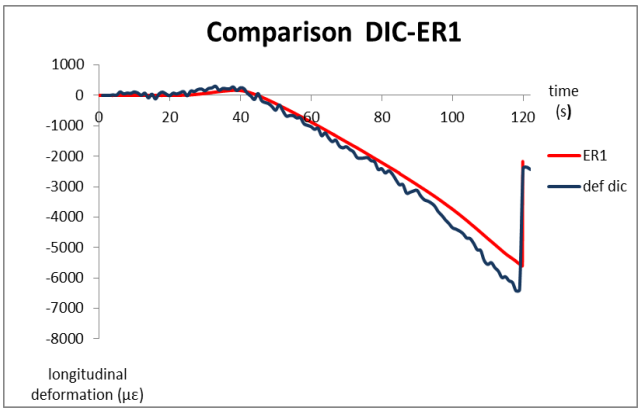

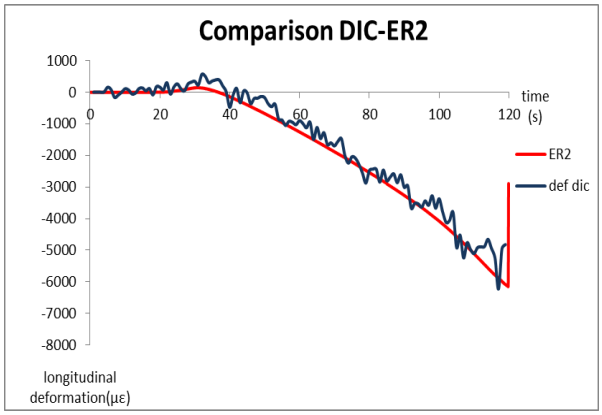

Figure 7. Comparison of longitudinal deformation reading between DIC and strain gauge

From the comparison between the two techniques it is possible to infer that there is some overlap in the deformation trends. For one of the two considered ER lower deformation where recorded; this may be due to a misalignment error in the mounting of the two strain gauges, in fact there is a certain shift between the left and right of the specimen with respect to the center of the latter in favor of the left area.

It should also be observed that higher level of noise affects the data obtained by DIC as reported in Fig.7 and this is due to the high luminance reflected by the bounding structure, on the right side where the ER2 is mounted.

In this case a "smoothing" operation is preferable.

In Fig.8 the trend of longitudinal deformation along the cross section of the specimen is shown, at the step t = 116s .

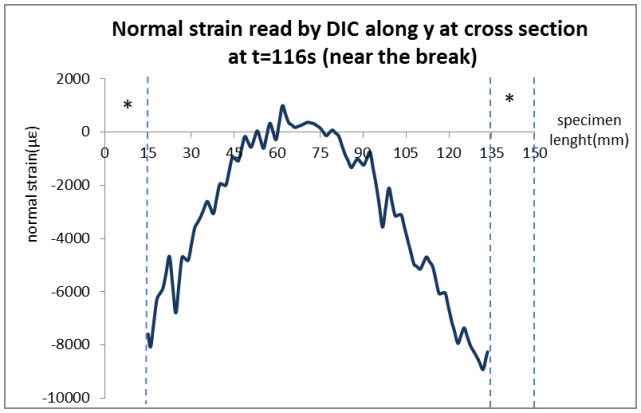

Figure 8. Normal strain ε_{yy} at t=116s

It can be noticed that the component has a normal strain ε_{yy} negative in the outer areas, according to a nearly symmetrical pattern with respect to the center of the specimen. At the center the deformations are positive then the specimen stretches slightly.

There is a certain shift towards the top, in fact it is precisely in that area, exactly 15 mm from the 0 that breaks. In Fig 9 the shear strain recorded after 116 s is reported

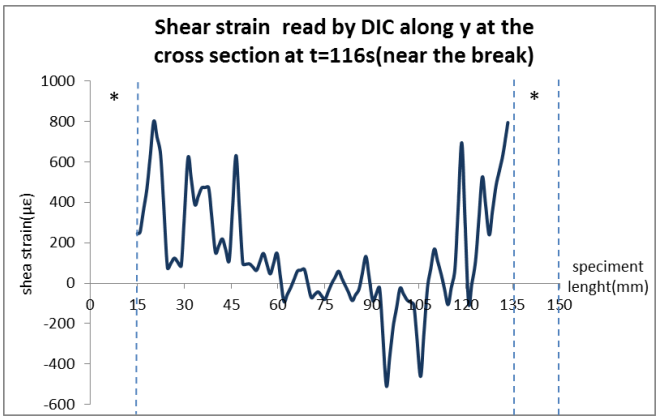

Figure 9. Shear strain γ_{xy} at t=116s

Interesting considerations can be made on the previous graph.

It was noted that the maximum shear strain value can be traced from 15 to 20 mm from the zero and that is the point where the sample starts to break.

This may be understood in the framework of the continuum mechanics theory. Such deformation, in fact, is due to the sum of the mixed derivatives of the x e y displacements in response to the angular deformation of the composite in that area that determines delamination effects.

Previously indicated asymmetry was also found by analyzing the out of plane z displacements (Figure 10), in fact despite of the trend being typical of a gaussian, the lower part has a different slope than the upper one.

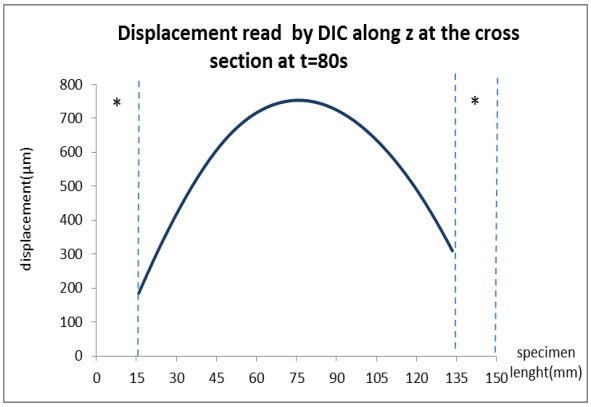

Figure 10. Out of plane displacement w at t=80s

The off-plane displacement behaviour indicates how the specimen goes in buckling exactly at the center with a value of w = 750 μm at $\frac{l}{2} = 75mm$.

It can be stated, however, that although the specimen was constrained to a structure designed to avoid buckling, the

phenomenon of elastic instability is, however, at a critical load which is certainly higher than that referenced by the bibliography for a simply anisotropic supported plate subject to uniaxial compression [7].

The areas indicated by * do not display information since in those areas the DIC was unable to recognize the speckle pattern and therefore could not read the u,v,w displacements along x, y, z.. The underlying reason for this lack of information is that the particular constrained structure creates shadow zone that do not allow the lenses to recognize the white and black points typical of the speckle pattern.

4 Conclusions

In this paper the mechanical behavior of composite subjected to compression loading was reported as analyzed by Digital Image Correlation.

Electrical strain gauges at known locations [5] were also used in order to compare local results obtained by ER and full-field results obtained by DIC. This comparison underlines the possibility to apply the 3D DIC technique as an integration or a replacement of traditional measuring instruments to calculate displacements and deformations on the whole surface of the specimen. Allowing also reduction of some experimental bias as those connected with ER misalignment. Moreover, DIC is able to capture asymmetries in the behaviour of the sample, and this is a fundamental aspect for materials that are non-homogeneous and anisotropic.

Acknowledgment

Research co-funded by *Fondo di Sviluppo e Coesione 2007-2013 – APQ Ricerca Regione Puglia* "Regional program to support smart specialization and social and environmental sustainability – FutureinResearch"

References

[1] F.C. Campbell Jr - *Manufacturing Technology for Aerospace Structural Materials*

[2] I.K.Varma, V.B.Gupta, - *Thermosetting Resin Properties, Volume 2*; (ISBN: 0-080437206); IIT, Delhi, India.

[3]Sutton, M.A., J.J. Orteu, and H.W. Schreier - *Image Correlation for Shape, Motion and Deformation Meaasurements.* Springer Science, 2009.

[4]Ajovalasit, A. - *Analisi sperimentale delle tensioni con la fotomeccanica*, 2009

[5] ASTM standard 7137 (Compression After Impact "CAI")

[6] Yong-Kai Zhu [1], Gui-Yun Tian [1,2,*], Rong-Sheng Lu [3] and Hong Zhang [2] - *A Review of Optical NDT Technologies*

[7]. N. S. Trahair - *Flexural torsional buckling of structures*, CRC Press, 1993

IMPROVING THE PRECISION OF PLANT RESPONSE BY MODELING THE STEADY STATE ERROR

MSc. Dushko Stavrov, Assist. Prof Goran Stojanovski, Prof. DSc Stojche Deskovski,

Faculty of Electrical Engineering and Information Technology – University of Ss Cyril and Methodius in Skopje, Republic of Macedonia

dushko.stavrov@feit.ukim.edu.com.mk

Abstract: *Nowadays, one of the most common problems in control system theory that should be tackled is how to improve the precision of a plant in steady state, under a change in the target value of the plant. Well known fact is that the models we use for designing controllers are not ideal. Thus, when the controller is applied to the real plant there is difference in between the expected and obtained results. Likewise, the controllers should be designed to be at the same time robust to uncertainties and also fast enough to drive the system to the desired value. The purpose of this paper is to describe and finally implement the approach in which the idea is to improve the precision of the system in steady state by adding an additive term to the control value calculated by the predesigned PID controller. The PID controller is designed in advance, and has poorly tuned integral term. Afterwards, when the desired target value is changed the PID controller is not aware of that change, so its performance starts to drop and as a result the steady state error starts to increase. Therefore, to preserve the exactness of the plant's output an additive term to the control signal is calculated out of a polynomial second order model derived from the error values obtained in the previous measurements of the plant. The results from MATLAB simulations have shown that the PID controller could not keep up good performance when the target value of the system is changed. Hence, by adding an additive term to the control signal we gave to PID the needed 'awareness' and as a result of that we could improve the steady state error by small margin.*

KEYWORDS: PID CONTROLLER, ADDITIVE TERM, POLYNOMIAL SECOND ORDER, EXACTNESS,

1. Introduction

In control literature, one can easily find a variety of different examples for industrial control, where contemporary control algorithms are implemented. Surprisingly, there are not much known examples where the state-of-art control algorithms have been implemented in real-time control systems, like for example: missiles, jets, drones, robots, etc. Instead as control techniques for such systems researchers usually implement algorithms that are proven to be reliable, fast and easy to implement. In the light of this discussion we can add that nowadays control algorithms are not a single or stand-alone solution, like the basic PID controller is. Instead contemporary controllers are supported by a bundle of additional procedures. For example, the MPC algorithm ([6], [7]) which is considered as main candidate to replace the much simpler, wholly grail of industrial control - the PID controller, uses a lot of background computations to generate the control signal.

The PID controller is in the heart of control engineering practice for more than seven decades. The PID controller is one of the most commonly used controllers in industry. Some of the reports show that PID controllers are being used in 90-95% of the control loops in industry ([1], [2]). Its simple structure has made PID controller one of the most widespread controllers in all technical systems. Over the long history of its use and development, the simple notation of PID control mechanism has been augmented with new features that aim to improve its efficiency. However, the key question that many scientists try to solve is - which is the best procedure to tune the PID parameters, in order to achieve the desired control object performance. One should mention that one of the most broadly used method of computing the PID coefficients, in industry, is Ziegler Nichols method ([3]). However, we should make a notice of a reference of the tuning of PI and PID controllers ([4], [5]) whose second edition published in 2006, shows that there are more than 400 versatile methods of PID synthesis. Even though there are a lot of synthesis methods of PID controller, some reports say that around 80% of the PID controllers are poorly tuned, where 30% of the the PID controllers operate in manual mode [9].

Although there are a lot of advantages of PID control, it cannot be successfully used when dealing with system with drifting parameters. It is well known that the industrial plants, are subject to change in time and the possibility of parameter drift in the plant drastically increases as the plant is being operated. We interpret this as parameter uncertainties in the control object which usually leads to worse performance of the control system. Hence, if the PID controller was initially designed to work for a particular operating point, after the parameters drift, the controller should be adapted to the new operating conditions. If there is not some kind of supervisory system that automatically takes care of the adaptation, we should track the parameter drift and occasionally tune the PID parameters.

The above mentioned problem of parameters drift can be solved with adaptive control algorithms, which are making continuous or periodic corrections in the PID coefficients [12]. The problem that arises in this situation is the speed of adaptation of the coefficients. Surely, we want to reduce the time of adaptation to the possible minimum.

Nevertheless, there are other possibilities for correction of the effects derived from the parameter drift. In this paper, we assume that the parameters are already obtained using trial and error. Therefore, we propose an improvement to PID controller in form of an additive term to the PID control value, as $u_{PID} + \Delta u$, aiming to improve the precision of the control object in the steady state. This is of great importance in control systems in chemical industry and manufacturing plants, where the precision in steady state is of great concern for safety and as well as for cost effectiveness.

Moreover, the additive term is calculated as a root of the quadratic polynomial model which is modelled out of the set of previously stored values of the steady state error and additive term values. In mathematical terms the error model is given by:

$$E_M = f(\Delta u). \tag{1}$$

The rest of the paper is structured as follows. Firstly, the mathematical background of the simple and enhanced PID is presented; then the PID enhancement is discussed in more details. Secondly, the case study of a CSTR control system is modelled. Afterwards, both PIDs are applied to the CSTR system and the obtained results are analyzed. Finally, conclusions and outlook for future work are given.

2. Mathematical formulation of simple PID and enhanced PID

Simple PID formulation

Despite the simplicity of the basic notion of a PID controller, we can distinguish several different forms of implementation of a PID control law. Likewise, in industry various forms of PID

controllers are used, more than ten in whole. For more information about different forms of PID realizations see references ([4], [5]).

In this paper we have focused on the simplest PID realization and that is the parallel form. The control signal with this PID form is generated by the following equation:

$$u_{PID}(t) = u_0 + K_p e(t) + K_i \int_0^t e(\tau)d\tau + K_d \frac{de(t)}{dt}. \quad (2)$$

Where, u_0 is a bias in the control signal and $e(t) = SP - PV$ is the current error, which is calculated as difference between set point (SP) also known as reference value and the process value (PV). The coefficients of the PID are, K_p- the proportional term, K_i - the integral term and finally K_d is the derivative term. By any means the generation of the control signal is done very fast and the control value only depends on the current as well as the past values on the error. On Figure 1, the control loop consisted of PID controller and control object is shown.

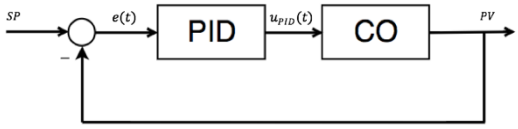

Figure 1 *PID control loop.*

Enhanced PID formulation

As we mentioned before, in the introduction, the simple PID controller doesn't have awareness of how good its parameters had been tuned. Accordingly, in this paper we have tried to give the needed awareness to the PID with the objective to deal with error in steady state as well as to improve the time needed to get in steady state. The principle schematic representation of the approach is given on the Figure 2.

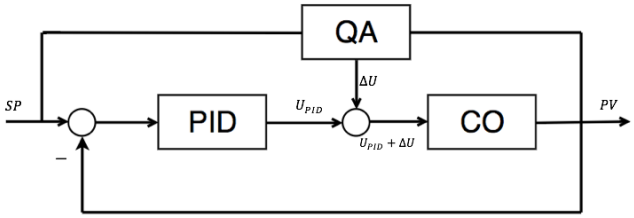

Figure 2 *PID control loop.*

On Figure 2 the change we have done on the simple PID structure is shown. As opposed to what is on the Figure 1 we can see that on Figure 2 there is an additional component named QA. It is an abbreviation of the word Quadratic Approximation. The main idea is, as the control system operates, in the background to have some kind of supervisory mechanism which principle purpose would be to model the steady state error in the system. Afterwards the same model presented with equation (1) will be exploited as apparatus out of which the additive term Δu will be calculated.

The whole process of plant control, calculation of the PID control value in addition to additive term is given with the flow chart on Figure 3. Where N_s is the number of simulation steps of the plant (control object). As long as the counter $i \leq N_s$ the plant is controlled in as presented on Figure 2. When the condition given with equation, (3) is true, the steady state error defined with the equation (4) is calculated and stored. The name, mod stands for function which gives information whether in division between i and DV there is residuum or not. If the residuum is zero that means that i is divisible with the number DV. The index j in the brackets, in (4), indicates how many times the condition given with (3), was fulfilled and in the same time, it gives the number of collected steady state error points which after that will be used for designing a quadratic model, equation (1). The variable PV_{ss} stands for steady state value of the process value. Further, DV stands for the Dynamical Variable, which defines on how many simulation steps an error point should be collected.

$$mod(i, DV) = 0, \quad (3)$$

$$E_{ss}(j) = SP - PV_{ss} \quad (4)$$

The next step is to check whether $j \geq 6$, if it is not, then a simple metric is used for producing the points needed for quadratic model fitting.

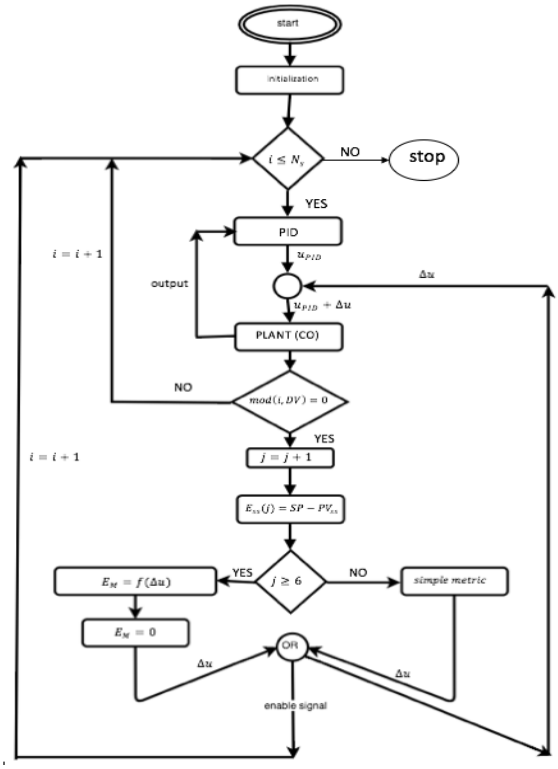

Figure 3 *Flow chart diagram of proposed algorithm.*

The metric that has been used is,

$$\Delta u = k_{ss} \sum_{m=1}^{j} E_{ss}(m). \quad (5)$$

where the parameter $\boldsymbol{k_{ss}}$ is obtained using the trial and error method. Afterwards, when 6 points are gathered, it is easy to fit a quadratic model like the one given with (6). To fit the model (6) we only need 3 points ([10], [11]). In other words, the sufficient number of points is equal to the number of unknown parameters. In this paper the model was dynamically generated out of the last 6 steady state error points. The equation of the model is given by***:***

$$E_M(\Delta u) = A(\Delta u)^2 + B(\Delta u) + C \quad (6)$$

The parameters A, B and C of the model are calculated by solving the next equation:

$$p = (M^T M)^{-1} M^{-1} \cdot J \quad (7)$$

Where $p \in \mathbb{R}^3$ is a vector of parameters,

$$p = [A, B, C]^T, \quad (8)$$

$M \in \mathbb{R}^{6\times 3}$ is a matrix of 6 points, which are considered to determine the parameters p.

$$M = \begin{bmatrix} (\Delta u_1)^2 & \Delta u_1 & 1 \\ \vdots & \vdots & \vdots \\ (\Delta u_6)^2 & \Delta u_6 & 1 \end{bmatrix} \quad (9)$$

At last, $J \in \mathbb{R}^6$ denotes the vector of error values. Equation (7) can be solved if the inverse $(M^T M)^{-1}$ exists, which means that the matrix M should have rank equal to the number of parameters, in

our case that number is 3. In other words, the points used for regression have to be distributed in a way that the rank of matrix M is not smaller than 3.

At first sight, 3 points seem to be enough to solve the equation (7). However, there are cases in which the chosen 3 points are not suitable. First of all, it is clear that two points should not be placed in the same location which leads to a reduced rank of M. Furthermore, it has to be ensured that the points are not distributed on a line. Anyway, if that is the case then the information provided by the points is not adequate to describe a quadratic function exactly.

3. Case Study: Nonlinear Non-isothermal Continuous Stirred Tank Reactor

Consider a simple liquid-phase, irreversible chemical reaction where chemical reactant A is converted to product B. The reaction that happens in the reactor can be written as follow $A \rightarrow B$. Also, we assume that the rate of reaction is first-order with respect to reactant A:

$$r = kC_A \tag{10}$$

where r is the rate of reaction of A per unit volume, k is the reaction rate constant and C_A is the molar concentration of reactant A. For a single-phase reaction as we are assuming here, the rate constant is typically a strong function of reaction temperature. The rate constant is given with the equation:

$$k = k_0 e^{-\frac{E}{RT}} \tag{11}$$

where E is the activation energy, R is the gas constant and k_0 is the frequency factor.

The graphical representation of the CSTR is given on Figure 4. The input in the system is the inlet flow which is consisted of reactant A with concentration C_A. Often, the reactions happening in CSTR system have significant heat effects. Thus it is important to be able to add or remove heat from them. Adding or removing heat from reactor depends on the temperature difference between the cooling jacket fluid and the reactor fluid.

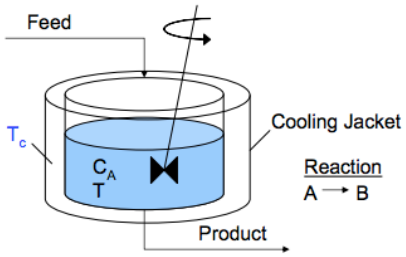

Figure 4 *CSTR system.*

The model of this control system is given by the following two equations [8]:

$$\frac{dT}{dt} = \frac{q}{V}(T_f - T) + \frac{\Delta H}{\rho C_p} k_0 e^{-\frac{E}{RT}} + \frac{UA}{V\rho C_p}(T_c - T) \tag{12}$$

$$\frac{dC_A}{dt} = \frac{q}{V}(C_{Af} - C_A) - k_0 C_A e^{-\frac{E}{RT}} \tag{13}$$

where T_c, the temperature of the cooling jacket fluid, is the manipulated variable and T, reactor temperature, is the controlled variable. Production of the desired component concentration depends on coolant flow rate, reactor temperature and reaction rate. It is assumed here that the cooling jacket flow is fixed. Other parameters values contained in equations (12) and (13) are given in Table 2.

For the purpose of simulating and also solving the equations (12) and (13) MATLAB has been used. More precisely for numerically solving of system equations the ode23t function was employed with integration step of T =0.01 min. The initial conditions of the system are given in the Table 1.

Table 1: *Initial conditions for temperature and concentration*

$\boldsymbol{T(0)}$	$\boldsymbol{296.6\ K}$
$\boldsymbol{C_A(0)}$	$0.98\ mol/m^3$

Table 2: *Model parameters.*

Parameter	Value	Parameter	Value
Volumetric flowrate $[m^3/sec]$	$q = 100$	Overall heat transfer coefficient $[W/(m^2K)]$	$UA = 5 \cdot 10^4$
Volume of CSTR $[m^3]$	$V = 100$	Feed concentration $[mol/m^3]$	$C_{Af} = 1$
Density of A-B mixture $[kg/m^3]$	$\rho = 1000$	Feed temperature $[K]$	$T_f = 350$
Heat capacity of mixture $[J/(kgK)]$	$C_p = 0.293$	Activation energy $[J/mol]$	$E/R = 8750$
Heat of reaction $[J/mol]$	$\Delta H = 5 \cdot 10^4$	Pre-exponential factor $[1/s]$	$k_0 = 7.2 \cdot 10^{10}$

4. Implementation of the discussed algorithms, PID and enhanced PID and results

In this part we will apply the two PIDs, discussed before, on the CSTR system. First of all, the parameters of both PIDs will be defined. Further, the two algorithms will be simulated in MATLAB, in the fashion given on Figure 1 and Figure 2, where the CO (Control Object) is the highly nonlinear system CSTR. To prove that, the CO is highly nonlinear, we have carried out an open loop simulation. The simulation of the algorithms was carried out over a period of 135 minutes or speaking in simulation steps $N_s = 1350$. The next, Figure 5 shows that at temperature of the 305 of T_c the CSTR system exhibits limit cycle behavior.

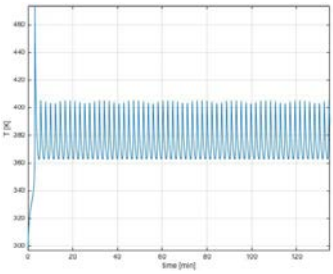

Figure 5 *Open loop simulation of the CSTR system at coolant temperature of 305 K.*

Furthermore, in this paper we assumed that all of the parameter in the system are constant and do not survive drift. Both controllers, simple PID and enhanced PID will be compared in two different scenarios. The first one (Scenario 1) is when the reference value (SP) changes from 300 to 305 K. The second one (Scenario 2) is when the reference value (SP) changes from 300 to 295 K. In both scenarios the responses of the PIDs will be compared. The IAE (Integral Absolute Error) metric given with the equation:

$$IAE = \frac{1}{N_s}\sum_{r=1}^{N_s} |e(r)|, \tag{14}$$

is used to estimate how well one of the controllers performs over the other. We should also mention that the parameters of the two controllers in both scenarios are the same and are given in Table 3,

Table 3: *both PID parameters*

$\boldsymbol{K_p}$	$\boldsymbol{4.5}$
$\boldsymbol{K_i}$	0.5

K_d	0.04

Let's first consider the Scenario 1, when the SP changes from 300 to 305 K, at 60 minute. On the next figure (Figure 6) are given the responses of both PIDs, the response of the simple PID is given in blue whereas the response of the enhanced PID is given in red.

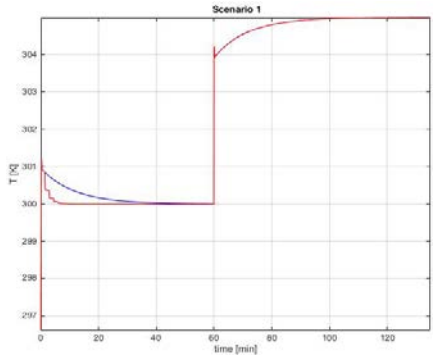

Figure 6 *Response of the CSTR system in cases when it is controlled by simple PID (blue line) and enhanced PID (red line) in Scenario 1.*

From the Figure 6 we can conclude that the overall response of the system has improved. Indication for that is the metric IAE, its values show that the enhanced PID is performing better than the simple PID. The IAE values, for Scenario 1, are given in the Table 4:

Table 4: *IAE values for the Scenario 1*

Simple PID	0.1801
Enhanced PID	0.1156

Let's now consider the Scenario 2, when the SP changes from 300 to 295 K, at 60 minute. On the next figure (Figure 7) are given the responses of both PIDs, the response of the simple PID is given in blue whereas the response of the enhanced PID is given in red.

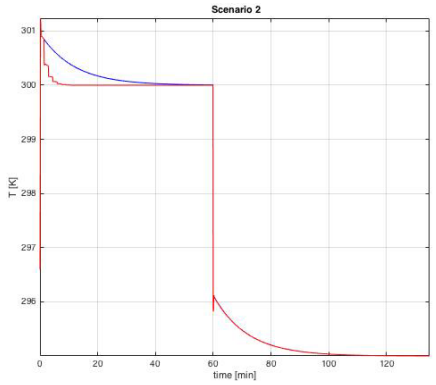

Figure 7 *Response of the CSTR system in cases when it is controlled by simple PID (blue line) and enhanced PID (red line) in Scenario 2.*

Figure 7 indicates that the enhanced PID controller in first phase of the simulation, until 60 minute, is able to converge very fast to the SP value, but after the 60 minute the enhanced PID and simple PID are performing equally bad. That was also the case in the first scenario. It is a problem that indicates that the quadratic model has not ability to adapt very well. A solution for this problem is already being considered; it is thought that the problem might be solved by adding additional information into the model, such as the temperature T or the SP value. However, the values of the IAE metric as in the Scenario 1 led us to the same conclusion in the Scenario 2. The enhanced PID performs better by small margin. The IAE values in Scenario 2 are given in the table that follows:

Table 5: *IAE values for the Scenario 2*

Simple PID	5.5467
Enhanced PID	5.4821

5. Conclusion and outlook for future work

In this paper we present an enhanced PID controller used to compensate for the steady state error. The presented controller is compared with a standard PID controller most commonly used in industry, with poorly tuned integral term. The proposed algorithm uses historical values for the steady state error and the additive control term to create a simple quadratic model of the plant's steady state error. The simulations have shown that the enhanced PID using the additive control term beats the performance of the simple PID by a small margin.

Future work will consist of implementing and afterwards comparing the same controllers presented here, in a case where they are used to control a system, possibly the same one CSTR system, which exhibits drift in some of the parameters. In such conditions, it is expected that the proposed control approach will have superior performances over the standard PID.

ACKNOWLEDGEMENTS

The work was funded by the Faculty of Electrical Engineering and Information Technologies in Skopje, Republic of Macedonia, through the ERESCOP Project.

REFERENCES

[1] Astrom, K. J. and Hagglund, T., Advanced PID control, North Carolina: ISA, 2006.
[2] Rotach, V.Ya, Teoriya avtomaticheskogo upravleniya: uchebnik dlya VUZov (Automated Control Theory: Univeristy Textbook), Moscow: MEI Publishing House, 2008.
[3] Ziegler, J.G. and Nichols, N.B., Optimum Settings for automatic controllers, Trans. ASME, 1942 vol.64, pp 759-768.
[4] O'Dwayer, A., Handbook of PI and PID controller Tuning Rules, London: Imperial College Press, 2009 3th ed.
[5] O'Dwayer, A., Handbook of PI and PID controller Tuning Rules, London: Imperial College Press, 2006 2th ed.
[6] Badwe, A. S., R. D. Gudi, R. S. Patwardhan, S. L. Shah, and S. C. Patwardhan, Detection of Model-Plant Mismatch in MPC applications, J. Process Control, 19, 1305 (2009)
[7] Camacho, E. F., and C. Bordons, Model Predictive Control 2nd ed., Springer-Verlag, New York, 2003
[8] D.E. Seborg, D. A. Mellichamp, T. F. Edgar, and F. J. Doyle III, Process dynamics and control: John Wiley & Sons, 2010.
[9] P. Van Overschee and B. De Moor, in Preprints, Proc. PID '00: IFAC Workshop, Terrassa, Spain, pp. 687-692, 2000
[10] G. Stojanovski, L. Maxeiner, S. Kramer, S. Engell, "Real-time Shared Resource Allocation by Price Coordination in an Integrated Petrochemical Site", 2015 European Control Conference (ECC), pp. 1492-1497, 2015.
[11] S. Wenzel, R. Paulen, S. Kramer, B. Beisheim, S. Engell, "Shared Resource Allocation in an Integrated Petrochemical Site by Price-based Coordination Using Quadratic Approximation", 2016 European Control Conference (ECC), June 29 – July 1, 2016 Aalborg, Denmark.
[12] Rania A. Fahmy, R. I. Badr, Farouk A. Rahman, "Adaptive PID Controller Using RLS for SISO Stable and Unstable systems", Advances in Power Electronics, Volume 2014, Article ID 507142.

Path Planning and Collision Avoidance Regime for a Multi-Agent System in Industrial Robotics

MSc. Ivan Gochev, MSc. Gorjan Nadzinski, Prof. DSc Mile Stankovski,

Faculty of Electrical Engineering and Information Technology – University of Ss Cyril and Methodius, Republic of Macedonia, Skopje

ivang@feit.ukim.edu.com.mk; gorjan@feit.ukim.edu.mk; milestk@feit.ukim.edu.mk

Abstract: *Industry 4.0 which creates "smart factories" present a recent trend in development. The area represents a merge of cyber-physical systems and Internet of Things, which aims to improve manufacturing technologies. Industry 4.0 strives to boost the algorithms and technologies used in industrial processes during the production processes, process preparations, and products delivery. Our intention is to improve the robotics transport system in factory floor. There are a lot of different research approaches in this area for further improvement. Our approach is to deal with multi-agent systems control, because of the great potential it has in practical applications in industrial robotics. The strive for minimizing the work time and maximizing the efficiency can be satisfied through the usage of multiple coordinated agents to achieve the end goal. The use of Automated Guided Vehicles (AGVs), combined with concepts for task planning of multiple agents broadened during the late 20th century. In this paper, the multi-agent system consists of several mobile robots, in other words platforms, which need to transport materials in a workhouse. The goal of each mobile platform is to carry the specified object to a set position. These appointed goals are not predefined and can be changed according to the needs of the user. Working in a dynamic environment, numerous agents with different tasks to complete can be exposed to many obstacles which may be the cause of accidents. For this reason, a careful path planning is required in such environments. The suggested path planning algorithm for this system is A*. A* is a fast path finder, which can navigate quite well in a planar environment, but it is not favorable for dynamical settings. Therefore, a combination of the A* algorithm with a collision avoidance method is proposed for overcoming these difficulties. By doing this, the A* algorithm is expanded to work in dynamical situations and can assure the convergence of any agent towards their goal. This fusion of both, the path finding algorithm and the collision avoidance method, can aid the cooperation of the agents and improve the efficiency of the system as a whole.*

Keywords*:* Industry 4.0, smart factory, factory floor, multi-agent systems, mobile robotics, A* algorithm, collision avoidance.

1. Introduction

Recent technological advances indicate that we are witnessing the dawn of an era of Internet of Things [1]. Internet of things is broadening its possibilities in industry as well, providing more flexibility and maneuverability in production. Intelligent agents creating multi-agent systems provide better performance instead of single agents completing different tasks. Not only that, but multi-agent systems can even found themselves in a situation to complete tasks which other individual agents would not be able. The control of multi-agent systems is presented in [2]. The industry strives to create manufacturing systems that would be fully autonomous, in order to increase the time and capacity of production. The first step to automate the environment is to plan the trajectory that each robot has to follow to reach the end goal. A* is one of the most used algorithms for finding optimal paths [3] [4].

In this paper, a small representation of a smart factory is presented where automatic guided vehicles (AGVs) are accomplishing different tasks. The main idea is to design an autonomous warehouse, where mobile vehicles (agents) deliver packages. For that very reason in this paper path planning in the environment and preventing collisions between agents of the multi-agent system is accented the most. In section 2, the environment (warehouse) layout and the multi-agent system working in those settings are presented. The following sections, Section 3 and Section 4 explain the planning and control algorithms used to create the autonomous work of the whole system, and the avoidance rules of agents and static environment obstacles. Section 5 briefly shows the function of the different aspects of in the whole project and the results from the implemented algorithms. In Section 6 a conclusion is given, as well as the outlook for future work.

2. Environment settings and Multi-agent system

V-REP and factory settings

The multi-agent system along with the environment in which it operates is represented in the programing package V-REP (Virtual Robot Experimentation Platform), a program for prototyping robotics systems. V-REP is the first step for system design and algorithm testing, because it offers a flexible program with a lot of possibilities. The free open source educational version of the robotics toolbox is provided by Coppelia Robotics. Robotic simulators represent the connection between artificial creatures' theory and robotics. They provide an additional guarantee that cognitive framework developed can be applied to real robots, with need of minor adjustments needed [5].

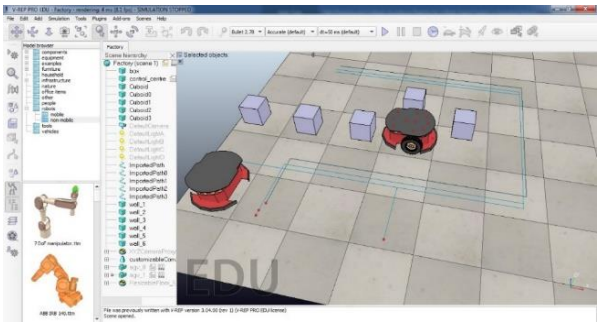

Fig. 1: V-REP Simulation interface

The simulator is running from Python code where most of the main algorithms are written. The basic idea is that the hardware aspects of the system are realized in the V-REP simulation interface, whereas the logic is implemented in Python. V-REP is the server side, and Python is the client side. Both programs are communicating through an Application Programming Interface (API). The remote API modus operandi represent a set of functions, subroutines, protocols and tools for building application software.

Multi-agent system

The multi-agent system consists of automatic guided vehicles (AGVs), which are by definition the agents of the system. They are equipped with 16 ultrasonic sensors and 10 force sensors. The end goal of each mobile robot of the multi-agent system is to hand out a specific object to the correct position in the warehouse. They need to navigate in a time differing and dynamic environment. The system is made up of *N* automatic guided vehicles which distribute certain goods in a warehouse and the best way to automate that is to implement some kind of planning logic. Having an optimal planning

algorithm would enhance the performance of the system as a whole and therefore a heuristic pathfinding algorithm is proposed. The suggested algorithm is A* (A-star) and this is only the first step in designing the whole factory floor. To ensure the convergence towards the final objective of the whole project, the pathfinding algorithm is enhanced with a collision avoidance regime, which prevents any accidents that might occur.

A multi-agent system is a system composed of multiple interacting intelligent agents in a specific environment. The agents of the system are small mobile robots generated in V-REP called the "Pioneer" model. (Fig. 2)

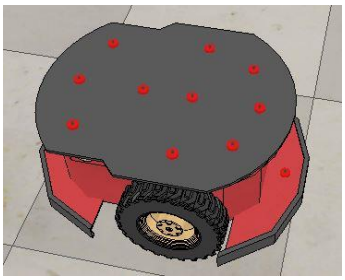

Fig. 2: Pioneer robot model

The mobile robot is equipped with ultrasonic and force sensors. Based on the information from the ultrasonic sensors the specific agent will either enter a collision avoidance regime or it will continue finishing the designated task. When the force sensors are activated, the agent will know that a specific object to transport is given to it and will start completing the task. The algorithms are tested for two agents in the environment, but there are no restrictions on how many agents can be involved if the hardware can endure.

The mobile robots work in a warehouse which is 60 meters long and 20 meters wide. The map of the environment is represented as a grid with 120x60 elements. One cell of the grid is 0.5x0.5m^2. Each vehicle has information about all other objects in the environment, including the other agents, all seen as rigid bodies. A rigid body in space is defined by 3 positions (*x, y, and z coordinates)* and 3 angles (α, β, γ) which give the orientation of the body around a specific coordinate system. When the position of the agent is known the cell coordinates can be obtained through the following equations:

$$\begin{cases} i = \left\| \left[\frac{x}{cell\_length} + environment_{length} - 1 \right] \right\| \\ j = \left\| \left[\frac{y}{cell\_length} + environment_{width} \right] \right\| \end{cases}, \quad (1)$$

where *x* and *y* are the agent coordinates, $cell\_length$ is the length of each cell in the grid, $environment_{length}$ and $environment_{width}$ are the length and width of the whole factory floor (an offset of the grid), and i and j are the obtained cell coordinates. Having the environment mapped as a 120x60 grid, and translated to a graph, the pathfinding algorithm can easily navigate in it and find the optimal trajectory [3].

3. Path planning

One of the most used algorithms for finding an optimal path in an environment is the A* (A-star) algorithm. This is a heuristic search algorithm for graph traversal. It minimizes a cost function for each neighboring node and expands to the nodes with the smallest function value. The algorithms' efficiency depends on the defined heuristic function. The heuristic function is the main decision maker in how the algorithm goes over the vertices of the graph. Because of the grid like representation of the environment, the chosen heuristic is the Manhattan heuristic, given with the equation:

$$h = \left| cell_{1_x} - cell_{2_x} \right| + \left| cell_{1_y} - cell_{2_y} \right| \quad (2)$$

The two parts which construct the A* algorithm are the heuristic and distance between the points in the graph. To complete the whole algorithm, it is needed to get the distance between the points. The distance is calculated as Euclidean with the equation:

$$d = \sqrt{(x_1 - x_2)^2 + (y_1 - y_2)^2} \quad (3)$$

To sum up everything, the A* is storing each neighbor in a priority queue and is looking for the nearest node with minimal f, where f is:

$$f(n) = d(n) + h(n), \quad (4)$$

where n is a neighboring node of the current node in the graph. Fig. 3 shows the generated path from the algorithm for specific settings.

However, there is a possibility for the A* algorithm to generate two or more trajectories for different agents that can intersect, leading to a collision between them. To avoid this the algorithm is enriched with a force model collision and obstacle avoidance regime presented in the following section.

4. Collision avoidance

To increase the certainty of the operation of the multi-agent system in the specific environmental settings, the planning algorithm is augmented with a collision avoidance method. The regime is divided into two parts: prevention of collision between the agents of the system and obstacles avoidance. In the following subsections the proposed methods are shown.

Collision avoidance between agents

Every agent of the system is equipped with ultrasonic sensors which construct a reaction zone around each agent. As soon as another agent is detected in the safe zone, both of them activate the code for collision avoidance. This upgrade enables the agents to quickly react when they are nearing each other and create a roundabout along the generated trajectory, instead of stepping back and changing directions which would be more time consuming. The collision avoidance is based on the force and momentum models of the agents seen as a rigid body [6]. This way the control rule is a whole of a fast path planning algorithm and a quick method for reaction if a potential collision is detected.

As said before, the method is based on the force and momentum models of the agents seen as a rigid body. This means that as soon as two or more agents enter each other's safe zones they become "risky neighbors", and based on the force vectors the new trajectory for the agents is updated with the following equation:

$$\overrightarrow{new_{position}} = \overrightarrow{current_{position}} + C * \widehat{new_{direction}}, \quad (5)$$

where the current position of the agent are the *x* and *y* coordinates. The new direction vector is determined from the direction of the force vector needed to be applied in order for the agent to reach the goal. The amount the new position is updated relies on the weight factor *C*, which is tuned by the user. Two force vectors are needed to complete the control law. Those are the external force vector and the force vector needed to reach the goal. The external force vector represents a sum of the force vectors of all agents in the reaction zone (risky neighbors).

To define whether a force or momentum model will be used, the formulated external force vector and the goal force vector are used to calculate the similarity between them. This similarity states how the agents are set in the environment and how they are moving. Having this information, both agents can move in a linear direction (force model) or rotate around each other (momentum model).

Obstacles avoidance

The obstacle avoidance rule is based on the Braitenberg approach for mobile robot navigation. This method can also be used instead of

the force and moment models for constructing a roundabout between agents, but both algorithms are implemented since the first method preserves the movement of the agents. The deviations from the original path with the first method do not have a large impact on the performance of the system, whereas the Braitenberg method would completely change the direction of the agents, leading to the need to regenerate a new path. The Braitenberg method is used for obstacle avoidance between an agent and other static objects in the environment, such as: walls, boxes, and conveyor belts. The outputs of the ultrasonic sensors directly affect the movement of the vehicle. When the detected obstacle is different than another agent, this part of the control code is activated. The measured distance affects the vehicle motors speeds proportionally to specific weight coefficients. The coefficients can be tuned in order to make the avoidance faster or slower. Although higher coefficients will make the avoidance faster, it will also make the movement of the vehicle more oscillatory. The motor speeds are modified as in the following equation:

$$\widehat{v_m} = v_m + B_c * \bar{s}, \quad (6)$$

where v_m is the motor speed, B_c is the braitenberg weight coefficient, $\bar{s}$ is the normalized data from a specific ultrasonic sensor. The normalization is a function of the minimum safety distance and the maximum detection radius.

5. Simulation

There are 3 aspects that have to be taken into consideration, which are: path planning, obstacle avoidance and agent avoidance. In Fig. 3 we can observe the generated path which the vehicle has to go over. It can be seen that the algorithm correctly finds the optimal path.

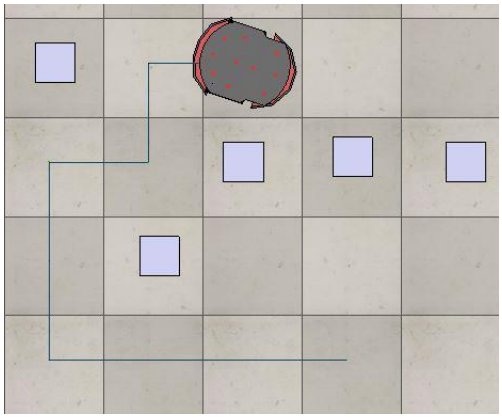

Fig. 3: Generated path from the algorithm

As it can be seen the mobile robot needs to reach the fourth cell in the bottom row. The A* algorithm generates the correct shortest path, instead of a longer one which would make the vehicle circle around the terrain.

Fig. 4 presents the Braitenberg algorithm for obstacle avoidance, where a vehicle switches the direction in order to escape the obstacle.

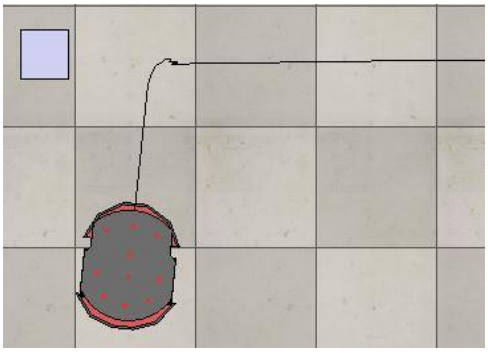

Fig. 4: The vehicle avoids the barrier in front of it

Fig. 5 shows the *x, y,* and *z* coordinates of the vehicle when it avoids the obstacle.

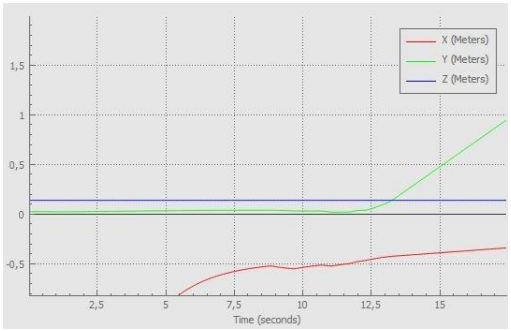

Fig. 5: x, y, and *z* coordinates of the vehicle avoiding the obstacle with the Braitenberg algorithm

The graph shows that the mobile robot successfully changes the path and avoids the static obstacle.

The avoidance between agents is shown on Fig. 6, where if two agents are moving in a direction they construct a roundabout each other and continue moving.

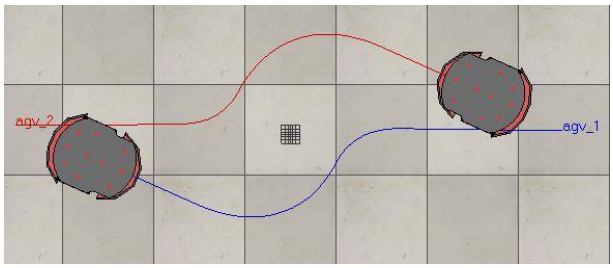

Fig. 6: Agent avoidance

The next figure (Fig. 7) shows the symmetry between the *x, y,* and *z* coordinates of the agents.

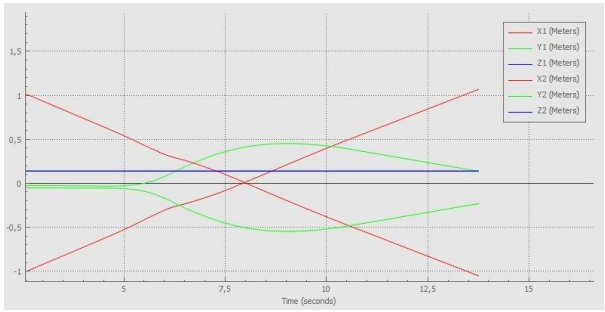

Fig. 7: Coordinates of the agents while avoidance

The symmetry of the mobile robots' coordinates follows the reconstructed path while avoiding other agents shown on Fig. 6.

Figures 3, 4, and 6, show that the algorithms are functioning correctly and giving the correct task for the agents to complete. This states that the three main aspects of the project are tackled, which leads to the project functionality.

6. Conclusion and outlook for future work

In this paper a prototype of a smart factory is presented with accent put on the path planning in the specific environment settings. The environment is mapped as a 2D grid represented as a graph where the objects are stationed and the automatically guided vehicles can operate. The proposed path planning algorithm is A*, a heuristic search algorithm which is used for graph traversal. The algorithm generates a path for each vehicle on factory floor, to the end position the vehicle needs to reach. To ensure the operation of the whole multi-agent system the A* algorithm is implemented together with a collision avoidance and obstacles avoidance rules.

Future work in this area consists of further upgrades of the proposed algorithms, or switching to dynamical pathfinding algorithms which can significantly improve the multi-agent systems' performance and even replace the collision avoidance regime. Another idea includes finding a way to modify the graph vertices which represent the environment in such way that the generated path will avoid the static obstacles [7]. The Braitenberg algorithm used for obstacle avoidance can be upgraded to be used in agent avoidance as well, which would lead to less computational power used if there are two algorithms instead of three. This can be achieved if the Braitenberg algorithm is modified so that the sensors values influence the actuators in a symmetrical way, which would lead to the same outcome as the force and moment model method. Furthermore, a wide variety of data can be obtained in the environment in which the multi-agent system operates. The information from those data sets can be used to improve the performance of the multi-agent system.

ACKNOWLEDGMENTS

The work was funded by the Faculty of Electrical Engineering and Information Technologies - University of Ss Cyril and Methodius, Republic of Macedonia, Skopje, through the ERESCOP Project.

References

[1] Feng Xia[1], Laurence T. Yang[2], Lizhe Wang[3], Alexey Vinel[4] "Internet of Things," [1]*School of Software, Dalian University of Technology, China,* [2]*Department of Computer Science, St. Francis Xavier University, Canada,* [3]*Indiana University, USA,* [4]*Tampere University of Technology, Finland*

[2] Shamma, J.S. (2007) *Cooperative Control of Distributed Multi-Agent Systems*, Wiley Online Library

[3] Peter Yap, "Grid-Based Path-Finding," Department of Computing Science, University of Alberta Edmonton, Canada

[4] Xiao Cui, Hao Shi"A*-based Pathfinding in Modern Computer Games," *School of Engineering and Science, Victoria University, Melbourne, Australia*

[5] Lucas Nogueira, "Comparative Analysis Between Gazebo and V-REP Robotic Simulators," School of Electrical and Computer Engineering Universidade de Campinas

[6] Victor Casas, Andreas Mitschele-Thiel, Mehdi Harounabadi, "On the Emergence of Virtual Roundabouts from Distributed Force/Torque-based UAV Collision Avoidance Scheme," 2017 13th IEEE International Conference on Control & Automation (ICCA) July 3-6, 2017. Ohrid, Macedonia

[7] Tomas Lozano-Perez, Michael A. Wesly, "An Algorithm for Planning Collision-Free Paths Among Polyhedral Obstacles," IBM Thomas J. Watson Research Center

MOVING TARGET DETECTION BY ACOUSTIC FORWARD SCATTERING RADAR SYSTEM

Prof. DSc Eng. Garvanov I., PhD student Vladimirov S., PhD student Geshev N.
University of Library Study and Information Technologies, 1784 Sofia, Bulgaria
i.garvanov@unibit.bg, stoyanvladimirov@yahoo.com

Abstract. *The paper explores the possibility of detection of moving target on the base of their sound shadow (sound blocking) when the target cross the baseline in the Acoustic Forward Scatter Radar System (AFSRS). Experimental sound shadows have been obtained from moving cars. The algorithm under investigation can be applied to create a network of sound barriers.*

KEYWORDS: TARGET DETECTION, FORWARD SCATTERING SYSTEM, SOUND SHADOW

1. Introduction

The paper is based on the theory of distribution of sound waves in the airspace and their interaction with moving targets. The idea of this article is to use the sound shadow to detect moving objects crossing the virtual line between the sound transmitter and the sound receiver. In our study, sound receiver and transmitter form bistatic system because are placed in different location, where the bistatic angle between the directions "receiver-target" and "transmitter-target" should be around 180^0. This bistatic system is called Forward scattering radar (FSR) system [1]. When the target moves close to the virtual line between the receiver and the transmitter it creates the diffraction of the transmitted signal. In this configuration, the receiver signal is received as a result of the phenomenon of diffraction of sound signals. The Forward Scattering (FS) effect has been studied by many scientists and it is the basis for the creation of different radio barrier systems. In [2], the authors used GSM signals to detect targets. In [3–8], GPS signals have been applied to detect moving targets using the principles of FSR. In [9], the authors proposed the usage of WiFi to detect moving targets by FS principles. Most of proposed technologies are used the principles of FS configuration or split receiver and transmitter and an object passing between them. In [10] are given the normal mode model for a waveguide to analyze the phenomena of forward scattering created by a target crossing the virtual line “transmitter-receiver”, and its physical significance. The experimental results demonstrated the capability of forward scattering detection for slow moving objects.

The diffraction of the sound signals is a well-studied phenomenon and it is similar to the diffraction of the electromagnetic signals. Despite the difference in the nature of the radio and acoustic signals, the shadow effect is present in both types of signals [11]. Such studies have been conducted by the team of this article but with GPS signals, which demonstrated the great potential in this field [3–8]. The purpose of this article is to apply the accumulated knowledge and skills from the field of radio signals in the field of sound signals and as a result to develop algorithms for detecting mobile targets using the sound shadows created by the targets. In this article, one possible algorithm for moving car shadow detection is studied by using the acoustic forward scattering effect.

The proposed algorithm can be used for in automated tracking and traffic management systems in the future smart cities [12, 13]. This algorithm is inexpensive and usable in real-time systems. The resulting audio shadows have specific characteristics and parameters that can be evaluated and used to classify moving objects. This algorithm can also be used to create border or object security systems. Both artificial and natural sources of sound signals as well as background sounds with constant parameters can be used as the sound source.

2. Acoustic Forward Scatter Radar System

Forward scattering system is a special case of bistatic configuration where the bistatic angle is close to 180 degrees. The bistatic angle is the angle between transmitter, target and receiver, as shown in Fig.1.

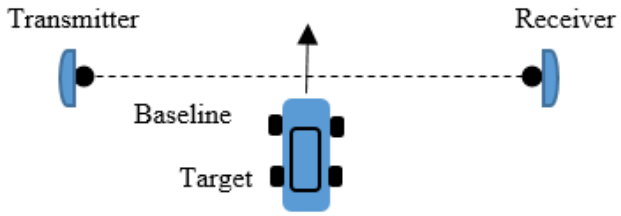

Fig. 1: *Illustration of acoustic forward scattering configuration.*

The FSR is based on the Babinet principle, which says that the shadow radiation in the optical case is completely determined by the size and geometry of the shadow contour [1, 2]. Thus scattering on the target with the rectangular cross-section is equivalent to the radiation by a rectangular aperture antenna. This principle is a theorem concerning diffraction, stating that the diffraction pattern from an opaque body is identical to that from a hole of the same size and shape except for the overall forward beam intensity. Diffraction of wave can be divided into two classes: Fresnel diffraction (when the target is close to the transmitter or the receiver) and Fraunhofer diffraction (when the target is far from the transmitter and the receiver) (Fig. 2).

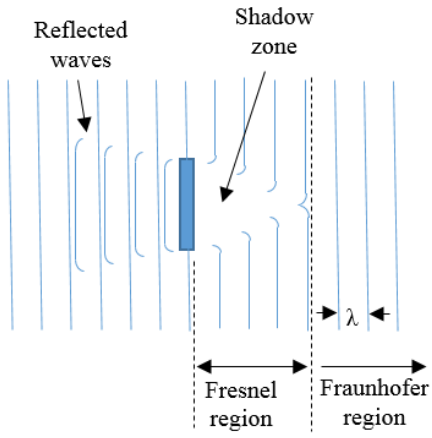

Fig. 2: *Sound diffraction.*

In Fresnel diffraction, the size of the target is comparable with the Fresnel zones, which takes place when the target is relatively close to

the receiver or the transmitter. Here, the diffraction pattern varies from high intensities to low intensities as the targets cross different Fresnel zones. These variations will depend on the coverage percentage of one or more Fresnel zones.

Sound waves are affected by the different targets that they come into contact with. For example, denser materials are better at absorbing sounds than thinner ones. Although materials can absorb sounds, they can also reflect and diffract them. Diffraction of a sound is when the wave gets to an object and propagates around it. The phenomenon of diffraction is the basis of the signal propagation in the in forward scattering system (Fig. 2). Our first goal is to confirm the possibility of signal blocking caused by moving target crossing the baseline in the Acoustic Forward Scatter Radar System (AFSRS).

Naturally, to ensure the registration of sound shadows the values of the sound signal in the sound shadow zone must be distinct from the noise of the receiver by a few decibels. That's why we chose to make the recordings of sound signals on a variety of distances, when target are very close to the receiver and are in the sound shadow area. For the simplicity of the experiment, we chose the moving object to be car crossing the radio barrier.

3. *Signal processing*

The paper presents a possible variant of signal processing in passive Acoustic Forward Scatter Radar System [11]. The general block-scheme of a possible algorithm for AFSR shadow detection includes: signal decimation and filtration, signal envelope evaluation and signal detection (Fig. 3).

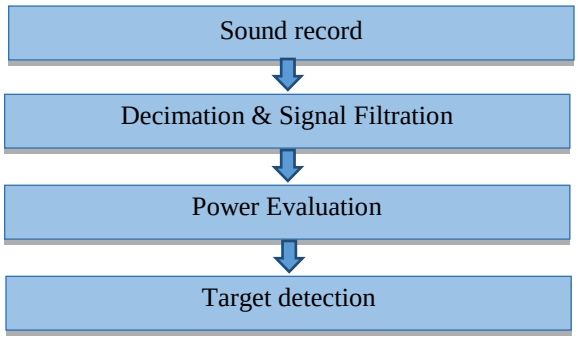

Fig. 3: *Blok-scheme of signal processing.*

The obtained target signature can be used for estimation of various target parameters in the time and frequency domains. In this experiment, the sound receiver samples the received signals at the sampling rate of 40 KHz. Therefore, the received signal is firstly decimated and next filtered by the bandpass filter in order to remove undesired signals. The next step is evaluation of the signal envelope. For the convenience of detection, the signal envelope is inverted and further is used for target detection by CFAR detector. The CFAR detector is a very important procedure and very often used especially in real systems, because it results in producing of precise target images separated from the existing interference. It is performed by removing clutter from the receive signals using the adaptive CFAR threshold.

4. *Experimental results*

During the experiments, the sound generator and the microphone are positioned on the two opposite sides of a street. The experiments include moving cars that cross the virtual baseline between the transmitter and the receiver. The acoustic system transmit signal with frequency 5 KHz (Fig. 6). The sound signal registrate at the sound frequency of 5 KHz when car crossing the baseline between the transmitter and the receiver is shown in Fig. 5.

Fig. 4: *Sound recording system.*

In this figure, it can be seen the areas with reduced signal power (signal blocking) of the received acoustic signal as a result of this crossing. The sound signal envelope is shown in Fig. 6, where the sound shadows due to the passage of car is clearly visible.

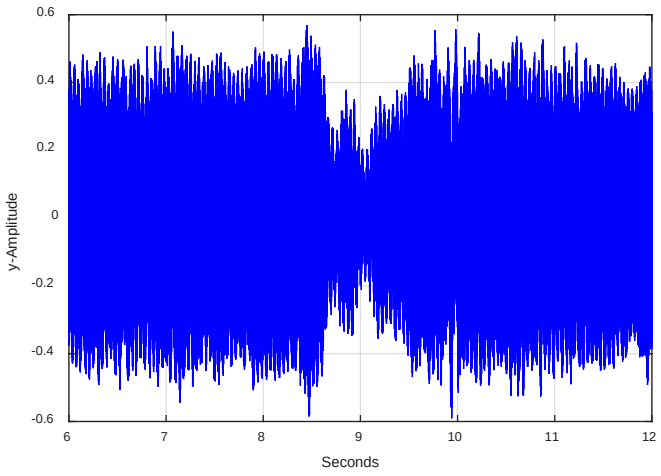

Fig. 5: *Sound record (5 KHz).*

During the experiment, both the useful sound signal and other sounds and disturbances are recorded. The spectrum of the recorded signal is shown in Fig. 7, where it is seen that the recorded signal contains a predominant signal at frequency of 5 KHz, but the lower and higher frequencies are interfering.

Through filtering the sound signal with a filter, whose frequency response is shown in Fig. 8, only the sound signal at frequency of 5 KHz is omitted. The filtered sound signal is shown in Fig. 9. The filtered signal envelope is shown in Fig. 10. From this figure can be seen that the sound shadow due to one passing car is well-shaped. A signal envelope inversion is applied before signal detection. The inverted signal envelope is shown in Fig.11.

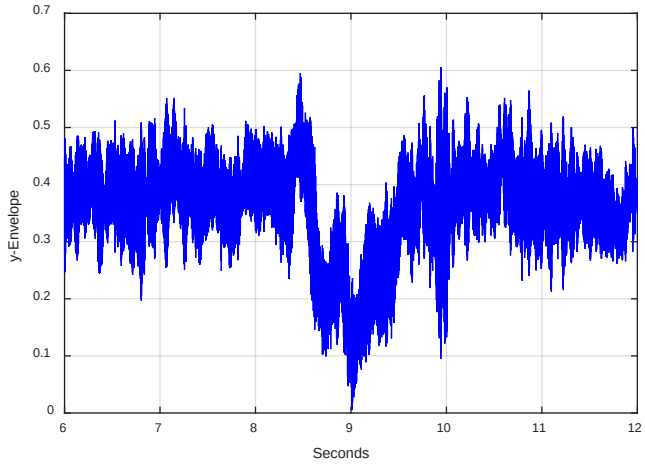

Fig. 6: *Envelope of sound signal (5 KHz).*

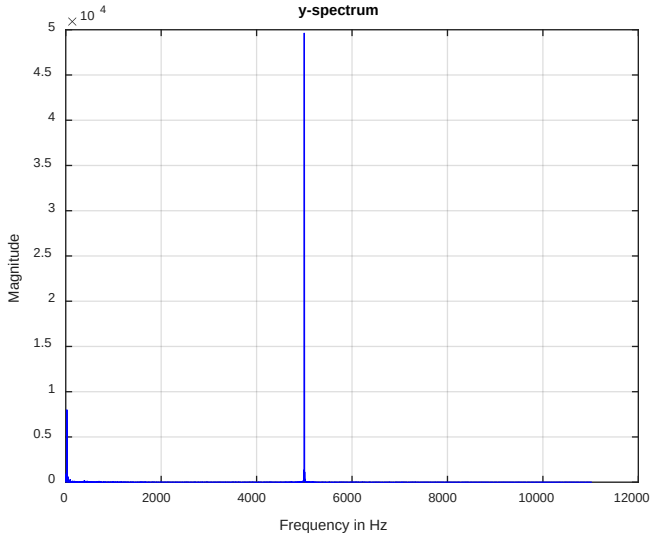

Fig. 7: *Spectrum of the recorded sound signal.*

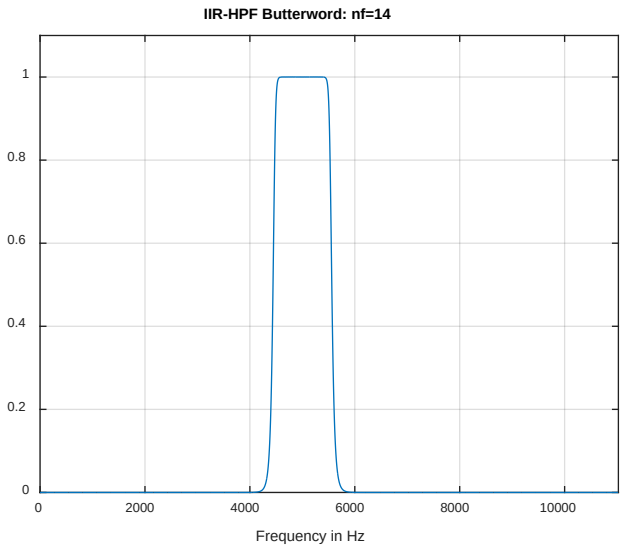

Fig. 8: *Frequency response of the bandpass filter.*

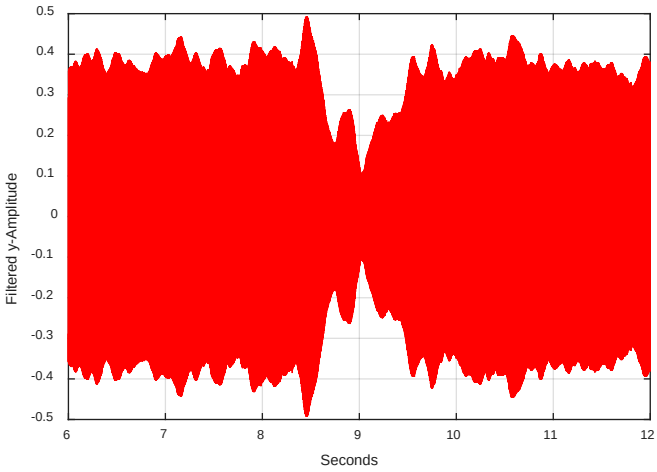

Fig. 9: *Filtered sound signal (5 KHz).*

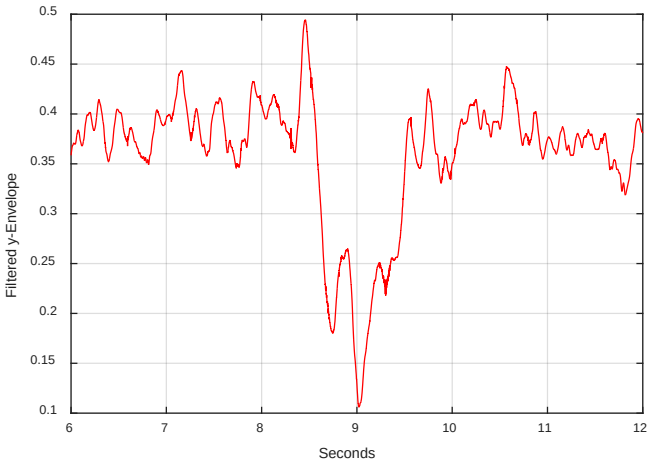

Fig. 10: *Filtered signal envelope.*

From figure 11 can be seen that the sound shadow due to one passing car is well-shaped. The CFAR detector is used to detect the sound shadow and the output of the detector is shown in Fig. 12.

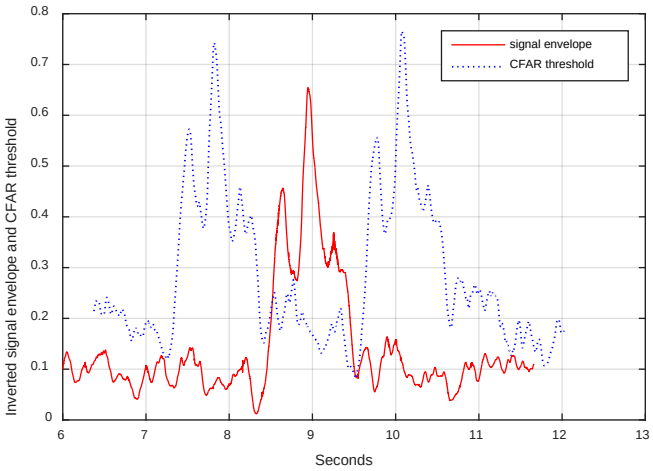

Fig. 11: *Inverted signal envelope.*

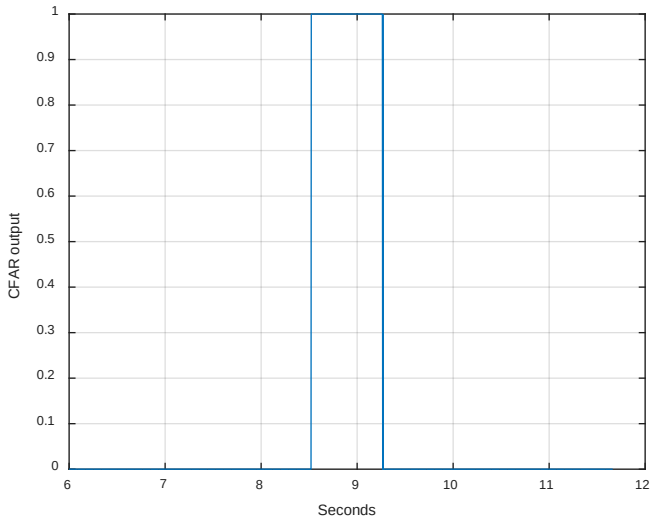

Fig. 12: *CFAR output.*

The example shows that sound signals can be used to create motion detection systems. Audio shadow parameters can be used to classify objects. A source of sound signals can be both artificial and natural sources of sound.

Conclusions:

An algorithm for detecting of moving cars crossing the baseline in the Acoustic Forward Scatter Radar System is proposed in the article.

The use of powerful, self-powered sound sources such as AFSRS will allow us in the future to explore the FS effect in the sound range, which appears when objects cross the virtual line between the receiver and the transmitter at very large distances from the transmitter and from the receiver.

The paper provides the opportunity to explore and use information of the audio shadows from sources of sound or noise (like radio shadows) to develop new applications as monitoring and management of urban road traffic.

Acknowledgement: This work was supported by Bulgarian Science Foundation, the project DFNI-T 02/3/2014.

References

[1] Cherniakov, M., (ed.), 2007. Bistatic Radar: Principles and Practice, Wiley & Sons.

[2] Krysik, P., K. Kulpa, P. Samczyński, 2013. GSM based passive receiver using forward scatter radar geometry, 14th International Radar Symposium, Dresden, Germany, pp. 637-642.

[3] Suberviola, I., I. Mayordomo, J. Mendizabal, 2012. Experimental Results of Air Target Detection With a GPS Forward-Scattering Radar, IEEE Geoscience and Remote Sensing Letters, vol. 9, no. 1, pp. 47-51.

[4] Kabakchiev C., I. Garvanov, V. Behar, H. Rohling, A. Lazarov, 2013. The Experimental Study of Target FSR Shadows Detection using GPS signals. Third International Symposium on Radio Systems and Space Plasma, Sofia, Bulgaria, pp. 64-73.

[5] Kabakchiev C., I. Garvanov, V. Behar, P. Daskalov, H. Rohling, 2014. Moving Target FSR Shadow Detection using GPS signals, Third International Conference on Telecommunications and Remote Sensing ICTRS- 2014, Luxembourg, pp. 34-40.

[6] Garvanov, I., C. Kabakchiev, V. Behar, P. Daskalov, 2016. Air target detection with a GPS forward-scattering radar, 19th International Symposium on Electrical Apparatus and Technologies (SIELA), Bourgas, Bulgaria, pp. 1-4.

[7] Kabakchiev C., I. Garvanov, V. Behar, D. Kabakchieva, K. Kabakchiev, K. Dimitrov, H. Rohling, K. Kulpa, A. Jarovoy, 2017, Experimental Parameter Estimation of Vehicles GPS Shadows by Forward Scattering Systems, International Radar Symposium IRS-2017, Prague, Czech Republic, pp. 4.

[8] Garvanov, I., C. Kabakchiev, V. Behar, M. Garvanova, 2015. Target detection using a GPS Forward-Scattering Radar. IEEE Pros. of the Second International Conference "Engineering & Telecommunications – En&T 2015", Moscow-Dolgoprudny, Russia, pp. 29-33.

[9] Martelli, T., F. Colone, P. Lombardo, 2016. First experimental results for a WiFi-based passive forward scatter radar, IEEE Radar Conference (RadarConf), Philadelphia, PA, pp. 1-6.

[10] Lei B, Yang K D, Ma Y L, et al. 2012, Forward acoustic scattering by moving objects, Theory and experiment. Chin Sci Bull, pp. 313–319.

[11] Garvanov I., K. Dimitrov, V. Behar, C. Kabakchiev, 2017. Comparative analysis of object shadows obtained by GPS and sound signals, Signal Processing Symposium SPS-2017, Jachranka, Poland

[12] Vladimir Ivanov., P. Stoyanov, "Monitoring and management of urban road traffic", Proceedings of the 23rd International Symposium Management of energy, industrial and environmental systems, Bankya, Bulgaria, 2015, pp. 103-107.

[13] Vladimir Ivanov. "Summary approach to designing management systems at intersections," Proceedings of the 24th International Symposium Management of energy, industrial and environmental systems, Bankya, Bulgaria, 2016, str.101-104.

AGENT-BASED DEVELOPMENT OF CYBER-PHYSICAL SYSTEMS FOR PROCESS CONTROL IN THE CONTEXT OF INDUSTRY 4.0

Prof. Dr. Batchkova I. A., Prof. D.Sc. Popov G.T., Eng. Ivanova Ts. A., Eng. Belev Y.A.
Dept. of Industrial Automation, University of Chemical Technology and Metallurgy
Bul. Kl. Ohridski 8, Sofia, Bulgaria

idilia@uctm.edu

Abstract: *In order to achieve its goal in using intelligent adaptive and predictive technical systems with self-X functions and cognitive information processing in continuous interaction with environment, the Industry 4.0 initiative implies integration of Cyber-Physical Systems (CPS), the Internet of Things (IoT) and cloud computing leading to what is called "smart factory". This, in turn, faces the CPS with new challenges in terms of increasing the degree of distribution, autonomy, mobility, communication and security of the systems and their components, as well as expanding their functionality in the direction of data analytics, information and knowledge extraction, and increasing their intelligence. This paper discusses and analyses the CPS in the context of Industry 4.0 and the main trends in the development of process automation and control in order to suggest an appropriate and advanced agent based approach for development of CPS for process control. The proposed approach is based on using the following standards – from one side the IEC61499 Standard for agent specification and from other side the IEC62264 and IEC 61512 Standards for defining the different kind of agents in the control system. The presented approaches are illustrated with a partly presented example of development of Injector control system. Finally some conclusions are made.*

Keywords*:* CYBER-PHYSICAL SYSTEM, INDUSTRY-4.0, AGENTS, PROCESS CONTROL, ONTOLOGY

1. Introduction

The European Commission's strategy for European Reindustrialization aims of increasing the industrial sector's share of gross value added in the European Union to 20% in 2020, based on European strengths in the fields of engineering, automotive, aeronautics, etc. [1]. The Industry 4.0 platform is an initiative of the German Federal Government to support German industry in the transition to digital production with intelligent, digital networks and systems that enable largely self-control and self-management of manufacturing processes [2, 3]. Especially strong is the focus of Industry 4.0 on the functions of future intelligent adaptive and predictive technical systems that need to be self-optimizing, self-configurable and self-diagnosable, enabling cognitive information processing and intelligent networking in continuous interaction with environment. That is why the strategic initiative Industry 4.0 implies integration of Cyber-Physical Systems (CPS), the Internet of Things (IoT) and cloud computing leading to what is called "smart factory".

CPS are physical and engineered systems whose operations are monitored, coordinated, controlled and integrated by a computing and communication core [4]. They are unique in that the components can be distributed both spatially and temporally, and include complex networks of feedback controllers and real time communication. The effective control, associated with achievement of a high degree of adaptability, autonomy, functionality, reliability, security and usability is the core of cyber-physical systems. The synergy between cyber and physical systems can be both at the nano-level and also at the level of "system of systems". The Strategic Research Co-operation Plan [5] points out that European industry should take advantage of the opportunities resulting from the wider application of the CPS concept as one of the key technological options (capabilities). Still, however the science is owed to CPS, the lack of theoretical foundation and methodologies creates barriers that may hamper the adoption, commercialization, and market success of new CPS applications [6]. The development of CPS is much more than the union of computation and physical systems and in order to apply the principles of CPS to new applications, new methods and tools are needed. Establishing an excellent science foundation and close cooperation between researchers in the field of CPS is a prerequisite for increased competitiveness and a means to address the major challenges.

CPS integrate computing, networking and physical dynamics, as distinguished by a high degree of heterogeneity and parallelism. As a result, the software design techniques are insufficient. New approaches, methods, algorithms and techniques are needed, which will support the process of analysis and design of CPS. The concept of CPS is tightly linked with agent based systems in respect to their basic properties such as: autonomy, sociability, reactivity, proactivity and mobility. Different approaches and methods are used in order to guarantee the useful features of agents in various applications areas of CPS, such as modeling, monitoring, control, diagnostics etc. An important conclusion to be drawn from the analysis of the approach is that the results are more successful when the agent based approach is combined with other approaches, methods and tools.

The main aim of the paper is based on an analysis of CPS in the context of Industry 4.0 and the main challenges in the field of process control and automation to summarize the basic assumptions and capabilities of using an agent based approach for development of CPS for process control. Some results are presented and discussed. The paper is organized in 4 parts. After the introduction, in part 2, a short analysis of the requirements to the CPS in context of Industry 4.0 is proposed. Part 3 discusses the main challenges to process automation and control according to the European Roadmap for process automation [7]. In the next part a short survey of the agent based approaches for control and automation is presented. The last part presents an idea for development of CPS for process control based on agents using IEC-61499, IEC-62264 and IEC 61512 Standards. Finally some conclusions are made.

2. An Analysis of the CPS in the context of Industry 4.0

The advent of control systems in industry started in the era of the first industrial revolution and was characterized by the use of mechanical devices, such as the steam engine governor. The growing number of implemented control systems has led to the emergence and development of the first analysis methods of control theory. The advent of electricity, which is connected to the second industrial revolution led to the replacement of mechanical control devices with electromechanical and their enormous and diverse use in the existing and new emerging industrial branches. With the emergence of the first microprocessors in the seventies began the development and introduction of digital control systems. This has led to the advent of the new levels of control such as DCS, SCADA, MES, the purpose of which is to process and aggregate huge amounts of data from various sensors, releasing the person from multiple control system setup operations, and set him more responsible tasks related to monitoring and optimization of production systems. Unfortunately, however, the theory of

computer-based control is underdeveloped. The main task of the theory of cyber-physical systems is to fill this gap.

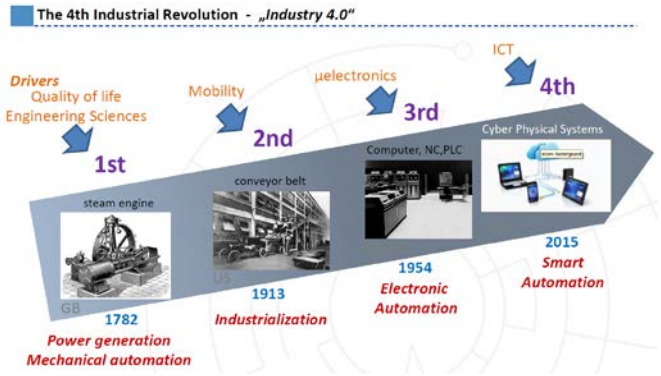

Fig.1: Industrial revolutions and Automation

The fundamental requirements for introducing CPS in industry are specified by [8] as follows:

- *Adaptable to heterogeneous environments:* integration with cutting-edge information systems, smart-devices and the existing environment (from old PLCs to smart object embedded in computing power).
- *Capable of working in distributed networks:* they should gather, transfer and store in a reliable manner all the information provided by smart sensors and actuators through the use of the IoT.
- *Based on a modular open architecture:* the interoperability has to be ensured across different platforms provided by several vendors along the value chain.
- *Incorporate human interfaces (HW & SW based):* integration of user-friendly and reliable service to make decision makers aware about the real time situation of the factory.
- *Fault tolerant:* given by the encapsulation of models to activate prediction control loop and correctness of automation systems.

The design of the CPS requires knowledge on the dynamics of computers, software, networks, and physical processes. The main challenges in the development of cyber-physical systems have different nature and may be grouped in different categories, such as technical, organizational and social. To organizational challenges belong the standardization and issues connected with regulations and legislation. Till now, there is no a reference framework for development of CPS. Different reference models and Standards for interoperability of different systems are needed. The most important social challenges are connected to the Computer – human interactions and interface design. The technical challenges in the design and analysis of CPS stem from the need to build a bridge between sequential semantics and parallel physical world and are connected with the following engineering domains:

- Modeling, development and realization of CPS components and systems;
- Validation, verification and testing of the models at different levels of abstraction;
- Maintenance and evolution of the introduced CPS components and systems.

Industry 4.0's vision requires revision of the approaches for development and use of CPS concerning the following areas:

- In respect to the decentralization in order to integrate the Cyber-Physical Systems (CPS) with cloud computing infrastructures using a high-level architecture for IoT systems, such as this of OpenFog Consortium or FAR-EDGE Reference Architecture [9].
- Empowering decentralization using edge computing that moves some part of computing from the cloud to its edge nodes supporting real-time interactions and scalable analytics;
- Application of new disruptive key enabling technologies in factory automation like DLT (Distributed Ledger Technology) and Smart Contracts (ISO-20022) changing the paradigm of messaging;
- Digital representation of all information and services from and about the physical systems using the concept of Administrative Shell and I4.0 component as a specific case of CPS [10].
- Need for new planning procedures for CPS;
- The Industry 4.0 vision requires smaller, more intelligent and modularized cyber-physical entities that are function-oriented.

3. *Main trends in process automation and control*

The European roadmap for industrial process automation is developed by the ProcessIT.EU Center of innovation Excellence and formulates the trends, visions and long range goals in industrial process automation, categorizes them into a set of research and development areas and concretises the visions and long range goals into a number of ideal concepts that form the direction of development, proposed in this roadmap [7]. The study also found that automation services predominate over hardware and automation software, which directs attention to the used engineering tools and their efficiency. The roadmap envisions also some technical solutions and methods, summarized in Fig.2, which are of high importance to meet the main challenges of process control and automation. Among these solutions, with particular luminance, three main points stand out:

- The future development of automation and process control systems relies on the use of approaches and methods of cyber-physical systems with a view to achieve collaborative automation and a dynamic virtual twin of the system, available in a real time;
- Secondly, the need for adapting and using the technologies of the Internet of Things to achieve distributed automation and control systems;
- The third major point is the massive need of standards and their use in the development of hardware, software, platforms, network communications and transparency of information.

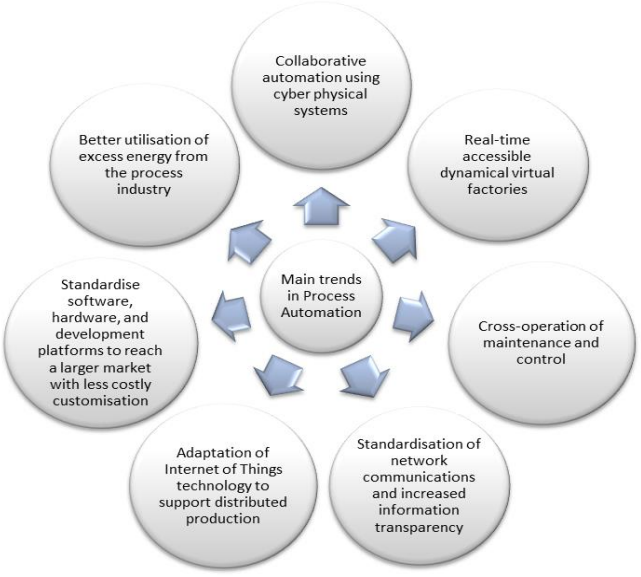

Fig.2: Main trends in Process automation

4. *Short overview of agent based development of control systems*

Jennings and Wooldridge [11] have defined an agent as "a computer system situated in some environment and capable of autonomous action in this environment, in order to meet its design objectives". Software agents may be seen as building blocks for virtual environments which augment the reality. They have the following main properties and characteristcs [12]:

- autonomy: agents encapsulate some state (that is not accessible to other agents), and make decisions about what to do, based on this state, without the direct intervention of humans or others;

- socialability (interactivity): agents interact with other agents (and possibly humans) via some kind of agent-communication language, and typically have the ability to engage in social activities (such as cooperative problem solving or negotiation) in order to achieve their goals;
- reactivity: agents are situated in an environment, (which may be the physical world, a user via a graphical user interface, a collection of other agents, the Internet, or perhaps many of these combined), and are able to perceive this environment (through the use of potentially imperfect sensors), and are able to respond in a timely fashion to changes that occur in it;
- pro-activeness: agents do not simply act in response to their environment, they are able to exhibit goal-directed behaviour by taking the initiative;
- mobility: agents can transport themself across different systems architectures and platforms.

CPS may be modeled as Multi Agent Systems (MAS), which may be defined as "a loosely coupled network of problem solvers (agents) that work together to solve problems that are beyond the individual capabilities or knowledge of each problem solver" [13]. The agent community has considerable interest in developing methods and techniques for specifying, modelling, implementing and verifying of MAS for development of CPS in the different applications domains, but so far no standardized methodology has been recognized. Several object-oriented methodologies have been suggested for agent-oriented analysis and design, based on UML. Important drawbacks of using UML to model MAS are the modelling of agent communications as method invocations and the absence of references to the mental state of the agents. To overcome these drawbacks, the UML notations are extended to reflect the characteristic properties of the agents. Successfully extensions of UML are achieved in AUML, GAIA, MESSAGE/UML, AgentUML, Prometheus, etc. Some of them are based on FIPA standard (http://www.fipa.org) suggesting an agent reference model for creation, registration, location, communication, migration and retirement of agents. Recently are also available some specialized tools for lightweight devices, such as DSML4MAS (http://dsml4mas.sourceforge.net/), FIPA-OS, ASEME (for Eclipse), Tropos (http://www.troposproject.org/), INGENIAS (http://sourceforge.net/projects/ingenias/), Jade-Leap, etc. However, there are limitations and drawbacks, associated with the variety of devices and communication protocols, specific for CPS. As well there are some agent-based development environments especially for the CPS domain, as for example: THOMAS, MaRV, ALZ-MAS, CodeBlu, etc.

The actually state of the industrial application of agent technology in CPS is proposed in [14] and the current efforts and challenges for their wider applicability are discussed. The review also shows that the adoption of agent technology in industrial applications is critical in respect to real time constraints and this implies the use of technologies for real-time control as for example the IEC-61499 standard. The agent based technologies are more appropriate for the higher levels in order to provide intelligence and responsiveness.

5. *An approach for agent based development of process control system as CPS*

As shown in the previous section the concept of CPS is tightly linked with multi-agent systems, however there is not an existing methodology for applying agents to the cyber-physical domain of process control. We suggest using the design principles for development of agent based CPS, defined in [14] and illustrated in Fig.3. They link the high level design abstraction and principles with the final implementation.

There are many different standards associated with the Industry 4.0 vision in order to achieve interoperable and scalable solutions based on the integration of smart agents in industrial CPS environments. This study uses three of them in order to start an approach for development of CPS for process control, connected with improving the adaptability, autonomy, efficiency, functionality, reliability, safety, and usability of such systems. For solving real time control tasks, the IEC 61499 standard [15] is adopted, which defines the basic concepts and models for design of distributed process measurement and control systems. It is based on the concept of function block as a main building block of an application and may be used in the design of re-usable intelligent software components. Distributed automation systems could be modeled in cyber-physical way by introducing concurrent model of computations in the IEC-61499 standard. By applying the cyber-physical view with the IEC-61499, control, communication and physical plant in distributed automation systems are covered in one graphical modeling langauge.

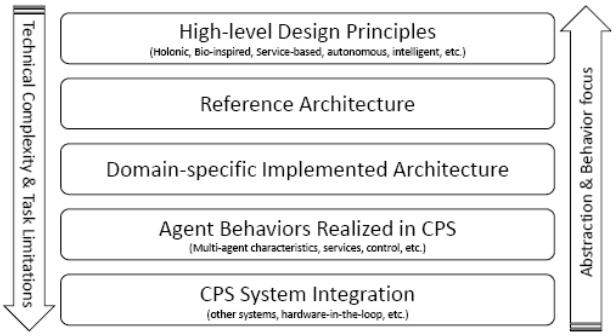

Fig.3: Design principles for agent-based CPS [14]

In cyber-physical systems, there are stronger communications between components and new communication standards and approaches are needed because of the exchange of heterogeneous information. A promising approach in this direction is the use of ontologies, describing the semantics of information and achieving a comprehensible exchange of information. It is extremely important to reuse existing ontologies in automation such as ontology of automation devices, reconfigurable mechatronic systems, diagnostics, and so on. Other important requirements for ontologies used are their modularity, enabling their efficient reuse, refinement and extension; the use of a common standard language for their description, as well as a common automation vocabulary that facilitates the alignment of individual modules to satisfy different requirements.

Both standards IEC-61512 and IEC-62264 are used to create ontology for the automation domain. The IEC-61512 standard [16] provides domain specific models and terminology for design and control of batch production processes and may help to explain the relationships between them. The standard also defined the data models that describe batch control as applied in the process industries, data structures for facilitating communications within and between batch control implementations and language guidelines for representing recipes. The IEC-62264 standard [17] for Enterprise-control system integration defines the terms and models between the enterprise business systems and factory floor control systems. The most important and old parts of the standard include models and terminology, objects and attributes for enterprise-control system and activity models of manufacturing operations management systems. In Fig.4 is shown the "equipment module" of the "manufacturing ontology", structured according to the hierarchical model of the equipment defined by the two standards: IEC-62264 and the IEC-61512.

In Fig.5 an intelligent agent based approach for process control of Injector, based on the IEC-61512 standard is partly illustrated. Common intelligent cyber components have been built and reused for different application. The components are managed in a control recipe that describes their execution schedule. Furthermore, IEC 61499 Standard is adopted as an application framework in which the functional components are implemented as IEC 61499 based function blocks (FB). The operation schedule of the controlled components is then implemented according IEC 61499, based on Scheduler-Selector-Synchronizer (S^3) architecture and a special

kind of Petri nets models describing the sequence of control execution may be used in order to verify of algorithm.

Fig.4: ''Equipment module'' of the "manufacturing ontology"

6. Conclusions

The presented approach is still at an early stage of development. There are a number of extensions to automation ontologies based on other existing standards and developed ontologies. An important step in the right direction is also related to the communication protocols and interfaces used. The discussion around the fusion of MAS and SOA is connected with enhancing some basic features of the CSP, such as adaptability, flexibility, interoperability and modularity. Moreover CPS systems must be improved in respect to service discovery, self-organization, rich knowledge representations and context-awareness.

References

1. European Commission, Digital Agenda, http://ec.europa.eu/digital-agenda/en/digitising-european-industry
2. Industry 4.0, http://www.plattform-i40.de/I40/Navigation/EN/Home/home.html
3. Kagermann H., Wahlster W., Helbig J., Recommendations for implementing the strategic initiative INDUSTRIE 4.0, Final report of the Industrie 4.0 Working Group, Akatech, April, 2013.
4. Rajkumar R., Lee I., Sha L., Stankovic J., Cyber-physical systems: the next computing revolution. In Proceedings of the 47th Design Automation Conference, ACM, New York, pp. 731-736, 2010.
5. Hafner-Zimmermann S., Henshaw M. J. C., The future of trans-Atlantic collaboration in modeling and simulation of Cyber-Physical Systems, A Strategic Research Agenda for Collaboration, Steinbeis-Edition, 2017, ISBN 978-3-95663-121-4.
6. CPS summit, Action Plan - Towards a Cross-Cutting Science of Cyber-Physical Systems for mastering all-important engineering challenges, Final Version 10th April 2016.
7. European Roadmap for Industrial Process Automation, http://www.processit.eu/roadmap
8. De Carolis A., Tavola G., Taisch M., Cyber-Physical Systems in Manufacturing: Future Trends and Research Priorities, XXI Summer School "Francesco Turco" - Industrial Systems Engineering, pp.12-17.
9. Isaja M., Soldatos J., Gezer V., Combining Edge Computing and Blockchains for Flexibility and Performance in Industrial Automation, UBICOMM 2017 : The Eleventh International Conference on Mobile Ubiquitous Computing, Systems, Services and Technologies, ISBN: 978-1-61208-598-2, pp.159-164.
10. Grangel-Gonzalez I., Halilaj L., Coskun G., Auer S., Collarana D., Hoffmeister M., Towards a Semantic Administrative Shell for Industry 4.0 Components, 2016 IEEE Tenth International Conference on Semantic Computing (ICSC), pp.230-237.
11. Jennings N. R. & Wooldridge M. (1998). Applications of Agent Technology, in: N. R. Jennings and M. Wooldridge, editors, Agent Technology: Foundations, Applications, and Markets. Springer-Verlag, March 1998.
12. Wooldridge, M., Jennings, N. R. & Kinny, D. (2000). The Gaia Methodology for Agent-Oriented Analysis and Design, International Journal of Autonomous Agents and Multi-Agent Systems, 3(3):285-312.
13. Durfee, E. H. & Lesser, V. (1989). Negotiating task decomposition and allocation using partial global planning, in: L. Gasser and M. Huhns, editors, Distributed Artificial Intelligence Volume II. Pitman Publishing: London and Morgan Kaufmann: San Mateo, CA, 1989, pp. 229–244.
14. Leitao P., Karnouskos S., Ribeiro L., Lee J., Strasser T., Colombo A. W., Smart Agents in Industrial Cyber-Physical Systems, 2016, Proceedings of the IEEE, (104), 5, 1086-1101.
15. IEC Technical Committee TC65/WG6, "IEC 61499 Industrial-Process Measurement and Control - Specification", IEC, 2012.
16. IEC (1997). IEC 61512 - Batch control - Part 1: Models and terminology.
17. IEC (2003). IEC 62264 - Enterprise-control system integration Part 1: Models and terminology.

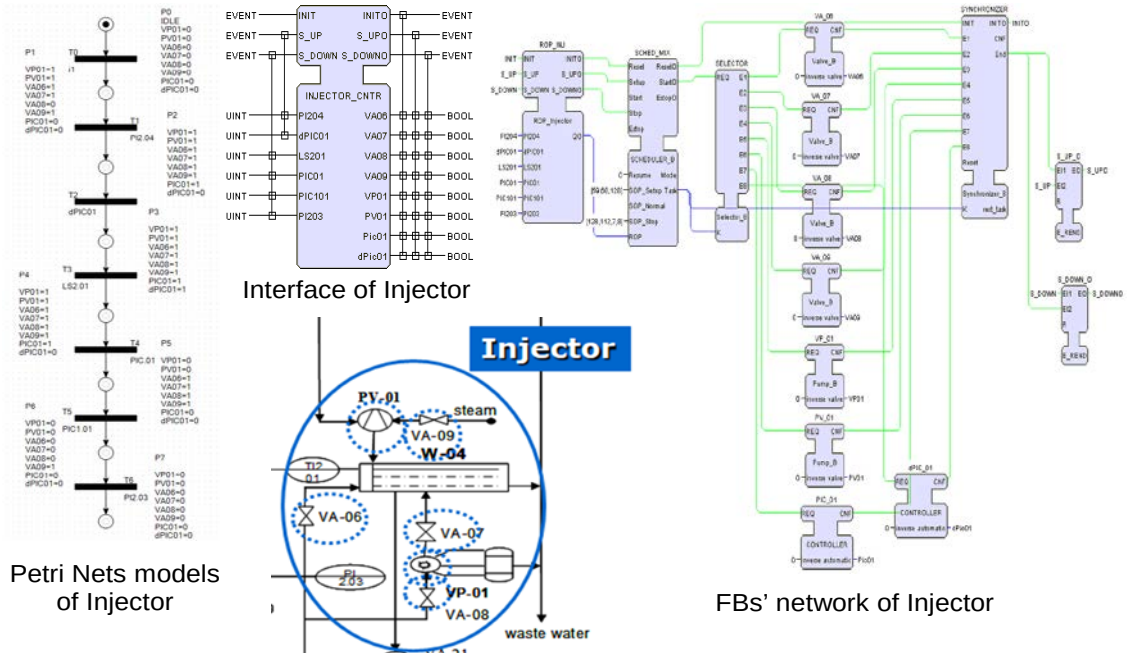

Fig.5: Control components of Injector CPS

NEW APPLICATIONS OF NANOSTRUCTURED MATERIALS IN THE PROSPECT ELECTRONIC DEVICES

Prof. Dr. Alexander G. SMIRNOV[1], Dr. Andrey A. STSIAPANAU[1], Barys A. Kazarkin[1],
Prof. Dr. Victor V. Belyaev[2], Dr. Denis N. Chausov[2]
[1]Belarusian State University of Informatics and Radioelectronics, Minsk, Belarus
[2]Moscow Region State University, Moscow, Russia

smirnov@bsuir.by

Abstract: *Nanostructured materials have unique properties which completely differ from the initial solid state condition. In this presentation we will discuss different techniques to fabricate such materials, their physical and optical parameters and characteristics, possible application areas. Main attention will be paid to aluminum and silicon nanostructured layers which are the promising alternatives of transparent semiconductors or metals as well as electroluminescent light emitting media.*

Keywords: INDUSTRY 4.0, NANOSTRUCTURED MATERIALS, OPTOELECTRONIC DEVICES

1. Aluminum nanostructured materials

Aluminum nanostructured layers are the promising alternatives of transparent semiconductors or metals. Main requirements for transparent conductive electrodes (TCEs) are good transparency in a limited and well-defined range as well as suitable conductivity. E.g., the wavelength interval constitutes 300 nm-2500 nm for photovoltaic and 400-700 nm for displays. Nowadays the best material to reach this goal is indium tin oxide (ITO). It is commonly used in many kinds of displays, light-emission diodes, solar cells and other optoelectronics devices.

The average transmission for ITO is approximately 80-90% depending on thickness variation. For smaller thickness, ITO has better transmission and resistance and vice versa. The range of ITO sheet resistance is 10-100 Ω/□ [1]. Assuming ITO is "ideal", novel TCEs should have the same properties or even better.

The metal-based thin transparent films are attractive due to their plasmonic properties and better flexibility. Planar metal films have poor optical performanse, however a special nanostructuring can increase the transmission. The cross-linked Cu layer with average 61 and 75% transmittance and sheet resistance 10 and 15 Ω/□ for 120 and 200 nm grating line width were demonstrated correspondently [2].

Another nanostructuring shape is a nano holey structure. The main feature of these structures is the independence on the light polarization at defined holes arrangement. In [3–5] data on transmission, reflection and absorption *vs* different hole size, inter hole distance and thickness are shown. In this paper, two simple methods of transparent conductive metal electrodes fabrication were proposed and realized. There optimal optical and electrical parameters were found and systematized.

2. Experimental results

A glass substrate with 200 nm aluminum (Al) is used for the first method of the TCEs fabrication [6]. The full process is illustrated on Fig. 1, where, for simplicity, the holey alumina (Al_2O_3) is not included.

When the electrochemical anodization of Al starts the holes grow with sphere shape. At time t_0 (step ***a***) the holes (sphere) contact with the substrate and an aluminum electrode is forming. At this position the transparency is small and a further anodization is required (step ***b***).

At time $t_1 > t_0$ the transmission increases and at time $t_2 > t_1$ has the biggest values. The conductance has opposite behaviour and has the smallest value at time t_2. Thus trade-off between transparency and conductivity is necessary.

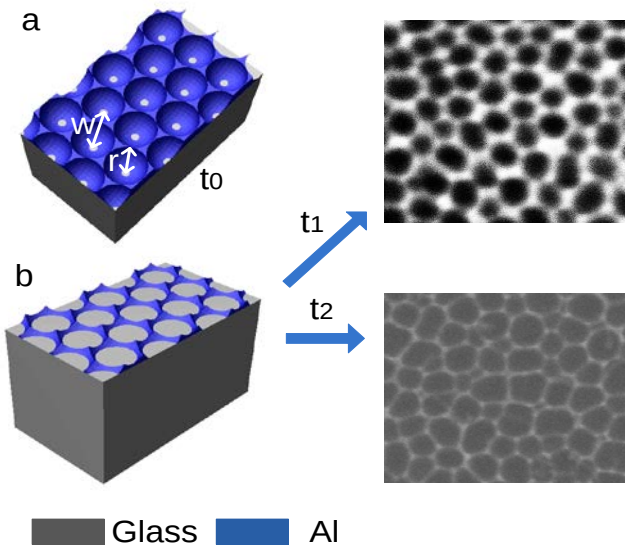

Fig.1. *First method of TCEs fabrication: a) The beginning of Al TCE formation (time t_0); b) The end of Al TCE formation (time t_1 or t_2)*

In order to find the optimal parameters the FDTD Lumerical [7] and COMSOL Multiphysics [8] packages are used for optical and electrical properties simulation accordingly.

The 10-20 Ω/□ sheet resistance for hole (sphere) radios *r*=60-70 nm and inter hole distance *w*=100 nm was obtained.

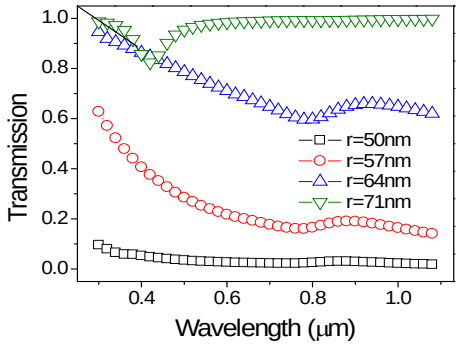

Fig.2. *Simulated optical properties for Al TCE with r = 50, 57, 64, 71 nm and w=100 nm.*

The simulated optical properties for hole (sphere) radii with r = 50, 57, 64, 71 nm and inter hole distance w = 100 nm is shown in Fig. 2. The r = 50 nm and r = 57 nm correspond to time t_0 and t_1 accordingly. The r = 57 nm is an intermediate time value and r = 71 nm is a value when conductance equals 0 Ω/□. In this case the trade-off between transparency and conductivity must satisfy condition 1.2-1.4r to obtain the average transmission 70-80% for range 300-1000 nm and 10-20 Ω/□ sheet resistance.

The second proposed TCE formation method includes three steps as illustrated on Fig. 3. The step ***a*** is aluminum deposition followed by anodization and holes widening in the solution containing phosphoric acid. Then the metal (gold Au in our case) is deposited by e-beam evaporation (step ***b***). The final step ***c*** is the transfer of obtained TCE to adhesive substrate.

Optical properties for Au TCE at different hole size r = 100, 150, 200 nm, inter hole distances w = 2r+25, 50, 75 nm and thickness d = 25, 50 nm are simulated using commercial software FDTD Lumerical [7]. The larger holes size provides better average transmission, when larger inter hole distance and thickness have opposite dependence. The Au electrode only absorbs a part of light for the range of 300-600 nm due to localized plasmonic resonance. At λ>700 nm the reflection increases.

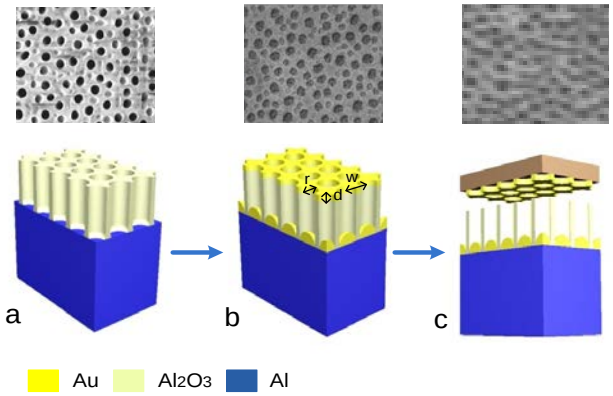

Fig.3. *Second method of TCEs fabrication:*
a) aluminum deposition, anodizing and holes widening;
b) metal deposition;
c) metal TCE transferring.

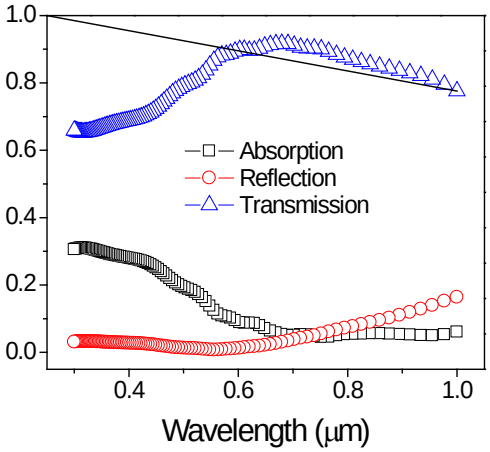

Fig.4. *Simulated optical properties for Au TCE with r=100, w=25 and d=25nm.*

The structure with r = 100 nm, w = 25 nm and d = 25 nm has better average transmission for the range 300-1000 nm (Fig. 4) and equals to 82.5%. The 10-20 Ω/□ values were obtained for 25-50 nm TCEs thickness by four probe method.

3. Silicon nanostructured materials

Integration of electronic and optoelectronic components on a silicon chip is the task of a great importance. One of the most difficult optoelectronic component to integrate onto a Si chip is a light emitting device because Si is an indirect band gap semiconductor, meaning that it normally can't produce light.

A standard technological method of high porosity nanostructured silicon formation as functional layer for light emitting devices is electrochemical etching in hydrofluoric acid solution. It is believed that the presence of two holes is necessary for the separation (or etch away) of one silicon atom. In our electrochemical process, after applying voltage, two fluorine ions approaching silicon atom (together with four molecules HF) etch away one Si atom from silicon surface.

The scheme of this process is illustrated by Fig. 5.

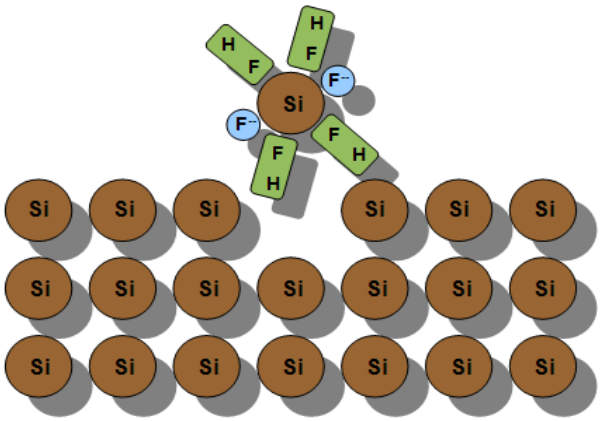

Fig.5. *The process of nanostructured silicon formation*

But this method has some inconveniences such as short anodizing time (few seconds for thin porous layers formation), toxic for operators and aggressive hydrofluoric acid which destroy aluminum interconnections. To avoid these inconveniences we propose to use a solution with low fluorine ions concentration. In this paper we are describing the stable and reproducible method for high porosity silicon formation in novel ammonium fluoride solution NH_4F:H_3PO_4:C_2H_5OH:H_2O.

By increasing of NH_4F concentration from 5 to 20 wt % the pore sizes are reducing from 20 to 10 nm. In addition, the reduction of current density also reduces the pores size. Thus, it is possible to change the pores size by varying of ammonium fluoride concentration and current density. Fabricated layers have a sponge like structure with the porosity in the range of 70-80 %.

Table 1. *The range of current densities and electrolyte concentrations*

Current density	Solution concentration NH_4F:H_3PO_4:C_2H_5OH:H_2O
0.01 - 0.1mA/cm^2	NH_4F – 1-3% H_3PO_4 – 20-70% C_2H_5OH – remaining

Therefore, highly uniform and ultrathin high porosity nanoporous silicon films can be fabricated under very low current densities and fluorine ion concentration in a reproducible manner. Structural and electro optical properties of nanoporous silicon films are also discussed.

4. Conclusion

Two methods of transparent conductive metal electrodes fabrication by electrochemical anodization technology are presented. The obtained transmission in the range of 300-1000 nm and its sheet resistance are the same as at ITO reference electrodes. These electrodes can be applied in the various optoelectronic devices.

In this work we also report the stable and reproducible regime of ultrathin nanoporous silicon layers fabrication under ultra small current density (down to 0.01 mA/cm^2) and fluorine ion concentration (1 % wt) by using NH_4F solution.

Acknowledgements

The work is partly supported by Belarusian Republican Foundation for Basic Researches (grant No T16P-200) and by Russian Foundation for Basic Researches, grant No 12-07-90006_Bel_a, 14-07-00574_a.

References

[1] A.L. Dawar and J.C. Joshi, J. Mater. Sci. Lett. **19,** 1-23 (1984)

[2] M.G. Kang and L.J. Guo, J. Vac. Sci. Technol. B, **25**, 2637-2641 (2007).

[3] W.A Murray and W.L. Barnes, Adv. Mater., **19**, 3771-3782 (2007).

[4] X. Shou, A. Agrawal and A. Nahata, Opt. Express, **13**, 9834-9840 (2005).

[5] Q. Wang, J. Li, C. Huang, C. Zhang and Y. Zhu. Appl. Phys. Lett., **87**, 091105-091107 (2005).

[6] A. Smirnov, A. Stsiapanau, A. Mohammed, E. Mukha, H.S. Kwok, A. Murauski, Proc. SID Symposium "Display Week-2011", Los-Angeles, 1385-1387 (2011).

[7] Trial Versions of FDTD Solutions http://www.lumerical.com

[8] Porous Silicon Avalanche LEDs and Their Applications in Optoelectronics and Information Displays // P.Jaguiro, P.Katsuba, S.Lazarouk, and A.Smirnov // Acta Physica Polonica A,Vol. 112, No. 5, 2007, pp. 1037–1042

БЕЗРАЗРУШИТЕЛЕН КОНТРОЛ НА СТРОИТЕЛНИ МАТЕРИАЛИ И КОНСТРУКЦИИ

NON DESTRUCTIVE TESTING OF CONSTRUCTION MATERIALS AND STRUCTURES

Hristova V., Ivanova D.
e-mail: veneta.christova@gmail.com e-mail: divanovaacomin@gmail.com
Institute of Information and Communication Technologies, Bulgarian Academy of Science, Sofia, Bulgaria

Abstract: *In this paper the attention is paid to the research of a* non destructive testing of construction materials and structures. *The mechanisms of audit and evaluation are described. Different methods and devices for non destructive testing are discussed.*

Key words*: non destructive testing, construction, material features*.

1. Увод.

За определяне състоянието на сградите, след началото на експлоатацоята им могат да бъдат използвани разрушителни или безразрушителни методи на изпитване. При повечето методи се използва зависимоста между различните характеристики на вградените материали. Разрушителните методи обикновено са свързани с изрязване на ядки от различни зони на сградата, които биват тествани според особеностите на конструкцията, в която са вложени или механичните им свойства. Заради сложността на техническото изпълнение и ограничения брой на пробите, този метод не винаги води до точни резултати.

Безразрушителните методи за контрол на строителни материали и конструкции могат да бъдат прилагани както при нови, така и при стари сгради и съоръжения от всякакъв тип. Тези методи са особено полезни в редица ситуации:

- Контрол на качеството на вложения материал;
- Контрол на качеството на изпълнение;
- Проверка на нормативните изисквания;
- Проверка за наличие на пукнатини, дефекти и нежелани отвори;
- Проверка на армировка;
- Наблюдение на поведението на конструктивните елементи.

Преди обследването на отделните елементи и материали от конструкцията, по нормативна уредба, се изпълняват следните стъпки за определяне актуалното състояние на изследвания обект, [1, 2]:

2. Конструктивно обследване за установяване актуалното състояние.

Обследването на конструкцията става на следните етапи:

1. Запознаване и анализиране на наличната проектна документация за носещата конструкция на сградата;
2. Технически оглед, визуално обследване (ако е възможно) и документиране на наличните дефекти, пукнатини и повреди в елементите на конструкцията на сградата, участъци с открита армировка, промени в структурата на бетона или стоманата, недопустими деформации и провисвания на отделни елементи и др., свързани с досегашния експлоатационен период;
3. Събиране на информация относно общите геометрични размери на носещата конструкция;
4. Установяване на основните размери на напречните сечения на главните конструктивните елементи от сградата (колони, греди, плочи, стени и др.) и сравняване с тези от проекта по част;
5. Установяване на якостните и деформационните свойства на вложените в конструкциите материали в главните елементи на конструкцията;
6. Установяване на дефекти и повреди в конструкцията.

3. Конструктивна оценка на сградата.

Оценката на сградата се извършва чрез:

1. Систематизиране на информацията относно нормите и критериите на проектиране;
2. Установяване на типа и значимостта на минали конструктивни повреди, включително и проведени ремонтни дейности;
3. Проверка на носещата способност на характерни елементи на конструкцията;
4. Обобщени резултати за конструктивната оценка.

Според направената предварителна оценка за състоянието на дадена конструкция, се набелязват зони и елементи които да бъдат допълнително изпитвани чрез най-подходящите техники за безразрушително обследване спрямо функцията и местоположението им [3, 4].

Съществуват различни методи за безразрушително обследване, които спрямо материала, конструкцията, местоположението и др. могат да бъдат обобщени в няколко раздела:

- Метод използващ повърхностната твърдост на материалите;
- Метод чрез използването на ултразвук;
- Инфрачервена термография;
- Метод с намагнетизирани частици;
- Електросъпротивителни методи;
- Радиометрични методи.

Безразрушителен метод за определяне на вероятна якост на натиск чрез повърхностна твърдост използвайки склерометър (чук на Schmidt) (БДС EN 12504-2) – фиг. 1.

Фиг.1. *Диагностика чрез чук на Schmidt.*

При този метод се използва правопропорционалната зависимост между повърхностната твърдост и якостта на материала. При взаимодействие на уреда с изпитваната повърхност се отчита отскока от скалата на уреда, спрямо който се определя якоста на материала и сравнява с нормативната.

Безразрушителен метод за изпитване на бетона чрез скоростта на разпространение на ултразвуков импулс (БДС EN 12504-4) – фиг. 2.

Фиг. 2. *Диагностика чрез ултразвуков бетоноскоп.*

При този метод се използва ултразвуков бетоноскоп. Целта е да се определи времето за преминаване на ултразвуков импулс през бетона, след което се изчислява скоростта на преминаване. Известно е, че в по-плътна среда скоростта на разпространение на вълната е по-голяма и обратното.

Разположението на предавателя и приемника на ултразвуквата апаратура може да бъде директно, полу-директно и индиректно, като директното разположение е за предпочитане ако има достъп от две срещуположни стени. Колкото времето за преминаване на импулса е по-малко, толкова скоростта е по-голяма, а плътността и якостта са по големи. Методът се използва и за проверка на структурата, еластичността, еднородността на материала в конструктивните елементи. Едни от най-често срещаните ситуации са – табл. 1:

Табл. 1*. Поведение на импулс от ултарзвуков бетоноскоп.*

Поведение на импулса	**Вероятно състояние на материала**
Преминава без смущения	Еднородна структура
Преминава с по-голяма скорост	Наличие на стомана
Преминава по-бавно	Наличие на пукнатина или кухина
Не преминава	Наличие на голяма пукнатина
Преминава значително по-бавно	Наличие на множество малки дефекти

4. Инфрачервена термография за определяне на дефекти в конструкцията.

Всички тела с температура над абсолютната нула излъчват инфрачервена радиация, която, за човешкото око става видима над 500 ^{o}C. Чрез инфрачервени термокамери радиацията може да бъде засечена и визуализирана (термограма) [5].

Благодарение на движението на топлината в телата, чрез термокамерата може да бъдат засечени и визуализирани зони с различни температури. При нееднородна структура, пукнатини, наличие на влага и др., на термограмата засегантия участък, заради температурната разлика, ще бъде оцветен по различен начин, което е сигнал за възникнал проблем. По този безразрушителен метод могат да бъдат засечени редица нередности в една конструкция като:

- Липсваща или повредена изолация;
-Загуба на топлинна енергия, заради пукнатини и непредвидени отвори;
- Наличие на мухъл;
- Термо мостове – фиг. 3;
- Задържаща се влага – фиг. 4.

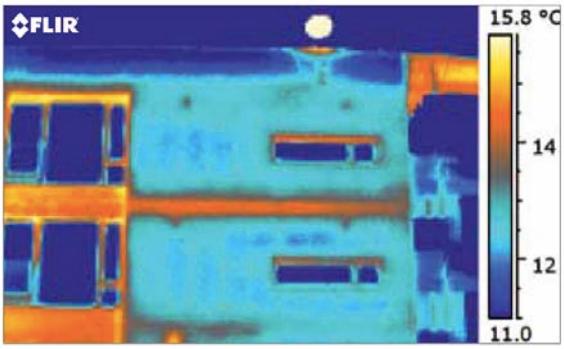

Фиг. 3*. Термо мост между етажи.*

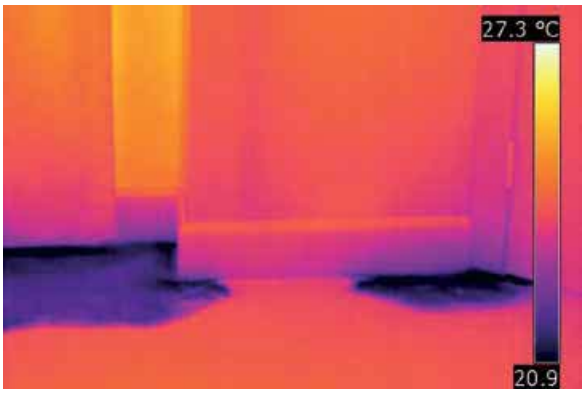

Фиг. 4. *Събираща се влага между под и стени.*

5. Метод с магнетизирани частици за измерване на покритието на армировката на втвърден бетон.

Инспекцията чрез магнетизирани частици (MPI – Magnetic Parts Inspection) е процес на безразрушително тестване за откриване на повърхностни прекъсвания в материалите и такива, които са плитко под повърхността, чрез използване на различни феромагнитни материали като желязо, никел, кобалт и някои от техните сплави. Процесът включва поставянето на материала под влиянието на магнитно поле, като той може да бъде магнетизиран чрез *пряка* или *непряка* магнетизация – фиг. 5. Пряката магнетизация се получава, когато електрическият ток преминава през тествания обект и в материала се образува магнитно поле. Непряката магнитизация се получава, когато материала няма свойства за преминаване на електрически ток и съответно магнитно поле не може да бъде директно образувано в него, но такова е налично във външен източник. Магнитните линии, които се образуват, са перпендикулярни на посоката на електрическия ток, който може да бъде или променлив ток (AC), или някаква форма на прав ток (DC) (изправен променлив ток).

Наличието на повърхностно или подземно прекъсване в материала позволява магнитния поток да изтече, тъй като въздухът не може да поддържа толкова магнитно поле на единица обем, колкото металите.

За да се идентифицира изтичането, металните частици, сухи или в мокра суспензия, се поставят върху материала. Те са привлечени от област на изтичане на потоци и формират това, което е известно като *индикация* (за проблем), която се

оценява, за да се определи нейната природа, причина и следващите действия, ако има такива [6].

Фиг. 5. *Машина за тестване чрез метода на магнетизираните частици.*

Магнитни методи могат да се използват за определяне на местоположението и покритието на армировката, вградена в закален бетон. Някои от моделите, които се предлагат на пазара, са Micro-cover meter, Pachometer, Profometer, Fe-Depth meter и т.н. Тези съоръжения се основават на принципа, че наличието на стомана влияе върху полето на електромагнита. Повечето уреди се състоят от източник на енергия, усилвател и измервателен уред, както и отделно устройство за търсене (сонда), съдържащо електромагнита, който е свързан към основното устройство чрез кабел.

Фиг.6. *Изследване с профометър.*

Профометърът е преносимо, снабдено с батерии, оборудване, използвано за измерване на дълбочината на покриващия бетон, местоположението и размера на стоманената армировка, закрепена в бетон – фиг. 6. Оборудването е полезно за изследване на структурите, където чертежите не са налични. Оборудването се състои от уред за регистриране на данни, сонда за диаметър и сонда за дълбочина, както и калибрационен блок.

Оборудването има достатъчно памет за съхраняване на сканираните данни. Иглата на измервателния уред се нулира и сондата се премества над повърхността на бетона, сондата се премества и завърта, за да се получи максимално отчитане и тази позиция съответства на местоположението на арматурната греда (минимално покритие). Използва се за: а) измерване на бетонния капак; б) откриване на усилващата лента; в) определяне на размера и посоката на лентата. В силно подсилена секция обаче ефектът на вторичната армировка не може да бъде напълно отстранен. Въпреки това, това оборудване дава справедлива представа за средната дебелина на слоя с максимална вариация + 5mm.

6. Електросъпротивителни методи

Уредите за измерване на съпротивлението в материалите за целите на безразрушителното тестване, са устройства за измерване на електрическата проводимост и / или електрическото съпротивление на твърдите носители, за да се определят характеристиките на съставните му материали. Обикновено измервателите на проводимостта и измервателите на съпротивление с NDT се използват с метали, но са възможни изследвания и на други материали. Електрическата проводимост измерва ефективността, с която атомите в метал (или друг материал) предават електрони. Електрическото съпротивление е електрическото съпротивление на тялото, на база единица дължина, единица площ на напречното сечение на материала, или единица тегло – фиг. 7. Ниското съпротивление показва материал, който лесно позволява движението на електрически заряд. Същевременно, в една и съща проба, вариации от съпротивлението, които се получават в зависимост от състава на материала и вътрешната структура, могат да помогнат за индикиране на дефектите в него [7, 8].

Фиг. 7. *Изпитване на бетонов блок чрез уред за електрическо съпротивление.*

Изпитването с индукционни токове използва електромагнитна индукция за откриване на позиции, форма, фрактури и пропуски в проводящи материали. Този метод може да се използва за оценка на стоманобетонни конструкции, позволяващ да се открият положението и диаметрите на арматурите. За да се постигне прецизно разпознаване на позицията на стоманените части и да се ограничат външни смущения, в системата може да се използва lock-in усилвател.

Ток на Фуко се индуцира в арматурни пръти (арматура), което създава вторично магнитно поле, което се противопоставя на магнитното поле, което го създава. Чрез измерване на промените в импеданса в серпентината може да се определи повърхността на бетона и / или диаметърът на арматурата – фиг. 8.

Изследването с уреди, работещи с вихрови токове, е ограничено от разстоянието между армировката и повърхността на бетона. Максималната дълбочина на проникване е около 15 см. Методът на тестване позволява откриване само на първия армировъчен слой. Измерването се влияе от наличието на други армировъчни пръти, колани, метални телове или двойни пръти. Освен това, методът на измерване изисква спецификация на входните променливи като например диаметър на арматурния прът и др. Най-малко един параметър трябва да бъде известен от плановете за подсилване или тестовите сондажи, за да се потвърди местоположението на арматурата.

Фиг. 8. *Измерване на покритието върху арматурата с вихрови токове.*

7. Радиометрични методи.

Когато се използва радиочестотно изпитване, през конструктивното тяло прониква електромагнитно излъчване. Това са рентгенови лъчи или гама лъчи. Отчитат се разликите в абсорбцията, които са в зависимост от плътността и дебелината на тествания материал. Това позволява подробен анализ на вътрешната структура на широк спектър от компоненти. Поради сложната система за измерване с достъпност от двете страни и персоналното оборудване / изисквания за безопасност, тестването с радиография се използва само в няколко специални случая, [9].

Използван е метод за предаване на гама-лъчи за изследване на изменението в плътността на бетона, причинено от утаяването в колони. Съдържанието на влага в бетона се определя чрез техниката на разсейване на неутроните и разпределението на цимента се изследва чрез радиоактивен трасиращ анализ. Използване на такива методи може да предостави необходимата информация за инженерния анализ на много проблеми.Структурата на бетона може да бъде изследвана чрез рентгенографиране на тънки резени от бетон. Образуването и разпространяване на пукнатини може да бъде изследвано от рентгенови снимки, взети на редовни интервали от време.

Може да се използват уреди за наземно проникващо радарно или импулсно радарно изследване, използвано за откриване на позицията на арматурни пръти или напречни канали. Този метод се използва вместо рентгенографска проверка за проверка на кабели, тръбопроводи в бетон и положение на армировъчни пръти.

8. Заключение.

В съвременното строителство, стандартно, качествата на строителните материали и конструктивни елементи се тестват лабораторно, с нормативни товари според изискванията на приложението им. Основен недостатък е, че в реална среда, върху конструкциите въздействат различни фактори като слънцегреене, климатични промени, корозия, температурни разлики, износване и пр. , които занижават якостните и поведенческите им свойства. Поради тази причина се използват различни техники за обследване на строителните конструкции и материали по безразрушителни методи извършвани на място. С напредването на научните изследвания, безразрушителните методи непрекъснато се усъвършенстват и спомагат за по-детайлно и точно диагностициране на съществуващите сгради с оглед на използваните материали. Тази прецизност на резултатите, от своя страна спомага за разработването на нови материали и конструктивни елементи и проектирането на по-сигурни сгради и съоръжения.

Литература

1. Наредба №5 от 28.12.2006г за техническите паспорти на строежите ДВ, бр.22 от 2010г.;

2. Guidebook on non-destructive testing of concrete structures — INTERNATIONAL ATOMIC ENERGY AGENCY, VIENNA, 2002

3. Non-Destructive Testing of Concrete: A Review of Methods — J. Helal, M. Sofi, P. Mendis, University of Melbourne, Australia

4.Безразрушителни изпитвания на строителни конструкции, С., 2011 — Проф. д-р инж. Д. Димов

5. Thermal Imaging Guidebook For Building and Renewable Energy Applications — FLIR Systems Co. Ltd.

6. Betz, C. E. (1985), Principles of Magnetic Particle Testing (PDF), American Society for Nondestructive Testing, p. 234, ISBN 978-0-318-21485-6.

7. Nondestructive Testing (NDT) Conductivity and Resistivity Meters Information.

http://www.globalspec.com/learnmore/test_measurement/nondestructive_test_equipment/conductivity_resistivity_instruments_earth_ground. Internet, Online.

8. Resistivity: Measure of the Quality of Metals quickly and accurately with Non Destructive Testing (NDT).

http://www.epandt.com/us/resistivite_us.html. Internet. Online

9. Taffe, Alexander, Stoppel, Markus und Wiggenhauser, Herbert. Zerstörungsfreie Prüfverfahren im Bauwesen - Übersicht der Verfahren. [Hrsg.] Bundesanstalt für Materialforschung und -prüfung. Betoninstandsetzung im Ingenieur- und Wohnungsbau. Filderstadt : s.n., 2010

Експериментално изследване на равномерността и дебелината на тънки покрития с 3D томограф.

EXPERIMENTAL STUDY OF THE EVENNESS AND THICKNESS OF THIN FILMS WITH 3D TOMOGRAPHY.

Stanislav Gyoshev, Nikolay Stoimenov
stanislavgyoshev@mail.bg, nikistoimenow@gmail.com

Институт по информационни и комуникационни технологии, София 1113, ул. акад. Георги Бончев, бл.2.

Abstract: *In the present work are obtained results of experiments for the study of thin coatings with computer tomography. There is an overview of the types of nickel and chromium coatings and the different ways of applying them. Options are proposed for testing thin and thicker coatings.*

Key words: *thin coatings, nickel coatings chrome coatings, coating thickness, coating evenness.*

1. Видове никелови покрития и методи за нанасяне.

Металните покрития намират широко приложение в антикорозийната практика. Тези покрития не само защитават от корозия, но и предават на повърхността редица ценни физико-механични свойства като: твърдост, износоустойчивост, електропроводимост, запояемост, добър външен вид и др. В зависимост от полярността на покритието по отношение на защитавания метал, те се групират в две групи – катодни и анодни. [1, 2]

През последните години интересът към „electroless" никел покрития се е увеличил значително. Това се дължи на свойството да се отлага по повърхността, както и способността му да се нанася равномерно и да влиза в добър контакт с нея. Свойствата на „electroless" никел покрития се определят от начина на отлагане, химичен състав и структура на сплавта.

2. Описание на основните методи за нанасяне на покрития.

Металните покрития се нанасят посредством следните основни методи: потапяне в разтопен метал, метализация чрез разпрашаване, термодифузионен метод, термомеханичен метод, галваничен метод, химично отлагане [1-5].

- потапяне в разтопен метал – нанасяне на цинкови, алуминиеви, калаени и оловни покрития върху стоманени изделия и полуфабрикати (лист, тел, тръби и др.

- метализация чрез разпрашаване (пулверизиране) на разтопен метал върху повърхността с помощта на сгъстен въздух или инертен газ. Разпрашаването се извършва, чрез специални пистолети – метализатори, в които се подава (във вид на тел или прах) нанасяния метал. Например нанасяне на цинк, алуминий, олово, калай, никел, месинг върху метални и неметални повърхности. В зависимост от източника на топлина за топене на метала, метализаторите биват: газови, електрически и плазмени.

- термодифузионен метод – нанасяне на покрития в резултат на дифузия на атомите на нанасяния метал при висока температура, при което се образува слой от сплав. Този метод на практика се реализира, чрез термодифузионни покрития на прахообразни смеси – цинкови, алуминиеви, хромови и силициеви покрития върху стомана.

- термомеханичният метод (плакирането) се прилага за производство на биметални ленти, листи, телове. Покритието се образува при съвместно валцуване, горещо пресоване или нагряване под налягане на два метала – на основния и на покриващия. Този метод осигурява много добро сцепление между покритието и основата, тъй като се извършва взаимна дифузия на двата метала при едновременното действие на високата температура и налягане.

- галваничен метод – нанасяне на покрития, чрез електролизно отлагане на метални слоеве върху токопроводяща основа. Извършва се в галванични вани за нанасяне на цинкови, кадмиеви, никелови, хромови, калаени и медни покрития.

- химично отлагане – представлява нанасяне на покритие върху метални и неметални материали, чрез химична редукция от разтвори. В състава на разтвора влизат йоните на отлагания метал и редуктор. Редукцията на металните йони се извършва (при определени условия) самопроизволно, при което редуцирания метал се отлага върху предварително подготвената повърхност на изделието. Извършва се за отлагане на редица метали, като никел, кобалт, мед, калай, сребро и др., върху метални или напоследък и пластмасови изделия и детайли за получаване за защитно декоративни и функционални покрития.

Освен тези методи съществуват и други методи за нанасяне на метални покрития като: вакуумно метализиране (отлагане на разтопен метал в условия на дълбок вакуум в специални камери); катодно разпрашаване (в условия на дълбок вакуум и електрично поле); парафазно отлагане (чрез термично разлагане на летливи съединения на отлагания метал); електрофорезно отлагане (чрез електрофореза на неводна сеспензия, съдържаща отлагания метал в прахообразно състояние).

Например измерването на линейното износване от порядъка на десети от микрона би могло да се измерва с помощта на хидравличния усилвател (фиг.1) с разработването на специализирана технология и автоматизирана система записване на пряко записване на линейното износване във функция на времето t, характерни за различните тънки покрития.

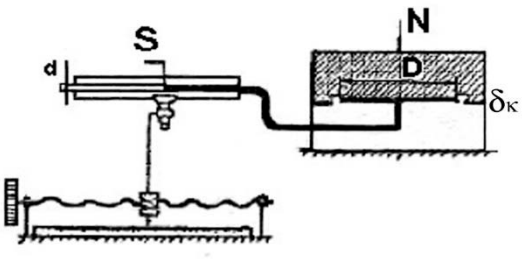

Фиг.1 *Схема на опитна установка за измерване и изследване на контактни деформации.*

За полагане на покрития биха могли да се използват и не метални материали например детайли получени на 3D принтер, като това ще повиши значително износоустойчивостта им, което е основен проблем при детайлите получени от 3D принтери. Като пример за такива детайли могат да се дадат брайлови плочи фиг.2, които се използват като картини за разпознаване от слабо виждащи или слепи хора. Основното приложение на тези плочи е разчитането им чрез докосване от незрящите хора, поради тази причина би било подходящо да бъдат покрити с износоустойчиво метално покритие.

Фиг.2. *Брайлова плоча за хора с нарушено зрение.*

3. Възможности за изследване износването на тънки покрития.

В много случаи на практиката се използват покрития с дебелина от порядъка на 10 ÷20 μm. Линейното износване на такива покрития, свързано с деформирането, приработването и разрушаването им поднася големи метрологични трудности. Например ако трябва да се проследи приработването на едно такова покритие, то по общия закон на трибологията би следвало линейното износване L да се представи аналитично като функция на времето t във вида:

$$\frac{dL}{L} = \eta_1 \frac{dt}{t} + \eta_2 \frac{dt}{t} + \eta_3 \frac{dt}{t}$$

където η_1, η_2, η_3 са парциалните контактни потенциали на износващото се покритие на съответните три епата на износване – приработване, стационарен режим, патология.

Задачата за изследване на износването се усложнява многократно, т.к. и без това тънкото покритие трябва да се разбие на три участъка и за всеки от тези участъци да се построи закона за износването. Всички това предполага наличие на оборудване с изключителна разделителна способност и възпроизводимост (компютърен томограф Nikon XTH 225, фиг.3)

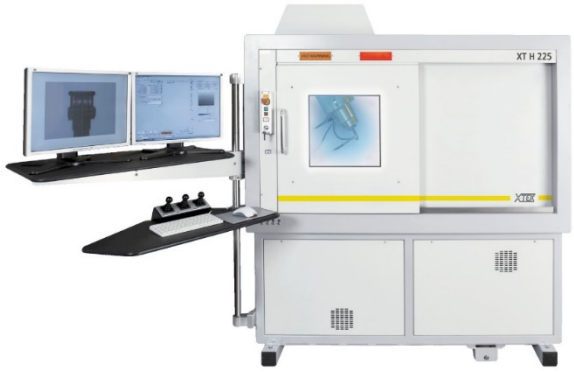

Фиг.3 *Компютърен томограф Nikon XTH 225.*

Чрез компютърния томограф биха могли да бъдат изследвани покрития с дебелина по-дебело от 5 μm (това е максималната разделителна способност на уреда), благодарение на томографа, такива покрития могат да бъдат изследвани по безразрушителен метод, детайлът който се изследва, след изследването може да работи нормално. Работната зона на уредът е 30x30x30 cm.

На фиг.5 са показани снимки на изследваните детайли, според производителя покритието е хромово с дебелина 20 μm, задачата е да се изследва дебелината и равномерността на покритието. След провеждане на експерименти за износване и последващо заснемане на детайла на компютърния томограф, може да се изведе закон за износване и по този начин да се определи и износоустойчивостта на металното покритие.

4. Основни подходи, представи и модели на износването и износоустойчивостта

Основните подходи и представи са: скорост на износване, интензивност на износване, износоустойчивост, относителна износоустойчивост, линейно износване. Основните схеми на контакт при изследване на износване на покрития са показани на фиг. 4. [4-8]

4.1. Скорост на износване – отношение на величината на износване към времето, за което протича. Различават се мигновена скорост на износване (в определен момент от времето) и средна – за определен интервал от времето.

4.2. Интензивност на износване – отношение на величината на износване за изминатия път, за което се е осъществило износването, или към големината на извършената работа.

4.3. Износоустойчивост – свойство на материала да оказва съпротивление на износване в определени условия на триене. Износоустойчивостта е реципрочна стойност на скоростта на износване или на интензивността на износване.

4.4. Относителна износоустойчивост – отношение на износоустойчивостта на изпитваното покритие и износоустойчивостта на материал, приет за еталон при тяхното износване при еднакви условия. Прието е еталонът да е от материал с по-ниска износоустойчивост.

4.5. Под линейно износване се разбира изменение на линейния размер на образеца в резултат на износване в посока, перпендикулярна на повърхнината на триене.

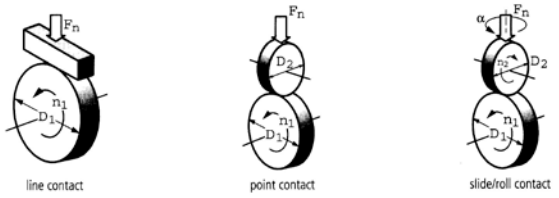

Фиг.4. *Основни схеми на контакт при изследване на износване на покрития.*

5. Експерименти

На фиг.5 са показани детайлите с хромово покритие, които са обект на изследването. Материалът от който са изработени е алуминиева сплав, благодарение на голямата разлика в пропускливостта на алуминия и хрома много лесно ще се „види“ чрез томографа равномерността и дебелината на покритието.

На фиг.6 са показани снимки от компютърния томограф на които се вижда равномерността на покритието - фиг.6а и дебелината на покритието в най-тънката част - фиг.6б

а)

б)

Фиг.5. *Снимка на изследваните детайли. А- детайл с 20 микрона хромово покритие, б- детайл с 30 микрона хромово покритие.*

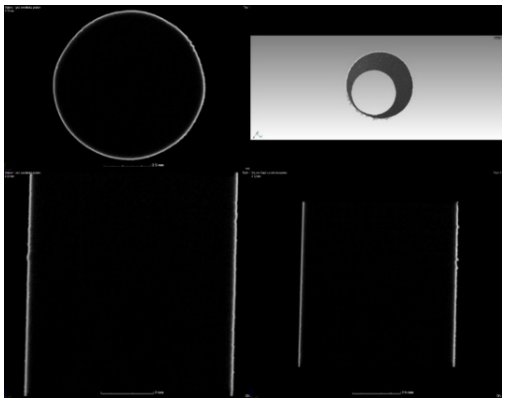

а) Изглед и сечения.

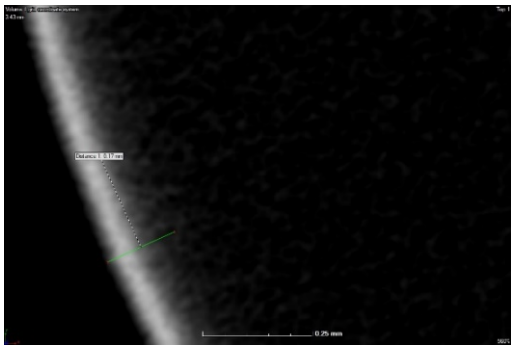

б) Отчитане на дебелина.

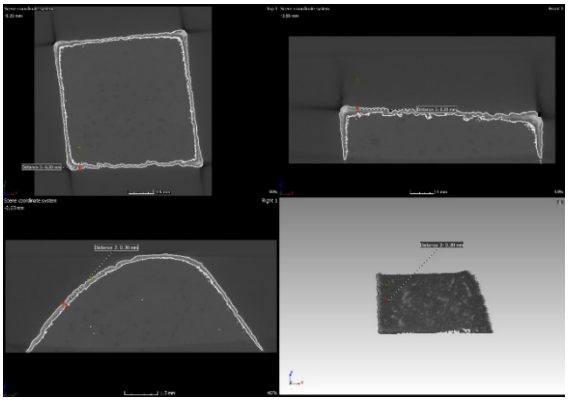

в) Томографски изображения.

Фиг.6. *а) 3д изглед и сечения на образеца от фиг.5а, б) дебелина на покритието в най-тънката част на покритието, в) томографски изображения на детайла от фиг.5б.*

Принципно новото в тази работа е възможността за построяване на закона за износване повърхностни покрития с отчитане на многофакторното влияние на параметри от експлоатацията им чрез отчитане на изменението дебелината на покритието, чрез компютърен томограф.

Благодарности.

Изследването в настоящата работа е осъществено с подкрепата на проект “Информационно-комуникационни технологии за 3D моделиране и 3D тактилна визуализация на обекти на културно-историческо наследство (изграждане на 3D модели от 2D източници и 3D принтиране)”, договор № ДФНП 17-98/29.08.2017, финансиран от „Програма за подпомагане на младите учени в БАН”.

Литература

1. Коваленко В. С., Технология и оборудование электрофизических и электрохимических методов обработки материалов., Киев, Вища школа, 1985

2. Маслов Е. П., Теория шлифования материалов., Москва, машиностроение, 1978

3. Gavrilov G., Chemical(electroless) Nickel Plating, England , 1979, Monography

4. Гаврилов , Г, Николов Ив. , Химическо никелиране и дисперсни покрития, София, 1985

5. Riedel , W . Funktionale Chemische Vernicklung, Saulgau , 1989

6. Karastoyanov D., Kandeva M., Vencl A.. Advanced Tribological Coatings for Heavy-Duty Applications: Case Studies. Prof. Marin Drinov Academic Publishing House, 2016, ISBN:978-954-322-858-4, 147

7. М. Кандева, Д. Карастоянов. Състояние и актуални въпроси на трибоквалиметрията в областта на износоустойчивите покрития., СЕДМА КОНФЕРЕНЦИЯ ПО ТРИБОЛОГИЯ БУЛТРИБ 2009, София, 30 октомври 2009 г, стр. 108-115

8. D. Karastoyanov, T. Penchev., New Methods for Renovating of Shafts for Folio Extrusion., JOHN ATANASOFF CELEBRATION DAYS, International Conference AUTOMATICS AND INFORMATICS ’09, Symposium ROBOTICS AND AUTOMATION, SOFIA, BULGARIA, 29.09 – 4.10. 2009, pp II – 25 – II – 28

ВИСОКОТЕМПЕРАТУРНИ ВАКУУМНИ ТЕХНОЛОГИИ ЗА ПРОИЗВОДСТВО НА МАТЕРИАЛИ И СПЛАВИ С ВИСОКА ТВЪРДОСТ И ИЗНОСОУСТОЙЧИВОСТ С ВКЛЮЧЕНИ НАНОЕЛЕМЕНТИ

HIGH TEMPERATURE TECHNOLOGIES FOR PRODUCING OF MATERIALS AND ALLOIS WITH HARDNESS AND WEAR RESISTANCE INCLUDING NANO ELEMENTS

Богомил Попов, Димитър Карастоянов, Николай Стоименов
Институт по информационни и комуникационни технологии – БАН
1113 София, ул. „ак. Г. Бончев“ бл. 2, e-mail: dkarast@iinf.bas.bg

Abstract: *The paper discusses the features of high temperature technology for the production of hard and wear resistant materials and alloys for instrumental equipment. Two technologies are proposed using nano elements.*

Key words: *high temperature technologies, hardness, wear resistance, materials and alloys, nano elements*

1. ВЪВЕДЕНИЕ.

Масово разпространените методи за термична и химико-термична обработка на инструментални и конструкционни стомани са газово навъглеродяване и газово азотонавъглеродяване. Използват се шахтови пещи с външно индиректно нагряване на изделията в реторти. За закаляване се използват други допълнителни съоръжения, в т.ч. пещи за второ нагряване за закаляване, транспортиращи устройства, маслени вани, съоръжения за обезмасляване, пещи за отвръщане и др. Тези методи се характеризират с редица недостатъци като голям разход на реактивни газове, неравномерност на дифузионните слоеве, висока степен на замърсяване на околната среда поради отделяне на отровни газове при закаляване, наличие на технологични отпадъци от маслото за закаляване и необходимостта от обезмасляване на изделията след закаляване чрез използване на органични и неорганични обезмаслители, частично обезвъглеродяване и окисляване на повърхността на изделията при транспортиране в нагрято състояние.

От извършено проучване се установи, че в много страни, вкл. България, се развива ползването на вакуумни пещи за разработване на нови процеси за йонно азотиране и карбо нитриране. Вакуумните пещи основно биват двукамерни (с две отделени камери - за загряване и охлаждане), фиг. 1, и еднокамерни (с две зони в една камера–за загряване и охлаждане), фиг. 2.

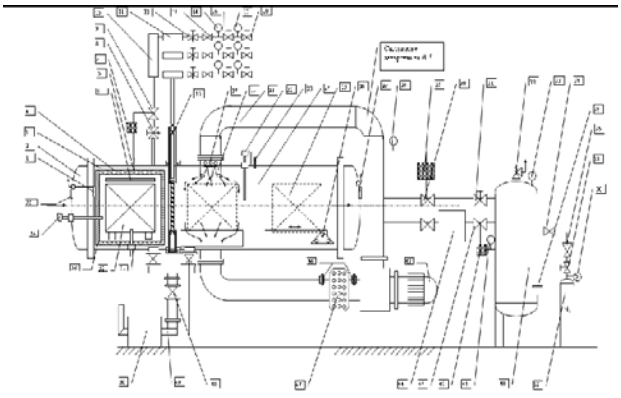

Фиг. 1. *Двукамерна вакуумна пещ.*

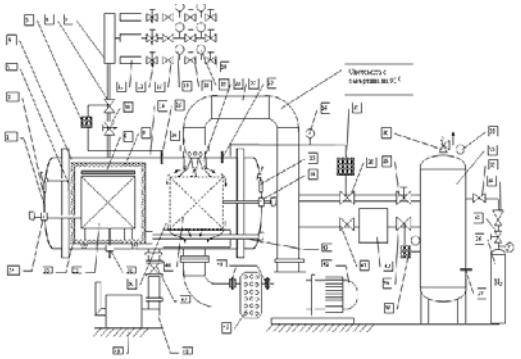

Фиг. 2. *Еднокамерна вакуумна пещ.*

2. ОСНОВНА КОНЦЕПЦИЯ.

Иновативността на предлаганото решение се състои в ползването на **Таманова и Вакуумна пещи** за получаване на титанов карбид и нано материали, смилането и пресоването на смес от титанов карбид и стоманен прах, спичането на заготовките във вакуумна пещ и отгряването им, а също така и хомогенизиране на борен карбид с нано активатори и спичане при температура 2260°C. Тези заготовки могат лесно да се обработват в наши предприятия (без внос) до желаните инструменти, след което да се закалят повторно.

Предимство на първия етап за разработване ще бъде усвояване на процес за изработване на заготовки от инструментални материали на основата на титанов карбид - легирани стомани с които да се задоволяват потребностите на машиностроителните предприятия в страната, внасящи скъпоструващи инструменти. Заготовките под форма на цилиндри, блокове и други форми ще се дообработват в машиностроителните заводи до многопрофилни специализирани инструменти, които след закаляване придобиват твърдост близка до тази на волфрам - титан карбидни инструменти, но притежават висока ударна жилавост.

Освен това предвиждаме да са разработи технология за изостатично пресоване на карбидни сплави и активирано спичане в **Таманова пещ** при температури 2240°C – 2260°C.

Използването на процеси при които ще се реализират високи температури, както и ползването за изработка на входящи материали **на Таманова пещ** с температури до 2 200° ÷ 2 300° C, както и **на Вакуумна пещ**, дава възможност за изработка на:

- инструментални материали без използване в тях на дефицитни метали като волфрам и кобалт /например сплави на основата на титанов карбид-стомана позволяващи

дообработване, до сложни конфигурации за режими и инструменти/;
- изделия за отбранителната промишленост;
- изделия за радиоактивна защита.

От особено значение е производството на материали, които широко се използват като армиращи елементи в ляти изделия от цветни и черни метали с оглед намаляване на масата на използваният материал при увеличаване на якостните характеристики на изделията:

1. Изделията на основата на титанов карбид-стомана намаляват количествата използван волфрам и особено вреднят кобалт – тежки метали, вредни за здравето;

2. Титановият карбид и легираната стомана са недефицитни материали, получавани в страната.

Спечените въглерод съдържащи материали, вградени в бронежилетки, в средства за предпазване от радиация са незаменими материали при работа в тежка криминална и радиационна среда.

1. Съществено предимство на инструменталните материали титаново карбидна стомана е възможността да бъдат обработвани сложни по форма изделия с използване на обикновени съоръжения. След закалка материалите придобиват твърдостта на волфрам-карбидни твърди сплави

2. Активираното спичане, което ще бъде предложено за уплътняване на трудно уплътняеми материали, ще увеличи рязко производителността при получаване на специални материали, тъй като ще замени трудоемкият процес на горещо пресоване, свързан с големи разходи на метериали за пресформи и енергия при пресоването (например борен карбид).

3. Технологиите предстои да се защитят евентуално в ЕС с патенти.

4. В процес на усвояване са подходи за точно поддържане на високи температури в тесен интервал от 2240^0C – 2260^0C.

Възможни са затруднения при получаване на титанов карбид без примеси от свободен въглерод.

3. ПРАХОВА МЕТАЛУРГИЯ, ПРЕДИМСТВА НА МЕТОДА.

Високата ефективност на праховата металургия (ПМ) се заключава в производството на материали или изделия, които е технологично невъзможно или икономически неизгодно да бъдат произведени по други методи. Отличителна особеност на ПМ е, че изделията се получават по практически безотпадни технологии. Независимо от по-високата цена на праховете от тази на летите метали, материалните разходи за единица изделие, получено по методите на ПМ са винаги по-ниски от тези за изделия, получени посредством рязане, щамповане, фрезоване и др. Така напр., при ПМ методите коефициентът на използване ма материалите е в границите 95-97%, докато при обработка посредством рязане тази стойност е едва 50-60%. Друго предимство на ПМ метода е сравнително неголемия брой операции - като правило не повече от 3-5, което позволява да се съсредоточи производството на изделия в едно предприятие, а това е свързано с повишаване производителността на труда, снижаване на енергийните загуби, намаляване броя на работещите и като резултат - снижаване цената на крайния продукт. Използваните процеси лесно се поддават на автоматизация, като при работа с прес-автомати количеството на праха, необходимо за получаване на заготовка с определена плътност е точно дозирано, като се избягват материални загуби, неизбежни при механична обработка на лети детайли. Методът е уникален при производство на композиционни материали на метална или керамична основа: мед-графит за тоководящи детайли, WC-Co за металообработващи инструменти, сплави W-Cu и мн. други. Към тези материали спадат и предлаганите за разработване методи включват композиционни материали на основата на титанов карбид TiC – стомана (феротик) и на основата на борен карбид (B4C).

Предлаганата методология е типична в прахово металургичното производство с тази *иновативна особеност, че се използват високо температурни процеси*. Предварително се правят изследвания за валидиране едрината на частиците и равномерността им по едрина в използваните железни и други прахове с **лазерен нано грануломер Analysette 22 Nano Tech+** с диапазон от 10 нано метра до 2000 микрона – фиг. 3.

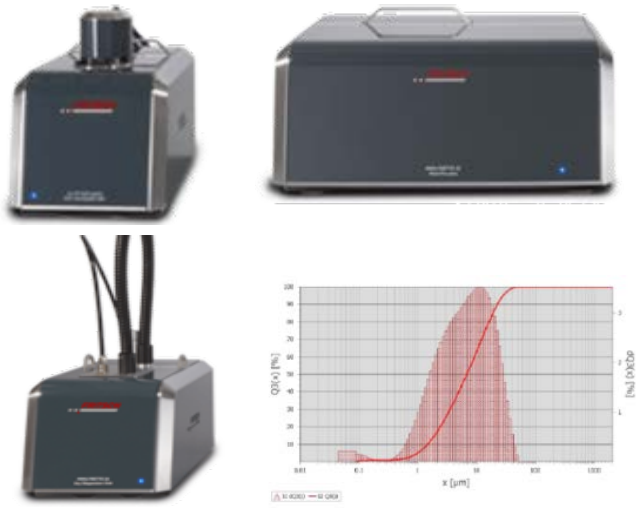

***Фиг. 3.** Лазерен нано грануломер.*

1. Получаване на чист титанов карбид от титанов оксид и сажди в **Таманова пещ.**

Изходните материали се насипват и смесват в графитни ладии и за загряват в пещта до 2300°C.

2. Получаване на нанопрахове в Тамановатата пещ за активирано спичане на борен карбид при 2240-2260°C – фиг. 4.

3. Получаване на стоманена сплав под формата на прах

За целта се ползва топкова мелница, предвидена за закупуване, съчетана с планетарна мелница за допълнително издребняване.

4. Пресоване на смес от титанов карбид и стоманен прах, пресоване на борен карбид.

За целта се ползва изостатична преса, предвидена за закупуване.

5. Спичане на пресовките от титанов карбид и стоманен прах във вакуумна пещ – фиг. 5.

6. Отгряване на изделията.

За целта се ползва пещ за отгряване.

За допълнителен контрол на температурните процеси, както и за термално обследване на детайлите през междинните етапи между пещите се използва **термо камера FLIR P 640** с измервателна точност 0.06°C и диапазон до 2000°C – фиг. 6.

След получаване на отгретите заготовки те се изследват финално за равномерност на вътрешната 3D структура, наличие на шупли, пукнатини и други дефекти с **3D индустриален томограф Nikon XT H 225 –** фиг. 7**.**

В технологичните процеси се ползват смесители, сушилня,пещ за отстраняване на пластификатора.

7. Пресоване изостатично на карбидни сплави и активирано спичане при температура 2240°C – 2260°C

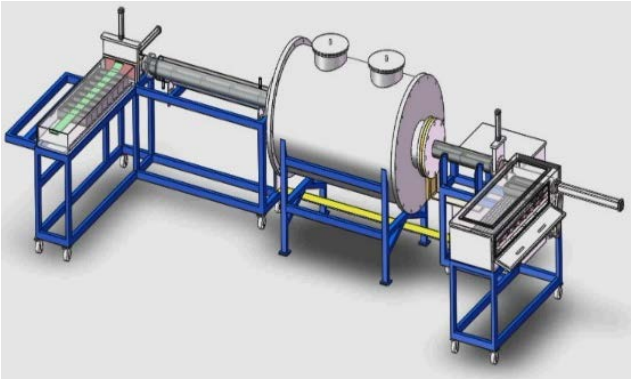

Фиг. 4. *Таманова пещ.*

Фиг. 5. *Вакуумна пещ.*

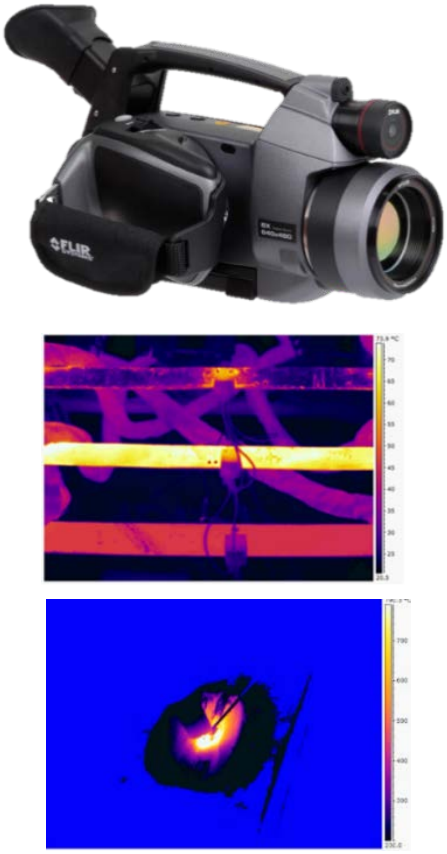

Фиг. 6. *Термо камера FLIR P640.*

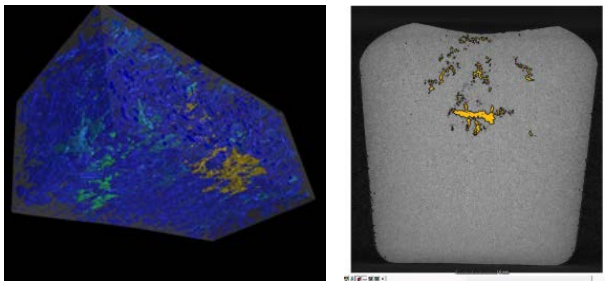

Фиг. 7. *Индустриален томограф Nikon XT H 225.*

4. *БОРЕН КАРБИД – СВОЙСТВА И ПРИЛОЖЕНИЕ.*

В йерархията на материалите по твърдост борният карбид заема на трето място след изкуствените диаманти и кубичната модификация на борния нитрид. За разлика от тези два материала, синтезът на B4C протича сравнително лесно. Синтезът на (BN)c от (BN)h протича при по – затруднени условия (температура, налягане), отколкото синтезът на диаманти от въглеродни материали. Освен към свръхтвърдите (~40 GPa), борният карбид принадлежи и към труднотопимите (2450°C) материали. Притежава висока химическа и добра устойчивост срещу високотемпературно окисление.

Продуктите не са радиоактивни, а лъчението е „меко" и може да се пренебрегне. **Приложения – фиг. 8.**

Таблетки от горещо пресован B4C намират приложение при изработването на регулиращите ядрената реакция системи на различни по конструкция (PWR, BWR) ядрени електроцентрали [1, 2]. Съчетанието от ниска плътност (2.52 $g.cm^{-2}$), изключителната твърдост и високите стойност на модулите на еластичност (E~400 GPa, B~200 GPa, G~200 GPa) обуславя приложението на B_4C във военната техника за изработване на противокуршумни жилетки, брони за танкове и хеликоптери. От борен карбид се изработват калибри, шаблони, заточващи инструменти, предпазители за термодвойки, хавани и др. От борен карбид се произвеждат висококачествени пясъкоструйни и дробеструйни дюзи с прилижение в металургията, машиностроенето, корабното дело, архитектурата, зъботехниката. Сравнението на износоустойчивостта спрямо корунд (Al_2O_3) на дюзи от различни свръхтвърди материали (корунд, самосвързан SiC, твърда сплав WC-Co, SiC) показва превъзходството на произведените от борен карбид. Наноразмерни прахове намират приложение в Boron Neutron Capture Therapy (BNC) на туморни заболявания [3]. Високата термична и химична стабилност обуславят приложението на B_4C в архитектурата на горивни клетки в качеството на каталитичен носител [4].

Фиг. 8. *Приложения.*

<u>Високотемпературна иновация:</u>

Технологичните особености на процесите на активирано спичане на високо температурни износоустойчив материал от **карбид на бора** са иновативна новост.

<u>Процедура на технологията:</u>

1. Хомогенизиращо смесване на нано прахове от борен карбид с волфрамов карбид в присъствие на течна фаза. Необходимо съоръжение – топкова мелница.

2. Вакуумно изсушаване на хомогенизираната смес (вакуумна сушилня).

3. Пластифициране / смесване на нано праховете с пластификатор. Използва се подогреваем смесителен Z образен смесител.

4. Изостатично пресоване на профилни заготовки с изостатична преса.

5. Депластифициране на отпресованите заготовки в нискотемпературна пещ в среда от водород или инертен газ (азот, аргон)

6. Високотемпературно спичане във водородна среда при температура 2240^0C – 2260^0C Таманова пещ.

5. ЗАКЛЮЧЕНИЕ

Високотемпературните технологии за получаване на материали и сплави с висока твърдост и износоустойчивост, при които се ползват нано елементи, представляват иновации за снабдяване на български предприятия с инструментални материали, без да се налага внос на скъпи материали, екипировка и технологии.

Литература:

1. M.Beauvy, F.Thevenot, L'Industrie ceramique, 734, 12 (1979), 811-814
2. M. Streinbruck, Journal of Nuclear Materials, 336, (2005), 185-193
3. T. Iwagami, Y. Ishikawa, N. Koshizaki, N. Yamamoto, H. Tanaka, Sh. Masunaga, et al.,"Boron Carbide Particles as a Boron Compound of Boron Neutron Capture Therapy," *J. Nucl. Med. Radiat. Ther*., 177 1-5 (2014).
4. E. Antolini, E.Gonzalez, "Ceramic Materials as Supports for Low-temperature Fuel Cell Catalysts," *Solid State Ionics, 180, 746-63, 2009*

НАДЛЪЖНИ ПУКНАТИНИ ВЪВ ФУНКЦИОНАЛНО-ГРАДИЕНТНИ ГРЕДИ

LENGTHWISE CRACKS IN FUNCTIONALLY GRADED BEAMS

Проф. д-р инж. Ризов В.
Университет по Архитектура, Строителство и Геодезия, София, България
E-mail: V_RIZOV_FHE@UACG.BG

Abstract: *The present paper analyzes the lengthwise fracture behavior of beam structures made by functionally graded linear-elastic material. The material is functionally graded along the height of the beam cross-section. It is assumed that a lengthwise crack is located arbitrary in the beam. Thus, the crack arms have different thicknesses. The fracture is analyzed in terms of the strain energy release rate. The solution to the strain energy release rate derived in the present paper is compared with the J-integral for verification. The analysis developed is very useful for parametric investigations of the lengthwise fracture behavior of functionally graded beams.*

Keywords: FUNCTIONALLY GRADED BEAM, LENGTHWISE CRACK, FRACTURE ANALYSIS

1. Увод

Функционално-градиентните материали са сравнително нови нехомогенни конструктивни материали, получени чрез смесване на две компоненти [1 - 19]. Свойствата на даден функционално-градиентен материал се променят непрекъснато по едно или повече направления в рамките на един конструктивен елемент или детайл. По този начин може да се оптимизира поведението на конструктивния елемент по отношение на различни натоварвания и външни въздействия. Функционално-градиентните материали разкриват много добри възможности и за намаляване на собственото тегло, което е предпоставка за снижаване на себестойността на конструкциите. Също така, функционално-градиентните материали са много подходящи за работа в екстремални условия (например, висока температура, радиация и др.). Тези съвременни материали намират широко приложение в аеронавтиката, роботиката, ядрените реактори, електрониката, автомобилната индустрия, оптиката, медицината и др. Появата на пукнатини е един от основните проблеми при използването на функционално-градиентните материали в носещи конструктивни елементи. Пукнатините водят до значително редуциране на носимоспособността на конструкцията. Освен това, пукнатините са причина за увеличаване на деформируемостта, което сериозно застрашава нормалното функциониране на конструкцията. В някои случаи пукнатините могат да предизвикат даже катастрофално разрушение на цялата конструкция. Същевременно трябва да се отбележи, че надлъжните пукнатини във функционално-градиентните конструктивни елементи са сравнително слабо проучени в специализираната научна литература. Ето защо, главната цел на настоящата статия е да се извърши изследване на надлъжна пукнатина във функционално-градиентна греда, която е натоварена на огъване.

2. Анализ на скоростта на освободената потенциална енергия на деформацията

Обект на изследване в настоящата статия е надлъжната пукнатина във функционално-градиентната греда, показана схематично на Фиг. 1. Гредата има правоъгълно напречно сечение с основа b и височина h (Фиг. 2). Дължината на гредата е означена с l. В гредата има надлъжна пукнатина с дължина a (Фиг. 1). Височините на долното и горното рамо на пукнатината са означени съответно с h_1 и h_2. Външното натоварване на гредата се състои от две правопротивоположни вертикални сили F, приложени върху крайните сечения на рамената на пукнатината. Гредата е изпълнена от функционално-градиентен материал с линейно-еластично поведение. Връзката между напреженията и деформациите се изразява със закона на Хук

(1) $$\sigma = E\varepsilon,$$

където σ е нормалното напрежение, E е модулът на еластичност, ε е линейната деформация.

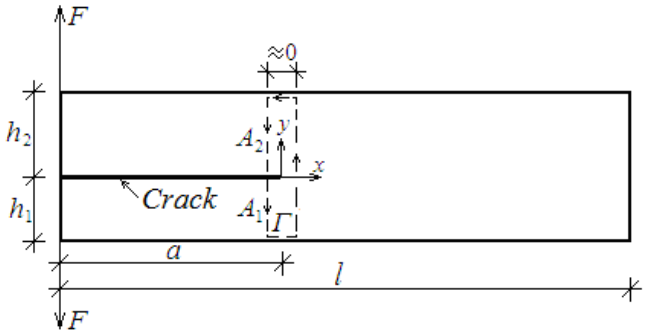

Фиг. 1*. Функционално-градиентна греда с надлъжна пукнатина*

Материалът е с градиент по височината на напречното сечение на гредата. Изменението на модула на еластичност по височината на напречното сечение се описва със следния косинусов закон:

(2) $$E = E_0\left[1 + q\cos\left(\frac{z+\frac{h}{2}}{h}\,\frac{\pi}{2}\right)\right],$$

където

(3) $$-\frac{h}{2} \le z \le \frac{h}{2}.$$

В (2), E_0 и q са материални свойства, z е вертикалната централна ос на напречното сечение на гредата (Фиг. 2). От (2) следва, че

(4) $$E\left(-\frac{h}{2}\right) = E_0(1+q)$$

(5) $$E\left(\frac{h}{2}\right)=E_0\ .$$

Основната цел на настоящата разработка е да се определи скоростта на освободената потенциална енергия на деформацията G .

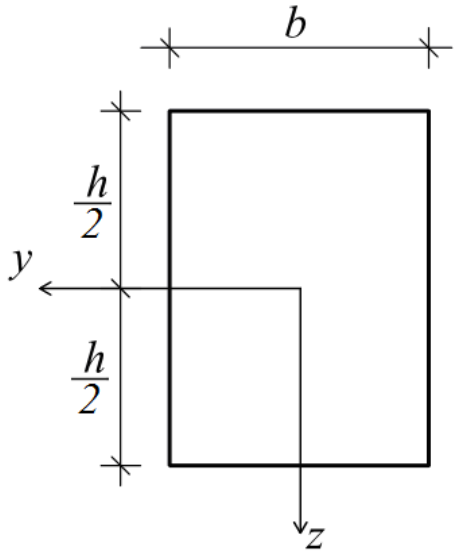

Фиг. 2. *Напречно сечение на функционално-градиентната греда*

Като е известно, скоростта на освободената потенциална енергия на деформацията има ключова роля в механика на пукнатините [2]. Ако се зададе едно малко нарастване Δa на дължината на надлъжната пукнатина, скоростта на освободената потенциална енергия на деформацията може да се изрази по следния начин:

(6) $$G=\frac{U_a-U_b}{\Delta A},$$

където U_a е потенциалната енергия на деформацията в участък от гредата с дължина Δa след нарастване на пукнатината, U_b е потенциалната енергия на деформацията в същия участък преди нарастване на пукнатината, ΔA е нарастването на лицето на пукнатината. Ясно е, че

(7) $$\Delta A=b\Delta a\ .$$

Потенциалната енергия на деформацията в ненапукания участък на гредата е нула. Ето защо

(8) $$U_b=0\ .$$

U_a се намира чрез сумиране на потенциалната енергия на деформацията в двете рамена на пукнатината

(9) $$U_a=U_a^{(1)}+U_a^{(2)},$$

където $U_a^{(1)}$ и $U_a^{(2)}$ са съответно потенциалната енергия на деформацията в долното и горното рамо на пукнатината.

Чрез интегриране на специфичната потенциална енергия на деформацията $u_0^{(1)}$ в участък от долното рамо на пукнатината с дължина Δa зад върха на пукнатината достигаме до следния израз за $U_a^{(1)}$:

(10) $$U_a^{(1)}=\Delta ab\int_{-\frac{h_1}{2}}^{\frac{h_1}{2}}u_0^{(1)}dz_1\ ,$$

където z_1 е вертикалната централна ос на напречното сечение на долното рамо на пукнатината.

За определяне на $u_0^{(1)}$ прилагаме следната формула:

(11) $$u_0^{(1)}=\frac{1}{2}\sigma\varepsilon\ .$$

Чрез комбиниране на (1) и (11) получаваме

(12) $$u_0^{(1)}=\frac{1}{2}E\varepsilon^2\ .$$

От (2) получаваме следното разпределение на E по височината на напречното сечение на долното рамо на пукнатинта:

(13) $$E=E_0\left[1+q\cos\left(\frac{z_1+h-\frac{h_1}{2}}{h}\ \frac{\pi}{2}\right)\right],$$

където

(14) $$-\frac{h_1}{2}\le z_1\le\frac{h_1}{2}\ .$$

Разпределението на ε по височината на долното рамо на пукнатината се намира по формулата

(15) $$\varepsilon=\kappa_1\left(z_1-z_{1n_1}\right),$$

където κ_1 е кривината, z_{1n_1} е разстоянието от нулевата линия до центъра на тежестта на напречното сечение на долното рамо на пукнатината (очевидно е, че нулевата линия се отмества от центъра, понеже модулът на еластичност на материала се изменя по височина на сечението).

Заместваме (15) в (12). Резултатът е

(16) $$u_0^{(1)}=\frac{1}{2}E\left[\kappa_1\left(z_1-z_{1n_1}\right)\right]^2\ .$$

За определяне на κ_1 и z_{1n_1} прилагаме следните условия за равновесие на напречното сечение на долното рамо на пукнатината:

(17) $$N_1 = b\int_{-\frac{h_1}{2}}^{\frac{h_1}{2}} \sigma dz_1 ,$$

(18) $$M_{y_1} = b\int_{-\frac{h_1}{2}}^{\frac{h_1}{2}} \sigma z_1 dz_1 ,$$

където N_1 и M_{y_1} са съответно надлъжната сила и огъващият момент в сечението на долното рамо зад върха на пукнатината. Очевидно е, че (Фиг. 1) $N_1 = 0$, $M_{y_1} = Fa$. Уравненията, получени след заместване на (1), (13) и (15) в (17) и (18), се решават по отношение на неизвестните κ_1 и z_{1n_1} с помощта на компютърната програма MatLab.

$U_a^{(2)}$ се намира по формулата

(19) $$U_a^{(2)} = \Delta ab\int_{-\frac{h_2}{2}}^{\frac{h_2}{2}} u_0^{(2)} dz_2 ,$$

където $u_0^{(2)}$ е специфичната потенциална енергия на деформацията в горното рамо на пукнатината, z_2 е вертикалната централна ос на нпречното сечение на горното рамо.

Формула (16) може да се приложи и за определяне на $u_0^{(2)}$. За целта, z_1, κ_1 и z_{1n_1} се заменят съответно с z_2, κ_2 и z_{2n_2}, където κ_2 е кривината на горното рамо зад върха на пукнатината, z_{2n_2} е разстоянието от нулевата линия до центъра на тежестта на напречното сечение на горното рамо. Освен това, от (2) получаваме следната формула за разпределението на E по височината на горното рамо:

(20) $$E = E_0\left[1 + q\cos\left(\frac{z_2 + \frac{h_2}{2}}{h}\,\frac{\pi}{2}\right)\right],$$

където

(21) $$-\frac{h_2}{2} \le z_2 \le \frac{h_2}{2} .$$

За определяне на κ_2 и z_{2n_2} използваме уравнения (17) и (18). За целта, заменяме z_1 и h_1 съответно с z_2 и h_2.

Заместваме (7), (8), (10) и (19) в (6) и получаваме следния израз за освободената потенциална енергия на деформацията:

(22) $$G = \int_{-\frac{h_1}{2}}^{\frac{h_1}{2}} u_0^{(1)} dz_1 + \int_{-\frac{h_2}{2}}^{\frac{h_2}{2}} u_0^{(2)} dz_2 .$$

Интегрирането в (22) се извършва с програмата MatLab.

За проверка на (22) се извършва анализ на пукнатината и с помощта на интеграла *J* [2]. Интегрирането се извършва по интеграционния контур Γ, показан с пунктирна линия на Фиг. 1. Ясно е, че интегралът има ненулева стойност само в участъци A_1 и A_2. Следователно, решението се намира по формулата

(23) $$J = J_1 + J_2 ,$$

където J_1 и J_2 са стойностите на интеграла съответно в участъци A_1 и A_2 на интеграционния контур.

Интегралът *J* в участък A_1 се записва така

(24) $$J_1 = \int_{-\frac{h_1}{2}}^{\frac{h_1}{2}} \left[u_0^{(1)}\cos\alpha_1 - \left(p_{x_1}\frac{\partial u}{\partial x_1} + p_{y_1}\frac{\partial v}{\partial x_1}\right)\right] ds_1 ,$$

където α_1 е ъгълът между външната нормала към контура за интегриране и направлението на пукнатината, p_{x_1} and p_{y_1} са компонентите на вектора на напрежението, *u* и *v* са компонентите на вектора на преместванията в координатната система *xy* (*x* е насочена по посока на пукнатината), ds_1 е диференциален елемент от контура на интегриране.

Компонентите на J_1 са определени по следния начин:

(25) $$p_{x_1} = -\sigma ,$$

(26) $$p_{y_1} = 0 ,$$

(27) $$ds_1 = dz_1 ,$$

(28) $$\cos\alpha_1 = -1 .$$

Производната $\partial u / \partial x$ в (24) е определена така

(29) $$\frac{\partial u}{\partial x_1} = \varepsilon = \kappa_1\left(z_1 - z_{1n_1}\right).$$

Интегралът *J* в участък A_2 на интеграционния контур (Фиг. 1) е записан по следния начин:

(30) $$J_2 = \int_{-\frac{h_2}{2}}^{\frac{h_2}{2}} \left[u_0^{(2)}\cos\alpha_2 - \left(p_{x_2}\frac{\partial u}{\partial x_2} + p_{y_2}\frac{\partial v}{\partial x_2}\right)\right] ds_2$$

Компонентите на J_2 се записват така

(31) $$p_{x_2} = \sigma ,$$

(32) $p_{y_2} = 0,$

(33) $ds_2 = -dz_2,$

(34) $\cos\alpha_2 = 1,$

(35) $\dfrac{\partial u}{\partial x_2} = \varepsilon = \kappa_2\left(z_2 - z_{2n_2}\right).$

Чрез заместване на (24) и (30) в (23) получаваме следния израз:

(36) $$J = \int_{-\frac{h_1}{2}}^{\frac{h_1}{2}} \left[u_0^{(1)} \cos\alpha_1 - \left(p_{x_1} \frac{\partial u}{\partial x_1} + p_{y_1} \frac{\partial v}{\partial x_1} \right) \right] ds_1 +$$

$$+ \int_{-\frac{h_2}{2}}^{\frac{h_2}{2}} \left[u_0^{(2)} \cos\alpha_2 - \left(p_{x_2} \frac{\partial u}{\partial x_2} + p_{y_2} \frac{\partial v}{\partial x_2} \right) \right] ds_2 .$$

Интегрирането в (36) се извършва с програмата MatLab.

Стойността на интеграла *J*, получена от (36), съвпада точно със скоростта на освободената потенциална енергия на деформацията, определена по формула (22). Този факт представлява една проверка на анализа на надлъжната пукнатина в разглежданата функционално-градиентна греда.

3. Заключение

Полученото решение на задачата за определяне на скоростта на освободената потенциална енергия на деформацията е много удобно за параметрични изследвания на надлъжната пукнатина във функционално-градиентната греда, показана на Фиг. 1. Резултатите от тези изследвания могат да се използват за оптимизиране на структурата на гредата с оглед намаляване на скоростта на освободената потенциална енергия на деформацията, което е важна предпоставка за осигуряване на гредата срещу поява на пукнатини. Освен това, решението може да се използва и за проверка за нарастване на съществуваща пукнатина. За целта, с помощта на полученото решение трябва да се определи скоростта на освободената потенциална енергия на деформацията за конкретна дължина и местоположение на пукнатината и за дадено външно натоварване. Така изчислената скорост на освободената потенциална енергия на деформацията трябва да се сравни с нейната гранична стойност, която се определя по експериментален път. Ако изчислената скорост на освободената потенциална енергия на деформацията е по-малка от граничната, конструкцията е осигурена срещу нарастване на съществуващата пукнатина. Също така, решението е подходящо и за определяне на скоростта на освободената потенциална енергия на деформацията въз основа на данни от експериментални изпитвания на надлъжни пукнатини във функционално-градиентни греди.

Благодарности

Настоящата разработка е финансирана от ЦНИП при УАСГ-София (Договор БН-198/2017).

Литература

1.Arani, Ali Ghorbanpour, Haghparast, Elham and Zarei, Hassan BabaAkbar. Vibration analysis of functionally graded nanocomposite plate moving in two directions, Steel and Composite Structures, An International Journal, 2017, 23 (5), pp. 529-541.

2. Bohidar, S., Sharma, R., Mishra, P. Functionally graded materials: A critical review. Int. J. Res., 1, 2014, 289-301.

3.Barka, Merbouha, Benrahou, Kouider Halim, Bakora, Ahmed and Tounsi, Abdelouahed. Thermal post-buckling behaviour of imperfect temperature-dependent sandwich FGM plates resting on Pasternak elastic foundation, Steel and Composite Structures, An International Journal, 2016, 22 (1), pp. 91-121.

4.Broek, D. Elementary engineering fracture mechanics, 1986, Springer.

5.Chen, Chun-Sheng, Liu, Fwu-Hsing and Chen, Wei-Ren. Vibration and stability of initially stressed sandwich plates with FGM face sheets in thermal environments, Steel and Composite Structures, An International Journal, 2017, 23 (3), pp. 251-261.

6.Galeban, M., Mojahedin, A., Taghavi, Y., Jabbari, M. Free vibration of functionally graded thin beams made of saturated porous materials, Steel and Composite Structures, An International Journal, 2016, 21(5), pp. 999-1016.

7.Hebali, Habib, Bakora, Ahmed, Tounsi, Abdelouahed and Kaci, Abdelhakim. A novel four variable refined plate theory for bending, buckling, and vibration of functionally graded plates, Steel and Composite Structures, An International Journal, 2016, 22 (3), pp. 473-495.

8.Houari, Mohammed Sid Ahmed, Tounsi, Abdelouahed, Bessaim, Aicha and Mahmoud, S.R. A new simple three-unknowns sinusoidal shear deformation theory for functionally graded plates, Steel and Composite Structures, An International Journal, 2016, 22 (2), pp. 257-276.

9.Lia-Liang Ke, Jie Yang and Sritwat Kitipornchai. Postbuckling analysis of edge cracked functionally graded Timoshenko beams under end shortening, Composite Structures, 2009, 90, pp. 152-160.

10.Madani, Hamid, Hosseini, Hadi and Shokravi, Maryam . Differential cubature method for vibration analysis of embedded FG-CNT-reinforced piezoelectric cylindrical shells subjected to uniform and non-uniform temperature distributions, Steel and Composite Structures, An International Journal, 2016, 22 (4), pp. 889-913.

11.Meftah, Ali, Bakora, Ahmed, Zaoui, Fatima Zohra, Tounsi, Abdelouahed and Bedia, El Abbes Adda. A non-polynomial four variable refined plate theory for free vibration of functionally graded thick rectangular plates on elastic foundation, Steel and Composite Structures, An International Journal, 2017, 23 (3), pp. 317-330.

12. Mokhtar Bouazza, Noureddine Benseddiq. Analytical modelling of thermoelastic buckling behaviour of functionally graded rectangular plates using hyperbolic shear deformation theory under thermal loadings, Multidiscipline Modelling in Materials and Structures, 2015, 11, pp. 558 – 578.

13. Shi-Dong Pan, Ji-Cai Feng, Zhen-Gong Zhou and Wu-Lin-Zhi. Four parallel non-symetric Mode –III cracks with different lengths in a functionally graded material plane, Strength, Fracture and Complexity: an International Journal, 2009, 5, pp. 143-166.

14. Tilbrook, M.T., Moon, R.J. and Hoffman, M. Crack propagation in graded composites, Composite Science and Technology, 2005, 65, pp. 201-220.

15. Tokova, L., Yasinskyy, A. and Ma, C.-C. Effect of the layer inhomogeneity on the distribution of stresses and displacements in an elastic multilayer cylinder, Acta Mechanica, DOI: 10.1007/s00707-015-1519-8, 2016, p. 1 – 13.

16. Tokovyy, Y. and Ma, C.-C. Axisymmetric Stresses in an Elastic Radially Inhomogeneous Cylinder Under Length-Varying Loadings, ASME Journal of Applied Mechanics, 2016, 83, DOI: 10.1115/1.4034459.

17.Tsukamoto, H. Mechanical properties of zirconia – titanium composites, International Journal of Materials Science and Applications, 2014, 3, pp. 260-267.

18. Upadhyay, A.K. and Simha, K.R.Y. Equivalent homogeneous variable depth beams for cracked FGM beams; compliance approach, Int. J. Fract., 2007, 144(2), pp. 209-213.

19. Zhang, H., Li, X.F., Tang, G.J. and Shen, Z.B. Stress intensity factors of double cantilever nanobeams via gradient elasticity theory, Engineering Fracture Mechanics, 2013, 105, pp. 58-64.

PHYSICO-CHEMICAL PROPERTIES OF DISSIMILAR WELD

M.F. Benlamnouar[1], N. Bouchnafa[1,2], A. Boutaghane[1], M. Ouadah[1], N. Bensaid[1], M. Iddir[1], A. kellai[1]
[1] Research Center in Industrial Technologies CRTI, P.O.Box 64, Chéraga 16014, Algiers, Algeria
[2] University of Saâd Dahleb Blida, BP 270, Route de Soumaâ, Blida 09000, Algeria
E-mail: csc.farid@yahoo.fr

Abstract: *Mechanical and electrometrical behavior of dissimilar welds between low Carbone steel (X70) and Carbone steel (42CrMo4), were studied using a combination of optical and electron microscopy. Thus, the influence of weld parameters on fusion zone and heat affected zone was investigated using two filler metals and two weld currents. The results of our work show that alternative TIG welding presents the butter combination between metallurgical and Mechanical comportment, also it was established in this study, that nickel alloy filler has the best electromecanical behavior for these types of welds.*

Keywords*: X70, TIG Welding, 42CrMo4, dissimilar weld*

1. Introduction

Dissimilar welds have been widely used in industrial applications and singing in their form of sheet metal, pipe or modified structures. They have found a wide range of applications especially in fusion welding processes thanks to their characteristics which can be adapted after heat treatments [1, 2]. Heterogeneous welds Stainless steel / steel, stainless steel / stainless steel, aluminum / steel and steel / steel are often obtained for different requirements [3,4], among which is a welding between a tempered steel tempering (42CrMo4) with a low steel on carbon (X70) which seems to be very interesting for the realization of a GMA crane in our center.

The main problem of heterogeneous welds is the formation of the metallic precipitations in the bonding zone between the two basic materials due to the difference between the tenants of the additive elements that exist in the two materials. that magnification of grain in the area thermally affect by thermal welding cycles [5,6].

Heterogeneous welding is the subject of several studies, Azizieh has evaluated the weldability between a quenching steel tempered (CK60) a low carbon steel (ST37) by a friction welding process[6]. It obtained very hard interfaces and mechanical and electromechanical properties that could be questioned through the microstructures presented and the welding method [7].

Our work is based on improving the physicochemical properties of heterogeneous welds by modifying filler metals and welding mode.

2. Materials AND METHODS

In this work, the base materials utilized are Carbone steel (42CrMo4) and low Carbone alloy steels (X70) (Table 1). Two filler metals were used to elaborate welded joints. It represents respectively Nickel alloy filler Ok60 and low Carbon E6010. The chemical composition of filler metals is given in Table 2. The base materials are welded using automatic tungsten arc welding (TIG) based on ASTM standard [8] (Table 3), According to moved table in order to set welding parameters. Sheet metal dimensions were fixed at 100x60x4mm (Fig. 1) (Fig. 2) with filler wire diameter of 1.5 mm. Standard polishing procedures were used for microstructural observations, Glycerine reactif was used with the conditions (20ml of nitric acid, 30 ml HCl acid and 30ml of glycerol) for 3min. The microstructure was characterized by optical microscopy. Hardness test was conducted using Vickers scale with a load of 0.2Kg ($Hv_{0.2}$). $Hv_{0.2}$ test was performed on the middle of weld joint, perpendicular to welding direction. Image J program was used to compute fractions and gain sizes.
To perform electrochemical tests, measurements have been done, these measurements comprise:
A EGC Princeton 263 Potentiometer / Galvanostat measures the potential difference between the working electrode (Et) and the reference of a three-electrode cell, passing a current Ic in the cell via the against electrode (Ec) and measure the current using the chemical drop across the resistor Rm. An electrochemical cell contains cylindrical thermostatic shape; it is formed by glass and double wall with a capacity of 250 ml. It is equipped with a conventional three-electrode mounting: Work (or sample), reference (a saturated calomel electrode (ECS) whose end is placed near the working electrode) and against electrode (or auxiliary electrode) which is a platinum grid (to ensure the passage of current).

Table 1. Chemical composition and mechanical properties of base materials

Elément	C	Si	Mn	P	S	Al	Cu	Cr	Mo	V	Nb	Ti	Ni
X70 (%)	0.08	0.7	2.39	0.01	0.001	0.06	0.01	0.04	0.1	0.05	0.4	0.09	0.02
42CrMo4 (%)	0.45	0.4	0.90	0.35	0.0.35	-	-	1.20	0.3	-	-	-	-

Table 2. Chemical composition of filler metals

Elément	Fe	Ni	C	Si	Mn
Ok 60 (%)	0.40	0.60	-	-	-
E6010 (%)	Rest.	-	0.10	0.20	0.50

Table 3. Welding parameters

Current	Electrode	Argon flowrate (L/min)	Medium voltage (V)	Average intensity (A)	Weld speed (mm/min)
CC	Ok60 (1)	6	10.65	100	35.24
	E6010 (2)	6	11.65	100	36.70
CA	Ok60 (3)	6	11.84	100	37.72
	E6010 (4)	6	12.4	100	37

3. Results And Discussion

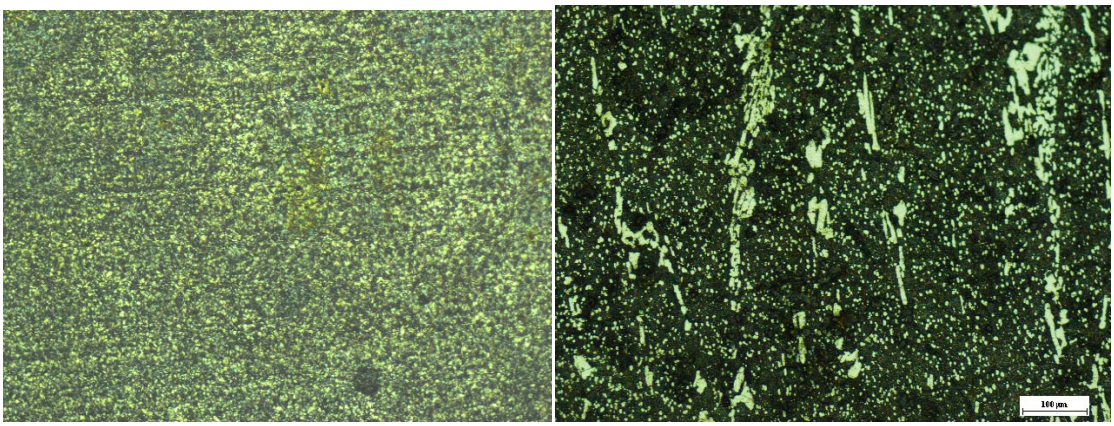

Figure1. Optical microstructure of the base materials X70 (right)

The micrograph of the two basic materials shows that: X70 microstructure is composed of ferrite and perlite, the latter consisting of ferrite and cementite, while 42CrMo4 steel is characterized by martensitic lattes in ferritic matrix with a small proportion of Cabrides (Figure1).

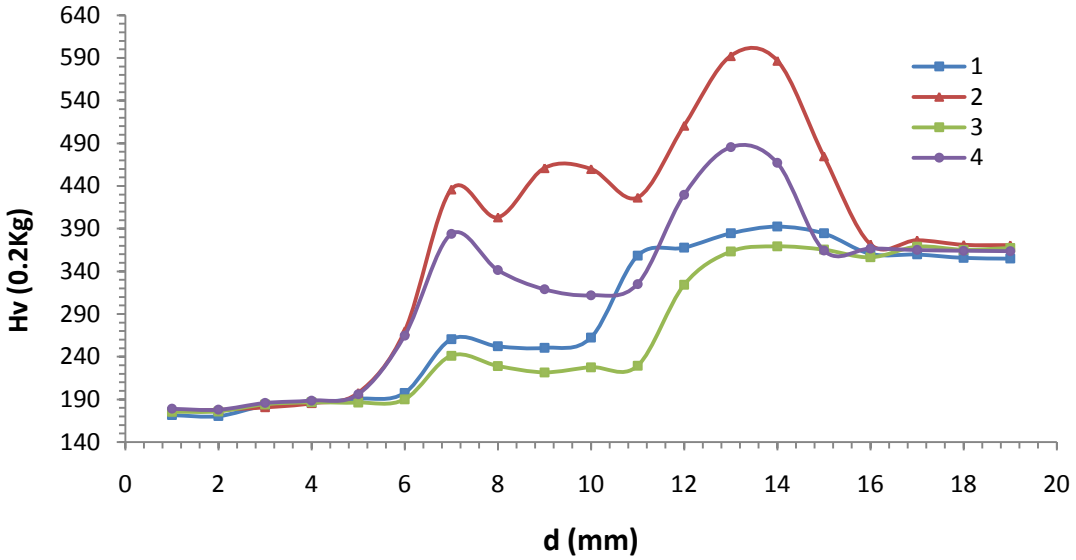

Figure2. Microhardness profile

Figure2 Shows the variation of the Vickers microhardness measured through fusion zone, both HAZ and the two basic materials. The four curves represent four samples, two samples (E3) and (E4) undergo alternating TIG welding and continuous TIG welding is applied to (E1) and (E2). When the microhardness curve stabilizes, it indicate the microhardness of steel, 175 Hv (X70) and 362 Hv for (42CD4).

From these graphs of microhardness profiles we can draw the following conclusions:

The welded samples undergo a large increase in microhardness in heat affected Zone (HAZ) compared to the two base materials, where there is a creation of relatively fragile structures rich in metal carbides (Widmanstatten, martensite ....) When from the welding operation, this wealth becomes huge in the 42CrMo4 side.

The variation of the microhardness is also related in a first degree by the carbon content, and second degree, by the effect of alloying elements which presents in each basic material. The role of the gamma elements (Mn, Ni) reduces significantly transformation temperatures of phases and moves the diagrams in continuous cooling to slow speeds. Manganese in particular has a important role on start temperature of martensitic transformations. The primary effect of the carburigenic elements (Cr, Mo) is to increase the quenchability, and more particularly for molybdenum, to increase the stability of the bainitic microstructure, by delaying germination of ferrite phase. In addition, these elements form carbides dispersed with iron in the course of the reciprocating cycles, whereas in the (CC) it forms dispersed carbides which are concentrated in the HAZ, which poses a risk of a sudden fracture.

In the case of AC current there, there is a decrease in the microhardness compared to the DC current, this reduction is due to the effect of thermal welding cycle which causes a rapid variation in the heating rate,

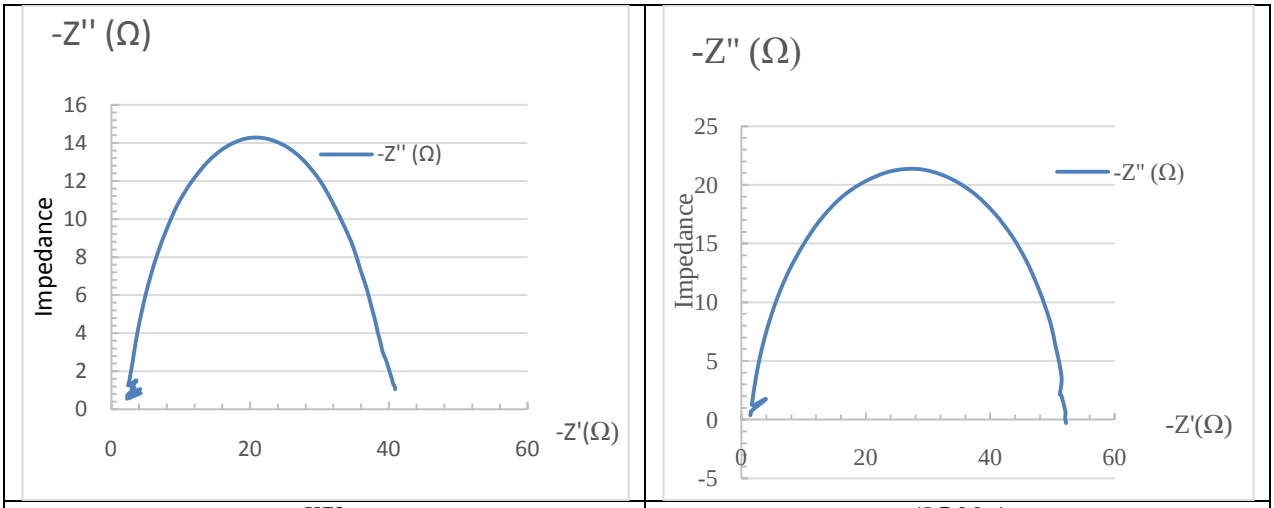

Figure 4. Impedance of base materials

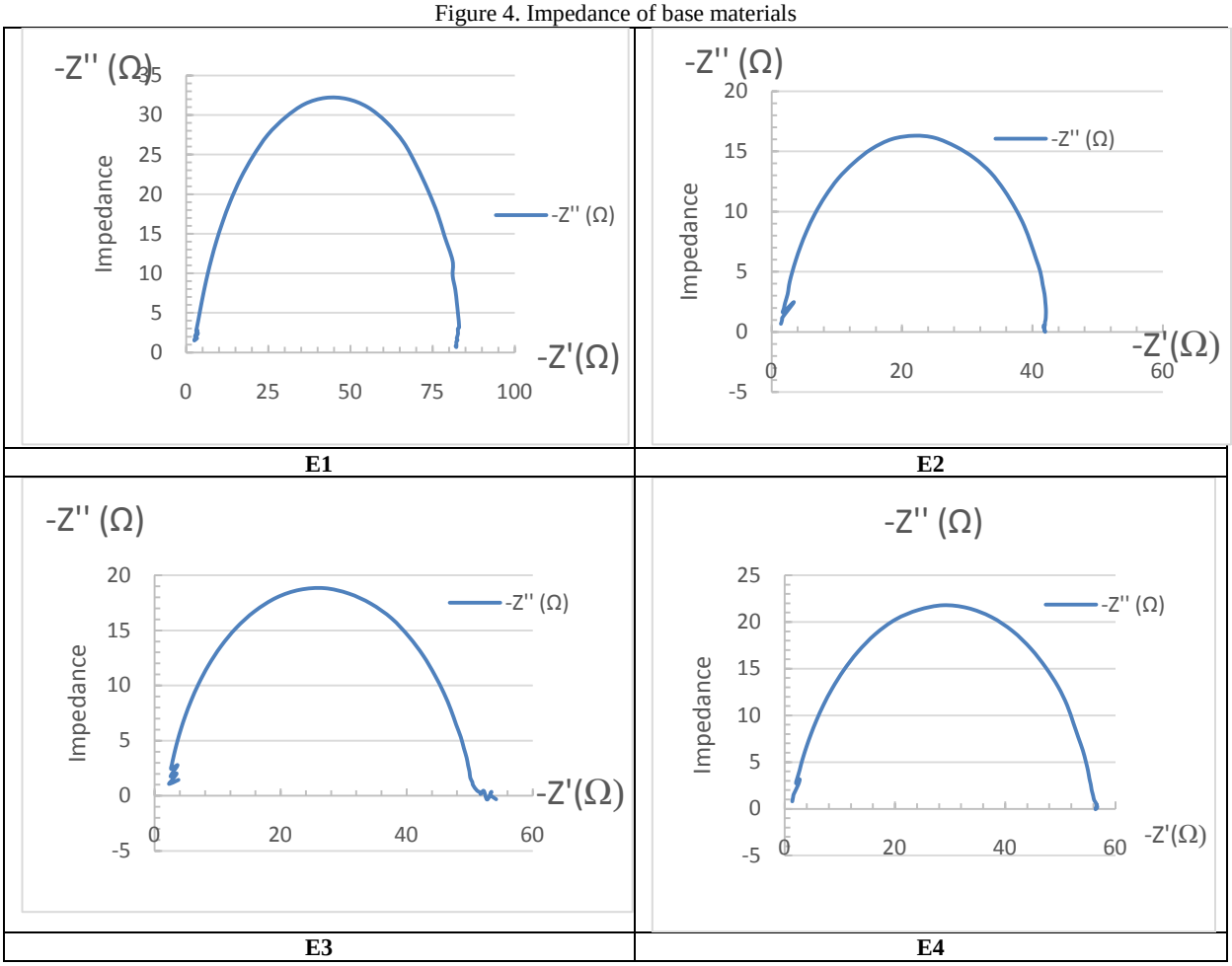

Figure 5. Impedance of weld joints

Figure 5 and Figure 4 show impedance diagrams of Nyquist Z plane at different welds joints in frequency range: 50 Hz - 100 mHz. the representation in the Nyquist plane was used here to determine Load Transfer Resistance and Sample Capacity. The interpretation of the diagrams makes it possible to determine the various processes that take place at the electrode and the charge transfer resistance.

From the impedance curves we can see that:

The impedance evolution in the Nyquist Z plane as a function of the welding parameters, the good electrochemical behavior results in an increase in the considerable resistance of charge transfer together with a decrease in the capacity of the sample. Electrochemical tests showed a good efficiency which observed in E3, as well as a good load transfer resistance observed in sample E1.

The polarization tests clearly show that the characteristics of the electrochemical behavior of the welds are generally found between the base material terminals except for the Ok.60 welded samples.

Corrosion rates significantly lower than the heterogeneous weld compared to carbon steel (42CD4). Thus the speeds in the welds (E1, E3) significantly lower compared to other samples. In addition, it is found that the weld (3) has a potential and a corrosion voltage lower than that of the sample (01). Compared to the other samples, the sample (E3) is passive and its polarization curve shows slight passivation levels, its corrosion current remains low. It is around

0.0022648 A and its corrosion potential is (-00.37561). From the linear polarization curves (Lp) we obtained the following results:

Table 4. Polarization results

Samples	ba (v/dec)	bc (V/dec)	E corr (V)	I corr (A)	Vitesse mm/an
X70	0.73402	0.21418	-0.37431	0.0025587	29.732
42CrMo4	1.1318	0.50853	-0.40282	0.0037302	43.345
01	0.47959	0.20530	-0.396	0.0018713	21.744
02	1.0276	0.46995	-0.40969	0.0032702	38
03	0.55053	0.19139	-00.37561	0.0022648	26.317
04	1.2367	0.42045	-0.39137	0.0035365	41.094

The polarization tests clearly show that the characteristics of the electrochemical behavior of the welds are generally found between the base material terminals except for the Ok.60 welded patterns (Table 4).

Corrosion rates significantly lower than the heterogeneous weld compared to carbon steel (42CD4). Thus the speeds in the welds (E1, E3) significantly lower compared to other enchantillons. In addition, it is found that the weld (3) has a potential and a corrosion voltage lower than that of the sample (01). Compared to the other samples, the sample (E3) is passive and its polarization curve (Figure III.8) shows slight passivation levels, its corrosion current remains low. It is around 0.0022648 A and its corrosion potential is (-00.37561).

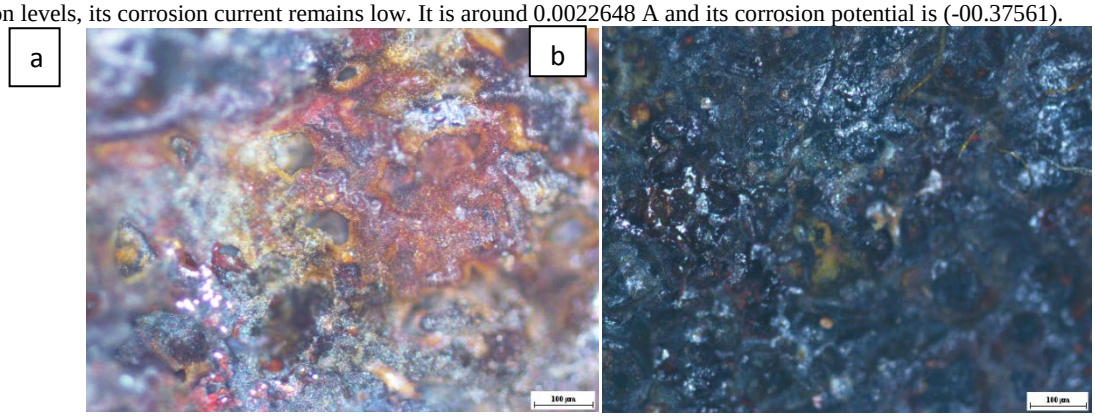

Figure 6. Micrographics of corroded base materials: (42CrMo4) and b (X70).

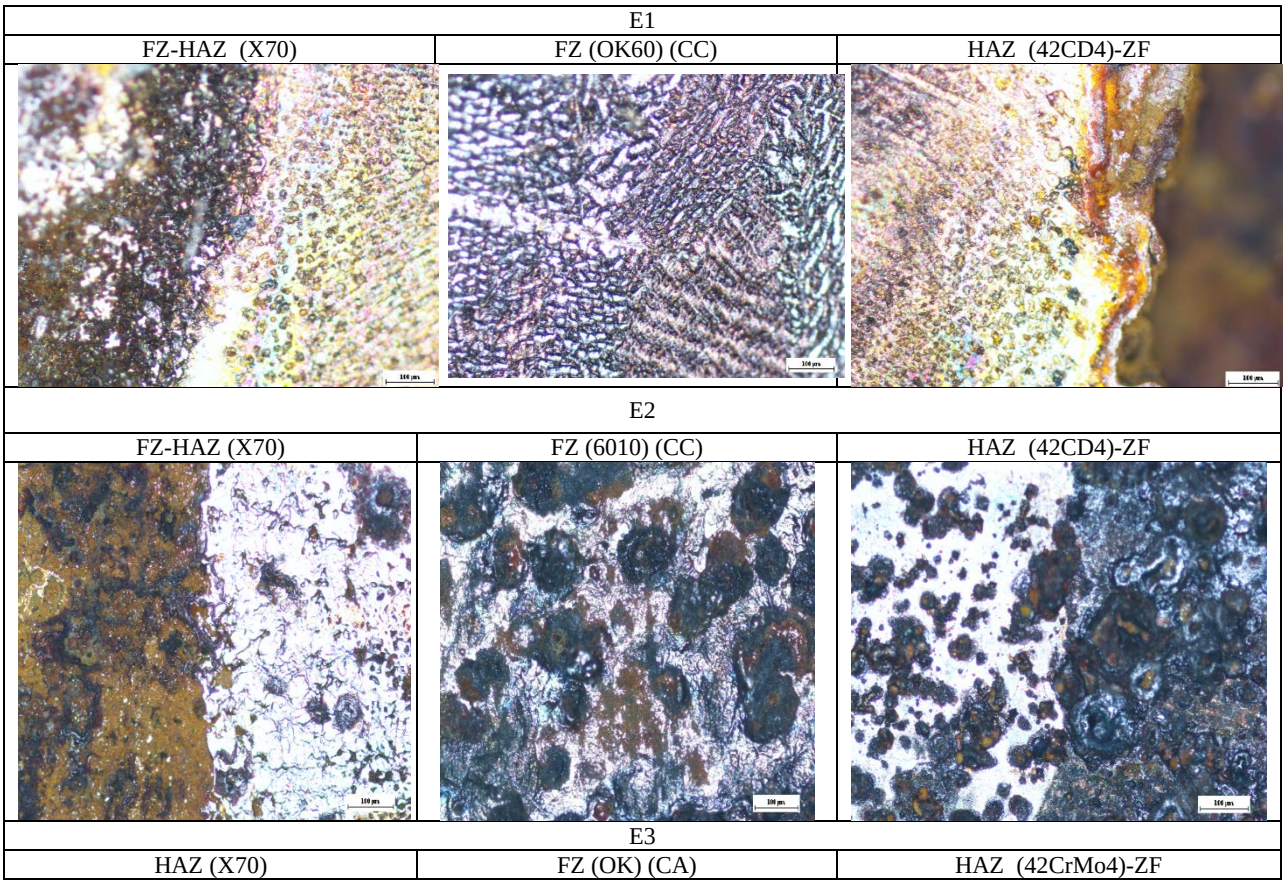

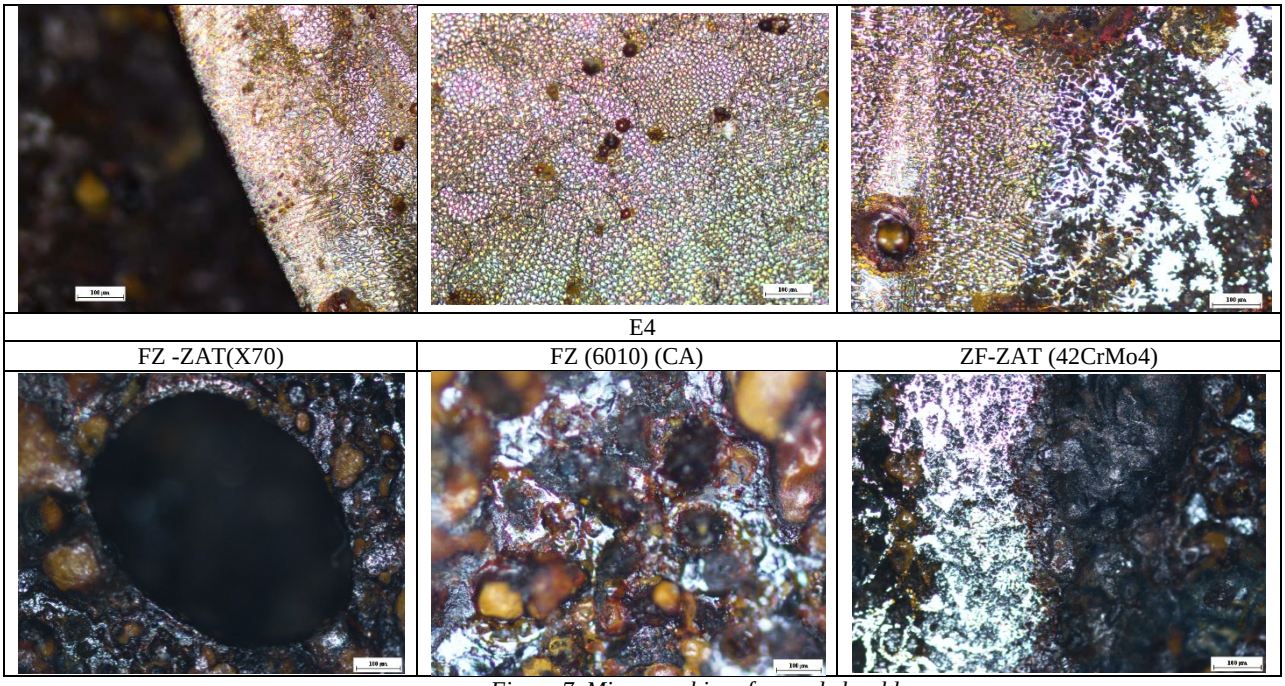

Figure 7. Micrographics of corroded welds

The figures (Figure 6, Figure 7) show the results of the optical observations of corrosion surfaces for magnifications (X100). These micrographs show a strongly etched structure in the 42CrMo4, with a high density of dissolution. On the other hand, the micrographs of the welds have strongly burned aspects in the welds (E4, E1). Also, the fusion zone of welds with Ok60 is the least to alter by the electrochemical tests. We also observe the presence of bites distributed randomly on the surfaces obtained, the number of these defects were too small in the samples welded by the Ok.60.

4. CONCLUSION

This work is only a modest contribution to understanding the different physico-chemical phenomena encountered related to the reliability of heterogeneous metal structures. In the ZATs of the carbon steel (42CD4) sides, the morphology of martensite became a dominant phase with an increase of the bainitic phase in the AC welded sample. This phase is favorable for the mechanical behavior. In addition, the ZATs of X70 steel have undergone a magnification of ferritic grains; this magnification becomes light in E3.

- Welding with E6010 low-alloy steel (E2, E4) allows to obtain melted zones with fine structures consisting of rough zones of solidification such as: proeutectoid and acicular ferrite, lamellar constituent of bainite and martensite.
- Nickel-based alloy welding induces melted zones consisting of columnar austenitic grains surrounded by ferritic precipitations; it is also observed that in the case of (CA) the austenitic grains undergo a grain coarsening.
- The use of the alternating current causes a decrease of the microhardness with respect to the direct current, this reduction is due to the effect of the welding thermal cycle which causes a fast variation in the rate of heating.
- The use of filler metal E6010 increases the microhardness compared to OK60 this is due to the effects of the additive elements.
- Polarization tests clearly show that the characteristics of electrochemical behavior of Ok.60 welded joints has the better comportment.

REFERENCES

[1] Guozhen WANG, Haitao WANG, Fuzhen XUAN, Shantung TU, Changjun LIU, Local fracture proprities and dissimilar weld intergrity in nuclear power plants (Eng. 2013 vol8(3) : 283-290.

[2] Jeong Kil Kim, Seung Gab Hong, Ki Boong Kang, and Chung Yum Kang, Microstructure ana High Temperature Properties of the Dissimilar Weld between Ferritic Stainless Steel and Carbon Steel, vo1 5, No5 (2009), pp :834-849.

[3] Jing Wang, Min-xu Lu, et al., Effect of weldin process on microstructure and proprities of dissimilar weld joints between low alloy steel and duplex stainless steel, International Journal of Metallurgy and Materials, Vol 19,No 6, june 2012 : p 518 .

[4] Anna Vyroslhova, Jan Kepic, Viera Homolova and Ladistlav Falat, Precipitation of Nobium Boride Phases at the Base Metal/Weld Interface in Dissimilar Weld joints, JMEPEG (2015) vol 24, 2699-2708.

[5] K.Bettahar, J H Schmitt, R Badji, et al., Microstructure and mechanical behavior in dissimilar 13Cr/2205 stainless steel welded pipes. Material and Design vol 85 (2015), 221-229.

[6] M Azizieh, M Khamisi, D J Lee, E Y Yoon, H S Kim, Characterizations of friction welding of ST37 and CK60 steels, Int J Manuf Technol (2016)85, 2773-2781.

[7] Herbert H. Uhlig, R. Winston Revie. Corrosion and corrosion control. Third edition / an instruction to corrosion science and Engineering, page 299-300, 1985.

[8] ASME “Qualification Standard for Welding and Brazing”, An International Code of ASME Boiler and Pressure Vessel Committee on welding and Brazing, USA, 2010.

HORIZONTAL AND VERTICAL INTEGRATION, AS A REQUIREMENT FOR CYBER-PHYSICAL SYSTEMS IN THE CONTEXT OF INDUSTRY 4.0

K.Chukalov. PhD Student.
Faculty of Mechanical Engineering – Technical University Sofia, Bulgaria

Konstantin_chukalaov@abv.bg

Abstract: *The development in the information and communication technologies conditions the beginning of the fourth industrial revolution(FIR) The current report considers the peculiarities of the cyberphisical systems, as the basis of the fourth industrial revolution (Industry 4.0) and the need of their inner horizontal and vertical integration.*

.**Keywords**: INDUSTRY 4.0 , INFORMATION-TECHNICAL SYSTÉM, STRUCTURAL REORGANIZATION

1. Introduction

The key elements of the fourth industrial revolution are the cyberphisical systems (CPS), through which networks are created for the self-regulation of spatially distributed production resources. The introduction of the principals of this revolution in production requires the creation of conditions for its normal functionality. The vertical and horizontal cooperation between the machine and the internet, machine – person, and machine - machine along the value chain in real time, are the basis of the production cyber system and determines the actuality of the problem.

2. Theoretical foundations

The cyberphisical systems are „intelligent systems", which cover the hardware and software, as well as the effectively integrated physical components, , which interact closely with each other, so they can detect any change in the state of the real world, as defined by the "National institute of Standards and Technology" (NIST). In the world's scientific literature there is no "sharp" restriction on the notion of cyber-physical systems regarding the tendencies and ways in the development of complex informational – communication technical systems. Cyber-physical systems refer to physically mechanical complexes with IT systems, hardware and software digital components with mechanical or electronic components that can autonomously communicate with each other.

The creation of a cybernetic environment is imperative so it can provide:

- Functional compatibility: The capability of cyber-physical systems (for example – intelligent machines), people and "intelligent factories" (Smart Factory) so they can exchange information between "the internet of things" and "Internet services";
- Virtual compatibility: The creation of a virtual copy of a "Smart factory", which is created by connecting the data collected from physical sensors with virtual models of the production processes, specialized software and so on;
- Decentralized management: The ability of Cyber-physical systems, Separate components and so on, within the margins of one "smart factory" to make independent decisions;
- Data transfer in real time: The ability of gathering and analyzing data while making decision in real-time;
- Service orientation: Through the Internet of Services, people and "smart users" are provided with services;
- Modularity: Flexible adaptation of "Smart factories" to the changing requirements, either by replacing or expanding of individual or accession modules;
- Flexibility: Individualization of mass production, by using the principals of mass production by a customized system of planning.

3. Implementing of cyber-physical systems on the basis of horizontal and vertical integration

Interaction between implemented systems based on highly specialized software and specialized user interface, which are integrated in digital networks create an entire new world of the systems functionality for the horizontal and vertical integration.

Horizontal integration: Trough the integration of the Network IT technologies and manufacturing systems an exchange of data and information must be established between the firms and the geographically remote sites across the value chain. Therefore by "Horizontal integration" an integration of various information technology systems in the production and automated equipment for various stages of the production and planning process is understood.

Vertical integration: The "internet of things" and services grant immediate access to IT and production systems. Trough vertical integration of data and information directly from the workplace by controlling and operating on a production and corporate level, the data is processed and as a result, adequate information about the management is returned. Therefore "Vertical integration" can be understood as the integration of information technologies in IT systems in various hierarchy levels in production and automation equipment. (For example: sensors, level of management, level of production management). The vertical and horizontal Cooperation between machine and internet, machine and person and machine to machine on the chain of value, in real time, is the basis of the production cyber system.

In the transition to cyber-physical systems, implemented systems, production, logistic, engineering, coordination and management processes as well as internet services can be added, which with the help of sensors gather physical data and interact with physical processes with the help of digital networks, connected with each other. They can use current data and services, as well as multimodel interfaces person – machine.

On fig.1 the stages of development of the cyber-physical systems.It can be assumed that this concept will be transferred by a single factory to a whole network of sited with added value in the future, for the manufacturing of intelligent products or for the compensating of the production capacities, acc. to Scheer[1].

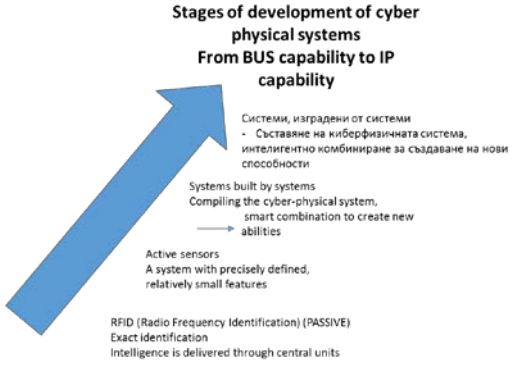

Fig.1. *Stages of development of the cyber-physical systems*

3.1 – Stages of development of the cyber-physical systems

The development of the cyber-physical systems can be characterized with three phases of implementation, namely:

- First Generation of CPS, which includes identification technologies, as RFID tags, which allow a unique identification.
- The storing and analyzing of information is a centralized service.
- The second generation of CPS is the equipped with sensors and executive mechanisms with a limited set of functions.
- The third generation can store, analyze data and is equipped with various sensors and executive mechanisms, all which are executed in compatible networks, acc. to Bauernhansl, Hompel, Vogel-Heuser [2].

This is a production revolution in terms of expense and saving time. The intelligent manufacturing brings with itself many advantages in comparison with the conventional manufacturing, or that is the intelligent production revolution. The cyber-physical systems require a network of informational technologic and production systems to be build, trough domains and hierarchy boundaries. The implementation of the cyber-physical systems in the production, for the establishment of an intelligent manufacturing is the second key moment.

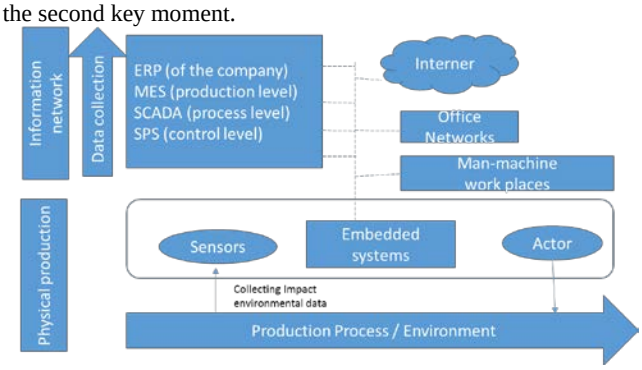

Fig,2 *Implementing of the cyber-physical system in manufacturing.*

Because of that, interoperable communication interfaces and standard protocols are required. Furthermore, the products of manufacturing are intelligent, they carry information from their own manufacturing in machine-readable form (for example RFID chips), that way they can coordinate their own manufacturing actions. In order to meet the requirements for communication in real time, and also so that the cyber-physical systems meet the requirements for high availability and for a longer life cycle they must be built with standard IT elements. In that way, in order to establish a decentralized data collection , they must be continuously integrated into IT systems – best case scenario, included in Enterprise Resource Planning (ERP), manufacturing management (MES), systems for supervision (supervisory control and data acquisition, SCADA), programmable controllers (SPS) and integrated systems for vertical and horizontal integration. The structure of informational streams and networks is of most importance for the cyber-physical manufacturing as a whole. On pic.2 the transition from existing to cyber-physical systems is shown.

In this transition the cyber-physical systems usually include: Embedded systems, production, logistics, engineering, coordination and management processes, as well as internet services, whom with the help of sensors gather physical data and interact with physical processes with the help of digital networks connected with each other. They can use all current data and services, as well as multimodel interface person - machine. The production systems gradually evolve from planning systems (ERP, MRP, MRPII) and operational management of production (MES) to an integrated working platforms, which encompass business tools, supply and asset management, production schedules and solutions for an optimization of the production processes.

The cyber-physical systems are an openly social-technical systems and allow a number of new features, services and properties to be performed. Therefore one of the most important tasks in the field of design, development and management of cyber-physical systems is the question of co-operation between the cyber-physical system and the human factor. The questions which are with most importance in the context are the identification and modeling “awareness of the situation” the human experience with such kind of systems, the environment, as well as reflecting the changes.

4. *Methodology for the research of the factors for vertical and horizontal integration.*

In relations to the better structuring of the problem of accounting for the requirements of Industry 4.0. , the influencing factors can be grouped in the following directions:

- Factors influencing on the physical wear and tear, which leads to reducing their capacity capabilities. This group of factors are directly related with the requirements for Modularity (flexibility);
- Factors influencing on the innovation aging, which can be only partial, without having any affect on the on the productivity, or full innovation aging, which has a relative impact on productivity. This group of factors are directly related with the requirements from for operational compatibility;
- Factors influencing on the level of elements of the technical system, such as automation devices (Level / degree of automation), automated complexes (Level / degree of automation), self-regulating systems, technical compatibility (Level / degree of elements in the system), Base and bonding models. These factors are directly related with the requirements from Industry 4.0 for Decentralization;
- Factors influencing on the level of the technical system, related to modules, complexes and systems such as a Modular Network, complex network and a system network. This group of factors is directly related to the with the requirements from Industry 4.0 for information in real time, virtualization and orientation towards services;
- Factors related to the flexibility of the system (flexible adaptation towards the changing requirements: replacement, expansion and more.) All those factors are connected with the requirements from Industry 4.0 for modality (flexibility);
- Factors related to the automation of the elements and components of the system. (CAD/CAM/CAE, vertical and horizontal diversification and software). This group of factors is related with modality (flexibility), information in real time, virtualization and decentralization.
- Factors related to the operational and functional compatibility of the elements and components of the system, decentralization and usage of the information in real time;
- Factors related to the horizontal and vertical compatibility of the system (technological and business operations in a horizontal direction, technological and business operations in a vertical direction, targeted network models for compatibility and communication of the elements of the system in a horizontal or vertical way, self-regulating components of the technical and manufacturing systems;

This way and this grouping define the methodological basis of the approach of studying the possibilities for adapting the requirements of Industry 4.0 in machine building companies, see fig.3.

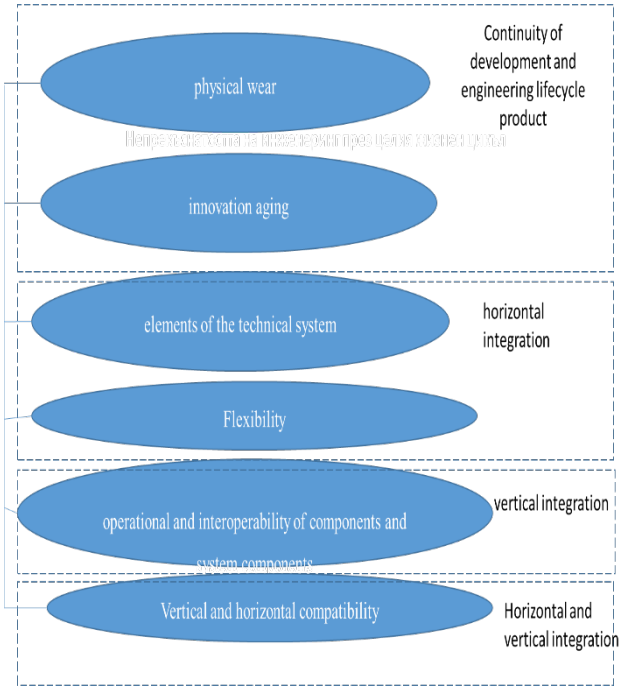

Fig.3 *Factors for the Horizontal and vertical integration*

The Innovative aging: is due to technology development and the speed of implementation of the innovations, physical wear is associated with machine parts without which the machine can not work.

Physical wear is a result of the constructive-technological and operational reasons. The development of new technologies is provoking innovation aging. A balance between the physical and innovational aging is necessary to be found.

Physical wear, can be considered in terms of changing the parameters of the equipment, without changing the productivity and with changing it (The change in physical condition of the details, machines, the quality, change in how it affects the environment, level of safety and so on.) or stopping work (cessation of operation).

The innovation aging is related with a delay due to technological reasons, for example: The appearance of a newer and more productive machine giving better quality of production.

The parameters and indicators that can characterize the conditions are:

Economically expressed in economic indicators: such as Operating costs, share of equipment per one unit of product, unit cost, depreciation costs.

Technical and technological parameters, expressed in technical parameters including operating life, reliability, efficiency, technological capabilities and more.

For the purpose of the study it is necessary to study the level of elements of the technical system in the enterprises: conventional type machines, machines with 2D control devices, machines with 3D control devices, automation devices (automation degree), automatic complexes (automation degree), self-regulating systems, technical compatibility (degree/level of elements in the system) and base and bonding models.

Degree of modularity through modular network, complex network and system network.

When creating a product, who is to be given to the costumer, there has to be a wide variety of options, as well as a big flexibility of the production capacities. The use if a “CPS” in the production process gives an opportunity for the firms to develop the different stages on a modular principal, as a result of that all the separate modules can be organized flexible and on their own. Thru a modular system, companies can make considerable savings in regards of the assembly and exploitation, but in the same time can offer optimal functionality when installing and maintaining the equipment. Often the importance of the full (or almost full) integration is underestimated and a decision is made for the purchase of software from different providers and also their assembly. This is when problems begin to show, the data exchange is not complete etc. Such an assembly of individual modules is only possible under certain conditions, such as unifies connection margins, implementation of certain geometric and constructive constrains, observance of certain conditions for a previously build system of block modules.

Regarding the flexibility of a system, it is represented by the degree of adaptation to different models, possibility of change regarding the needs of the costumer, system adequacy to the changing requirements (replacement, expansion and so on.)

Regarding the degree of automation of the elements and components of the system (CAD/CAM/CAE), vertical and horizontal diversification, software (models) etc.:

Regarding the operational and functional compatibility of the elements and components of the system as a decentralization and transfer of information in real time.

Regarding the horizontal and vertical compatibility of the system, as technological and business operations in a vertical state, network models targeted for compatibility and communications of the elements is the system in a horizontal and vertical state. Self-regulating components of the technical and manufacturing system.

The challenges of the cyber-physical systems include:

Reducing complexity in the development of the stabilizing architecture of management for the cyber-physical systems:

Distributed sensor networks;

Conclusion

- A systematization was made of the factors, regarding the horizontal and vertical integration.

- The functions if the cyber-physical systems was analyzed.real-time information, flexibility, interoperability, modularity, decentralization and virtualization.

References

As a result of the shown above, the following conclusions can be made:

- The key element of the fourth industrial revolution are the cyber-physical systems, through which networks are created for the self-regulation of allocated production recourses.

- Introducing the principals of “Industry4.0” in the manufacturing requires the creation of an environment for its normal functionality. This means that the horizontal and vertical co-operation between machine and internet, machine - person and machine – machine on the chain of value in real time. This is the basis of the cyber-physical production system.

Literature

[1] Scheer A. (2013) Industrie 4.0: Wie sehen Produktionsprozesse im Jahr 2020 aus?

2]. Bauernhansl, Thomas. Industrie 4.0 in Produktion, Automatisierung und Logistik. Anwendung, Technologien und Migration. Wiesbaden: Springer Vieweg, 2014

[3] Plattform Industrie 4.0 2014: Industrie 4.0: Whitepaper FuE-Themen, http://www.plattform-i40.de/sites/ default/files/Whitepaper_Forschung%20Stand%203.%20April%20 2014_0.pdf (12.3.2015).

[4 Promotorengruppe Kommunikation der Forschungsunion Wirtschaft – Wissenschaft. Deutschlands Zukunft als Produktionsstandort sichern. Umsetzungsempfehlungen für das Zukunftsprojekt Industrie 4.0. Abschlussbericht des Arbeitskreises Industrie 4.0., 2013

[5.]Nikolowa, I. Upravlenie na kachestvoto, King, 2016

[6.]Roth, A. Einfuehrung um Umsetzung von Industrie 4.0, Springer,2016

DIESEL ENGINE EXHAUST GAS EMISSIONS INVESTIGATION BY USING MEASUREMENT DATA AND NUMERICAL ANALYSIS

PhD. Mrzljak Vedran[1], Student Žarković Božica[1], PhD Student Eng. Poljak Igor[2]
Faculty of Engineering, University of Rijeka, Vukovarska 58, 51000 Rijeka[1], Rožići 4/3, 51221 Kostrena[2], Croatia
E-mail: vedran.mrzljak@riteh.hr, bozica.zarkovic@gmail.com, igor.poljak2@gmail.com

Abstract: *Paper presents an exhaust gas emission investigation for a high speed turbocharged direct injection diesel engine MAN D0826 LOH15 during the fuel and air mass flow variation. Emission analysis is based on a two measurement sets at two different engine rotational speeds (1500 rpm and 2400 rpm). The analyzed diesel engine operates with a standard diesel fuel. Measured emissions were nitrogen oxides (NO_x), unburned hydrocarbons (HC) and soot emissions. Calculated emissions were carbon dioxide (CO_2) emissions by using equations from the literature. For the observed diesel engine, much higher NO_x and HC emissions were obtained at the lower engine rotational speed. Soot emission of the analyzed engine, in general, does not have to depend on engine rotational speed. Calculated CO_2 emissions depend primarily on the fuel mass flow and the carbon mass fraction in used fuel.*

Keywords: *DIESEL ENGINE, EMISSIONS, ENGINE MEASUREMENTS, FUEL MASS FLOW, AIR MASS FLOW*

1. Introduction

Engine measurements are unavoidable in internal combustion engines operating parameters analysis [1].

Investigation of diesel engines can be performed in several different ways [2]. Experimental analysis of diesel engines requires proper engine management [3] and repairing processes [4]. Along with diesel engine measurements, numerical simulations have been developed to make easier, faster and cheaper investigations of engine operating parameters. But still, each numerical model must necessarily be validated in a few measured operating points of the diesel engine, [5] and [6].

Emissions from the diesel engines are intensively explored [7] and researchers investigated ways for their reduction [8].

Instead of standard diesel fuels, alternative fuels and its blends with standard diesel fuels represent an alternative which can significantly reduce engine emissions [9]. A review of alternative fuels for diesel engines can be found in [10] while a review of performance, combustion and emission characteristics of bio-diesel fuels used in diesel engines is presented in [11].

Diesel engine optimization can provide further emissions reducing. Optimization methods are multi-objective optimization [12], genetic algorithm optimization [13] and optimization by using Artificial Neural Networks (ANN) [14].

This paper presents exhaust gas emissions of a turbocharged high speed direct injection diesel engine during the fuel and air mass flow variation. Emissions measurement and calculation were performed in two measurement sets, on two different engine rotational speeds. Measurements were obtained with a standard diesel fuel D2. Measured exhaust gas emissions were nitrogen oxides (NO_x), unburned hydrocarbons (HC) and soot emissions. By using equations from the literature, CO_2 emissions for each engine operating point were calculated. The aim was to examine the behavior of all mentioned emissions at different engine rotational speeds.

2. Turbocharged diesel engine specifications

The investigated diesel engine is turbocharged high speed direct injection diesel engine MAN D0826 LOH15. The main engine specifications are presented in Table 1.

Table 1. *Engine specifications*

The total operating volume	6870 cm^3
Number of cylinders	6
Peak effective power	160 kW
Cylinder bore	108 mm
Cylinder stroke	125 mm
Nozzle diameter	0.23 mm
Number of nozzle holes	7
Compression ratio	18

3. Diesel engine measurement results and measuring equipment

Engine measurement was performed in the Laboratory for Internal Combustion Engines and Electromobility, Faculty of Mechanical Engineering, University of Ljubljana, Slovenia.

The engine was connected to an eddy current brake Zöllner B-350AC, Fig.1. Measurements control was secured with a control system KS ADAC/Tornado. Cylinder pressure was measured with pressure sensor AVL GH12D, placed in an extra hole in the cylinder head. The cylinder pressure signal was led to a 4-channel amplifier AVL MicroIFEM. The crankshaft angle was measured by crank angle encoder Kistler CAM UNIT Type 2613B.

The heated measuring tube (tube temperature was maintained constant at 195 °C) was used for guidance of "wet" exhaust gases into the Horiba OBS-2200 exhaust gas analyzer [15]. Horiba OBS-2200 exhaust gas analyzer measure unburned hydrocarbons (HC) in FID cell (FID = Flame Ionization Detector) and nitrogen oxides (NO_x) in CLD cell (CLD = ChemiLuminescence Detector).

Soot emission was measured by Bosch EFAW 65A/6 smoke detector [16]. Obtained soot measurement results were re-calculated into the BSU (Bosch Smoke Unit).

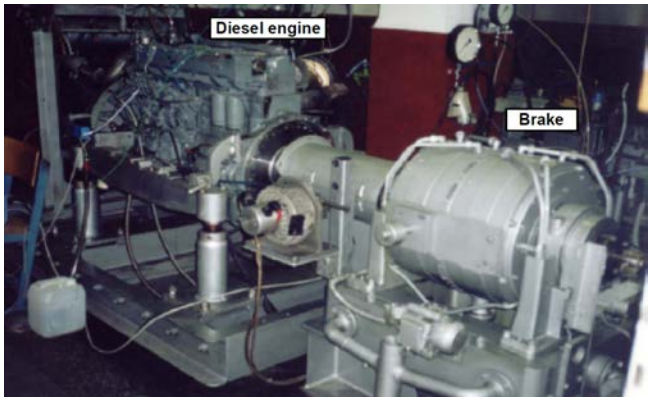

Fig.1. *Diesel engine MAN D0826 LOH15 during measurements*

From several obtained measurement sets, two measurement sets presented in Table 2 and Table 3 are selected for exhaust gas emissions analysis. Measurement Set 3 has almost constant engine rotational speed of 1500 rpm while measurement Set 4 has constant engine rotational speed of 2400 rpm. Fuel and air mass flow were varied in each observed measurement set, for every observed engine operation point. In each measurement set was used standard diesel fuel D2 with a lower heating value 42700 kJ/kg and with the carbon mass fraction of 85% in its chemical composition.

Table 2. *Engine measurement results - Set 3*

	Measurement No.	Fuel mass flow (kg/h)	Air mass flow (kg/s)	Rotational speed (rpm)	Effective power (kW)	BMEP* (bar)
SET 3	1	9.743	0.09761	1501	41.93	4.88
	2	13.977	0.10337	1498	61.82	7.21
	3	18.673	0.12048	1501	86.12	10.02
	4	23.358	0.13943	1500	108.66	12.65

***** BMEP = Brake Medium Effective Pressure

Table 3. *Engine measurement results - Set 4*

	Measurement No.	Fuel mass flow (kg/h)	Air mass flow (kg/s)	Rotational speed (rpm)	Effective power (kW)	BMEP* (bar)
SET 4	1	16.045	0.18775	2400	56.76	4.13
	2	21.961	0.21650	2400	87.92	6.40
	3	30.086	0.25726	2400	123.49	8.99
	4	36.001	0.28798	2400	145.56	10.60

***** BMEP = Brake Medium Effective Pressure

4. Engine measured and calculated emissions with discussion

Fig.2 presents nitrogen oxides (NO_x) emission change in ppm (ppm = parts per million) for measurement Set 3 and Set 4. In those two measurement sets trend lines of NO_x emission change are not the same and in both sets were not found continuous and permanent change of NO_x emissions during the increase in fuel mass flow.

In Set 3 NO_x emission for the lowest fuel mass flow of 9.743 kg/h amounts 1958 ppm. With an increase in fuel mass flow from 9.743 kg/h to 13.977 kg/h, NO_x emission increases from 1958 ppm to 2449 ppm. Further increase in fuel mass flow resulted with a decrease in NO_x emission. Therefore, for the fuel mass flow of 18.673 kg/h NO_x emission amounts 1897 ppm, while the lowest NO_x emission in this measurement set amounts 1647 ppm for the fuel mass flow of 23.358 kg/h.

Measurement Set 4 showed different behavior in NO_x emissions change in comparison with measurement Set 3. For the fuel mass flow of 16.045 kg/h NO_x emission amounts 995 ppm. With an increase in the fuel mass flow on 21.961 kg/h NO_x emission amounts 955 ppm, what is the lowest value in Set 4. With further increase in fuel mass flow, NO_x emission increases, firstly at 1082 ppm for the fuel mass flow of 30.086 kg/h and then at 1211 ppm for the highest fuel mass flow in this measurement set of 36.001 kg/h.

If compared measurement Set 3 and Set 4 for the same fuel mass flow (fuel mass flow range from 16 kg/h up to 23 kg/h), it can be seen from Fig.2 that much higher NO_x emissions were obtained in Set 3, at the lower engine rotational speed (1500 rpm).

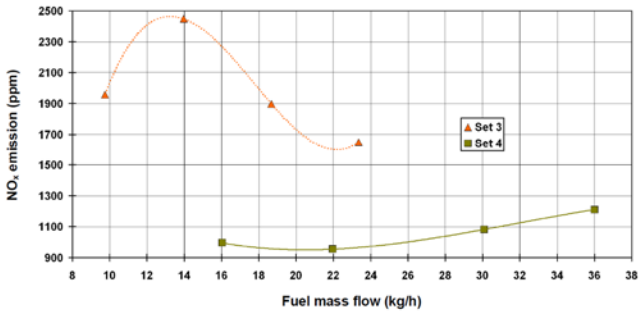

Fig.2. *Measured NO_x emissions for measurement Set 3 and Set 4*

For measurement Set 3 and Set 4 unburned hydrocarbons (HC) emission is presented in Fig.3. Trend lines of HC emissions are not the same in both measurement sets. In both measurement sets HC emission have no continuous and permanent change during the increase in fuel mass flow.

In measurement Set 3, HC emission for the lowest fuel mass flow amounts 107 ppm. With an increase in fuel mass flow, HC emission increases to 114 ppm for the fuel mass flow of 13.977 kg/h and to 126 ppm for the fuel mass flow of 18.673 kg/h. In the last operating point in Set 3, for the fuel mass flow of 23.358 kg/h, HC emission decreases to 115 ppm in comparison with the previous observed operating point.

An HC emission in measurement Set 4 has a different trend in comparison with measurement Set 3. At fuel mass flow of 16.045 kg/h, HC emission amounts 94 ppm, after which decreases to 61 ppm at fuel mass flow of 21.961 kg/h. With the further increase in fuel mass flow, HC emission firstly increases to 80 ppm at fuel mass flow of 30.086 kg/h, after which decreases to 62 ppm at the highest fuel mass flow in this measurement set.

When compared HC emissions in measurement Set 3 and Set 4 for the same fuel mass flow, from Fig.3 can be seen that at lower engine rotational speed (1500 rpm - Set 3) HC emissions are significantly higher in comparison with Set 4 (2400 rpm).

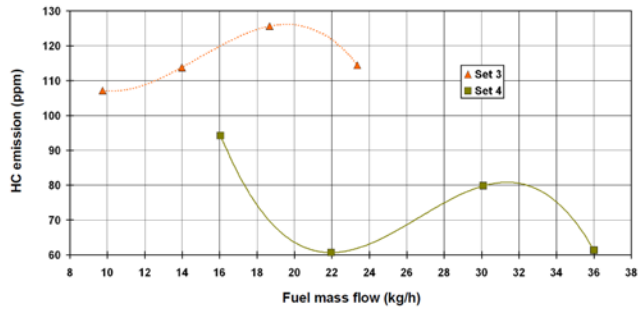

Fig.3. *Measured HC emissions for measurement Set 3 and Set 4*

In measurement Set 3, soot emission continuously increases during the increase in fuel mass flow, from 0.1 BSU at fuel mass flow of 9.743 kg/h up to 0.45 BSU at fuel mass flow of 23.358 kg/h, Fig.4. The trend line of soot emission change in Set 3 is not nearly similar to trend line of soot emission change in measurement Set 4.

Soot emission in measurement Set 4 amounts 0.3 BSU at the lowest observed fuel mass flow of 16.045 kg/h. During the increase in fuel mass flow in Set 4, soot emission firstly increases to 0.65 BSU at fuel mass flow of 21.961 kg/h, after which follows decrease to 0.45 BSU (fuel mass flow of 30.086 kg/h) and to 0.2 BSU (fuel mass flow of 36.001 kg/h).

When compared above mentioned emissions (NO_x, HC, soot), soot emission is the only one where for the same fuel mass flow, higher emissions were obtained at higher engine rotational speed of 2400 rpm (Set 4) in comparison with the lower engine rotational speed of 1500 rpm (Set 3).

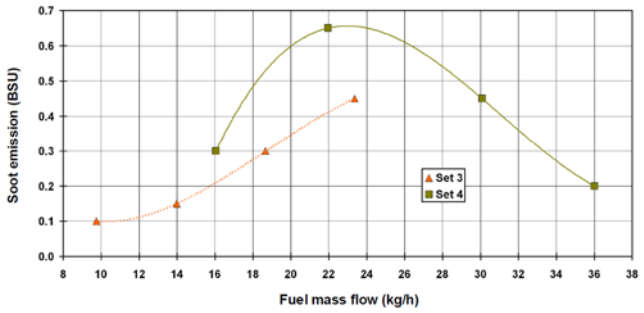

Fig.4. *Measured soot emissions for measurement Set 3 and Set 4*

Carbon dioxide (CO_2) emissions were calculated by using equations from [17] and [18]. The main components of these equations are the fuel mass flow and the carbon mass fraction in used fuel during the engine measurements.

CO_2 emissions in kg/h were presented in Table 4 for measurement Set 3 and Set 4. From Table 4 can be seen linear dependence of CO_2 emissions on fuel mass flow. With the increase in fuel mass flow, CO_2 emissions proportionally rise.

In measurement Set 3 the lowest CO_2 emissions were 30.366 kg/h at the lowest fuel mass flow and then continuously rises up to 72.798 kg/h at the highest fuel mass flow. In measurement Set 4, CO_2 emissions were much higher, due to higher fuel mass flow if compared with measurement Set 3. In Set 4, CO_2 emissions were in the range from 50.006 kg/h up to 112.203 kg/h from the lowest to the highest used fuel mass flow.

CO_2 emissions can be significantly reduced by using fuels with higher heating values or by using fuels with lower carbon mass fraction in its composition. Research and development of bio-fuels and other alternative fuels for use in diesel engines can fulfil the goal for CO_2 emissions reduction.

Table 4. *Calculated CO_2 emissions for measurement Set 3 and Set 4*

	Fuel mass flow (kg/h)	**CO_2 emission (kg/h)**
SET 3	9.743	30.366
	13.977	43.562
	18.673	58.197
	23.358	72.798
SET 4	16.045	50.006
	21.961	68.446
	30.086	93.767
	36.001	112.203

5. Conclusion

Change in exhaust gas emissions for a high speed direct injection turbocharged diesel engine MAN D0826 LOH15 during the fuel and air mass flow variation was presented. Analysis is based on a two measurement sets at two different engine rotational speeds (1500 rpm and 2400 rpm).

During the engine laboratory experiments were measured nitrogen oxides (NO_x), unburned hydrocarbons (HC) and soot emissions in each observed measurement point. Carbon dioxide (CO_2) emissions for the all measurement points were calculated by using equations from available literature.

Presented measurement and calculation results showed that much higher NO_x and HC emissions are observed at the lower engine rotational speed (1500 rpm) in comparison with the higher engine rotational speed (2400 rpm).

Soot emissions change for the observed measurement sets are opposite to NO_x and HC emissions. On a wide range of fuel mass flow rates, soot emission is higher at engine rotational speed of 2400 rpm - Set 4 in comparison with the lower engine rotational speed of 1500 rpm - Set 3.

According to equations from the literature, CO_2 emissions depend primarily on the fuel mass flow and the carbon mass fraction in used fuel. This fact was confirmed also for the engine analyzed in this paper.

In future research of this diesel engine will be interesting to compare the same emissions with those obtained when engine uses alternative fuels or its blends with standard diesel fuel.

6. Acknowledgments

The authors express their thankful regards to the whole team at the Laboratory for Internal Combustion Engines and Electromobility (LICeM), at the Faculty of Mechanical Engineering, University of Ljubljana, Slovenia. This work was supported by the University of Rijeka (contract no. 13.09.1.1.05) and Croatian Science Foundation-project 8722.

7. References

[1] Merker, G. P., Schwarz, C., Teichmann, R.: *Combustion Engines Development - Mixture Formation, Combustion, Emissions and Simulation*, Springer-Verlag, Berlin, Heidelberg, 2012. (doi:10.1007/978-3-642-14094-5)

[2] Mollenhauer, K., Tschoeke, H.: *Handbook of Diesel Engines*, Springer-Verlag, Berlin, Heidelberg, 2010. (doi:10.1007/978-3-540-89083-6)

[3] Reif, K.: *Diesel Engine Management - Systems and Components*, Springer Fachmedien, Wiesbaden, 2014. (doi:10.1007/978-3-658-03981-3)

[4] Dempsey, P.: *Troubleshooting and Repairing Diesel Engines*, Fourth Edition, The McGraw-Hill Companies, Inc., 2008. (doi:10.1036/0071493719)

[5] Mrzljak, V., Medica, V., Bukovac, O.: *Volume agglomeration process in quasi-dimensional direct injection diesel engine numerical model*, Energy, 115, p. 658-667, 2016. (doi:10.1016/j.energy.2016.09.055)

[6] Mrzljak, V., Medica, V., Bukovac, O.: *Simulation of a Two-Stroke Slow Speed Diesel Engine Using a Quasi-Dimensional Model*, Transactions of Famena, 2, p. 35-44, 2016. (doi:10.21278/TOF.40203)

[7] Park, S., Kim, Y., Woo, S., Lee, K.: *Optimization and calibration strategy using design of experiment for a diesel engine*, Applied Thermal Engineering, 123, p. 917–928, 2017. (doi:10.1016/j.applthermaleng.2017.05.171)

[8] Ramesh, N., Mallikarjuna, J. M.: *Low Temperature Combustion Strategy in an Off-Highway Diesel Engine – Experimental and CFD study*, Applied Thermal Engineering, 124, p. 844–854, 2017. (doi:10.1016/j.applthermaleng.2017.06.078)

[9] Liu, J., Sun, P., Huang, H., Meng, J., Yao, X.: *Experimental investigation on performance, combustion and emission characteristics of a common-rail diesel engine fueled with polyoxymethylene dimethyl ethers-diesel blends*, Applied Energy, 202, p. 527–536, 2017. (doi:10.1016/j.apenergy.2017.05.166)

[10] Othman, M.F., Adam, A., Najafi, G., Mamat, R.: *Green fuel as alternative fuel for diesel engine: A review*, Renewable and Sustainable Energy Reviews, 80, p. 694–709, 2017. (doi:10.1016/j.rser.2017.05.140)

[11] Tamilselvan, P., Nallusamy, N., Rajkumar, S.: *A comprehensive review on performance, combustion and emission characteristics of biodiesel fuelled diesel engines*, Renewable and Sustainable Energy Reviews, 79, p. 1134–1159, 2017. (doi:10.1016/j.rser.2017.05.176)

[12] Park, S., Cho, J., Park, J., Song, S.: *Numerical study of the performance and NOx emission of a diesel-methanol dual-fuel engine using multi-objective Pareto optimization,*

Energy, 124, p. 272-283, 2017. (doi:10.1016/j.energy.2017.02.029)

[13] Navid, A., Khalilarya, S., Taghavifar, H.: *Comparing multi-objective non-evolutionary NLPQL and evolutionary genetic algorithm optimization of a DI diesel engine: DoE estimation and creating surrogate model*, Energy Conversion and Management, 126, p. 385–399, 2016. (doi: 10.1016/j.enconman.2016.08.014)

[14] Channapattana, S.V., Pawar, A.A., Kamble, P.G.: *Optimisation of operating parameters of DI-CI engine fueled with second generation Bio-fuel and development of ANN based prediction model*, Applied Energy, 187, p. 84–95, 2017. (doi:10.1016/j.apenergy.2016.11.030)

[15] http://www.horiba.com (accessed: 20.08.2017.)

[16] https://de-ww.bosch-automotive.com/en_GB/ (accessed: 24.08.2017.)

[17] Klingenberg, H.: *Automobile Exhaust Emission Testing - Measurement of Regulated and Unregulated Exhaust Gas Components, Exhaust Emission Tests*, Springer-Verlag, Berlin, Heidelberg, 1996. (doi:10.1007/978-3-642-80243-0)

[18] Blanco-Rodriguez, D.: *Modelling and Observation of Exhaust Gas Concentrations for Diesel Engine Control*, Springer International Publishing, Switzerland, 2014. (doi:10.1007/978-3-319-06737-7)

MARINE SLOW SPEED TWO-STROKE DIESEL ENGINE - NUMERICAL ANALYSIS OF EFFICIENCIES AND IMPORTANT OPERATING PARAMETERS

PhD. Mrzljak Vedran, Student Žarković Božica, Prof. PhD. Prpić-Oršić Jasna
Faculty of Engineering, University of Rijeka, Vukovarska 58, 51000 Rijeka, Croatia
E-mail: vedran.mrzljak@riteh.hr, bozica.zarkovic@gmail.com, jasna.prpic-orsic@riteh.hr

Abstract: *This paper presents numerical analysis of efficiencies and non-measured operating parameters for the marine two-stroke slow speed turbocharged diesel engine 6S50MC MAN B&W with direct fuel injection. Numerical analysis was based on a measurement set performed at different engine loads. Calculated efficiencies were mechanical, indicated and effective efficiency, while the calculated important operating parameters were power of engine mechanical losses, mean effective pressure, effective engine torque and specific effective fuel consumption. Engine load was presented in percentage of maximum continuous rating (MCR). The highest engine mechanical efficiency of 94.52 % was obtained at the highest engine load, while the highest engine effective efficiency of 49.34 % was obtained at the engine load 75 % of MCR. Available engine effective torque was from 267380 Nm on the lowest up to 643594 Nm on the highest engine load, while effective fuel consumption was between 171.18 g/kWh and 186.83 g/kWh.*

Keywords: *MARINE DIESEL ENGINE, TWO-STROKE PROCESS, EFFICIENCIES, OPERATING PARAMETER ANALYSIS*

1. Introduction

Experimental measurements are the basis of internal combustion engines operating parameters analysis [1], regardless of the engine type. By using several engine measured variables can be obtained a complete insight into engine general operating parameters, in a wide load range [2]. Numerous researchers are involved in the investigation of the diesel engines from the several points of view [3].

Marine slow speed two-stroke diesel engines, compared to the other diesel engines, are characterized by their construction, dimensions, operating processes and start-up process. Because of the high pressures and temperatures, the materials used in such engines for a large number of engine components, cannot be conventional ones [4].

Several researchers were involved in the development of numerical models for marine two-stroke diesel engines [5], in order to predict their operating parameters during the propulsion [6] or to get an insight into the details of in-cylinder processes [7] such as convective heat transfer [8].

Marine two-stroke diesel engines are turbocharged engines and it is interesting to investigate turbocharging process and its influence on engine performance [9].

To improve marine two-stroke diesel engine operating parameters and reduce emissions, numerous investigations were performed in order to implement alternative fuel combustion [10], using bio-fuel blends for combustion [11] or using standard diesel fuels with some additives [12] in this type of engines.

For this type of diesel engines were also investigated some of the known techniques from automotive diesel engines for reducing nitrogen oxides (NO_x) emissions, as for example Exhaust Gas Recirculation (EGR) [13]. It is also important to know maximum NO_x reduction potential of two-stroke marine diesel engines [14] by using EGR. Along with nitrogen oxides, for marine slow speed two-stroke diesel engines was also investigated soot emission [15] and possibilities of soot emission reduction.

This paper presents change in efficiencies and the main operating parameters of marine slow speed two-stroke diesel engine 6S50MC MAN B&W. Operating parameters and efficiency analysis was based on a measurement set performed at different engine loads (from the lowest to the highest load). For each engine operation point, by using measured parameters, was performed calculation of mechanical losses power, mean effective engine pressure, engine effective torque and engine specific effective fuel consumption. On this way was gained an insight into the change of these engine operating parameters during the whole range of observed loads. Calculated engine efficiencies and their change during the change in engine load were engine mechanical efficiency, engine indicated efficiency and on the end engine effective efficiency. This analysis confirmed that marine slow speed two-stroke diesel engines are the internal combustion engines with the highest effective efficiency and the lowest specific effective fuel consumption, during the complete load range.

2. Slow speed marine diesel engine specifications

Analyzed marine diesel engine is a slow speed turbocharged two-stroke engine with direct fuel injection 6S50MC MAN B&W. The main engine specifications are presented in Table 1.

Table 1. *Specifications of marine slow speed two-stroke diesel engine 6S50MC MAN B&W [16]*

Number of cylinders	6 in line
Cylinder bore	500 mm
Cylinder stroke	1910 mm
Firing order	1-5-3-4-2-6
Maximum continuous rating (MCR)	8580 kW
Engine speed at MCR	127 rpm
Maximum mean effective pressure	18 bar
Maximum combustion pressure	143 bar
Compression ratio	17.2
Crank mechanism ratio	0.436
Exhaust manifold volume	6.13 m^3
Inlet manifold volume (with intercooler)	7.179 m^3
Cumulative engine mass	232000 kg

A cross section of the analyzed marine diesel engine 6S50MC MAN B&W is presented in Fig.1. In Fig.1 can be seen all of the housing and cylinder main elements. The engine was built in a diesel engine factory in Split, Croatia, according to the license MAN B&W.

3. Engine measurement results

The main operating data of the marine diesel engine 6S50MC MAN B&W were obtained by test-bed measurements in Shipyard Split, Croatia. Engine load was presented in percentage of maximum continuous rating (MCR), Table 1. The measured values for the engine steady state operation at engine loads 25 %, 50 %, 75 %, 93.50 % and 100 % of MCR was presented in Table 2.

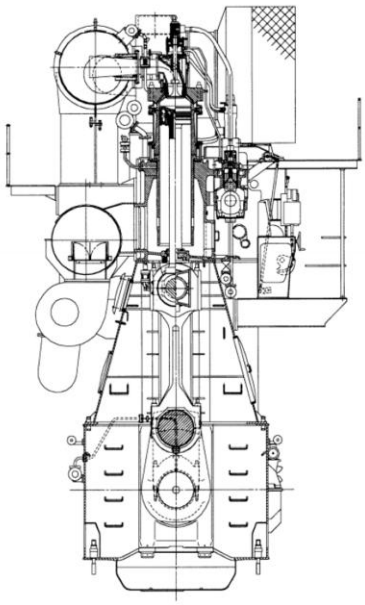

Fig.1. *Cross section of marine slow speed two-stroke diesel engine 6S50MC MAN B&W [17]*

Table 2. *6S50MC MAN B&W measured data [16]*

Load (% of MCR)	Indicated power (kW)	Effective power (kW)	Mean indicated pressure (bar)	Rotational speed (rpm)	Fuel mass flow (kg/h)
25 %	2401	2142	8.37	76.5	400.2
50 %	4406	4099	12.24	96.0	713.5
75 %	6580	6160	15.89	110.4	1054.5
93.50 %	8170	7667	18.38	118.5	1317.3
100 %	8656	8182	19.01	121.4	1429.1

The measurements were performed during the following environmental conditions:

- Ambient temperature 30 °C,
- Ambient pressure 1005 mbar,
- Relative humidity 50 %.

The engine was tested with a standard marine diesel fuel, whose properties are:

- Density 844.7 kg/m^3,
- Kinematic viscosity 3.03 mm^2/s,
- Sulfur content 0.45 %,
- Lower heating value 42625 kJ/kg.

4. Equations for calculating engine efficiencies and operating parameters

Power of mechanical losses for each operating point of the analyzed engine should be calculated as a difference between measured indicated and effective power, Table 2:

$$P_{\mathrm{ml}} = P_{\mathrm{ind}} - P_{\mathrm{eff}} \tag{1}$$

where P_{ml} (kW) is power of mechanical losses, P_{ind} (kW) is measured indicated power and P_{eff} (kW) is measured effective power.

Engine mechanical efficiency was calculated by using an equation:

$$\eta_{\mathrm{m}} = \frac{P_{\mathrm{eff}}}{P_{\mathrm{ind}}} \cdot 100 \tag{2}$$

where η_{m} (%) is engine mechanical efficiency.

Indicated engine efficiency is the ratio of engine indicated power and heat released by fuel. Indicated engine efficiency was calculated according to the equation:

$$\eta_{\mathrm{ind}} = \frac{P_{\mathrm{ind}}}{\dot{m}_{\mathrm{f}} \cdot H_{\mathrm{low}}} \cdot 3600 \cdot 100 \tag{3}$$

where η_{ind} (%) is engine indicated efficiency, $\dot{m}_{\mathrm{f}}$ (kg/h) is measured fuel mass flow - Table 2 and H_{low} (kJ/kg) is used fuel lower heating value.

Effective engine efficiency is the ratio of engine effective power and heat released by fuel. Effective engine efficiency was calculated according to the equation:

$$\eta_{\mathrm{eff}} = \frac{P_{\mathrm{eff}}}{\dot{m}_{\mathrm{f}} \cdot H_{\mathrm{low}}} \cdot 3600 \cdot 100 \tag{4}$$

where η_{eff} (%) is engine effective efficiency.

Engine mean effective pressure was calculated by using an equation:

$$p_{\mathrm{me,eff}} = \frac{P_{\mathrm{eff}} \cdot \tau}{2 \cdot z \cdot n \cdot V_{\mathrm{op}}} \cdot \frac{6}{10} \tag{5}$$

where $p_{\mathrm{me,eff}}$ (bar) is engine mean effective pressure, τ (-) is engine stroke - analyzed engine is two-stroke engine so τ = 2, z (-) is number of engine cylinders - Table 1, n (rpm) is measured engine rotational speed - Table 2 and V_{op} (m^3) is operating volume of one engine cylinder which can be calculated according to the equation:

$$V_{\mathrm{op}} = \frac{D^2 \cdot \pi}{4} \cdot s \tag{6}$$

where D (m) is cylinder bore - Table 1 and s (m) is cylinder stroke - Table 1.

Engine effective torque, which drives the ship's propeller was calculated according to the equation:

$$M_{\mathrm{eff}} = \frac{P_{\mathrm{eff}}}{2 \cdot \pi \cdot n} \cdot 60000 \tag{7}$$

where M_{eff} (Nm) is engine effective torque.

Specific effective fuel consumption was calculated by using an equation:

$$b_{\mathrm{eff}} = \frac{\dot{m}_{\mathrm{f}} \cdot 1000}{P_{\mathrm{eff}}} \tag{8}$$

where b_{eff} (g/kWh) is engine specific effective fuel consumption.

5. Engine calculation results for various observed loads and discussion

Fig.2 presents the power of mechanical losses calculated by using equation (1) and mechanical efficiency calculated by using equation (2) for all observed loads of the analyzed engine.

Engine power of mechanical losses is the lowest at load 25 % of MCR and amounts 259 kW, while the highest power of mechanical losses can be seen at load 93.5 % of MCR where it amounts 503 kW. At the highest engine load 100 % of MCR, power of mechanical losses decrease from the highest value and amounts 474 kW.

The mechanical efficiency of the analyzed engine continuously increases during the increase in engine load. At the lower engine load 25 % of MCR, mechanical efficiency is the lowest and

amounts 89.21 %, while on the highest engine load 100 % of MCR mechanical efficiency of the engine is the highest and amounts 94.52 %. This is an important fact, because for the analyzed engine it can be expected that the majority of its operation will be obtained at the highest load. Therefore, during the majority of engine operation, mechanical efficiency will be the highest.

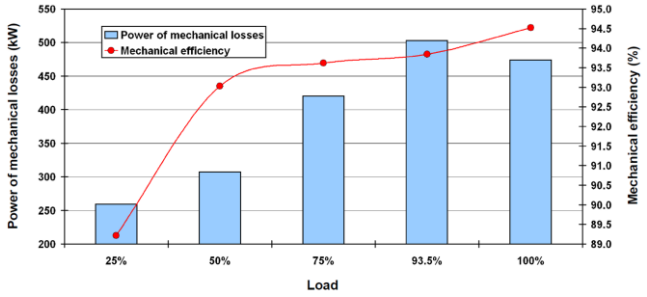

Fig.2. *Change in engine power of mechanical losses and mechanical efficiency for all observed loads*

Analyzed engine indicated efficiency change, calculated according to equation (3) and engine effective efficiency change, calculated according to equation (4) are presented in Fig.3. From the lowest to the highest engine load, both efficiencies have the same trend - they increase until the engine load 75% of MCR after which both of them decreases.

Indicated engine efficiency is the ratio of the engine indicated power and heat released by fuel, so this efficiency presented amount of energy which is transferred from fuel to the engine pistons. At the lowest engine load 25 % of MCR indicated efficiency is the lowest and amounts 50.67 %. Increase in engine load firstly causes an increase of indicated efficiency to a maximum value of 52.70 % at the engine load 75 % of MCR after which follows a decrease in indicated efficiency to 52.38 % (engine load 93.50 % of MCR) and to 51.16 % (engine load 100 % of MCR).

Engine effective efficiency has the lowest value of 45.21 % at the engine load 25% of MCR while the highest effective efficiency amounts 49.34 % at the engine load 75 % of MCR. At the highest engine load 100 % of MCR, effective efficiency amounts 48.36 %. In comparison with all the other types of internal combustion engines, marine slow speed two-stroke diesel engine has significantly higher effective efficiency, which can nowadays reach above 50 % (maximal obtained effective efficiency of marine two-stroke diesel engine is 55 %). Effective efficiency of analyzed diesel engine does not reach 50 % for any observed load, but is very close to that value.

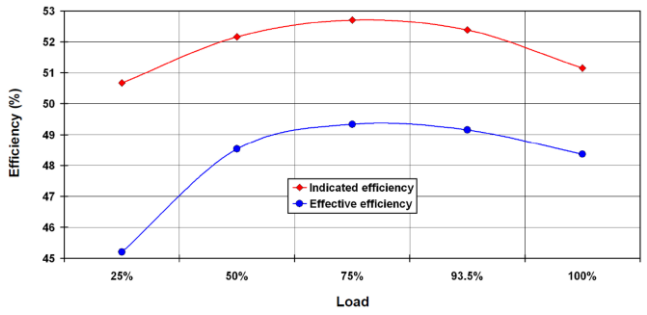

Fig.3. *Change in engine indicated and effective efficiency for all observed loads*

The change in mean effective pressure of the analyzed engine, for all of the observed engine loads was presented in Fig.4. Mean effective engine pressure was calculated according to equation (5) and in Fig.4 was presented along with measured mean indicated engine pressure.

During the increase in engine load, mean effective pressure continuously increases from 7.47 bar at the engine load 25 % of MCR up to 17.97 bar at the engine load 100 % of MCR. At the maximum engine load 100 % of MCR was obtained almost the maximum mean effective pressure, which amounts exactly 18 bar, Table 1.

Measured indicated and calculated effective pressures of the analyzed engine have the same trends during the increase in engine load from the lowest to the highest loads.

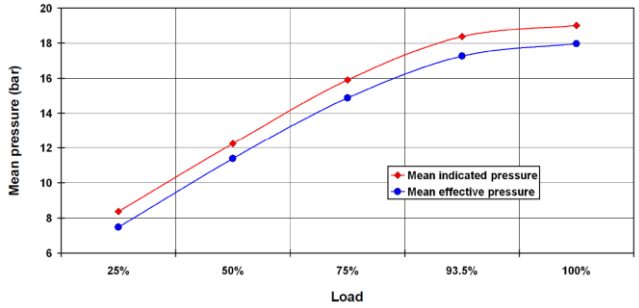

Fig.4. *Change in engine mean indicated and effective pressure for all observed loads*

Engine effective torque, calculated by using equation (7) continuously increases during the increase in engine load, Fig.5. In comparison to other diesel engines, marine slow speed two-stroke diesel engines develop significantly higher engine effective torque which will be used for propulsion propeller drive. One of slow speed marine diesel engine advantages is direct propeller drive, without usage of gearbox, so the developed effective torque was directly transferred to the main ship propeller.

The lowest effective torque analyzed engine develops on the lowest observed load 25 % of MCR, and that effective torque amounts 267380 Nm. On the highest observed engine load 100 % of MCR was developed the highest engine effective torque which amounts 643594 Nm. For marine two-stroke diesel engine, with cylinder bore of 500 mm, this is an expected range of developed effective torque. The highest developed effective torque must be obtained at the highest engine load, because at the highest engine load can be expected the majority of ship operation (maximum ship speed).

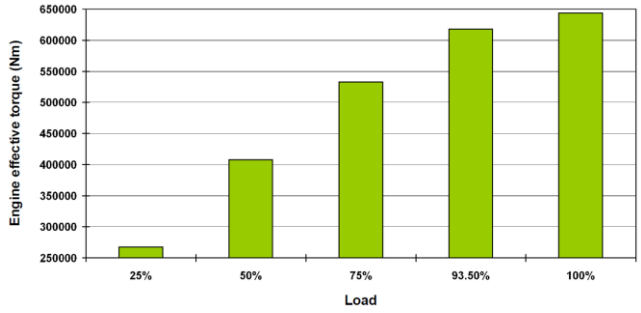

Fig.5. *Change in engine effective torque for all observed loads*

When compared specific effective fuel consumption of the analyzed engine with other diesel engines, for example, with a high speed direct injection turbocharged diesel engine MAN D0826 LOH15 presented in [18], it can be calculated that marine two-stroke diesel engine has much lower specific effective fuel consumption. This is not a fact only for two compared diesel engines, marine two-stroke diesel engines have the lowest specific effective fuel consumption of all diesel engines or of all engines in general. This fact is valid if compared diesel engines which use standard diesel fuel, if diesel engine use the alternative fuels, this conclusion does not have to be correct.

Specific effective fuel consumption of the analyzed engine, calculated by using equation (8), has the same trend like the other diesel engines - during the load increase specific effective fuel consumption firstly decrease to the lowest value, after which

follows slight increase, Fig.6. The highest specific effective fuel consumption of the analyzed engine was obtained at the lowest load 25 % of MCR and amounts 186.83 g/kWh. Increase in engine load causes that specific effective fuel consumption decreases and the lowest value were obtained at the engine load 75 % of MCR and amounts 171.18 g/kWh. A further increase in engine load causes an increase in specific effective fuel consumption and at the highest engine load 100 % of MCR specific effective fuel consumption of the analyzed engine amounts 174.66 g/kWh.

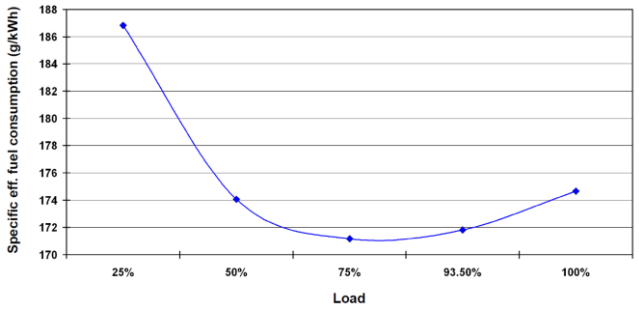

Fig.6. *Change in engine specific effective fuel consumption for all observed loads*

6. Conclusion

Calculated operating parameters and efficiencies of marine slow speed two-stroke diesel engine 6S50MC MAN B&W was analyzed in this paper. Analysis was based on a measurement set performed at different engine loads in order to obtain complete range of main engine parameters and efficiencies change.

Presented calculation method gives for result that the highest engine mechanical efficiency of 94.52 % was obtained at engine load 100 % of MCR. The highest indicated engine efficiency of 52.70 % and the highest engine effective efficiency of 49.34 % were obtained at the engine load 75 % of MCR. In comparison with the other types of internal combustion engines, marine slow speed two-stroke diesel engines have significantly higher effective efficiency which can nowadays reach above 50 %.

The highest power of engine mechanical losses was obtained at engine load 93.50 % of MCR and amounts 503 kW. During the engine load increase, mean effective pressure continuously increases from 7.47 bar at the lowest up to 17.97 bar at the highest observed engine load. The range of available engine effective torque was from 267380 Nm on the lowest up to 643594 Nm on the highest engine load, what is an expected range of developed effective torque for this kind of diesel engine.

The range of analyzed engine specific effective fuel consumption was between 171.18 g/kWh and 186.83 g/kWh. Obtained range of specific effective fuel consumption proves the fact that marine two-stroke diesel engines have the lowest specific effective fuel consumption of all diesel engines or of all engines in general.

7. Acknowledgments

This work was supported by the University of Rijeka (contract no. 13.09.1.1.05) and Croatian Science Foundation-project 8722.

8. References

[1] Martyr, A. J., Plint, M. A.: *Engine Testing - Theory and Practice*, Third edition, Butterworth-Heinemann, Elsevier Ltd., 2007.

[2] Merker, G. P., Schwarz, C., Teichmann, R.: *Combustion Engines Development - Mixture Formation, Combustion, Emissions and Simulation*, Springer-Verlag, Berlin, Heidelberg, 2012. (doi:10.1007/978-3-642-14094-5)

[3] Mollenhauer, K., Tschoeke, H.: *Handbook of Diesel Engines*, Springer-Verlag, Berlin, Heidelberg, 2010. (doi:10.1007/978-3-540-89083-6)

[4] Olander, P., Jacobson, S.: *Scuffing resistance testing of piston ring materials for marine two-stroke diesel engines and mapping of the operating mechanisms*, Wear, 330-331, p. 42–48, 2015. (doi:10.1016/j.wear.2015.01.074)

[5] Mrzljak, V., Medica, V., Bukovac, O.: *Simulation of a Two-Stroke Slow Speed Diesel Engine Using a Quasi-Dimensional Model*, Transactions of Famena, 2, p. 35-44, 2016. (doi:10.21278/TOF.40203)

[6] Yum, K. K., Taskar, B., Pedersen, E., Steen, S.: *Simulation of a two-stroke diesel engine for propulsion in waves*, International Journal of Naval Architecture and Ocean Engineering, Vol. 9, Issue 4, p. 351-372, 2017. (doi:10.1016/j.ijnaoe.2016.08.004)

[7] Tang, Y., Zhang, J., Gan, H., Jia, B., Xia, Y.: *Development of a real-time two-stroke marine diesel engine model with in-cylinder pressure prediction capability*, Applied Energy, 194, p. 55–70, 2017. (doi:10.1016/j.apenergy.2017.03.015)

[8] Sigurdsson, E., Ingvorsen, K. M., Jensen, M. V., Mayer, S., Matlok, S., Walther, J. H.: *Numerical analysis of the scavenge flow and convective heat transfer in large two-stroke marine diesel engines*, Applied Energy, 123, p. 37–46, 2014. (doi:10.1016/j.apenergy.2014.02.036)

[9] Sakellaridis, N. F., Raptotasios, S. I., Antonopoulos, A. K., Mavropoulos, G. C., Hountalas, D. T.: *Development and validation of a new turbocharger simulation methodology for marine two stroke diesel engine modelling and diagnostic applications*, Energy, 91, p. 952-966, 2015. (doi:10.1016/j.energy.2015.08.049)

[10] Sun, X., Liang, X., Shu, G., Wang, Y., Wang, Y., Yu, H.: *Effect of Different Combustion Models and Alternative Fuels on Two-stroke Marine Diesel Engine Performance*, Applied Thermal Engineering, 115, p. 597-606, 2017. (doi:10.1016/j.applthermaleng.2016.12.093)

[11] Senatore, A., Buono, D., Frosina, E., Prati, M. V., Valentino, G., Poles, F.: *PERFORMANCES AND EMISSIONS OF A 2-STROKE DIESEL ENGINE FUELED WITH BIOFUEL BLENDS*, Energy Procedia, 81, p. 918 – 929, 2015. (doi:10.1016/j.egypro.2015.12.147)

[12] Ryu, Y., Lee, Y., Nam, J.: *Performance and emission characteristics of additives-enhanced heavy fuel oil in large two-stroke marine diesel engine*, Fuel, 182, p. 850–856, 2016. (doi:10.1016/j.fuel.2016.06.029)

[13] Wang, Z., Zhou, S., Feng, Y., Zhu, Y.: *Research of NOx reduction on a low-speed two-stroke marine diesel engine by using EGR (exhaust gas recirculation)-CB (cylinder bypass) and EGB (exhaust gas bypass)*, International Journal of Hydrogen Energy, In Press, Corrected Proof, 2017. (doi:10.1016/j.ijhydene.2017.06.009)

[14] Raptotasios, S. I., Sakellaridis, N. F., Papagiannakis, R. G., Hountalas, D. T.: *Application of a multi-zone combustion model to investigate the NOx reduction potential of two-stroke marine diesel engines using EGR*, Applied Energy, 157, p. 814–823, 2015. (doi:10.1016/j.apenergy.2014.12.041)

[15] Pang, K. M., Karvounis, N., Walther, J. H., Schramm, J.: *Numerical investigation of soot formation and oxidation processes under large two-stroke marine diesel engine-like conditions using integrated CFD-chemical kinetics*, Applied Energy, 169, p. 874–887, 2016. (doi:10.1016/j.apenergy.2016.02.081)

[16] Račić, N.: *Simulation of performance of the ship propulsion system with slow speed diesel engine in aggrivated conditions*, Doctoral Thesis, University of Rijeka, Rijeka, 2008.

[17] http://marine.man.eu (accessed: 12.09.17)

[18] Mrzljak, V., Medica, V., Bukovac, O.: *Volume agglomeration process in quasi-dimensional direct injection diesel engine numerical model*, Energy, 115, p. 658-667, 2016. (doi:10.1016/j.energy.2016.09.055)

INFLUENCE OF FRICTION COEFFICIENT ON MECHANICAL PROPERTIES IN PROCESS OF COLD BULK FORMING

Ass. Prof. dr. Leo Gusel, Ass. Prof. dr. Rebeka Rudolf
University of Maribor; Faculty of Mechanical Engineering, Maribor, Slovenia
leo.gusel@um.si

Abstract. *Bulk forming is one of the most effective and efficient manufacturing processes. Mass production of many of the items without any defects has been possible because of the advancements in cold bulk forming. The characteristic of a lubricant, especially coefficient of friction influences the interfacial friction during the forming process. This friction causes defects and many difficulties and has to be kept within limits so the proper choice of lubrication is very important for the quality of the formed product. The influence of lubricant's coefficient of friction on different mechanical and electrical properties of cold extruded material has been investigated and described in this paper by performing many different tests and measurements for mechanical properties and electrical conductivity of the formed material. Coefficients of friction for four different lubricants were first obtained by ring test, and then these lubricants were used in cold extrusion process. The obtained experimental results describing the effect of lubrication on material properties were presented in a form of diagrams and have shown that choice of lubrication could influence some material properties.*

***Keywords**: BULK FORMING, FORWARD EXTRUSION, LUBRICANTS, FRICTION COEFFICIENT, RING TEST, MECHANICAL PROPERTIES*

1. Introduction

Mass production of many of the products without any defects, in different fields has been possible because of the advancements in cold bulk forming, extrusion for example. During extrusion process, there is a relative movement between the tool and die setup, and the billet formed; Due to this friction arises in the interface between them. [1]

This friction causes defects and difficulties like inadequate filling up of metal in the cavity, cracks and porous surfaces, subsurface defects in the formed part, premature wear and tear of the tool and die setup, increased energy requirements [1]. Therefor the interfacial friction has to be kept within limits, though cannot be eradicated. The lubrication problems are one of the most delicate problems in cold forming. The influence of lubrication on wear, friction, forming force, temperature, material and geometrical properties and finally costs are very important [2]

In a bulk metal forming, the characteristic of a lubricant (especially coefficient of friction) influences the interfacial friction during the process. It is generally expressed in two terms, coefficient of friction, μ and shear friction factor, m. In metal forming analysis, two friction models namely Coulomb friction model and Tresca friction model are used to describe friction. In Coulomb's theory, frictional shear stress, τ is expressed as follows [1]:

$$\tau = \mu \, \sigma_{n,} \tag{1}$$

where σ_n is the normal stress or pressure that acts perpendicular to the surface and μ is the coefficient of friction.

Tresca's friction model relates the shear stress to a constant shear friction factor, m as given below [1]:

$$\tau = m \, \sigma_f / \sqrt{3} \tag{2}$$

where σ_f is the flow stress of the material.

The flow stress, a property of the material, in turn depends upon the strain, strain rate and temperature of the billet.

The value of shear friction factor varies from 0 to 1, where $m = 0$ represents frictionless interface and $m = 1$ represents sticking friction.

In the majority of metalworking processes the material is deformed by means of a contacting die. The pressure required for deformation generates a normal stress to the die surface, and movement of the specimen relative to the die surface generate a shear stress at the interface [3, 4]. Thus a classical tribology situation arises, with friction at the die-specimen interface, and with potential for wear of both die and specimen materials. The first step in controlling this friction is to quantify it, and then properly apply a suitable lubricant for the extrusion process [5, 6].

The success or failure of such lubrication has important consequences on the quality of the issuing product, and also on pressures, forces and on the mechanical properties as well as some other properties of the product. The choice of the right lubricant and its proper application is very important. There are some articles describing new lubrication technologies [6, 7, 8] with new lubricants and also optimization of application of known and widely used lubricants [9, 10]. Authors in [11] describe numerical analysis of lubrication while in papers [12] decreasing of friction during cold forming by using a nano-molecular layer or adding a nano particles [13] was investigated. Despite the extremely wide range of conditions under lubricants must function, some systematic approach to selection can be made.

Final selection is almost always a matter of compromise, but there exists some fairly general, desirable attributes which must be taken into account when choosing the optimal lubricants for bulk forming processes [14]:

- separation of die and specimen surfaces,
- prevention of cold welding (pressure welding),
- controlled friction,
- control of surface temperature,
- easy handling, safety,
- low costs, ecological friendly.

2. *Experimental work*

In the frame of the experimental work the process of cold forward extrusion of a cylinder from the copper alloy CuCrZr was analysed. This is a copper-chrome-zirconium alloy with high electrical and thermal conductivity and excellent mechanical and physical properties also at elevated temperatures. It is used as electrode material in spot, seam and butt resistance welding of low carbon steel sheets. Further it is used for manufacture of various components for resistance welding equipment.

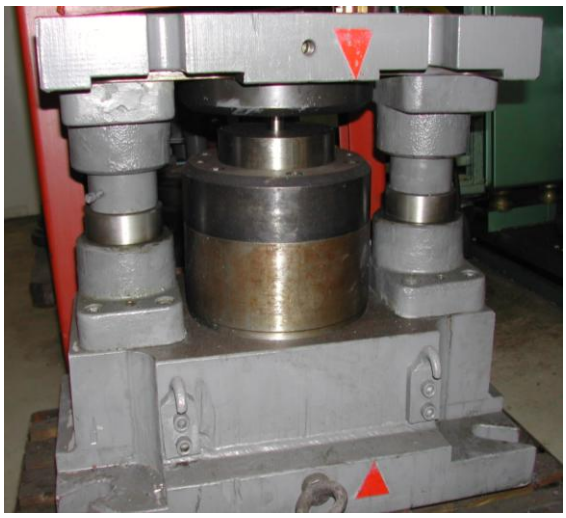

Fig. 1. *Experimental tool for cold forward extrusion*

The cylinders of dimension Φ22 mm x 32 mm were extruded in a special tool for forward extrusion (Fig.1) at 20°C temperature and four different lubricants coefficients of friction (μ = 0,05, 0,07, 0,11 and 0,16). The effective strain was in all cases ε_e = 1, 29. The measurements of coefficient of friction for each of the four different lubricants were carried out by using the ring-compression test. It is a very simple test. There is no need for load measurement or knowledge of material yield stress. This test is most suitable for processes with low effective strains. A ring-shaped billet is compressed by two plates in several increments. Deformation of diameter and height is measured after each increment [15]. Friction is evaluated by comparing obtained results (curve) with friction calibration curves given in literature [16, 17, 18, 19]. Increasing friction presents increasing resistance to free expansion of the ring, resulting in a decrease of the ring internal diameter (Fig. 2).

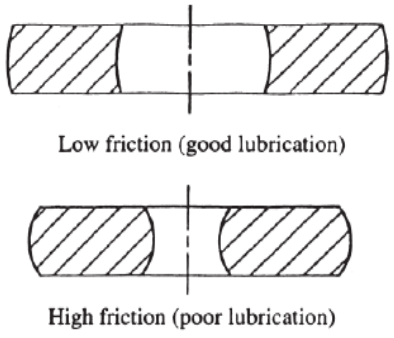

Fig. 2: *Effect of friction on metal flow during the ring compression test [17]*

Thus lubricants can be ranked simply by measuring the change in internal diameter and height of the ring. For each lubricant three ring tests were performed and then average values of coefficients of friction were calculated. The results of the ring-compression test for all four lubricants gave us these average values:

- Lubricant No. 1 (oil) μ = 0, 05
- Lubricant No. 2 (oil) μ = 0, 07
- Lubricant No .3 (oil) μ = 0, 11
- Lubricant No. 4 (grease) μ = 0, 16

To determine the influence of the coefficient of friction on mechanical and electrical properties of cold forward extruded specimens, tensile tests, Brinell hardness measurements and electrical conductivity measurements were carried out.

Tensile strength, yield stress, reduction of area and elongation were determined with the tensile tests. Brinell hardness was measured by using the measuring instrument WPM, electrical conductivity of extruded specimens was measured by the Sigmatest instrument. Many experiments were done to provide reliable results.

3. *Results and discussion*

The diagrams on the Fig. 3 and Fig. 4 present the change of tensile strength R_m, yield stress $R_{p0,2}$, reduction of area Z and elongation A_5 as a function of lubrication friction factor μ at the constant tool speed v_{tool} = 12 mm/s. The results at different coefficients of friction are very similar but the difference between them range from 2% to 7%.

Although this difference in mechanical properties could be of importance in some specific cases, in general it is possible to say that the value of lubricant's coefficient of friction does not affects significantly the measured mechanical properties of the cold extruded alloy. Of course this conclusion can be made only for lubricant friction factor interval from μ= 0, 05 to 0, 16.

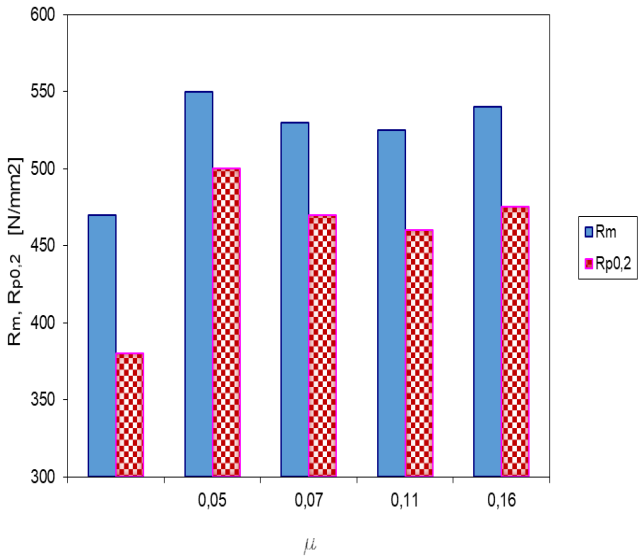

Fig. 3. *Influence of lubricant's friction coefficient μ on tensile strength (R_m) and yield stress ($R_{p0,2}$)*

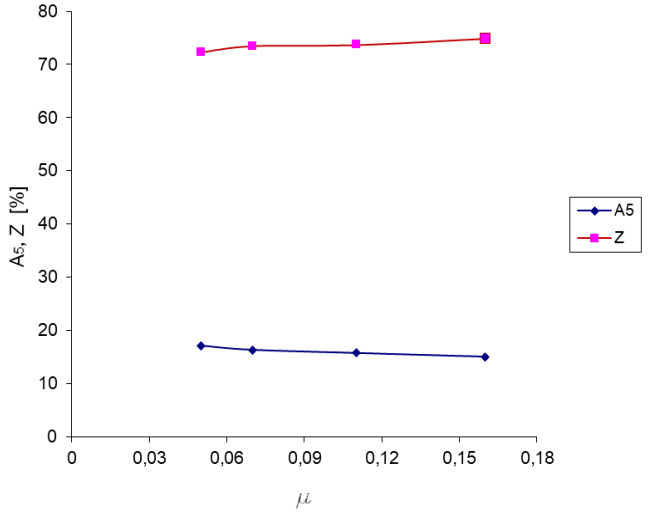

Fig. 4. *Influence of coefficient of friction μ on reduction of area (Z) and elongation A_5*

If we compare the results for tensile stress R_m and yield stress $R_{p0,2}$ measured at different values of coefficient of friction very interesting thing can be observed. By using lubricator with the lowest coefficient of friction (μ = for lubricator Nr.1) the highest tensile strengths and yield stresses were measured. With increasing coefficient of friction (μ= 0, 07 and) both, tensile and yield stress decreases, although insignificantly. The biggest difference in yield stress measurement was obtained when we compared results for lubricant's coefficient of friction μ= 0, 05 and μ= 0, 11. The yield stress measured at μ= 0, 11 was 7% lower compared to yield stress at μ= 0, 05. We could expect a further decrease of both stresses when using lubricant with the highest value of coefficient of friction (μ= 0, 16). But tensile strength and yield stress increase for about 2% to 4% compared with stress values when lower coefficient of friction was used.

The same phenomenon can be observed with elongation A_5 and reduction of area Z on Fig. 4. But the change of values for elongation and reduction of area measured at different coefficients of friction is even smaller (less than 4%) than the change of tensile strength and yield stress.

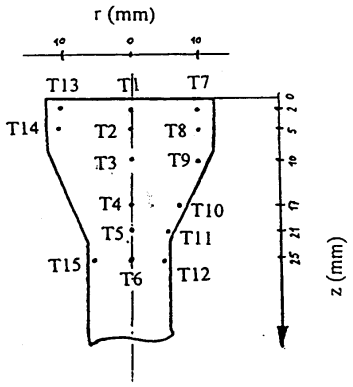

Fig. 5. *Measuring points for Brinell hardness*

By means of Brinell hardness measurements in several measuring points of the cold extruded part (Fig. 5), it was possible to determine the influence of the strain and lubricants coefficient of friction factor on the hardness. Fig. 5 presents the measuring points on the extruded alloy CuCrZr.

Fig. 6 shows the influence of lubricant friction factor to Brinell hardness of the extruded alloy, measured at points according to Fig. 5.

According to diagram on Fig. 6 the influence of lubricant friction factor on Brinell hardness has no big importance but it is obvious that with increasing coefficient of friction there is an increase of hardness (especially in measuring points T1, T3 and T5, which are all in the middle axis of the specimen) although this increase is relatively small.

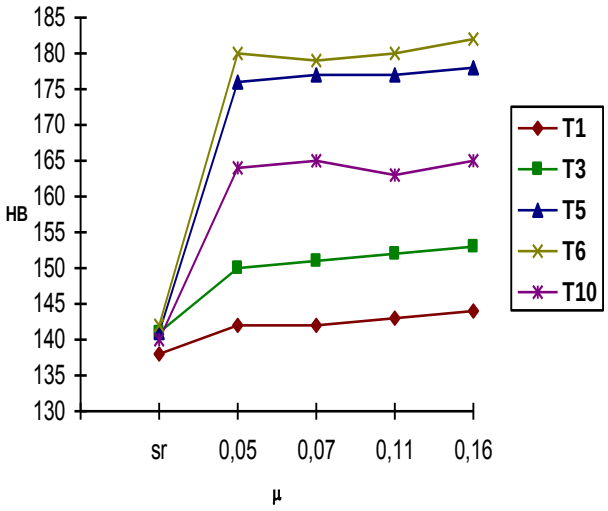

Fig. 6. *Brinell hardness HB measured in different points T as a function of lubricant's coefficient of friction μ (sr. = unformed alloy)*

The differences between values of Brinell hardness in the same measuring point of the extruded alloy but at different lubricant coefficients of friction μ are less than 4%. Of course, this conclusion can be made only for lubricant's coefficients friction interval from μ = 0,05 to 0,16.

Measurement of the electric conductivity was performed on the cylinders taken from the root of the cold extruded alloy. Dimension of these cylinders was Φ 11mm x 16mm and the conductivity was measured by special Sigmatest instrument with measuring frequency of 120 kHz. Many measurements were done to provide reliable measuring results of electric conductivity. The influence of coefficient of friction on the electrical conductivity of the cold extruded material is presented in Fig. 7.

Electrical conductivity is decreasing with higher strain. When measured on the specimen which was extruded with lubricant's coefficient of friction μ = 0,05, the electrical conductivity is about 20% lower than the electrical conductivity of unformed material (0 on x-axis in the Fig. 7). It is obvious that the electrical conductivity increases with increased lubricant's coefficient of friction, the difference between electrical conductivity values when using smallest (μ = 0,05) and highest (μ = 0,16) coefficient of friction is less than 6 %.

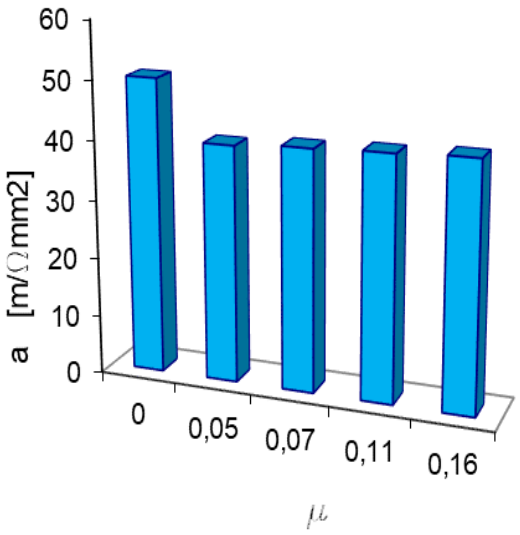

Fig. 7. *Effect of coefficients of friction on electrical conductivity a of the extruded specimens (No. 0 on x-axis represents the value of unformed alloy)*

4. Conclusion

Friction is a very important parameter in all metal forming processes. It affects in unfavourable way all main process parameters and product quality. The magnitude of friction needs to be known for several reasons. Pressures, forces and energy requirements can be calculated only if interface conditions can be described by shear strength or friction factor. For this, a numerical value must be established. In most cases reduction of friction by lubrication has a beneficial effect by lowering the forces required for a given operation. This reduces the stresses imposed on tooling and may allow the use of smaller and less costly equipment. Effective lubrication can also improve product quality by eliminating surface defects such as scoring or cracking through the reduction of metal-to-metal contact and avoiding harmful residual stresses and internal defects through promoting more homogeneous deformation conditions.

The values of lubricant's coefficient of friction can also have effects on the material properties during and after forming process. Although this influence is in general not very significant, it could be of importance when very precise information of mechanical and other properties of the extruded specimen is necessary.

One of the reasons for small difference in measured mechanical properties when using different lubricators with different coefficients of friction could be the fact that we have done our experiments with lubricants with rather low coefficients of friction. By using lubricants with higher coefficients of friction, the influence on the mechanical and electrical properties of the formed material could be more significant.

5. References

[1] R. Velu, M. R. Cecil: Quantifying Interfacial Friction in Cold Forming using Forward Rod Backward Cup Extrusion Test, Journal of The Institution of Engineers (India), Series C, Volume 93, Issue 2, pp 157–161, 2012

[2] K. Lange: Handbook of Metal Forming, McGraw Hill Book Company, New York 1998, Chapter 6;

[3] Qi Zhang, M. Arentoft, St. Bruschi, L. Dubar, E. Felder: Measurement of friction in a cold extrusion operation: Study by numerical simulation of four friction tests, LaMCoS, INSA de Lyon. 11th ESAFORM Conference on Material Forming, April 2008, Lyon, pp. 1267- 1270, 2008

[4] P. Tiernan, M.T. Hillery, B. Draganescu, M. Gheorghe: Modelling of cold extrusion with experimental verification, Journal on Materials Processing Technology 168, pp. 360–366; 2005

[5] I. Anzel, L. Gusel: *Forming processes*, University of Maribor, Faculty of Mechanical, Engineering, Maribor, 2005,

[6] R.S. Takhautdinov, R.T. Latypov, S.Yu. Spirin, A.I. Antipenko et. al.: Efficient new lubrication technologies for the production of cold - rolled sheet; Metallurgist, Vol. 45, 5-6, pp. 241 – 244, 2001

[7] M. Gariety, G. Ngaile, T. Altan: Evaluation of new cold forging lubricants without zinc phosphate precoat. Int. J. Mach. Tools Manuf **47**, pp. 673–681, 2007

[8] R. Ebrahimi, A. Najafizadeh: A new method of evaluation of friction in bulk metal forming. J. Mater. Process. Technol. **152**, pp. 136–143, 2004

[9] H.R. Le, M.P.F. Sutcliffe: The effect of surface deformation on lubrication and oxide scale fracture in cold metal rolling; Metallurgical and Materials Transections B, Vol. 35, pp. 919-928, 2005

[10] H. Yamin, L. Zhoui, Z. Yucheng: The study of cup-rod combined extrusion processes of magnesium alloys, J. Mater. Process. Tech. 187–188, pp. 649–652, 2007

[11] M. B. Hanamantraygouda. M.B, B. P. Shivakumar, S. B. Halesh, P. N. Siddappa, D. Chethan, S. H. Prashant: Numerical Analysis of Cold Forging Effect on Mechanical Properties of Al/Sic Metal Matrix Composites, IOSR Journal of Mechanical and Civil Engineering (IOSR-JMCE) Volume 14, Issue 1, Ver. VII, pp. 26-35, 2017

[12] S. Prüntea, D. Music, J. M. Schneider: Decreasing friction during Al cold forming using a nanomolecular layer, Journal of Vacuum Science & Technology A: Vacuum, Surfaces, and Films, Volume 35, Issue 2, pp. 1-5, 2017

[13] J. Padgurskasa, R. Rukuizaa, I. Prosyčevasb, R. Kreivaitis: Tribological properties of lubricant additives of Fe, Cu and Co nanoparticles, Tribology International, Volume 60, April 2013, pp. 224-232, 2013.

[14] N. Gil Azevedo, J. Sá Farias, R. Pereira Bastos, P. Teixeira, J. P. Davim, R. J. Alves de Sousa: Lubrication Aspects during Single Point Incremental Forming for Steel and Aluminum Materials, International Journal of precision engineering and manufacturing Vol. 16, No. 3, pp. 1-7, 2015

[15] M. Plančak, Z. Car, M. Kršulja, D. Vilotić, I. Kačmarčik, D. Movrin: Possibilities to measure contact friction in bulk metal forming, Tehnički vjesnik 19, 4, pp. 727-734, 2012

[16] H. Sofuoglu, J. Rasty: On the measurement of friction coefficient utilizing the ring compression test. Tribology International, Vol. 32, pp. 327-335, 1999.

[17] R. K. Ohdar, P. Talukdar, M. I. Equbal: Evaluation of friction coefficient of 38MnVS6 medium carbon micro-alloyed steel in hot forging process by using ring compression test, Technology Letters, Vol. 2, No. 3, pp. 12-16, 2015.

[18] L. Gusel, I. Anzel, M. Brezocnik: (2005), Effect of lubrication on the stress distribution in an extruded material, International Journal of Advanced Manufacturing Technology, Vol. 25; pp. 288 – 291, 2005

[19] V. Marušić, I. Opačak, B. Nedić, D. Jovanović, G. Rozing: Investigation of the tribological characteristics of the stainless steel x20cr13, Innovations in engineering 2016 - 2nd Scientific Congress, Proceedings, XXIV, Vol. 15/201, Varna, Bulgaria, pp. 26-28, 2016.

INFORMATION - CALCULATION METHOD FOR ENERGY EFFICIENCY RADIANT HEATING SYSTEMS IN INDUSTRIAL PREMISES

Hristozov Daniel Eng. [1], Madzharova St. Asst. Prof PhD., Eng.[1], Bozukov N. Prof. PhD, Eng[1], Petrova T. Assoc. Prof. PhD[2], Bakalov I. Asst. Prof. PhD[2],
Dept. of Informatics and Statistics, Faculty of Economics, University of Food Technologies, Plovdiv, Bulgaria[1]
Food Research and Development Institute - Plovdiv, Plovdiv, Bulgaria[2]
d_hristozov@uft-plovdiv.bg, nitani@abv.bg[1], bozukovnanko@abv.bg[1], dorrapetrova@abv.bg[2], ivvanbakalov@abv.bg[2],

Abstract: *The paper considers a model and an algorithm for predicting the thermal regime in work (home) accommodation with radiant heating. The algorithm allows the analysis and design of cost-efficient option for realization of this type of heating.*

Keywords: INFORMATION-CALCULATION METHOD, ENERGY EFFICIENCY, RADIANT HEATING SYSTEM

1. Introduction

Temperature, relative humidity, air mobility in the occupied areas, the surface temperature of the surrounding building elements, and the temperature of the equipment in the facility prove essential to the flow of vital processes in the human body.

The multifactor system determining the thermal conditions is the basis for choosing a heating system of the manufacturing facilities. Serious attention should be paid to all these factors, since not only the quality and functioning of the equipment situated in the production room depends on this, but also has an impact on the effectiveness of workers who spend most of their time indoors.

Constant temperature of the air in the manufacturing facilities is usually needed, without radical changes which could have a negative impact on the installed equipment and the employees. It is also necessary to take into account regulatory requirements in terms of explosion and fire safety. The production facilities themselves usually occupy a considerable area, on which the different production or technical equipment is installed. Ceiling height is not small, which creates additional difficulties when choosing a suitable heating system.

2. Solutions for radiant heating

The use of radiant heating allows the obtaining of better results in the heating of production premises with respect to the uniformity of the temperature distribution of air in the vertical and horizontal [1]. The increased surface temperature of the surrounding elements allows the maintenance of a lower air temperature while preserving the thermal comfort of the workers. With these, the heating is via infrared heat energy radiated from emitters situated directly above the work area. By reflectors, this energy is directed to the heated area, while both the air and the surrounding surfaces are heated. Part of the indicated advantages of radiant heating also includes the short period necessary to achieve thermal comfort. In radiant heating with radiating bands is advisable to bear in mind that they are not recommended for premises, which are expected to accommodate high equipment and bulk materials. They are considered very inappropriate for low premises.

Infrared emitters can work with gas or electricity. Depending on the surface temperature there are light and dark emitters.

High temperature tubular heaters are also considered very appropriate for production halls. The heating fixture consists of a bundle of tubes coated with heat-insulated tin jacket. The number of tubes in a bundle can vary, and it is typically from 2 to 6, and their diameter usually ranges from 180 to 600 mm. Their length is determined depending on the shape and dimensions of the room.

The heating is by direct combustion of gas or diesel. The emitted flue gases are disposed outside the premise. In practice, systems with recirculation or direct current systems are used in heating of premises with high temperature piping.

Sizing of heating systems

Heating systems are sized for indoor air according to design regulations. These parameters are determined on the basis of a set of hygienic and economic considerations. Thermal comfort is defined by temperature conditions satisfying the occupants of the room. It cannot be unequivocally that is why, permissible temperature conditions are admitted, which underline in the basic methodologies for calculating HVAC (heating, ventilation and air conditioning) systems [2].

An important point in the sizing of the heating system is the determination of heat losses. It is customary to calculate them in stationary conditions of constant temperatures, the characteristic of structural elements, etc. In their determination it is necessary to take into account the fact whether the heating will be with or without interruption.

It should be kept in mind that the operation of heating systems is associated with high costs, formed mainly from energy consumption.

It is recommended even at the design phase to take measures to reduce them. Among the possible measures are to allow for good thermal insulation of buildings; regeneration and recuperation of the heat of the exhaust air; choice of secure system for automatic regulation and others.

3. Research method and results

The idea is to develop an approximate mathematical model of the complex heat and mass transfer processes occurring in a room with radiant heating and ventilation. The mathematical model constitutes a system of equations for the air and heat balance in the specific volume and the surrounding surfaces of the room. The site is a production room, in which a radiant heating system is installed, without other heat sources. The heat flows from the radiating sources are: convective currents which are located in the top part of the room and give warmth to the interior walls and radiant component. The interior surfaces transfer heat by convection and radiation in the closed premises. Part of the heat is lost by transmission through the outer wall of the building.

The air is fed in the direction of the work service area in quantity M_{nr} and is given to the upper area with an expenditure $M_b = M_{nr}$. At the level of the upper work service area the expenditure of air in the stream is M_{str}. The increase of air flow is due to air circulation, which constitutes a drop in the flow. The cross-border flows are shown by dashed lines in figure 1. The calculated volumes are chosen: region (an area with a constant

presence of people); the volume of the supplied air flow and the wall convective flows. The direction of the wall convective flows depends on the ratio of the temperature of the inner and outer surfaces and the ambient air.

The air temperature in the service area t_{wz} is formed by mixing the air from the air flow for heating, the wall convective flows and the convective heat from the inner surfaces of the floors and the walls. In reporting the developed scheme for heat exchange and circulation of air flow (figure 2, 3) the algorithm is drawn for calculating the heat and air balance for the given volume.

The air flow in the range [4], defined by the convective flow is:

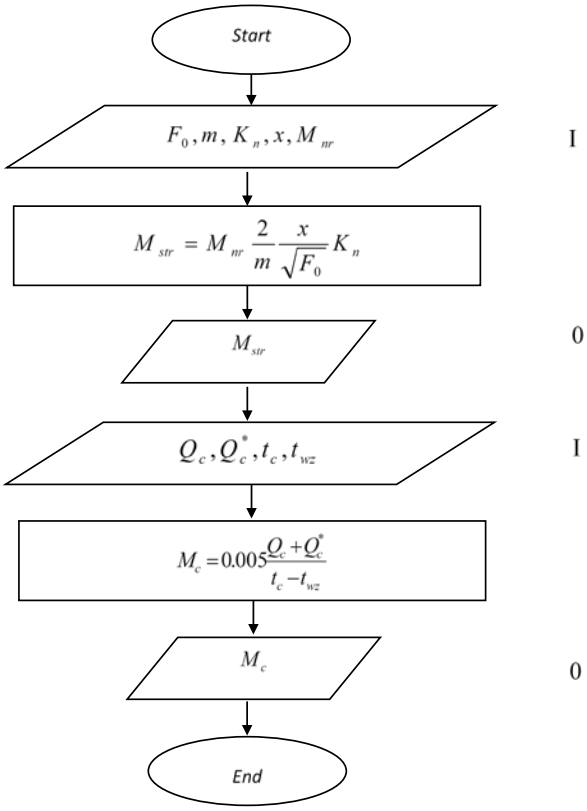

Figure 2

m - damping ratio

F_0 - section of the inlet air-distributing diffusers, [m^2]

x - the distance from the diffuser to the point of basic service area, [m]

t_c - temperature of the inner surface of the external wall, [^{0}C]

c - specific heat capacity, [J/(kg.°C)]

Q – power of the gas radiant system, [W]

Q_c и Q_c^* - convective heat transfer from the inner surfaces of the walls in the service area, and of the wall above the service area, [W]

t_{str}, t_c, t_{wz} - air temperature in the inflow into the work area in the wall convective flows and work area, [^{0}C]

Q_{mn} - heat loss in the room, [W] (equal to the amount of heat loss through the building envelope).

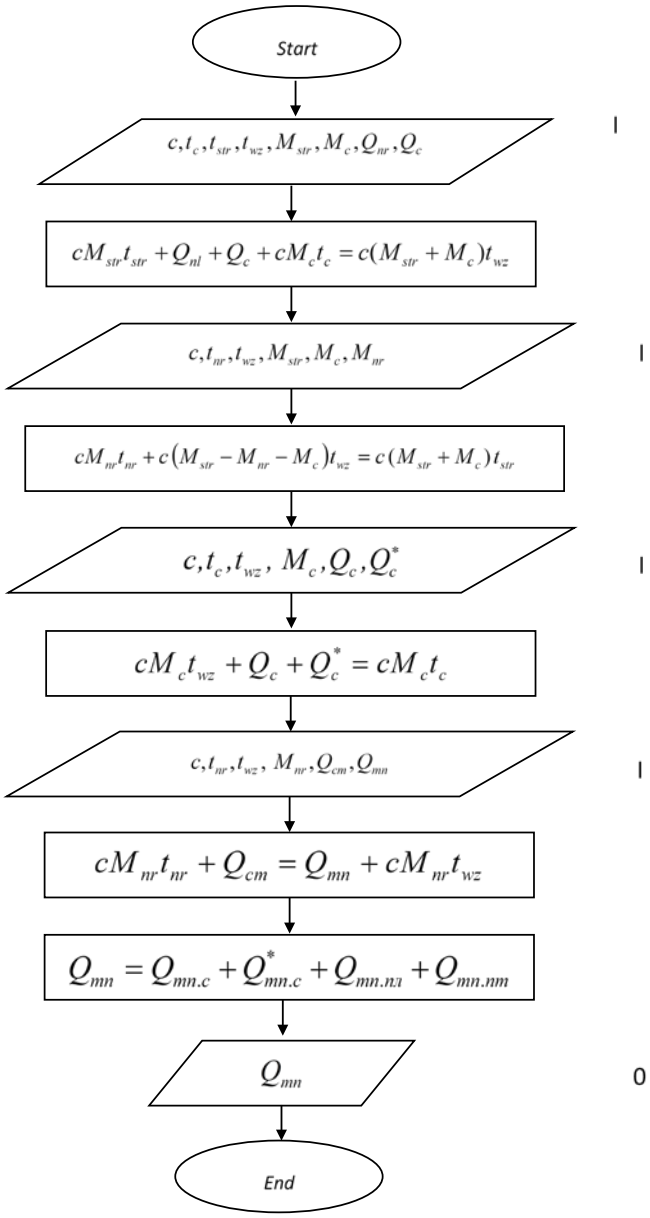

Figure 3

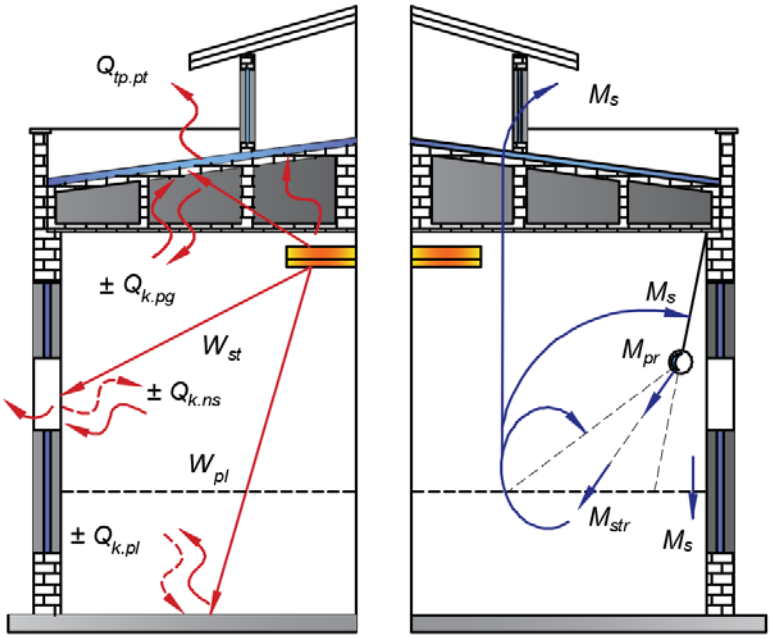

Figure 1

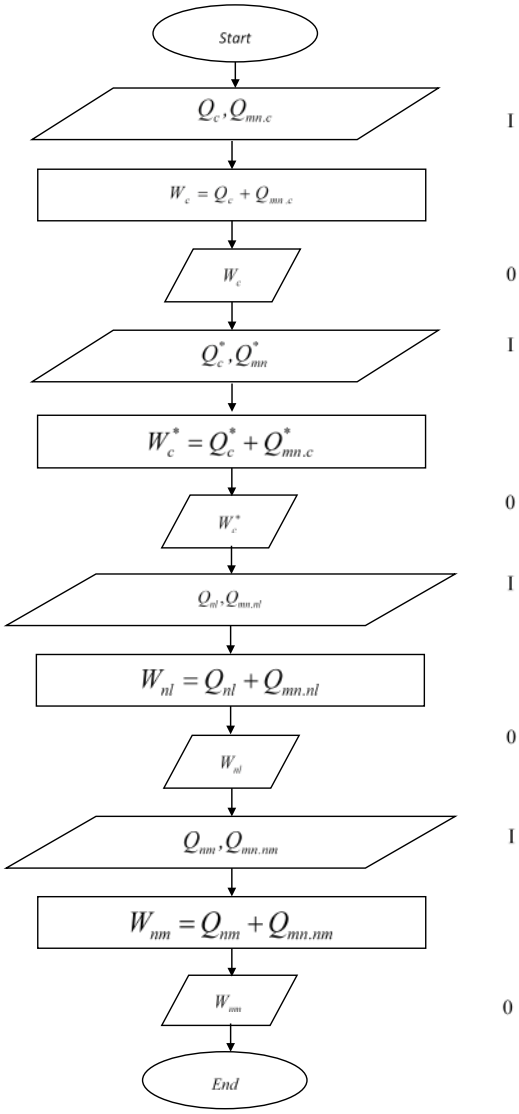

Figure 4

Q_c, Q_c^*, Q_{nl} и Q_{nm} - convective heat transfer from the inner surfaces into the service area - walls over the service area, the floor and the surrounding walls, respectively, $Q_{mn.c}$, $Q_{mn.c}^*$, $Q_{mn.nl}$, $Q_{mn.nm}$, - heat losses from the relevant structures, W_c, W_c^*, W_{nl} и W_{nm} - radiant heat flows from the source flowing into these surfaces.

Convective heat loss is determined by:

$$Q_j = m_j F_j \Delta t_j^{4/3}, \qquad (1)$$

m_j - factor determining the direction of heat flow with reference to surfaces, F_j - surface area, [m^2], Δt_j - temperature differential between the environment and the surfaces, [^{0}C], j - index indicates the type of surfaces.

Heat loss can be expressed through:

$$Q_{mj} = F_j \frac{\tau_j - t_н}{R + R_н}, \qquad (2)$$

$t_н$ - outside air temperature, [^{0}C], t_j - the temperature of the inner surfaces of the outer walls, [^{0}C], R и $R_н$ - resistances of heat transfer, [m^{2}K/W].

The radiant heat flow from the source of radiation W_j at an arbitrary orientation of the radiating system and the surrounding surfaces is calculated by:

$$W_j = c_0 \varepsilon_{ij} H_{ij} \left[\left(\frac{T_i}{100} \right)^4 - \left(\frac{T_j}{100} \right)^4 \right], \qquad (3)$$

c_0 - emission ratio of blackbody, [W/(m^2 K^4)], ε_{ij} - degree of blackness, H_{ij} - area of the radiating surfaces, [m^2].

The solutions of the resulting mathematical models of the processes of heat and mass transfer [3] under the joint action of radiant heating and ventilation allow the obtaining of basic characteristics of the thermal regime in the design of systems for radiant heating of various buildings equipped with ventilation systems.

4. Conclusion

Heating systems with infrared emitters are the preferred solution for heating of premises in which organic dust or fire hazardous aerosols are not emitted.

They are recommended for buildings with low thermal insulation and for heating of separate areas in unheated premises. Among their advantages are small heat inertia, the ability to operate in the mode of a general or zone heating, economical operation, the ability to heat open areas, high reliability and easy maintenance.

Their disadvantages are mostly related to the high temperature of the radiating plate, the need of ventilation for removal of waste products from the combustion in using gas emitters. It should be kept in mind that it is not recommended to install infrared emitters in premises with increased fire hazard and in areas where there are materials which under the influence of infrared radiation modify their properties.

References

1. Банхиди А. (1985) Лучистое отопление. А. Банхиди, Л. Мачкаши -М .: Стройиздат, pp. 464
2. Григорьев В.А. (1988) Теоретические основы теплотехники/ В. А. Григорьев, В. М. Зорин// Справочник.- М.: Энергоатомиздат, pp. 560
3. Джалурия Й. (1983) Естественная конвекция/ Й. Джалурия// Тепло- и массообомен. -М: Мир, pp. 399
4. Наумейко А.В., П.В. Кузнецов, Ю.И. Толстова, Р.Н. Шумилов (2003). Энергоэффективные системы отопления: Учебное пособие. Екатеринбург

ВИРТУАЛНО ПРЕДПРИЯТИЕ ЗА ПРОИЗВОДСТВО НА ДЕЙТАЛИ ЧРЕЗ ШПРИЦВАНЕ

VIRTUAL ENTERPRISE FOR THE PRODUCTION THROUGH INJECTION MOLDING

Associate prof. Pavel Vitliemov PhD
Faculty of Business and Management – University of Ruse Angel Kanchev, Ruse, Bulgaria
pvitliemov@uni-ruse.bg

***Abstract**: The paper presents the virtual enterprise as an organizational form that provides opportunity for increased competitiveness through co-operation between organizations representing key knowledge, skills and technology for the productions of products. The structure and organization of virtual enterprise for the production through injection molding is described.*

Keywords: VIRTUAL ENTERPRISE, INJECTION MOLDING, PRODUCTION

1. Увод

Засилените процеси на глобализация на икономиката и пазарите, наблюдавани през последните години с развитието на информационните технологии и бързият темп на технологични иновации, както и постоянно изменящите се предпочитания и потребности на клиентите създават непрестанно изменяща се и силно конкурентна външна среда за предприятията. В условията на несигурност и нестабилност за организациите е от решаващо значение да бъдат гъвкави и адаптивни към новите условия, а постигането на конкурентоспособност все повече зависи от развитието на знанията и иновациите в рамките на предприятието. Това се налага поради все по-засилената конкуренция, скъсяването на жизненият цикъл на продукта и нарастващото търсене на иновативни изделия – фактори, изискващи бърз темп на технологични иновации при разработването на нови продукти, с които да се отговори на изискванията на клиентите и предизвикателствата, поставени от конкурентите.

Създаването на нови продукти, достигащи бързо до пазара с минимална себестойност, изисква интегриране на знания и технологии с висока стойност, които често предприятието не притежава. Това обстоятелство спомага за развитието на нов вид сътрудничество и изграждането на т.нар. мрежи за сътрудничество. Благодарение на мрежите за сътрудничество се развива широка разновидност от организационни форми, среди които и виртуалните предприятия- обект на настоящата разработка. Виртуалното предприятие интегрира принципите на подвижното производство, свързвайки ключови знания, умения и компетенции, притежавани от участниците за създаване на продукти въз основа на сътрудничество и споделяне на ресурси и технологии.

Иновативността на концепцията за виртуалното предприятие, предоставяща му предимство пред традиционното предприятие, лежи в отличителните му характеристики, а именно на организационна форма, основана на сътрудничество въз основа на знания и технологии, притежаваща гъвкава и адаптивна структура, в рамките на която се споделят знания, умения, технологии, ресурси, разходи и печалба за създаването на конкурентоспособни продукти в динамични и силно променливи пазарни и икономически условия.

2. Същност и характеристики на виртуалното предприятие

Съставянето на единно определение на термина "виртуално предприятие" се превръща в продължителна тема на дискусия както в академичната среда, така и в практическата сфера [9] още от момента на зараждането на концепцията. До момента не съществува единно прието определение в научните среди на термина „виртуално предприятие“ (който в зависимост от областта на приложение и литературният източник се среща и като *виртуална компания, виртуална корпорация, виртуална фабрика, виртуално производство* и т.н. [5]).

Някои автори дори твърдят, че виртуалното предприятие (ВП) не представлява новост като организационна форма, а като стратегическа насоченост [7]. Характерните особености на концепцията за виртуалното предприятие, които го различават от традиционната организация и допринасят за иновативността на концепцията могат да се обобщят както следва:

1) Динамика на пренастройване на мрежата от предприятия – темп на преразпределение с цел постигане на конкурентоспособност в динамичен и непредсказуем пазар, т.е. гъвкавост и подвижност;

2) Виртуалност;

3) Външни обекти (други предприятия) като помощна среда, която подпомага интегрирането на виртуалното предприятие [9].

Според други автори [5] поне два подхода са в основата за съставяне на определение на виртуалното предприятие:

1. Първият подход определя като най-важна характеристика на концепцията за виртуалното предприятие динамичната мрежова свързаност на фирмите.

2. Вторият подход подчертава виртуалността на обединението от предприятия като по-голямо общо цяло, което "не съществува реално (физически), но изглежда реално чрез помощта на софтуер" (Oxford Dictionary).

Според първият подход, мрежите от предприятия са в основата на модела на виртуалното предприятие. Идеята за виртуалното предприятие като динамична мрежа от предприятия идва от трудовете на Питър Дракър [5]. Проблемът при съставянето на определение до известна степен лежи в термина "виртуален" [9] и неговото интерпретиране от авторите [5].

На база различни публикации, свързани с виртуалните организации може да се посочат следните общи характеристики на виртуалното предприятие:

- временно мрежово обединение на независими предприятия и специалисти;
- сътрудничество между партньорите-виртуалното предприятие се формира за да се възползва от обединението на ключови умения, компетенции и ресурси, притежавани от група от предприятия, които си сътрудничат за да се възползват от конкретна пазарна възможност, която не биха могли да оползотворят самостоятелно;
- гъвкава организационна структура - използват се общи ресурси, активи, помещения, фабрики и складове. Виртуалното предприятие не притежава собствен персонал, а управлението се извършва от екип, съставен от служители от участващите предприятия. Предприятията могат да се включат и да напуснат ВП по всяко време;
- гъвкавост и адаптивност на организацията към външните условия;
- приложение на информационни технологии за организация и управление на процесите;
- фокус върху основната цел или проект;
- споделяне на умения, разходи, печалба, риск и пазар;
- географска дисперсираност на участниците;

- временен характер на организацията – виртуалното предприятие съществува докато съществува конкретната пазарна възможност;

- едноличност и разпознаваемост - за клиента виртуалното предприятие е единично, самостоятелно предприятие без значение, че в действителност представлява съдружие от предприятия [3;6;7;8].

3. Организация на виртуалното предприятие

При създаване на организационния модел на виртуалното предприятие голямо значение се отдава на определяне на главен координиращ орган. Възприети са два подхода- йерархичен подход, при който координиращ орган става един от участниците, и нейерархичен подход, при който ролята на координиращ орган се възприема от съвет, съставен от участващите в рамките на виртуалното предприятие организации. При йерархичният подход, показан на фиг.1, едно от участващите предприятия възприема ролята на главно предприятие, т.е. вид координиращ център, който осъществява връзката между виртуалната организация и външната среда. Това предприятие отговаря за разпределението на необходимите ресурси, осигуряване на условия за работа и производствените резултати. Този подход е характерен за високотехнологични производства [4].

Фиг.1 *Йерархичен подход на организация на виртуалното предприятие.*

Нейерархичният подход, показан на фиг. 2, се състои в създаването на съвет, в който участват всички съставящи виртуалното предприятие организации. Административните и организационни функции се прехвърлят на съвета, който координира и определя начина на създаване на виртуалното предприятие и неговата функционалност. Този подход се използва при стандартно производство при наличието на варианти за алтернативно производство на продукта и възможност за поръчки през интернет [4].

И при двата подхода координационният орган отговаря за създаване и използване на обща система от стандарти и механизми за вътрешна и външна координация и сътрудничество [4].

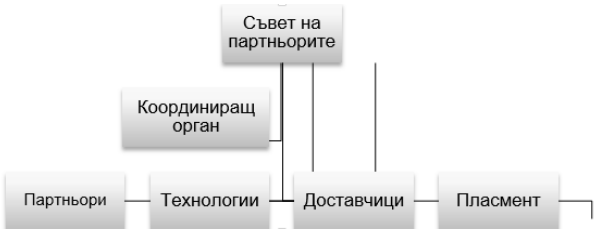

Фиг.2 *Нейерархичен подход на организация на виртуалното предприятие*

Разработването на система за управление на виртуалното предприятие се усложнява от особеностите, характерни за виртуалното предприятие, като например: необходимостта от гъвкавост на управлението и структурата, високата степен на сложност на изпълнение на задачите и процесите, вследствие от участието на няколко предприятия, наличието на множество източници на информация, които трябва да бъдат синхронизирани в реално време [5].

При организацията на виртуалното предприятие трябва да се решат следните задачи:

- определяне на бизнес-процесите с помощта на методологии за комплексно моделиране на процеси;

- разработване на динамична система с помощта на методи за решаване на задачи;

- анализ на ефективността на получените модели [4].

4. Структура и организация на виртуално предприятие за производство на детайли от пластмаса чрез шприцване

Според Reid [10] създаването на виртуалното предприятие преминава през шест стъпки (фиг.3):

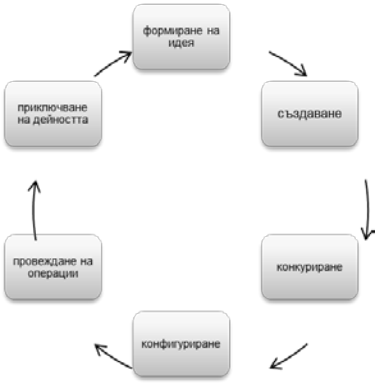

Фиг.3 *Стъпки за създаване на виртуално предприятие*

1) Идеята за виртуалното предприятие се *формира* когато пазара предостави определена възможност. При тази стъпка е необходимо разбиране на нуждите и очакванията на клиентите и необходимите за задоволяването им дейности. Изгражда се визия за предприятието, което ще може да задоволи възникналите потребности и се изгражда стратегия за формиране на новото предприятие. Тази стъпка се разглежда като концептуално проектиране на виртуалното предприятие и може да бъде извършена от индивидуална фирма или съществуващо виртуално предприятие;

2) На този етап фирмите, създаващи виртуалното предприятие развиват и внедряват нови или подобрени процеси и системи за да се подготвят за следващия етап на цикъла. Основните задачи включват създаване на подробен проект за новото виртуално предприятие и пълна подготовка за изпълнението по проекта;

3) Предприятието може да предложи нови или алтернативни решения на съвременните потребителски нужди или да намери и реализира конкретна възможност за да произведе и достави продукта си. Друг вариант е привличането на нови клиенти за съществуващи продукти;

4) Придобиване на активи, умения, компетенции и инфраструктура, които се използват за постигане на целите на предприятието. Всички придобити активи, знания и умения за процесите се използват за създаването на проектираният продукт;

5) Производство, доставка и сервиз на продукта;

6) Приключване на дейността когато поставените цели бъдат постигнати като се прекъсва връзката между участващите предприятия и се връщат придобитите активи [10].

Създаденото виртуално предприятие ще се реализира с краткосрочна структура, която позволява основната дейност да бъде разделена на отделни проекти и задачи, които да бъдат разпределени за изпълнение между участниците.

В конкретният случай, необходимите основни дейности за производство на детайли от пластмаса са както следва:

- създаване на прототип на детайла;

- проектиране на шприцформа за производството на детайла;

- създаване на прототип на проектираната шприцформа;

- изпълнение на проекта за шприцформа - физическо производство на формата;

- производство на детайлите.

За краткосрочната структура на виртуалното предприятие е характерно, че е необходимо само някои или част от дейностите да бъдат извършвани с помощта на паралелното проектиране. По-голямата част от необходимите задачи могат да се изпълнят с несъгласувани съвместни дейности (асинхронно).

Най-подходяща форма на организация за конкретното виртуално предприятие е базираната върху йерархичния подход. Във виртуалното предприятие ще участват четири предприятия, както е показано на фиг. 4:

Фиг. 4 *Организация на виртуално предприятие за производство на детайли чрез шприцване, базирана на йерархичният подход на организация.*

1) Главното предприятие е с основна роля за координацията между дейностите, извършвани от останалите участници. Освен координиране на процесите, ръководна дейност и контрол на изпълняваните от другите предприятия задачи, ще отговаря за анализ на пазара и пазарните възможности, както и за привличане на клиенти.

2) Задачите на Партньор 2 ще обхващат дейностите по изготвяне на проект за щприцформа за производство на детайла. Проектните данни за шприцформата ще бъдат предоставени от Главното предприятие. След създаване на проекта за инструменталната екипировка, той ще бъде изпратен на Партньор 1 за изготвяне на прототип. След одобряване на прототипа от Главното предприятие, задачата на Партньор 2 ще бъде реализирането на проектираната вече шприцформа, т.е. нейното производство.

3) Партньор 1 ще разработи прототип на подходяща шприцформа чрез технологията за бързо прототипиране въз основа на създаденият от Партньор 2 проект. Другата задача на Партньор 1 ще бъде изготвяне на прототип на продукта, отново чрез използване на технологията за бързо прототипиране.

4) Задачите на Партньор 3 ще включват фактическото производство на продукта чрез технологичният процес шприцване чрез впръскване на разтопен термопластичен полимер в изготвената от Партньор 2 шприцформа.

Информационното осигуряване на виртуалното предприятие ще се извърши посредством т.нар. Cloud-технологии (Cloud Computing). „Cloud computing“ е модел за предоставяне на удобен достъп при поискване до споделени конфигурируеми компютърни ресурси (например мрежи, сървъри, пространство за съхранение, приложения и услуги). “Cloud computing” услугите са платформи или инфраструктури, които позволяват изпълнение на код (услуги, приложения и др.) по управляван и еластичен начин [2]. „Cloud computing“ технологиите ще позволят визуализиране на протичащите в реално време процеси във виртуалната организация, предоставяйки информация на участниците и възможност за по-ефективна координационна дейност на главното предприятие.

Заключение

При прилаганите до сега технологии на проектиране, новите продукти се въвеждат на пазара чрез цикъла „Техническа подготовка – производство – продажба” [1]. Този цикъл нараства във времето със сложността на продуктите, а за постигане на конкурентно предимство в съвременните динамични пазарни условия е от решаващо значение новите продукти да бъдат проектирани и произвеждани бързо. Тези предпоставки, а и все по-взискателните клиентски изисквания променят условията, при които се внедряват нови продукти - посоченият по-горе цикъл „Техническа подготовка – производство – продажба” се замества от нов цикъл „Конструиране – продажба – производство” [1]. Конструирането (проектирането) на продукта и ролята на създаването на прототип придобиват все по-голяма важност от гледна точка на успешното реализиране на продукта на пазара.

Създаването на прототип е от значима полза както за производителите, така и за клиентите. Прототипирането намалява броя на итерациите по създаването на продуктите, като спомага за избягване на допълнителни разходи, а също и за покриване на специфицираните от клиента характеристики без последващи корекции. Създаването на бърз прототип на шприцформата ще намали разходите и времето на всички етапи по подготовката, разработването и производството на продукта. Разработването на бърз прототип на формата не само спестява времето, което би било необходимо за нейното създаване по конвенционалните методи, но и дава възможност за изчистване и коригиране на проектни грешки още преди производството на шприцформата. Това създава голямо предимство на виртуалното предприятие, тъй като разходите по изработване на инструментална екипировка по традиционните методи са значителни и евентуални корекции след създаването на формата биха довели до допълнителни разходи, а също така и до забавяне при реализиране на продукта на пазара. Паралелното и съвместно разработване на задачите по създаването и производството на продукта между участниците във виртуалното предприятие допринася за намаляване на необходимото време от създаването на концептуалният дизайн до стартиране на фактическото производство. Съвместната работа и възможността всички извършвани дейности и задачи да бъдат видими за участниците в реално време създава предпоставки за по-ефективно сътрудничество и по-бързо и точно изпълнение на поставените задачи.

Виртуалното предприятие обединява за времето на съществуването си знанията, уменията, технологиите и компетенциите, притежавани от участващите в него предприятия, като по този начин създава предпоставки за разработване на иновативни продукти, които отделните участващи фирми не биха могли да разработят самостоятелно.

Споделянето на разходи, ресурси и технологии води до синергичен ефект и постигане на по-ефективно и печелившо производство от това в традиционната компания, където не само разходите, но и риска се поема изцяло от една фирма. В границите на виртуалното предприятие се създава възможност за оптимизиране на избора на ресурси, производствена технология и производствена база, а също така и планиране на най-ниски разходи за производство.

Литература

1. ВИТЛИЕМОВ П.,Обновяване на бизнес процесите,записки Иновационен мениджмънт, РУ „Ангел Кънчев“, 2011;

2. ЕМАНУИЛОВ И.,Правни аспекти на “cloud computing” услугите. Проблеми на договорите между доставчици и потребители и защита на данните в „облака“, сп. „Съвременно право“ бр.2, 2011;

3. ТАШЕВ А.,Т. ГИГОВА, Визия за виртуалната компания в началото на 21 век, Journal of the Technical University at

Plovdiv“Fundamental Sciences and Applications”,Vol.13(9),Anniversary Scientific Conference’2006BULGARIA, 2006

4. ШАТОХИН М.А.,Основы построения организационно-функьиональной модели управления виртуальными предприятиями,в-к „Машиностроения“ бр. 1,2008

5. CUNHA M.M., GORAN PUTNIK, Agile Virtual Enterprises:Implementation and Management Support. Idea Group Inc. p.36-42, 2006;

6. GOEL A., HEINZ SCHMIDT, GILBERT DAVID, Formal Models Of Virtual Enterprise Architecture: Motivations And Approaches.RMIT University, Melbourne, Australia;

7. HALES, K. R. and J R BARKER, Searching for the Virtual Enterprise, 2000;

8. PETERSEN S. A., RAO JINGHAI, TVEIT AMUND, Virtual Enterprises: Challenges in Selecting and Integrating Computational and Human Resources. Norwegian University of Science & Technology Trondheim, 2002;

9. PUTNIK G., MARIA MANUELA CUNHA– Virtual Enterprise Integration: Technological and Organizational Perspectives, p.3-9, 2005;

10. REID R. LEIGH & K.J.ROGERS, MARY E. JOHNSON, and DONALD H. LILES – Engineering the Virtual Enterprise, 1996.

MATHEMATICAL MODELING OF ENERGY INTEGRATED ATAD SYSTEM FOR THEIR SUSTAINABILITY IMPROVEMENT

МАТЕМАТИЧНО МОДЕЛИРАНЕ НА ЕНЕРГИЙНО ИНТЕГРИРАНА ATAD СИСТЕМА ЗА ПОДОБРЯВАНЕ НА НЕЙНАТА УСТОЙЧИВОСТ

Prof. Dr. Vaklieva-Bancheva N. G., Assist. Prof. Dr. Vladova R. K., Assist. Prof. Dr. Kirilova E. G.

Institute of Chemical Engineering at Bulgarian Academy of Sciences,
Sofia, Bulgaria

vaklieva@bas.bg, raika_vladova@abv.bg, eshopova@gmail.com

Abstract: *Autothermal Thermophilic Aerobic Digestion (ATAD) is a technology for municipal waste water treatment where Class A Biosolids is produced. ATAD systems characteristic with the simplicity of the process, the higher reaction rate and smaller bioreactors. Systematic observations carried out on conventional ATAD systems have shown that their major disadvantage is the thermal shock that occurs in first bioreactors stages due to uncertainties regarding to the quantities, composition and temperatures of the incoming into the system raw sludge. This study focuses on opportunities for the thermal shock reduction in conventional ATAD system through recovery the heat from the effluent stream. It can lead to substantial savings of the time required for operating temperature recovery and quicker bio-degradation. To reduce the impact of the stochastic parameters and to ensure efficient using of the waste heat for the sustainable operation of the ATAD system, two mathematical models of energy integration with one and two heat storage tanks are proposed which will be suitable to be involved in a stochastic optimization framework.*

Keywords: MODELING, ENERGY INTEGRATION, HEAT STORAGE TANKS, ATAD WWTP, UNCERTAINTIES

1. Introduction

Autothermal Thermophylic Aerobic Digestion (ATAD) is a novel technology for wastewater treatment. It uses aerobic microorganisms with exothermic energy metabolism. Conventional ATAD processes (Fig. 1) take place in parallel series of two batch bioreactors where the wastewater is treated at different temperatures with aeration and mixing for 20-24 hours.

Fig. 1. *Conventional ATAD system (source Fuchs Gas- und Wassertechnik GmbH web page)*

Once per day part of the treated sludge from the last bioreactors is discharged to “a product” storage. Then the partially treated wastewater from the previous stage is displaced to the next one and the system is fed with the fresh sludge from the feed tank. The required operational temperature for the bioreactors from the first stage is around 55°C, which is optimal for bacterial growth, while for the second one it is ~65°C – which is the best one for pasteurization.

The process of biochemical oxidation of organic substance results in releasing of energy in the form of heat, water, carbon dioxide, ammonia and etc. Heat retention within the system leads to increasing the operating temperature and increasing the rate of degradation of volatile organic as well as killing the pathogenic microorganisms. ATAD systems benefit by the simplicity of the process, a higher reaction rate and consequently smaller bioreactors. Main problems in ATAD facilities arise during loading each new portion of raw sludge which leads to a sharp decline in temperature in the first stage bioreactors. The latter provokes a thermal shock (TSk) on the thermophilic microorganisms resulting in a decrease in the operating temperatures in the first bioreactor and often in the second bioreactor stage; prolongs treatment process and increases energy consumption for mixing and aeration. Depth of the thermal shock depends on variety of parameters that are subjected to daily uncertainties such as the volumes and temperatures of loaded raw sludge, ambient temperature, sludge properties etc. Due to the thermal shock the reactors from the first stage usually operate at about and below 50°C.

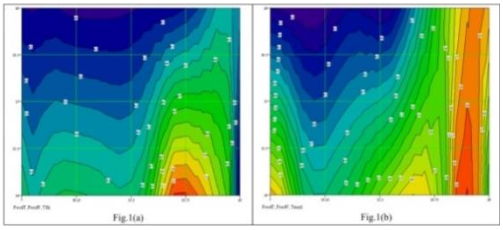

Fig. 2. *Depth of the TSk (2a) and maximal temperatures achieved at the end of the process (2b) in bioreactors from the first stage depending on the temperature and quantity of loaded fresh sludge.*

Reduction of the temperature drop in the first bioreactor and its impact on the microorganisms can improve the energy efficiency of ATAD systems and lead to more sustainable operating temperatures in the bioreactors. Having in mind that heat production and its retention into the system have a great importance for the ATAD process many researchers have analyzed the possibilities for energy efficiency improvement of ATAD systems.

Firstly, Layden et al. have found that re-using the heat released with outgoing from the ATAD system end product can reduce the fluctuations of the operating temperatures in the first bioreactors stages [1]. Based on this idea, Zhelev et al. have proved that this heat has a sufficient energy potential which can be used for preheating the raw sludge [2], [3]. It was proved that substantial

quantity of low grade heat at the exit of the second-stage bioreactors, under certain conditions could be used for preheating the fresh sludge supplied to the first one. Recovery and utilisation of this heat is obstructed by the fact that the system operates in a batch mode and the streams candidates for heat integration are shifted in time.

The aim of this study is development of an approach for the thermal shock reduction in conventional ATAD system. To ensure efficient using of the waste heat for the sustainable operation of the ATAD system, two mathematical models of energy integration with one and two heat storage tanks are proposed which will be suitable to be involved in a stochastic optimization framework.

2. Mathematical description of the process of energy integration of streams in the ATAD system with one heat storage tank

In 1993, Ivanov et al. [4] have proposed a method for heat integration of the flows outgoing in different time intervals from two, hot and cold, batch reactors by using one heat storage tank. We have implemented this method in the conventional two-stage ATAD system with two series (*A* and *B*) of bioreactors. The heat integration framework is shown in Fig. 3, [4]. Its general purpose is to integrate hot flows that appear during partial discharge of hot stabilized and pasteurized sludge from the second stage bioreactors - *2-A* or *2-B,* with the cold ones, appearing during loading of the raw sludge to the first stage bioreactors, *1-A* or *1-B*. Service, (loading and discharging) of each series is independent of each other.

The proposed heat integration scheme comprises two heat exchangers: *HE-c* for preheating the cold sludge, incoming from the feed tank toward *1-A* or *1-B,* and *HE-h* – for cooling the hot stabilized sludge discharged from the bioreactors *2-A* or *2-B* and as well as one heat storage tank. Intermediate fluid storing in the heat storage tank plays the role of heating or cooling agent at different time intervals. During loading the bioreactors *1-A* or *1-B,* the intermediate fluid stored as a hot agent in the heat storage tank, passes through *HE-c*, preheats the cold sludge, cools and returns back to it. Due to mixing the hot and cold intermediate fluids in the storage tank, the heat exchange in both *HE-c*, and the heat storage tank, is unsteady state. Accordingly, during discharging *2-A* or *2-B,* the cooled intermediate fluid, which is already placed into the heat storage tank, is used in *HE-h* for cooling the hot stabilized sludge, outgoing from the bioreactors *2-A* or *2-B*. This process is also unsteady state. Two sludge pumps transport the flows from the feed tank and bioreactors *2-A* or *2-B* toward corresponding heat exchangers, while the transport of heating/cooling intermediate fluid from the heat storage tank toward corresponding heat exchangers is carried out by one regular pump.

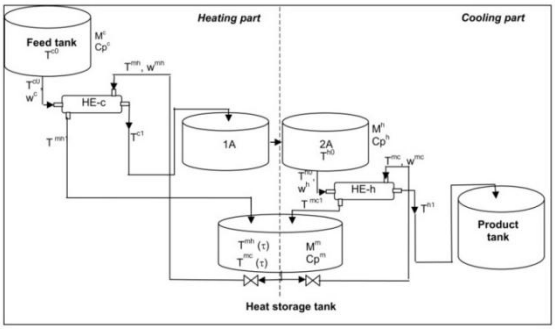

Fig. 3*. Heat integration framework of batch ATAD system using one heat storage.*

Mathematical model of the proposed scheme includes the following equations:

$$(1)\quad T^{c1}(\tau^c) = T^{c0} + [T^{mh}(\tau^c) - T^{c0}]R^c\Phi e^c,$$

$$(2)\quad T^{mh1}(\tau^c) = T^{mh}(\tau^c) - \left[T^{mh}(\tau^c) - T^{c0}\right]\Phi e^c,$$

$$(3)\quad T^{mh}(\tau^c) = T^{c0} + \left(T^{mh0} - T^{c0}\right)\exp(-G^{mh}\Phi e^c\tau^c),$$

$$(4)\quad T^{h1}(\tau^h) = T^{h0} - \left(T^{h0} - T^{mc}(\tau^h)\right)\Phi e^h,$$

$$(5)\quad T^{mc1}(\tau^h) = T^{mc}(\tau^h) + \left(T^{h0} - T^{mc}(\tau^h)\right)R^h\Phi e^h,$$

$$(6)\quad T^{mc}(\tau^h) = T^{h0} + \left(T^{mc0} - T^{h0}\right)\exp\left(-R^h\Phi e^h G^{mc}\tau^h\right)$$

(1-6) determine the temperatures of the inputs and outputs of the respective heat exchangers at the end of the energy integration of the streams in the ATAD system as well as the equations

$$(7)\quad T^{mh0} = \frac{b^{22} + b^{12}b^{21}}{1 - b^{11}b^{21}};\quad T^{mc0} = \frac{b^{12} - b^{11}b^{22}}{1 - b^{11}b^{21}}$$

to determine the initial temperatures in the heat storage tank at which it began to play the role of "hot" or "cold" respectively. The model is supplemented with constraints providing the feasibility of the heat exchange in the heat exchangers:

$$(8)\quad \Delta T^c \geq \Delta T^{\min}$$

$$(9)\quad \Delta T^h \geq \Delta T^{\min},$$

where ΔT^c and ΔT^h are minimal temperature differences at the end of heat integration process for heat exchangers *HE-c* and *HE-h*. The temperatures values obtained by the model allow to determine ΔT^c and ΔT^h. There are equal to the smaller temperature difference at the end of the heat exchangers:

$$(10)\quad \Delta T^c = \min\left\{\left(T^{mh1}(\tau^c) - T^{c0}\right),\ \left(T^{mh}(\tau^c) - T^{c1}(\tau^c)\right)\right\}$$

$$(11)\quad \Delta T^h = \min\left\{\left(T^{h0} - T^{mc1}(\tau^h)\right),\ \left(T^{h1}(\tau^h) - T^{mc}(\tau^h)\right)\right\}$$

3. Mathematical modeling of heat integrated ATAD system with one intermediate heating/cooling fluid and two heat storage tanks.

The proposed model of heat integrated ATAD system consists of a common intermediate heating/cooling fluid and two heat storage tanks, called *"H-Storage"* for heat and *"C-Storage"* for cold and two heat exchangers *HE-c* to heat cold fluid and *HE-h* to cool hot one, Fig. 4 [5].

At the beginning of the integration process, before loading the bioreactor 1-A(B), the cold sludge income into the heat exchanger *HE-c* with initial temperature T^{c0} [^{0}C]. It is heated counter-currently by the intermediate fluid coming from *"H-Storage"* tank, with an initial temperature T_m^{h0} [^{0}C] and leaves the heat exchanger with temperature T^{c1} [^{0}C]. After heat exchange the cooled intermediate fluid goes in the *"C-Storage"*. At the end of the integration process τ_c [h] the temperature in the cold storage tank becomes T_m^{c0} [^{0}C]. Likewise, the hot "product" with an initial temperature T^{h1} [^{0}C] passes through the heat exchanger *HE-h* and it is cooled by the intermediate fluid coming from the *"C-Storage",* with an initial temperature T_m^{c0} [^{0}C]. Then the cooled "end product" leaves *HE-h* with final temperature T^{h1} [^{0}C].The intermediate fluid

is stored in *"H-Storage"* and at the end of the integration process τ_h [h] the temperature in the hot storage is T_m^{h0} [^{0}C].

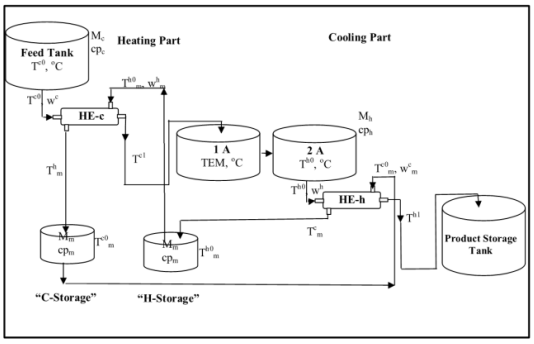

***Fig. 4**. Heat integration framework using two heat storage tanks.*

Determination of the temperatures at inputs and outputs of both heat exchangers at the end on the integration process τ_c and τ_h is represented by the following equations:

$$(13)\quad T^{c1} = T^{c0} + (T_m^{h0} - T^{c0})R^c \Phi e^c,$$

$$(14)\quad T_m^h = T_m^{h0} - (T^{h0} - T_m^{c0})\Phi e^c,$$

$$(15)\quad T^{h1} = T^{h0} - (T^{h0} - T_m^{c0})\Phi e^h,$$

$$(16)\quad T_m^c = T_m^{c0} + (T^{h0} - T_m^{c0})R^h \Phi e^h.$$

where T_m^h [^{0}C] is the final temperature of cooled hot intermediate fluid in *HE-c;*

T^{h1} [^{0}C] and T_m^c [^{0}C] are the final temperatures of cooled "end" product and heated intermediate fluid in *HE-h.*

The terms used in equations (13) and (14) are following:

$$R^c = \frac{w_m^h cp_m}{w_c cp_c};\ w_c = \frac{M_c}{\tau_c};\ w_m^h = \frac{M_m}{\tau_c}\ \text{[kg/s];}$$

$$\Phi e^c = \frac{1-\exp(-y_c U_c A_c)}{1-R^c \exp(-y_c U_c A_c)};$$

$$y_c = \frac{1}{w_m^h cp_m} - \frac{1}{w_c cp_c}$$

M_c and M_h are the masses of the cold sludge and hot "end product", M_m is the mass of the intermediate fluid in [kg] and A_c and A_h are the heat exchanger areas of *HE-c* and *HE-h* in [m^2]. The initial temperatures T_m^{h0} [^{0}C] and T_m^{c0} [^{0}C] in the "hot" and "cold" heat storage tanks calculate as follows:

$$(17)\quad R_m^{h0} = \frac{\Phi e^c (R^h \Phi e^h - 1)T^{c0} - R^h \Phi e^h T^{h0}}{(R^h \Phi e^h - 1)(\Phi e^c - 1) - 1}$$

$$(18)\quad T_m^{c0} = \frac{(\Phi e^c - 1)R^h \Phi e^h T^{h0} - \Phi e^c T^{c0}}{(R^h \Phi e^h - 1)(\Phi e^c - 1) - 1}$$

Thus, at given integration times τ_c and τ_h [h] initial temperatures T_m^{h0} and T_m^{c0} [^{0}C] and the values of A_c, M_c, A_h, M_m, the temperatures at the inputs and outputs of both heat exchangers can be exactly calculated using the model (13)-(18).

4. Conclusions

The study deals with the problems of energy efficiency and sustainability improvement of the ATAD system for municipal wastewater treatment operating under uncertainties. For that purpose two mathematical models of heat integrated ATAD system with one heat storage tank and two heat storage tanks are presented.

Acknowledgement:

The study has been carried out by the financial support of National Science Fund, Ministry of Education and Science of the Republic of Bulgaria, Contract № ДН07-14/15.12.16.

References

[1] Layden, N.M., (2007). *An Evolution of Authotermal Thermophilic Aerobic Digestion (ATAD) of Municipal Sludge in Ireland*, J. Environ. Eng. Sci., 6(1), 2007, pp. 19-29.

[2] Zhelev, T., Vaklieva-Bancheva, N., Jamniczky-Kaszás, D., (2008). *About Energy Efficiency Improvement of Autothermal Thermophilic Aerobic Digestion Processes*, Comput. Aided Chem. Eng., 25, 2008, pp. 1-6.

[3] Zhelev, T., Vaklieva-Bancheva, N., Rojas-Hernandes, J., Pembroke, T., (2009). *"Smelly" Pinch, Proceedings of the 10th International Symposium on Process Systems Engineering: Part A.* Comput. Aided Chem. Eng., 27, 2009, pp. 933-938.

[4] *B. Ivanov, K. Peneva, N. Bancheva,* Heat Integration in Batch Reactors Operating in Different Time Intervals. Part II. A Hot-Cold Reactor Systems with a Common Storage Tank, *Hungarian Journal of Industrial Chemistry*, Volume 21, 1993, pp. 209-216.

[5] Gomez, J., de Gracia, M., Ayesa, E., Garcia-Heras, J. L. *Mathematical Modeling of Autothermal Thermophilic Aerobic Digesters*, Wat. Res., 41(5), 2007, pp. 959-968.

НОРМАТИВНА УРЕДБА В РЕПУБЛИКА БЪЛГАРИЯ СВЪРЗАНА С КИБЕРСИГУРНОСТТА ПРИ ИНДУСТРИЯ 4.0

LEGAL REGULATION IN THE REPUBLIC OF BULGARIA RELATED TO THE CYBERSECURITY IN INDUSTRY 4.0

Дочева М., доц. д-р Цокев А.
Машинно-технологичен факултет, Технически Университет-София, София, България
maria.docheva@ict-academy.bg, alextz@tu-sofia.bg

Abstract: *We have started the new fourth step in the industrial revolutions hence labelled "Industry 4.0". The ubiquitous use of smart sensors, intelligent robots, wired and wireless networking, cloud technologies, big-data, smart robots and AI have transformed the manufacturing processes. Some of the most important challenges in this model are the IT security issues, related to communication, Internet access and the use of IoT devices in "Industry 4.0". A variety of technologies, algorithms, protocols and devices are currently available and are developed to secure the specific security IT needs of "Industry 4.0", and they form the engineering part of the solution. On the other hand, the local legal regulation for each country is very important. This paper considers the current state of the Bulgarian laws and implemented EU directives which are related to the cybersecurity field in "Industry 4.0".*

Keywords: INDUSTRY 4.0, CYBERSECURITY, LEGAL REGULATION, EU DIRECTIVES

1. Въведение

Концепцията „Индустрия 4.0“ описва достигнатото ниво на индустриално развитие и в частност посочва, че успешно преминахме прага на четвъртата индустриална революция. Включването на актуални информационни и комуникационни технологии (ИКТ) в този модел дава възможност за увеличаване на гъвкавостта, повишаване на качеството, намаляване на разходите и стратегическо предимство пред компаниите, които са го интегрирали.

Основните технологии, на които се базира концепцията „Индустрия 4.0“ са обобщени на фиг. 1.

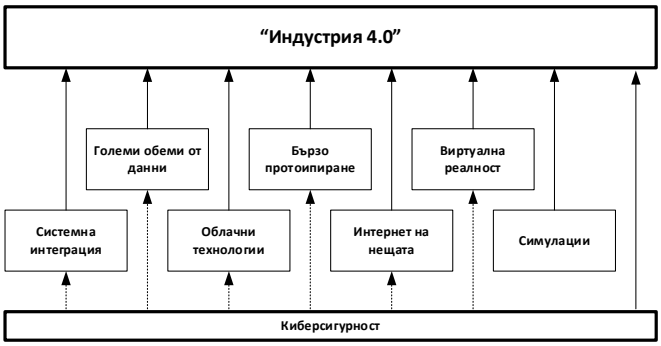

Фиг. 1 Основни технологии, включени в концепцията „Индустрия 4.0“

От фиг. 1 ясно се вижда и значимата роля на ИКТ. За облачните технологии, интернет на нещата (IoT), системната интеграция и от части симулациите на процеси и виртуалната реалност може да се каже, че попадат под ударите на кибератаките, насочени към индустриални устройства и системи, които в последните месеци значително се увеличиха като брой, вид, извършители и чиято сложност значително нарасна. Анализът и превенцията от кибератаки изисква екип от специалисти, работещи в областта на ИКТ, както и на юристи, запознати в дълбочина с нормативната база на Република България, относима към киберзаплахите и киберсигуността, имащи отношение към подобен тип злонамерени действия. Също така е важно да се посочи, че това е изключително динамична област (от гледна точка на използваните технологии за атака и защита), но правната рамка в общия случай значително изостава.

В настоящата статия е направен кратък преглед на текущата правна рамка (законова и подзаконова) в Република България, имаща отношение към киберсигурността и в частност към „Индустрия 4.0“.

2. Атаки на индустриални системи

В проучване на Форбс [2], са посочени 5^{те} най-често атакувани сектора (индустрии) през 2016 година, а списъкът е следния:

1. Здравеопазване;
2. Производство;
3. Финансови институции;
4. Правителствени институции;
5. Транспорт.

В своята статия [2] авторът Майкъл Надау обобщава някои от прогнозите, свързани с кберсигурността при индустрията:

1. Годишният размер на загубите, нанесени на индустрията от киберпрестъпления през 2021 година се очаква да бъде около 6 трилиона USD. Това е увеличение с почти 100% от нивата през 2016 година;
2. За периода 2017 година до 2021 година се очаква да бъдат направени инвестиции в размер от над 1 трилион USD, които да са свързани с киберсигурността на индустриални компании и системи;
3. Броя на работните позиции, свързани с киберсигурност през 2021 година се очаква да достигне 2.3 милиона;
4. През 2022 година, кибератаките, насочени към индустрията ще оказват влияние върху повече от 6 милиарда жители в световен мащаб;
5. Зловредният код от тип "ransomware" ще донесе най-голям процент загуби на индустрията.

От горните прогнози, ясно се вижда, че към момента киберзаплахите и киберсигурността оказват и ще продължават да налагат значително влияние върху индустрията.

Друга интересна статистика е публикувана в специалния доклад за първото полугодие на 2017 година [3] от лидерът в комуникационните технологии Cisco Systems. Там е посочено, че около 46% от анализираните индустриални компании използват ИКТ решения на 6 или повече производителя, а 20% имат системи, разработени от повече от 10 производителя. Въпреки че това може да се разглежда като нормална тенденция, то погледнато от страна на киберсигурността е възможно да се предположи, че защитата на голям брой разнородни системи и модули значително се усложнява, което е предпоставка за неоткрити потенциални проблеми или

налични конфигурационни грешки (водещи до успешни злонамерени атаки). В същият доклад е посочена и друга сравнително тревожна цифра – приблизително 60% от компаниите, работещи в областта на производството посочват, че разполагат с по-малко от 30 служителя (специалисти), които да отговарят за киберсигурността.

Броят на целенасочените атаки към индустрията зачестява, както и се увеличава и дела на Advanced Persistent Threats (APT) – изключително сложни, имащи ясна цел и извършвани от добре подготвени и компетентни хакери зловредни действия, попадащи под наказателна отговорност в редица държави в световен мащаб.

Ако се направи кратко обобщение на горе написаното, от инженерна гледна точка може да се заключи, че увеличаването на използваните ИКТ при „Индустрия 4.0“ ще доведе до значително увеличаване и на броя на злонамерените атаки, насочени към индустриални компании, а към момента те рядко разполагат с подготвен персонал, който успешно и адекватно да може да противодейства на подобни атаки.

3. Преглед на нормативната уредба в Република България

Броят на неправомерни достъпи и дейности се увеличава поради бързото развитие и разширяването на обхвата на компютърните системи и интернет, както и приемането им в ежедневието на обществото. Обектите на атаки по целия свят са от национални и международни инфраструктури, правителствени, образователни и военни организации, малки и средни предприятия, както и компании, предлагащи интернет продукти и услуги, и техните потребители и това е една от причините, правораздавателните органи се сблъскват в борбата си с международните компютърни престъпления с едно от най-големите предизвикателства, а именно тяхната ефективна координация в разследването, предвид различните правораздавателни и съдебни системи.

През месец юни 2001 г. Европейският комитет по проблемите на престъпността прие на своето 50^{то} заседание окончателен проект на Конвенция за престъпления в кибернетичното пространство, която е първият международен договор за престъпления, извършени по Интернет и други компютърни мрежи. Тя регламентира главно правонарушенията, свързани с детската порнография, компютърната измама, авторските права, сигурността на мрежите. Основната цел на Конвенцията е постигането на „обща наказателна политика, насочена към закрила на обществото срещу кибернетичните престъпления, включително и чрез прилагане на съответното законодателство и поощряване на международното сътрудничество“ [5].

В съответствие с Конституцията на Република България, с Наказателно-процесуалния кодекс (НПК), със Закона за специалните разузнавателни средства, и с вътрешното си законодателство, нашата страна е направила допустимата резерва по чл. 14, ал. 3 на Конвенцията, че ще прилага разпоредбите, предвидени в чл. 20 от същата, а именно прихващане на данните за трафика на компютърните съобщения, само по отношение на тежките престъпления, така, както те са определени в българския Наказателен кодекс (НК).

Според разпоредбата на чл. 9, ал. 1 от НК „престъпление е това обществено опасно деяние (действие или бездействие), което е извършено виновно и е обявено от закона за наказуемо“, а в ал. 2 е предвидено, че „не е престъпно деянието, което макар формално и да осъществява признаците на предвидено в закона престъпление, поради своята малозначителност не е обществено-опасно или неговата обществена опасност е явно незначителна“ [6, 7].

С промените от 13.09.2002 г., публикувани в ДВ, бр. 92/2002 г., в НК бяха очертани отделните видове компютърни престъпления, които се съдържат в Глава 9 „а“ от НК. Освен компютърните престъпления, НК визира и престъпления, свързани с използването на компютър и други електронни устройства.

Тъй като обществото става все по-доверчиво и зависимо от компютърните мрежи и информационните потоци, движещи се по тях, както и от неизбежната нужда от автоматизирането на много дейности, се стига до увеличаване на възможността за нарушаване, манипулиране, разрушаване, унищожаване и кражба на данни, намиращи се и разпространяващи се в тези системи. Това от своя страна изисква наличието на адекватна правна рамка, която да осигури ефективна защита от престъпните действия, насочени към кибер пространството, които търпят постоянно развитие.

Съгласно чл. 23, ал. 1 от Правилник за функциите, задачите и организацията на работа на Съвета по сигурността при Министерския съвет, „министър-председателят определя национален координатор по киберсигурността, който координира дейностите по изпълнението на Националната стратегия за киберсигурност и плана за действие по киберсигурността и изпълнява други задачи, свързани с киберсигурността, съобразно правилата за функциониране на Националния киберситуационен център”. В следващата ал. 2 е предвидено, че „националният координатор по киберсигурността е съветник към политическия кабинет на министър-председателя“, а видно от ал. 3 той „организира Национален киберситуационен център, който се създава в Националния ситуационен център“. В последната ал. 4 е посочено, че „националният координатор по киберсигурността може да участва в заседанията на Съвета по сигурността по решение на председателя на съвета“.

В тази връзка е приета Национална стратегия по киберсигурност „Кибер устойчива България 2020” [6]. Тя предвижда създаването на Съвет по кибер устойчивост към Министерския съвет като нещатен постоянен консултативен орган. Той ще има основни направляващи и стратегически функции, които ще бъдат свързани с изработването и обосноваването на позицията на България пред международни институции и организации по въпросите на кибер сигурността

На следващо място в чл. 54 и чл. 55 от Раздел III „Информационна сигурност“ на **Закона за електронното управление** е регламентирано, че административните органи осигуряват информационната сигурност на използваните от тях информационни системи. Изискванията и стандартите за сигурност, на които трябва да отговарят информационните системи за въвеждане, изпращане, обработка, достъп, обмен, съхраняване и архивиране на данни, както и общите мерки за сигурност, които трябва да се предприемат от административните органи, се определят с наредба на Министерски съвет.

В чл. 60, ал. 1 от същия закон е регламентирано, че „председателят на Държавната агенция „Електронно управление“ упражнява контрол за спазване на изискванията за мрежова и информационна сигурност и оперативна съвместимост“, а съгласно ал. 2 той „може да осъществява проверки на информационната сигурност и оперативната съвместимост на определена информационна система или на предприетите от административния орган мерки чрез овластени от него лица и дава предписания за подобряването им”.

От 1 януари 2018 г. страната ни ще председателства „Хоризонтална група по кибер сигурност“, която е работен орган към Съвета на ЕС. Работната група ще разглежда предложение за ревизия на регламента за Европейската агенция за мрежова и информационна сигурност и сертификация на софтуерни продукти, както и ревизията на европейската стратегия за кибер сигурност [6, 7, 8].

4. ОРЗД и „Индустрия 4.0“

Концепцията „Индустрия 4.0“ изисква значителна промяна и дори преосмисляне на индустриалните процеси, инфраструктурата и обмяната на информация в рамките на индустриалната компания. При нея едни от основните ИКТ са облачните технологии, които налагат внимателен анализ и подсигуряване срещу неправомерен достъп до конфиденциални или лични данни.

Към момента в ЕС влиза в сила регламент (ЕС) 2016/679, свързан със защитата на физическите лица във връзка с обработването на личните данни и относно свободното движение на такива [4], позната като GDPR. Изискванията промени на този регламент са значителни и налагат специално внимание при тяхното внедряване, което се явява и добра възможност за начало на поетапно преминаване към „Индустрия 4.0“. Също така част от основополагащите технологии на концепцията имат пряко отношение към GDPR, например облачни технологии, големи обеми от данни, интернет на нещата и други.

5. Изводи

Концепцията „Индустрия 4.0“ обхваща редица актуални ИКТ, които се интегрират към производствените процеси. Именно тяхното приложение се явява както значително предимство, така и сериозен проблем, свързан със сигурността на информационните системи в индустриалната организация.

Проучване на Cisco Systems [3] показва, че процентът на индустриалните компании, използващи ИКТ на повече от 6 различни производителя надвишава 45%, което е сериозна пречка за изграждане на адекватна защита от все по-сложните целенасочени хакерски атаки, целящи кражба на информация или отказ на услуги.

При потенциален пробив в системите за сигурност, както и при доказване на такъв е необходимо да се предприемат стъпки, регламентирани в различни законови и подзаконови нормативни актове.

Правната уредба в РБ е необходимо да бъде изменена и допълнена, за да съответства на бързо развиващите се ИКТ. Националното ни законодателство следва да се актуализира, за да отговаря на промените на условията за сигурност, тъй като целите на все по-честите кибератаки са насочени към кражба на информация и нарушаване на правилната работа на информационните системи както към атакуваните индустриални сектори, така и към частната сфера. НК обхваща само малка част от компютърните престъпления и не може в пълна степен да предпази потребителите (ФЛ и ЮЛ) от множеството вредни последици от успешни (или дори само проведени) кибератаки.

В момента в ЕС се провеждат редица инициативи, свързани с разработване на нови актове, изменение и допълнение на съществуващи с цел гарантиране на електронната сигурност. Това е ясен показател за важността на киберсигурността при концепцията „Индустрия 4.0“.

Необходимо е да се търси мнението на специалисти от различни области, сред които инженери, юристи и икономисти, които да приложат законовите разпоредби в Република България и в ЕС с цел да се реализира адекватна защита срещу кибератаки насочени към компании интегрирали концепцията „Индустрия 4.0“.

6. Благодарности

Изследванията, свързани с настоящата работа, са финансирани по Договор № ДУНК-01/3 ”Създаване на Университетски научно-изследователски комплекс (УНИК) за иновации и трансфер на знания в областта на микро/нанотехнологии и материали, енергийната ефективност и виртуалното инженерство” между НИС при ТУ-София и Фонд „Научни изследвания”, МОН на РБ.

7. Използвана литература

1. “Top 5 Industries At Risk Of Cyber-Attacks” - https://www.forbes.com/sites/stevemorgan/2016/05/13/list-of-the-5-most-cyber-attacked-industries/#17219b35715e, последно посетен на 11.2017
2. “State of Cybercrime 2017: Security events decline, but not the impact’, https://www.csoonline.com/article/3211491/security/state-of-cybercrime-2017-security-events-decline-but-not-the-impact.html, последно посетен на 11.2017
3. “Cisco 2017 Mid-Year Cybersecurity Report” - https://www.cisco.com/c/en/us/products/security/security-reports.html, последно посетен на 11.2017.
4. “Регламент (ЕС) 2016/679 на Европейския парламент и на съвета от 27 април 2016 година” - http://eur-lex.europa.eu/legal-content/BG/TXT/PDF/?uri=CELEX:32016R0679&from=BG, последно посетен на 11.2017.
5. Национална стратегия по киберсигурност „Кибер устойчива България 2020” - http://www.cyberbg.eu, последно посетен на 11.2017.
6. http://www.government.bg/cgi-bin/e-cms/vis/vis.pl?s=001&p=0228&n=8393&g=, последно посетен на 11.2017.
7. http://www.government.bg/cgi-bin/e-cms/vis/vis.pl?s=001&p=0228&n=9710&g=, последно посетен на 11.2017.
8. Методики за разследване на престъпления, следствена практика, том II, НСлС, 2005 г.

COMPUTED TOMOGRAPHY IN FORENSIC RESEARCH

Ing. Kysela M.[1], Ing. Baburek E., PhD.[2], Ing. Kolar M.[1], Ing. Kolinova M., PhD.[1], prof. Ing. Richter A., CSc.[1]
[1]Technical University of Liberec, Liberec, Czech Republic, [2]EUROSEAL a. s., Liberec, Czech Republic
martin.kysela@tul.cz, evzen.baburek@euroseal.cz, matej.kolar@tul.cz, marcela.kolinova@tul.cz, ales.richter@tul.cz

Abstract: The paper is focused on using computed tomography in forensic research and the performance of computed microtomograph Skyscan 1272. Computed tomography due to its non-destructive analysis of the internal structure of materials can be applied in many fields. This method also provides information on the distribution of fillers, pores, fibers and defects in the tested sample and their 3D visualization using specialized software. Computed microtomograph Skyscan 1272 can be successfully used in forensic investigation of an attacked seals. For example, during unauthorized consumption of energy and water supply, in the tempering with security seals and a consequent theft, in logistics, in the transport of cargo and money, in the counterfeit goods (trademark protection, seals, stamps) etc. Computed tomography is able to verify and detect unauthorized tempering with the security seal, stamps and envelopes.

Key words: computed tomography (micro-CT), 3D visualization (3D model), forensic research, security components

1 Introduction

Computed tomography is a radiological examination method that allows displaying an internal structure of materials using x-ray radiation. CT can be translated into imaging in cuts, in other words displaying the structure without physical disruption of the whole. This method is currently widely used, for example in medicine, archeology, biology, geophysics and many other fields of science. It is based on a mathematical method known as tomographic reconstruction [1]. The resulting image quality is dependent not only on time the data are processes, but also on other factors. X-rays weaken while penetrating various materials. The degree of their absorption is either smaller or greater depending on the density of the material and depends mostly on the properties of the examined material.

This X-ray diagnostics can be successfully applied in forensic examination of a damaged seal in these situations:

- *Unauthorized access of energy and water grid* – deliberate attack of measuring instruments (water, electric and gas meters), damage to security seals (led, plastic, self-adhesive) in order to eliminate or limit measuring equipment and to illegally withdraw the medium.
- *Forensic science* – manipulation with security seals in order to enter into secured premises and subsequent theft.
- *Logistics, freight and money transfer* – manipulation with security seal in order to enter into secured premises and subsequent theft.
- *Hunting – manipulation with security seal for the purpose* of stealing the game, poaching (in the Czech Republic and in a number of European countries it is mandatory to mark the killed game by a seal with the number of a hunting association on whose territory the game was hunted down).
- *Product forgery* – brand protection, seals, stamps.

The aim of this article is to present particular equipment of the computer tomography Skyscan 1272 and demonstrate its utilization in the field of forensic science [2].

2 Methodology and means for solving the problem

Using computer tomography, we can easily and nondestructively visualize structures of the observed objects, such as composite materials, tissue, bones, spacer knitted fabric, non-woven textiles, biological materials etc. [4]

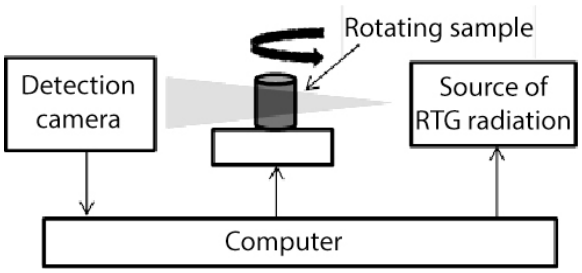

Fig. 1 The diagram of x-ray microtomography function

Figure 1 presents x-ray microtomograph function [4]. X-ray RTG imaging is achieved by the rotation of the tested sample and x-ray radiation emitted under various angles. CCD detection camera is localized opposite of the x-ray emitter. Thin stream passes through the sample and its intensity is detected and transferred into electrical

signals. X-rays weaken while passing through various materials. The degree of absorption is smaller or greater depending on the density of the material and depends mostly on the properties of the examined material [3]. Absorption represents the ability of various substances to absorb x-ray radiation. In case the emitted energy is constant, the absorption of x-ray radiation depends only on the material they pass through. The output of the tomograph is represented by 2D images (cuts).

This method can be used to check the material, localize defects and faults of the inner material structure, material density, relative content of components in different sections of the cut, pore or object distribution, visualization of the examined structures etc. [2].

2.1 Experimental technique

Desktop microtomograph Skyscan 1272 (fig. 2) contains an x-ray emitter with the output of 10 W max, 16 Mpx detection CCD camera, support to fix the sample and a computer terminal. The resolution of the device is 0.5 µm, maximum size of the tested material is 70 mm in diameter and 70 mm in length.

Method of testing the inner material structures is as follows:

Skyscan 1272 scans the object in the form of 2D images and transforms the object into 3D form using specialized software (reconstruction software NRecon). Obtained dataset and scanning results can be verified using program Dataviewer, allowing for detailed inspection of the inner structures of the tested sample from three axes – transaxial, sagittal and coronary. Part of the tomograph is also a software suite for complete 2D and 3D quantitative analysis, for morphometry (measurement of shapes) and densitometry (for the measurement of optical densities of the computed photographic images), for realistic 3D visualizations of the examined objects (creation of 3D models), etc. [4].

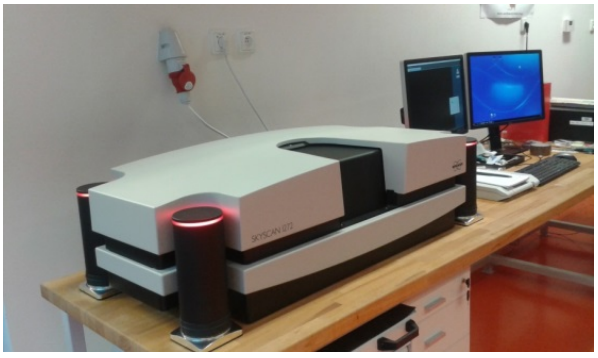

Fig. 2 Microtomographic device SkyScan 1272 including the workstation

2.2 Used materials and methods of measurement

Security components by the company Euroseal a. s. were used for the evaluation and visualization:

- indicative plastic seals of the PL type with wide range of use, manufactured from high quality plastic material,
- plastic seals of the ES type manufactured from high quality plastic material with the addition of metal collet,
- metal cable seals, with body made of aluminum and a seal sealed by metal cable,
- metal container seal made of high quality steel.

One group of security seals was modified in order for the sample dimension to correspond with the required parameters suitable for microtomograph Skyscan 1272. Samples were inserted into the scanner and fixed with rotational support. Scanning process was initiated after setting respective scanning parameters. After the scanning finalization, an obtained 2D dataset was transferred into 3D dataset using NRecon software. Such transformed data were further processed using Dataviewer and CTVox programs. Second group of the selected security seals was exposed to heat, mechanical or chemical deformation. Those damaged seals were scanned and the obtained data processed by special software. Plastic seals were subjected to temperatures of 185 °C and 120 °C or chemically deformed using technical petrol and polyoxymethylen, metal cable seals were mechanically strained by 1, 2, 3, and 4,4 kN. Several obtained images of the undamaged and damaged security seals are presented in the following chapter 4.2.

3 Results and discussion

3.1 Visualization of the undeformed security components

A. Plastic security seals of the PL type

Fig. 3 Plastic security seal of the PL 91 type

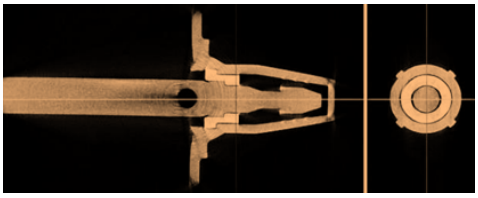

Fig. 4 Plastic security seals of the PL 95 type

Scanning parameters for the PL type security seals:

- ✓ X-ray voltage 50 kV, current 200 µA, resolution 20 µm, exposition 464 ms, scanning duration 35 minutes.

B. Plastic security seals of the ES type

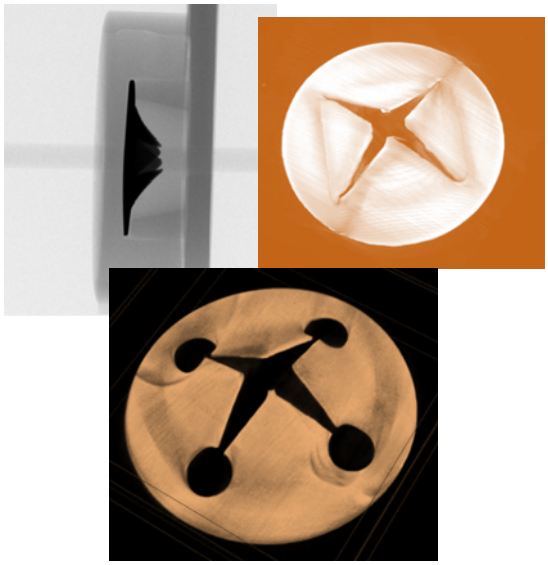

ig. 5 Sample of the plastic security seals of the ES type

Scanning parameters for the ES type seal:

- ✓ X-ray voltage 80 kV, current 125 µA, resolution 20 µm, exposition 1129 ms, scanning duration 200 minutes.

C. Metal cable seals

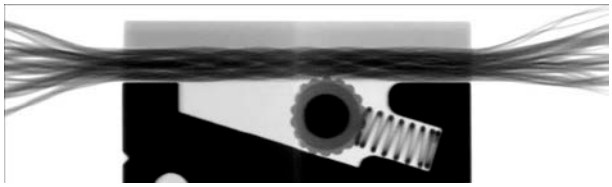

Fig. 6 Visualization of the metal cable seals

Scanning parameters for the metal cable seals:

- ✓ X-ray voltage 100 kV, current 100 µA, resolution 20 µm, exposition 2130 ms, scanning duration 70 minutes

D. Metal container seals

Fig. 7 Image provided by the scanner – metal cable seal

This security component cannot be tested by the tomograph because of insufficient output of the X-ray. An image provided by the scanner is available.

3.2 Visualization of the deformed security components

A. Thermal deformation of the security components at 120 °C

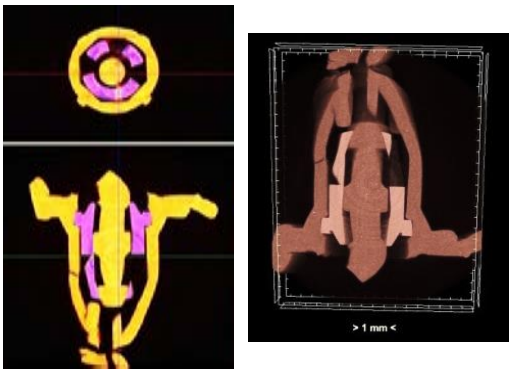

Fig. 8 A cut through seal of the PL type deformed by heat (120 °C) and a 3D model of the destroyed seal

B. Thermal deformation of the security components at 185 °C

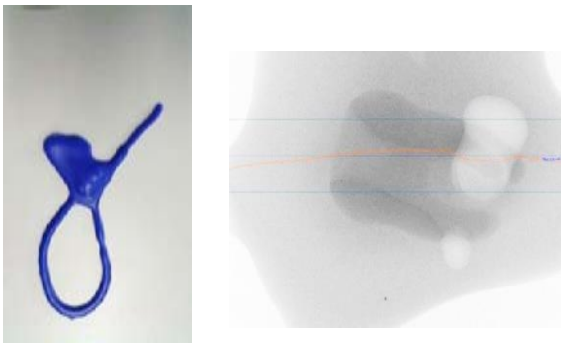

Fig. 9 Photo of a badly damaged seal of the PL 91 type and a view provided by the tomograph into the structure of the security component damaged by thermal deformation (185 °C)

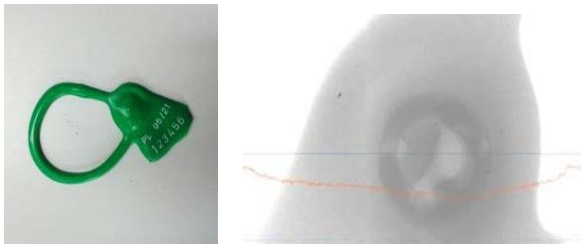

Fig. 10 Photo of the damaged PL 95 type seal and a view into the structure of the security component after thermal deformation (185 °C)

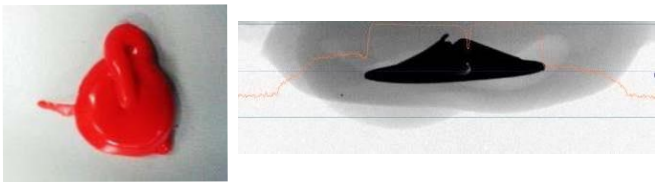

Fig. 11 Photo of the damaged ES type seal and a view provided by the tomograph onto the structure of the security component after thermal deformation (185 °C)

C. *Tensile deformation of the security components*

Fig. 12 Visualization of the tensile deformation of the metal security components (strained by 1, 2, 3 and 4.4 kN – from left to right)

D. *Chemical deformation of the security components*

- deformation by the technical petrol

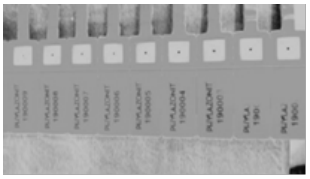

Fig. 13 Seal visualization marked by thermal print and damaged by technical petrol

- deformation by the Polyoxymethylen

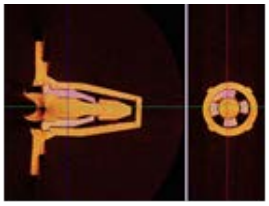

Fig. 14 Visualization of the PL 95 type security seal after chemical damage cause by Polyoxymethylen

4. Conclusion

Three levels of examination are applied while examining potentially attacked security seals in order to find out their actual state. The first level is a visual examination, taking place at the location of an attack and doesn't usually use any other means. The second level is an inspectional examination, which takes place at the location of an attack or in laboratory conditions. It is possible to use other equipment (such as magnifiers, microscopes and reference sample). This research is conducted by specially trained person. The third level is a forensic research conducted in laboratory conditions with a specially trained researcher using special equipment. Conclusions of forensic research can be used as proof during a lawsuit. A sophisticated computed microtomograph was presented here as one of the ways of non-destructive examination, detection and verification of unlawful tempering with security components.

5. References

[1] Kak, A.C., Slaney, M.: Principles of Computerized Tomographic Imaging, California, Siam, 2001.
[2] Kolinova, M., Richter, A., Baburek, E., Kolar, M., Kysela, M.: Computed tomography in forensic research (in Czech), Jemna mechanika a optika, num. 6-7/2017, p. 190–193.
[3] Petru, M., Syrovatkova, M., Kolinova, M. a Novak, O.: Materials Science Forum, 2015, p. 295-298.
[4] Ullmann, V.: Detection and spectrometry of ionizing radiation (in Czech), http://astronuklfyzika.cz/JadRadMetody.htm.

Acknowledgement

This article was created under the project "Methods for verifying of ensuring the detection of an unauthorized breach of security seals, signets and envelopes", registration number VI20152018023 within the framework of the "Security research program of the Czech Republic in 2015-2020" (BV III/1-VS) of the Ministry of Interior.

The research was supported by the project LO1201 through the financial aid from the Ministry of Education, Youth and Sports under the specific support of the "National Sustainability Program I" and the OPR & DI project "Center for Nanomaterials, Advanced Technologies and Innovations", registration number CZ.1.05/2.1.00/1.0005.

This work was supported by Student Grant Competition of Technical University of Liberec.

REACHABILITY PLANNING OF INDUSTRIAL ROBOT IN CONCEPT OF DIGITAL FACTORY

doc. Ing. P. Košťál, PhD. & doc. Ing. Š. Václav, PhD. & Ing. D. Michal & Ing. Š. Lecký
Faculty of Materials Science and Technology in Trnava – Slovak University of Technology, the Slovak Republic
peter.kostal@stuba.sk, stefan.vaclav@stuba.sk, david.michal@stuba.sk, simon.lecky@stuba.sk

Abstract: *One of the factors that influence the production and assembly systems based on robotic cooperation is the reachability of the required locations as well as the design of the robotic arm paths without the need for initial testing at a real workplace, which could lead to damage of some parts in the workplace. The resulting robot paths must be collision-free, they cannot correlate with other elements of the automated workplace, they should also follow the set production cycle. The trajectory time described by the industrial robot end effector influences the overall production cycle time. For this reason, it is necessary to create a trajectory which represents the shortest path described by the industrial robot. The design of the end effector path of an industrial robot must in general meet many criteria, either in terms of tact or safety. By simulating multiple path trajectory variants in the digital environment, it is possible to select the ideal trajectory of motion of the industrial robot depending on the layout of individual elements of the production or assembly system and the elimination of collisions. When designing a robotic workstation, the main parameters of the industrial robot are range and load capacity. By implementing CAD data and customer requirements into the digital environment of the selected software, we can verify the data and choose the most appropriate solution. The main benefits of industrial robot application and the use of available software to efficiently design a robotic system include benefits such as shorter production times and associated higher productivity, labor cost savings and wage costs reduction, robots are used in other applications after the end of the production cycle of the original product, thereby achieving savings in investment costs.*

Keywords: TECNOMATIX, PROCESS SIMULATE, DIGITAL FACTORY, INDUSTRIAL ROBOT, WELD POINT,

1. Introduction

Nowadays, efforts are being made to shorten the cycle of products, to increase the usability of production systems and to reduce the complexity of products, requiring changes in the technical preparation of production as well as in the production process. The number of newly-developed and upgraded products in the industry is large and will be further enhanced by the improvement of technical solutions. A partial solution is the application of industrial robots to manufacturing or assembly systems.

Industrial robots are used in various industries such as welding, pressing, machining, painting, painting, etc. Pressure to increase quality, productivity and cost reduction opens space for industrial robots, including machine handling and material handling. Industrial robots can move with high precision repeatability and trajectory of handling moves compared to conventional solutions, making cycle times shorter. The advantage is that the robot is not a dedicated device, for example, on machine operation, e. g. within the cycle time can do other additional operations in addition to the primary operation.

The main technical advantages of the industrial robot are undoubtedly the stability of the process and hence the achievement of high quality requirements for the final product, as well as the flexible production process change and the rapid incorporation of the technical change of the product. The major economic benefits include shortening production times and bringing together higher productivity, labor cost savings and lower wage costs, the ability to use robots in other applications after the end of the production cycle of the original product, and thereby achieve savings in investment costs. When designing a robotic workstation, the main parameters are the industrial robot, its range and load capacity.

Optimization of a robotic workstation can be analyzed from multiple angles, regardless of the area. Optimization can occur in:

- production,
- communication,
- management,
- logistics,
- ATC.

Optimizing these and other areas is geared to the main goal of increasing efficiency, saving costs, increasing productivity. Maintaining the right to maintain high quality and production stability is a matter of course. The possibility and scope of optimization of the robotic workplace is given by sufficient flexibility, which is achieved using appropriate technologies at the very design of the workplace. Availability visualization is done in a 3D software environment where it is possible to determine the cycle time, the reachability of the industrial robot and at the same time to verify the functionality of the proposed workplace. With the increasing demands on the efficiency of production, its reliability and the quickest putting into operation are an important part of the design of the production and assembly lines, becomes a computer simulation.

Computer simulation enables virtual verification of plans and assembly lines before the start of production, helping to mitigate risks, whether cost or real-estate safety. It is a comprehensive tool that can verify the feasibility of the assembly process by controlling the reachability and eliminating possible collisions. This process is performed by simulating the whole assembly procedures of the product and the required tools and their interaction. Using computer simulation, it is possible to design the most optimal way of these processes and to incorporate all the necessary means necessary for the planned production process. The main advantages of computer simulations include the possibility of early detection of errors in the design and optimization phase of production, the possibility of making analyzes of the feasibility of a given solution or examining ergonomics of manual works.

2. Literature analysis

The effectiveness of robotization lies in the rapid integration of robots into production processes and, above all, in their economic and social benefits. Under economic benefits, we mean increasing labor productivity, stability and improving production quality, improving production management, and saving resources. In addition to the benefits that can be quantified to save production costs, the introduction of robots generates many secondary effects that only assist in deployment, such as lowering the technical preparation of production, reducing the need for operative production planning, and shortening production lead times.

2.1 Robotized workplaces

Robotic applications for Smart Manufacturing, whose definition and ideas constitute the current development trend in robotic systems, define new requirements for the technical level of in-use equipment. Innovating current solutions puts emphasis on the development of fully integrated and interoperable manufacturing systems that can respond in real time to conditions and requirements changing in real time. An integral part of the successful development of the Smart Manufacturing Application vision is industrial robots that provide the user with a high level of

functionality, flexibility and mobility. Their ability to collaborate safely in direct interaction with humans or other industrial robots, on the other hand, provide simple parameterization and definition of the tasks performed, which will allow the rapid and seamless integration of new devices into existing infrastructure within the production process. [4]

The geometry description aims at defining the movement of the end effector of the industrial robot over time and excluding force effects, determining its path, velocity and acceleration. The operation of the industrial robot consists in adjusting the discrete positions of the working head or in the continuous motion of the working head after a generally defined spatial trajectory, whereby the orientation of the working head is also controlled. Thus, the working head is a functional part which, depending on the nature of the desired activity, determines the use of the motion robot movement system. Due to the kinematic scheme of industrial robots and the scope of their workspace, emphasis is placed on the trajectory itself to eliminate the risk of interaction with the robot peripherals, and therefore emphasis is placed on workplace layout and ease of accessibility. [4]

*2.2 Simulation soft*ware

Simulation software allows simulation of all activities from product design, assembly techniques, production planning, operational management, manufacturing of parts, inspection, assembly, packaging through to dispatch, in order to reduce material and energy consumption, increase productivity, reduce inventory, shorten the interim development and production times, increase time and power utilization of production facilities, and increase product quality. The potential of using simulation software is high. To select the software, you need to have a clear idea of the usability and suitability of the selected software, and it is necessary to correctly define the criteria and the objective of the project.

Issues and errors detected during simulation:

• large transport points,

• small storage capacity,

• Insufficient storage capacity,

• excess or shortage of workers,

• poor layout of workplaces,

• downtime.

• high caries,

• Insufficient maintenance,

• Unusable workplaces during breaks,

• Verification of functionality, reliability and performance,

• poorly planned progress of individual operations in the project.

There are models that are built for single use only (eg when analyzing processes to confirm the correctness of our hypotheses). Next are the models whose use is repeated. These are, therefore, simulation models of production and logistics systems that are still available to the user. Such models are used, for example, to verify the availability of system capacities, production plans, and the number of workers depending on the plan. An important part of the reuse of the model is its updating. The user not only changes the production plan but needs to constantly update the basic process data in the simulation model (e.g. machine failure, cycle times, sorting times). Today's simulation software can communicate with different databases or spreadsheet editors. Therefore, process data can be maintained in MS Excel spreadsheets or automatically downloaded from the enterprise information system. This greatly reduces the simulation model user's expertise. Although the construction of the model is performed by an expert, it can also be used by a scheduler in the production, and may not be able to control the programming language. [3]

2.3 Tecnomatix Process Simulate

Process Simulate is one of the major modules for simulating manufacturing processes that helps minimize startup costs and change the production program. It enables the virtual verification of plans and assembly lines before the start of production, thus helping to mitigate risks, whether cost-related or in real-life safety. It is a comprehensive tool that can verify the feasibility of the production or assembly process and eliminate possible collisions. This process is carried out by simulating the entire assembly or production procedures of the product and the required tools and their interaction. Its task is to design the most optimal solution of the processes and to involve all the necessary means necessary for the planning of the production process. This module is fully integrated with the Teamcenter platform, allowing engineers and designers to reuse data that has been used in past designs and re-process, validate, edit, and use in the future. This archiving enables easy return to data, facilitates and accelerates the design of production systems and links. It also simplifies the simulation of human processes, mechanical processes, tools, devices and robots. Process Simulation creates complex and realistic views of the look and course of production through relatively detailed and credible simulations. [1, 2]

Process Simulation is the solution to minimize the risk of manufacturing change or the rise of new production lines. It will allow you to verify practically plans from the concept to the start of production to help mitigate these risks. The ability to use 3D data of products and resources, facilitates virtual verification, optimization and introduction of complex manufacturing processes, resulting in faster startups and higher production quality. Tecnomatix - Process Simulation can verify the feasibility of the assembly process by verifying availability and collisions. This is done by simulating the complete order of assembly of the product and its working tools. Tools such as cutting, measuring, and collision detection allow detailed control and optimization of production and assembly scenarios.

The main features include activities such as 2D and 3D view, 3D simulation, static and dynamic collision detection, 3D measurement, assembly planning, line design and workspace, filtering and displaying products and production information. There are advantages [2]:

• Reduce the risk of changing the production system,

• shortening planning time for new production systems,

• Reduce change costs with early error detection,

• Analysis of ergonomic processes,

• selecting the best option, by deducting several production alternatives [2]

When using the Tecnomatix - Process Simulate software correctly, the given robot simulation can be used as off-line programming and PLC code generation. The off-line industrial robot programming method offers several benefits, shortening the time of deployment of the robot, detecting collisions and detecting unrealizable and dangerous situations. The actual working range of the robot is known before the physical realization, which allows the selection of a suitable industrial robot. In addition to the advantages when introducing a new workstation, it is advisable to apply the off - line programming method to the process of changing the workplace, during which the delays occur during reprogramming of the robot during operation. [2, 5]

3. The example of Tecnomatix Process Simulate application

At first, we need to define what kind of research question we are going to solve by simulation.

Research question:

What are the limitations of the new proposed production system, and how can the production system be put into practice realistically and to what extent?

In the following example, we will introduce a digital model that defines a manufacturing system focused on spot welding process. A key element is the creation of a trajectory of an industrial robot with an end effector. This model is designed by Tecnomatix Process Simulate from SIEMENS.

To create the simulation of the digital model itself, it is necessary to define the correct kinematics of the CAD model of the industrial robot and scoring welding pliers.

The Process Simulate system distinguishes between passive items and those having joints enabling them to move; the latter are kinematic and are designated mechanisms. Mechanisms have links connected by axes to constitute joints. Links are hierarchically related to each other such that every link is either a parent link or a child link relative to another link, or both: an intermediate link may be a child link to one link and a parent link to another link. If the links of a mechanism are connected such that no link has more than one parent or more than one child, the mechanism is a chain. Every joint is either prismatic (linear) or rotational, and has limits of maximum and minimum movement (distance of travel), and maximum speed and acceleration. Every mechanism is either a device or a robot. If it has only links and joints, it is a device. If in addition it has a base frame and a tool frame, it is a robot. A robot also has a tool center-point frame (TCPF) which initially is superimposed on the tool frame, and a reference frame (REFRAME) to which the coordinates of all robot frames except the base frame are referenced. These frames are identified by names and have six numerical values expressing the X-Y-Z coordinates of position and the Rx-Ry-Rz coordinates of orientation; the Rx coordinate is a rotation around the X axis, the Ry coordinate is a rotation around the new Y axis, and the Rz coordinate is a rotation around the new Z axis. [6]

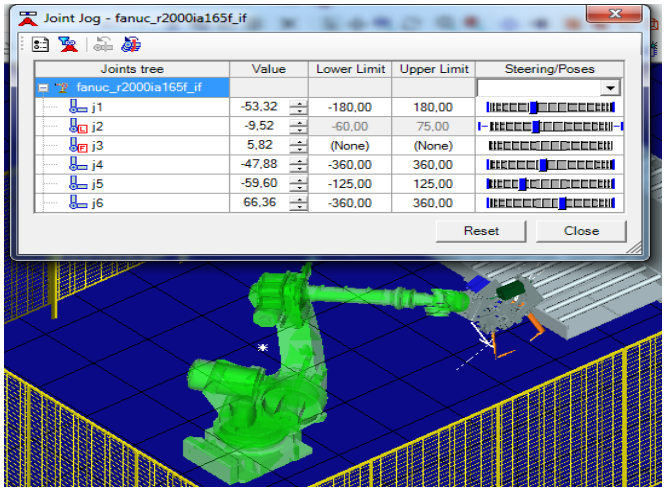

Fig. 1 Value of joint

When we have a CAD model of an end-effector industrial robot and a kinematics created, simulation can be created. In this example, New Weld Operation is used, which involves designing welded points. Subsequently, auxiliary points are created to guide the industrial robot with the welding point ticks to the desired location. To create the right trajectory and simulation, it is necessary to identify the technological points and points. Technological points are specific places where the technological process takes place. In this case, it is spot welding. The welding point pliers are attached to the industrial robot arm. The auxiliary points serve to accurately guide the welding scoring pliers on the industrial robot arm to the point of the first welded point, through the intersections between the welded points and to leave the space after the welding operation is completed. These help points are important to correctly determine that no collision occurs because the robot automatically selects the shortest path when starting a process with the Home position to the point of the first welded point or when passing between the welded points.

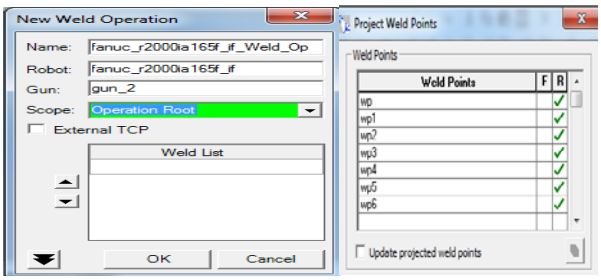

Fig.2 Project Weld Points

The next step for guiding welding scoring pliers mounted on the arm of the industrial robot is the orientation of the created technological and auxiliary points. It is necessary to set correct points orientation in the coordinate system with axes x, y, z to avoid collisions of the industrial robot with welding pliers with other objects in the vicinity. It sets the direction and angle of access of the industrial robot's tool (welding point pliers) to a predefined point, such as a technological or auxiliary access point.

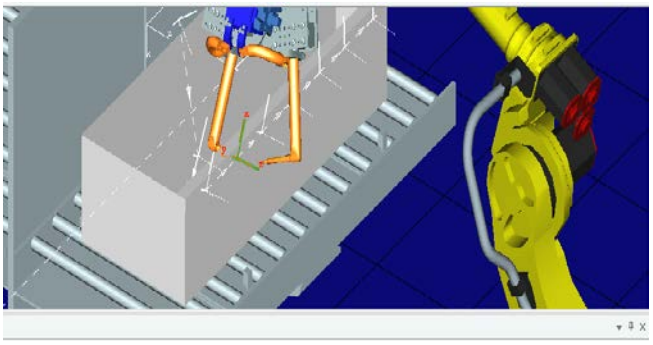

Fig.3 Trajectory of motion weld gun

After creating the trajectory of the industrial robot path with the end effector, adjusting the orientation of the technological and auxiliary points, and removing the collision states, it can create a simulation.

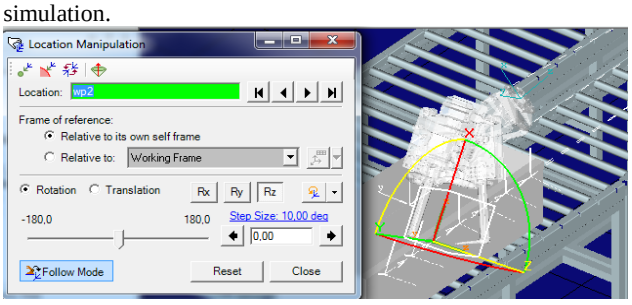

Fig.4 Location and orientation weld gun

In this part, it is possible to simulate a technological process with different speed parameters of the movement of an industrial robot where it is possible to observe the change of the time character of the technological process and eventually the collision. Before running the simulation, it is necessary to sort the operations

in the Operation Tree according to the time sequence. In the case of creating a simulation consisting of multiple operations, it is possible to create groups and subgroups that will include individual operations.

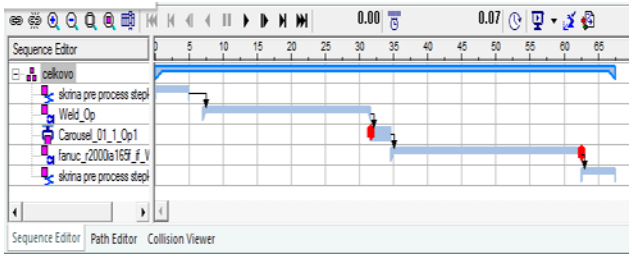

Fig.6 Sequence Editor

4. Results and discussion

The proposed digital model must be tested in terms of the reachability of the industrial robot and the distribution of the individual components of the production system. This prevented the collision between the parts of the production system and the industrial robot with the end effector resp. to remove collisions.

In addition to the interaction of the components of the production system, the load characteristics of each joint were verified. In Fig. 7 Joint value, it is possible to see the measured values in terms of time. Among other things, it is possible to read the actual movement range of individual joints at the proposed trajectory from the overall motion range of individual joints.

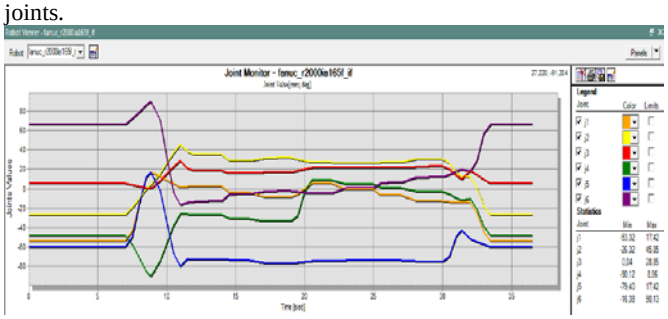

Fig.7 Joint Value

In addition to the load characteristics of the joints, it is possible to read out the greatest speed of movement of individual joints. Thanks to it, it is then possible to retroactively refine the simulation of the process to provide realistic information for implementation into real production.

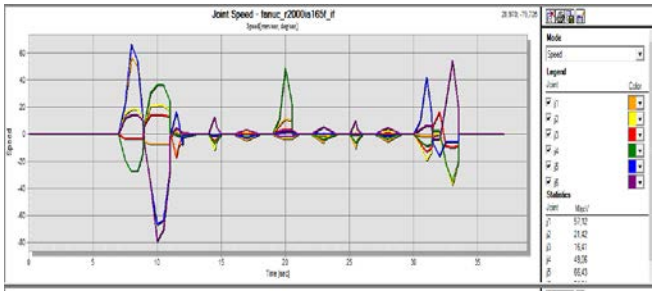

Fig. 8 Joint Speed

This is an option to show the complexity or simplicity of the path when designing larger ranges of joints means consuming more time and energy to perform the operation

5. Conclusion

With an increasing number of industrial robot installations, processes related to automated application design and the use of CAx systems that target different levels of their development are at the forefront. Software solutions allow you to create simulations across the range of tasks from simple object availability testing within the robot workspace to virtual plant simulation including process, production, logistics, product, and more.

The result of the example used is to verify the reachability of the industrial robot while creating the optimal trajectory of the industrial robot. Using simulation, you can test the kinematic and dynamic properties of mechanisms and systems. Movement of a mechanism or system is controlled by a time sequence. The output is a dynamic simulation that carries information about the movement speeds of individual parts and the trajectory of the industrial robot, the length of the technological operation, the collisions and the layout of the workplace. The total length of the trajectory time interval is the sum of the individual lengths of the time intervals of the industrial robot movements from which the technological operation is composed. The time interval is affected by the speed of movement of the operational and inter-operation processes. The speed of movement of the industrial robot must not affect the accuracy and quality of the technological operation. Consideration must also be given to factors such as inertia, movement, strength or structural strength. An important element is the dispositional distribution of the individual components of the production system, which to a certain extent affects the finding of the optimal trajectory of the industrial robot. The accuracy of the input data and the geometric accuracy of the CAD models influence the credibility of the information obtained.

The creation and more frequent introduction of simulations of various processes in manufacturing, logistics or other industries is an integral part of the Digital Factory concept, which falls under the Industry 4.0 strategy. Simulation facilitates decision making when designing new and optimizing existing production systems. Assuming the correct creation of the kinematic CAD model of the industrial robot and the welding pliers, the obtained simulation data can be considered as data obtained in a real production process, but without significant financial investment.

Acknowledgements

The article was written as part of the Young Researcher project 1383“Influence of selected attributes in manufacturing systems and sub-systems planning in digital enviroment” supported by the scientific program - Motivation and support in quality and effectivity elevation of young researchers and scientists. Slovak University of Technology.

6. References

[1] KLIMENT, M., TREBUŇA, P.: Prínosy softvérového portfólia TECNOMATIX, jeho moduly a súčasti využívané pri modelovaní a simulovaní podnikových procesov a ich optimalizácii. In: Transfér inovácií. 2013, þ. 25, 158-161.

[2] Tecnomatix – Process Simulate, Internet source: http://www.plm.automation.siemens.com/en_us/

[3] Burieta, J. – Kakačka, S. - Fraunhofer IPA Slovakia: Simulácia výrobných a logistických procesov. Internet source: http://archiv.ipaslovakia.sk/UserFiles/File/ZL/Uspech/2007-%20Uspech%20Simulacia%20vyrobnych%20a%20logistickych%20procesov.pdf

[4] NIST, Robotic Systems for Smart Manufacturing Program, 2014, Internet source: http://www.nist.gov/el/isd/ms/rssm.cfm

[5] Trebuňa, P. , Popovič R., Klos S.: Methodology of the Creation of Human and Robot Operation in the Tecnomatix Process Simulate. Procedia Engineering. Volume 96, 2014, Pages 483-488

[6] Siemens PLM Software – TECNOMATIX: Motion Planning Definition File "motionparameters.e". 2015. Pages 4-8.

ANALYSIS OF MANUFACTURING SYSTEMS WITH USE OF SIMULATION SOFTWARE

doc. Ing. P. Košťál, PhD. & doc. Ing. Š. Václav, PhD. & Ing. D. Michal & Ing. Š. Lecký
Faculty of Materials Science and Technology in Trnava – Slovak University of Technology, the Slovak Republic
peter.kostal@stuba.sk, stefan.vaclav@stuba.sk, david.michal@stuba.sk, simon.lecky@stuba.sk

Abstract: *Knowledge gained from the Digital factory field needs to be expanded and further disseminated. The use of the Digital factory concept is mainly in laboratory conditions. It is essential for new knowledge to be made it more accessible for further experiments and for acquiring new knowledge for faster and easier deployment. The visualization of machines, devices, and entire manufacturing systems allows for almost faultless design of such systems. It is an expense saving and time-efficient solution. The article represents an experiment aimed at exploring simulation methods used in design and development of production systems by use of simulation digital tool. Comparison of the results obtained by examining the simulation model and real model will be made for acquisition of deviation between virtual model and real model. The task of optimization is, in this case, to create an optimal timetable for individual production lines by increasing flexibility and lowering costs, with prediction that the conditions are met and all orders will be made on time, minimize downtime, reduce production of waste and consider the efficient use of electricity.*

Keywords: SIMULATION, MANUFACTURING, TECNOMATIX,

1. Introduction

Among the current priorities in the field of production is the effort to shorten product cycle cycles, to increase the usability of production systems and to reduce the complexity of products, which requires changes in the technical preparation of production as well as in the realization of production. Optimizing these and other areas is geared to the main goal of increasing efficiency, saving costs, increasing productivity. Maintaining the right to maintain high quality and production stability is a matter of course. The scope and scope of workplace optimization is given by sufficient flexibility, which is achieved using appropriate technologies already at the design of the workplace itself. With increasing demands for production efficiency, reliability and the quickest start-up, an important part of the design of production and assembly lines is the computer simulation.

Empirical experience confirms that the most expensive decisions to change production and products are those that arrive late in the last stages of product development and the process of putting products and production systems into operation. It can be stated that any change introduced into production needs to be prepared and reliably tested in all aspects of production in the early stages of the design and development of production systems. Testing the production process in production systems is one way of preventing late changes in production systems. Simulation methods, as well as the virtual introduction of production systems into the digital enterprise concept, are a tool that verifies the functionality of the individual models together with the systems and verifies the functionality of the elements of automation technology in the early stages of product development and manufacturing processes. The current way of introducing new production systems has its drawbacks, and by means of new software tools for simulation and modeling of process systems, the time needed for the preparation and deployment of real systems will be shortened and thus considerable savings will be saved. Start of production or the introduction of new production, the production line is time-consuming. With these tools, there is a significant reduction in the start-up time of production. The virtualization of production systems by virtue of the future of technology and the "Industry 4.0" concept.

Computer simulation enables virtual verification of plans and assembly lines before the start of production, thus helping to mitigate risks, whether in terms of cost or real-world safety. It is a comprehensive tool that can verify the feasibility of the assembly process by controlling the reachability and eliminating possible collisions. This process is performed by simulating the whole assembly procedures of the product and the required tools and their interaction. Using computer simulation, it is possible to design the most optimal way of these processes and to incorporate all the necessary means necessary for the planned production process. The main advantages of computer simulations include, in particular, the possibility of early detection of errors in the design phase and optimization of production, the possibility of making analyzes of the feasibility of a given solution or examining ergonomics of manual works.

2. Literature analysis

At present, a large part of the production is realized in medium and small-lot or piece production. Many ranges of flexible assembly of manufacturing machines and handling equipment from production cells to flexible production systems (hereinafter referred to as PVS) are designed for these production series. The efficiency of the work of such flexible clusters of production and handling technology does not achieve the efficiency of mass production. The lower efficiency is particularly evident in the higher percentile of bypass and non-production times due to the frequent change in production. As a result, the Lean Manufacturing requirement has grown in recent years, i.e. the slimming of production strategies and the design of products and equipment itself. These requirements will need to be implemented in new production strategies, product design support and production facilities. [1]

CAx technologies have become self-evident in the design process of manufacturing systems and processes. These technologies make it possible to streamline the process of designing and designing production systems with a view to improving quality through virtual simulation and testing of individual kinematic patterns. However, these kinematic models need to be integrated and integrated into the process control itself within the simulation. On the basis of the analysis, it can be stated that the process of decontamination of the production system and its processes is often lengthy and not always predefined solutions are right. This process is demanding, costly and increases the total time needed to complete the project. The big advantage for the implementation of this process is the ability to use new technologies that allow engineers to build a complete production equipment and also they realized processes in an interactive virtual 3D environment, which are implemented as complete mechanical, electrical, hydraulic and pneumatic systems and include the production process the process into operation weeks or months before building a real production system. By creating a simulation model in a virtual environment within the Industry 4.0 concept, it is possible to simultaneously control and monitor material flow that can be tested and optimized by means of simulation tools. The expected benefit of using virtual simulation tools is to shorten the time to redeploy production systems to operational status at the planning stage. The author (Lee Ch.G. and Park S.C., 2014) addresses the idea of linking the virtual model of a production system with a real-time control system to achieve virtualization of systems. [2]

Based on the information from published works by authors (G. Kovács and S. Kot, 2017; Hoffmann et al, 2010; Reinhart, G. and

Wunsch, G., 2007,) it is possible to conclude that simulation tools have high application in the design and the design of new production systems, but it is important to evaluate methodologies interaction between platforms, a new production system in the simulation environment and verification of production equipment in a real environment and compare the simulation model with the real environment of the production system. [3, 4, 10]

Innovating current solutions emphasizes the development of fully integrated and interoperable manufacturing systems that can respond in real time to conditions and requirements changing in real time. [5]

Simulation software enables simulation of all activities from product creation, manufacturing processes, production planning, operational management, component manufacturing, inspection, assembly, packaging to shipping, to reduce material and energy demands, increase work productivity, reduce inventory, shorten ongoing development and production times, increase time and power utilization of production facilities, and increase product quality. The potential of using simulation software is high. To select the software, you need to have a clear idea of the usability and suitability of the selected software, and it is necessary to correctly define the criteria and the objective of the project.

Problems and Errors Detected During Simulation:

• large transport points,

• small storage capacity,

• Insufficient storage capacity,

• excess or shortage of workers,

• poor layout of workplaces,

• downtime.

• high caries,

• Insufficient maintenance,

• Unusable workplaces during breaks,

• Verification of functionality, reliability and performance,

• poorly planned progress of individual operations in the project.

There are models that are built for single use only (eg when analyzing processes to confirm the correctness of our hypotheses). Next are the models whose use is repeated. These are, therefore, simulation models of production and logistics systems that are still available to the user. Such models are used, for example, to verify the availability of system capacities, production plans, and the number of workers depending on the plan. An important part of the reuse of the model is its updating. The user not only changes the production plan but needs to constantly update the basic process data in the simulation model (eg machine failure, cycle times, sorting times). Today's simulation software can communicate with different databases or spreadsheet editors. Therefore, process data can be maintained in MS Excel spreadsheets or automatically downloaded from the enterprise information system. This greatly reduces the simulation model user's expertise. Although the construction of the model is performed by an expert, it can also be used by a scheduler in the production, and may not be able to control the programming language. [6]

2.1 Tecnomatix Plant simulation

Tecnomatix Plant Simulation of workplaces and assembly systems helps in planning new systems or improving current systems. It is also often used in decision-making processes such as return of investment, cost of planned changes, project confirmation, production process analysis, and so on. Simulation in assembly systems facilitates the design phase and enhances the smoothness of project design and execution through its outputs. At present, simulations are up to 99% accurate. Of course, it depends on the input parameters and the validity of the model.

Benefits of simulation:

• testing innovative strategies in risk-free virtual environments,

• maximum use of production resources,

• reducing investment risk through rapid simulation,

• optimizing the size of systems and storage space,

• rapid identification of sources of problems in logistics and production spheres,

• 20-60% reduction in inventory due to system size,

• 5 - 20% reduction in investment costs for the new system,

• reduction of capacities for personnel and handling equipment,

• quickly achieve positive results and identify impacts [7].

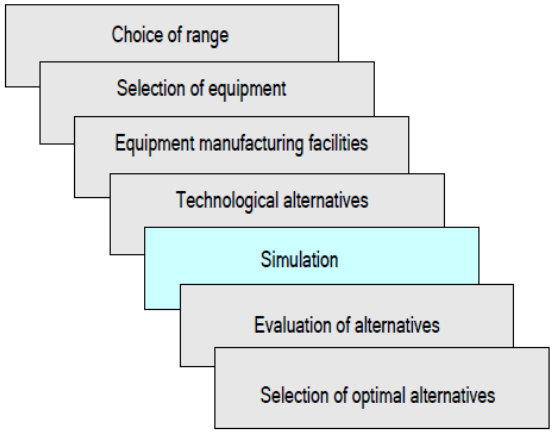

Fig.1 *Integration of simulation in designing of production cells [11]*

2.2 Tecnomatix Process Simulate

It is a comprehensive tool that can verify the feasibility of the production or assembly process and eliminate possible collisions. This process is carried out by simulating the entire assembly or production procedures of the product and the required tools and their interaction. Its task is to design the most optimal solution of the processes and to involve all the necessary means necessary for the planning of the production process. [8]

Main functions:

- 3D simulation.
- static and dynamic detection of collisions,
- 2D and 3D view,
- 3D measurement,
- scanning operations
- planned assembly operation.
- 3D geometry and kinematics. [7]

Process Simulation is the solution to minimize the risk of changes in the production and launch of new production system. It allows to verify the plans from design concept to start of production. It helps allay these risks. Ability to use 3D data makes easier virtual validation, optimization and commissioning of production processes. This results in faster launches and better production quality. Tecnomatix - Process Simulation can verify the feasibility of the assembly process by verifying reachability of the robot or human, and collisions between moving devices or between

man and machine. This is done by simulating complete assembly sequence of the products and their working tools. Tools such as measurement and detection of collisions allows detailed control and optimization of assembly processes. The software is fully integrated with the platform Teamcenter. Technology can be reused and can verify the production processes. Makes easier simulation of assembly processes, human operations and mechanical methods of tools, devices and robots [7, 8].

Advantages:

- reduce the risk in the production system,
- shortening the planning of new production systems,
- reduce the cost of change thanks to the early detection of errors,
- analysis of ergonomic process.
- choice of the best production variant[7].

3. The example of Tecnomatix application

At first, we need to define what kind of research question we are going to solve by simulation.

Research question:

How does the impact / insufficiency of information gained from simulation with respect to real-process operation?

In this study, the proposed digital model is used to represent the production and transport system. Dynamic simulation data can be used to verify the layout of individual production machines, conveyors, industrial robots and to determine the working range of the workers.

In addition, it is possible to verify the selection of the industrial robot and to verify its working range. It is necessary to verify the collisions and the reach of the industrial arm. From Fig.1 "Collision warning of industrial robotic arm with CNC milling machine doors" it is obvious that a collision state arises. It is necessary to review the time sequence of the event and at the same time to change the choice of the industrial robot due to the inaccessibility of the robotic arm.

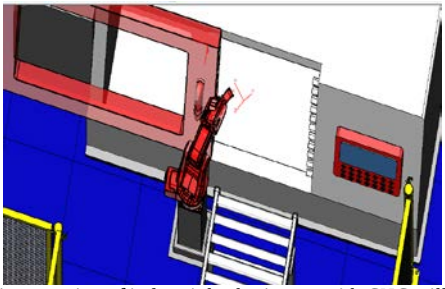

Fig.2 *Collision warning of industrial robotic arm with CNC milling machine doors*

Among other things, I know to gain the load characteristics and speed characteristics of the industrial robot joints. In figure 2, "Joint value", it is possible to see the characteristics of the rotation of individual joints in relation to time, where it is possible to check the applicability of the range of joints. We can use the information to make it easier for the production system to be put into real operation.

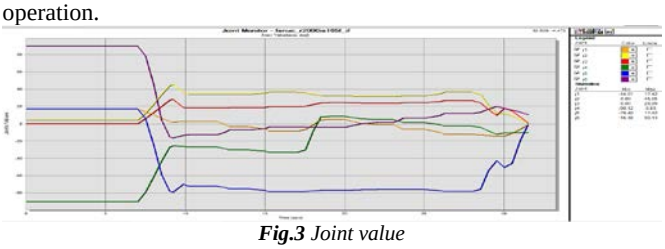

Fig.3 *Joint value*

4. Results and discussion

Simulation is suitable tool for experimenting with the structure of work and modernization of the production system. Simulation allows detection and the subsequently reducing collision situations in the design of the production system in the digital space and the help to find unfeasible and dangerous situation.

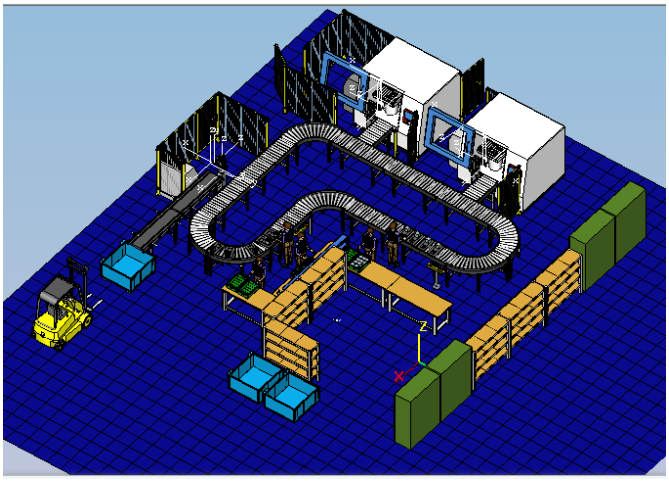

Fig.4 *Designed production system*

Same production system made in Tecnomatix Plant simulation can be analyzed for bottlenecks or throughput, labor time management, conveyor usage etc. On figure below is shown 3D model visualized in Tecnomatix Plant Simulation software.

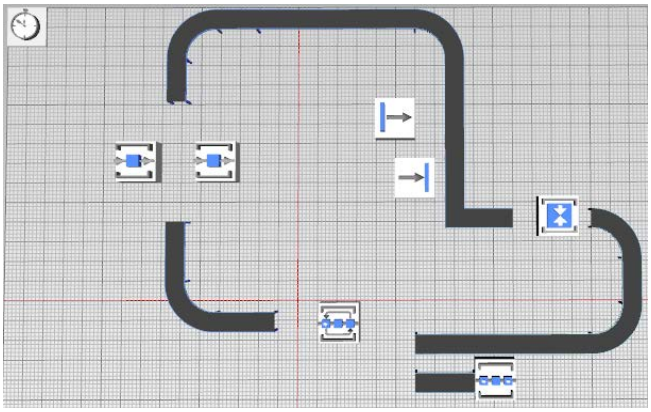

Fig.5 *Designed production system in Tecnomatix Plant Simulation (3D view)*

By analyzing this model, we can get resource statistics about each station. Based on that production line stations can be managed or time management on stations can be adjusted.

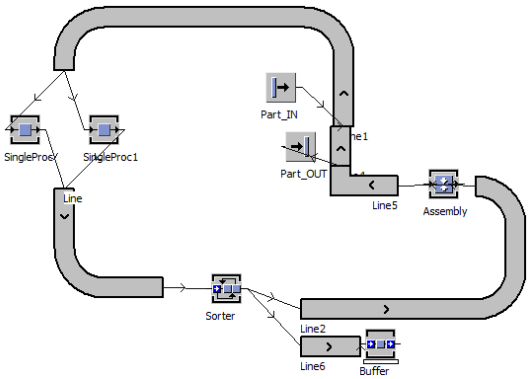

Fig.6 *Designed production system in Tecnomatix Plant Simulation (2D view)*

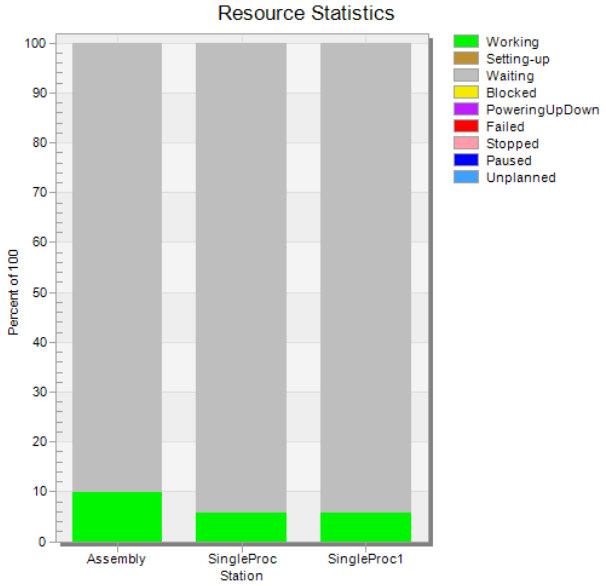

***Fig. 7** Resource statistics before implementation of changes*

Between figure seven and eight we can see difference in productivity of stations. In figure eight is much better productivity and working time on stations because of adjustments to model based on simulation results.

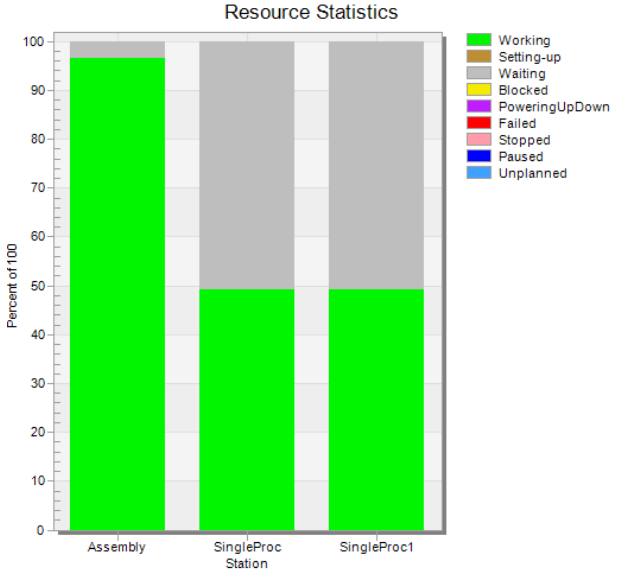

***Fig. 8** Resource statistics after implementation of changes*

5. Conclusion

The use of simulation tools in the design and implementation of production systems is highly sought after by the professional public and in the field of design and design of production systems and by the automatic service, and the results of the research will be expected from the point of view of the transfer. The creation and more frequent introduction of simulations of various processes in manufacturing, logistics or other industries is an integral part of the Digital Factory concept, which falls under the Industry 4.0 strategy. Simulation facilitates decision making when designing new and optimizing existing production systems.

Simulation methods are used for evaluation different aspects of production systems or subsystems. Repeatability is important and basic attribute of computer simulation. Because of exact values and parameters which have their own values assigned to them can be the same process executed many times. In real life, this is not possible [9].

Production planning ensures the efficient use of material resources, production capacities of the company and external cooperation with a view to meeting the deadline by the customer in the required quantity and quality. Data is very important for production planning. These are input data, which are usually output from the majority of processes in individual departments, which are then joined and evaluated. Further research in this field is the possibility of integrating available information from the simulation model to automate the generation of mechanisms and the automatic selection of production facilities or decision-making solutions.

Software solutions allow you to create simulations across the range of tasks from simple object availability testing within the robot workspace to virtual plant simulation including process, production, logistics, product, and more.

Acknowledgements

The article was written as part of the Young Researcher project 1383“Influence of selected attributes in manufacturing systems and sub-systems planning in digital enviroment” supported by the scientific program - Motivation and support in quality and effectivity elevation of young researchers and scientists.

References

[1] Baozhong, Qu, and Wang Hongying. 2012. “The Application of FCS-Based Architecture in the Flexible Manufacturing System.” Energy Procedia 17: 1395–1400. doi:10.1016/j.egypro.2012.02.258.

[2] Lee Ch.G. and Park S.C., Survey on the virtual commissioning of manufacturing systems. Journal of Computational Design and Engineering, Volume 1, Issue 3, July 2014, Pages 213-222.

[3] Hoffmann P., Talal M.A. Maksoud, Schumann R., Virtual commissionng of manufactoring systems a review and new approaches for simplification. Simulation meets global challenges. 2010. ISBN: 978-0-9564944-0-5, p. 175-181

[4] Economic application of virtual commissioning to mechatronic production systems. Production Engineering - Research and Development. ISSN: 0944-6524 (Print) 1863-7353 (Online). December 2007, Volume 1, Issue 4, pp 371–379

[5] NIST, Robotic Systems for Smart Manufacturing Program, 2014, Internet source: http://www.nist.gov/el/isd/ms/rssm.cfm

[6] Burieta, J. – Kakačka, S. - Fraunhofer IPA Slovakia: Simulácia výrobných a logistických procesov. Internet source: http://archiv.ipaslovakia.sk/UserFiles/File/ZL/Uspech/2007-%20Uspech%20Simulacia%20vyrobnych%20a%20logistickych%20procesov.pdf

[7] Tecnomatix – Process Simulate, Internet source: http://www.plm.automation.siemens.com/en_us/

[8] KLIMENT, M., TREBUŇA, P.: Prínosy softvérového portfólia TECNOMATIX, jeho moduly a súčasti využívané pri modelovaní a simulovaní podnikových procesov a ich optimalizácii. In: Transfér inovácií. 2013, þ. 25, 158-161.

[9] KLOSOWSKI, G., 2011. Zastosowanie symulacji komputerowej w sterowaniu przepływem produkcji mebli, Zarządzanie Przedsiebiorst-wem / Polskie Towarzystwo Zarządzania Produkcją 2: 29–37.

[10] G. Kovács and S. Kot, “Facility layout redesign for efficiency improvement and cost reduction,” J. Appl. Math. Comput. Mech., vol. 16, no. 1, pp. 63–74, Mar. 2017.

[11] L. Pachniková, Ľ. Šidlovská: Simulation as support tool for design of manufacturing systems. 2010. Transfer inovácií 18 (2010)

PRODUCTION STATE IDENTIFICATION USING RAW ETHERNET DATA OF TOTAL POWER CONSUMPTION IN A CYBER-PHYSICAL FACTORY

Meltem Dincer, Aleksei Kharitonov, Prof. Dr. Axel Zimmermann, Dr. Thomas Burghardt
Department of Industrial Engineering– Aalen University, Germany

axel.zimmermann@hs-aalen.de, aleksei.kharitonov@hs-aalen.de, thomas.burghardt@hs-aalen.de, meltemd@hotmail.de

Abstract: *Complex production systems are increasingly using Industrial Ethernet for connecting MES, PLCs, Touch Control, and even sensors and actors within the industrial control network. While today's production is still process driven under MES control, digitalization requires a data driven approach with cyber physical systems acting autonomously in a connected production world. Moving away from a centralized control architecture has the advantage of more flexibility but eliminates the implicit knowledge on global parameters such as the current condition or state of the overall machinery. This paper describes a methodology to retrieve these global parameters independently from any control system and fully transparent to the control network. A data sensor device is introduced that can listen to any Ethernet data traffic. Together with a specialized packet rules engine it is used to extract and combine information out of a raw Ethernet data stream to build up a virtual sensor device. A production state identification sensor is described as an example application of the virtual data sensor device.*

Keywords: CONDITION MONITORING, DATA ANALYSIS, DATA SENSOR, MAINTENANCE, VIRTUAL SENSOR

1. Introduction

Industrial control systems and process control systems are dominating today's factory floors. The centralized information on all production parameters enable supervisory functionality that is used to monitor the machinery condition for example [1]. However, migration to a smart cyber physical factory requires a more distributed control scenario and therefore prevents a centralized condition monitoring.

In this paper, we describe a way to retrieve virtually all relevant information on production parameters even in a smart cyber physical factory environment. As an example, we describe the identification of the working state on a drilling station in a cyber-physical factory (CP-Factory). An approach for transparent condition monitoring (CM) will be introduced. In order to permanently monitor the state of a system it is necessary to measure and analyze one or more physical values in real-time. Often the realization of a forward-looking state-oriented maintenance of an equipment is intended. The challenge in this strategy consists of the search of relevant sensor data, effective signal analysis, pattern recognition and control over the data flow. It was already shown that motor current signatures can be used to detect faults [2]. In this work, the application of a single physical energy data sensor for state identification is considered. The sensor measures the electrical power of all components in a production unit and provides periodically measured data on a digital interface to a cable-connected network (Ethernet). The energy sensor works as a Modbus Slave service and sends measured data upon request over Modbus/TCP protocol. [3] The goal is to reliably identify operational state and state transition from the total power consumption. For that purpose a data sensor (network sniffer) for the recognition of the MODBUS packets, their processing and evaluation of captured energy data was integrated at the network site. The electrical power for nine practice-oriented operational states was measured and saved as reference table values. Hereupon a data model for the state recognition and state transition was developed. It was implemented and validated in a user-friendly rule-based language in the data sensor. This rule-based interpreting language is a formal programming language for rule description and for analysis of the Ethernet data flow. In different tests, it was proven that the identification of an operational state was reliable with an error rate of 0.8 %. A use case of the application is the recognition of irregularities, detection of impermissible states and accordingly the identification of the state transition of a production module at the CP-Factory. The analysis- and evaluating tool consists of the data sensor with implemented rule interpreter. Thereby realizable data capture and evaluation can be implemented in existing networks. Further industrial use cases are discussed in this work.

2. Cyber-physical factory and virtual sensor

Cyber-physical factory (CPF) is a small-scale factory which is used for laboratory experiments and Industry 4.0 production process simulation. It offers a modular construction and modern communication between parts of the factory. The modular structure allows to composite the production process depending on the quickly changing manufacture requirements. Furthermore it allows to replace production units in a minimal time, reducing factory idling and avoid losses. It features radio frequency identification (RFID) for full control of the manufacturing process and to write production data directly onto the production unit, which enables to follow the whole production chain anytime in the future. Module units of the CPF are connected in a chain over industrial Ethernet. A manufacturing execution system (MES) is connected to the internal production network as well. The MES controls the manufacturing process of production units over all production steps. [4]

A power monitoring device SENTRON PAC3200 [5] is built into every production module.

Fig 2.1 Power monitoring device SENTRON PAC3200. [6]

It measures voltage and current, and based on these data it computes other electrical parameters such as total power consumption, active power consumption, etc. All data can be read on the front panel. The device provides all measured and calculated parameters to the Ethernet port over the Modbus/TCP protocol. It works in Modbus-slave mode and receives commands from Programmable Logic Controller (PLC), which has a Modbus-master role. The PLC monitors electrical values and reads them with a period of one second.

The data communication between PLC and Power monitoring device is sniffed using a data sensor device. Sniffing is fully transparent so that the original communication is not changed by any means. In addition to the sniffing capability a data sensor can also process the captured data, extract measurement values, and finally implement a virtual sensor functionality.

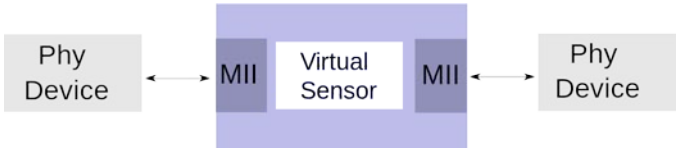

Fig. 2.3 Virtual sensor implemented in a data sensor device.

For implementing the capture unit and the virtual sensor an embedded XMOS parallel processor architecture is used. An embedded rule-based engine is developed on this platform, which makes it possible to define rules for every Ethernet packet of OSI layer 2. Thereby each of the passing Ethernet frames is going to be sequentially processed by the rules engine to filter out important information defined in the rules.

In the current work only the active power for the state monitoring was used, the rules for the Ethernet packets were written to filter out Modbus/TCP packets containing the value of the active power of the production module being monitored. In the next steps the encoded value of a floating point type was extracted from a specific place in an Ethernet frame. This preprocessing stage supplies the data for the further data analysis and for the state monitoring of the manufacturing module.

3. Solution of the examined problem

As a data sensor application example the identification of working states on a drilling machine in a cyber-physical factory was investigated. The working station consists of three actors, the conveyor and two drilling units, which can be moved in an X- and Z-direction. The working station detects a production part using light barrier sensor. The position of the production part is checked and the station can drill up to four holes on it. [4] The objective is the detection of the working states of the actors by measuring and analyzing the active electrical power of the drilling machine.

There are two possibilities to control the actuators, by the Manufacturing Execution System (MES) or manually via a touch panel. All working states are shown in figure 3.1. In state Z2, only the conveyor belt is switched on. During a drilling process, the conveyor belt runs and both drill units are active (state Z9). This corresponds to the production mode (order processing) when the plant is controlled by the MES. The permissible operating state transitions are also shown in green in the figure 3.1.

initial state \ final state		Z1 base load	Z2 TB	Z3 B1	Z4 B2	Z5 B12	Z6 TB + B1	Z7 TB + B2	Z8 TB + B12	Z9 TB + drilling process
Z1	base load		+TB	+B1	+B2	+B12	+TB +B1	+TB +B2	+TB +B12	
Z2	TB	-TB		-TB +B1	-TB +B2	-TB +B12	+B1	+B2	+B12	+ drilling process
Z3	B1	-B1	-B1 +TB		-B1 +B2	+B2	-B1 +TB +B1	-B1 +TB +B2	+TB +B2	
Z4	B2	-B2	-B2 +TB	-B2 +B1		+B1	-B2 +TB +B1	-B2 +TB +B2	+TB +B1	
Z5	B12	-B12	-B12 +TB	-B2	-B1		-B2 +TB	-B1 +TB	-B12 +TB +B12	
Z6	TB + B1	-B1 -TB	-B1	-B1 -TB +B1	-B1 -TB +B2	+B2 -TB		-B1 +B2	+B2	
Z7	TB + B2	-B2 -TB	-B2	-B2 -TB +B1	-B2 -TB +B2	-TB +B1	-B2 +B1		+B1	
Z8	TB + B12	-B12 -TB	-B12	-TB -B2	-TB -B1	-B12 -TB +B12	-B2	-B1		
Z9	TB + drilling process		- drilling process							

permissible operating state transitions
impermissible operating state transitions
TB = conveyor belt, B1 = drill 1, B2 = drill 2, B12 = drill 1 and 2

Fig. 3.1 State table with permissible and impermissible state transitions.

For example a state transition from state 1 to state 2 is valid. A transition from state 2 to states 3 to 5 (shown in red) would not be permitted. This is caused by the fact that the conveyor belt and the two drilling units may not be simultaneously switched over due to different control mechanisms.

The energy measurement step includes the measuring of the active power of the production module in the nine operating states. For data collection the data sensor (network sniffer) was integrated into the data network running in forward mode. This has the task of detecting and forwarding the Modbus telegrams containing energy data to a desktop computer. In this phase no processing was done within the data sensor. On the desktop computer the energy data could be evaluated in offline mode with the software tool Wireshark.

With the help of Wireshark the collected energy data was exported into a text based network capture data format K12. In this data format every captured network data packet is saved into a single row in form of a time stamp and a sequence of bytes as hexadecimal numerical values represented in text form. In order to make this usable for state detection, data conversion from the hexadecimal to the decimal number system was performed. Finally the recorded data was exported to an Excel spreadsheet.

The data were recorded over a temporal measuring range of 15 to 30 minutes (see figure 3.2).

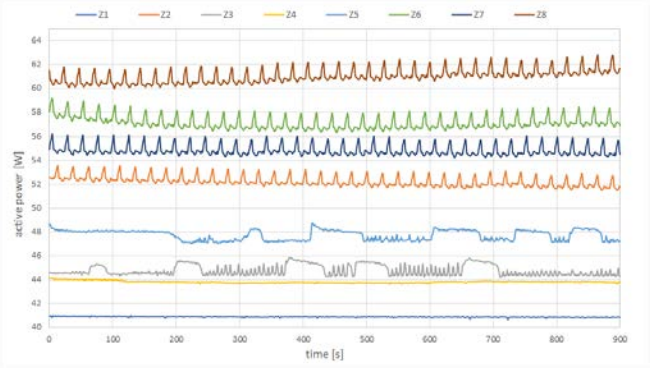

Fig. 3.2 Active power over a temporal measuring range of 15 minutes.

The procedure for measuring the energy values during the state transitions was identical. The active power during operating process and transitions between states were measured and recorded as reference values in tabular form.

A feature-based data model was developed for automatic state detection. For this purpose, the measured average active power values were used as characteristics of the states.

In the case of state transitions the differences between the individual states were calculated and recorded in a matrix.

In order to meet the cybernetic behavior of the plant, the recorded reference values were dynamically adjusted to current consumption in the nine operating states. Thus, possible fluctuations in energy consumption were counteracted. These may be due to load and temperature changes or mechanical wear. In order to enable robust state detection, the reference values have been adapted to the changes via the formation of the moving average.

The reference value of the current state as well as the reference values of the other directly accessible states are continuously adapted to the changes. Another challenge was to recognize the state transitions. For this purpose, the consumption in the operating conditions must be constantly measured and monitored for characteristic changes.

It has been found useful to aggregate the individual active powers readings over a short period of time from a few seconds to a mean value and to use them as a temporarily comparison value. If the

difference between the comparison value and the reference value is outside a permissible range, a change of state is assumed. For safety, the status change is checked for validity by comparing it with the valid state changes.

In the second step for online analysis of production states, the above described model was implemented on the data sensor in a proprietary rule-based language with a total of 120 queries and instructions. The following is an explanation of the first two statements (see figure 3.3).

```
// intercept the relevant data packets
1."pass(if:*ETYPE=kIPV4; if:*I4PROTO=kTCP; if:*TCPSPORT=%502;
if:*MODBUSSIZE=%232; cont:%1)\0",
2."pass(set:$break=%1)\0",
```

Fig. 3.3 Example statements of the rule-based language.

The first nested statement checks whether the data packet is relevant to the model-based state detection. All IPv4 packets encapsulating the TCP protocol addressed to the port number 502 and having a length of 232 bytes are relevant. If all conditions are met, the cont:% 1 statement causes the 2nd statement to be skipped. Otherwise, statement 2 is executed, causing the next data packet to be analyzed. With these two commands, a filtering of relevant data packets is implemented. The subsequent instructions for the evaluation of relevant data packets are not explained in detail, as this would be beyond the scope of the present article.

4. Results and discussion

After the transformation of the model into an algorithm, it was implemented into the data sensor using the rule-based language. Following to that an evaluation regarding reliability of the state detection was performed. For this purpose, the data sensor was plugged into the Ethernet connection between the energy data sensor of the drilling station and the local Ethernet switch. The actual power values transmitted by the energy sensor in the data stream are detected by the data sensor and processed to conclude the current operating state of the drilling station.

In order to be able to fully validate the recognition of nine relevant states, all possible state transitions were carried out in a specific cycle during the test runs and production orders were commissioned via the MES. The deduced working states identified by the data sensor were compared with the actual operating states observed. (see figure 4.1 and 4.2).

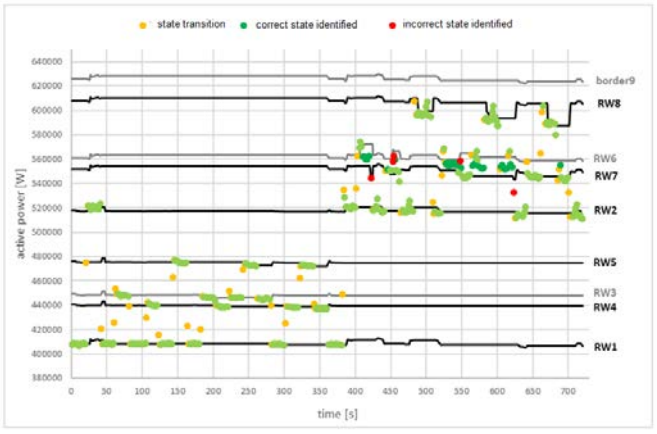

Fig. 4.1 Result of validation (states Z1 to Z8).

During the tests, 842 active power values were evaluated, wherein only 7 of them were identified incorrectly. Thus the error rate is 0.8%. Thereafter the state transition detection was tested. From the totally tested 68 state transitions 65 of them were recognized correctly, and besides none of them was classified as impermissible. The validation result of the commissioned production orders can also be shown: out of 14 orders, 13 were correctly recognized by the data sensor. In 12 of these orders, the data sensor could even distinguish between two different production order types.

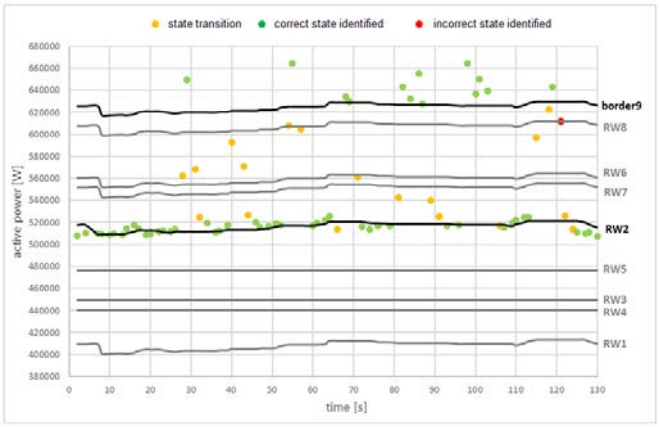

Fig. 4.2 Result of validation (states Z2 and Z9).

The validation result shows that in the case of sufficiently complex production processes, a condition monitoring system with certain level of reliability can be implemented by analyzing the Ethernet data with a single hardware.

5. Conclusion

In this work an algorithm for detection of operation states and state transitions was tested on a production line. Within this project, nine relevant operating states of the drilling station were defined. The total power consumption data of a drilling station in the cyber-physical factory was extensively analyzed and characteristics that represent a correlation between the energy data and the operating states were identified.

The analysis showed that using only the active total power value can be used to identify the operating state of the drilling station. In addition to that, a distinction between different production orders based on current power consumption and a time interval can be drawn. To develop a virtual sensor based on identified features and correlations, a model was derived. The model can recognize operating states and state transitions as well as distinguish between different production order types. In addition, the model includes the detection of impermissible state transitions, in which case an alarm message is issued.

To use the model in a real-time environment, the algorithm was implemented into a data sensors device using a rule-based language. Thus the data sensor represents a virtual sensor which determines the current operating state from the energy data in real-time and outputs it for online monitoring. After successful commissioning, the software was able to validate its reliability. The operating states determined during the tests were compared with the real operating states and an error rate of 0.8% was determined. Therefore, the developed condition monitoring system has a very high reliability. In this application, the virtual sensor was used in transparent mode where no interference with the actual data stream takes place. Due to the permanent monitoring of the production states in real-time, disturbances and irregularities as well as impermissible states or state transitions can be detected. This is important for the development of predictive maintenance applications. The data acquisition and evaluation method describe here can be embedded into any existing data networks.

6. References

[1] Patrick Jahnke: Machine Learning Approaches for Failure Type Detection and Predictive Maintenance, Master Thesis TU Darmstadt, June 19, 2015

[2] Chaitali S. Kalaskar, Vitthal J. Gond: Motor Current Signature Analysis to Detect the Fault in Induction Motor, Journal of Engineering Research and Applications, ISSN : 2248-9622, Vol. 4, Issue 6(Version 1), June 2014, pp.58-61

[3] Festo: Energiemonitoring CP Factory. Systembeschreibung Inbetriebnahme Anwendungsbeispiele, Denkendorf, 11/2015, p. 4.

[4] Festo: Qualifikation für Industrie 4.0, URL:http://www.festo-didactic.com/download.php?name=brochure_Qi4_screen_full_56758de.pdf&c_id=1100&file=brochure_qi4_screen_full_56758de.pdf, p. 10.

[5] Festo: Energiemonitoring CP Factory. Systembeschreibung Inbetriebnahme Anwendungsbeispiele, Denkendorf, 11/2015, p. 1.

[6] Siemens: SENTRON Multifunktionsmessgerät SENTRON PAC3200, Gerätehandbuch, 02/2008, A5E01168664A-04

INFLUENCE OF SELECTED ATTRIBUTES IN ASSEMBL SYSTEMS PLANNING ITH USE OF SIMULATION SOFTWARE

Doc. Ing. Václav Š. PhD.[1], Doc. Ing. Košťál P. PhD.[1], Ing. Lecký Š. [1], Ing. Dávid M.[1]
Faculty of Materials Science and Technology – Slovak University of Technology, the Slovak Republic [1]

simon.lecky@stuba.sk

Abstract: *At present, there is an increasing emphasis on planning production and assembly systems. In the planning phase, it is important to eliminate as much as possible, ideally all deficiencies and errors of the intended system. Simulation software helps to find shortcomings in production or assembly systems. Using simulation, we can analyze individual parts of production systems in a virtual environment before they are implemented. This all leads to cost savings in the implementation of production systems. The article deals with simulation of production systems and their planning. The case study will illustrate the simulation process in choosing the right manufacturing system.*

Keywords: ASSEMBLY PLANNING, SIMULATION, ASSEMBLY SIMULATION

1. Introduction

Based on the competition of the international manufacturing network, it is felt to increase pressure to improve the efficiency of production systems. International logistics networks need a linked logistical concept. These requirements can be managed only by using the right digital business tools in the context of the product lifecycle management environment (PLM). This allows the resulting data to be used as the basic support for cooperation between different departments and offers everyday relevant data for every user who needs them. Simulating a complete material flow, including all major manufacturing, storage and transport activities, is a key component of a digital enterprise in the industry. A 20-60% reduction in inventory and production throughput and a 15-20% increase in the productivity of an existing production process can be achieved in real projects. Reasons for using simulations can be strategic or tactical operational goals.

Fig. 1 Product lifecycle management

From a strategic point of view, users answer questions about which plants in which countries are best suited to producing a new product, with regard to factors such as logistics, workforce, time lags, flexibility, warehouse costs, this is all about production from the years to come. In this context, users also assess the flexibility of the production system and, therefore, the significant change in production figures (statistical data - a topic that is becoming more and more important today).

Simulation models make evaluation of different variant of production and effectiveness measurement possible [1]. "In addition, the simulation allows to use new strategies and procedures, verification of the production in the revised system, locate bottlenecks in the flow of materials, increase productivity while reducing inventory and reduce the cost of the implemented changes [1]."

"A bottleneck is defined as a workstation limiting the production efficiency of the entire process (Betterton, 2012; Hsiao et al., 2010). It is the enterprise's workstation or a production cell that is characterized by the lowest level of a specific production parameter
among all co-participating parameters in the manufacturing process. This can lead to a situation, in which a workstation before the bottleneck completes processing, but it cannot forward materials, as the workstation that follows it, being the bottleneck of the process, is still engaged in processing earlier orders. Bottlenecks can also extend the time of the standstill in the processes occurring at subsequent stages (Li, 2009), prolonging the waiting time for further orders. Bottlenecks mark the pace of the entire process. All definitions are consistent in one sense – bottlenecks have an adverse effect on the efficiency of production systems, the flow of materials in the process as well as even burdening of workstations. [2]"

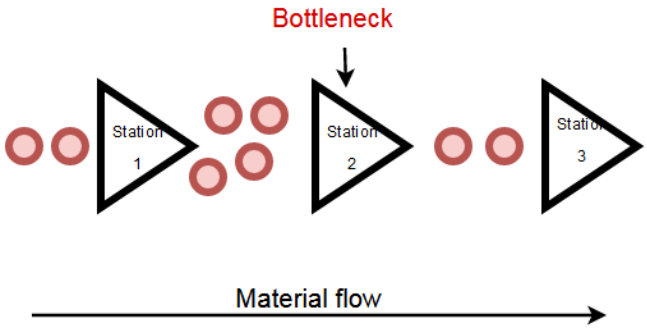

Fig. 2 Bottleneck characteristics

Application/ benefit

Plant Simulation (formerly eM-Plant, Simple++) is a standard software for the simulation of highly complex production systems and control strategies. The tool features object-oriented, graphic and integrated modelling, simulation and animation of systems and business processes [3].

It is an important component and entry tool for the Digital Factory in the software portfolio of Siemens PLM.

Typical questions that Plant Simulation can help to answer

- How can investment costs be minimized?
- Is the required output reached?

- What happens in case of quantity changes?
- How can stocks be reduced?
- What is the best control strategy?
- What effect do rush orders have?
- What is the best planning alternative [3]?

Statistical Evaluation

Plant Simulation offers different statistics for model parameters: Interval statistics, overall statistics and momentary statistics. Comprehensive analysis tools such as automatic bottleneck analysis, Sankey diagram and Gantt chart (planning chart) [3]

Structure / Modules

All Plant Simulation basic and user modules are visible and accessible in the modular library, which can be configured freely. Arbitrary user modules are graphically and interactively created from basic modules by the user himself. These include:

- Integrated neuronal networks
- Factor analysis
- Experiment administration
- Automated optimization of system parameters
- Batch size and sequence planning (sequencing)

The complex production lines and manufacturing processes of today's manufacturers are best understood through a rigorous, analytical framework. It is no surprise that digital modeling and simulations are becoming essential pieces of the manufacturing IT toolbox. Industrial simulation software provides insight into potential problems and presents opportunities for improvement in plant and production line layout, process flow, and other aspects of a manufacturer's operations [3].

2. Simulation with Tecnomatix Plant Simulate

Tecnomatix Plant Simulation software makes the simulation and optimization of production systems and processes easy and effective. By use of Plant Simulation, material flow can be optimized, utilization of resources and logistics for all levels of plant planning from global production facilities, through local plants, to specific lines is effective and time efficient [4].

Benefits

– Enhance productivity of existing production facilities by as much as 20 percent

– Reduce investment in planning new production facilities as much as 20 percent

– Cut inventory and throughput time by as much as 60 percent

– Optimize system dimensions, including buffer sizes

– Reduce investment risks through early proof of concept

– Maximize use of manufacturing Resources

– Improve line design and schedule Features

– Simulation of complex production systems and control strategies

– Object-oriented, hierarchical models of plants, encompassing business, logistic and production processes

– Dedicated application object libraries for fast and efficient modeling of typical scenarios

– Graphs and charts for analysis of throughput, resources and bottlenecks [4]

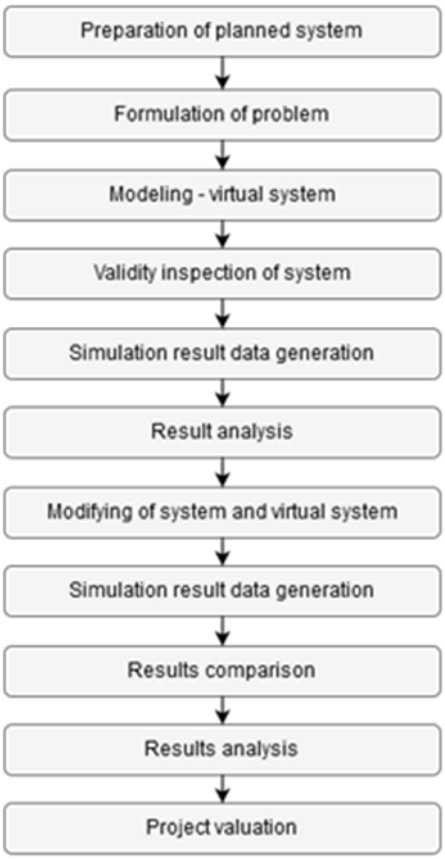

Fig. 3 Simulation workflow steps

3. Simulation case study

In this section will be discussed and shown case study. This case study is aimed on simulation solutions for production lines and systems with use of simulation software Tecnomatix Plant Simulate from company SIEMENS. Tecnomatix Plant Simulate is based on discrete simulation.

Basics of every simulation is to solve some problem or answer some of the questions mentioned before. In this case assembly/production system is tested if there is some room for update or improvement of throughput.

That means for this example that adjusted version of system will be tested and compared with base model of system. The point is to find improvement that would increase throughput or decrease resources.

This case study deals with assembly/production system which consist of input station, pick and place mechanism, three work stations, three assembly stations, four buffers and two conveyors.

First in Tecnomatix Plant Simulate every station, assembly station, conveyor or pick and place mechanism must have time management setting done before running the simulation.

Table 1: *Time management of stations*

Station	Time (seconds)
Pick and place	50
Preparation	300
Assembly	300
Assembly 2	240
Assembly 3	240
Packing	120
Preparation and handling	120

Time management for stations mentioned in Table 1 is between 50 seconds and 300 seconds. Buffers capacities are 1000 pieces except buffer 3 where capacity is 500 pieces.

Table 2: *Capacity management of buffers*

Buffer	Capacity (pieces)
Buffer	1000
Buffer 1	1000
Buffer 2	1000
Buffer 3	500
Failed parts buffer	1000

Table 3: *Speed settings of conveyors*

Conveyor	Speed (m/s)
Line	1
Line 1	1
Line 2	0,5

All the information in tables are parameters that can be changed with respect to technological limits of production/assembly system. By changing parameters, we can adjust model and analyze different output characteristics or behavior of system. Based on that can be chosen the right set up for system.

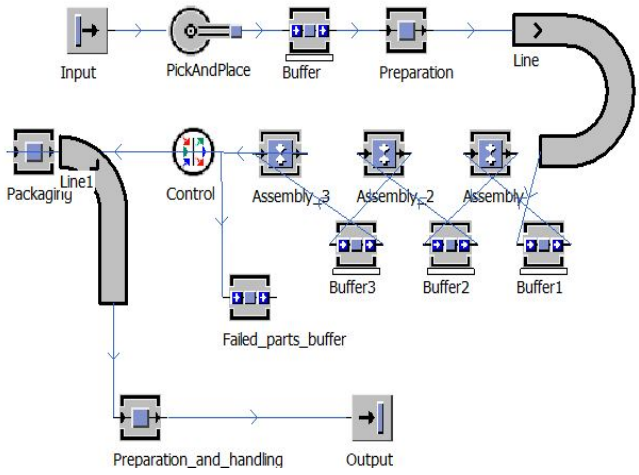

Fig. 4 Base model of system (Tecnomatix Plant Simulate)

In figure number 4 is show production/assembly model which starts at input station where pick and place mechanism moves units to buffer. Pick and place mechanism sets the speed of whole input. Next in preparation station, units are prepared for assembly line. To assembly line are units transported by conveyor with speed 1 m/s.

Assembly part of system consists of three assembly workstations with three buffers. At control point are units sorted and failed parts are moved to failed parts buffer, other parts are transported to preparation and handling station to get ready for output.

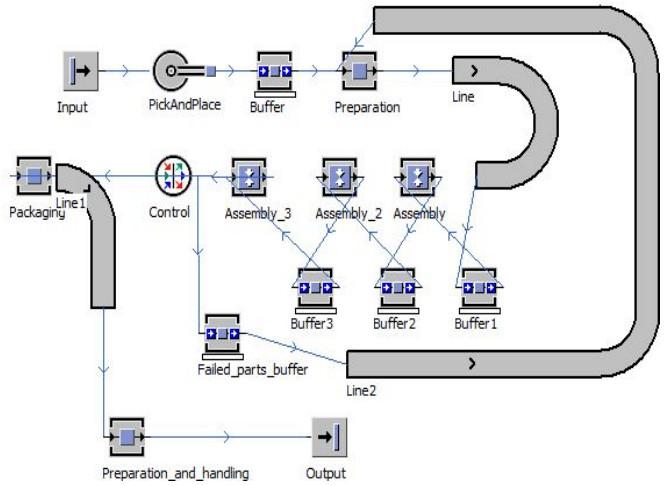

Fig. 5 Adjusted model of the system (Tecnomatix Plant Simulate)

Difference between base model and adjusted model in figure number five is that failed parts buffer is connected to conveyor. Through conveyor failed parts transport to preparation station again, so they are disassembled and ready for next assembly process.

Simulation models work usually with failure settings of 95% working time to 5% failure. In pick and place mechanism was calculated fail time 1% based on real model information.

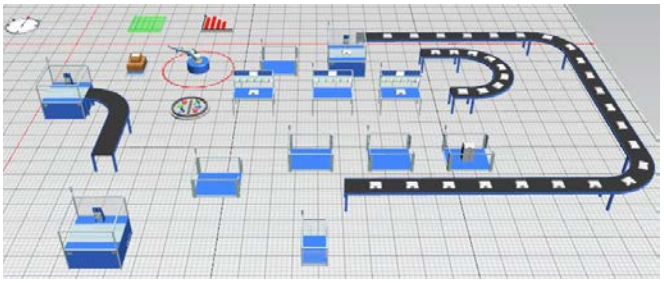

Fig. 6 3D model of adjusted system (Tecnomatix Plant Simulate)

In figure six we can see adjusted model in 3D view of Tecnomatix process simulate window. 3D models in simulation will be important in future as concept of industry 4.0 is becoming more popular nowadays.

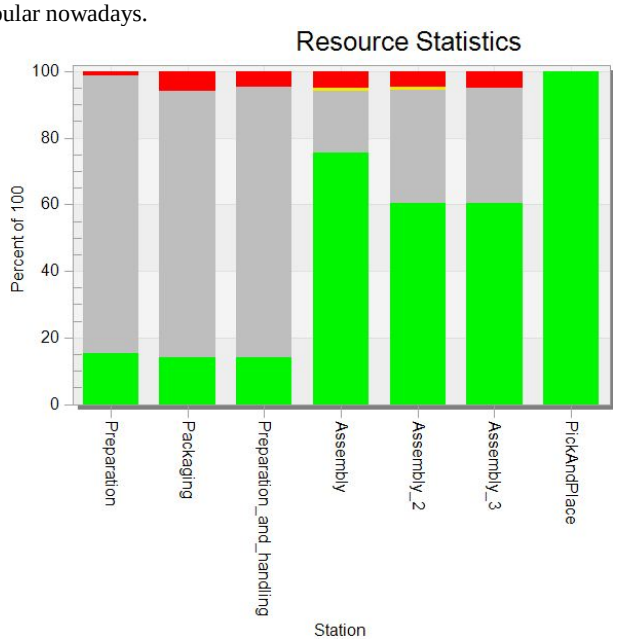

Fig. 7 Resource statistics of base model

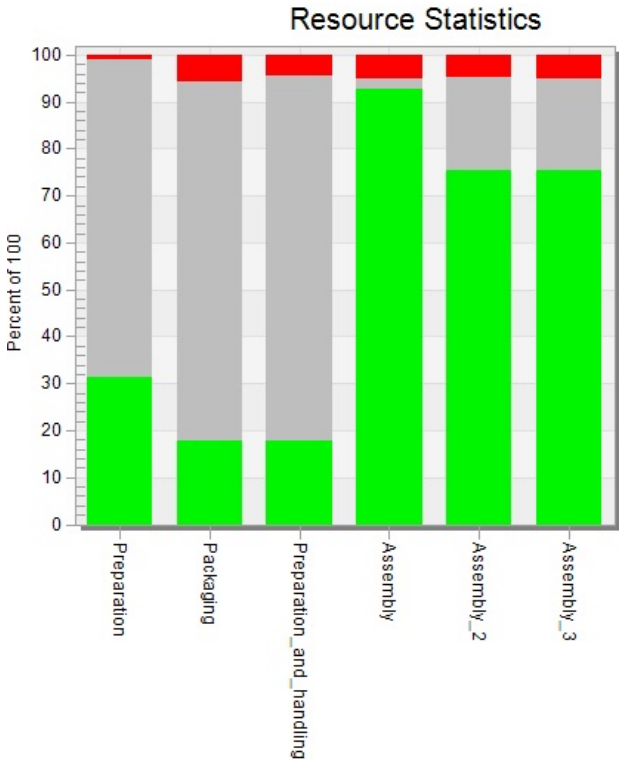

Fig. 8 Resource statistics of adjusted model

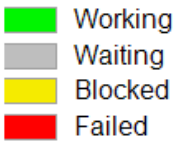

Fig. 9 Legend for resource statistics

Based on figure seven and eight we can see how working time of assembly stations increased only by managing the material flow and better timing on pick and place and conveyors.

Cycle time of five working days was tested for throughput evaluation. As is shown in table four, throughput in adjusted model is higher by 136 pieces of products.

Table 4: *Throughput of models in five working days*

	Base model	Adjusted model
Throughput	1064	1200

4. Conclusion

Computer simulation with IT tools is currently an essential activity to support the design of new production and logistics systems or even existing systems [5]. Simulation methods are used to evaluate different aspects of manufacturing systems or subsystems. Repeatability is an important and fundamental feature of computer simulation. Because of the exact values and parameters that have inherent values, the same process can be executed many times. In real life it is not possible [6].

The application of innovative design methods is one of the factors that has positively influenced the process of introducing fast, modern assembly systems [7].

This article describes the application of Tecnomatix Plant Simulation from SIEMENS in computer design and manufacturing process planning. Simulated production systems, created as examples, have shown that if the production system has some shortcomings, it can be improved by simulation. The simulation experiment can be tested with different characteristics and different modification types. It is a user choice when it is necessary to change the base model or just some features of the production model.

Major benefit of simulation like the one made in case study is that adjustments or improvements of production/assembly systems are made without shutting down the production. Real system work without changes and adjustments are made just after simulation shows that these adjustments will increase production or decrease spending etc.

The information obtained from the simulation results is influenced by the accuracy of the input data and model. The use of simulation methods of different processes in production, logistics or planning of new production systems is an element of Industry 4.0. It simplifies the planning of production systems and the optimization of existing systems.

Acknowledgement

The article was written as part of the Young Researcher project 1383“Influence of selected attributes in manufacturing systems and sub-systems planning in digital enviroment” supported by the scientific program - Motivation and support in quality and effectivity elevation of young researchers and scientists. Slovak University of Technology.

References

[1] Hromada, J., & Plinta, D. (2000). Modelowanie i Symulacja systemów produkcyjnych [Modelling and simulation of production systems]. Bielsko-Biała, Poland: Wydawnictwo ATH.

[2] Kikolski M., (2016). Identification of production bottlenecks with the use of Plant Simulation software. Economics and Management Volume 8 Issue 6.

[3] Plant Simulation: Product overview. SIEMENS, ©2017 [quotation 2017-11-11]. Internet source: www.plm.automation.siemens.com/

[4] Soble, B., Tecnomatix Manufacturing and Plant Simulation: Case study. SIEMENS, ©2014 [quotation 2017-11-11]. Internet source: https://www.hylasoft.com/en/posts/tecnomatix-plant-simulation

[5] SIDERSKA, J., 2016. Application of Tecnomatix Plant Simulation for modeling production and logistics processes. VGTU, ©2016 [quotation 2016-11-10]. Internet source: http://www.bme.vgtu.lt/index.php/bme/article/view/316

[6] KLOSOWSKI, G., 2011. Zastosowanie symulacji komputerowej w sterowaniu przepływem produkcji mebli, Zarządzanie Przedsiebiorst-wem / Polskie Towarzystwo Zarządzania Produkcją 2: 29–37.

[7] MADARÁSZ, L., KOVÁČ, J., SENDERSKÁ, K., 2008. Selection of assembly system type. SAMI 2008 6th International Symposium on Applied Machine Intelligence and Informatics - Proceedings, art. no. 4469196, pp. 44-47. ISBN 978-1-4244-2105-3

IMPROVEMENT OF TECHNOLOGIES FOR THE DEVELOPMENT OF MODERN RAIL AUTOMATION SYSTEMS

СОВЕРШЕНСТВОВАНИЕ ТЕХНОЛОГИЙ РАЗРАБОТКИ СОВРЕМЕННЫХ СИСТЕМ ЖЕЛЕЗНОДОРОЖНОЙ АВТОМАТИКИ

Assos. prof. Ph.D.(eng.) Kameniev Oleksandr, Assos. prof. Ph.D.(eng.) Lapko Anton, post grad. Shcheblykina Elena,
Department of automatic and computer remote control of train traffic – Ukrainian State University of Railway Transport, Ukraine

Abstract: *Until Currently in the countries of Europe there is an intensification of the introduction of modern microprocessor systems of railway automation and the increase of their functional capabilities. The introduction of additional functions of control and monitoring systems, tightening of the requirements for the safety of their operation, mutual integration and unification of systems for various purposes, the complication of the implementation of processing of logical dependencies require fundamentally new approaches to the development of software and hardware of a new generation. In this regard, scientific and applied research aimed at the development of appropriate technologies is being conducted, based on the common methods and tools used in the formation of control and monitoring systems for various objects of the railway transport infrastructure. The proposed material contains the main results of such studies conducted over the past five years, as well as the main directions for further improving the development of microprocessor-based rail automation systems.*

***KEYWORDS**:* RAILWAY AUTOMATION, DEVELOPMENT, TECHNOLOGY, INTEGRATION, LOGICAL DEPENDENCIES, CONTROL SYSTEM, TRANSPORT INFRASTRUCTURE

1. Introduction

Currently, in Europe, there is an intensive development of rail automation systems involved in the management and regulation of train traffic, as well as the implementation of shunting work. Modern systems are built on a microprocessor-based element base with application of programmable logic. Several generations of such systems have already changed. Systems of the first generation, which appeared in the late 70's - early 80's of the last century, used symbiosis of the microelectronic and relay-contact element base, laying on the latter almost 100% of the responsible functions. Those. full responsibility for ensuring the conditions of traffic safety is assigned in such systems to relay-contact logic elements and finite state machines. The second generation of transport automation systems (90s of the last century), similar to the first generation, also represented a combination of a microprocessor and a relay-contact logic component. However, unlike the previous generation, there is a division of responsibility for the safety of the functioning of systems between relay and microprocessor components. The degree of distribution depends on a number of factors, among which: the functional purpose of the system, the type of technological control object, the type of microelectronic components used, the way of reserving information-control channels, etc. The third generation of rail automation systems (late 90s - early 2000s) is characterized by the fact that all the logic of functioning in them is programmable, while the switching of power circuits is performed by means of relay components connected to the windings and contacts of the modules O and input. In such circuits, the relays perform the function of exclusively contactors, without participation in the implementation of the dependency logic. In the systems of the fourth generation (2000s - present), all the logic of the functioning and implementation of the execution of commands are performed on programmable microprocessor components - without the use of relays. In such a system, the implementation of the dependency logic is performed by a separate subsystem, and the execution of commands by specialized object controllers [1 – 3].

The most interesting are the systems of the fifth generation, which began to develop actively after 2010. They are characterized by mutual integration and unification of systems for various purposes on the basis of a single core of management and control [4, 5].

For automation systems of different generations, fundamentally different approaches to the preparation of the turnkey management complex are applied, including design, production, safety proofing and commissioning. At the same time, it is the design and proof of security that, in the opinion of most experts in the field of knowledge, are the most important components of the technology for developing such responsible systems.

At the same time, for systems of the last two generations, which are the most economical and efficient from the point of view of performance indicators, many aspects of the above components are fundamentally unresolved. The task of the conducted research is to form preliminary bases for the subsequent solution of an important scientific and applied problem of improving technologies for the development of modern rail automation systems.

2. Preconditions and means for resolving the problem

2.1. Methodological and practical basis for the development of methods and design tools

Automated design of modern railway automation systems involves the following main areas: software design (configuration) and design of technical documentation. For these purposes, specialized application packages of CAD systems are used. The basis for the development of such systems used for transport infrastructure facilities is the principle of their territorial distribution.

In [5], experimental-static models of distributed process objects were proposed as a mathematical basis for improving methods and tools for computer-aided design. They are based on the graphic and analytical representation of the initial design object with the subsequent block decomposition of the graphic model. As a result, the implementation of the design scheme using this method looks like the diagram shown in Fig. 1.

The disadvantage of this approach is the excessive complexity for the user, primarily due to the inconvenience of the user interface and the need for specialized knowledge in the field of graph theory and matrix analysis.

At the same time, classical methods and means of computer-aided design are not in all cases acceptable for rail automation systems, taking into account their specificity. Thus, combining the method of forming a design object using experimental-static models and classical graphical shells (human-machine interfaces) is a method of solving this problem in the field of computer-aided design.

2.1. Methodological and practical basis for the development of methods and design tools

The main methods of proving the safety of railway automation systems are: methods of expert evaluation, calculated, experimental and calculation-experimental methods.

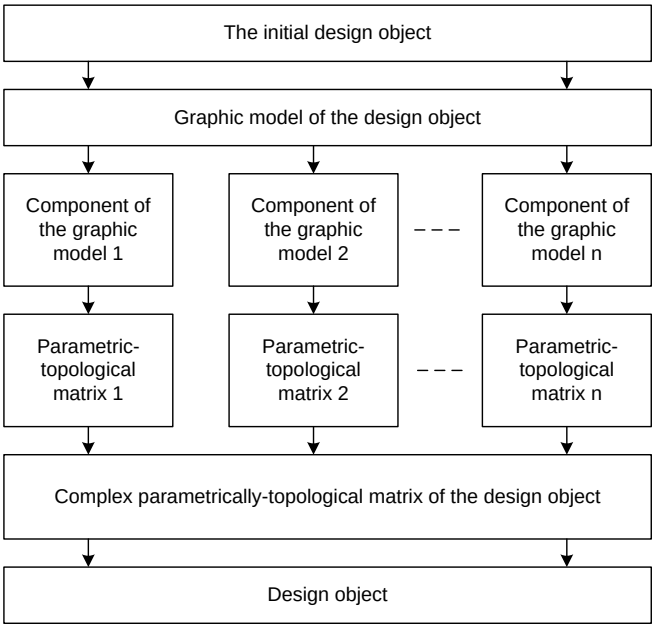

Fig.1. *Scheme of graphical-analytical design*

Of decisive importance are the experimental methods, which consist in the imitation, bench, combined and operational tests. Simulated and combined tests carried out in the laboratory conditions bear the main burden for revealing the features of the system's behavior, including failures, errors, etc.

It is these tests that can be automated as much as possible using specialized software test automation (robot testers) and test scripts that are put into these tools and implement the corresponding programs and techniques. An approximate simplified procedure for performing such tests is shown in Fig. 2.

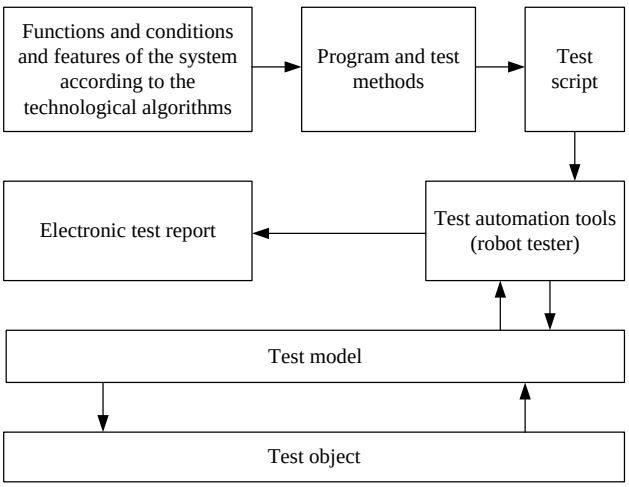

Fig. 2. *The existing simplified procedure for automating tests*

The main disadvantage of this approach is the complexity of providing and evaluating the test coverage of the functions, conditions and conditions of the control system. This is due to the fact that the program and test methodology, on the basis of which the test script is formed, is compiled by engineers on the basis of technological algorithms (technical specifications). At the same time, all possible combinations of states of the elements of the system, as well as "covered" (unintended) manifestations of the program and methodology may not be taken into account. Thus - an adjustment of the test automation method is required taking into account the objective evaluation of the test coverage and its provision.

Together, the solution of the two agreed problems in the direction of improving the technologies for the development of modern railroad automation systems of the fourth and fifth generations should increase the economic and technical efficiency of their creation. The evaluation of the corresponding effect depends on the purpose and specific modification of the control system.

3. Solution of the problem under consideration

3.1. Synthesis of the method and interface of computer-aided design

The solution of the problem of computer-aided design is the synthesis of the user's shell (user interface) with the means of forming the experimental-static model of the design object (the subsystem for processing logical dependencies, technical documentation, software, etc.). For this, a graphic editor with an external interface of an acceptable CAD package is created. This editor forms a modified graph of the experimental-static model, which together with the editor represents the custom shell of the advanced CAD system (Fig. 3).

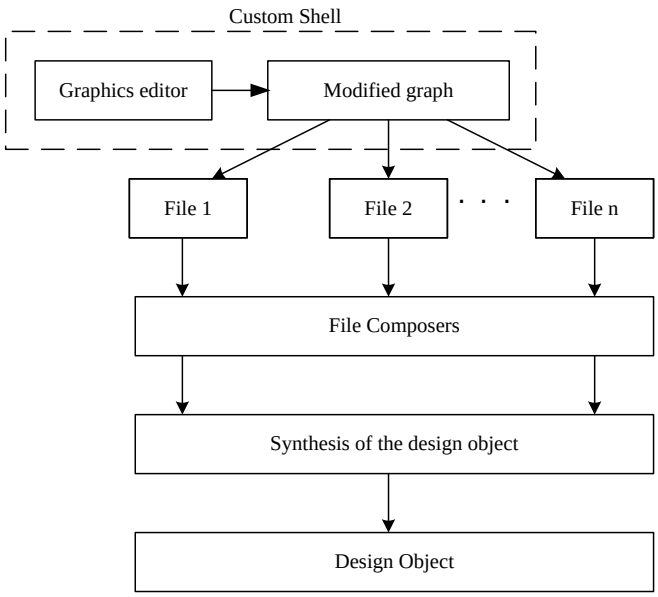

Fig. 3. *The scheme of computer-aided design taking into account the synthesis of the graphic shell and the experimental-static model*

In contrast to the classical experimental-static model proposed in [5], the proposed approach does not presuppose the preliminary formation of the components of graphs and blocks of parametrically-topological matrices in explicit form. Instead of them, files File 1 - File n, reproducing data blocks are generated directly on the basis of the modified graph. After composing these files, the synthesis of the design object is performed - similar to how it is done when using the classical experimental-static model.

The most important advantage of the proposed approach is the maximum adaptation to a user who does not have a special mathematical preparation, and the use of standardized human-machine interfaces.

The most promising environment for automated design, which is taken as the basis for the formation of the user's shell, is a CAD-type E-plan. The advantage of such an application package is maximum user adaptability, the ability to accelerate the design of large-scale objects, the use of convenient tabs and links, a sufficiently high speed. Taking as a basis the shell of this CAD will make it possible to create a universal means of automated design of railroad automation systems of any complexity.

Thus, the issue related to the effective use of graphic models and their analytic interpretations (in the form of matrices) in the problems of computer-aided design is solved.

3.2 Creation of self-learning system of automated tests

As it was noted earlier, the most important advantage of imitation and bench tests is the possibility of their maximum automation - with the exception or minimization of human participation in the trial process. At the same time, however, the human factor is not completely excluded under the existing approach (Figure 2) in connection with the design of the program and the test procedure followed by its interpretation into a test script by a test engineer (a group of engineers). In this regard, at least it is not guaranteed to provide 100% of the test coverage of the functions, conditions and properties of the control system.

The solution to this problem is the implementation of self-learning test scripts (Fig. 4).

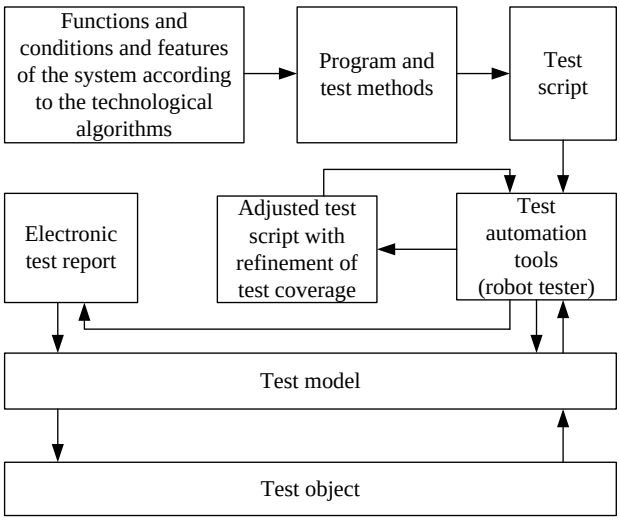

Fig. 4. *The procedure of automated tests with self-learning test script*

With this approach, the procedure for performing automated tests is generally similar to the original version (Fig. 3). However, in the scheme (Fig. 4) it is stipulated that only the basic (initial) test script is formed on the basis of the program and the test procedure by the test person. It is formed and used only before the first test cycle.

On subsequent cycles, the test automation tool generates a corrected test script, taking into account the actual coverage of the functions, conditions and properties of the control system. For this test script, feedback is provided to the test automation facilities, in accordance with which the technological information of this script is written to the memory devices of these means. Thus, a system is formed in which the automation tools independently form a test scenario using some initial data (the initial test script) and dynamic test coverage results.

In turn, the evaluation of the test coverage is formed on the basis of information obtained on the basis of the dynamic (test) analysis of the test object (control system) through the information channels of feedback. Only when determining the complete (100%) coverage of all functions, conditions and properties of the system is the feasibility of testing determined. This is done by a special algorithm (Fig. 5).

The initial data in this algorithm are the sets of input signals of the control system, on the basis of which, in turn, the sets of output signals and internal states are formed. On the basis of these sets, sets of combinations of functions, conditions and properties of the system are formed, which actually represents a test coverage without taking into account the reaction of the system to such combinations. After the initial test script is formed, the above combinations are cycled through according to their indexing. Only after this is done, the test coverage is checked (branch operator in Figure 5). Only after the positive test results is formed a dynamic test script. Otherwise, the cyclic operation is repeated until a complete test coating is provided.

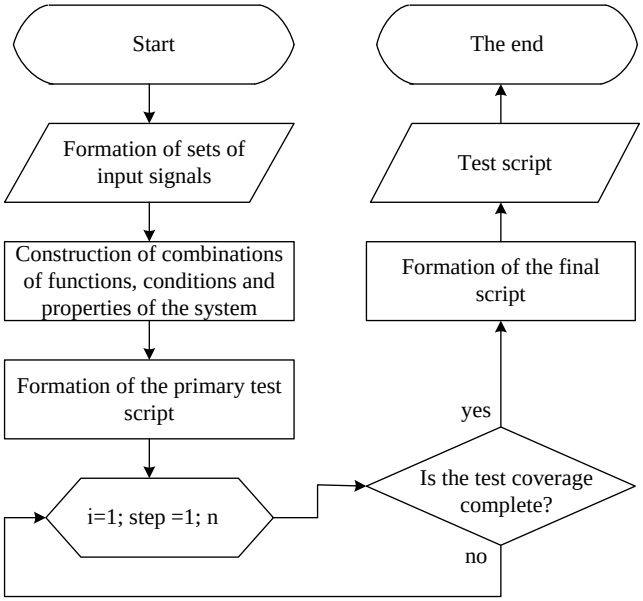

Fig. 5. *Algorithm for generating a dynamic test script, taking into account testing of the test coverage*

Performing the process shown in Fig. 5 of the cyclic procedure is realized during the direct execution of automated tests with subsequent testing of the test coating. Thus, the first few test cycles serve not to reveal the properties of the system (including failures and failures), but to provide self-learning test scripts. The number of these cycles depends, first of all, on the scale of the transport infrastructure object, which is subject to testing. For control systems for various purposes and for a particular application, this number of cycles can vary within fairly wide limits.

However, however, the methodology (procedure) for evaluating the test coverage, which is performed on the basis of combinatorial analysis, remains unclear. The algorithm for its implementation is shown in Fig. 6.

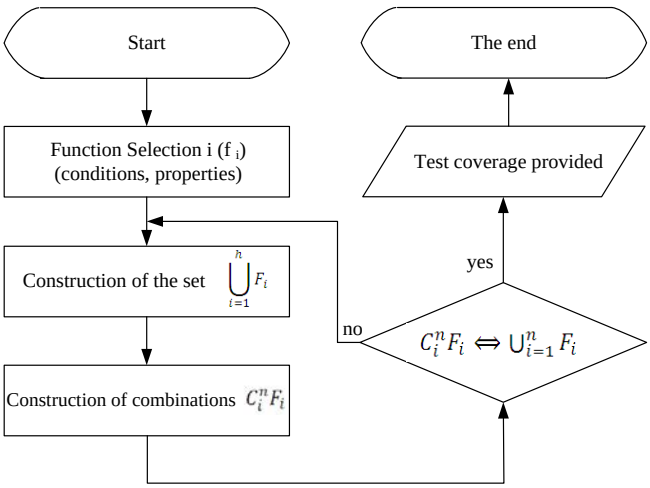

Fig. 6. *Algorithm of combinatorial evaluation of test coverage*

The algorithm works as follows. At the first stage, the union of the sets of all functions, conditions and properties of the system $\bigcup_{i=1}^{n} F_i$.

After that all their possible combinations are determined $\tilde{N}_{i=1}^{n} F_i$.

The completeness of the test coverage is determined on the basis of a one-to-one correspondence of the specified combination of sets and combinations of functions, conditions and properties of the system. In fact, the algorithm in Fig. 6, is an embedded algorithm for Fig. 5. Completely executed test coverage is a guarantee of

verification of all functions, conditions and properties of the system.

However, even as a result of the procedure in Fig. 6 the test coverage problem is not completely solved, which may be due to the identification of additional system properties in the testing process. These properties should also be taken into account in the assessment of the test coating. The corresponding algorithm is shown in Fig. 7.

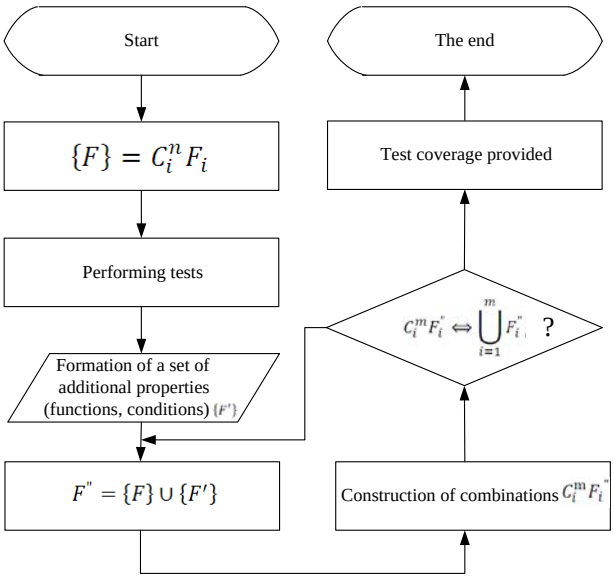

Fig. 7. *Algorithm of combinatorial evaluation of test coverage, taking into account the identification of new systems*

Initially, the initial set of combinations of functions, conditions and properties of the system $\{F\} = \tilde{N}_{i=1}^{n} F_i$. In the process of testing, an additional set is formed, identified during their conduct $\{F'\}$. As a result, a set of initial and additional (revealed in the test) properties of the control system is formed $F'' = \{F\} + \{F'\}$. The subsequent operations with the resulting set are carried out in a manner analogous to the algorithm in Fig. 6.

Another important aspect of carrying out automated tests in conditions of self-learning test scripts is the correction of the original program and the test procedure taking into account changes in these scripts. The fact is that according to the current normative and technical documentation for testing, it is the program and methodology that is the guiding document, according to which the order and conditions of testing are regulated. This is especially true for the certification of control systems, in which the technical documentation for the system (including the program and test procedure) is an integral attribute of the object of certification. In such circumstances, the guidance document must necessarily be aligned as an updated test script, and in accordance with the current regulatory technical documentation. However, adjusting the program and test methodology only on the basis of the test script does not guarantee unambiguous compliance with regulatory requirements, since certain aspects and results of self-learning test scripts may not correspond to these requirements. At the same time, these discrepancies must be taken into account both in the guidance document and in the script itself. This should be taken into account in the final test cycle. The algorithm for performing the corresponding check and making corrections based on it is shown in Fig. 8.

As a result of the implementation of the above algorithm, if there are any inconsistencies in the test script, the corresponding normative and technical requirements are corrected.

The final results can only be the results of the latest spraying cycles, under which the program and methodology for their implementation have not changed.

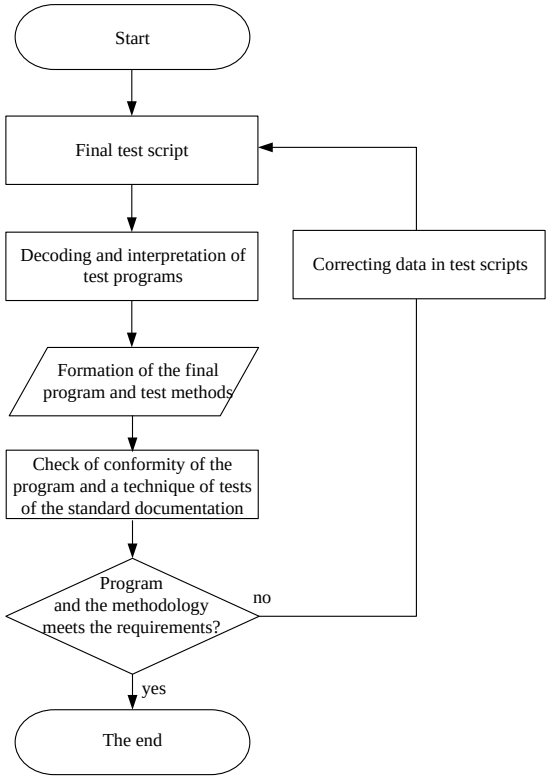

Fig. 8. *Algorithm for adjusting the program and test methodology, taking into account changes in the test script and regulatory requirements*

The resulting electronic test report must be consistent with the final versions of both the test program and methodology, and the test script.

4. Conclusion

Thus, in the technology of the development of modern systems of rail automation there are two main problems - the automation of design and automation of safety tests. Within the framework of solving the first problem, an approach based on the synthesis of the graph-analytic design method and the graphical user shell is proposed. To solve the second problem, an approach based on self-learning test scripts is proposed. Additionally, a set of procedures for verifying the correctness of the results of self-study is proposed. The results of the research are practically applied in the conditions of the development and implementation of a microprocessor system for the electric interlocking of pointers and signals at a number of railway stations.

5. Literature

1. Karevs, V. Railway automation and telematics system's monitoring and diagnostic/ V. Karevs. – Saarbrücken: LAP LAMBERT Academic Publishing, 2015. – 192 p.

2. Pereira, J. RAMS analysis of railway track infrastructure (Reliability, Availability, Maintainability, Safety) / J. Pereira, P. Teixeira, J. Viegas. – Paris: International Union of Railways (UIC), 2015. – 44 p.

3. Moiseenko, V. Predicting a technical condition of railway automation hardware under conditions of limited statistical data / V. Moiseenko, O. Kameniev, V. Gaievskyi // Eastern-European Journal of Enterprise Technologies. – 2017. – №3/9(87) . – P. 26-35.

4. Arlat, J. Composants COTS et sûreté de fonctionnement / J. Arlat. – Atelier thématique n°5, LAAS-CNRS Toulouse, 2003. – 12 ñ.

5. Kamenyev, A. Isomorphism classes of tolerance at different levels of hierarchical control systems / A. Kamenyev, A. Lapko // Scientific works of Donetsk National Technical University. Series: "Computer Science and Automation". – 2016. – No. 1 (29). – P. 8-11. – 2016. – №4/3(82). – P. 25-30.

ANALYSIS OF OPERATING MODES AND ENERGY EFFICIENT PRACTICES DURING THE OPERATION OF INDUSTRIAL INDUCTION FURNACES WITH NETWORK AND MIDDLE FREQUENCY

Assist. Prof. Dimitrina Koeva PhD [1], Assoc. Prof. Rachev S. PhD. [1], Assist. Prof. Lyubomir Dimitrov PhD [1],
Technical University of Gabrovo [1], Republic of Bulgaria

dkoeva@abv.bg

Abstract: *Among the main problems of the induction furnaces are the clearly manifested worsened power factor during operation, the asymmetry, the deflection and the variance of the supply voltage in their power supply. Induction furnaces in all their operating modes are a non-linear load with significant and varying consumption of active and reactive energy. Compensation devices are set for the heaviest mode of operation - metal melting. There remains a question of the limits of the low inherent power factor for individual regimes, the size of the penalties for this on an annual basis, and the potential energy saving measures taking into account the possibilities of waste heat utilization. In this connection, the task of implementation of modern optimal management according to predefined criteria is current.*

Keywords: INDUCTION HEATING, INDUCTION FURNACES, NON-LINEAR LOAD, POWER FACTOR, ENERGY EFFICIENCY

1. Introduction

Metal casting in the industry is a highly energy-intensive process characterized by a low inherent power factor and wide range of changes in the consumption of active and reactive energy. Achieving high energy efficiency is associated with technical risks associated with disruption of the production process, the application of inappropriate technology, lack of time and qualified personnel and increased capital costs. Energy savings can be realized in two ways - direct savings through lower energy consumption and indirect savings - through less consumption of material resources. Therefore, the goal is to achieve a certain amount of quality output with less energy and fewer raw materials. In order to do this, energy and material flows in the metal casting process should be explored and understood.

2. Research tasks

The object of the research and analysis is the operation of two induction furnaces (IF), one operating at a network frequency $f = 50Hz$ and the other one with an middle operating frequency $f = 250Hz.$ One of the advantages of the crucible furnaces is the short melting times due to the high specific power, with the minimum melting times of the metal depending on the frequency [1].

It is known that the energy emitted by the inductor depends on the frequency of the current, the ratio between the geometric dimensions of the crucible and the inductor, the dimensions and the electrophysical properties of the melting material. There are dependencies between the required thickness of the pipe walls of the inductor Δ_i and the size of the pieces of burst material from the operating frequency. Recommended at operating frequency $f = 50Hz,\ \Delta_i = 13-20mm,$ and the pieces dimensions have to be $200-350mm$. At operating frequency $f = 250Hz,\ \Delta_i = 2-4mm,$ and smaller pieces sizes – $150-2000mm$, [2, 3].

The dependences of the inductor's energy on the size of the crucible and the electro-physical properties of the process are of great importance for the operation of the induction furnaces in terms of their power supply and efficient operation. Changing the temperature of the metal pieces in the crucible changes both their geometrical dimensions and the contact area between the individual pieces, as well as their magnetic permeability and their specific electrical resistance. This dependence determines a continuous change in the energy emitted by the inductor and requires a flexible control system that ensures that optimum process parameters are maintained throughout its duration. The electrical parameters through which the metal melt process can be controlled are the magnitude and frequency of the supply voltage. Failure to comply with certain conditions in the construction and operation of the crucibles may result in severe accidents which will remove the furnaces for a long time and create an immediate danger to the service personnel. The principle of inductive energy transfer requires, if possible, the smallest wall thickness of the crucible, since it decreases the electrical efficiency factor along with its increase [4]. This thickness cannot be reduced below certain limits in order not to shorten the life of the crucible and to break through. Every 120-150 melts the crucible is beated out and imbed again according to strict requirements followed by sintering. Induction sintering is a process of switching on and off the furnace at a minimum power to achieve a rate of increase in temperature $100^oC/h$ to reach a temperature $t = 800^oC.$ Then, increase the rate of temperature rise to $150^oC/h \div 200^oC/h$ until the temperature reaches in the crucible $t = 1000^oC.$ The sintering temperature is then maintained for 1-2 hours at 50°C above the working temperature, after which the metal can be spilled.

3. Measurements and results obtained

Data of the induction furnaces with network frequency research

The object of the analysis is the operation of the TDM 3150-20 induction furnace with operating frequency $f = 50Hz,$ rated power $S_N = 2500kVA,$ 9-degree adjustment of the capacitor battery, capacity of the furnace - 10 *t.* At the beginning of the melting, when the molten metal is in a smaller quantity and the burden is still solid, all the stages of the capacitor bank are included. As the melting speed increases, some of the capacitors are turned off. The main disadvantage of these furnaces is the low melting speed and the need for symmetry to increase the efficiency of the furnace. Therefore, these furnaces are always allowed to work with a 'marsh', that is, leaving molten metal from the previous melt. The most economical mode of operation occurs when 25% - 35% of the molten metal is left. Then the duration of the melting is reduced to 1.5 - 2 *h,* with an energy consumption of 550 - 800 *kWh /t* [5, 8]. According to the aforesaid dependence, when left over from the previous melt 'marsh' 10, 25 and 40%, the power of the furnace required for the next melting process is reduced by (0.25; 0.48; 0.65) S_N. The electrical supply of such furnaces is carried out with the so-called Steinmetz scheme. Due to the low natural power factor, compensation is a must and should not be interrupted during the melting process. Since the consumption of active and reactive energy during the melting process is highly variable, therefore the symmetrical power needs to be altered by a similar load schedule.

Measurements of active, reactive and full power, consumed by the furnace in basic and finishing mode have been carried out. The duration of the process is 6 h. 25 measurements have been carried out, Fig. 1. For the purposes of the research, data from electric

meters with specialized software EMH-Combi Master 2000, [6] are available for graphical representation of the current state of the network (current and peak current and voltage values, active, reactive and full power, power factor, frequency; load schedules).

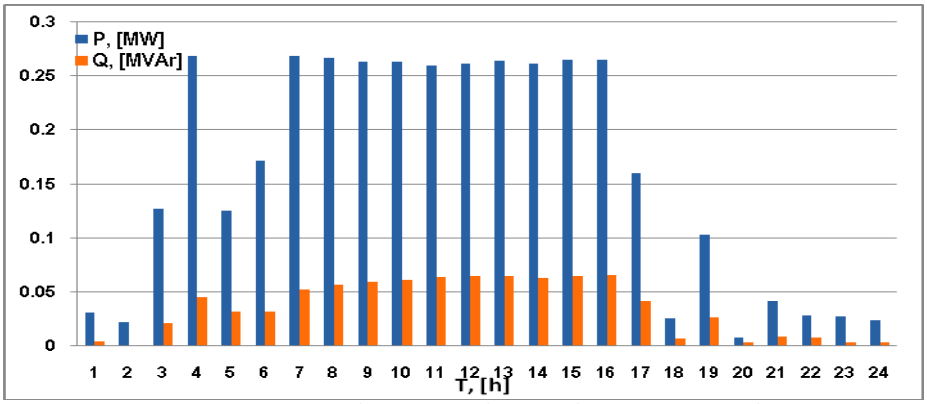

Fig. 1. *Active and reactive powers of an industrial-frequency furnace in basic and finishing mode.*

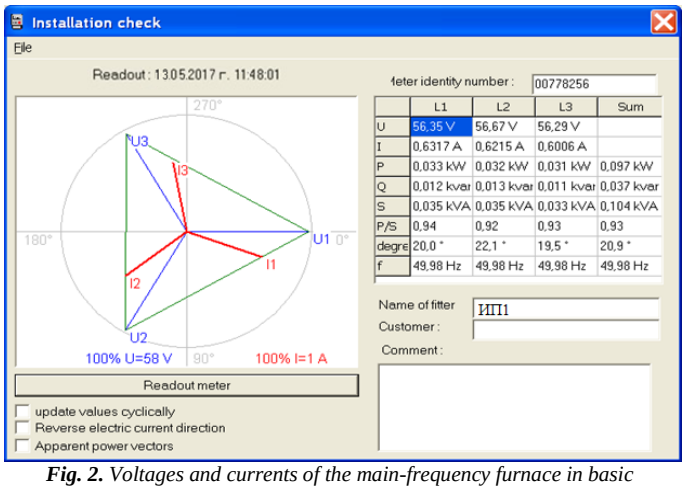

Fig. 2. *Voltages and currents of the main-frequency furnace in basic mode.*

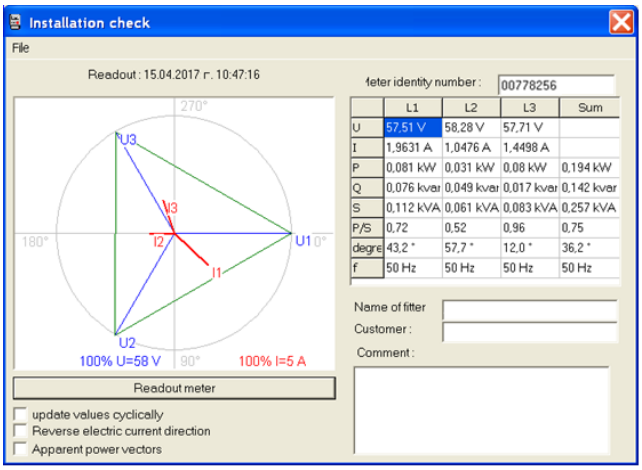

Fig.3. *An unbalanced induction furnace with a network frequency.*

Data of induction furnaces with middle frequency research

This kind of furnaces are mostly used for smaller parts and cold bent steel materials. Compared to induction furnaces with a mains frequency, these furnaces have a higher melting speed at the start of the solid burden process, therefore cosφ is easier to adjust.

The object of the analysis is the operation of the same type of induction furnace TDM with operating frequency $f = 250Hz$, rated power $S_N = 2 \times 2505kVA$, with thyristor rectifier and inverter, capacity of the furnace – 7.5 *t*. The furnace is controlled by changing the unlocking angle of the inverter thyristors. The researches have been carried out for the following furnace operating conditions: sintering mode - 16 *h* 30 *min*, 70 measurements recorded, Figures 4 and 5; basic melting and finishing mode with "marsh" 40% with duration 3 *h* 15 *min*, 15 measurements recorded, Figures 6 and 7; basic melting and finishing mode with "marsh" 10% with duration 3 *h*, 13 measurements recorded, Figures 8 and 9.

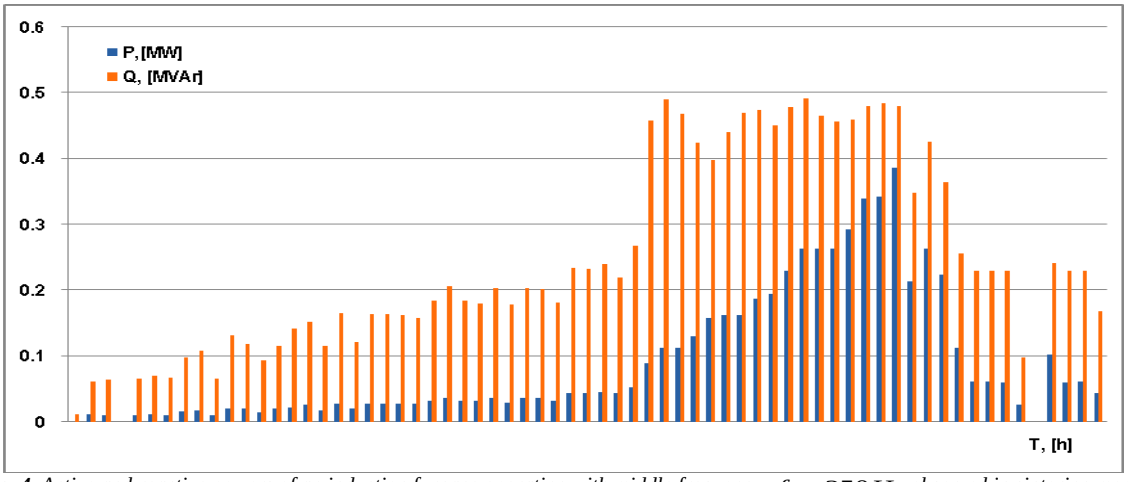

Fig. 4. *Active and reactive powers of an induction furnace operating with middle frequency* $f = 250Hz$ *observed in sintering mode.*

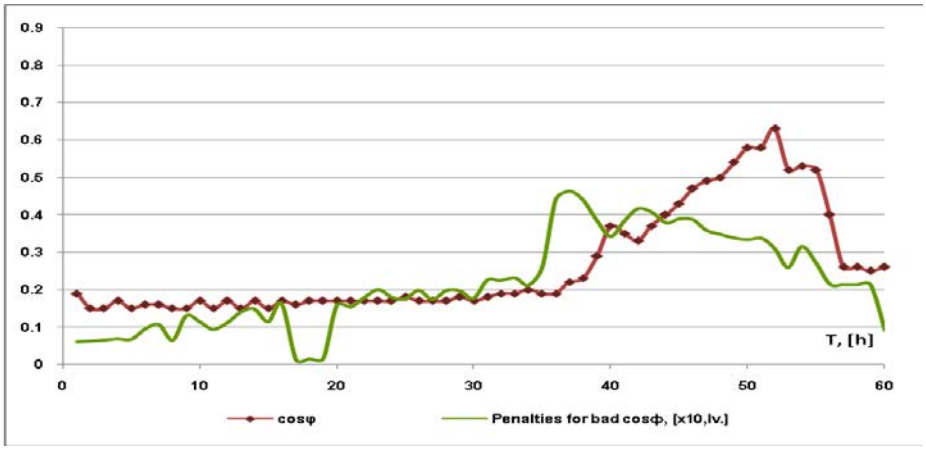

Fig. 5. *Modification of power factor in sintering mode and penalties for bad cosφ.*

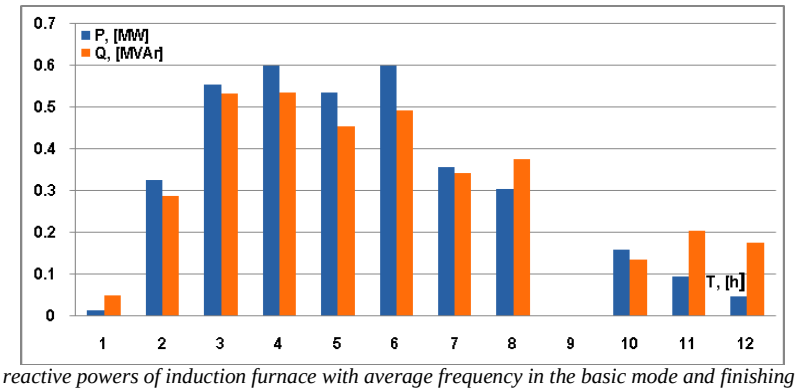

Fig. 6. *Active and reactive powers of induction furnace with average frequency in the basic mode and finishing with 'marsh' 40%.*

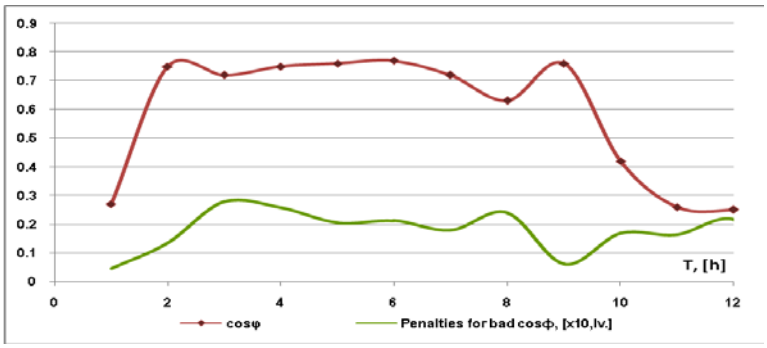

Fig. 7. *Modification of power factor in basic mode and finishing with 'marsh' 40% and penalties for bad cosφ.*

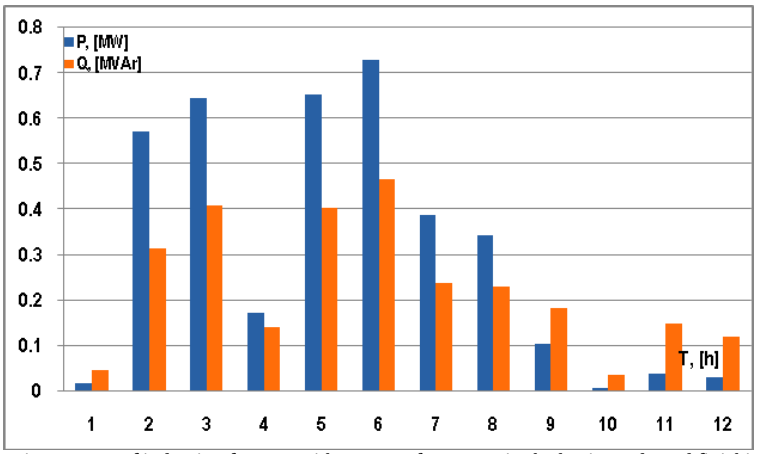

Fig. 8. *Active and reactive powers of induction furnace with average frequency in the basic mode and finishing with 'marsh' 10%.*

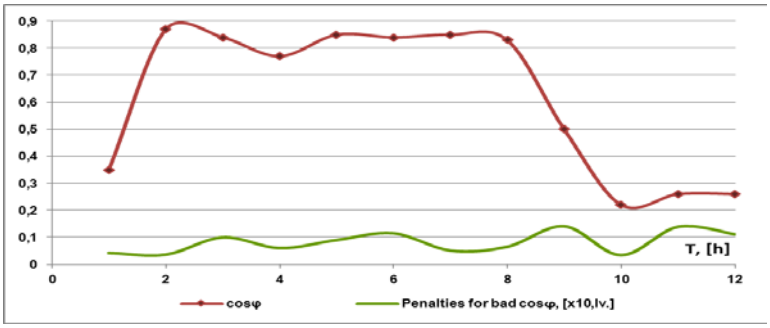

Fig. 9. *Modification of power factor in basic mode and finishing with 'marsh' 10% and penalties for bad cosφ.*

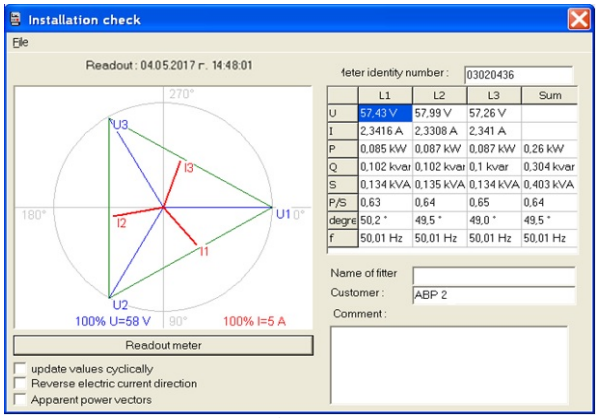

Fig. 10. *Graphics in basic and finishing mode with 'marsh' 10% and increased consumption of the furnace.*

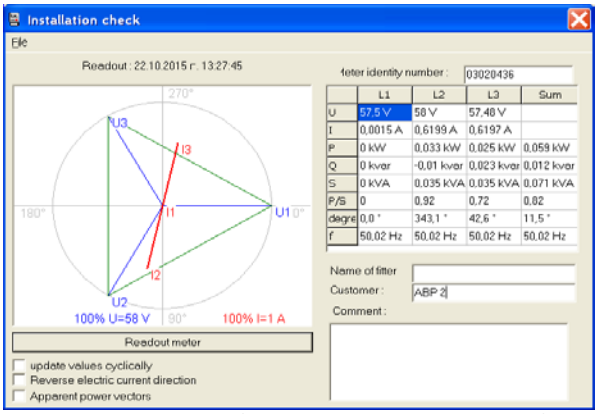

Fig. 11. *Graphics of emerging asymmetry as a result of an emergency situation (burnt thyristor).*

4. Conclusions

The load asymmetry in the operating modes of the induction crucible furnace with a thyristor converter is minimal. Fragrant deflections occur in emergency situations, Fig. 11. This is not the case with the power factor. Data analysis shows that drying (sintering) mode is the most severe mode of influence on the power supply and power system due to the deterioration of the power factor. In the case at hand it varies $\cos\varphi = 0.15 \div 0.19$. During the setting of the sintering temperature and then cos increases, but not enough, because the power supply becomes smooth and reaches only 40% of the installed one. From the load schedules, it is observed that during the induction melting process there is a strong uneven consumption of active electrical energy. The same applies to the size of the supply voltage, where the induction crucibles furnaces with network frequency are clearly expressed, Fig. 3. According to [7] the process can be divided into three distinct stages: 1st stage - melting of the metal pieces placed in the crucible, followed by zero electricity consumption, refining and sampling of the metal to be tested in a laboratory; Stage II - overheating of the metal up to 1520°*C*, correction of the metal, if needed, followed by zero consumption; Stage III - preheating and spilling the metal from the crucible. Thus, it is clear that the greatest amount of electricity consumption is in the basic mode of operation about 70-75%, which includes this first stage. The supply voltage during this mode changes to small limits (varies in the range 1300-1500*V*). In this mode of induction crucibles furnaces operation with a mains frequency is the most advantageous time for performing compensation and carry out symmetry of the load.

Data analysis for basic and finishing modes with 'marsh'

Under Basic Mode (First Stage): duration 1.4 hours (about 84 minutes); active power - an average of 2624 *kW*; power factor - average $\cos\varphi = 0.67.$

The second and third stages are in the finishing mode.

On finishing mode: overheating time - second stage (1420°*C* to 1520°*C*), about 21 minutes; active power 500 *kW*; power factor - average $\cos\varphi = 0.41.$

In the third stage: d uration 1.5 hours (about 90 minutes) in this case and active power 380 *kW*.

The energy required for melting and overheating is 3141 *kWh*, hence about 698 *kWh /t* of molten metal - a relatively high value of the specific power. This is not the case when using more power at the remaining 'marsh' 10%. Total energy consumed for melting and overheating is increased to 3520 *kWh*, hence about 521 *kWh /t* of molten metal. Consequently, the specific furnace power drops by 25.4%. In the 'marsh' 40% is used almost 55% of the power through the basic mode is maintained average $\cos\varphi = 0.72.$ With a 'marsh' of 10% this process is maintained with a higher power output of about 70%. During the first stage of the process, $\cos\varphi$ increases to an average value for the basic mode $\cos\varphi = 0.88.$

If there is a very good symmetry achieved of the furnace with a network frequency (which leads to a high $\cos\varphi \geq 0.9$) there are no financial penalties.

References

[1] Conrad H., R. Krampitz. *Elektrotechnologie*. Berlin, Verlag Technik, 1983.

[2] Sluhotskoy, A. E. *Induction heating plants*. Leningrad, Energoizdat, 1981.

[3] Todorov T. S., I. Mechev. *Induction heating with high frequency currents*. Sofia, Tehnika, 1970.

[4] Mineev R., A. Miheev, Y. Rizhnev. *Increase of energy efficiency of electrical supply of electric furnaces.* Moscow, Energoatomizdat, 1986.

[5] Kirov R., I. Iliev. *Electrical energy efficiency.* Varna, ENA Publishing House, 2017, ISBN 978-619-7255-05-8.

[6] EMH-Combi-Master, *Operational Manual*, 2000.

[7] Bogorov V., I. Valev, Compensation and symmetry of electrical loads of induction crucibles furnaces, Journal of University of Mining and Geology 'St. Ivan Rilski', Sofia, vol. 50, part III, Mechanization, electrification and automation of mines, 2007.

[8] Iliev I., N. Kaloyanov, Pl. Gramatikov, A. Terziev, I. Palov, S. Stefanov, K. Sirakov, V. Kamburova, *Energy Efficiency and Energy Management Handbook*, 'Angel Kanchev' University of Ruse, ISBN 978-619-90013-8-7, 2011.

APPLICATION OF CAD DESIGN OF TECHNOLOGICAL PROCESSES IN THE FIELD OF MATERIAL SCIENCE

Emil Hr. Yankov [1] Nikolay Tontchev [2] Simeon Yonchev

[1]"Angel Kanchev" University of Ruse, Bulgaria
[2] "Todor Kableshtov" Higher School of Transport, Sofia, Bulgaria

Abstract. *A review of the existing methods applied to multi-criteria decision aiding has been made as well as the multi-criteria approach to a class of problems in the field of material science has been defined. The multi-criteria decision aiding has been successfully applied to determine appropriate compromise decisions about the examined parameters of a number of technological processes of welding, chemical thermal processing, iron covering, etc. The approach presented determines the values of technological factors satisfying the requirements of users simultaneously to a number of values examined and proposes a solution for the relatively highest thresholds at one and the same time*

KEY WORDS*. SIMULATION, ANN, MODELING, OPTIMIZATION TECHNOLOGICAL PROCESES.*

1. INTRODUCTION

The modern problems of examining the parameters of new and conventional materials and technological processes are multi-criterial and conflict in principle. This nature of the problems is grounded by the fact that, with there examination, it is necessary to provide a certain set of parameters that have to satisfy users' requirements. The solution sought usually consists in determining those combinations of controlling parameters that provide the set of quality parameters specified. The choice of the assessment system of criteria and their rating according to the degree of significance is a problem difficult to formalize. It does not have unambiguous interpretation inevitably causes subjective decisions.

The problem of multi-criteria decision aiding could be most generally defined as a process with:

- a great number of parameters of the solution with a complex interaction among themselves;
- complex cause-and-consequence relations of the solution parameters and the attributes or aims;
- a set of alternatives, which could be reduced to a limited number and in this case the form of cause-and-consequence has to be used.

Due to that reason, looking for an appropriate model to solve a certain multi-criteria problem, one should define first the type of the situation, which is most suitable for solving the problem. An important element of the information base is the component implementing the method of planning the experiment. The main instrument and means of the modern scientific technologies is modeling as by it one can formulate the multi-criteria problem. The models of the complex objects and phenomena are often integrated including contents-describing and formal mathematical parts.

Hence, the study mainly emphasizes on different indices of quality providing including the following groups of criteria: strength (with static and dynamic loading), stiffness (E-module) and toughness (of the material/article), wear-out resistance and hardness, high temperature resistance, appropriate primary cost, compatibility with environment and the possibility of recycling.

2. ANALYSIS OF EXISTING METHODS

An approach to solving the problem (1) is to find the complete set of effective points on the basis of which the decision maker /DM/ chooses one solution. Such algorithms of linear continuous multi-criteria problems have been developed [1], [2]. They have a complex structure and operate slowly. On the other hand, the number of the effective points could be very big and thus make difficult the choice of a decision by the DM.

Another possible approach is to interact directly with the user and his/her preferences to obtain different compromise decisions. In that case, the DM should have a possibility to assess and compare the different solutions obtained. Independently of the method used to find out an effective point, this point has to reflect the DM's preferences to a certain extent. That is why in the multi-criteria decision aiding (MCDA) generally there are two stages: the stage of a dialog with the DM and the stage of computing the effective point. They are interactive procedures [3], which comprise great part of the well-known methods of solving a MCDA problem.

The criteria thus formulated are directly connected with high serviceability (functionality) and quality (constructional and operational properties) as well as economic efficiency.

The optimal matching of all these trends defines the efficiency of materials, i.e. their capability to meet the challenges of engineering in the best way on each stage of its development. Thus a set of problems of multi-criteria compromise decision-making could be formulated also by multi-criteria compromise optimization of one and the same class for which to is necessary to build an appropriate modern instrument in the process of study.

According to the information available about the DM's preferences, the methods of solving MCDA problems can be divided into three main groups:

1. when the DM is able to give a complete information about his/her preference;
2. when there is not such information available;
3. when this information is given by the DM in the process of solving the problem.

The criteria thus formulated are directly connected with high serviceability (functionality) and quality (constructional and operational properties) as well as economic efficiency.

The optimal combining of all these trends defines the efficiency of materials. The optimal matching of all these trends defines the efficiency of materials, i.e. their capability to meet the challenges of engineering in the best way on each stage of its development. Thus a set of problems of multi-criteria compromise decision-making could be formulated also by multi-criteria compromise optimization of one and the same class for which to is necessary to build an appropriate modern instrument in the process of study.

With the problems in the field of material science, the DM does not have information about his/her preference and for that reason the methods developed within the first group cannot be used.

The second group of methods is characterized by generating the whole set of effective solutions. The set of effective solutions is presented partially or entirely by the DM. Such methods are: the method of weight coefficients or *P* problem [4],[5],[6], the method of limitations [7],[8]; the method of weighed Chebishev's standard [9]. These methods are able to generate the whole set of effective solutions of the MCDA. However, their disadvantage lies in the big calculation resources necessary for generating and the impossibility

or difficulty of the DM to choose a solution from that set. However, they serve as a base of the interactive methods.

The third group of methods does not require knowledge on the function of preference by the DM. They are the base of the interactive man-computer procedures. The DM interacts with the computer (the algorithm set) on the purpose of clearing and giving additional information about the way of reaching a compromise decision.

The methods consist of three basic steps:

1. Giving the DM's requirements;
2. Finding a compromise solution;
3. Checking if the solution found satisfies the DM.

These methods have been developed most intensively for the past few year and are the base of further studies on the problem of MCDA.

The method of limiting planes [10] is very useful for the peculiarities of the problems in the field of material science. This method can be examined as a variation of the method of the admissible destinations. The methods of this class are unique with the approach, which they use to find the best compromise decision. They reduce the area of criteria iteration reflecting the planes and thus eliminating the stage of looking for a destination. Here precise information about trade-off coefficients is required.

3. APPROACH TO SOLVING MULTI-CRITERIA PROBLEMS IN THE FIELD OF MATERIAL SCIENCE.

The multi-criteria approach [10] proposed is characterized with the peculiarity of defining only one effective point of the whole set, which, according to its nature, turns to be fully sufficient for the different processes examined. That solution is characterized with the peculiarity of the problem class being solved and the solutions are with the highest thresholds of the quality indices examined. Their determination is usually assisted by the nature of the multi-criteria problem defined by the regression models of particular parameters of quality. In the field of material science, the latter require relatively one and the same preferences to all criteria as a whole. The solution presented meets the requirements mentioned and corresponds to the maximal effective point. It is determined after the discretization of the variables with certain exactness and building a transformation containing the lowest value of the criteria examined.

Applying this computation technology, technological solutions important for a number of technologies have been obtained and proved in practice [11]-[14].

The approach has been developed in the form of suitable software [10] that automates the calculations and determines the solutions necessary in a extremely easy way.

Before being visualized, the criteria have been put on a normally distributed scale by finding the discrete extremes and excluding the areas where the function has infinite or indefinite values. The movable limits move along this scale filtrating the visualized multi-dimensional spaces and giving a possibility to focus exactly on the decisions, which the researcher is interested in. The multiple criteria approach is used to visualize the numerical transformation of criteria and this visualization is called a filter. Experiments have been made with geometric mean, arithmetic mean, max and min filters and all decisions found out by these filters are non-dominated. The approach visualizes the symbolic data, transforming it into geometric information that helps to form a real picture of the data. The movable limits are a tool, which is used to focus on some details of the picture, thus finding the decisions looked for. The approach helps the decision-maker to get access to the limits as much as possible from the point of view of criteria. This information aids the participation of the decision-maker's intuition towards the problem and helps him/her to identify and fulfill the aim intentionally

In previous studies, team members conducted research that is summarized in Fig. 1 - Fig.4.

References.

1. Zeleny, M., "Linear Multiobjective Programming", LNEMS, vol. 95, Springer Verlag, Berlin, (1974).
2. Steuer, R., "Multiple Criteria Optimization: Theory, Computation and Application", John Wiley, N.Y., (1986).
3. Rosinger, E., "Interactive algorithm for multiobjective optimization", Journal of Optimization Theory and Applications, vol. 35, No. 3, (1985).
4. Geoffrion, A. M., "Proper efficiency and the theory of vector maximization", J. of Mathem. Analysis and Appl., vol. 22, No. 3, pp. 618-630, (1968).
5. Geoffrion, A. M., "Strictly concave parametric programming. Part I Basic Theory". Mgmt. Sci. No. 13(5), pp. 244-253, (1966).
6. Geoffrion, A. M., J. S. Dyer, and A. Feinberg, "An Interactive Approach for Multicriteria Optimization with an Application to The Operation of an Academic Department", Management Science, 19, pp. 357-368, (1972).
7. Bacopoulas, A., I. Singer, "On convex vectorial optimization in linear spaces". J. Optimization Theory and Applic. 21, pp. 175-188, (1977).
8. Yu, P. L., "Cone convexity, cone extreme points, and nondominated solutions in decision problems with multiobjectives", Journal of Optimization Theory and Applications, No. 49, pp. 430-468, (1974)
9. Bowman, V., "On the relationship of the Chebishev's norm and efficient frontier of multiple-criteria objectives". In: Thiriez H., S. Ziontis (eds.) Multiple criteria decision making (LNEMS vol. 130), Springer, Berlin, pp. 76-85, (1976).
10. Tontchev, N. T. & D. L. Dimitrovski.(1997) Software Providing of Compromise Optimization of Technology processe, Scientific Collections , Vol.1, Aviation and Spaceship, pp.583-589.
11. Toshkov. V., Tontchev, Ziumbilev. A.On Some Aspects of Minimizing the Energy Expenses at Nitriding of Steels in Glow-Discharge, Jubilee Scientific Session on 50th anniversary of the Technical University in Sofia, 1995, pp.32-36 /in Bulgarian/.
12. Dragolov D. N. Tontchev, Multi-factor Optimization at Technological Regimes Allowing Maximum Precipitation of Manganese and Nickel in Electrolytic Iron – Manganese – Nickel Coverings, Proceedings of the Maritime Scientific Forum, Varna, Volum 1, 1996, pp. 272-277 /in Bulgarian/.
13. Tontchev, N., Toshkov, V & A. Zyumbilev. Multi-Criteria Approach and Computer System of Defining Properties of Alloys Processed Thermally and Chemically-and-Thermally, Proceeedings of AMTECH, 97 Scientific Conference, Gabrovo, 1997, pp. 175-182 /in Bulgarian/..
14. Tontchev, N. & G. Valtchev. Multicriterial Optimization of the Properties of Plasma-Sprаued Coatings, Proceedings of Transcom' 97, University of Zilina, pp. 241-244
15. Dimitrov D., Implementation of Contemporary Technologies in Virtualization and Construction of an Information Cloud of Systems for University Needs in the Field of Transport Education, , Proceedings of International Conference on Application of Information and Communication Technology and Statistics in Economy and Education – ICAICTSEE-2014, UNWE, Sofia, 2014г.
16. T.Razmov T., D. Dimitrov , Laboratory Exercise and Course Design on "Project Management" - Third Edition, Todor Kableshkov University of Technology, 2012.

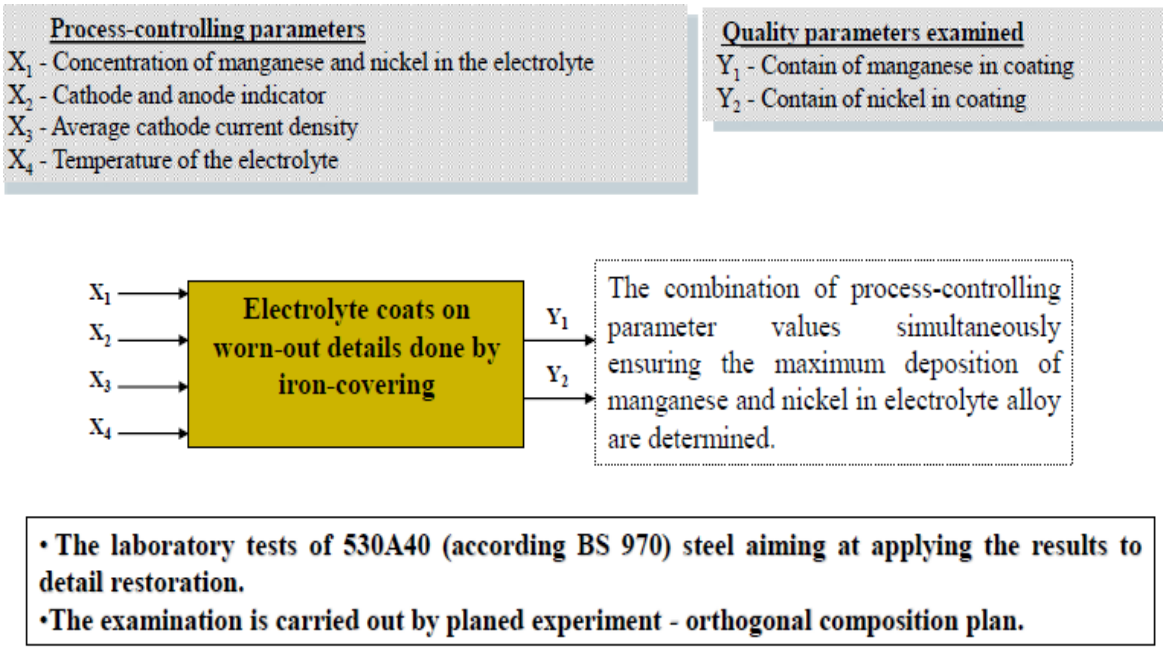

Fig 1. *Electrolyte coats on worn-out details done by iron-covering [12]*

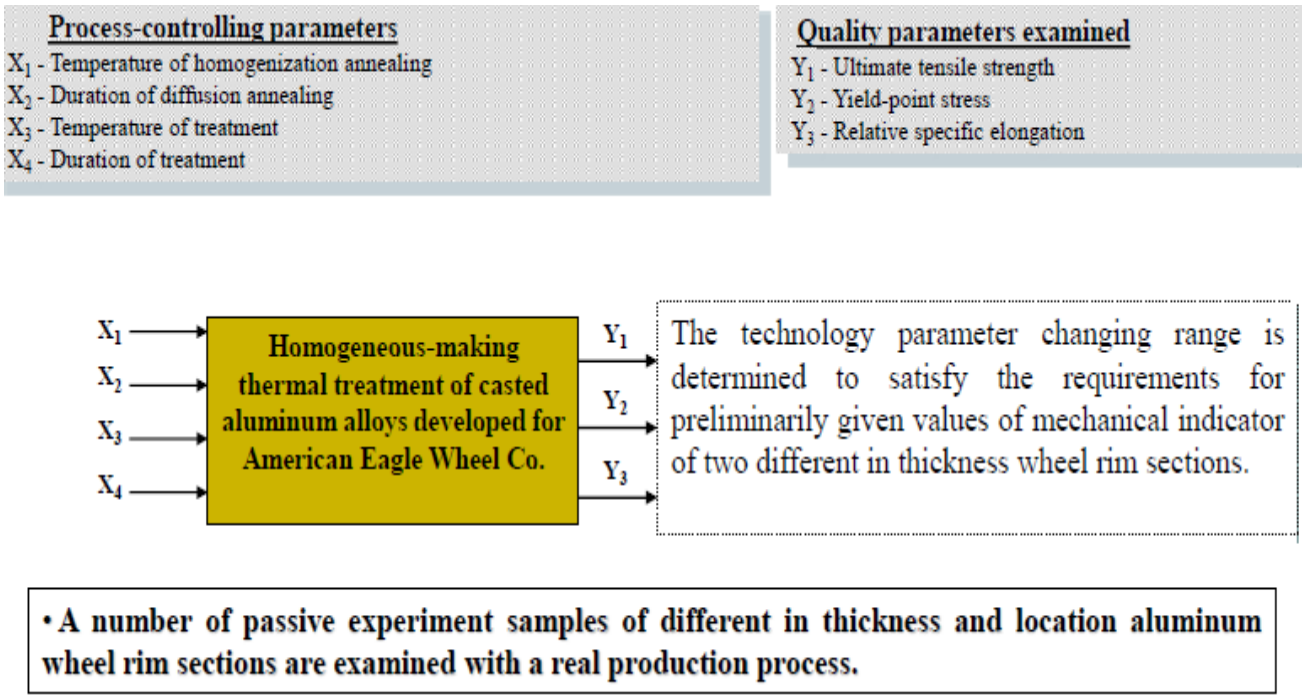

Fig. 2. *Homogeneous-making thermal treatment of casted aluminum alloys developed for American Eagle Wheel Co. /Ordered Company Survey/*

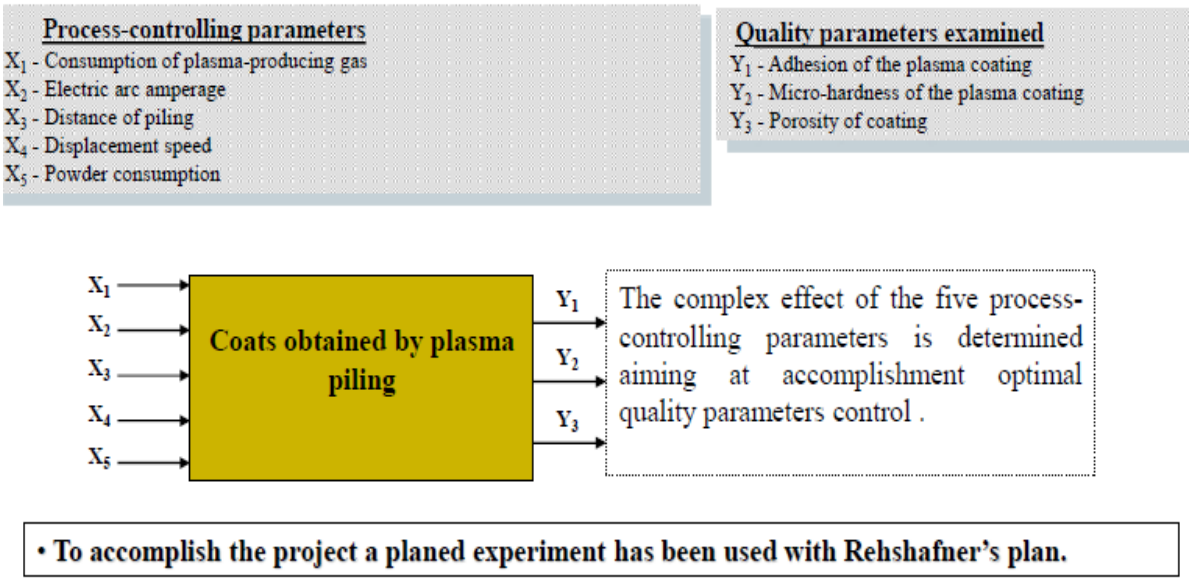

Fig 3. *Coats obtained by plasma pilling [14]*

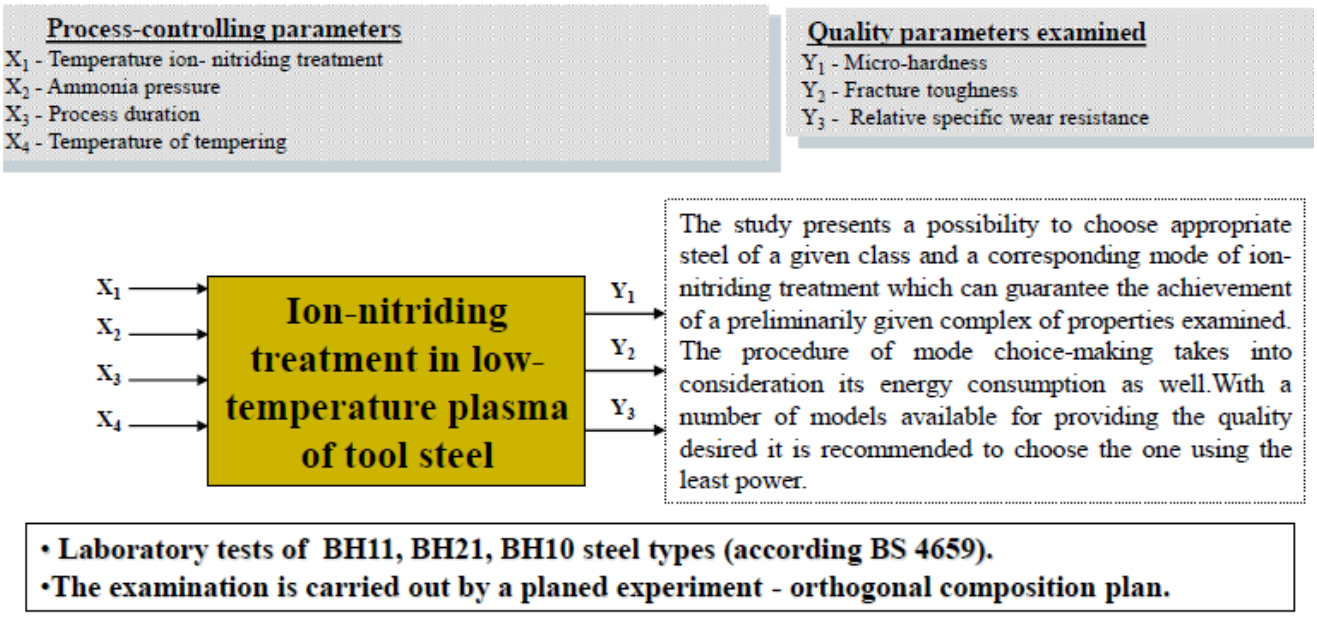

Fig 4. *Ion-nitriding treatmentin low-temperature plasma of tool steel [11, 13]*

STUDYING SIDE-EFFECTS OF GAMMA-IRRADIATION PROCESSING OF LEATHER MATERIALS

Assoc. Prof. P. Kovacheva PhD.[1)], M.Sc. N. Boshnakova[2)], M.Sc. Eng. D. Zhekov[1)]

[1)] University of Sofia "St. Kliment Ohridski", Faculty of Chemistry and Pharmacy, Sofia, Bulgaria

[2)] BULGAMMA, Sopharma JSC, Sofia, Bulgaria

kovacheva.petya@gmail.com

Abstract: *The paper describes part of the results of the first year of the IAEA Coordinated Research Project F23032, Contract № 20567 on "Studying Side-Effects of Gamma Irradiation Treatment for Disinfestation of Cultural Heritage Artefacts". Calf leather, calf suede and pig skin patterns were selected and analyzed by Scanning electron microscopy (SEM), and Thermal gravimetric analysis (TGA) before and after the gamma-irradiation treatment with 5 kGy, 10 kGy and 15 kGy absorbed doses at low dose rate. The irradiation of the leather materials was performed in the gamma-irradiation facility BULGAMMA based on JS-850 ^{60}Co type gamma irradiator at Sopharma JSC. No significant changes in the leather morphology and thermal decomposition were observed as a result of the gamma-irradiation treatment. Conclusions on the applicability of gamma-irradiation treatment for preservation of leather items with insecticide and fungicide doses were done.*

Keywords: GAMMA-IRRADIATION, LEATHER, LOW DOSE RATE, MORPHOLOGY, THERMAL DECOMPOSITION

1. Introduction

Preservation of cultural heritage artefacts is one of the major objectives of archaeologists, restorers and museum workers. Biological attack of insects, larves, fungi and bacteria is a serious problem in the preservation and long-term keeping of natural materials (wood, paper, leather, textiles, religious icons, etc.) when stored in improper conditions. Successful application of nuclear techniques (gamma irradiation and electron beam treatment) for disinfestation of archives and cultural heritage artefacts has been demonstrated in the last decades. There are several advantages of radiation disinfestation, compared to the traditional chemical treatment, including higher effectiveness, reliability, lack of toxic residues, applicability on large amount of objects etc [1-7]. However there are not enough data on the side-effects of gamma irradiation on leather items, especially at fungicide radiation doses. This impedes the development of methodology for gamma irradiation treatment for their disinfestation and preservation. Cultural heritage artefacts are often unique and their structure can not be simulated easily. Studies of the effects on irradiated items require the different extent of aging to be considered. Investigations of the side-effects on leather samples will contribute to clarify the structural and morphological changes and select appropriate doses for treatment and allow widening the preservation of leather-containing items by gamma- irradiation. Gamma-irradiation at low radiation dose rate is found to cause accelerating aging of the items, due to radical formations [2, 8]. The radiation induced oxidative degradation is observed to increase at low dose rate values due to increased time for oxygen diffusion [8]. Thus the application of low dose rate gamma-irradiation might contribute to determine the effects of gamma irradiation on artefacts by using model samples.

The Co-60 industrial radiation facility BULGAMMA, situated at Sopharma JCS is used for sterilization of health care products, disinfection of pharmaceuticals, drugs, cosmetics and food irradiation. However gamma-irradiation treatment until now is not regularly accepted for disinfestation of cultural heritage artefacts in the country. The aim of the current study is to increase knowledge on side-effects of gamma-irradiation treatment of leather materials in order to implement the radiation disinfestation of leather artefacts in the country. This paper presents part of the results, obtained during the first year of Contract № 20567 "Studying Side-Effects of Gamma Irradiation Treatment for Disinfestation of Cultural Heritage Artefacts". Side effects of gamma-irradiation treatment of leather materials with 5 kGy, 10 kGy and 15 kGy at low dose rate (0.006 - 0.06 Gy/s) were investigated. The radiation induced changes in the thermal decomposition and morphology of the samples were studied by using Scanning electron microscopy (SEM), and Thermal gravimetric analysis (TGA/DTG).

2. Materials and Methods

2.1. Samples description

Three natural leather patterns were chosen for this study: calf leather, calf suede and pig skin. Pictures of their both sides are presented in Figure 1. No chemical treatment of the leather samples was performed before and after the gamma-irradiation.

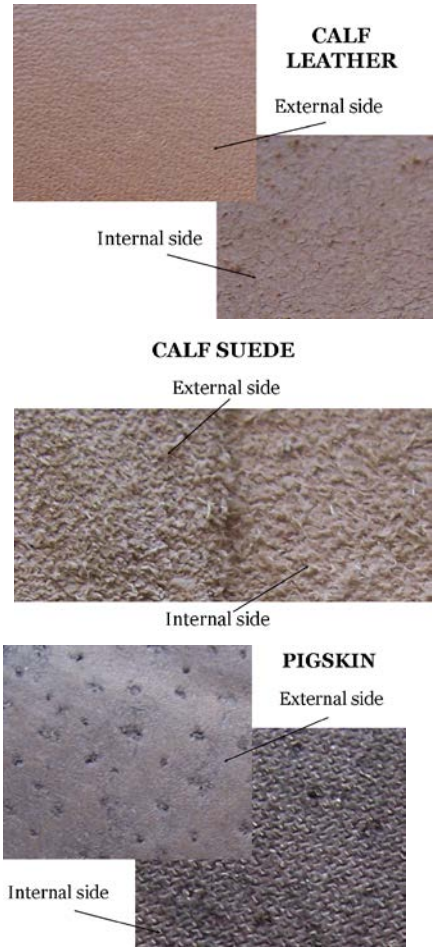

Fig. 1*. Physical observation of the selected leather patterns.*

2.2. Gamma irradiation

The irradiation of the leather patterns was performed in the gamma-irradiation facility BULGAMMA based on JS-850 ^{60}Co type gamma irradiator at Sopharma. JS-850 ^{60}Co gamma irradiator is a wet storage, tote-box irradiator, produced by MDS Nordian, Canada. JS-850 is an elevator type irradiator. It was replenished in 2007 with total irradiator activity 98.484 Ci after source reloading.

The absorbed dose distributions were measured with Ethanol Chlorobenzene routing dosimeters, consisting of dosimetric solution encapsulated in glass ampoule with diameter 10.7 mm and volume 2 mL. The absorbed dose was calculated from a calibration curve connecting it with the electric conductivity of the dosimetric solution measured with oscilotitrator. This dosimeter consists of an aerated solution of Chlorobenzene and water in ethanol to which a small quantity of acetate was added. The absorbed dose was calculated from a calibration curve connecting it with the electric conductivity of the dosimetric solution measured with oscilotitrator.

The maximum of the combined uncertainty of dose determination did not exceed 7.2 % (for 2 standard deviations).

Irradiator BULGAMMA is certified by the Quality Management System ISO 9001: 2008, applicable to Processing, decontamination and sterilization of products by gamma-irradiation for industrial, medical and scientific purposes. The samples (calf leather, calf suede and pig skin) were packed in plastic bags separately, closed in paper envelopes and irradiated by: 5 kGy, 10 kGy and 15 kGy absorbed doses at low dose rate (0.037 Gy/s).

2.3. Methods of investigations

The general morphology of the non-irradiated and gamma-irradiated leather samples was studied by SEM. A scanning electron microscope Lyra 3 XMU (Tescan with Quantax EDS detector - Bruker) was employed. Prior to the measurements, the samples were covered with a thin film of carbon. Analysis of the non-irradiated leathers was performed by SEM-EDX in order to obtain information on the elemental composition of the samples and the tanning methods.

The thermal properties of the samples were studied by thermogravimetry (TG/DTG) in pure argon, using Perkin-Elmer TGS-2.

3. Results and discussion

3.1. Morphology

The morphology of carbon-coated leather samples before and after gamma-irradiation at dose rate of 0.037 Gy/s with 5, 10 and 15 kGy was observed in several SEM images, at three different magnification ranges: x 200, x 500 and x 2000. Selected SEM images of the leather patterns before and after gamma-irradiation with 5, 10 and 15 kGy at low dose rate are presented on Figs. 2 - 7.

The SEM images of the external and internal surfaces of the studied leather samples did not show changes of the morphology as a result of the gamma-irradiation treatment. Despite the non uniformity of the leather surfaces, no irradiation induced damages on them; neither on the fibers could be noticed as a result of gamma-irradiation treatment up to 15 kGy.

The results of SEM-EDX analysis, revealed that the calf suede and the pig skin samples were chrome tanned and contained 4.56 % Cr (suede) and 6.74 % Cr (pig skin). The calf leather did not show elements, untypical for natural leather content and considering that it is light in color, harder and less flexible than the suede and pig skin, we supposed that it has been vegetable tanned.

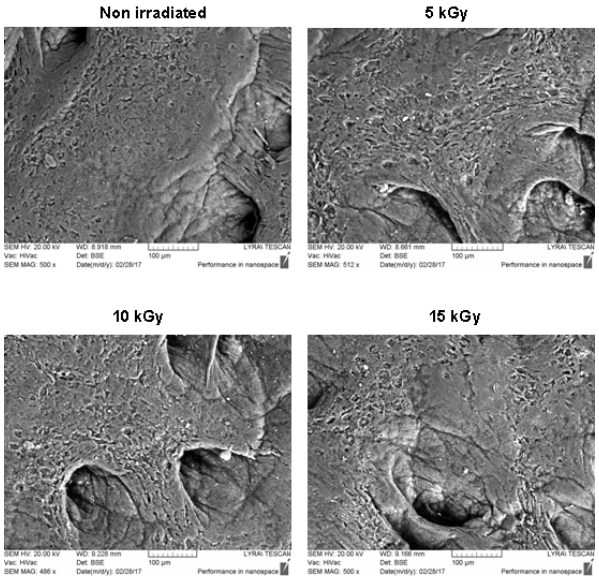

***Fig.2**. SEM images of calf leather (external side) before and after gamma- irradiation with 5, 10 and 15 kGy dose at 0.037 Gy/s.*

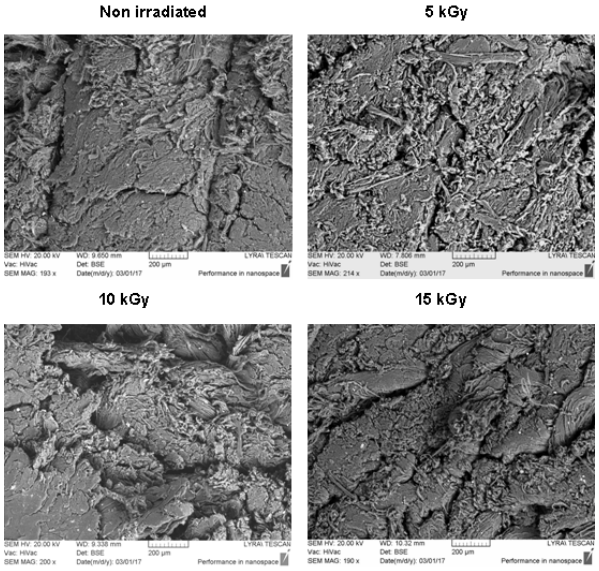

***Fig.3**. SEM images of calf leather (internal side) before and after gamma- irradiation with 5, 10 and 15 kGy dose at 0.037 Gy/s.*

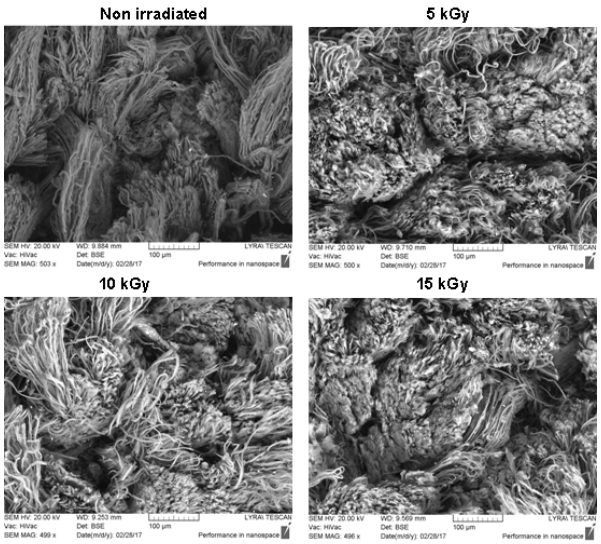

***Fig.4**. SEM images of calf suede (external side) before and after gamma- irradiation with 5, 10 and 15 kGy dose at 0.037 Gy/s.*

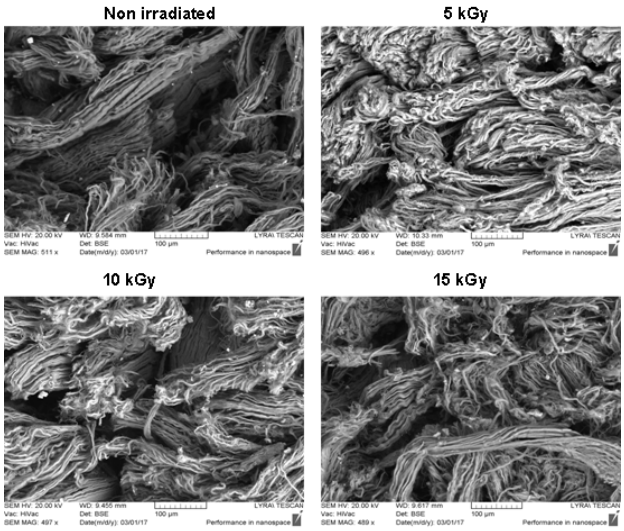

***Fig.5**. SEM images of calf suede (internal side) before and after gamma- irradiation with 5, 10 and 15 kGy dose at 0.037 Gy/s.*

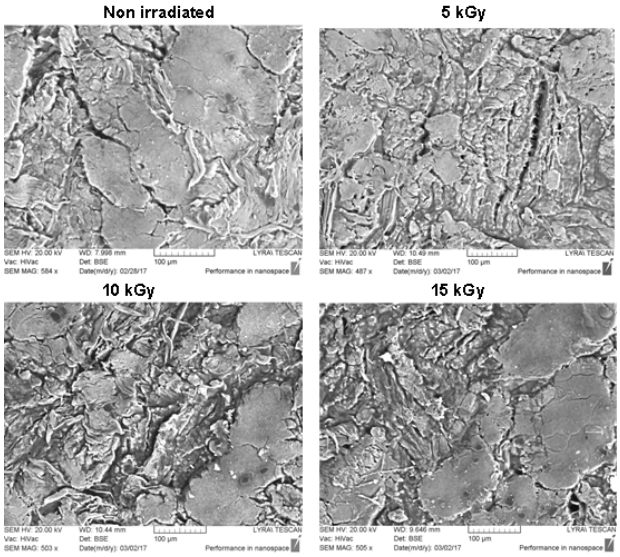

***Fig.6**. SEM images of pig skin (external side) before and after gamma-irradiation with 5, 10 and 15 kGy dose at 0.037 Gy/s.*

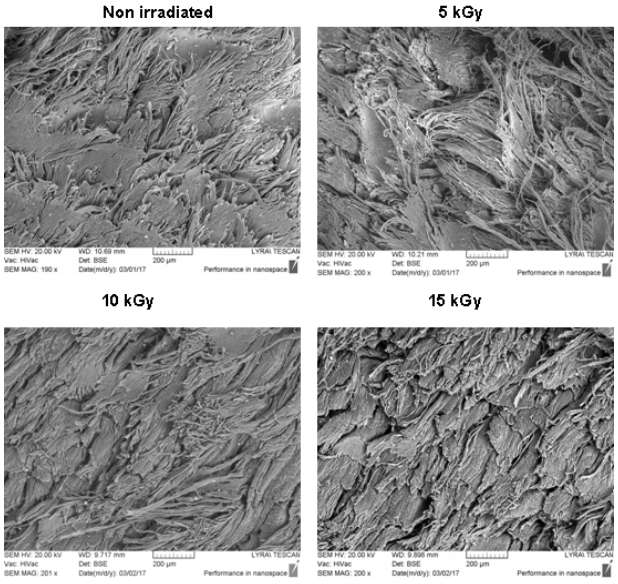

***Fig.7**. SEM images of pig skin (internall side) before and after gamma-irradiation with 5, 10 and 15 kGy dose at 0.037 Gy/s.*

3.2. Thermal decomposition

The data, obtained from the TG/DTG analysis of the initial leather samples and irradiated samples with 15 kGy at low dose rate (0.037 Gy/s) are presented on Figs. 7-11.

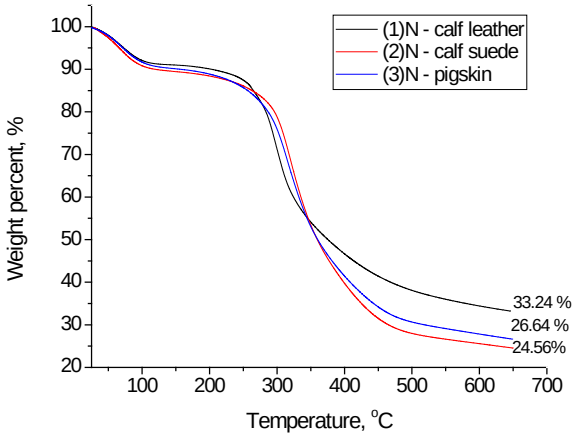

***Fig.8**. Thermal decomposition of the non-irradiated leather samples.*

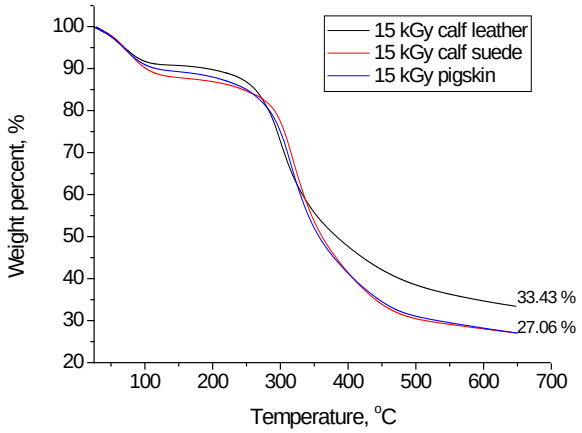

***Fig. 9.** Thermal decomposition of the leather samples, irradiated with 15 kGy at low dose rate.*

The TG curves of the three leather patterns have similar shapes (Figs. 8, 9). Highest weight percent remained in the calf leather after heating up to 650 °C (33.24 %), followed by pig skin (26.64 %) and calf suede (24.56 %). The irradiated samples of calf suede showed slight increase of the weight percent remained after heating up to 650 °C, as compared to the non-irradiated sample (from 24.56 % to 27.06 %). This effect can be due radiation induced changes in the molecular structure, e. g. cross-linking of the collagen.

As can be seen from Figs. 10-12, the DTG curves of the non-irradiated and irradiated samples practically overlap, which indicates no influence of gamma-irradiation with 15 kGy at dose rate 0.037 Gy/s on the weight loss of the studied leathers. The initial weight loss in the temperature range of 40 – 120 °C can be ascribed to the moisture volatilization or evaporation of some residual tanning solvent. The temperatures of maximum weight loss rate, corresponding to the main weight loss step was observed at 298 °C for calf leather, 317 °C for calf suede and 320 °C for pig skin patterns.

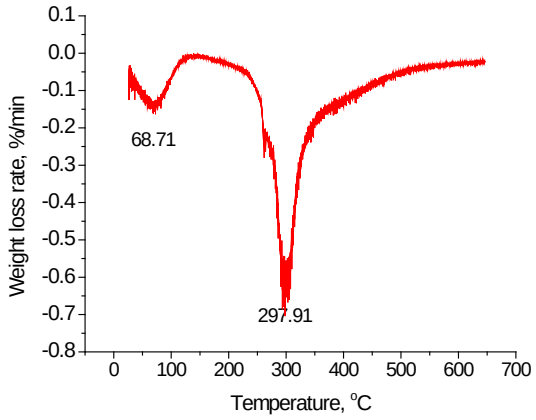

Fig.10. *DTG curves of calf leather, non-irradiated and after irradiation with 15 kGy at low dose rate.*

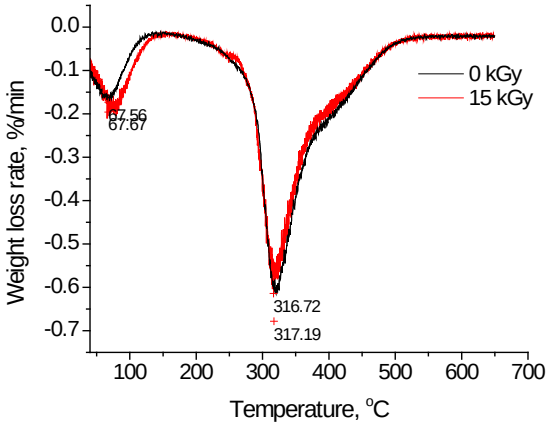

Fig.11. *DTG curves of calf suede, non-irradiated and after irradiation with 15 kGy at low dose rate.*

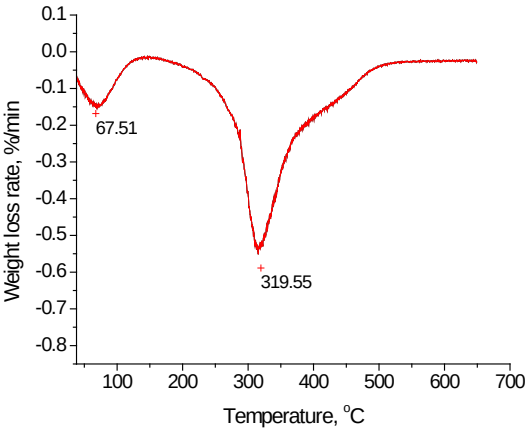

Fig. 12. *DTG curves of pigskin, non-irradiated and after irradiation with 15 kGy at low dose rate.*

4. Conclusions

The studies on the effects of gamma-irradiation treatment of calf leather, calf suede and pig skin with 5 kGy, 10 kGy and 15 kGy at low dose rate showed no significant changes in the morphology and thermal decomposition of the selected leather materials, as revealed by the scanning electron microscopy and thermal gravimetric analysis. Further investigations on the side-effects of gamma-irradiation on the molecular structure and radical formation in leather materials would contribute to development of radiation treatment methodology for their disinfestation and preservation.

Acknowledgements

This study was performed with the financial support of the International Atomic Energy Agency, Coordinated Research Project F23032, Research Contract № 20567 “Studying Side-Effects of Gamma Irradiation Treatment for Disinfestation of Cultural Heritage Artefacts”.

References

1. Cortella, L., Tran, K.Q., Głuszewski, W.J., Moise, I.V., Ponta, C.C., 2011. Nuclear Techniques for Preservation of Cultural Heritage Artefacts. IAEA Technical Cooperation Project – RER 8015: Using Nuclear Techniques for the Characterization and Preservation of Cultural Heritage Artefacts in the European Region.
2. Adamo, M., Baccaro, S., Cemmi, A., 2015. Radiation processing for bio-deteriorated archived materials and for consolidation of porous artefacts, ENEA Technical Report RT/2015/5/ENEA.
3. Katušin-Ražem, B., Ražem, D., Braun, M., 2009. Irradiation treatment for the protection and conservation of cultural heritage artefacts in Croatia. Rad. Phys. Chem. 78, 729–731.
4. Magaudda,G., 2004. The recovery of biodeteriorated books and archive documents through gamma irradiation: some considerations on the results achieved. J. Cultural Heritage 5(1), 113–118.
5. Moise, I. V., Virgolici, M., Negut, C. D., Manea, M., Alexandru, M., Trandafir, L., Zorila, F.L., Talasman, C. M., Manea, D. ,Nisipeanu, S., Haiducu, M., Balan, Z., 2012. Establishing the irradiation dose for paper decontamination. Radiat. Phys. Chem. 81(8), 1045–1050.
6. Da Silva, M., Moraes, A.M.L., Nishikawa, M.M., Gatti, M.J.A., Vallim de Alencar, M.A., Brandão, L.E., Nobrega, A., 2006. Inactivation of fungi from deteriorated paper materials by radiation, Int. Biodet. Biodegr., 57, 163-167.
7. Baccaro, S., Cemmi, A., Ferrara, G., Fiore, S., 2015. Calliope gamma irradiation facility at ENEA-Casaccia R.C. (Rome), ENEA Technical Report RT/2015/13/ENEA.
8. Baccaro, S, Caccia, B., Onori, S., Pantaloni, M., 1995. The influence of dose rate and oxygen on the irradiation induced degradation in ethylene-propylene rubber, Nucl. Insrr. and Meth. in Phys. Res. B 105(1-4), 97-99.

DISTRIBUTION OF NANODIAMONDS IN ELASTOMERIC MIXTURES.

Associate Prof. PhD eng. Tzolo Tzolov – University of chemical technology and metallurgy - Sofia (tzolovtz@abv.bg)
PhD eng. Aleksandar Stoyanov – Aviodetachment 28 (anstoianov@abv.bg)
Mas.deg.eng.Margarita Trencheva Маргарита Тренчева, University of chemical technology and metallurgy - Sofia (margarita_trencheva@abv.bg)

Annotation: *In the present work the distribution of ND in standard mixtures of natural rubber without the use of stearin acid was studied.*
KEY WORDS: *NANODIAMOND (ND), ELASTOMER, RUBBER, COMPOSITE MATERIAL*

I. Introduction

Nowadays, polymeric materials are applied practically in all areas of human activity and replace the increasingly used traditional metals and alloys from the modern fields of engineering, machine building, etc. The dynamic development of nanotechnology in the field of the processing of elastomers, determines the great importance of studying the structure of the elastomeric material.

One of the important components of a composite material (CM) - an elastomeric mixture (EM) is the filler. The importance of fillers is related to the production of materials with specified properties necessary for certain branches of the economy, research, medicine, etc.

II. Experiment

As regards nanotechnologies and fillers for elastomeric mixtures, the influence of nanodiamants (ND) as an element of the nanoparticles on the EM must first be studied before the formation of the supermolecular structure of the mixture and the vulcanization process preceding the manufacture of the rubber article. The influence of ND on the EM should be focused on the interfacial processes and superficial phenomena of the elastomer - filler, because precisely the changes occurring in them determine the emergence of a new complex of properties of CM. The diamond modification of carbon has the highest values of free surface energy [1], which leads to a high activity of nanoparticles in the modified material but is found in a powdery state in air, ND tends to agglomeration, leading to a reduction in excess surface energy deactivation. In order to increase the ND's modifying effect on the NR, in order to preserve the values of free surface energy, NDs should be introduced together with their inert storage environment, as they fall into the EM to maintain their activity.

The problems with the NR with ND are:

- developing methods for introducing ND into the mixture;
- Achieving the even distribution of ND in the mixture.

The following embodiments of the inert environment in the mixture are shown Fig 1:

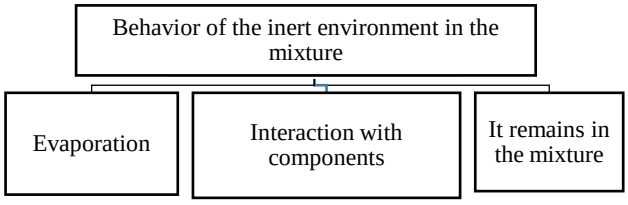

Fig 1: *Behavior of the inert environment in the mixture*

Confirmation of the claim is the [2] found in the ND of connected and sorbed water. It is not even released when drying at 393 K.

Ideally, we accept:

- ND do not chemically react with the individual components of the mixture;
- The values of free surface energy remain unchanged.

On the other hand, the dimensions of ND and their surface hardness will contribute to the formation of their own hierarchy of supramolecular structures, averaging the density of the packings of the macromolecule chains over the entire volume of the polymer matrix (PM) [3].

According to [4] the matrix is modified under conditions that the particle of the modifier (ND in the present case) exhibits its activity in the adjacent layer of the polymer with a thickness,

$$L = r\sqrt[3]{\frac{\rho_н}{C_н \rho_n}}$$, where:

L – film thickness,
r-particle size,
pn-density filler,
pp - density polymer,
CH-density filler

The formula follows that the amount of carbon cloud particles is in the range of 30-50 nm.

A natural rubber (NR) was used to carry out the experiment as an elastomeric matrix.

The EU has been developed in options:

- not filled without stearin with ND - 1,5 weight fraction per 100 weight fraction NR (C-1);
- not filled without stearin with introduced ND - in 3 weight fraction per 100 weight fraction NR (C-2);

As a method for demonstrating the distribution of ND in the mixture based on their size, the X-ray diffraction analysis method is used to study the structure of the substance in the Delay-Sderder distribution space.

Figure 2 *shows the results of both samples.*

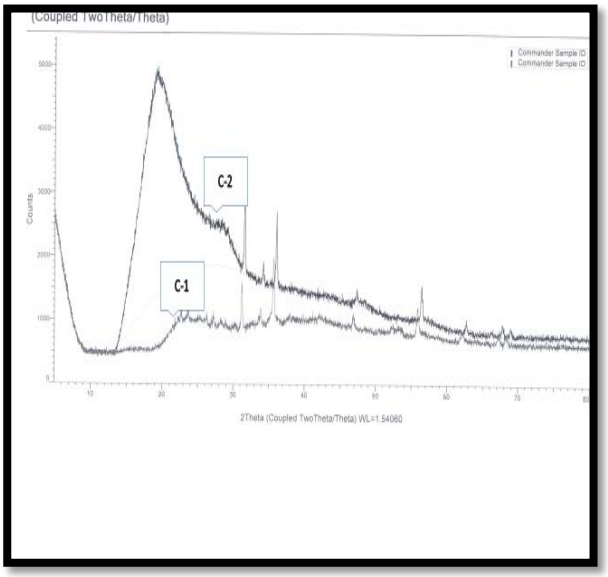

Fig. 3 and 4 *show the results of samples C-1 and C-2*

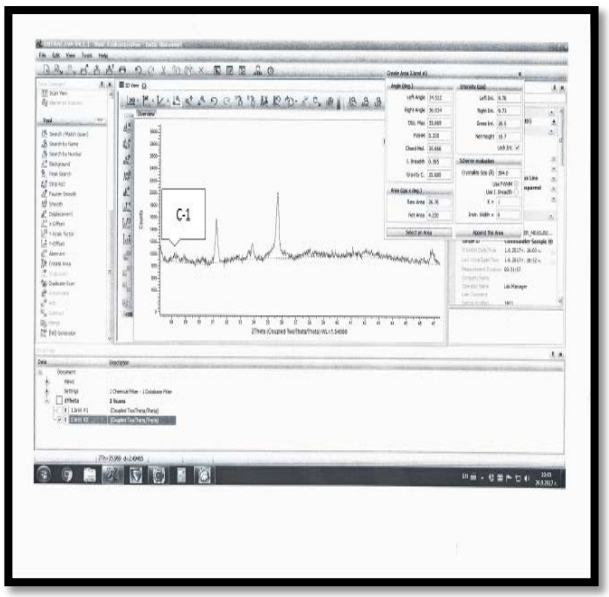

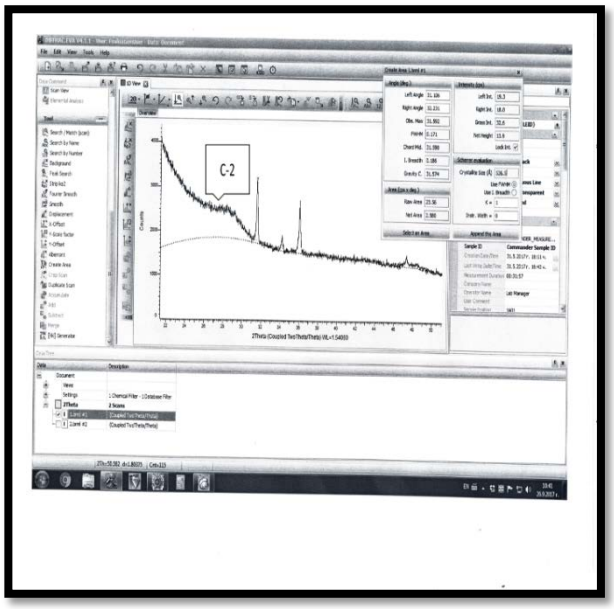

From the sample results shown, it can be seen that the size of the crystals is within the range, respectively:

- For sample C-1 at 1.5 weight fraction ND per 100 weight fraction NR, the crystals have a size of 394 Ä-39 nm
- For C-2 sample at 3 weight fraction ND, per 100 weight fraction NR, the crystals have a size of 536 nm - 54 nm

III.Conclusion

By using the above-mentioned composition and method of ND introduction into the EM together with the inert storage medium, a uniform distribution of ND is achieved by forming an own hierarchy of supramolecular structures with dimensions of 39-54 nm by:

- averaging the packing density of the macromolecule chains over the entire polymer matrix volume:
- uniform distribution of ND in the polymer mixture;
- enhancing the modifying effect of ND.

IV.References:

1. Мокочунина Т.В., диссертация Упрочняющее модифицирование продуктов нефтепереработки углеродными наночастицами, "Российский государственный университет нефти и газа имени И. М. Губкина", 2015г.

2. Сверхтвердые материалы 3, Г.В.Сахович, В.Ф.Комаров, Е.А.Петров, 3-2002г.

3. И.М.Цыпкина, А.П.Вознаковский, Л.Ю.Матвеева, Влияние наноуглерода детонационного синтеза на эксплоатационнъе свойства, резин на основе каучуков общего назначения, УДК:678.044:678 063

4. Наноалмазы детонационного синтеза /получение и применение/,П.А. Витязь, ,Александр Ильющенко,Виктор Жорник, Белоруская навука,2013, ISBN 978-985-98-1637-5

МЕТОДИКА ЗА ПРОЕКТИРАНЕ НА ПРИСПОСОБЛЕНИЕ ЗА ОГЪВАНЕ НА ЧЕТИРИ-ЧЛЕННИ ДЕНТАЛНИ МОСТОВЕ

METHODOLOGY FOR DESIGNING OF APPLIANCE FOR BENDING TEST OF FOUR-PART DENTAL BRIDGES

Head Assist. Dr Vasilev T. [1], Assoc. Prof. Dr Dikova T.[2], Head Assist. Dr Ivanova E.[1]
[1] Nikola Vaptsarov Naval Academy, Varna, Bulgaria
[2] Faculty of Dental Medicine, Medical University of Varna, Bulgaria
E-mail: t.vasilev@abv.bg, tsanka_dikova@abv.bg, elisa.d.ivan@abv.bg

Abstract: *The four-part dental bridges from 1st premolar to 2nd molar are the most loaded during the chewing process. In addition, they are characterized by complex geometry of the teeth surface and complicated way of load distribution. The aim of the present paper is to develop a methodology for designing of appliance for bending test of four-part dental bridges that achieves the load of the bridge bodies close to the actual load. The using of CAD software allowed determining the shape and sizes of the pistons, the distance between the centers in the two main directions and the angle, at which the device must be located relative to the test specimen. The designed device provides contacts between the spherical tips of the punches and the teeth - bridge bodies in the most loaded areas in occlusion and a loading scheme that only produces normal stresses in the bridge construction during bending. As a result, appliance for bending test of four-part dental bridges was designed, produced and used in the next experiment.*
KEYWORDS*:* FOUR-PART DENTAL BRIDGES, BENDING TEST, APPLIANCE, CAD DESIGN

1. Увод

Неснемаемите протезни конструкции – дентални мостове и коронки се изработват основно от метални сплави, инкрустирани с пластмаса, композит или керамика, както и от чиста керамика. По време на дъвкателния процес те са натоварени циклично на огъване или натиск в зависимост от вида на реставрацията. Затова и якостните свойства на материалите, от които са произведени, са от особена важност за техния клиничен успех.

За дълготрайността на денталните мостове от особена важност е якостта на огъване. Този параметър на денталните материали може да се измери по три начина – чрез три-точков, четири-точков или би-аксиален експерименти на огъване [1-5]. Най-често се използва три-точковия тест, защото е лесен за изпълнение и формата на образците е сравнително проста – планки с правоъгълно сечение [2, 3, 6, 7]. Четири-точковият експеримент обикновено се прилага, когато се изследват двуслойни конструкции като стъкло-керамична фасета върху основа от метал или керамика [3], а би-аксиалният тест е за изследване на материали, от които се изработват сравнително големи образци [2, 3]. Трябва да се отбележи, че стойностите на якостта, измерена чрез три-точков и би-аксиален тестове, е по-голяма от якостта на огъване, изследвана с четири-точков експеримент [2, 4, 5].

Изследването якостта на огъване на денталните материали е стандартизирано [1, 5, 7], но поради многообразието и сложността на формите на неснемаемите протезни конструкции, стандартизиран метод за изпитания при тях е трудно да се разработи. Стремежът при изучаване якостните свойства на денталните мостове и коронки е условията на експеримента максимално да се добижат до тези на експлоатация. Повечето автори изследват на огъване три-членни мостови конструкции от различни части на съзъбието. В своята работа Filser F. и кол. [8] изпитват на огъване три-членен мост от най-натоварената част (5-ти до 7-ми зъб), изработен от цирконий. Извършени са два различни експеримента: единият е с анатомична форма на денталните мостове, като натоварването е осъществено със стоманена съчма, а при другия образецът има опростена форма с плоска, изпилена и полирана оклузална повърхност. Натоварването при втория тест е извършено с поансон с плосък връх и с подложка от тефлон. Seo J.Y. и кол. [9] също изпитват на огъване три-членен мост от най-натоварения участък – от втори премолар до втори молар. Тъй като те изучават якостта на връзките между короните и мостовото тяло, използват опростен модел и варират с напречните размери на най-опасните сечения. Натоварването е приложено в центъра на мостовото тяло. Yoon J.-W. и кол. [10] изследват якост на огъване на три-членни мостове от металокерамика, включващи от ляв централен резец до десен страничен резец. Натоварването е приложено чрез поансон с плосък край и Ф6 mm върху режещия ръб на мостовото тяло, успоредно на дългата ос на зъба. Между поансона и ръба на моста е поставено алуминиево фолио с дебелина 1 mm.

Четири-членните дентални мостове от първи премолар до втори молар са най-натоварени по време на дъвкателния процес съгласно разпределението на услията по Filtchev A. и Kalachev Y. [11]. Освен това те се характеризират със сложни геометрия на повърхността на зъбите и начин на разпределение на натоварването. До този момент липсват подробни данни за изпитания на огъване на този вид неснемаеми протезни конструкции. Целта на настоящата статия е да се разработи методика за проектиране на прибор за огъване на четири-членни дентални мостове с помощта на CAD софтуер, при който натоварването на мостовите тела да се осъществи максимално близко до действителното.

2. Предпоставки и начини за разрешаване на проблема

2.1 Основни положения при изпитване на огъване

При изпитания на огъване, според стандартите, се използват правоъгълни образци, към които се прилага усилие чрез поансон с определен диаметър. В зависимост от броя на поансоните, с които се прилага усилието, се различават две схеми на огъване. Първата е три-точково огъване (фиг.1–а), а втората, четири-точково (фиг.1–б). Оста на поансона и при двете схеми е кръстосана спрямо образеца, който се изпитва, а диаметърът му трябва да е съобразен с размера на образеца. Усилието се прилага до достигане на определен ъгъл на огъване или до разрушаване. Като резултат от огъването се приема наличието или отсъствието на пукнатини.

Основната разлика при двата вида огъване е показана на графиките на разпределение на нормалните напрежения по дължина на изпитвания образец (фиг. 1). При три-точковото огъване има повишаване на напреженията (огъващия момент) до максимална стойност, действащи само в сечението, в което е приложено усилието чрез поансона (фиг.1–а), докато четири-точковото огъване се характеризира с нормално напрежение, действащо с постоянна стойност в зоната от образеца, разположена от единия до другия поансон (fig. 1-б)[2, 3, 12].

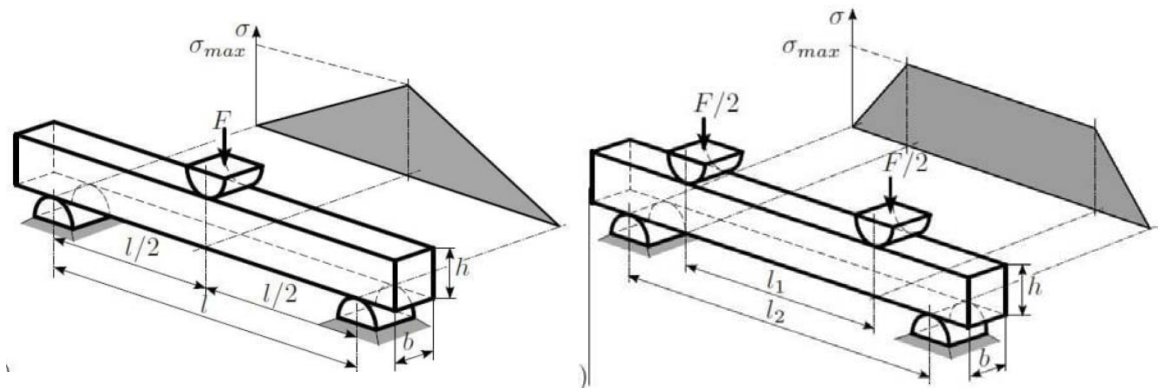

а) *б)*

Фиг.1 *Схеми на разположение на дорниците и изменение на напреженията спрямо изпитвания образец при двата основни метода на изпитване при огъване: а) три-точково огъване и б) четири-точково огъване [12].*

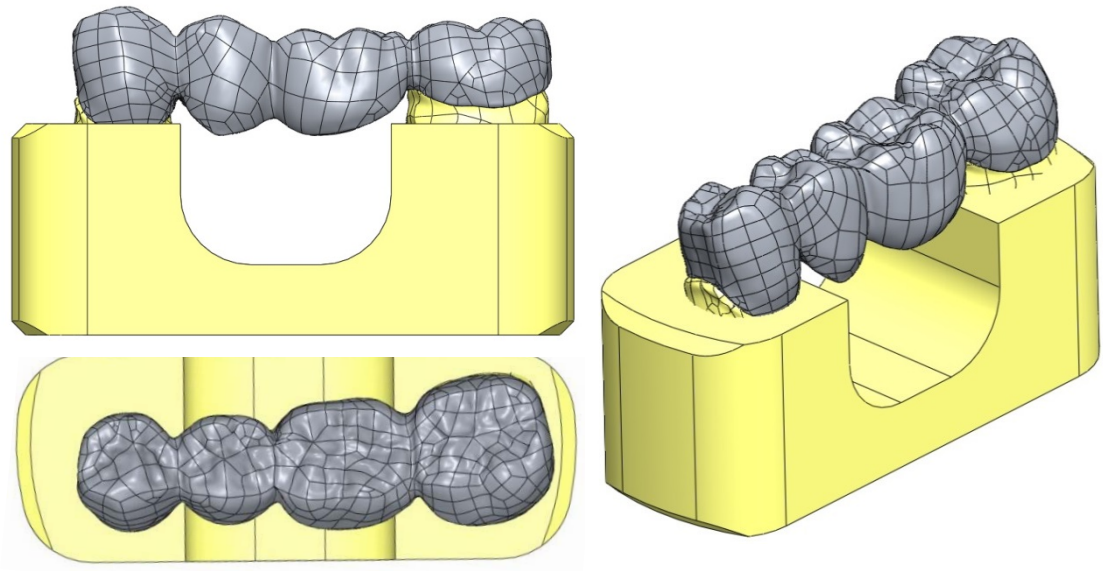

Фиг.2 *Виртуален модел на четири-членен мост разположен върху опорите и плочата.*

2.2 Изходни данни при проектиране на инструментална екипировка за огъване

За изходни данни при проектирането на инструментална екипировка за изпитания на четири-членни мостове на огъване е използван виртуален модел на основния мост-модел, получен по методиката, описана в [13]. За опори, върху които да се разположи моста, служат виртуални модели на изпилените зъби от реалния гипсов модел, генерирани по начин, разгледан в [14]. Общ вид на модела, поставен върху опорните зъби, е показан на фиг.2. Мостът, заедно с опорите, са разположени върху плоча с разстояние, което осигурява безпроблемно провисване по време на изпитване. По време на проектирането се работи с CAD софтуер Solid Works.

Ако се вземат съображенията, разгледани в точка 2.1, относно максималните напрежения (разпределението на огъващия момент), четири-точковото огъване би осигурило следните предимства пред три-точковото:

- по-голяма част от мостовата конструкция ще бъде натоварена с еднакъв по големина огъващ момент [3];
- натоварването по време на огъване би се доближило максимално до реалното натоварване, имайки предвид дъвкателното усилие, приложено в оклузалните контакти на всеки зъб;
- в участъка между двете сили има само нормални напрежения от огъване, без наличието на тангенциални напрежения, характерни за триточковото огъване.

Тези предимства са причината за проектиране на екипировка за четири-точково огъване.

Изпитанията на огъване трябва да бъдат проведени до тогава, докато образецът се разруши вследствие максимални нормални напрежения, достигащи максимални стойности в зони с малка площ на напречните сечения и превишаващи якостта на опън на материала. Различията между усилията, при които се разрушават мостовете, ще дадат основание за предпочитание на една технология пред друга.

За да се определи ориентировъчно какво ще бъде усилието при което ще се разруши образец от изследвания материал с механични свойства (якост на опън), получени при предходни изследвания [15], разглеждаме следната класическа схема на натоварване (фиг.3).

За максималния огъващ момент имаме:

$$M_{\text{ог}} = P.a \tag{1}$$

Където: P – сила, действаща върху образеца, N; a – разстояние от точката, в която действа силата, до точката, в която е разположена опората, m.

Разглеждаме какви ще са максималните огъващи напрежения, породени от получения огъващ момент, и ги сравняваме с напреженията на опън на съответния материал, които са известни, или може да се запише:

$$\sigma_{max} = \frac{M_{\text{ог}}}{W_{\text{ог}}} > \sigma_{\text{оп}} \tag{2}$$

Напреженията на опън за образеца, произведен от Co-Cr сплав чрез избирателно лазерно стопяване, показва якост на опън 720 MPa [15]. За приблизително определяне на съпротивителния момент на огъване ползваме конкретни

стойности от триизмерния модел, като предполагаме, че образеца е с правилна форма фиг.4.

От където за съпротивителния момент на огъване изчислен за конкретния образец имаме:

$$W_{\text{ог}} = \frac{b.h^2}{6} = \frac{4{,}5.4{,}3^2}{6} = 13{,}87\ mm^3$$

Ако заместим зависимости (1) и (3) в (2) ще получим:

$$M_{\text{ог}} = P.a > \sigma_{\text{оп}}.W_{\text{ог}} = 9986{,}4\ N.mm$$

$$P > \frac{9986{,}4}{a} = \frac{9986{,}4}{8{,}7} = 1147{,}8\ N$$

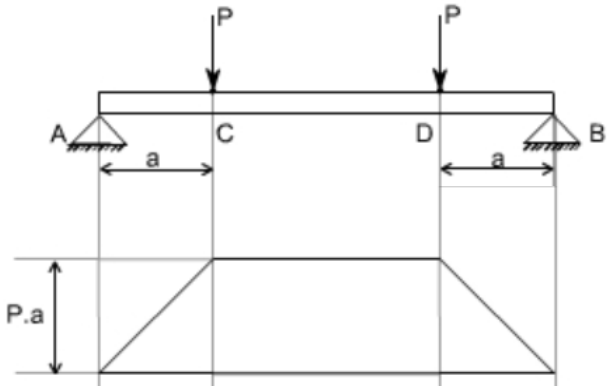

Фиг.3 *Класическа схема на натоварване на греда, разположена на две опори, с две еднакви по големина сили, разположени на еднакво разстояние спрямо опорите [16].*

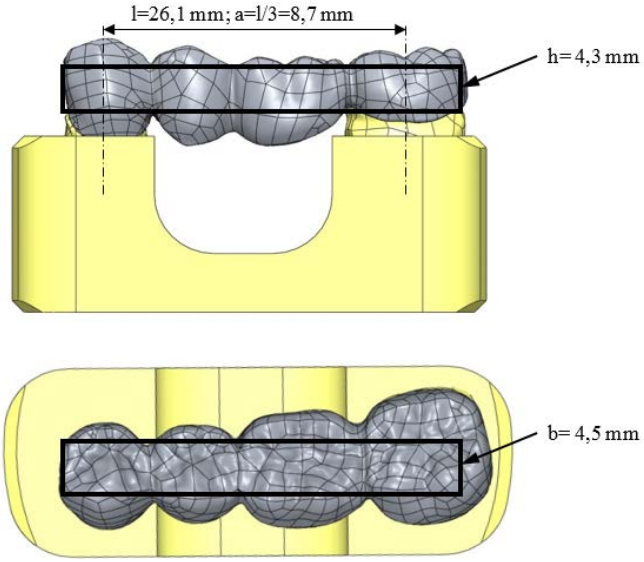

Фиг.4 Заместване на четири-членния мост със стандартен образец, за който можем да определим съпротивителния момент на огъване.

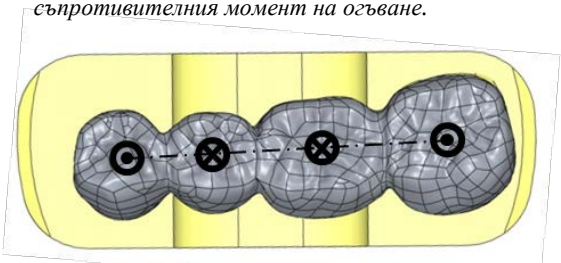

Фиг.5 *Схема на натоварване, при която в изпитвания образец ще се пораждат само нормални напрежения*

Получената стойност за усилието, при което ще се разруши образецът, е с допускането, че разстоянието между опорите и точките в които са приложени силите е едно и също. Това условие, обаче, зависи от конкретната геометрия на съответния зъб и дали в действителност усилието ще може да се приложи там.

2.3 Проектиране на инструментална екипировка според конкретния 3D модел

За да се получат вследствие огъването на образците само нормални напрежения е необходимо директрисите на прилаганите чрез поансоните сили, както и директрисите на получаваните реакции да лежат на една права линия, съгласно схемата, показана на фиг.5. В противен случай ще има условия за създаване на тангенциални напрежения породени от неизбежното усукване на образеца.

Поради сложната геометрия на повърхността на зъбите и начина на разпределение на натоварването [11, 17], както и извършен анализ за възможните форми на върха на поансоните [8-10], се установи като най-ефективна сферичната форма,

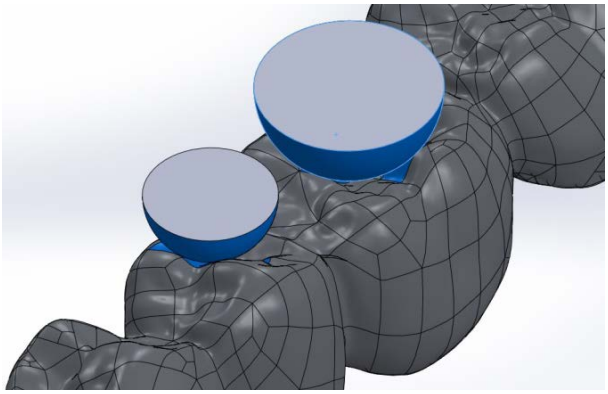

Фиг.6 *Снимка на избраната комбинация при напасване на сферичните дорници с повърхността на зъбите*

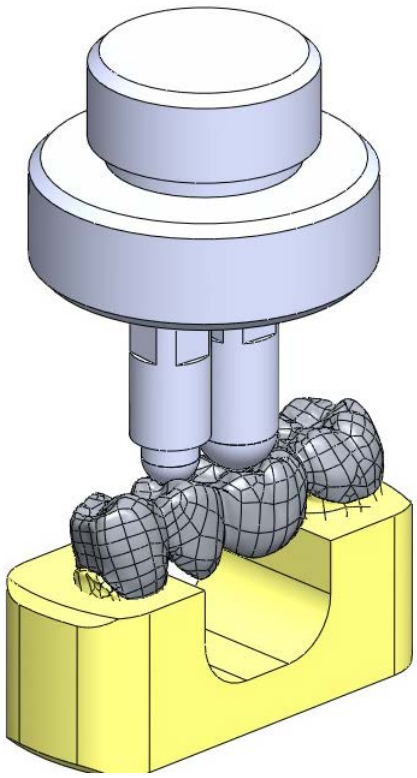

Фиг.7 *Общ вид на проектираното приспособление за огъване на четири-членни мостови конструкции.*

защото осигурява максимален брой от три точки на контакт. Сферичната форма е за предпочитане и от друга гледна точка – тя позволява максимално да се доближи натоварването до действителното по време на дъвкателния процес, като се отчитат и оклузалните контакти по схемата на *Lundeen* [17, 18].

За да се проектира приспособление за огъване са създадени модели на сфери с диаметри съответно 3, 5 и 7 mm, като са поставяни върху всеки един от зъбите, по които е необходимо да се осъществи натоварването (фиг. 6). За да се установи контакт между сферите и съответния зъб в CAD среда на Solid Works е използвана командата Move Components с под команда Collision Detection. В резултат са подбрани такива диаметри на сферите, при които схемата на натоварване на образеца наподобява тази от фиг.5, т.е. при огъване в мостовата конструкция възникват само нормални напрежения, и контактите между сферите и зъбите (мостови тела) се осъществяват в най-натоварените местата при действителна оклузия. Общ вид на проектираната екипировка е показана на фиг. 7.

Разработената методика и използването на CAD софтуер дадоха възможност да се определят диаметрите на сферичните накрайници на огъващите поансони, разстоянието между центровете в двете основни направления, както и ъгъла, на който трябва да бъде разположено приспособлението спрямо образеца на изпитване.

3.Заключение

Четири-членните дентални мостове от първи премолар до втори молар са най-натоварени по време на дъвкателния процес. Освен това те се характеризират със сложни геометрия на повърхността на зъбите и начин на разпределение на натоварването. В настоящата работа е представена методика за проектиране на приспособление за огъване на четири-членни дентални мостове с помощта на CAD софтуер, при което натоварването на мостовите тела се осъществява максимално близко до действителното. Конструираният прибор осигурява контакти между сферичните накрайници на поансоните и зъбите - мостови тела в най-натоварените места при действителна оклузия и схема на натоварване, при която възникват само нормални напрежения в мостовата конструкция при огъване. Проектираното приспособление е изработено и изпробвано в следващи наши експерименти.

4. Благодарност

Настоящата работа е извършена с помощта на катедра „Механика и машинни елементи“, Машинно-технологичен факултет при Технически Университет-Варна.

5.Литература

1.Wang L., D'Alpino P.H.P., Lopes L.G., Pereira J.C. Mechanical Properties of Dental Restorative Materials: Relative Contributions of Laboratory Tests. J Appl Oral Sci 2003; 11(3):162-169;
2.Sadighpour L., Geramipanah F., Raeesi, B. In Vitro Mechanical Tests for Modern Dental Ceramics. Journal of Dentistry of Tehran University of Medical Sciences 2006; 3(3): 143-152;
3.Mijoska A., Popovska M. Evaluation of Different In Vitro Testing Methods for Mechanical Properties of Veneer Ceramics. CONTRIBUTIONS, Sec. Med. Sci., MASA. 2015: XXXVI (1): 225-232;
4.Jin J., Takahashi H., Iwasaki N. Effect of Test Method on Flexural Strength of Recent Dental Ceramics. Deantal Materials Journal 2004; 23(4): 490-496;
5.Fischer J., Stawarczyk B., Hammerle C.H.F. Flexural strength of Veneering Ceramics for Zirconia. Journal of Dentistry 2008; 36: 316-321;
6.Fonzar R.F., Carrabba M., Sedda M., Ferrari M., Goracci C., Vichi A. Flexural resistance of heat-pressed and CAD-CAM lithium disilicate with different translucencies. Dental Materials. 2017 Jan; 33(1): 63-70;
7.De Kok P., Kleverlaan C.J., de Jager N., Kuijs R., Feilzer A.J., Mechanical Performance of Implant-Supported Posterior Crowns. J Prosthet Dent 2015 Jul; 114(1): 59-66;
8.Filser F., Luthy H., Scharer P., Gauckler L. All-Ceramic Dental Bridges by Direct Ceramic Machining (DCM). In: Materials in Medicine, Materials Day, Department of Materials, Eds. M.O. Speidel, P.J. Uggowitzer, vdf Hochschulverlag AG, ETH Zurich, May 1998, p.165-189;
9.Seo J.Y., Park I.N., Lee K.W. Fracture strength between different connector designs of zirconia core for posterior fixed partial dentures manufactured with CAD/CAM system. J Korean Acad Prosthodont. 2006 Feb; 44(1):29-39;
10. Yoon J.-W., Kim S.-H., Lee J.-B., Han J.-S., Yang J.-H. A Study on the Fracture Strength of Collarless Metal-Ceramic Fixed Partial Dentures. J Adv Prosthodont 2010;2:134-41;
11. Filtchev A., Kalachev Y., Phenomenon of domination of the strongest contacts in centric occlusion, Quintessence International 2008; 39(3): 99-106;
12. XYZTEC, Wafer and Die Testing – A Guide to Fracture Strength Testing, 14.06.2017, https://www.azom.com/article.aspx?ArticleID=14095,
13. Dzhendov Dzh., Pavlova D., Simov M., Marinov N., Sofronov Y., Dikova Ts., Todorov G., Kalachev Y., Геометрична точност на неснемаеми мостови конструкции, изработени посредством адитивни технологии, Сборник на 8 МНК за млади учени "Technical Science and Industrial Management", 15-16.09.2014, Варна, България, Vol.1, 13-17с.;
14. Vasilev T, T Dikova, D Dzhendov, E Ivanova, Нова методика за измерване на хлабини на дентални мостови конструкции с използване на CAD софтуер, Proceedings of 3-rd Int. Sci. Conference "Materials Science. Nonequilibrium Phase Transformations", 11-14 Sept 2017, Varna, Bulgaria, STUME. 2017 Sep;1(1):88-91;
15. Dolgov N.A., Dikova Ts., Dzhendov D., Pavlova D., Simov M., Mechanical Properties of Dental Co-Cr Alloys Fabricated via Casting and Selective Laser Melting, Int J Materials Science. Non-Equilibrium Phase Transformations. 2016;3:3-7;
16. http://www.nptel.ac.in/courses/112107146/lects%20&%20picts/image/lect27/lecture27.htm;
17. Vasilev T., Dikova T., Dzhendov D., Ivanova E. Simulations of Cast and Selective Laser Melted Dental Bridges with Chewing Load, Scripta Scientifica Medicinae Dentalis. 2016, 2(2): 7-11.
18. Ralev R., Filtchev A. Propedeuthics of prosthetic stomatology, Textbook for students in stomatology, [in Bulgarian], Sofia, 2000, 392 p.

CONFIGURING CUSTOMIZED PRODUCTS IN VR USING HMD

Assist. Prof. Angel Bachvarov[1], Stefan Georgiev M.Sc.[1], Prof. Stoyan Maleshkov[2]
Faculty of German Engineering and Management Education – Technical University Sofia, Bulgaria [1]
Department of Informatics – New Bulgarian University, Bulgaria [2]
a_bachvarov@tu-sofia.com

Abstract: *Until recently the Virtual Reality (VR) and its related technologies, e.g. Augmented Reality, Mixed Reality etc., were often thought of separately. However, in the Industry 4.0 model all they are observed as key elements and enablers. It is expected that the combination of VR related technologies with the advancements of Industry 4.0 will disrupt the traditional manufacturing, the existing business models and value creation chain and will reshape dramatically the industrial environment. According to White Paper of IDC considering the Digital Transformation in the Manufacturing industry published in 2016 a third of the industrial enterprises worldwide aims to use VR in their production and engineering environment in the upcoming five years aiming at applying VR for retail showcasing, customized products development, on-site assembly, engineering design, training, etc. Within this context, the so-called Head Mounted Displays (HMDs) represent a significant interest as promising end user devices that enable the wide penetration of VR into the engineering routines such as design activities, product configuration and validation. We make a brief overview of the common HMDs, their features and limitations. Further, a generic process for configuring the customizable product features using of HMD and its programming implementation are presented following by discussion of the results from the usability testing of the proposed interaction paradigm.*

Keywords: VIRTUAL REALITY, PRODUCT CONFIGURATOR, PRODUCT CUSTOMIZATION, HMD,

1. Product Customization and Virtual Reality

Nowadays the trend for creating the products precisely according to specific requirements of each customer is already a common practice of the product manufacturing companies. In order to be successful and competitive they, regardless of their scale or specialization, have to seek diverse innovative ways in order to adapt their products satisfying the individual needs of each customer while keeping the costs at the mass production level. Here, the innovation management has moved from a manufacturer to a customer centric process leading to anticipation of a new design and manufacturing paradigm for customization of the products wide known as Mass Customization. Nowadays the trend for creating the products precisely according to specific requirements of each customer is already a common practice of the product manufacturing companies. In order to be successful and competitive they, regardless of their scale or specialization, have to seek diverse innovative ways in order to adapt their products satisfying the individual needs of each customer while keeping the costs at the mass production level. Here, the innovation management has moved from a manufacturer to a customer centric process leading to anticipation of a new design and manufacturing paradigm for customization of the products wide known as Mass Customization.

According to [Dellaert & Stremersch 2005] two most serious issues related to the implementation of product customization from the customer perspective are the **cognitive cost** and the **complexity**. When the customer has a significant number of alternatives for making a choice, the cognitive effort for their evaluation may exceed the increased benefit from the availability of options to select from. This creates frustration due to so-called "paradox of choice". The existence of too many alternatives decreases their subjective value to the customer, which in turn shall lead to a postponement of the decision or shall classify this product as a "difficult" and undesired [Piller & Tseng 2010]. The most commonly used approach to avoid this is the use of a product configuration system also referred to as product configurator. The customer is given the opportunity to build a structured model of their needs and to obtain information on appropriate solutions based on interactive test between the model and the options available.

The product configurators can be observed as software tools that are used for performing “co-design” activities in an act of manufacturer-to-customer interaction [Khalid & Helander 2003]. The customer selects the attributes and attribute values from a finite set of options and combines them into a final customized product. The configurator systems perform various tasks and contain much more than calculating algorithms. The configurators check the specification of an individual product configuration for *completeness* (that all the necessary selections are made) and for *consistency* (that no rules are violated). Additional functionalities such as price and delivery time calculation, layout drawing etc. may be provided.

In the context of the product configuration the Virtual Reality (VR) and its related technologies respectively are considered as enablers for proactive participation of the customers in defining their needs, requirements and boundary conditions and for interactive multimodal validation of the configured product and its properties in near-real conditions and showcasing. By using VR the customers are allowed to carry our more efficient “mapping” of their requirements into the physical domain and they are able not only to observe or simulate the individual creation, but also to experience the product (through multiple sensorial modalities).

2. Product Customization and Virtual Reality

Head-mounted display or HMD is a display device worn over the user’s head. It features a display in front of one or both of the eyes that stream data, images and other information. Additionally, HMDs may feature position tracking and stereo sound, providing high level of immersion for the user. There are many variants of implementation of the head-mounted display system for various purposes with different characteristics starting with the very simple cardboard box and ending with sophisticated wireless devices [Romanova, 2017].

The VR HMDs as a concept and implementation are definitely not new, but in the last three years (2015-2017) there is a growing interest to head mounted displays (HMD) as end-user devices for immersive presentation of Virtual Reality. This is mainly caused by the investments in the sector from the major companies (e.g. Facebook, Alphabet, Sony, Samsung etc.) and the introducing on the market of a third wave of new affordable devices of different producers featuring acceptable performance characteristics including low-cost head-sets which integrate smart phones as display technology together with the correspondent SDI’s. However, the main focus for practical use of these HMDs are limited only to gaming, social VR, entertainment, showcasing and other similar topics. Engineering applications, in particular related to the product customization such as in [Yuan, 2017] are not commonly reported, but highly promising. According to the reports, it is expected that the Head-Mounted Display will reach USD 25.01 Billion by 2022 at an average annual growth rate of 38.8%. That implies high penetration in all spheres of the globalized economy, including Engineering. That means that HMDs have a significant potential to become a valuable tool for supporting engineers in performing their routines and decision making and bringing new dimensions for application of traditional CAD and CAE. In this term, the exploration of the specifics of the HMD interaction and

user interface is of big importance. The analysis of the available on the market devices shows that the producers are experimenting intensively with various approaches and try to find the best relation of these properties for their customers. Another clear trend is the introduction of 3D audio components that become an obligatory aspect of the HMD device. However, the performance characteristics are still not optimal and there is a long way before reaching the required maturity.

4. Functionality and Architecture

For the purpose of this work, a simple VR-based product configurator functionality and architecture was defined as shown on Fig. 1. In term of these, it is adopted that the product, which is the main subject of the configuration process, constitutes an assembly built from multiple subassemblies and/or single parts presented in different variations (instances). The software application that implements a configuration process is known as a Product Configurator. It provides two main roles for the participants in the process: Administrator (Engineer) and User (Customer).

Fig. 1 *General architecture of VR-Based Product Configurator*

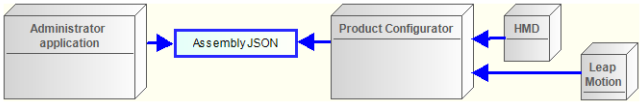

The Engineer prepares the assembly (Product) and creates a hierarchy of objects. Each object (assembly, subassembly, single part) has its own different properties that can be handled. An instance of a given subassembly can be incompatible with another instance from another subassembly. Beside other, the Engineer can configure this compatibility in order to enable implementation of real world scenarios. Upon the end of the configuration process, the Engineer can export Customer's configuration of the product as a Bill of Materials (BOM). The use of standard formats like JSON and XML enables an easy integration of the product configurator with existing or newly created upstream systems.

The Customer configures the Product based on the object hierarchy defined by the Engineer, handles it in the Virtual Reality environment and finally stores the configuration made. The configuration process can be restarted or performed multiple times. Thus, different configurations can be created, tested and compared. This provide better user experience, improved configurations and satisfaction. Both participants, the Engineer and the User, perform various tasks, which require different interactions and user interfaces. Therefore, the Product Configurator is divided in two sub-applications, which communicate through the standard JSON format. Because of this, they can be implemented using technologies that are best suited for the specific requirements. All properties of the assembly are stored in the JSON data such as id, name, color, label, position. Similar properties are available for the subassemblies and their instances. The Administrator application enables handling of this data, which is critical for the successful execution of the subsequent configuration process.

The main part of the Product Configurator is presented by the application, which provides a Virtual Reality environment accessed with a Head-Mounted-Displays (HMD) and interacted through a hand tracking system. In this environment, the user can look in arbitrary direction, move and resize the configured assembly object, change its properties (e.g. color, form, label, etc.) and undo and redo previous operations. The product configuration scenario is intended to be performed in a suitable virtual room that is near real furnished considering the specifics of the respective product as shown on Fig.2. This will provide better immersion for the users. Each operation is accompanied with appropriate sound for an optimal user experience. The user interaction with a hand tracking technology, which enables the Customer to execute most of the operations using virtual, hands (Fig. 2 *left*). The virtual hands are a graphical avatar of the Customer and represent the continuation of his/her hands in the virtual world. They react on every movement of the real hands and fingers of the Customer and repeat it in the VR. By using special gestures, the Customer can easily move the configured object, change its size and perform zoom-in and zoom-out operations. A user menu is integrated in one of the virtual hands as shown on Fig. 2 *right*. It provides access to variety of options and functions. Further, a text input is available through a virtual keyboard. The virtual room, virtual hands, virtual menu and basic gestures are presented in the following diagrams.

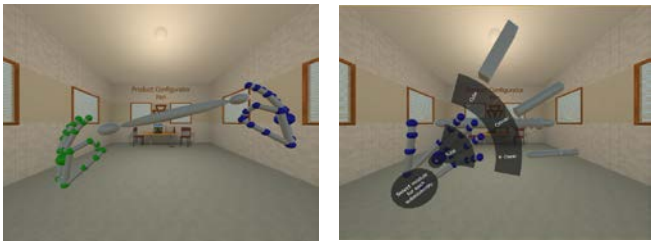

Fig. 2 *VR-based product configuration environment featuring virtual hands.*

The virtual hand menu has hierarchical structure and provides additional information to facilitate its use. It works intuitively and has a section with hints for the possible next operations. For some of the operations (like loading of previously saved configurations) an interaction with statically positioned menu is provided. The complete menu structure with possible options is shown on Fig. 3.

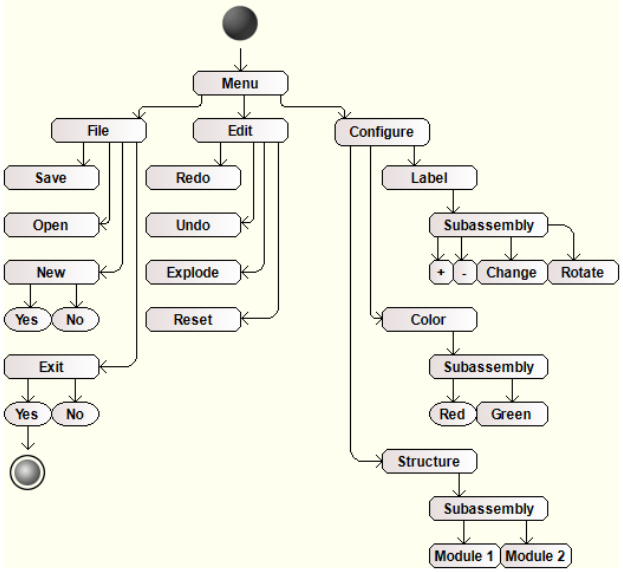

Fig. 3 *Configurator's menu structure*

5. Implementation and Integration

The Product Configurator application uses two interface devices: Leap Motion for user input and *Oculus Rift* HMD in its version *Development Kit 1* for immersive visual presentation. The Leap Motion device is placed on the front side of the HMD. In this way, the sensors can identify both hands also when the user moves his head in different directions. Both devices are connected to the computer through USB ports. The HMD is connected also through HDMI. Both require additional driver software to be installed. It was found that Oculus Rift has some compatibilities issues related to the used video cards, especially in the mobile computers. For the purpose of the development and testing the minimal computer setup with following parameters was determined: Windows 8.1 Pro 64bit, 8GB RAM, AMD A8 PRO7600B R7, 10 Compute Cores 4C+6G 3.10GHz (Fig, 3). This configuration is not powerful enough. Therefore, most of the elements of the virtual room are static and are calculated at compile time, which provides significant performance improvement and influences positively the user experience.

Fig. 4 *Minimal hardware setup*

It was found that Oculus Rift has some compatibilities issues related to the used video cards, especially in the mobile computers. For the purpose of the development and testing the minimal hardware setup with following parameters was determined: Windows 8.1 Pro 64bit, 8GB RAM, AMD A8 PRO7600B R7, 10 Compute Cores 4C+6G 3.10GHz (Fig, 4). This configuration is not powerful enough. Therefore, most of the elements of the virtual room are static and are calculated at compile time, which provides significant performance improvement and influences positively the user experience. The developers of Leap Motion and Oculus Rift provide software API for application development. This enables easy and fast beginning in the development process. Most of the basic functionalities come out of the box. As the technology is relatively new, often there is not backwards compatibility between releases and previously working code can malfunction. Therefore, version migration should be performed carefully dictated by the provided documentation.

The Administrator application is organized using the Model-View-Controller paradigm. Different packages are created to implement this separation. Under the models package all classes defining an assembly are created: Assembly, Subassembly and Module. A separate class is defined that contains the configuration information for each object. A singleton instance of *ConfigurableObjectManager* is provided, which implements all configuration operations. Fig. 5 presents its class diagram.

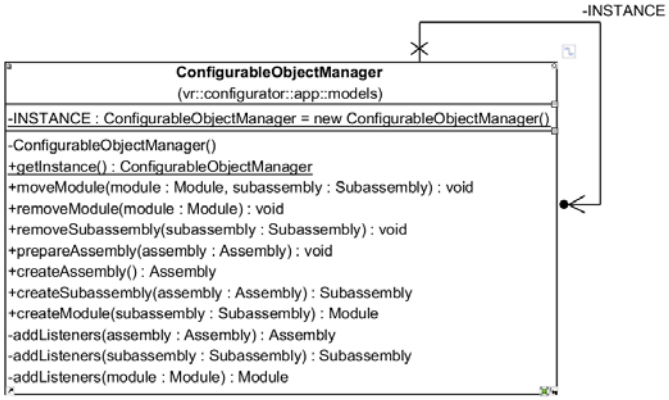

Fig. 5 *ConfigurableObjectManager class diagram*

The User application has more complex structure, because it models different kinds of interactions in the VR environment. The components are organized in packages based on their role in the overall architecture. The *Behavior* package contains again the definitions of all assembly related objects, but this time from the perspective of their manipulation and configuration. The *Config* package provides all settings prepared by the Administrator application. The architecture of the VR application is mostly event-driven. The user can perform operations in any order. Therefore, the Service package contains services, which are called when a specific event is fired. Fig. 6 shows the facade used for access to the object, text-material, sound, message and redo-undo services.

The Menu package contains definitions of all kinds of elements used for the VR interactions. They build an object hierarchy (Fig. 7), which is constantly manipulated and changed through the execution of the program.

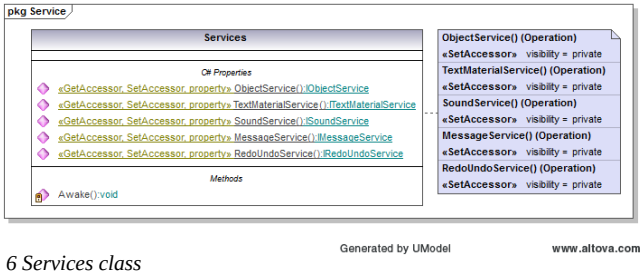

Fig. *6 Services class*

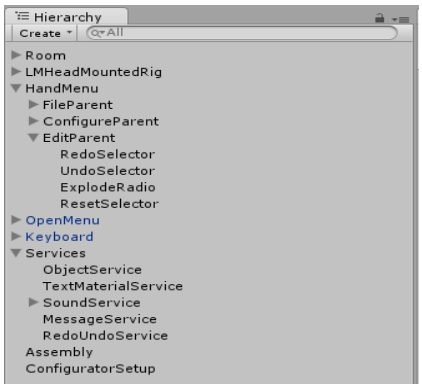

Fig. 7 Object hierarchy

6. Usability Testing

A simplified usability evaluation based on predefined testing procedure is performed to evaluate the proposed interaction paradigm as shown on Fig. 8. 16 participants took part in the testing with equal count of males and females. The age distribution is presented on Fig. 9. The participants of age of 18 - 24 years prevail.

Fig. 8 *Performing testing of the product configuration using HMD*

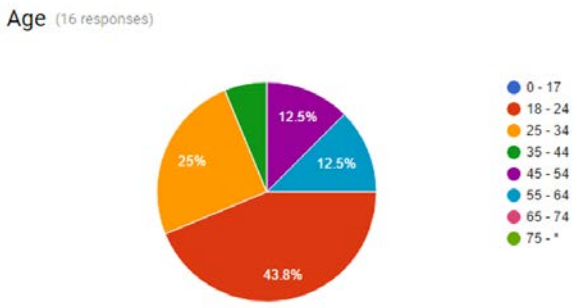

Fig. 9 *Age distribution of the participants in the usability study*

In the performed study, every testing person should configure his/her individualized version of a simple consumer product (a pen). The product consists of three subassemblies, each of them has three different variants (instances) as shown on Fig.13. Additional compatibility constraints are defined between some of them. At the beginning of test procedure, the purpose of the study is explained to the testing person. After that, he/she receives instructions about the way of use of the configurator and the virtual hands mechanics is explained. Each participant puts on the HMD by himself/herself and performs following tasks: assembly move, size change, configuration of the structure, color selection, defining and positioning of a label, saving the configuration. The first impressions are registered trough a personal interview upon completion of the testing procedure and then the user should complete a usability questionnaire.

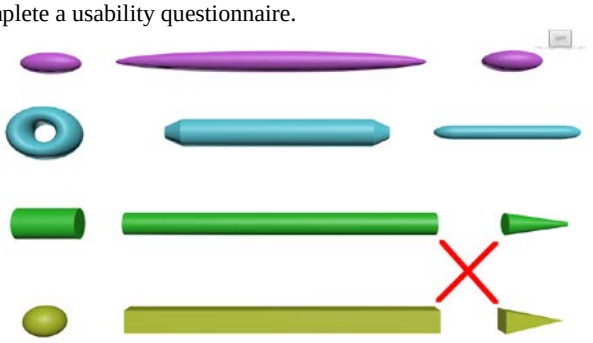

Fig. 10 *Test product structure*

The most of the user have good experience with the system as shown on Fig. 11. A half of them is completely satisfied with the product. One of the most important issue related to the Virtual Reality is the physical comfort of the user. Often after longer exposure to a virtual environment users show symptoms of so called cyber sickness such a general discomfort, headache, stomach awareness, nausea, vomiting, pallor, sweating, fatigue, drowsiness, disorientation. Manifestation of some of these symptoms with different extent are reported from five of the participants. The symptoms were severe only in one case.

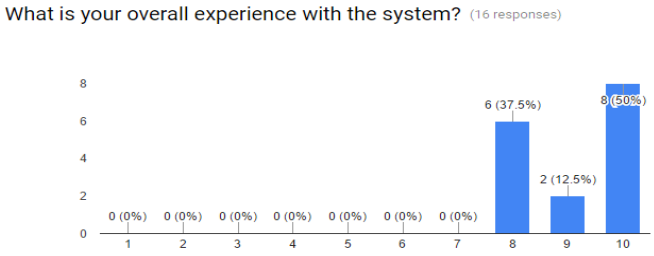

Fig. 11 *Overall experience with VR-based Product Configurator*

One aspect that plays important role is the resolution of the HMD. The experiments is performed by using the first Oculus Rift model and shows expected results. For most of the participants is the text with low readability and this hinders the interaction with the system. Nearly two-thirds of the participants like the control with the virtual hands. The rest report difficulties, which they overcame after a short period of time. This is valid for the most of the older participants who have problems to use the virtual hands. The size of the hand menu should not be so big because it is considered as an integral part of the hand. According to the majority of the users the menu is well structured and organized, but not perfect. It has to many options and is regarded as difficult. One possible solution of this issue is the use of voice commands or gestures related to additional tracking sensor. The menu icons and the menu colors facilitate the work. In the first version of the Product Configurator no icons or meaningful colors were used. Based on the feedback of the testing person these were implemented and 70% of participants find that the icons and colors provide them with important support into the configuration process.

Other important component for VR are the sounds. In the Product Configurator various sounds and audio effects are used for the occurring events. 60% of participants find these for appropriate and meaningful. According to the most of the participants, the immersion in VR environment enhances the experience as a whole. However, the opinions here varies in a wide range. On the one hand, VR supports and augments the configuration process and alters the user experience in disruptive way. On the other hand, some of the participants (10 %) rate the VR environment as distractive. Evident here is the problem for keeping balance between photorealistic appearance and functional requirements.

Generally, the results from the testing are positive and motivate the future development of the system. The negative aspects are not provoked form the Product Configurator itself, but from the performance characteristics of the user hardware equipment itself. The technology is improving continuously, therefore the low resolution, the latency and related to them sickness symptoms can be gradually overcame. In order to get better understanding the Product Configurator should be tested systematically with other HMD models. In our opinion the most of the reported issues can be avoided by the use of headset with better performing characteristics, e.g. HTC Vive. Based on the collected information from the testing the application can be improved in various ways. The user interface can be extended with new components, e.g. better color selector. The hand menu should be revisited, because it cannot support subassemblies with more than five modules. More optimal feedback mechanism should be provided for the single operations, e.g. when a given instance has been chosen it can change its appearance VR. The virtual room can be also improved. Additional spaces should be designed that support configurations of different assembly types. Another improvement that can provide a better immersion is the introduction of voice commands.

7. Conclusion

The field of Virtual Reality is rapidly going forward and givens new opportunities for software applications. Its integration in the Mass customization process involves even more the user and provides unique user experience. A new set of challenges arise from this innovation. The lack of standards and well-established methodologies motivates the experiments with new platform independent architectures, which should utilize all existing and future VR technologies. This work studies and proposes a generic architecture for product configuration, which can be easily deployed in an existing IT environment. It implements different approaches for the interaction between the user and the system. The described goals and principals are tested using a usability test. This evaluates the created system and gives guidance for the possible improvements. The overall positive results can be used as evidence for the growing potential of the VR technologies and strengthen its position in the constantly changing and evolving information technology world.

The results presented in this paper are obtained in the framework of research activities funded by the National Science Found at the Bulgarian Ministry of Education and Science received through grant DUNK-01/3.

8. Literature

[Khalid & Helander 2003] Khalid, H., & Helander, M. (2003). Web-based do-it-yourself product design. In M. Tseng & F. Piller (Eds.), The Customer Centric Enterprise (pp. 247-265). New York/Berlin: Springer.

[Dellaert & Stremersch 2005] Dellaert , B.G.C. and Stremersch, S. (2005). Marketing Mass-Customized Products: Striking a Balance between Utility and Complexity. Journal of Marketing Research, 42 (2), 219-227.

[Romanova, 2017] G. E. Romanova, A. V. Bakholdin, V. N. Vasilyev, Optical schemes of the head-mounted displays, Proc. SPIE 10374, Optical Modeling and Performance Predictions IX, 103740I (6 September 2017)

[Yuan, 2017] Yuan & Yu, Shiqiang & Zheng, Pai & Qiu, Liming & Wang, Yuanbin & Xu, Xun. (2017). VR-based Product Personalization Process for Smart Products. Procedia Manufacturing. 11. 1568-1576. 10.1016/j.promfg.2017.07.297.

COMPUTER SIMULATION OF WITHIN-YEAR CYCLE OF AN AQUATIC ECOSYSTEM LIFE

ИМИТАЦИОННОЕ МОДЕЛИРОВАНИЕ ВНУТРИГОДОВОГО ЦИКЛА ФУНКЦИОНИРОВАНИЯ ВОДНОЙ ЭКОСИСТЕМЫ

Ass. prof., Ph. Dr. Tretyakov V.Yu., Prof., Dr. Dmitriev V.V., Prof., Dr. Sergeev Yu. N.,
Ass. prof., Ph. Dr. Kulesh V.P.
Institute of Earth Sciences – St. Petersburg State University, St. Petersburg, Russia
E-mail: v_yu_tretyakov@mail.ru

Abstract: *We consider some experience of computer simulation of within-year cycles of aquatic ecosystems, which has group of lecturers and scientists of St. Petersburg State University. The experience includes designing point, reservoir and spatially non-homogeneous simulation models of aquatic ecosystems functioning, and carrying out numerical experiments with the models. The models are applied for investigations in the sphere of ecology, nature protection and nature management. Main attention in the report is devoted up-to-date state of the simulation.*
KEYWORDS*: AQUATIC ECOSYSTEM SIMULATION, ANTHROPOGENIC EUTROPHICATION, TOXIC CONTAMINATION*

1. Introduction

Modern global ecological crisis has been mainly caused by the Earth biosphere poisoning by anthropogenic contaminants. Oil is one of the most harmful one. Prognosis of an ecosystem behaviour and revealing of the weakest chains of the ecosystem is impossible without application to the computer simulation approach [1]. Institute of Earth Sciences of St. Petersburg State University has some experience in designing computer simulation models of aquatic ecosystems. The models were applied for investigations in the sphere of ecology, nature protection and nature management. Thus, Dr. Yuri Sergeev offered the general approach to the creation of simulation models of aquatic ecological systems in 1972 [2].

During 1970-1980s Dr. Yuri Sergeev leaded investigations in the direction. A very active participation in the investigations had Valery Kulesh, and Vasily Dmitriev. In 1970s the North Sea was studied, and as the result of the investigations in 1974 there was built a spatially non-homogeneous simulation model of the ecosystem [3]. Later, in 1980s, there appeared a number of simulation models of ecosystems of eastern part of the Finnish Gulf and the Neva Bay [4]. Victor Tretyakov built an aquatic-bottom reservoir model of the Neva Bay. His next computer model in 1994 was devoted to determination of specific features of Lake Ilmen ecosystem by means of computer simulation. It was a computer reservoir model of the ecosystem, which included blocks of the floodplain and bottom [5, 6]. At the same time Yuri Sergeev and Valery Kulesh designed spatial nonhomogeneous simulation model of Lake Ilmen ecosystem and model of economic and ecological development of Russia [6].

It should be said that all anthropogenic contaminants might be divided into two groups: those of total ecological influence and those of individual toxic impact. The first contaminants do not have any harmful effect on an organism but they change biogeochemical cycle of ecosystems. Eventually this can lead to the change of the ecosystem parameters and even structure. As an example of these contaminants, anthropogenic biogenic elements (that is nitrogen and phosphorus) may be considered. The contaminants of the second group affect directly some vital functions of the hydrobionts. The contaminants in turn may be divided into two groups: those, which stimulate some vital functions at low concentrations and depress these functions at higher concentrations and those, which depress the functions at any concentrations [7, 8, 9].

In 1999, V. Tretyakov designed a simulation model for the prognosis of the sea ecosystem behaviour in conditions of building and functioning of new industrial zone near Byorke-Zund Strait between Karelian Isthmus and Berezoviye islands in the Finnish Gulf. The zone includes a plant for producing liquid ammonia and granulated carbamide obtained from natural gas. In the model, a possible response of the ecosystem was investigated for the increasing of the anthropogenic impact. The model is the system of 102 non-linear differential equations, which are solved by Runge-Kutta method.

Later the model was modified for investigation of consequences of volley of toxicant sewage that is an abrupt discharge of considerable amount of the toxic substance into ecosystems of flowing water reservoirs with changeable volume, depth and river run-off. In addition, the model can reflect consequences of constant discharge of a toxic substance into an aquatic ecosystem. The model may be used for determination of ultimate acceptable anthropogenic impacts on aquatic ecosystems.

2. The model description

The alive components of the model are several groups of phyto- and zooplankton; bacteria, associated with detritus; babies of plankton-eater fishes, predatory fishes, benthos-phage ones, worms of Oligochaete class and molluscs.

The lifeless components of the model are plankton genic detritus, suspended mineral and organic matter, suspended matter of bottom silt; dissolved organic carbon, nitrogen, phosphorus, dissolved ammonia, nitrites, nitrates, phosphates; dissolved oxygen and carbon dioxide; concentrations of toxic contaminant in the organisms bodies, suspended organic matter and water body.

The model can be used for investigations of consequences of the following anthropogenic impacts: 1) Anthropogenic eutrophication of an aquatic ecosystem; 2) Constant discharge of a toxic substance into an aquatic ecosystem; 3) Volley of toxicant sewage that is an abrupt discharge of considerable amount of the toxic substance into an aquatic ecosystem; 4) A toxicant accumulation in the trophic chain of the simulated ecosystem; 5) Joint effect upon an aquatic ecosystem both anthropogenic eutrophication and the ecosystem poisoning by a toxic pollutant.

The model at present can simulate functioning of an aquatic ecosystem of an abstract flowing water reservoir with changeable volume, depth and river run-off. The simulated water body may be divided into two layers: the upper one that is epilimnion and the lower one – hypolimnion, or it can be non-separated aquatic ecosystem considered as a whole.

Temporal variability of the model components ensues both due to translocation processes within the ecosystem that is changes by matter between the model components and by reason of intermixing of the water body with inflowing river run-off which contains some of the ecosystem components.

The translocation processes are influenced by external ecological factors, such as temperature of water environment, solar radiation and so on. Concentrations of some ecosystem components in the inflowing river run-off can be also considered as external ones.

The external ecological factors which temporal dynamics affects the model ecosystem behaviour are: 1) Temperature of the upper layer or all water body as a whole if the model ecosystem consists of only a layer; 2) Temperature of the lower layer; 3) Share of the upper layer thickness relatively to the maximum depth of the reservoir; 4) Share of the river inflow entered into the upper layer; 5) Share of the outflow from the upper layer in the total outflow from the reservoir; 6) Photosynthetically active radiation – PAR; 7) Atmospheric pressure; 8) Wind velocity; 9) Run-off or level of the river inflowing into the reservoir; 10) Concentrations of the three groups of the river phytoplankton; 11) Concentrations of the two groups of the river zooplankton; 12) Concentration of the river bacteria; 13) Concentration of the river detritus; 14) Concentrations of the river dissolved organic carbon, nitrogen and phosphorus; 15) Concentration of the river dissolved organic matter excepting organic carbon, nitrogen and phosphorus; 16) Concentration of the river ammonium, nitrite and nitrate nitrogen; 17) Concentration of the river phosphate phosphorus; 18) Concentration of the river dissolved carbon dioxide; 19) Concentration of the river dissolved oxygen; 20) Concentration of the river suspended mineral matter; 21) Concentration of the river suspended organic matter; 22) Concentrations of the toxic pollutant in the first, second and third groups of the river phytoplankton; 23) Concentrations of the toxic pollutant in the first and second groups of the river zooplankton; 24) Concentrations of the toxic pollutant in the river bacteria; 25) Concentrations of the toxic pollutant in the river detritus; 26) Concentrations of the toxic pollutant in the river terrigenous suspended matter; 27) Concentrations of the toxic pollutant in the river water.

Within-year (annual) variability of the factors must be written into textual files separately for each month. Therefore, annual dynamics of each external factors have to written into 12 files. Extensions of the files must correspond to the month's numbers: January – "01", February – "02" and so on. Before a numerical experiment with the model, a user must prepare files of the initial values of the model components.

The model simulates the following processes: 1) Biosynthesis of the phytoplankton with consumption of biogenic elements in mineral forms and CO2 from the water and oxygen abjection; 2) Breathing and extracting processes of the phyto-, zooplankton, bacteria including destruction of the organisms tissues at metabolism, oxygen consumption, CO_2 and excretes abjection; 3) Bacterial detritus destruction, growth of the bacteria biomass, dissolved organic matter entering into the water; 4) Dissolved organic matter, NH_4 и NO_2 mineralization, oxygen consumption; 5) Zooplankton feeding; 6) Vital processes in the fish fauna including hatching, feeding, growth, breathing and metabolism with excretion, migration between the layers; 7) Vital processes in the benthic society including its influence upon the water body; 8) Turbulence interchange by the dissolved and suspended components between the layers; 9) Bottom silt stirring-up due to wind and waves; 10) Bottom silt organic matter destruction; 11) Change of the components concentrations due to the reservoir water body intermixture with the inflowing river; 12) Toxicant influence upon the vital processes; 13) Organisms dying off.

Formalization of the each simulated process demands setting of values of the process parameters and coefficients. Therefore, a user must prepare files of parameters of the simulated processes.

Besides that, a user must prepare the file of the reservoir parameters. In order to simplify the numerical experiments processing and escape possible mistakes it is better to prepare file of the data configuration. The file contains full addresses of all external data files and their names. The configuration file has rigid structure. A user can edit the file by means of any textual editor. He must not insert and delete the strings and delete in the strings the symbol of hyphen ("-"). Name and full address of a data file is written in each string to the right of the hyphen. In each string to the left of the hyphen, there is a brief explanation of the information, which is stored in the data file. A user can edit the explanation and even change its language. In addition, a user can edit the data file name and address to point new prepared file of data, template or the ones of a new file for the experiment results recording. Results of the numerical experiments are written into files of Microsoft Excel books format according to prepared files of templates. A user by the program interface must set the following features of a numerical experiment: 1) The reservoir type. The possible variants are: flowing, stagnant ones, marine estuary. By default, it is set the variant of a flowing reservoir. The variant of a marine estuary is now in stage of elaboration. 2) The type of the reservoir level. There is no a default variant: a user must make choice. In case of the stagnant reservoir this stage of the experiment features setting is skipped. 3) Simulation of a toxic matter cycle in the ecosystem. By default the feature is skipped. To switch on the feature a user have to switch on the corresponding checkbox in the program interface. 4) If the experiment includes simulation of the toxicant cycle, a user have to set the toxicant type. In case of the first type of toxicants a toxicant does not stimulate vital processes of the aquatic organisms at low concentrations of the toxicant in the organisms' tissues. In case of the second type of toxicants a toxicant stimulates vital processes of the aquatic organisms at low concentrations of the toxicant in the organisms' tissues. By default, the simulated toxicant is one of the first type. A user can set change the toxicant type on the second one. 5) Shape of the reservoir hollow. The possible variants are: cone, frustum of cone, ellipsoid, three-axial ellipsoid, cylinder, spherical segment. The variant of a spherical segment is set by default. 6) Number of the water body layers: one or two. 7) In the case of two layers a user have to select the variant of the layers thicknesses ratio. It can be constant or changeable one. 8) Share of the inflowing river water entering into the upper layer. It also can be constant or changeable during a year. 9) Share of the water from the upper layer in total outflow from the reservoir. It also can be constant or changeable during a year. 10) Windy stirring-up of the bottom silt. By default, the process simulation is checked on. In case of a one-layer ecosystem simulation the stages 7-9 are automatically skipped. After the stage 6 a user passes to the stage 10. In case of simulation of a two-layer ecosystem of a stagnant reservoir the stages 8 and 9 are skipped. 11) Taking into account the flood-plain influence upon the aquatic ecosystem (in the case of flowing reservoir). By default, the influence is checked off. The block of the influence has not yet been included into the program. Therefore, a user passes directly from the stage 10 to the stage 12. 12) Taking into account influence of atmospheric precipitation on the reservoir mirror. By default, the influence is checked off. The block of the influence has not yet been included into the program.

When the determination of the experiment specificity has been performed, a user have to input the experiment identifier into the textual field of the interface. The identifier can include any symbols. Then a user have to check on in the frame "To write the dynamics results" the checkboxes of the parameters sets which will be recorded into the external files of the experiment results. By default the checkboxes are checked off that is no any recording of the experiment results.

A user can check on recording of the following sets of the ecosystem functioning parameters: temporal dynamics of the non-toxic components values, toxic components values, and intensities of the non-toxic components matter interchange processes, intensities of the toxicant interchange processes, parameters of the environment quality estimation. A user can check on the sets in any combinations including all sets or no one.

Then a user by means of the interface have to point the data configuration file. After that, a user clicks the button "All parameters have been set" and the experiment starts.

The model simulates within-year cycle of an aquatic ecosystem life. The cycle begins on January 1 and finishes on December the 31-st. At the very beginning of the iteration body of the cycle the program determines if the ice cover exists or not. Then the program determines the number of the month. The program sets the number of splitting of daily step of the decision of the differential equivalences system by the month number. During the January-March period number of within-day steps is equal to 16, April-October period – 64, and in November and December – 32.

Then the program determines the number of the day within the month. If the day is the first day of a month then the program loads from external files into the main memory arrays of the external ecological factors values for a coming month. Then the program remembers the values of the external factors and the model components at the beginning of this and next day. If the day is the last day of the month, then the main program runs "Sledm" subroutine, which determines the extension of the files of the external factors for the next month. In this case, the next day is the first day of the next month. For the 31 of December it is January 1. The values of the external factors at the beginning of the next year are set as equal to the values at the beginning of this year. Then the main program examines if the temperature of the upper layer or the water body as a whole is enough for spawning or not. If it is enough then this day is set as the date of the beginning of the spawning. Of course, the temperature required for initiation of the spawning of various fishes may differ.

Then in the program, there is a block of automatic doubling of number of fractional steps within a day at the decision of the system of differential equations. This block is only performed in the case when during decision of the equations system at least a component becomes negative. Then the program returns the values of the components to the beginning of the day. At the initial calculation of the equations system for each day, the program skips the block. After that, the program performs the data preparation for decision of the equations system within a day. It is necessary to stress that the realization of the decision within a day does not refer to simulation of diurnal dynamics of the ecosystem processes. The diurnal cycle is necessary for decision of the differential equations system by the numerical Runge-Kutta method. At first, the program determines the size of a fractional step in part of a day by division of one by the number of the fractional steps in the day.

To ensure smoothness of the decision the program determines values of changes on the fractional step of the external ecological factors: water temperature, solar radiation, and atmospheric pressure, wind speed and so on. Then in the program, there is a block of simulation of within-year dynamics of individual weight of Oligochaete worms. This process is realized on the base of data for ecosystem of Ilmen Lake. Here the program also calculates change of the individual weight on a fractional step.

Then the program performs diurnal cycle of the equations system decision by means of iteration Runge-Kutta method of the fourth degree.

This method has the fourth degree of accuracy that is the total error at the final interval of integration is directly proportional to the value of the fractional step in the fourth degree. The above-mentioned method is realized in the subroutine «drob». The main program calls the subroutine 4 times according to the stages of calculation by the Runge-Kutta method. The subroutine calculates values of the external ecological factors. If the model simulates ecosystem of running water body ecosystem the subroutine also calculates values of parameters of the water body flowage and concentrations of the simulated substances in the inflowing river run-off for each fractional step and stage of calculation by the Runge-Kutta method. If the model simulates a cycle of a toxic matter, the subroutine calculates concentration of the toxic matter in the model components flowing into the water body with the run-off and in the river water itself.

Thus, we set the change within a day the following parameters of the model: the water temperature (if the water body has two layers, then in two layers separately), solar radiation, atmospheric pressure, wind velocity.

If we simulate ecosystem of a water body with changeable level then the model likewise calculates the change of the water body volume, its maximum and average depth, and surface area within a day. If the water body ecosystem divides into two layers then the model likewise sets changes within a day the ratio between the upper layer width and the maximum depth of the water body, maximum width of the upper and lower layers, volumes of the layers, and average widths of the layers. If we simulate change within a year the ratio between the input of the river water into the upper and lower layers of the water body then the model also sets change within a day share of the river inflow inputting into the upper layer. Likewise, the model sets change within a day share of water from the upper layer in the total outflow from the water body. At simulation of an ecosystem of a flowage water body the model likewise sets change within a day concentrations of the model components inflowing with the river inflow including a toxic substance, of course, if the model includes simulation of a toxic matter cycle.

After the end of a diurnal cycle of the calculation of the intensities and values of the model components in the main program there is block of the current values setting into cells of tables of Microsoft Excel format.

3. Results and discussion

Let us present some results of computer simulation by the model of functioning of an abstract flowing water reservoir ecosystem under various anthropogenic impacts and without any impacts that is at natural regime of the simulated ecosystem. In the standard (benchmark) numerical experiment with the model, the intra-annual dynamics of biogenic elements and organic matter concentrations in the inflowing river's water reflects generalized seasonal dynamics of the substations upon condition of absence of anthropogenic impact. The reservoir parameters and external ecological factors correspond to conditions of the Russian part of the Finnish Gulf watershed. Parameters of the simulated water reservoir are the following: the rate of conventional water exchange – 4, the maximum depth at average water level of the reservoir – 5 m. As data for building of intra-annual dynamics of biogenic elements and organic matter concentrations in the inflowing river's water, we used data of multi-year monitoring at 25 stations on medium and small rivers within Russian part of the Finnish Gulf watershed. According results of statistical analysis, we divided the rivers into four groups and separately the Mshaga River. There were carried out five benchmark experiments with the intra-annual dynamics of biogenic elements and organic matter concentrations in the inflowing run-off corresponded the generalized dynamics in the four river groups and the Mshaga River because biogenic and organic matter content in these rivers run-off practically does not include anthropogenic component. In the model experiments with anthropogenic eutrophication simulation, we increased the biogenic and the organic matter contents in few times. Intra-year dynamics of the toxicant content in the inflowing run-off was similar the one of chrome in the Smolyachkov stream in the Kurortnyiy district of St. Petersburg. The numerical experiments with the model included both separated simulation of anthropogenic eutrophication and toxic substance inflow, and joint impact of the eutrophication and the toxicant inflow.

4. Conclusions

Simulation of natural regime of the aquatic ecosystem with the intra-year dynamics of the biogenic elements and organic matter in the inflowing river water, which correspond the ones in the four groups of rivers of the Finnish Gulf watershed, shows intensive spring growth of the phytoplankton biomass. The reason of it is increased content of the biogenic elements during flood caused by streams of snowmelt water [10].

Dynamics of the biogenic elements content in these four groups of rivers show decrease of the content in the beginning of June. It results decrease of the phytoplankton biomass. Die-away of the phytoplankton leads to increase of the bacterial plankton biomass. There is autumn increase of the phytoplankton biomass caused by increase of inflowing run-off with the biogenic elements that is autumn flood. The maximum average annual phytoplankton biomasses were registered in the numerical experiments with simulation of the biogenic elements inflow from the Karelian and Central groups of the rivers. The average annual concentrations of total nitrogen and phosphorus in river water are maximal in these groups of rivers.

The numerical experiments with simulation of anthropogenic inflow of the biogenic elements have given the following conclusions. In all the numerical experiments, there were two blooms of the phytoplankton – spring-summer and summer-autumn ones. In all cases, the first spring-summer bloom is greater than the summer-autumn one for diatomic and blue-green algae. The group of rest algae shows inverse picture. The increase of the biogenic elements inflow influences at the beginning of the spring-summer bloom of the diatomic algae. The increase of the biogenic elements inflow leads to increase of primary production of the all phytoplankton groups. There is growth of the zooplankton biomass during periods of its maximum values without change of the peaks time. At increasing of the biogenic elements inflow there is decrease of dissolved oxygen concentration during summer and autumn due to the oxygen consumption for molding of the defunct organic matter [11].

The numerical experiments with simulation of toxic substance inflow have given the following conclusions. The toxic substance inflow leads to decrease of the phyto- and zooplankton biomasses. The benchmark numerical experiment with absence of anthropogenic impacts and the numerical experiment with minimal inflow of the toxic substance according to the intra-annual dynamics of chrome in the Smolyachkov stream shows very close dynamics of the model components. The experiment with minimal toxic matter inflow shows decreases of maximum biomasses of the plankton groups. Increase of the toxic substance in inflowing river water in three and five time leads to significant decrease of the plankton for the year, and peaks of the plankton blooms are essentially lower in comparison with the ones in the benchmark experiment. All the numerical experiments show evident spring peak of diatomic algae bloom. However, the autumn peak does not evident. The spring-summer peak of blue-green algae and other groups of the phytoplankton is below than the summer-autumn one. The spring-summer peak of the zooplankton biomass development is greater than the summer-autumn one. The toxic substance makes the feature more evident. Increase of the toxic substance concentration in three and five times the summer-autumn peak disappears [12].

The numerical experiments with joint simulation of anthropogenic eutrophication and toxic substance inflow have given the following conclusions. The toxic substance inflow leads to decrease of the phytoplankton biomass. Diatomic algae is most sensitive to the increase of the biogenic elements. The increase in three times leads to increase of the diatomic algae maximum summer biomass at 47%. The increase of the biogenic elements inflow accelerates the beginning of the spring-summer bloom of the diatomic algae. Additional inflow of the biogenic elements neutralizes the toxic substance negative influence upon the primary production [13].

The numerical experiments have given the following conclusions about the toxic substance distribution within the trophic net. In the experiments with simulation of the toxic substance inflow, there are insignificant decrease of the diatomic algae biomass with disappearing of the autumn bloom. Toxic pollution of the ecosystem leads to increase biomasses of the blue-green algae and other groups of the phytoplankton except diatomic algae. The maximum accumulation of the toxic matter in the phytoplankton organisms shows the experiment with the maximum concentration of the inflowing toxic substance. The toxicant inflow suppresses the autumn peaks of the phyto- and zooplankton. The phytivorous zooplankton and bacteria plankton shows the maximum average annual concentrations of the toxic substance in the ecosystem organisms. All the components of the biota except two-year age predatory fishes show increase of the average annual concentration of the toxic substance in the organisms at increase of the toxic substance inflow in the ecosystem. The two-year age predatory fishes show the minimal average annual concentration of the toxicant at its maxima inflow into the ecosystem [14].

References

[1] S.E. Jorgensen. Handbook of Ecological Modelling and Informatics. London, 2009, 35 p.

[2] V.V. Dmitriev. Diagnostics and modelling of aquatic ecosystems. Publishing house of St. Petersburg State University, St. Petersburg, 1995, 215 p.

[3] Yu.N. Sergeev, V.P. Kulesh, O.P. Savchuk, V.V. Dmitriev, T.S. Komarova. Mathematical modelling of the pelagic ecosystem of the North Sea. The Works of AtlantNIRO, Kalilingrad, "Kalilingradskaya Pravda", 1982, p.103-116.

[4] V.V. Dmitriev, V.P. Kulesh, Yu.N. Sergeev. Spatially non-uniform vertical model of aquatic ecosystem of the eastern part of the Gulf of Finland. *Application of methods of simulation modelling in ecology and fisheries studies on inland waters. Collection of research papers*, Vol. 302 (1989), p.115-125.

[5] V.V. Dmitriev, V.Yu. Tretyakov, V.Yu. Vasilyev. Simulation of the annual cycle of the aquatic ecosystem of Ilmen Lake. *Application of methods of simulation modelling in ecology and fisheries studies on inland waters. Collection of research papers*, Vol. 302 (1989), p.85-92.

[6] Yu.N. Sergeev, V.P. Kulesh, V.V. Dmitriev, V.Yu. Tretyakov and others. The ecosystem of Ilmen Lake and its floodplain. St. Petersburg State University, St.Petersburg, 1997, 276 p.

[7] V.Yu. Tretyakov, L.V. Alexandrova, V.V. Dmitriev. Simulation of toxic pollutant spreading in a trophic web of river mouth ecosystem. Land-Ocean Interaction in the Coastal Zone Second International Symposium on: Functioning of Coastal Ecosystems in Various Geographical Regions. Sopot, Poland, September 5-7, 1996. Abstracts, p. 14.

[8] V.Yu. Tretyakov. Research conception of natural evolution of aquatic ecosystems. Land-Ocean Interaction in the Coastal Zone Second International Symposium on: Functioning of Coastal Ecosystems in Various Geographical Regions. Sopot, Poland, September 5-7, 1996. Abstracts, p. 66.

[9] V.Yu. Tretyakov, L.V. Alexandrova, V.Yu. Vasilyev, V.V. Dmitriev, V.P. Kulesh, A.N. Ogurtsov. Parametrization of cascade geosystems and coevolution of its biotic and abiotic components with man-made load. International ecological congress. September 22-28, 1996, Voronezh, Russia, Manhattan, Kanzas, U.S.A. Proceedings and abstracts. Section: Science and Environment, p.84-85.

[10] V.Yu. Tretyakov, P.I. Boldyreva. Influence of intra-annual dynamics of biogenic elements inflow upon functioning of an abstract flowing water reservoir ecosystem. *Meteorologicheskiy Vestnik*, Vol. 7 (2015), N 2, p.1-47.

[11] V.Yu. Tretyakov, M.A. Zheltyshev. Simulation of flowing water reservoir eutrophication. *Meteorologicheskiy Vestnik*, Vol. 7 (2015), N 1, p.1-45.

[12] V.Yu. Tretyakov, E.V. Kruglov. Simulation of toxic pollution impact upon functioning of an abstract flowing water reservoir ecosystem, *Meteorologicheskiy Vestnik*, Vol. 7 (2015), N 3, p.1-57.

[13] V.Yu. Tretyakov, P.A. Bodrov. Joint effect of eutrophication and toxic contamination of aquatic ecosystems. *Meteorologicheskiy Vestnik*, Vol. 8 (2016), N 1, p.88-112.

[14] V.Yu. Tretyakov, O.A. Sverdlova. Simulation of toxicant dynamics in biocenosis of an abstract flowing water reservoir ecosystem, *Meteorologicheskiy Vestnik*, Vol. 8 (2016), N 2, p.1-42.

FOURTH INDUSTRIAL REVOLUTION. ROBOTS AND PRODUCTION AUTOMATION WITH ELEMENTS OF ARTIFICIAL INTELLIGENCE

Prof. Pavlov, V, Phd[1], Avishay, D. Phd[2], Pavlova, G [1]
Technical University of Sofia, Sofia, Bulgaria[1]
Afeka, Academic Engineering College in Tel Aviv, Department of Mechanical Engineering, Bnei Ephraim Street No 218 - Israel
vpavlov@u-sofia.bg, davishay@afeka.ac.il, raicheva@tu-sofia.bg

Abstract: *The present research is devoted to the coexistence and communication of a person with machines, equipment and robots that possess elements of artificial intelligence. The new conditions lead to revolutionary changes in the automation of various activities in and outside the industry. Changes are multifaceted and the disclosure of trends allows planning and protecting of legal long-term activities to achieve useful outcomes effectively.*

KEYWORDS: INDUSTRIAL REVOLUTION, ROBOT, ARTIFICAL INTELLIGENCE, PERSON, COEXISTENCE, AUTOMATION, EDUCATION, SELFTRAINING

1. Introduction

1.1. Motives for the Human Society Development and Revolutionary Steps

The evolution of human society creates tools of labor to satisfy ever-increasing needs of the people. The man king are forced to create tools that initially were driven by the energy of their muscls. Subsequently, the mental development is directed to the use of other kinds of energy – directly the natural (the power of water, fire, wind) and later - other types (electricity and other). The essence of satisfying human needs (consumption) most accurately and briefly is defined in the theory of Abraham Maslow [1], an American scholar psychologist in the publication „A Theory of Human Motivation", He defined the needs of humans as a hierarchical pyramid (fig. 1).

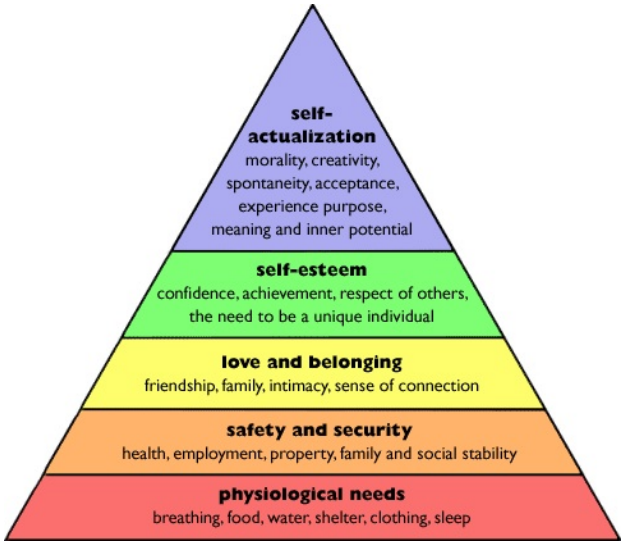

Figure 1: *Distribution of needs according to Maslow's pyramid*

According to Maslow, if the lower-level needs are not met, the person can not focus on fulfillhng higher level needs. If the hierarchical structure of the pyramid is considered in detail, the importance of technological evolution with appropriate tools could be determined. As we progress to hugher levels in the pyramid it could be seen how consumption increases. The hard to satisfying human nature drives him from what he has got, to what he has not or has not yet achieved. Passion for prey and survival tolerates violence The warriors have created and perfected instruments (armaments) for years and centuries. When neighbors are conquered, the distant countires become a next/new goal. Expanding their territories and conquesting the peoples, the economically developed countries - conquerors, draw resources and goods from conquered territories and increase their wealth. As a result, a society with distributed functions and migration of the Earth population from poorer to richer countries is created. The number of people in the world is increasing and most often in less developed countries and the basic needs of these people are growing. Economically, the society is oriented towards change and modernization. The purpose of change is to give hope for the future. Society has reached its inflexion point. The change is revolutionary. The revolution comes to satisfy the increased consumption and is based on one or a group of discoveries.

1.2. Characteristic features of industrial revolutions

As a beginning of the industrial revolution (IR) is considered:

- for the first IR - invention of the steam engine, as well as improvement of the weaving and spinning looms;
- for the second IR - invention of electricity, the internal combustion engine, the radio and the production line;
- for the third IR - the emergence of: electronics, robotics, computer chip (microprocessor), flexible automation, new materials, information and communication technologies, Internet.

Recently there is a change in economic reality and political authority [2,3,4], which is considered as the fourth industrial revolution. The "country and market behavior" is the main topic that was discussed at the World Economic Forum in Davos in 2016. There is growth of convergence between three spheres - the techno-sphere (the digital world and everything materially created by humans), the natural world (the eco-sphere) and the human sphere (socio-informational, everything not material created by people). A new point in the interconnection and interaction between man and machinery accures – people and robots are allowed to work together in one job (place), as well as different machines (robots) and people from different cultures (multicultural). The relationship between physical, digital and biological systems (bioengineering) is developing. This new stage of the economic development is based on: new technologies, AI robots, 3D printing (4D printing, for now is modestly mentioned, but in the near future it is expected to create structures, that can "grow in time", by analogy with biological ones), nanotechnologies (including nanorobots), big data processing (super intelligence), and AI-based automation. The speed with which the world is developing is unprecedented. The future comes soon and this imposes new demands on education and training of people [8,9] because of coexistence and action with robots with artificial intelligence.

2. Artificial intelligence and robots

The first obstacle encountered by technological revolutions is the need for qualified specialists for the new type of work. The new professions set different conditions from the previous ones. The intellectual human potential, allowing quick adaptation to the new, is still limited.

This gives the opportunity of biological spieces to survive (providing food and nutrition, surviving in a dynamically changing environment, and procreation through breeding), and people and human society, that in addition to the three activities for survival also needs spiritual life, to reach the current stage of development.

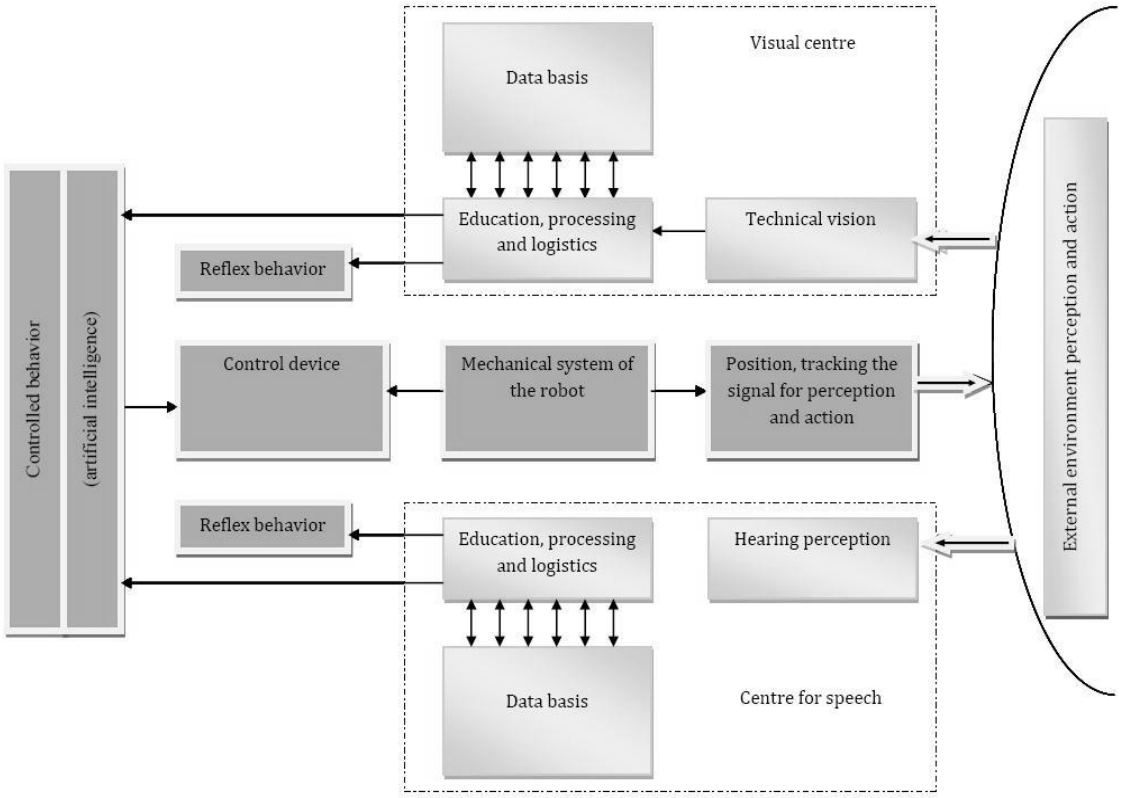

Figure 2. *Architecture of robot with artificial intelligence*

By analogy with the natural intelligence of humans and living creatures, inhabiting our planet, artificial intelligence (AI) is created due to increased abipities of computer technologies to solve complex tasks not only in the industry but also in the intangible sphere. The new digital environments are constructed by analogy to the biological world and are defined as artificial intelligence systems (AIS). In the architecture of the robots with AI (Figure 2), units for perception of the external environment must be included by analogy with the human brain and sensory organs, that allow solving tasks using global databases and knowledge (cloud technologies and super computers) [10]. This makes it possible for people and robots to work together (at the same workstation without collisions), which on the other hand reveals new opportunities in automation in the industry and beyond.

Robots nowadays are a product based on the latest physical theories, mechanical and physico-chemical technologies, theories and techniques for assessment of their own state and perception of external environment, technologies and techniques for collecting and processing of information and forming controlled behavior, including elements of AI. But in the near future, a qualitative change in intellectual capabilities is expected. New means for obtaining and transforming energy are expected. Such a product implies a need for knowledge in many scientific fields. Bionics and cybernetics are the theoretical basis of robotics. Biomechatronics (integration of biology, mechanics and electronics) is the future of robotics. This integration has appeared in the form of "Biologically Inspired Robots". For entrepreneurs, the dilemma "man or robot" will stand, as their qualities will get closer and in most cases the comparison will be in favor of the robots.

On one hand, human uses biological (zoological) analogies to improve the robots, and on the other hand man (and in the future, animals) has to be artificially “repaired” by implanting (including "added intelligence"). While, on the one hand, scientists (biologists and doctors) are progressing rapidly on the way of "humans robotisation", scientists-engineers are running along the same way striving to "humanize the robots". While the "artificial man," replacing human parts with artificial ones is creating, robotics aims to create a robot with artificial intelligence. The result of these efforts will occur at the so-called singularity point. According to the latest forecasts, a complete "technical singularity" will occur in 2045, i.e. the Turing test will be passed by computer, although according to some authors [7, 8], now there are partial cases of passing the test.

Thus, two tendencies are emerging for the future development of robotics: fear (robo-fear) and hope (robo-hope). What are the aspects of "human fears"? A lot of researchers believe that the three leading technologies for the 21st century are now unpredictable - robotics, genetic engineering and nano technologies.

They may be far more dangerous than previous technologies in the 20th century because a 20th-century bomb may explode "only once", but for example a reproductive robot may "get out of control" and to reproduce through multiplier technology "countless" copies of himself. The danger of the new technologies of the 21st century is that they are based exclusively on knowledge and do not require heavy equipment, rare raw materials and large capital investments. For this reason, both positive (beneficial) and negative (harmful and dangerous) technological products could be created by a smaller group of people. However, humans and, above all, the government elite of the states have to be prepared to avoid of harmful products and the negative consequences of the development of the leading technologies of the 21st century. Actually, as the bombs of the 20th-century have failed to destroy population, human society and the nature of the Earth, the negative consequences of new technologies in the 21st century could be possible also to be prevented. Since the fourth revolution concerns the highly developed countries (there are places on the Earth where they have not passed the first three stages), we must hope that they will not allow human society to be restarted from the beginning (from the primitive).

What are the optimistic forecasts?

• Robots have a great merit in the development of industrial technologies and technology in turn contribute to development and improvement the quality and ability of the robot;

• Robots gradually become indispensable and excellent assistents in the lifestyle of people, for example in the performance of precise and complex surgical operations (telecontrolable robot Da Vinci, cyber knife, etc.);

• Robotics provides modern adaptive and intelligent dentures, orthoses (mechanical compensator for physical disabilities), artificial limbs and artificial organs;

• It is possible to implant the robot-techical components in a person's body, which is related to the idea of turning people into "robot people", ie. in cyborgs;

• Robots help people and society to fight terrorism, crime and road accidentst;

• Robots create new jobs - directly and indirectly.

3.· What kind of changes could be expected in automation

Modern society is at a stage of immense automation, that undoubtedly increases the productivity and quality of human activity. Essential criteria for modern automation in industry is flexibility - the ability without reconstruction to produce new products. Productivity and versatility are the antithetic features. The highest productivity can be obtaine when the versatility is low (zero) and vice versa. The highest productivity comes from a fully-organized work environment that accurately determines all the elements involved in the manufacturing process (machines, basic and auxiliary equipment, robots, billets, details, assemblies and finished products) in space and time. The rhythm of production, if it is not the same or continuous, imposes intermediate storage in specialized facilities (intermediate warehouses). In order to shorten the transport times, the ordering is by the sequence of the technological process (less often by group technology). The efficiency of all devices for the highest productivity is when they are developed for the specific production, which is contrary to the flexibility.

The flexibility is imposed due to the individualization of consumption and, in particular, due to the constantly increasing requirements for the realization of the production on the market. The competitive environment requires offering new products with improved quality and competitive price. That is why an optimal and dynamic ratio between productivity and flexibility is needed and the change is in favor of flexibility.

The digitization of machinery and equipment, the new technologies, newly discovered materials and modern science dynamize industry and modern society. Metaphorically, the automation could be presented as an "orchestra with conductor artificial intelligence" to obtain a finite intelligent product. The robots in industry called "industrial" or "stationary robots" are used to fulfill their assigned functional task - to perform both technological (welding, painting, cutting, etc.) or ancillary (moving of blanks and finished parts, tools, equipment) operations. Therefore, the movements, actions and intellect that they have to possess are related to the respective task. They replace a man-worker with a robot-worker, and it is logical for these robots to be called "technological robots." The next higher level of robots, which will have a more developed AI, will cover a certain specialization like human engineers and will be a robots engineer-specialist. This class of specialized robots could be used not only in industry, but also in the automation of all human activities, which will ensure high quality and precisity of the execution processes. All this is a prerequisite for a new organization of automation - from a fully organized environment that requires a large number of auxiliary equipment, specific for each product to semi-organized one, where the production object (another type of product) occupies one of the possible stable positions and the position could be changed over the time.

There are still hypotheses about the spheres and / or segments where the fourth revolution will find a field of expression and to what extent the production will change. Bold is the forecast of Chief Executive Officer of AutoDesk, Carl Bass, "future factories will have only two employees: one man and one dog. The work of a man will be to feed the dog, and that of the dog - to prevent the person from touching the equipment. "

Of course, it should be haven in mind that AI (for now elements of AI are considered) can not fully cover the creative abilities of the human individual.

4. Education of people and robots in the new situation

4.1 A mix between traditional education and open education methods of people

Nowadays there are no boundaries for information due to the internet, so the need for education in general could be reconsidered and organized in different way. The physical boundaries are no longer barriers for education dues to the nationally and globally enlargement of networking services.

A modern approach in education is open education, which is one of the greatest challenges for future of learning. One of such type of education is Massive Open Online Courses (MOOCs). Except traditional course materials such as filmed lectures, readings etc., MOOCs provide interactive user forums among students, professors, and teaching assistants. The number of participants has doubled in 2015 from 16-18 million students to 35 million students across all MOOC providers.

The mix between MOOCs and traditional education methods in the future can provide higher education institutes and universities the opportunity to expand services to offer credentials using the experiences of the lecturers and teachers from all over the world.

4.2 Education of robots

Training of specialists in robotics is conducted nowadays. Here is payed attention of the need for another type of training for robots and people who train robots. Robots will receive hardware and basic knowledge from manufacturers, but they will not be enough for effective usage. Both people and robots have to go through specialized training to solve "class problems". At this stage, a bold prognosis is to talk about "schools and teachers for robots" but in the near future the need of such schools will grow up. The robots that could reproduce themselves will have very high basic capabilities of their "memory", which have to be "filled with knowledge", according to the needs of using the newly created product. By "image and likeness of its creator," the robots will have to resemble their "parent", but the knowledge about the surrounding environment and what is its job to do, the robots must acquire these knowledge through education and self-education. A rough analogy for this process can be made with modern computers. The manufacturer installes only the basic software and each user adds software and knowledge (accumulates knowledge) according to what they need to solve a certain set of tasks. If necessary, the hardware of the computer is upgraded, but the activity of the computer is mostly determined by the specificity of the software and by the knowledge of its full use, which so far remains only for the humans. It is often necessary to use the services of specialists when something unusual happens to particular computer, both with its software and hardware. The memory of robots in the near future, as well as of future computers, will probably be built on another basis (physical, biological, or a combination of both), and will be with grater abilities.

By analogy with education of people, robot training stations can once again be called "schools", and specially educated people will be called "teachers" or "roboteachers". It is not possible for the robots to adopt the other analogue referring to the conventional modern technique. The places where the technique is repaired are called "repair shops," and people who carry out this activity are called "masters" so far. The reproductive robots will need not only simple repairs but also for obtaining new knowledge that will not only be done by changing programs, but in ways that resemble human learning, such as MOOCs modules.

5. Conclusion

The development of human society is becoming more dynamic. The future comes soon and often people are unprepared in many directions. People have long been cohabiting with machinery and equipment, but in the near future **these** devices will have intellect and communication shoul be realized in an different way. This is large extend concerns communication between a human and a robot in jointly performing different activities within and without of the industry. That is why it is necessary to create united creative teams for project development, preparation of new type of specialists with higher and secondary qualification. Legislative changes will be needed to avoid conflicting situations during design and usage of innovations to solve the problems for the benefit of man and human society.

6. References

[1] A.H. Maslow, A Theory of Human Motivation, Psychological Review 50(4) (1943):370-96.

[2] Клаус Шваб, Четвъртата индустриална революция, Хермес, 2017.

[3] Хр. Проданов, Щрихи от политическата икономия на четвъртата индустриална революция, Икономически и социални алтернативи, брой 4, 2016.

[4] Четвърта Технологична революция – Роботи & Хора…..или Роботи vs. Хора (продължение), SIS investment intermediary, 03/10/2016

[5] Tim Urban The AI Revolution: The Road to Superintelligence, January 22, 2015.

[6] https://www.class-central.com/report/moocs-2015-stats/

[7] Kevin Kelly, Out of Control. The new biology of Machines, Social Systems, and the Economic World. 1994

[8] Dominik B., O. Boesl, Bernd Liepert*, 4 Robotic Revolutions - Proposing a holistic phase model describing future disruptions in the evolution of robotics and automation and the rise of a new Generation 'R' of Robotic Natives, IEEE/RSJ Intern.l Conf. on Intelligent Robots and Systems (IROS) Daejeon Convention Center October 9-14, 2016, Daejeon, Korea

[9] The Robotics Revolution: The Next Great Leap in ... – CIRCABC https://circabc.europa.eu/.../BCG_The_Robotics_Revolution_Sep_2015_tcm80-197133....Sep 3, 2015

[10] What role will education play in the Fourth Industrial Revolution? https://www.weforum.org/.../what-is-the-fourth-industrial-revo...

[11] Pavlova, G., V. Pavlov, R. Trifonov. Technical Parameters Integration of Mechanical and Computer Systems in Robotics; Proc. of VII International Scientific Conference Computer Science'2015, 8-10 September 2015, Duras, Albania, pp. 274-279, ISBN: 978-619-167-177-9

STRENGTHENING OF SURFACE LAYERS OF STEELS AND ALLOYS BY BORIDE COATINGS FORMED UNDER THE CONDITIONS OF AN EXTERNAL MAGNETIC FIELD

Prof. Dr. Chernega S., Grinenko E., Krasovskiy M.
National Technical University of Ukraine "Igor Sikorsky Kiev Polytechnic Institute", 03056, Ukraine, Kiev, Polytechnique st., Bldg. 9, e-mail: smchernega@ukr.net;

Abstract: *It was dedicated to solution of scientific and technical problem to increase the level of physical and mechanical and operational properties of the surface of steels by forming strengthened layers diffusion boriding and complex saturation boron and copper in a magnetic field.*

KEYWORDS: *BORON, BORIDING, BORON LAYER, COPPER, STRUCTURE, DIFFUSION, MICROSTRUCTURE, MICROHARDNESS, EXTERNAL MAGNETIC FIELD.*

INTRODUCTION

Diffusive multicomponent boriding quite energy consuming process, therefore to reduce energy consumption necessary to use methods for intensification the process saturation. One of these methods is the application of an external magnetic field (EMF), the so-called magnetic thermo chemical treatment [1-3].

To solve this problem, we used a complex diffusive saturation of the surface layer of carbon steel boron or boron and copper at simultaneous action of EMF.

The aim of this work was to study diffusive boride coatings and coatings obtained after saturation with boron and copper on carbon steel,

MATERIALS AND EXPERIMENT

The paper presents the results of the study of the influence of external magnetic field (EMF) on the structure, phase and chemical composition, microhardness, growth kinetics, roughness, crack resistance and wear resistance of boride coatings obtained with complex boron or boron and copper saturation.

RESULTS AND DISCUSSION

It was found that the use of EMF in diffusion saturated for 2 hours allows to increase the thickness of the diffusion boride layer in 1,5-2 times, compared with the coatings obtained without the action of EMF with a saturation time of 2 hours. So for 2 hours of diffusion saturation with EMF on medium carbon steel the thickness of the coating reached up to 200 μm (Fig. 1, c), compared with the boron layers obtained without

EMF - up to 110 microns (Fig. 1, a). It has been shown that the use of EMF can reduce the duration of saturation of steels and alloys by 2 times. So the thickness of the diffusion boride layer on medium carbon steel without the action of EMF grows to 160 μm for 4 hours of diffusion saturation.

The same pattern is observed for boride coatings obtained with complex boron and copper saturation. So with a whack for a while

For 4 hours without EMF, coatings with a thickness of 165 - 200 μm are formed (Fig. 1, r), whereas, when diminished under the action of EMF, 2 hours of diffusion saturation, borate phases grow in the thickness 180 – 225 μm. Investigation of the microhardness of the boride phases after boring at the simultaneous action of EMF showed that the microhardness of the phase of FeB is 19-20 GPa, and the Fe_2B phase is 17 - 18 GPa, without the action of a magnetic field, FeB - 17 - 18 GPa, Fe_2B - 15-16 GPa . At complex saturation with boron and copper using EMF, we obtain boride layers with a microhardness - for phase (Fe, Cu) B - 17 - 18 GPa, and for phase (Fe, Cu) 2B - 15-16 GPa, without magnetic field action (Fe , Cu) B - 15.5 - 16.5 GPa, and for the phase (Fe, Cu) 2B - 13.5 - 14.5 GPa. Thus, there is an increase in the microhardness of FeB, Fe_2B and (Fe, Cu) B, (Fe, Cu) 2B phases at 1.5-2 GPa, obtained under magnetic field conditions, which is probably due to the shredding of the block structure boride grains up to 38.3 nm compared to 66.1 nm for the FeB phase obtained without the action of EMF. At complex saturation with boron and copper, we observe a decrease in the microhardness of boride layers compared to boring.

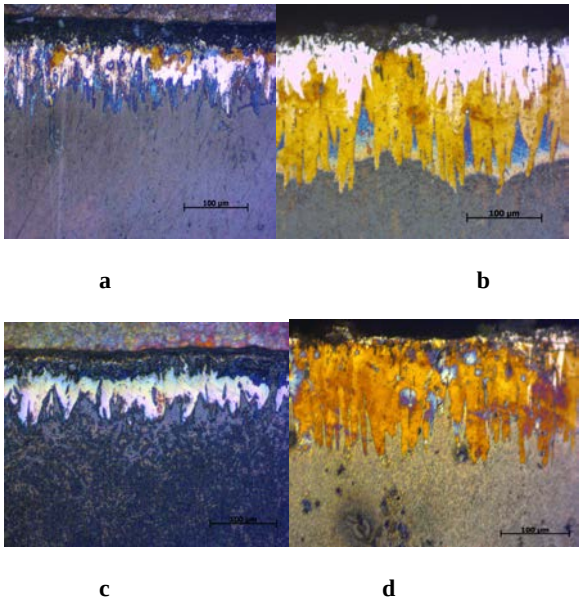

Fig.1 Microstructures of complex boride coatings on steel 45 obtained in different physical - chemical conditions: a – boriding without action EMF, the duration of saturation 2 hours, x200;b – boriding in EMF, the duration of saturation 2 hours, x200; c – complex saturation with boron and copper without action EMF, the duration of saturation 2 hours, x200; d – complex saturation with boron and copper with simultaneous action EMF, the duration of saturation 2 hours, x200, (thermal etching)

The study of the phase composition of boride coatings obtained in different physical and chemical conditions was carried out. It was shown that in the case of boronization without EMF in the surface layer of boride coating to 15 - 20 μm, the FeB phase (Fig. 2, a), and with complex boron and copper saturation without the action of EMF - the FeB, Fe2B, and Cu phases (Fig. 2, b).

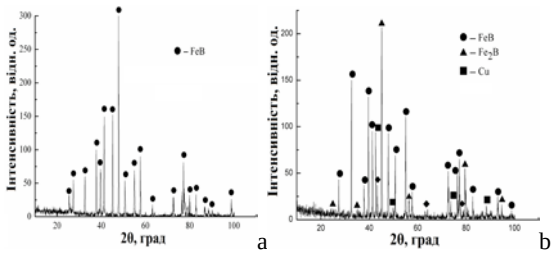

Fig.2. X-ray diffraction picture taken from the surface of the carbon steel 45 *with boride coatings obtained without action EMF after: a – boriding, the duration of saturation 2 hours; b – complex saturation with boron and copper, the duration of saturation 2 hours complex saturation with boron and copper without action EMF, the duration of saturation 2 hours*

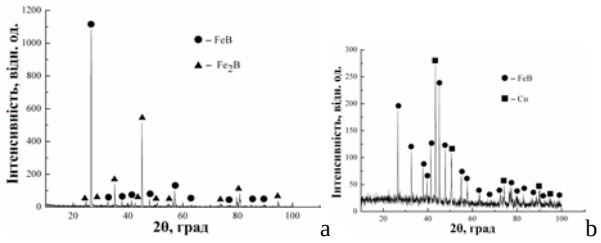

Fig.3. X-ray diffraction picture taken from the surface of the carbon steel 45 *with boride coatings obtained after: a – boriding at the simultaneous action EMF, the duration of saturation 2 hours; b – complex saturation with boron and copper with simultaneous action EMF, the duration of saturation 2 hours. Diffraction peaks Cu correspond crystallographic planes: (111) (200) (220) (311) (222)*

The diffractograms (*Fig.2*, *Fig.3*) were taken from the surface of steel 45 with boride coatings obtained after boriding (a), complex saturation with boron and copper (b) without the action of EMF and boriding (c), dimming (d) under the action of EMF.

When applying EMF in boride layers, the decrease in the volume of the phase of FeB and on the diffractograms of the surface layers of the boride coatings, and the presence of the FeB and Fe2B phases is observed in the diffractograms (Fig. 3, a). After complex saturation with boron and copper, under the action of EMF, the phases of FeB and Cu (Fig. 3, b) are fixed. An overlay of EMF leads to a redistribution of the quantitative ratio of boride phases in the surface layers, changes in the periods of the crystal lattice, and a decrease in the volume of the elementary lattice of the phase of FeB. Local microscopic analysis has established a discrete distribution of copper in a surface layer of FeB phase up to 20 microns of coating. Copper impregnations can accumulate in the pores of boride coatings and surround their walls (Fig. 4, a, Table 1). An overlay of a magnetic field at a complex saturation with boron and copper leads to an increase in the diffusion coefficient of copper in the surface layers of boride coatings from 7.8 · 10-11 cm^2 / s to 4.1 · 10-10 cm^2 / s, which leads to a faster penetration of copper in surface layers of the phase of FeB. Therefore, copper with this method of saturation penetrates to a depth of 30 micrometer (Fig. 4, b, Table 2), compared with 20 micrometer in the traditional complex saturation with boron and copper without EMF.

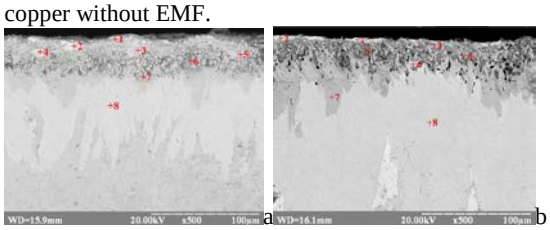

Fig. 4. Structures of a cross-section with a diffusion boride coating obtained with complex boron and copper saturation without the action of EMF (a) and under the conditions of the action of EMF (b) on steel 20 (chemical analysis was determined at points +1,+2, +3, +4, +5, +6, +7,).

Table 1*.The chemical composition of the diffusion layer obtained after complex saturation with boron and copper on steel 20 without the use of EMF*

Elements	Position						
	+ 1	+ 2	+ 3	+ 4	+ 5	+ 6	+ 7
	мас. %						
Fe (K)	2,38± 0,06	2,69± 0,07	76,66± 1,50	95,37± 1,65	57,75± 1,09	93,42± 1,71	100± 2,15
Cu (K)	97,62± 1,50	97,31± 1,80	23,34± 0,70	4,63± 0,31	42,25± 1,01	6,58± 0,29	0,00

Table 2.*The chemical composition of the diffusion layer obtained after the complex saturation of boron and copper on steel 20 at the simultaneous action of EMF*

Elements	Positions							
	+ 1	+ 2	+ 3	+ 4	+ 5	+ 6	+ 7	+ 8
	мас. %							
Fe (K)	1,33± 0,05	22,09± 0,74	1,40± 0,05	66,29± 2,59	77,44± 2,32	82,76± 2,59	83,28± 2,08	100± 2,60
Cu (K	98,67± 2,53	77,91± 2,19	98,60± 2,47	33,71± 1,34	22,56± 0,87	17,24± 1,59	16,72± 0,53	0,00

The research of roughness of complex boride layers obtained in different physical and chemical conditions has shown that the lowest level of roughness Ra = 0,0553 is achieved at the complex boron and copper saturation using EMF, compared with Ra = 0,0650 with dimming without EMF. When pounding in EMF Ra = 0,0855, compared with Ra = 0,0961 in the absence of EMF.

CONCLUSIONS

The investigation of the crack resistance of diffusion boride coatings obtained in various physical and chemical conditions was carried out. It has been established that the highest cracking strength is achieved in the boride phases obtained in powder environments with the use of copper powder when applied to EMF, and on steel 20, respectively, is 2.23 MPa • $m^{0.5}$, with the shearing stress of 345 MPa. Then, when scattering without the action of EMF, the crack resistance of the steel is 20 - 1.24 MPa • $m^{0.5}$, and the stresses of shearing - 181 MPa. An increase in the magnitude of the stresses in the complex bromide layers is due to the formation of phases of greater viscosity, for which the crack resistance K1C in 1,4 - 1,7 times higher than the output boridephase (FeB, Fe2B).

The study of wear resistance of boride coatings obtained in various physical and chemical conditions was conducted. It has been established that diffusion boride coatings obtained with the use of an external magnetic field have higher tribotechnical characteristics. Thus, the average linear wear in the boride coatings obtained in the EMF is reduced by 2.4 times, and the coefficient of friction is 0.63 versus 0.66. In the case of the production of gloomy coatings obtained in EMF, the average linear deterioration is reduced by 1.8 times, the coefficient of friction decreases to 0.60 compared with 0.64 for gloomy coatings without EMF.

REFERENCES

[1] Chernega S. Structure and properties of surface layers metals on the basis of high solid boride obtained in conditions of an external magnetic field / S. Chernega, I. Poliakov, M. Krasovskiy. // Machines. Technologies. Materials. – Sofia, Bulgaria. – 2015. – No.12. – P. 52 – 55.

[2] S. Chernega, I. Poliakov, M. Krasovskiy. Increasing wear resistance of machines details from carbon and Cr–Mn–N steels of the complex boride coating// Nonequilibrium phase transformations. – Sofia, Bulgaria. – 2016. – No.3. – P. 31 – 34. – ISSN 2367 – 749X.

[3] Chernega S. I. Poliakov, C. Grinenko, M. Krasovskiy. Increase wear resistance hard alloys T15K6 boride coatings // XII International congress «Machines, technologies, materials 2015». – Bulgaria, Varna, 16 – 19 September 2015. – Vol.II. – P. 109 – 111.

COLLECTORS SYSTEM - SOLAR WATER HEATING

M.Sc. Radeva T. PhD.[1]
Faculty of Electrical Power Engineering – Technical University of Sofia, Bulgaria
tania_rr@abv.bg

Abstract: *The scopes of this paper are the transformation of solar radiation into heat and transfer that heat to water. Using a solar collector, there is a constant provision of hot water and at the same time helps to protect the environment. It is necessary to develop and implement environmentally friendly and highly efficient solutions for heating and domestic hot water, which will make a significant contribution to nature conservation and improvement of living conditions. The system under consideration gives us a good example of the benefits of using solar energy.*

Keywords: SOLAR COLLECTORS, ENERGY EFFICIENCY, DOMESTIC HOT WATER

1. Въведение

Слънчевите колектори събират и приемат топлинната енергия на слънцето, като я използват за отопление и топла вода, която се съхранява в специален водосъдържател-бойлер. Колекторите придобиват все по-голяма популярност и намират все по-широко приложение в много сгради и домакинства. С помощта на слънчев колектор се разполага постоянно с гореща вода и едновременно се спомага за опазването на околната среда. Значително се намаляват разходите за загряване на гореща вода в сравнение с конвенционалния тип бойлер. Необходимо е разработване и прилагане на екологични и високоефективни решения за отопление и битова гореща вода, които ще допринесат в значителна степен за опазването на природата и подобряване условията на живот.

Слънчевите колектори са ефективен и евтин начин за загряване на водата използвана за нуждите на бита, селското стопанство дори малки промишлени предприятия. Домакинствата имат почти постоянна нужда от топла вода за задоволяване на различни нужди. Слънчевите колектори обикновено се използват в съчетание с традиционен бойлер, тъй, като метеорологичните условия се отразяват на ефикасността на производство на топла вода. При избора на такава система, традиционният бойлер допълва слънчевия нагревател. Добавянето на слънчеви колектори с водна отоплителна риза може да намали сметките за ток и съответните емисии на въглероден диоксид на половина, а понякога дори и с повече[1].

Наред с ултрамодерните технологии, има и простички решения, носещи изключителни ползи на обществото и околната среда в световен мащаб. Именно такива са слънчевите системи за добив на гореща вода. Всеки ден, тази технология пести милиони евро и тонове въглеродни емисии на човечеството. Европейските политики за чиста енергия и енергийна сигурност, превърнаха Стария континент в лидер в областта на ВЕИ технологиите, в частност слънчевата термия. В последното десетилетие водещите страни от ЕС създадоха мощни инструменти в подкрепа на зелените технологии и това мотивира милиони домакинства и бизнеси да инвестират в тези решения [2].

Всяка една система е изградена от допълващи се и работещи в синхрон елементи. Така е и при термичните системи за топла вода, които са съставени от:

Слънчев/и колектор/и за топла вода;

Управление, контролиращо и управляващо работата на инсталацията с дигитален дисплей за визуализиране на функциите и възможност за индивидуални настройки;

Слънчева помпена станция, състояща се от циркулационна помпа, спирателни кранове, термометър, дебитомер, манометър, предпазен клапан и др.

Тръбно трасе, пренасящо топлина – колектор топлообменик на бойлер – колектор, изградено, най-често, от медни или гъвкави неръждаеми тръби.

Бойлер с един или два топлообменника, т.н. серпентини.

Принцип на работа на слънчевите термични системи:

Слънчевите системи за топла вода оползотворяват слънчевата лъчиста енергия (т.н. радиация), преобразувайки я в топлинна енергия за битови, обществени и бизнес нужди, най-често за санитарно-хигиенни нужди: миене, къпане, нискотемпературно отопление, но понякога и за загряване на вода за обезпечаване промишлени и селскостопански процеси. Основен принцип при функционирането на слънчевите термични системи е цикличността на извършвания топлинния пренос. Този процес стартира при отчетена определена разлика (индивидуално зададена, най-често 5-7º С) между температурата на водата в бойлера и флуида в колектора. Например, ако температурата на слънчевия колектор е по-висока с 5ºС, това се отчита от електронното управление, което подава сигнал към помпената станция да стартира охлаждане на слънчевия колектор и паралелно загряване на топлообменника, чрез циркулиране на топлоносеща течност от колектора към бойлера. Цикълът продължава до изравняване на двете температури. Температури се отчитат, чрез термодатчици, монтирани в специални "гнезда" в тези два компонента. Самата слънчева система е защитена от прегряване, тъй като стандартно електрониката прекъсва топлинния пренос при постигане температура на бойлера 60-70º С. При тази система, налягането в тръбната мрежа се поема от разширителен съд с точно оразмерен индивидуален обем, който поема разширението на топлоносещата течност до идването на нощта, когато системата се самоохлажда.

Оптимално място за монтаж на слънчевите колектори е покривът на съответната сграда или площадка върху носеща метална конструкция. Важно условие е колекторът да се постави на открито и незасенчено място. Друго добро решение за монтаж на слънчевите колектори е интегрирането им в конструкции – покрив, стена, вкл. като ограждащ елемент, което ги превръща в елемент от архитектурата на дадената сграда. За тази цел са разработени специални колектори, които функционират дори при монтаж на 90 или 180º.

Препоръчително е колекторът да се ориентира на юг. В случай че е невъзможно да се спази това условие, е допустимо колекторът да се ориентира на югоизток или югозапад в отклконение от няколко градуса. Оптималният наклон на слънчевите колектори е в диапазона от 30 до 60°, като за оптимален се счита наклонът от 45 °. Счита се, че при тази ориентация и наклон, сумарната денонощна трансформация на енергия има максимум.Приложение и възвръщаемост на инвестицията.[2]

Слънчевите системи за топла вода са приложими, както в жилища и вили, така и в:туристически комплекси: хотели, къщи за гости, спа центрове, комплекси с басейн;обществени сгради - болници, училища, детски градини, др.; търговски центрове;индустриални предприятия;селскостопански обекти – ферми, оранжерии, сушилни.[2]

2. Обследване на хотелски комплекс

При заснемането на сградата е установено, че не е положена топлоизолация върху водопроводните тръби за гореща вода за битови нужди. Топлоизолация по тръбите няма и в техническите помещения още на изхода от бойлерите. В котелното помещение изолацията е стара и изгоряла, на места дори липсва. Това е предпоставка за големи загуби на енергия още на изхода, както и по цялата тръбна мрежа.

Предложена енергоспестяваща мярка 1:

Мярката включва поставяне на топлоизолация от микропореста гума с дебелина 13mm на всички тръбни разводки за пренос на гореща вода в сградата и на топлоизолация от микропореста гума с дебелина 19mm, обшиване с поцинкована ламарина на тръбните разводки разположени на открито.

Енергоспестяваща мярка 2:

Изграждане на инсталация за подгряване на вода за битови нужди оползотворяваща слънчева енергия

Съществуващо положение

В сградата е изградена система за централно снабдяване с гореща вода. За всеки корпус е изградено самостоятелно бойлерно помещение в което са разположени водосъдържатели произведени от Термотехника „ЕООД“ през 2001г. с електрически нагреватели, както следва:

ЗОНА 1 – КОРПУС СРЕДНА ГОРА 1;

В бойлерното са монтирани два бойлера, всеки с вместимост 4m3 и всеки е окомплектован с ел. нагревател 60kW.

ЗОНА 2 – КОРПУС СРЕДНА ГОРА 2

В бойлерното са монтирани три бойлера, всеки с вместимост 4m3 и всеки е окомплектован с ел. нагревател 60kW.

ЗОНА 5 – КОРПУС ГАЛЕОН

В бойлерното са монтирани четири бойлера, всеки със вместимост 4m3 и всеки е окомплектован с ел. нагревател 60kW.

ЗОНА 3 и ЗОНА 4 – ЦЕНТРАЛЕН КОРПУС

За захранване с гореща вода за битови нужди на Централен корпус, системата е подвързана директно към скоростен топлообменник „вода-вода“.

Основен източник на топлина за подгряване на водата за битови нужди за всички корпуси е водогреен газов котел Viessmann Vitoplex 200 с мощност 350-380kW работещ на пропан-бутан, монтиран в котелно помещение ситуирано до Централен корпус. Топлоносителят, получен от газовия котел посредством скоростен топлообменник „вода-вода“, подгрява водата за битови нужди. Подгрятата вода постъпва във водосъдържателите в бойлерните помещения на отделните корпуси. Електро - нагревателите към бойлерите доподгряват водата при недостиг на мощност или в аварийни ситуации.

Така изградената схема за загряване на вода за битови нужди е предпоставка за загуби още на изхода от топлоизточника, т.к. топлоносителя не постъпва директно в обема който трябва да бъде загрят (не са използвани бойлери със серпентина), а загуби са налице още при скоростния топлообменник.

Схемата предполага и по често подгряване на водата посредством инсталираните електро нагреватели при повишена консумация.

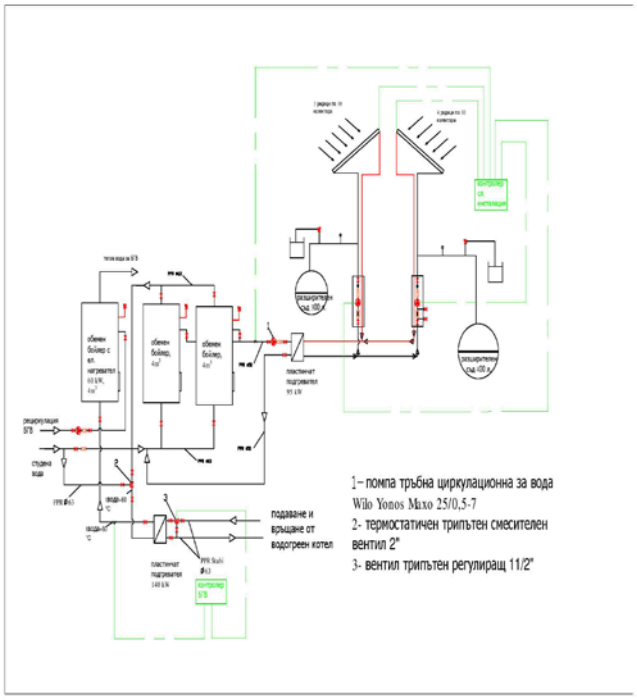

Fig. 1 *Разположение на колекторите и подгряване на водата Средна Гора 1.*

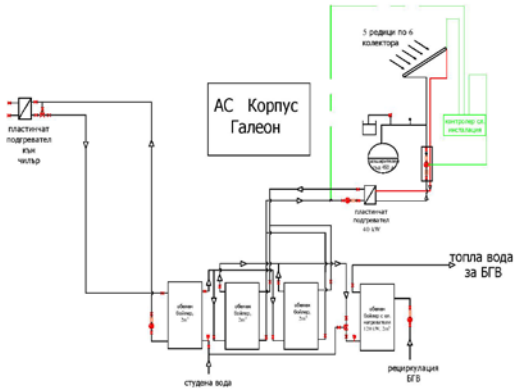

Fig. 2 *Разположение на колекторите и подгряване на водата Галеон.*

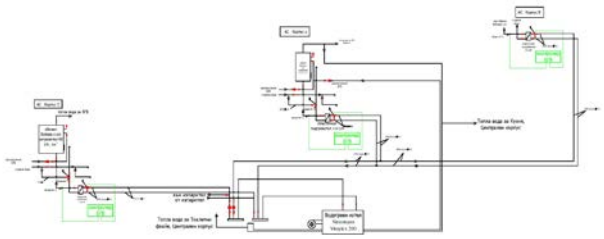

Фиг. 3 *Схема на котелно.*

3. Предложена мярка

Използваният модел е в съответствие с "Ръководство за анализ на разходите и ползите от инвестиционни проекти", анализите на финансовите показатели и паричните потоци на проекта са направени със специализирания софтуер "ENSI финансови изчисления". Този софтуер е приет като легитимен от АУЕР и за изготвяне на финансовата част на енергийните одити.

Обект на анализ в тази част на одита са техническите и екологичните рискове, които могат да възникват вследствие внедряване на енергоспестяващите мерки, предвидени в одита.

- Технически рискове

В енергоспестяващите мерки е избрана изпитана и ефективна технология за загряване на гореща вода за битови нужди на хотелския комплекс. Вероятността за неправилен избор на оборудване и проблеми при монтажа е минимална.

Икономически и търговски рискове

Извършените технически проучвания, заснемането на обекта и анализиране на техническата изпълнимост на мерките, както и подробните количествено-стойностни сметки от енергийният одит, са предпоставка за минимален риск от превишаване на разходите над предвидените. Заложените цени са пазарни (определени на база взети оферти от доставчици и изпълнителски фирми) и няма вероятност за повишаването им за периода на изпълнение на проекта.

Предвидените срокове за доставка са на база утвърдената практика. Рискът забавянето на доставките да доведе до цялостно забавяне на изпълнението на инвестиционния проект е малък.

- Рискове за околната среда

Предвидените енергоспестяващи мерки не противоречат на действащата нормативна уредба за опазване на околната среда. Изпълнението им води до намаление на емисиите на CO2.

Оборудването е от модерен тип и не представлява опасност за околната среда.

- Административни и управленски рискове.

Съгласно информацията за предишни ремонти, преустройства и строително-монтажни работи в хотела може да се заключи, че ръководството на хотела е в състояние да изпълни проекта.

4. Изводи

Изградена е инсталация за подгряване на вода за битови нужди оползотворяваща слънчева енергия в хотелен комплекс „Еврика“.

След внедряването на такава система при правилна поддръжка и експлоатация се отчитат спестявания от водогреен газов котел - пропан-бутан 45% и електрическа енергия 8%, което показва намаляването на разходи и положителната страна от внедряването на подобни интегрирани системи.

5. Литература

[1]. Петкова П., „Използване на слънчевата енергия за подгряване на вода“, Брой 08-2014, ka6tata.com

[2]. Петров П., „Възвращаемост на инвестицията – слънчеви колектори“, Брой 08-2014, ka6tata.com

[3]. Information Engineering

KEY COMPONENTS OF THE ARCHITECTURE OF CYBER-PHYSICAL MANUFACTURING SYSTEMS

M.Sc. Juhás P. [1], M.Sc. Molnár K. [1]
Merchant, Inc., the Slovak Republic [1]
peter.juhas@merchant.sk, karol.molnar@merchant.sk

Abstract: *The future of industry contains many challenges. Necessity is to increase the degree of digitization and achieve a new level of productivity. The rise emergence of modern production lines operating in accordance with the concept of Industry 4.0 foresees the creation and implementation of new technologies and the emergence of autonomous production units capable of independent existence within the manufacturing process. They must closely communicate with other elements and cooperate with all the elements in the production process. In this article we describe architecture of theoretical cyber-physical system and give components and technologies necessary to implement a modern enterprise designed according to Industry 4.0 standards.*

Keywords: INDUSTRY 4.0, PROCESS, MANUFACTURE, STANDARDS, ARCHITECTURE

1. Introduction

The result of implementing new technologies and new ways of communicating between industrial facilities is the fact that the boundaries between the real environment and the virtual world are being wiped out. New technologies in industry are well known as Industry 4.0 concept or Cyber-physical production systems. The main target of successful application of the concept of Industry 4.0 into practice is the realization of intelligent, interconnected production systems that can dynamically respond to changing conditions during production and are able to vary their physical and logical structure during the work cycle.

Cyber-physical systems are represented by a set of electronic and mechanical components linked to each other by means of sensors and networks that provide intelligent platform for flow and analysis of data (6).

The complexity of these production systems is significant and essential part of modern equipment in addition to physical facilities and operations are software tools to enable research in integration of information and management systems and solving problems in the field of acquiring knowledge (data mining), simulation of production and service processes and logistics systems with the possibility of their optimization, planning and management of production (ERP systems) and business intelligence tools (BI). Using these technologies, it is possible to create a combination of virtualized production environments to physical - Digital Twins (DT).

2. Architecture of Cyber-Physical systems

Due to the complexity of the industries, design of the structure of intelligent factory must meet a number of criteria and consider the applicability in different sectors and different types of manufacturing processes. There are a number of works dealing with issues of structure and standardization in the area of cyber-physical production systems. The work of the authors (12) describes a method of realization through a five-level architecture, referred to as 5C. The proposed model is based on a standardized model that extends with new features. The core of work of authors in article (6) describe the implementation of intelligent manufacturing systems in the Industry 4.0, and define the modern elements necessary for the existence of such production units. Several different approaches to managing and defining the structure of the CPS is described in article (10), while there are analyzed possibilities of centralized and decentralized management of production processes. In the author's work (1), a categorical and hierarchical framework is proposed in which the Industry 4.0 concept is described as achievable by the continuous and incremental development process, the main parameters of which are automation and intelligence: the intelligent manufacturing system is highly automated at the manufacturing company level and is self-repairing, self-optimizing and self-configuring.

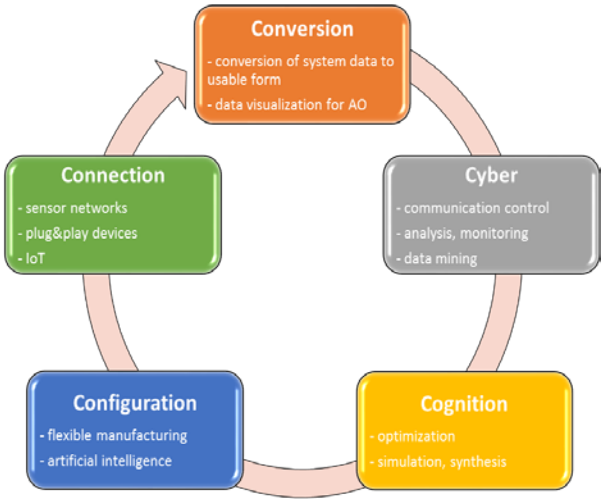

Fig. 1 *Basic parts of CPS architecture 5C*

It is clear that the autonomous intelligent manufacturing subsystems and the relationships between them are too complicated to manage human operators in real time. The solution is to control production process using an intelligent software with artificial intelligence using neural networks technology.

Decisions relevant to management in modern factories will be obtained through a real-time simulation that includes all the states, processes and components of the real world. The technology of digital twins (DT), virtualization and simulation of processes in a virtual environment is an important aspect in the management of production systems. By using DT, it is possible to predict the machine settings and parameters in a simulation environment in the virtual world, whereby switching to a different product (any change in the production process) allows the devices to be set up to configuration based on simulations in the virtual world. This approach significantly reduces machine setup times, improves quality and prevents malfunctions and outages (11).

In the pyramid model (Fig. 2) is assumed architecture of the manufacturing enterprises realized in accordance with the Industry 4.0 concept represented by layers, where the lower level consists of intelligent sensors and regulators interconnected by IoT technology (12). The process of obtaining accurate and reliable data from devices and their components is the first step in the implementation of cyber-physical system. Data can be directly measured by sensors in the production process or obtained from management or enterprise production systems (ERP, MES).

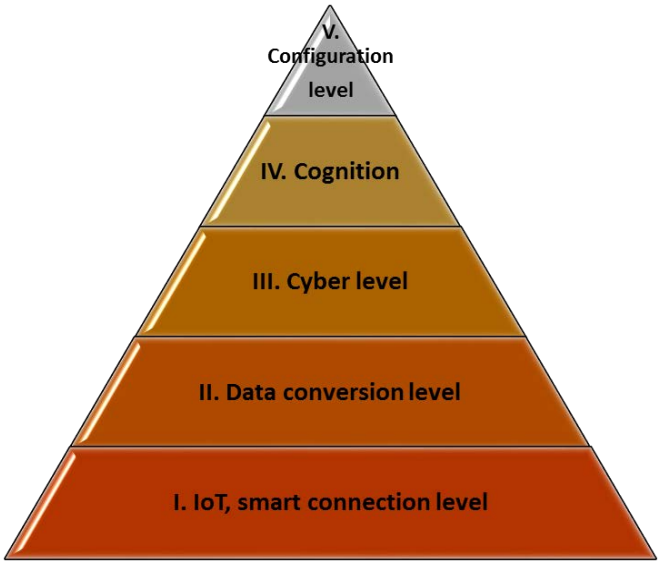

Fig. 2 *CPS – implementation architecture (12)*

Because these are data representing a number of variables of different kinds (time dependent / independent), it is important to choose a suitable method of interpreting the measured data and to select the appropriate form of recording. As a result of the ever increasing use of sensors and machines in the network, it results in the continuous generation of a large data volume (Big Data) (3). For processing of such amount of data are used special techniques and technologies and proper processing and evaluation of these data is very important for softness and quality simulation model twin digital production process.

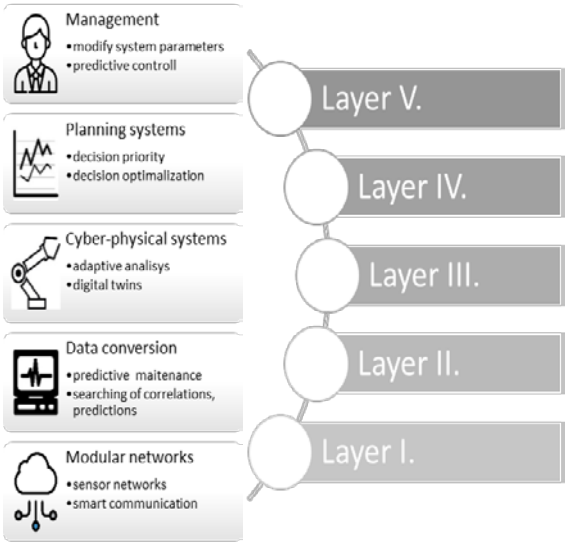

Fig. 3 *Techniques associated to layers in 5C pyramid model*

3. Technology platforms in Cyber-Physical systems

Based on the above information, we can summarize the components and technologies necessary for the implementation of a modern enterprise conceived in accordance with Industry 4.0 and exploiting the potential offered by the proposed technology (6). The future of flexible production and Cyber-physical manufacturing is the use of all modern approaches, communication between all components and the autonomy and intelligence of all elements in production.

- Advanced (autonomous) robotized production lines
  - modern automated and robotized production lines maximize efficiency, modern technology, accuracy and speed of production are an essential element in the implementation of CPS
- Autonomous supervisory/service mobile units (drones with camera system or handlers to carry light objects)
  - drones are easy to use as independent mobile supervisory units (equipped with a camera) or as highly mobile transport units with the appropriate equipment for the transfer of objects
- Industrial 3D printing
  - technology of 3-dimensional printing (additive manufacturing) is able to provide a high degree of efficiency and variability in the production of a wide range of products. By creating 3D objects based on data from materials such as plastic or metal, it is possible to create complex, easily customizable products whose design is impossible to carry out with classic production techniques.
- Autonomous traffic units (autonomous carts and manipulators)
  - ground handlers and vehicles for transporting heavy loads are forming a connection between the individual modules of CPS
- Intelligent management and control system
  - central management and control of all production processes and units must be implemented in such a way as to eliminate the possible errors in the management of complex and time-dependent production processes. This presupposes the exclusion of classical control centers with human service. Manufacturing and manufacturing processes should be managed by an appropriate intelligence management system with an ERP and CRM connection management interface.
- Distributed communication systems – sensor networks + IoT
  - all objects in the production process have to communicate with the control system wirelessly. Together with the sensor system they create an information data network. Based on these data, the central management system is able to analyze production procedures and processes and optimize them to achieve even greater production efficiency.
- Intelligent final inspection - 3D scanner
  - an intelligent control system that accurately identifies the parameters of complex elements and products through a set of cameras camera and 3D scanner.
- Augmented operator
  - in the case of excessively complicated manufacturing processes, the physical capabilities of human staff need to be improved using an additional technical solutions
- Energy-efficient production
  - a modern manufacturing enterprise must use renewable energy sources such as solar panels, energy passive buildings, recycling of raw materials and the like.

4. Conclusion

Modern manufacturing facilities of future are represented by highly automated production lines including sophisticated management and control computing systems. However, the manufacturing process is still dependent on the operators. The future lies in a combination of increasing device autonomy, applying new technologies and improving operators' capabilities, plus increasing the interoperability of all elements.

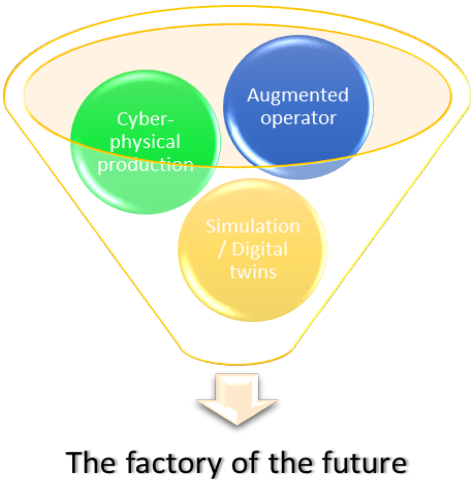

Fig. 4 *New technology in future factories*

In addition, it is necessary to improve interaction in the man-machine context, not only by enhancing and introducing smart technology on the machine side but also by the human abilities, possibly using other electronic specialized circuits implemented directly at the operator. Together with virtualization technologies (predictive simulation), the aforementioned possibilities offer interesting perspectives on the management of production processes in the upcoming period.

Acknowledgement

This article was created with the support of the Ministry of Education, Science, Research and Sport of the Slovak Republic within the Research and Development Operational Program for the project "Industrial research technology autonomic production cycle in accordance with the concept of Industry 4.0", 2015-10869/19439:15AA, co-funded by the European Regional Development Fund.

References

(1.) Longoa, F., Nicolettib , L. , Padovanoa, A. : „Smart operators in industry 4.0: A human-centered approach to enhance operators' capabilities and competencies within the new smart factory context" in Computers & Industrial Engineering, Volume 113, November 2017, Pages 144-159, ISSN: 0360-8352

(2.) Bagheri, B., Yang, S., Hung-An, K., Lee, J. : „Cyber-physical Systems Architecture for Self-Aware Machines in Industry 4.0 Environment" in IFAC-PapersOnLine 19th IFAC World Congress. Volume 48, Issue 3, 2015, Pages 1622-1627 ISSN: 2405-8963

(3.) Schroeder, G. , Steinmetz, Ch., Pereira, E.C., Espindola, D.: „Digital Twin Data Modeling with AutomationML and a Communication Methodology for Data Exchange" in IFAC-PapersOnLine.Volume 49, Issue 30, 2016, Pages 12-17 ISSN: 2405-8963

(4.) Weyer, S., Meyer., T., Ohmer, M., Gorecky., D., Zühlke, D.: „Future Modeling and Simulation of CPS-based Factories: an Example from the Automotive Industry" in IFAC-PapersOnLine, Volume 49, Issue 31, 2016, Pages 97-102. ISSN: 2405-8963

(5.) Rosen, R., Wichert, G., Lo, G., Bettenhausen, K.D.: „About The Importance of Autonomy and Digital Twins for the Future of Manufacturing IFAC-PapersOnLine, Volume 48. Issue 3, 2015, Pages 567-572

(6.) Yeo, N.C.Y., Pepin, H., Yang, S.S.: „Revolutionizing Technology Adoption for the Remanufacturing Industry" inProcedia CIRP, Volume 61. 2017. Pages 17-21, ISSN: 2212-8271

(7.) Cai, Y., Starly, B., Cohen, P., Lee, Y.S.: „Sensor Data and Information Fusion to Construct Digital-twins Virtual Machine Tools for Cyber-physical Manufacturing" in Procedia Manufacturing, Volume 10. 2017. Pages 1031-1042, ISSN: 2351-9789

(8.) Schleicha, B. , Anwer. B.,Mathieu, L., Wartzacka, S.: „Shaping the digital twin for design and production engineering" in CIRP Annals Manufacturing Technology, Volume 66, Issue 1. 2017. Pages 141-144. ISSN: 0007-8506

(9.) Zezulka, F., Marcon, P., Vesely, I., Sajdl, O.: „Industry 4.0 – An Introduction in the phenomenon" in IFAC-PapersOnLine, Volume 49, Issue 25. 2016. Pages 8-12. ISSN: 2405-8963

(10.)Meissner, H., IlsenJan, R., Aurich, C.: "Analysis of Control Architectures in the Context of Industry 4.0 in Procedia CIRP, Volume 62. 2017. Pages 165-169. ISSN: 2212-8271

(11.)Soderberg, R., Warmefjord, K., Carlson, J.S., Lindkvist, L.: „Toward a Digital Twin for real-time geometry assurance in individualized production" in CIRP Annals, Volume 66, Issue 1. 2017. Pages 137-140. ISSN: 0007-8506

(12.)Lee,J., Bagheri, B., Kao, H.A.: „A Cyber-Physical Systems architecture for Industry 4.0-based manufacturing systems" in Manufacturing Letters, Volume 3. January 2015. Pages 18-23. ISSN: 2213-8463

ИЗСЛЕДВАНЕ ПЛЪТНОСТТА НА ДЕНТАЛНИ МОСТОВИ КОНСТРУКЦИИ, ИЗРАБОТЕНИ ЧРЕЗ ИЗБИРАТЕЛНО СТОПЯВАНЕ С ЛАЗЕР

DENSITY INVESTIGATION OF DENTAL BRIDGES, PRODUCED BY SELECTIVE LASER MELTING

Assoc. Prof. Dr Dikova T.
Faculty of Dental Medicine, Medical University of Varna, Bulgaria

tsanka_dikova@abv.bg

Abstract: *Present paper deals with density investigation of four-part dental bridges, produced from Co-Cr alloy by Selective Laser Melting (SLM). Two methods were used: measuring the samples' density by liquid displacement method and defining the dense structure/pores ratio by CAD software. The comparative analysis was done with the density of bridges, cast conventionally with wax or 3D printed patterns. It was established that the density of the dental bridges, measured by the displacement method, was lower than the alloy's density and close for the three technologies - 7.86 g/cm^3 of the conventionally cast, 8.03 g/cm^3 of the constructions, cast with 3D printed patterns, and 8.13 g/cm^3 of the SLM samples. The investigation of the dense structure/pores ratio by CAD software showed presence of dense structure 95.94% and 94.77% in the bridges, cast with wax or 3D printed patterns respectively. While this parameter for the SLM constructions was 87.47%, as 12.53% of the volume were pores. These results were proved by observation of the microstructure, which is porous of the SLM bridges and comparatively dense of the cast ones. Therefore, the liquid displacement method is not suitable for measuring the density of porous structures. For obtaining reliable results it is necessary to be combined with other methodologies.*

Keywords: DENTAL BRIDGES, Co-Cr ALLOY, SELECTIVE LASER MELTING, DENSITY

1. Увод

В последните години технологиите за изработване на детайли с добавяне на материал (*additive technologies*) намират широко приложение в различни сектори на индустрията, строителството, медицината [1-7]. Това се дължи на изключителното многообразие от технологии и материали, с които се работи, на възможността почти безотпадно да се изработват детайли със сложна конфигурация и на автоматизацията на процесите, осигуряваща висока точност и добра повторяемост на продукцията. Процесът на избирателно стопяване с лазер (ИСЛ) се използва за изграждане на обекти от прахове на метали и сплави: цветни сплави, аустенитна стомана, а за медицински цели - чист Ti, титанови или Co-Cr сплави [2,8,9]. Изработването на детайла се извършва по виртуален 3D модел чрез последователно стопяване на слоеве метален прах с помощта на лазер.

В денталната медицина този технологичен процес намира приложение за изработване на скелети за протези, инфраструктури за коронки и мостове, дентални импланти и индивидуални импланти за лицево-челюстната хирургия [10-14]. Докато за повишаване биосъвместимостта и остеоинтеграцията на имплантите е необходимо повърхността им или в някои случаи целият обем да са порьозни, то при инфраструктурите за протезни конструкции плътната структура, която осигурява високи механични свойства, е наложителна. Averyanova et al. [10] изследват възможността за производство на 3-членни дентални мостове от Co-Cr сплав чрез ИСЛ и установяват, че всички образци са с необходимата плътност и са с по-малко от 1% порьозност. Vandenbroucke B. и Kruth J.-P. [12] осигуряват плътност от 99.9% на ИСЛ Co-Cr-Mo сплав, работейки с оптимални технологични режими. Takaichi A. et al. [15] варират с количеството внесена енергия и стъпката между сканираните следи и установяват, че плътна структура на Co-29Cr-6Mo сплав, изработена чрез ИЛС, може да се получи при енергия на лазерното сканиране по-голяма от 400 J/mm^3, а порьозна - при енергия по-малка от 150 J/mm^3.

Денталните мостови конструкции са натоварени циклично на огъване, като стойностите на усилието се увеличават от резците към моларите [16]. Най-голямо натоварване изпитват мостовите тела на четиричленни мостове от 1-ви премолар до 2-ри молар. Затова при изработване на такива конструкции чрез ИСЛ е необходимо да се направи оценка на тяхната плътност и получените резултати да се използват за оптимизиране на технологичните режими. В настоящата статия с помощта на две методики е изследвана плътността на четиричленни мостови конструкции от Co-Cr сплав, произведени чрез ИСЛ. Направен е сравнителен анализ с плътността на мостове, отлети по конвенционална технология с восъчни модели и с 3D принтирани модели.

2. Методика на експеримента

2.1. Материали и методи за изработване на образците

Изработени са три групи четири-членни дентални мостове от Co-Cr сплав. Първата група е отлята по конвенционална технология от восъчни модели, втората е отлята с 3D принтирани модели, а третата е изработена чрез избирателно лазерно стопяване. За генерирането на виртуален модел за последните две технологии и за изработване на матрица за отливане на еднотипни восъчни модели, първоначално е изработен един основен мост-модел от сплав *Biosil-F*. Последователността на изработване на образците е описана в [17]. Отливките са изработени от сплав *Biosil-F* (*Degudent*) с химичен състав, даден от производителя: Co 64.8; Cr 28.5; Mo 5.3; Si 0.5; Mn 0.5; C 0.4 (mass %) и плътност 8.4 g/cm^3. ИСЛ образци са произведени съответно от сплав *Co212-f* ASTM F75 с близък химичен състав: Co 65.2; Cr 28.3; Mo 5.48; Si 0.754; Fe 0.164 (mass %).

2.2. Изследване плътността на мостовите конструкции

Изследването е направено по две методики: 1) експериментално е определена плътността на мостовите конструкции по метода на водоизместимост и 2) изчислено е количественото съотношение плътна структура/пори с помощта на CAD софтуер.

2.2.1 Изследване плътност по метода на водо-изместимост

При този метод се използва закона на Архимед и се определя масата на обема течност, изместен от тялото. Използвана е прецизна електронна везна 200 g с точност 0.001 g, а за течност – дестилирана вода с плътност ρ_{fl}=1 g/cm^3. Първоначално се претегля всеки образец, а след това се определя масата на изместения от него обем вода. Плътността се изчислява по формула (1) [18].

$$\rho_s = \frac{m_s}{m_{fl}} . \rho_{fl}, \quad (1)$$

Където: ρ_s и m_s са съответно плътност и маса на твърдото тяло, а ρ_{fl} и m_{fl} са съответно плътност и маса на флуида, който потопеният образец измества.

По този начин е определена плътността на по 5 образеца от всяка една група. С помощта на софтуер *Excell* са изчислени средната аритметична стойност и статистическото отклонение.

2.2.2. Определяне количественото съотношение плътна структура/пори

При определяне съотношението плътна структура/пори в обема на образците се изхожда от твърдението, че плътността на дадена сплав се определя от нейния химичен състав и се допуска, че тя е постоянна за 100% плътна структура. Изхождайки от класическата формула за плътност на дадено вещество и при налични данни за масата на всеки един от образците и плътността на сплавта, може лесно да се изчислят обемите със 100% плътна структура по формула (2):

$$V_{dens1} = \frac{m_s}{\rho_a}, \quad (2)$$

Където: V_{dens1} е обем на плътна структура, изчислен след измерване масата на образците, cm^3; ρ_a – плътност на дадената сплав, g/cm^3; m_s – измерена маса на денталния мост, g.

За да се намери обемът на мостовите конструкции при 100% плътна структура е използван CAD софтуер *Inventor Professional 2016*. При наличен виртуален 3D модел и заложени данни за съответната сплав, той дава информация за обема, площта на обвиващата повърхност, център на тежестта, инерционни моменти и др., но при допускане за 100% плътна структура. За целта на нашето изследване по един от денталните мостове от трите групи е сканиран, генериран е виртуален 3D модел и информацията е превърната в *stl*-формат по методиката, описана в [19]. Информацията е използвана за създаване на 3D модел за съответната среда на използвания софтуер. От файла на съответния образец са взети данни за неговия обем - V_{dens2}, които са изчислени с допускането, че структурата е 100% плътна. С тяхна помощ е определено относителното количество плътна структура по формула (3):

$$V_{dens\%} = \frac{V_{dens1}}{V_{dens2}} \times 100, \quad (3)$$

Където: $V_{dens\%}$ е относителното количество плътна структура, %; V_{dens1} е обем на плътна структура, изчислен след измерване масата на образците, cm^3; V_{dens2} е обем на денталния мост при 100% плътна структура, изчислен от CAD софтуер, cm^3.

3. Получени резултати и анализ

При изследване плътността на неснемаеми протезни конструкции, произведени чрез технологии с добавяне на материал, в [20] е установено, че няма голяма разлика между плътността на денталните мостове, произведени чрез ИСЛ и леене – 8.13 g/cm^3 и 8.15 g/cm^3 съответно. Вижда се, че тя е по-малка от дадената 8.4 g/cm^3 за сплавите, от които са произведени. Заключението е, че това е вследствие на дефекти в микроструктурата, породени от вида технологичен процес. Това твърдение по принцип е правилно, защото наличието на неплътности от различен характер в обема на образците винаги води до по-ниска плътност.

Едно по-подробно изследване на микроструктурата, обаче, показа плътна структура в обема на мостовите конструкции, изработени чрез леене с восъчни и 3D принтирани модели (фиг. 1). В подповърхностите слоеве и на двата образца се забелязват газови шупли – сравнително големи при конвенционално отлетите (фиг. 1-а) и с по-малки размери при моста, отлят с 3D принтиран модел (фиг. 1-б). Докато при мостовите конструкции, изработени чрез ИСЛ, се наблюдават пори и неплътности в целия обем (фиг. 2-а). Размерите им варират от няколко микрона до 0.6 mm. По повърхността няма добро сплъване на последните слоеве метал (фиг. 2-б). Наблюдават се и частично разтопени прашинки както вътре в порите, така и по повърхността. Ясно се забелязват пукнатини, вероятно в местата на препокриване на слоевете или на отделните разтопени следи в даден слой (фиг. 2-в, фиг. 2-1 и фиг. 2-2).

Това несъответсвие между микроструктура и плътност бе причина да се направи допълнително изследване на плътността с комбинирано използване на две методики. При повторното определяне на плътността чрез Архимедовия закон се получиха подобни резултати, показани в таблица 1. Плътността на отлетите образци е по-ниска от тази на сплавта и варира в близки стойности - от 7.97 g/cm^3 на базовия мост-модел, 7.86 g/cm^3 на конвенционално отлетите мостове и 8.03 g/cm^3 на конструкциите, отлети с 3D принтирани модели. Противно на очакванията, мостовите конструкции, изработени с ИСЛ, имат най-висока плътност 8.13 g/cm^3. Направеният анализ показа, че наличието на вътрешни пори в тяхната микроструктура е решаващият фактор за това несъответствие. Оказва се, че при използване метода за водоизместимост за определяне на плътността, течността не може да проникне в порите, които са вътре в обема, и така не може да се получи точен резултат.

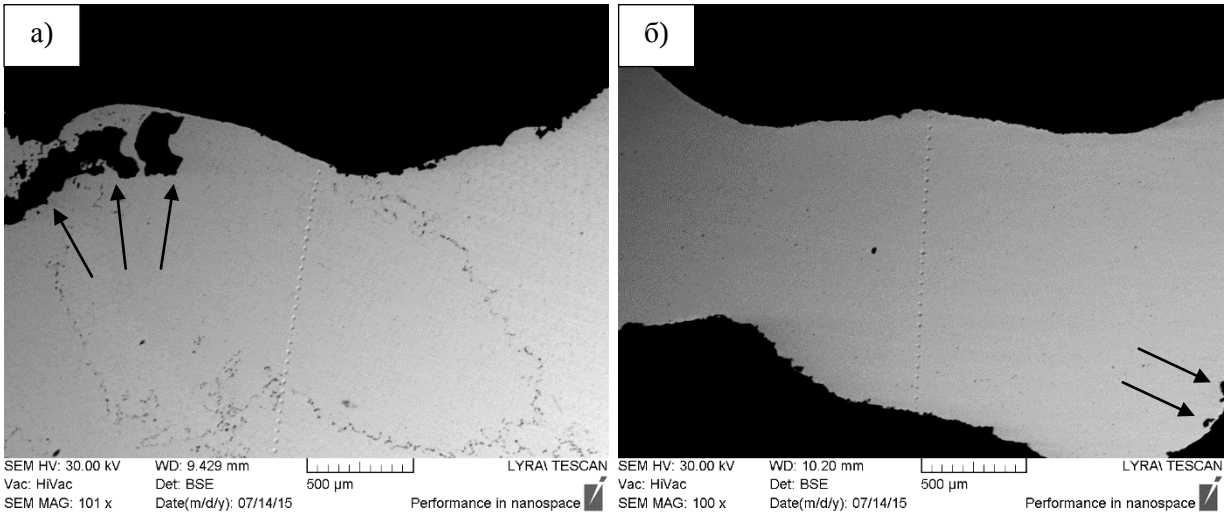

Фиг. 1 Дефекти в микроструктурата на мостови конструкции, отлети по конвенционална технология – а) и с 3D принтиран модел – б).

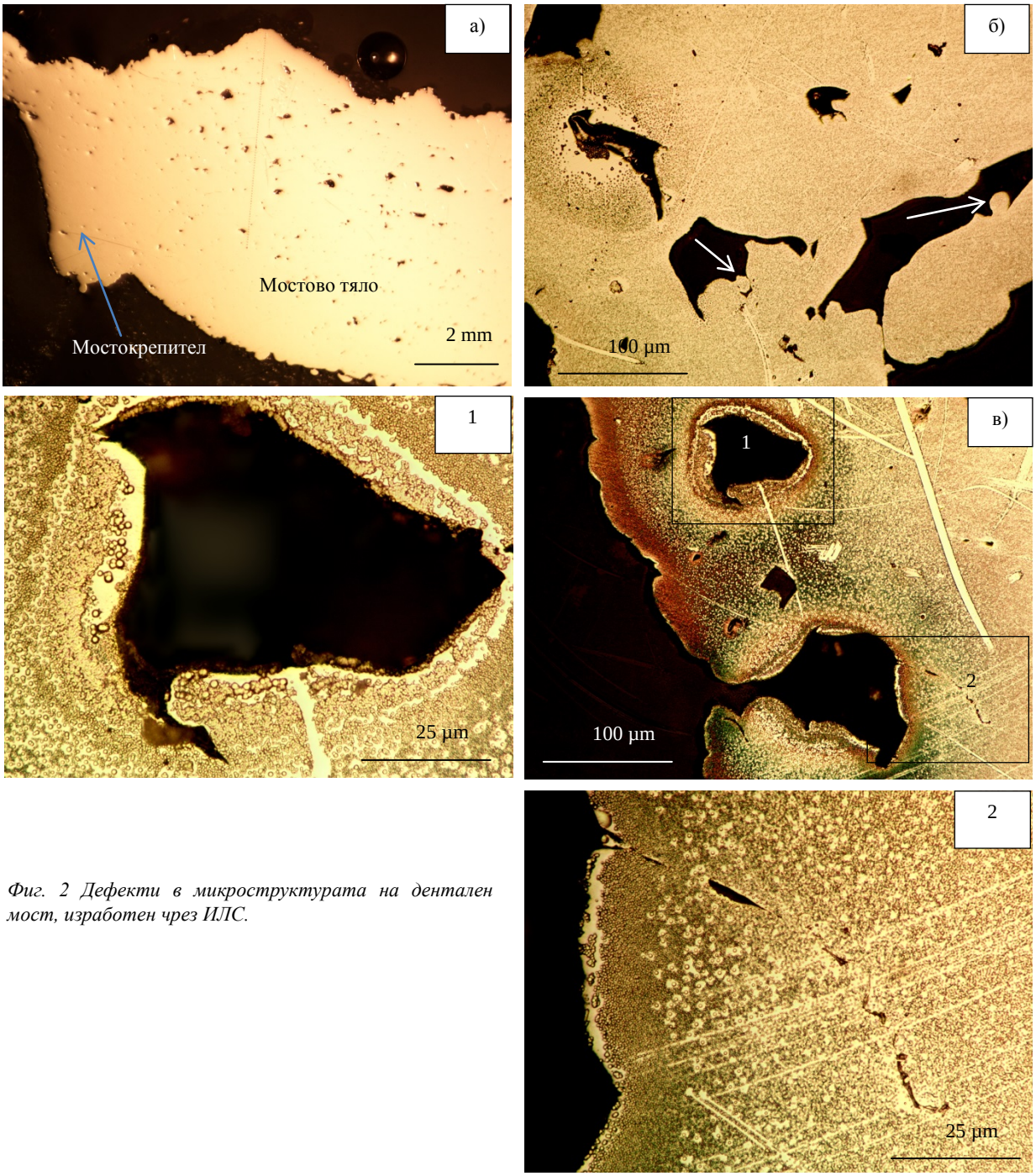

Фиг. 2 Дефекти в микроструктурата на дентален мост, изработен чрез ИЛС.

Затова се прибегна до втори метод за определяне съотношението между плътна стурктура и пори в обема на определени образци, който да даде по-реална преценка за относителната плътност. Резултатите на фиг. 4 показват плътна структура на отливките от 92.76% за базовия модел, 95.94% и 94.77% за отлетите с восъчни и 3D принтирани модели съответно. Ако сравним тези резултати с относителната плътност, посочена в таблица 1, виждаме едно добро съотношение (94.88%, 93.57% и 95,60% за базов модел, отливка с восъчни и отливка с 3D принтирани модели съответно). Не така стоят нещата с мостовите конструкции, произведени чрез ИСЛ. При тях плътната структура е едва 87.47%, а останалата част – 12.53% от обема са пори. Разликата между количеството плътна структура и относителната плътност от 96.79%, дадена в таблица 1, е сравнително голяма – около 10%. При използване на метода за определяне съотношението плътна стурктура/пори с помощта на софтуер трябва да се отчитат евентуалните грешки, свързани със сканиране на обектите, генериране на виртуалните модели и конвертиране на файловете. Но, имайки предвид порьозната структура на мостовите конструкции, произведени с ИСЛ, този метод дава по-точна оценка на относителната им плътност в сравнение с метода на водоизместимост.

Таблица 1.

Плътност на дентални мостови конструкции, изработени чрез различни технологии.

Образец	Плътност, g/cm^3	Стандартно отклонение	Относителна плътност, %
Базов модел, отливка	7.97		94.88
Отливка с восъчен модел	7.86	0.24	93.57
Отливка с 3D принтиран модел	8.03	0.29	95.60
ИЛС	8.13	0.17	96.79

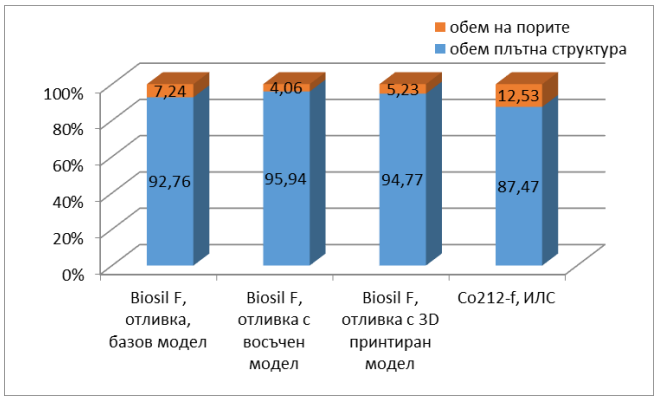

Фиг. 3 Относителен дял на порите и плътната структура в структурата на мостови конструкции, изработени чрез различни технологии.

Тъй като денталните мостове са натоварени циклично на огъване, наличието на пори и дефекти в микроструктурата би довело до по-бързото им разрушаване. При конструкции, изработени чрез ИСЛ, разслояванията и пукнатините между две следи в даден слой или между отделните слоеве биха ускорили процеса. Затова при този технологичен процес получаването на детайли с плътна структура е от голямо значение. Необходимо е да се осигури по-голяма енергия, достатъчна за разтопяване на целия обем метал по дълбочина на слоя и по ширина на стопената вана [8, 15, 21]. Това може да стане чрез намаляване скоростта на сканиране на лазера или увеличаване на неговата мощност.

4. Заключение

С помощта на две методики е изследвана плътността на четиричленни мостови конструкции от Co-Cr сплав, произведени чрез ИСЛ. Сравнителният анализ показа, че:

- Плътността на денталните мостове, измерена по метода на водоизместимост, е по-ниска от тази на сплавта и много близка за трите технологии - 7.86 g/cm^3 на конвенционално отлетите, 8.03 g/cm^3 на конструкциите, отлети с 3D принтирани модели, и 8.13 g/cm^3 за изработениете с ИСЛ.
- Изследването на съотношението плътна структура/пори с CAD софтуер показа наличие на плътна стурктура 95.94% и 94.77% за мостовете, отлети с восъчни и 3D принтирани модели съответно. Докато този параметър за изработениете с ИСЛ конструкции е 87.47%, а 12.53% от обема са пори.
- Резултатите от изследването с CAD софтуер се потвърдиха от наблюдението на микроструктурата, която е порьозна при мостовете, изработени с ИСЛ, и сравнително плътна при отлетите.
- Методът на водоизместимост за определяне на плътност не е подходящ при изследване на порьозни образци. За получаване на достоверни резултати е необходимо комбинирането му с други методики.

5. Литература

1. Wohlers T. Recent trends in additive manufacturing. *Proceedings of AEPR'12*, 17th European Forum on Rapid Prototyping and Manufacturing, Paris, France, 12-14 June 2012, 6p.
2. Dovbish VM, Zabednov PV, Zlenko MA. Additivnie tehnologii I izdelia iz metala, 57 p.[in Russian].
3. Vasilev T. Delta 3D wire printer for building objects – theoretical prerequisites for prototype design, *Industry 4.0*, 2017; 2(3):127-130.
4. Vasilev T. Analysis of the Deformations in „Delta Wired 3D Printer", *ACTA TECHNICA CORVINIENSIS – Bulletin of Engineering*. 2017;Tome X (3):93-98.
5. Василев Т. Оптимизиране на конструкцията на 3D принтер за строителни обекти, *Машиностроене и Машинознание.* 2017; XII(1):105-109.
6. Bandyopadhyay A, Bose S, Das S. 3D printing of biomaterials. *MRS bulletin*. 2015 Feb;40:108-115, www.mrs.org/bulletin.
7. van Noort R. The future of dental devices is digital. *Dental Materials.* 2012;28:3–12.
8. Thomas D. The Development of Design Rules for Selective Laser Melting [PhD thesis]. [Cardiff]: University of Wales Institute; 2009. 318 p.
9. Strietzel R. Selective Laser Melting in Dentistry. *Informatics in Oral Medicine: Advanced Techniques in Clinical and Diagnostic Technologies.* IGI Global, 2010. 111-125. doi: 10.4018/978-1-60566-733-1.ch008, Accessed Nov 14, 2017.
10. Averyanoiva M, Bertrand P, Verquin B. Manufacture of Co-Cr dental crowns and bridges by selective laser melting technology. *Virtual and Physical Prototyping.* 2011 Sept; 6(3): 179-185.
11. Bibb R, Eggbeer D, Williams R. Rapid manufacture of removable partial denture frameworks. *Rapid Prototyping J.* 2006; 12: 95-99.
12. Kruth J-P, Vandenbroucke B, Van Vaerenbergh J, Naert I, Rapid Manufacturing of Dental Prostheses by Means of Selective Lsser Sintering/Melting. In: Proceedings of the AFPR, S4. 2005, http://doc.utwente.nl/52914/1/Wa1025.pdf, Accessed Nov 14, 2017.
13. Dobrzański LA, Dobrzańska-Danikiewicz AD, Malara P, Gaweł T, Dobrzański L, Achtelik-Franczak A. Fabrication of scaffolds from Ti6Al4V powders using the computer aided laser method. *Archives of Metallurgy and Materials.* 2015; 60(2): 1065-1070.
14. Dobrzański LA, Dobrzańska-Danikiewicz AD, Gaweł TG, Achtelik-Franczak A. Selective laser sintering and melting of pristine titanium and titanium Ti6Al4V alloy powders and selection of chemical environment for etching of such materials. *Archives of Metallurgy and Materials.* 2015; 60(3): 2039-2045.
15. Takaichi A, Suyalatu, Nakamoto T. et al., Microstructures and mechanical properties of Co–29Cr–6Mo alloy fabricated by selective laser melting process for dental applications. *Journal of the Mechanical Behavior of Biomedical Materials* 2013;21:67–76;
16. Filtchev A, Kalachev Y. Phenomenon of domination of the strongest contacts in centric occlusion. *Quintessence International* 2008; 39(3): 99-106.
17. Dzhendov D, Pavlova D, Simov M, Marinov N, Sofronov Y, Dikova T, Todorov G, Kalachev Y. Геометрична точност на неснемаеми мостови конструкции, изработени посредством адитивни технологии. *Сборник на 8 МНК за млади учени* "Technical Science and Industrial Management", Варна, България,15-16.09.2014;1:13-17.
18. Manual of Weighing Applications, Part 1, Density. *Sartorius. Marketing, Weighing Technology*, February 1999, 62p., BK - 07.07.99 - VORWOR_E.DOC, http://www.dcu.ie/sites/default/files/mechanical_engineering/pdfs/manuals/DensityDeterminationManual.pdf ;
19. Dikova T, Vasilev T, Dzhendov D, Ivanova E. Investigation the fitting accuracy of cast and SLM Co-Cr dental bridges using CAD software. *J of IMAB.* 2017 Jul-Sep;23(3):1688-1696;
20. Джендов Д. Неснемаеми протезни конструкции от Co-Cr сплави, изработени чрез технологии с добавяне на материал [Автореферат на дисертационен труд за придобиване на ОНС „доктор"].[Варна]:МУ-Варна; 2017.50с.;
21. Dikova T, Dzhendov D, Simov M. Microstructure and Hardness of Fixed Dental Prostheses Manufactured by Additive Technologies. *Journal of Achievements in Mechanical and Materials Engineering*. 2015 August; 71(2):60-69.

FULL USE OF MATHEMATICS – FOUNDRY

Bushev S., Associate Professor, PhD, Eng.
Institute of metal science, equipment and technology with hydro- and aerodynamics center "Acad. A. Balevski"
Bulgarian academy of sciences, Sofia 1574, 67 "Shipchenski prohod" Str. Bulgaria Republic
stbushev@abv.bg

Abstract: In this work, we present the necessity of using the full mathematics in the industrial branch of machine building of the example of the foundry. Obtaining the necessary structures is accompanied by research work even in micro-foundries, which is provided by powerful and new software products, i.e. knowledge transfer with computational mathematics, physics and education.

Keywords: MACHINE BUILDING, FOUNDRY, CASTING STRUCTURES, MATHEMATICS, EDUCATION

1. Introduction

The importance of mathematics is represented by a general block diagram of "The History of the Development of Knowledge of Civilization from Antiquity to Today" of Fig. 1

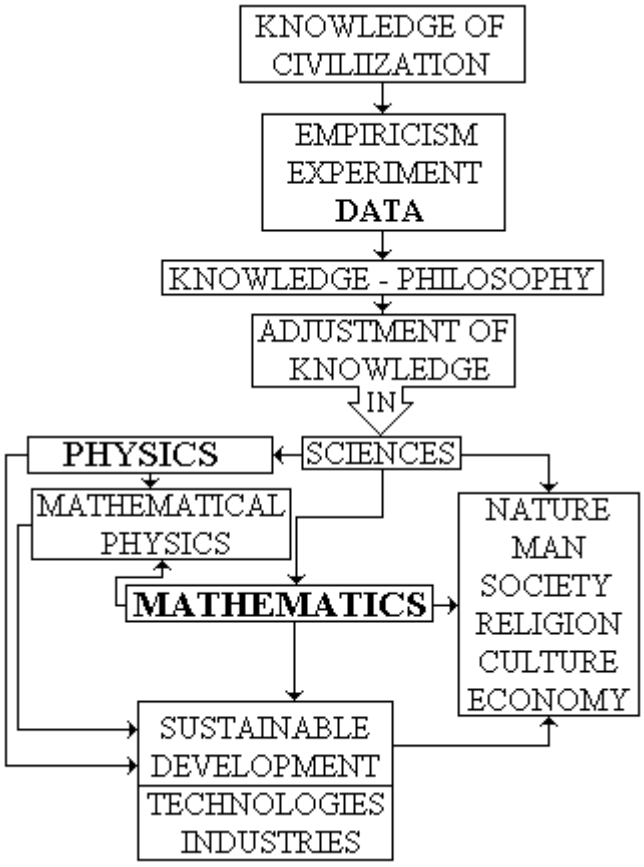

Fig. 1 *Block diagram - Developing the knowledge of civilization from antiquity to today [1, 3, 4].*

1 follows: 1. Initial knowledge is obtained through empiricism - obtaining and classifying experimental data; 2. Collecting knowledge in philosophy; 3. Knowledge is divided into separate sciences after Christ: 3.1 Physics - 18th Century; 3.2 Mathematics - the 19th and the beginnings of the 20th century; 3.3 Mathematics - Self Development; 3.4 Mathematics - a powerful tool for research: Description of physical processes and phenomena. Any theory is obtained only by using mathematics; 3.5 The term mathematical physics includes natural and theoretical physics; 4. Mathematics is in every area of human activity; 5. Sustainable development of civilization is based on: a sustainable society and economy - a challenge for every government; 6. Civilization only evolves by overcoming crises in society and the economy; 7. The challenge is the restructuring of the world by the fourth industrial revolution [1], involving education throughout every person's life, environmental technologies and industries.

The natural systems and the four main types of interaction forces in nature are classified in Fig. 2

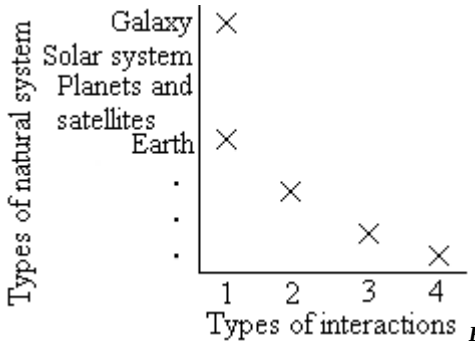

Fig. 2 *Scheme - Natural systems and types of interactions [2]: 1 - gravitational interaction (large-scale events in the Universe), 2 - electromagnetic interaction (holds electrons in atoms and binds atoms to molecules and crystals (chemistry, biology)), 3 - strong interaction connects the nucleons (it unites protons and neutrons in the nucleus of all elements), 4 - weak interaction determines the forces acting between the light particles (leptons: electrons, neutrinos and muons) and between leptons and heavier particles).*

The purpose of this work is to present the necessity of the complete mathematics in the foundry.

2. Foundry - physical and technological processes of structure formation

The casting structures are obtained in phase transition of 1st order is shown with the characteristic scale of the scheme of Fig. 3

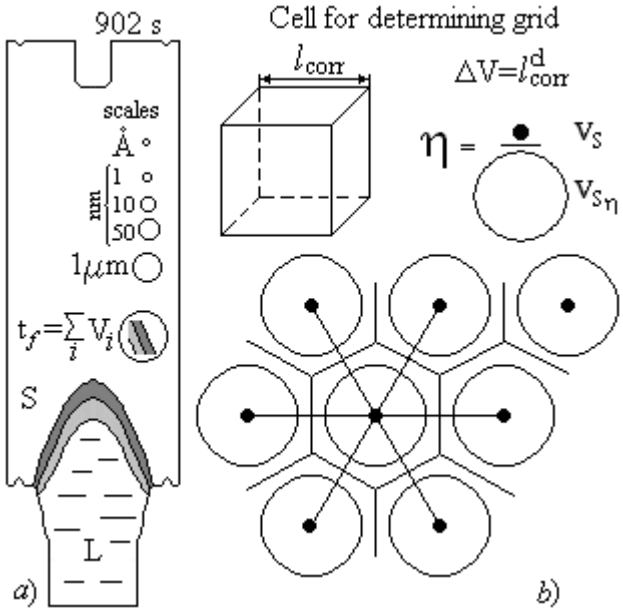

Fig. 3 *The casting structures are obtained in phase transition of 1st order (solidification) [5]: a) Numerical experiment: technological solidification of a cylindrical cast at 902 s, graphically represented by the geometry of the solidification zone (front) – between the liquid (L) and the solid (S) phases. Scales Å, nm, 1μm. t_f – local time of solidification. V_i – chosen local volume for description of structure formation; b) Cell for determining grid – l_{corr} for V_i, ΔV_i – changing the volume V_i from melting*

(solidification), d – direction of growth 1D, 2D or 3D, η – pacing density coefficient, v_S – volume of atom, $v_{S\eta}$ – volume cell, Wigner-Zeitz cell and structure.

The technological system of foundry we introduced on the example by the machine – Gas counter-pressure casting method Fig. 4

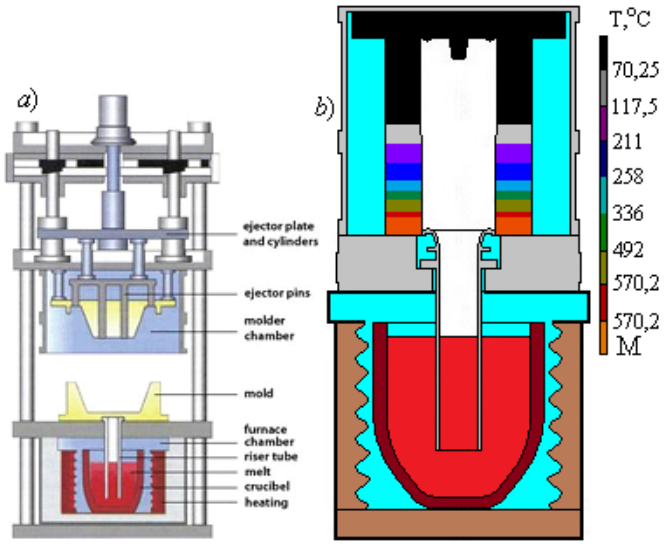

Fig. 4 *Casting technology system - Gas counter-pressure casting machine: a) General appearance of the casting machine; b) Technology for producing counter-pressure cylindrical castings. The technological regime shown (see Fig.2 a) is obtain with initial temperature of the mould without taking into account the filling process.*

The technological system (see Fig. 4) provides of macro-level to obtain the desired structure *average diameter of polycrystalline grains* [12]. The macro-parameters of the casting technology are **the overcooling of the melt** and **scattering of the latent heat of melting** [3, 5, 11, 12].

3. Mathematics in Foundry

It is well known, that the mathematics application in foundry is theoretical and applied thermodynamics [1, 2, 3]. The separation of each set of knowledge into science is achieved only by using mathematics, which definition is [3]: *Mathematics contains mathematical knowledge, foundation of mathematics, methodology of mathematics and philosophy of mathematics in a complex interconnectivity and continuous development.*

3.1 Mathematics in Thermodynamics and Foundry

The crystals are arranged in a solid state where the atoms or molecules are arranged in the form of a crystal lattice (structure). The crystals are obtained by a phase transition of first order by changing the aggregate state of the initial phase to the new solid phase. Bearer of the working properties of the castings is the crystalline structure, which is obtained in the phase transition of first order. Thermodynamics system in foundry is alloy (pure metal) (see Fig. 3 and Fig. 4). Casting is a fundamental branch of material science. It is known that the most advantageous technology for making castings with complex geometry is casting.

The description of the first-order phase transition is presented here in its historical development, i.e. the development of the classical theory of crystallization in atomistic approach. Table 1 presents: the description of thermodynamics; the theoretical description of nucleation like: thermodynamics and kinetics; crystal growth theory: Surface energy; Dyffusion; Surface nucleation; Screw dislocation

Table 1: *Phase transition in foundry: Liquid(L) ↔(S)Solid.*

Liquid (L) ⟵ *phase transition of* 1^{st} *order* ⟶ **Solid (S)**
THERMODYNAMICS OF THE TRANSITION L↔S

$G = H - TS$, *Gibbs free energy at* $T_e \rightarrow G_L = G_S$, (1,1,2)

$\Delta G = \Delta H - T\Delta S$; *and* $\Delta G = G_L - G_S, \Delta H = H_L - H_S, \Delta S = S_L - S_S$, (1,3,4,5,6)

$\Delta G = 0$ *is equilibrium at* $T_e \Rightarrow \Delta H = T_e \Delta S$, (1,7)

$\Delta G = \Delta H \Delta T / T_e$, *and* $\Delta T = T_e - T$, (1,8,9)

$\Delta G = \Delta S \Delta T$ *for melt growth,* (1,10)

$\Delta G = RT \ln(S_R)$ *growth depend to* supersaturation ratio S_R. (1,11)

In foundry the basic thermodynamics system is material from two phases; G – Gibbs's free energy of the system; H – enthalpy; S – entropy; T – temperature; $T_e = T_L = T_S$ – equilibrium temperature; $T_e - T$ – supercooling; Δ – change of G, H, S; R – gas constant.

NUCLEATION – IMPORTANT PHENOMENON IN CRYSTAL GROWTH

$$\Delta G = 4\pi r^2\sigma - \frac{4}{3}\pi r^3 \Delta G_v; \quad r^* = \frac{2\sigma}{\Delta G_v}, \quad \Delta G^* = \frac{16\pi\sigma^3}{3\Delta G_v^2} \quad (1,12,13,14)$$

$$\Delta G^* = \frac{16\pi\sigma^3\Omega^2}{3(kT\ln S_R)}, \quad Gibbs - Tomson \quad equation \quad (1,15)$$

$$J = J_0 \exp\left[-\frac{\Delta G^*}{kT}\right], J = J_0 \exp\left(\frac{16\pi\sigma^3\Omega^2}{3(kT\ln S_R)}\right), S_{R|Cri} = \exp\left[\frac{16\pi\sigma^3\Omega^2}{3k^3T^3\ln J_0)}\right], (1,16,17)$$

where ΔG_v – change the Gibbs free energy of nucleus volume of new phase (L or S); r – nucleus radius; r*, ΔG* - critical parameters; σ – surface energy; Ω – atomic (molecular) volume; J – nucleation rate per *unit* volume; J_0 – is the total number of particles in the new phase; $S_{R|Cri}$ – critical supersaturation ratio; k is Boltzmann's constant.

CRYSTALS GROWTH THEORY

1. **Surface energy theory** is on the based to thermodynamics equilibrium state with minimal total surphace energy for given volume. There is contradiction theory-experiment: supersaturation and growth sides of crystal. At high supersaturation the growth is not uniformly of all directions and only of some sides.

2. **Diffusion theory** is on the base that there is a concentration gradient in the vicinity of the growing surface

$$\frac{dm}{dt} = \frac{D}{\delta} A(C - C_0) \quad (1,18)$$

where dm/dt is the rate the mass deposited on the crystal surface with area A; D – diffusion coefficient; δ - thickness layer adjacent to the crystal surface; C and C_0 – actual and equilibrium concentration.

3. **Surface nucleation theory** is developed by Kossel [18], Stranski [19], Volmer [21], and Kaishev [23] (model KSVK): crystal growth on the surface with inhomogeneties of the type terrace, ledge and kink; guess that the growth is discontinues process of absorption of the material layer by layer on the crystal surface. The arriving atoms (molecules) do not get directly into the grid, but they migrate over the surface in a random walk process and finally get absorbed on these sites, where its energy is a minimum. Migration distance x_s is

$$x_S^2 = D_S \tau_S, where \quad x_S \approx a\left[3\phi/2kT\right] \quad (1,19,20)$$

where D_S – coefficient of diffusion; τ_S – life time of the absorbed particle on the crystal surface; ϕ is the nearest interaction parameter. Migrate atoms create diffuse flow at the surface of the growing crystal, and they are called adatoms. Migrate atoms create diffuse flow at the surface of the growing crystal, and they are called adatoms. For adsorption of adatoms on the crystal surface is need description of interaction between one adatom and elements of surface relief: one adatom at kink site have three chemical bonds for six first neighbor's atoms from of the crystal lattice surface; adatom and ledge have two chemical bonds; adatom and terrace have one chemical bond. Barton-Cabrera-Frank model (BCF) [22] gives: 1. the rate of diffusion flow of migrate adatoms V_{ST}: distant migration step is much higher than distant between two kinks (or middle migration distance is much higher than the mean distance between two adjacent kinks); 2. When the movement step covers the whole surface completely, further growth is only possible by creating a two-dimensional nucleus circle with a radius r and a height h with the necessary energy change ΔG_{td}. According to Volmer [21], this is possible due to heat fluctuations; 3. The growth rate of a single side is generally controlled by the degree of germ formation and the rate of step advancement $R_{J_{td}}^{V_{ST}}$

$$V_{ST} = 2S_{X_S} x_S \gamma \exp(-W/kT), \quad (1,21)$$

$$\Delta G_{td} = 2\pi r h\gamma - \pi\tau^2 h\Delta G_V, \quad \Delta G_{tg}^* = 2\pi h\gamma - \pi\tau^2 h\Delta G_V, \quad (1,22,23)$$

$$J_{td} = C_l \exp\left[-\pi h\gamma^2\Omega / k^2T^2 \ln S_{X_S}\right], \quad (1,24)$$

$$S'_{X_S|Cri} = \exp\left[\pi h\gamma^2\Omega / k^2T^2 \ln C_l\right], \quad (1,25)$$

$$R_J^V = hJ_{td}^{1/3}V_{ST}^{2/3}, \quad (1,26)$$

where γ is a frequency factori in (1,21) and the edge free energy in (1,22

and 23); W is the **total** evaporation energy; S_{X_S} is supersaturation for the mean migration distance x_S, and index cri is for critical supersaturation; C_l – concentration of liquid.

4. Burton, Cabrera and Frank [23] (BCF model) **screw dislocation theory**: on the surface of the crystal in the dislocation point a screw component with a height of the Burger vector projection acts as a continuous source of steps; the step provided by the screw dislocation is fixed at the point of displacement; growth is only by rotation around the point of dislocation, like the inner parts of the tread moving faster than the outer parts of the tread. This mechanism can provide a relation between the rate of growth R and the relative supersaturation s which are expressed with the equations

$$R = C(s^2 / s_1)\tanh(s_1 / s), \quad (1{,}27)$$

$$s_1 = 19\gamma\Omega/2kTx_S; \quad C = D_S \cap_{SE} \beta\Omega/x_s^2,$$

where s – relative supersaturation; s_1 – a const for BCR model; $\cap_{se}$ - equilibrium concentration of growth units on surface; β - retardation factor; Ω – volume of the growth unit. The variation R with supersaturation thus depends on two parameters, C which determines the absolute value of growth rate and s1 which determines actual growth rate. The BCF model predicts nucleation at edge dislocation predicts that the growth rate is proportional (∝) to the square of the supersaturation for low supersaturation if $s\langle\langle s_1 \Rightarrow R \propto s^2$ and changing to a linear dependence at higher supersaturations if $s\rangle\rangle s_1 \quad R \propto s$.

Crystal growth in casting methodology – atomistic approach

1. Thermodynamics – thermodynamic driving force and work of nucleation.
2. Kinetics – nucleation rate and supersaturation number.

MACROSCOPIC LEVEL – SOLIDIFICATION [5]

1. **Heat Conductivity analytical solution:** 1.1 1D Stephan's problems; 1.2 1D Stephan-Schwartz problems;
2. **Numerical Solidification's Problems:** 2.1 1D Stephan's problems and 1D Stephan-Schwartz problems; 2.2 3D Stephan's problems and **the most important 3D Stephan-Schwartz problem**; 2.3 Numerical Methods: 2.3.1 Finite differentials method; 2.3.2 Finite elements method; 2.3.3 Boundary elements method.

Chemical bond short history introduction on the base table 7 page 199 in [13]: MendeIeev (1871) Eight as a maximum valence rule and the sum of me hydrogen and oxygen valences for higher types; Abegg (1904) Electrochemical interpretation of Mendeieev's rule of eight in terms of electron gain and loss; Thomson: (1904, 1907) Concept of chemical periodicity in terms of recurring outer electron configurations. Rule of eight as striving for completion of stable rare gas shells; Kossel (1916) Extension of ionic model. Eight as a maximum valence rule for polar corn pounds only; Lewis (1916) Continuity of bond type and electron pair bonding mechanism for octet completion; Langmuir (1919-1921) Elaboration and popularization of the Lewis model. Mathematical formulation of the octet rule.

As it is known, Koseel offers a kinetic theory of crystal growth [18] and Stranski offers the same model [19]. At their meeting at the suggestion of the Stranski model is a well-known Kossel-Stranski model. The 1930s saw the publishing of several important articles which Stranski co-authored with Kaishev [20, 23] and Krastanov [30], which is called Stransk-Krastanov's growth mechanism. Stranski [28] and Kaishev [23] have developed the method of average separation work, a molecular kinetic method, which has played a role in the development of the theory of crystal growth and growth. Kaishev and Stranski create: the model of the crystalline growth (layered crystalline growth); have merit clarifying the relationship between the two-dimensional germ formation and spiral growth of the crystals. Kaishev summarizes Wulff's theorem of the equilibrium crystal's form, Kaishev summarizes Wulf's theorem about the equilibrium shape of the crystal formed on a foreign substrate (Wulf-Kaishev's rule); Develops thermodynamics and kinetics of electro-crystallization and electrolyte nucleation. Application the Kossel-Stranski mechanism is [17].

Nucleation. Kashchiev's book [25] presents at the same time an introduction to the theory of nucleation; the new results, their role and the interaction of the new results with the full theory of crystalline growth; the directions of the development of the complete theory. Thermodynamics and kinetics are directed to saturation (driving force), nucleus size dependence and work of nucleation. Regular spiral growth and known mechanisms of crystal growth are considered. Regular layered, spiral growth and known mechanisms of crystal growth are considered. A great potential for the application of the results in [25] to describe the first-order phase transition in the foundry methodologically is: the theorem of nucleation; and the basic kinetic equation of the formation of new phases for variable saturation. **Epitaxy.** Markov's book [26] considers in four parts the nucleation at obtaining of thin films in epitaxial growth, on the base of equilibrium between crystal and ambient phase, nucleation and crystal growth. The crystal growth mechanisms are examined, and the barrier effects on crystal growth mechanisms and on morphology analysis of the growing crystal surface are also considered. The mechanisms of Frank and van der Merwe and Stranski–Krastanov are discussed. The Mechanism of Stranski-Krastanov is the formation of several complete monolayers followed by the growth of isolated 3D islands and is well known to all epitaxial growth researchers. Barrier effects reporting require rewriting of the nucleation theory. An atom in a barrier effect like Ehrlich–Schwoebel has less close neighbors, which is important for morphology of surface growth. **Morphology.** The morphology of growing surface is part of the crystal growing. In [14] is presented graphical method generalized by general theorem. Has developed a new model of interaction between an internal structure and the morphology of a growing crystal surface [15]. In work [16] is study the growth and the morphology of Study of growth and morphology of precious stones.

An important moment for the foundry (but also for material science) is the natural boldness between the works of Balevski [6] and Borisov [7]. By definition [6] – By definition [6] – Metal science is the science of the relationships between structure and properties, as well as the influence that thermal, mechanical and other impacts have on the structure, and hence on the properties of metals and alloys. Metal science as a science emerges in the second half of the 19th century, originated in physics, metal physics, and so on. The introductory first part is Theory of Metals and Alloys: electronic struction of atoms; interatomic connections; crystal structure of metals; crystallization; physical - properties and methods of measurement; due to the engineering direction of [6]: deformation (elastic and plastic), mechanical properties and tests. These rigorous scientific terms clearly show the required minimum number of scientific fields in metal science, and only by the engineering need It is further clarified that the scientific ideas in [13] are not only in the theory of metal science but also in the theory of all **material science**. Изключително важен момент е: *за описание свойствата на металите е създадена квантовата механика*; използва се във фундаментални изследвания на физиката и техниката, които вече са съвпадат. An extremely important point is: *quantum mechanics has been created to describe the properties of metals*; used in fundamental studies of physics and technology that have already coincided. The full theory of crystalline growth covers applications such as semiconductor materials and structures for nanoelectronics [...].

In [7] the introduction of solid state physics is based on quantum chemistry, i.e. the application of quantum mechanics for explanation of the chemical connection (electromagnetic interaction see Fig. 2). The interaction of the electron (atomic core) is coulon and the state of the electron in the atom lies as a solution to Schrödinger's amplitude wave equation. Types of solid bodies according to the type of interatomic connections [7]: ionic crystals - crystalline lattice consists of oppositely charged ions; valent crystals - the atoms are connected in a crystal lattice with a covalent (homoeopolar) bond; metals - a crystal lattice is made up of positive ions, the repulsive forces between them being equalized by the free electrons; molecular crystals - the lattice is made up of individual molecules or atoms interconnected with intermolecular (vandervals) forces. Metal alloys are the simplest chemical compounds - solutions. The crystal lattices of the alloys according to the size of the atoms are: solid substitution solutions; solid solutions of deployment. It can be said that work [7] binds work [6] with

quantum mechanics. Work [6] and [7] are expanded by [9] for electron theory in metals.

Full mathematics is called upon to create new purely mathematical theories. The new theories are evolving because Gödel's theorems of "incompleteness" clearly show that there is no complete mathematical theory. The history of mathematics shows the need for the development of pure mathematics, but it is challenging to suggest the assessment of the development of the necessary, for example, a "new mathematical field".

A scale of 1μm is a macro-scale. Scale for nm or Å requires modern methodologies based on [8, 9, and 10]. Generalized this is the mathematics, the theoretical and the mathematical physics presented in Fig. 5

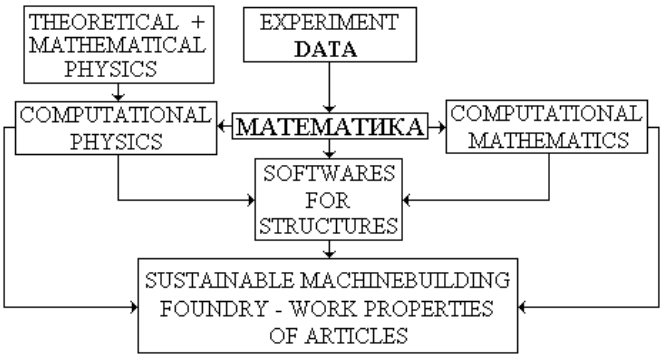

Fig. 5 *Scheme - Full mathematics is needed in Micro-Foundry and Industry 4.0.*

4. Conclusion

Mathematics is a powerful tool for research. Mathematics is needed in public development, for example "virtual factories", apart from technological, legal relations between companies, based on new experimental data, evaluations are also made for research ideas for development from "artificial intelligence". Hence Industry Change 4.0: "factories without people", and people naturally need life-long education.

5. References

1. S. Bushev, Knowledge transfer Industry 4, International Scientific Journal "INDUSTRY 4.0", No 4, p.51-54, Year I, ISSUE 1/2016

2. Ch. Kittel, W. Knight, M. Ruderman, Mechanics, Berkeley Physics Course, v. **I**, "Nauka", Moscow, 1975. (In Russian)

3. S. Bushev, Industrial mathematics – phase transitions, scattering, structures, International Scientific Journal "INOVATIONS", p.57-62 Year V, ISSUE 2/2017, Sofia.

4. K. Schwab, The Fourth Industrial Revolution, "Hermes", 2016, ISBN 978-954-26-1630-6 (In Bulgarian)

5. S. Bushev, Theoretical model of structureformation in die casting, XXII International scientific technical conference "FOUNDRY 2015", 16-17.04.2015, Pleven, Bulgaria, Year XXIII, ISSUE 3(166), April 1015, p.60-63, ISSN: 1310-3946 (In Bulgarian)

6. A. Balevski, Metaloznanie, „Tehnika", Sofia, 1962. (In Bulgarian)

7. M. Borisov, K. Marinova, Uvod vav fizikata na tvardoto tialo, I chast, „Nauka i izkustvo", Sofia, 1977. (In Bulgarian)

8. E. Pavarini, E. Koch, F. Anders, and M. Jarrell (Eds.) Correlated Electrons: From Models to Materials, Autumn School organized by the Forschungszentrum Jülich and the German Research School for Simulation Sciences, 3 – 7 September, 2012. ISBN 978-3-89336-796-2

9. U. Mizutani, Introduction to the electron theory of metals, Cambridge University Press, 2003, ISBN 0 511 01244 6

10. U. Landman, Materials by numbers: Computations as tools of discovery, PNAS, May 10, 2005, vol. 102, no. 19, 6671–6678

11. S. Bushev, Multyscales evaluation structure formation – casting, Proceed. Forth national conference with international participation "Materials science, hydro- and aerodynamics and national security'2014", p.19-23, 23-24, October, 2014, Sofia, Bulgaria

12. S. M. Bushev, Controllability problems of crystallization process in casting, Thesis of PhD, TU, Sofia, 1993.

13. W. B. Jensen, Abegg, Lewis, Langmuir, and the Octet Rule, Journal of chemical education, Volume 61, Num. 3, March, 1984.

14. P. Terpstra, W. J. van Weerden, Graphical methods for the determination of reticular densities and lattice parameters, *www.minsocam.org/ammin/AM19/AM19_531.pdf*

15. E. Dowty, Crystal structure and crystal growth: I. The internal structure on morphology, American Mineralogist, Volume 61, pages 448-459, 1976.

16. I. Sunagava, Growth and morphology of crystals, *Forma*, **14**, 147–166, 1999. Reprinted with permission from Mathematical Sciences, No 358, 1993, (in Japanese)

17. G. Wranglén, Bravais' and Kossel-Stranki's Theories of Homopolar Crystals and their Applications to Elements, Acta Chemica Scandinavica, **9** (1955) 661-676.

18. W. Kossel, Nachr. Ges. Wiss. Göttingen, Math. Phys. K1 11A (1927) 135.

19. I. N. Stranski, Z. Phys. Chem., 136 (1928) 259.

20. I. N. Stranski, and R. Kaischew, *2.* Phys. Chem., (B) 26 (1934) 31

21. M. Volmer, Die Kinetik der Phasenbildung (Steinkopff, Dresden, 1939).

22. W. K. Burton, N. Cabrera, F. C. Frank, Phil. Trans. Roy. Soc., A243 (1951) 299.

23. R. Kaishev, Selected Works, Publishing House of the Bulgarian Academy of Sciences, Sofia, 1980. (In Bulgarian)

24. M. C. Flemings, Solidification processing, Peace, Moscow, 1977. (In Russian)

25. D. Kashchiev, Nucleation: basic theory and application, Butterworth-Heinemann, Oxford, 2000. ISBN 0 7506 4682 9

26. I. Markov, Crystal growth for beginners: fundamentals of nucleation, crystal growth and epitaxy, World Scientific, Singapore, 2004.

27. Crystal growth: Theory and techniques, www.shodganga.inflibnet.ac.in./bitstream/10603/.../08_chapter1.pdf

28. I. Stranski, www.revolvy.co/main/index.php?s=Ivan%20Stranski

29. https://bg.wikipedia.org/wiki/Ростислав_Каишев

30. Stranski, Ivan N.; Krastanow, Lubomir (1938). "Zur Theorie der orientierten Ausscheidung von Ionenkristallen aufeinander". Abhandlungen der Mathematisch-Naturwissenschaftlichen Klasse IIb. Akademie der Wissenschaften Wien. **146**: 797–810

31. A. Popov, Semiconductor materials and structures for nanoelectronics, University Publishing house "St. Kliment Ohridski", Soffia, 2007. ISBN 978-954-07-2539-0 (In Bulgarian)

MESURMENT OF FOUNDRY STRUCTURES – MATHEMATICS

Maneva A., Chief Assistent, PhD, Eng., Bushev S., Associate Professor, PhD, Eng.
Institute of metal science, equipment and technology with hydro- and aerodynamics center "Acad. A. Balevski"
Bulgarian academy of sciences, Sofia 1574, 67 "Shipchenski prohod" Str. Bulgaria Republic
anna13@abv.bg , stbushev@abv.bg

Abstract: Mathematics is a technological necessity for manufacturing but casting in micro-foundry. The need to describe the first-order phase transition process is based on physical experiments with this transition based on theoretical and mathematical physics. The natural basis of any science is the use of mathematics, which is a basic motivation for its self-development.

Keywords: MATHEMATICS, FOUNDRY, MICROSTRUCTURE, INFRASTRUCTUR OF KNOWLEDGE TRANSFER

1. Introduction

The capabilities of foundries and computational mathematics are presented very clearly in Fig. 1

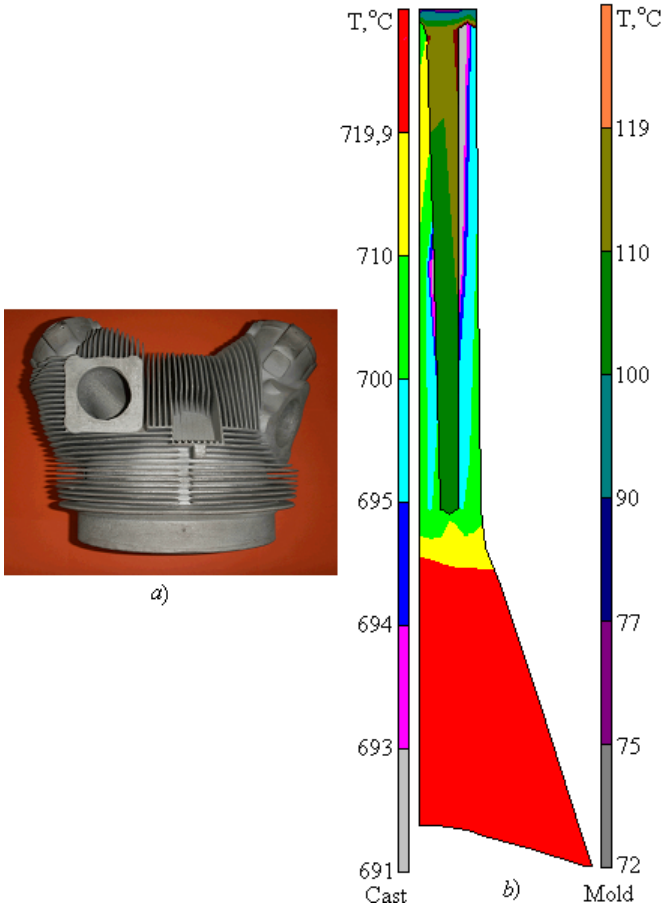

Fig. 1 *The possibilities of die-casting and computational mathematics:a) Cast cylinder head for an aircraft engine produced by the gas counter-pressure process according to [1]; b) Non-stationary temperature field cooling of a local melt volume (rib) and an adjacent local volume of format at the start of a melt cooling process. Computational mathematics allows detailed numerical study of contact heat transfer in volume with complex geometry according to [2]*

This communication presents the need to use computational physics through the necessary software for foundry structures of the meso- level (Quantum Mechanics) and in micro-foundry.

2. Computational physics – foundry structure formation

The structure of metals and alloys at the micro-level we present through the location of the atoms in 2D an ideal crystal lattice composed of Wigner-Seitz cells. By definition, it is well known that the volume of this cell may be located only a single atom. The degree of density of the atomic locations in the crystal lattice is represented by the density of the packing density coefficient in Fig. 2

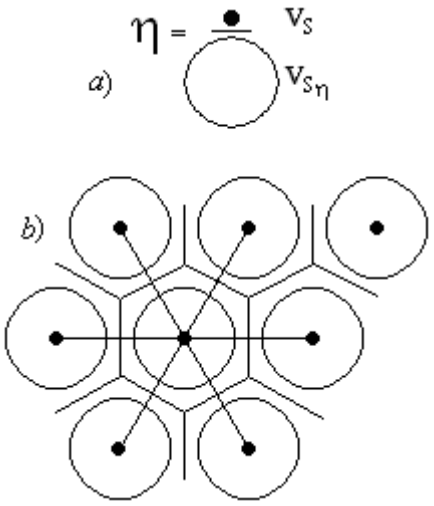

Fig. 2 *Scheme – casting structure of meso- level [3]: a) η – packing density coefficient, v_S – volume of atom, $v_{S\eta}$ – volume of cell, where have only one atom; b) 2D an ideal crystal lattice composed of Wigner-Seitz cells.*

The calculations of the casting structure at the meso-level are carried out at scales of Å and nm. It is well known that a scale of 1 μm is a macro size. The theoretical model [3] includes the tasks: Stephan and Stephan - Schwarz; the atomic level is the model of Kosel-Stranski-Folmer-Kaishev and the basic equation of Kashchiev with variable thermodynamic driving force and thermodynamics of supesaturation (supercooling). This is the classical theory of crystallization, but an important nuance applicable to a certain minimum scale. The classical theory of atomic crystallization is applied to the nuclei of ten atoms through the Kashchiev equation.

In the [4] mathematical theory of heat conduction it is proposed to use these nuclei sizes when it is possible to apply the postulates of quantum mechanics.

M. Borisov makes the main step for metal science by associating it with the physics of the solid body [5]. In particular, it shows „the metal bond" and the need for quantum mechanics in the engineering of metals and alloys. It should not be forgotten that quantum mechanics arises to describe the properties of metals - Drude's theory.

In the textbook of U. Mizutani is presented the electronic theory of metals [6]. Electrons are responsible for the physical, chemical and transport properties of metals. This textbook gives a complete account of electron theory in both periodic and non-periodic metallic systems.

At the Correlated Electrons: From Models to Materials Conference [7], mathematical modeling and simulation of correlated electrons in the electronic structure of quantum systems in materials is presented.

Def. Electronic correlation is the interaction between electrons in the electronic structure of a quantum system.

Work [8] presents the capabilities of computational physics as a research tool especially and for nano-sized materials. This work has a methodological significance.

Opportunities for observation and measurement of structures of electron microscopy materials are known. At work [9], single atom observation and a specific defect are presented in a 3D aberration-corrected electron microscope, with information being limited to 0.5-Å.

Let us summarize: Fundamental knowledge is needed directly in the details of the market in the particular consideration these are micro-foundries. Knowledge requires specification of the specific requirements for each manufacturer.

3.1 Computational physics in Materialscience

The theory of metals [10] spreads us to the physics of the solid body [5]. The phase transition from the first order creates the structure that carries the working properties of each cast. The description of the first-order phase transition processes requires scientific areas: the classical theory of crystal growth in the present state; quantum mechanics, which is used to describe the chemical bond and structures.

The types of solids according to the chemical bond in the crystal lattice are 5: ionic crystals; valent crystals; metals; molecular crystals. The metallic connection [5]: the crystal lattice is made up of positive ions, the repulsive forces between them being equalized by the free electrons. The description of the chemical bond is obtained after the decision of the amplitude wave equation of Schrödinger we show no relativistic time-dependent (Schrödinger, 1, 2) and time-independent (Schrödinger, 3, 4) view

$$i\hbar\frac{\partial\psi(r,t)}{\partial t}=\left[\frac{-\hbar^2}{2\mu}\nabla^2+V(r,t)\right]\psi(r,t), \quad \text{(Schrödinger, 1 and 2)}$$

$$i\hbar\frac{\partial\psi(r,t)}{\partial t}=\hat{H}\psi(r,t)$$

$$\left[\frac{-\hbar^2}{2\mu}\nabla^2+V(r)\right]\psi(r)=E\psi, \quad \text{(Schrödinger, 3 and 4)}$$

$$\hat{H}\psi(r)=E\psi$$

where ħ - Planck's constant; μ – particle reduced mass; ∇^2 is the Laplacian; ψ is wave function; $\hat{H}$ – Hamiltonian operator; V - potential energy; E – energy of the state ψ.

For real crystals it is necessary to describe the defects [5]: Schottky (1), Frenkel (2) and dislocations (3)

$$p=\frac{Z!}{(Z-x)!x!}, \quad (Schottky) \qquad \text{(Points Defects)}$$

$$x=\sqrt{ZZ'}\exp\left(-\frac{E_2}{2kT}\right), \quad (Frankel)$$

where Z – total number of atoms occupying places in the crystal lattice; Z' – number of gaps in the crystal lattice; p – Schottky's defects; x – Frenkel's defects; E_2 – the energy of the atom to pass from its normal to the intermediate state of the crystal lattice, k and T – Boltzmann's constant and temperature; Degression of ionic crystals from the ideal crystal lattice and the stoichiometric ratio by two parameters [5]: Degree of deviation of ionic crystals from the ideal crystal lattice and stoichiometric ratio by two parameters: μ – degree of deviation of the actual grid from the ideal, ν – degree of deviation from the stoichiometric ratio and criteria for observing the stoichiometric number

$$\mu = (Y_M/Z_M+X_R/Z_R) + (X_M/Z_M+Y_R/Z_R) \quad \text{(Grid deviation)}$$

$$\nu = (Y_M/Z_M+X_R/Z_R)–(X_M/Z_M+Y_R/Z_R) \quad \text{(Stoich. ratio deviation)}$$

$$\nu = N_M/Z_M – N_R/Z_R, \quad \text{(Stoichiometric ratio criteria)}$$

where X_M and X_R are the number of cations and anions vacantions; Y_M and Y_R – the number of ions and metal and the metalloid in the gaps; Z_M and Z_R – the total number of metal and metalloid ion sites in the ideal crystal lattice; N_M and N_R – the total number of metal and metalloid ions in the ideal crystal lattice. Example [5]: Let the crystal lattice consist of (m) the number of metals (M) and (r) the number of metalloid (R) ions and the grid composition and that of the molecules of the substance being determined by the formula M_mR_r. (Grid and molecules formula)

In pure ionic relation m/r = p/q, where p and q are the charges of the positive and negative ion in elementary electric charges.

There are various combinations of point defects in crystal crystals of ionic crystals [5]. For example, [5]: anion vacation with a connected electron called the F-center; pair adjacent in the direction $[e_1e_2e_3]$ the F-center (M-center); triple adjacent to the plane $(e_1e_2e_3)$ the F-center (P-center), etc.

Other defects in the lattices of real crystals are dislocations [5, 10]. This term means a heterogeneous elastic strain centered on a line to explain the plasticity properties of the crystals. The two simplest dislocations are threshold and screw. *Threshold dislocation* [5, 10] is characterized by the presence of an "excess" atomic plane in a part of the crystal lattice. *Screw dislocations* [5, 10]. Crystal in the form of a cylinder with a height H and a radius r is cut in a plane defined by the height ... and the radius ... and is perpendicular to the two bases. Then the two crystal parts are slid against each other along the plane of cut, with the outer parallel to the height side being offset at a distance equal to the Burger's $\vec{b}$ vector. Finally [5], the two parts of the crystal are glued and the outer forces are removed again. As a result, a non-uniform deformation, centered on the center height of the cage, occurs. As a result, a non-uniform deformation, centered on the center height of the cage, occurs. As a result of the screw dislocation the family of parallel crystallographic planes, perpendicular to the axis of the screw dislocation. When only one screw dislocation occurs, growth is due only to it, because it is much more energy efficient. Random dislocations in crystal lattices [5]: In general, the line of dislocation is a random curve, and the "sliding plane" is an arbitrary spatial surface. Dislocation defects: *energy* of dislocations such as a hollow cylinder (Dis. Def. 1), occurrence of *threshold* dislocation (or *movement*) (Dis. Def. 2), *interaction* of two dislocations (Dis. Def. 3)

$$E_S \approx \int_0^{2\pi}\int_{r_0}^{r_\infty}\frac{1}{r^2}rdrd\vartheta=2\pi\ln\frac{r_\infty}{r_0}, \quad \text{(Dis. Def., 1, 2, 3)}$$

$$F=\tau\vec{b},$$

$$dW\approx(\tau_1+\tau_2)^2=(\tau_1^2+2\tau_1\tau_2+\tau_2^2),$$

where E_S – energy of dislocations; r_∞ and r_0 – outer and inner radius of dislocation; F – force for occurrence of threshold dislocation; τ – the limit voltage required for plastic deformation of the crystal sliding; $\vec{b}$ – vector of Bürges; τ_1^2 and τ_2^2 – the energies of the individual deformations; $2\tau_1\tau_2$ – the energy of their interaction.

Crystal lattice of the alloys [5 and 10]: Metal alloys can be regarded as the simplest chemical compounds. They are solid solutions which can be obtained by replacing the atoms of the crystal lattice of one metal with other metal alloys or by introducing atoms of the second metal between the atoms of the crystal lattice of the parent metal.

The shortest can be said that work [5] is the development of work [10] in the direction of fundamental knowledge of foundry. This is confirmed by the current state of economic development - **the fourth industrial revolution**.

Summary: Fundamental knowledge is needed directly by the market-makers who are the micro-foundries. Knowledge requires specific specification for each manufacturer, which has to be

implemented by a specific infrastructure – such as R. Georgiev's office [14] for transfer of knowledge presented in Fig. 3

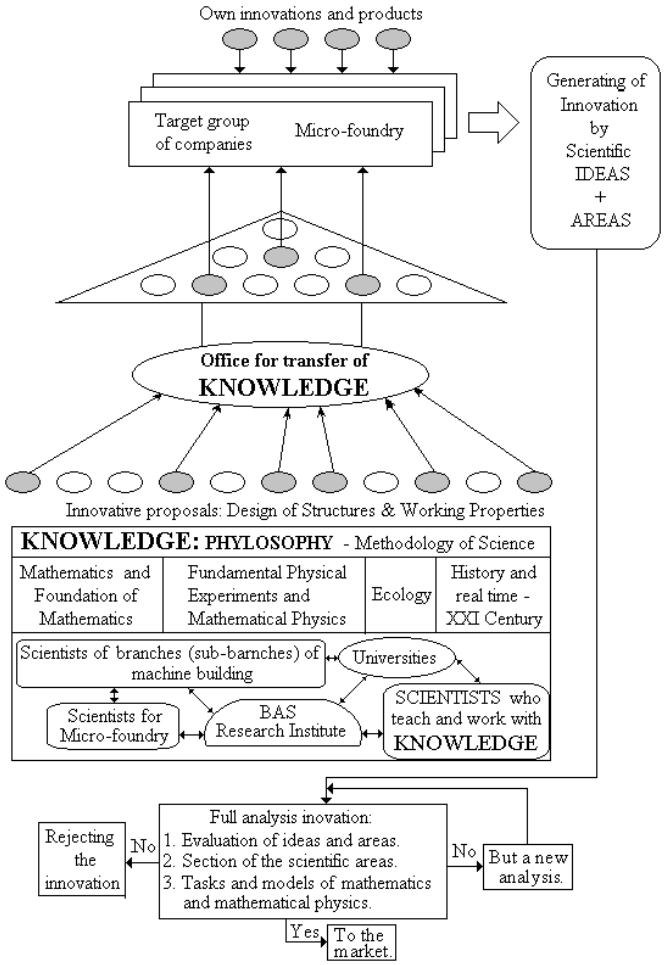

Fig. 3 *Principle scheme of Georgiev's office of knowledge transfer to innovation the subject of cast technology – Design of structures & Working properties. Knowledge: philosophy – methodology of science of: Mathematics and Foundation of mathematics; Fundamental experiments and Mathematical Physics; Ecology; History and real time of XXI century; Scientists, who teach and work with knowledge; Institutions - Universities and thoroughly Researches Institutes of the Bulgarian academy of sciences; Business branches; Office for transfer of knowledge; full knowledge are whites and innovations ideas + areas of our transfer are the grays; Target group of companies; Full analysis of generated innovation – micro-foundry [14].*

Date for phase transition of first order in foundry process:

Experiment and measurements: Alloy composition; Obtaining the alloy – fresh or using secondary alloys; Phase transition process of first order: melting; casting – thinness, degassing; pour temperatures, temperature range transferred to the melt; temperature interval of filling the mold cavity; true phase transition – precise thermocouple measurement of the hardening temperature field; Differential thermal analysis – solidification of the alloy in small volume; obtained polycrystalline structure – micro-, macro-grinding and medium grain diameter; measuring the temperature field of solidification in a large volume – an experimental task of Stefan-Schwarz.

Phase Transition Process of First Generation: Classical Theory of Crystal Growth – Mechanism; Contemporary Description Quantum Mechanics - Postulates; The polycrystalline structure of the cast material: mean grain diameter; Crystal lattice - parameters; A full description of the properties of the solid in the alloy, i.e. the working properties of the castings.

Scientific areas related to the description of the processes of formation of the structures of new phases Meso-level is **Quantum mechanics**. Nano-level are: **Quantum nanoscience** [11] is the research area and the branch of nanotechnology and physics that uses methods of quantum mechanics to the design of new types of nanodevices and nanoscale materials, where functionality and structure of quantum nanodevices are described through quantum phenomena and principles such as discretisation, superposition and entanglement; **Nanomechanics** [12] is a branch of *nanoscience* studying fundamental *mechanical* (elastic, thermal and kinetic) properties of physical systems at the nanometer scale. Nanomechanics has emerged on the crossroads of classical mechanics, solid-state physics, statistical mechanics, materials science, and quantum chemistry. As an area of nanoscience, nanomechanics provides a scientific foundation of nanotechnology.

On the basis of work [14], the data on the micro - foundry are presented on Fig. 4

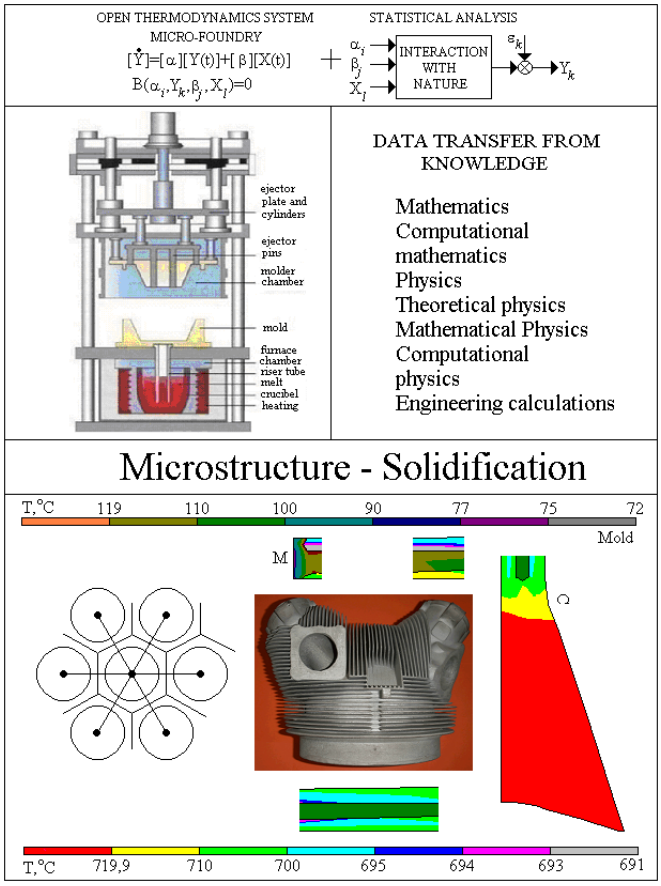

Fig.4 *Date from Knowledge transfer to Ecology–economics complex of "Smart Micro-foundry" for Phase transition of first order in Gas counter pressure casting method – Industry 4*

Micro-foundry is Open Thermodynamics System (OTS) is describe by stochastic differential equation in the subject of Ito – Stratonovich, which introduce transformation input materials and energies flows, where matrixes α_i, β_j – physical and constructive parameters, and i, j =1,…, m; matrixes column X(t), Y(t) – input, output parameters, and k, l = 1,…n; equation B is operator of controllability of OTS, which is support in zero by change of some parameters of control ; Statistical analysis ε_k – ecological complexity interaction micro-foundry with nature , Date transfer from office to micro-foundry.

It is clear that the information interesting for the particular technology should use the infrastructure (see Figure 3) and economic restructuring through serious investments such as the change – INDUSTRY 4.0. Filtering the necessary information is only possible through mathematics.

The methodology is work-based [8]: software for computing physics is continually being created by a new one based on the development of mathematics. Using mathematics to describe the meso-level is working [6, 7 and 8].

An example of the role of mathematics in quantum mechanics is work [13]. From the works [6, 7, 8 and 13] follows that every

question posed by a physical experiment passes a long and complicated mathematical interaction with theoretical and mathematical physics.

Measurements of example structures are works [9 and 15]. It has long been known to see the bottom, according to Feynman [15], the development of measuring instruments follows the development of the necessary technological possibilities, non-standard creation of equipment. A direct example of Bulgarian participation is a work [9], electron microscope with optimized aberration and monochromatic source with high brightness is a significant resolution of the instrument and contrast. Achieved is an information limit of 0.5-Å (angstrom).

Finally, in this paragraph, we need to say that a macro-level (solidification) relation and meso-level (quantum mechanics) is mathematics.

3. Conclusion

Mathematics is a complex technological necessity in the field of education and knowledge transfer infrastructure.

4. Reference

1. Y. Arsov, E. Momchilov, K. Daskalov, G. Bachvarov, Theoretical and technological fundamentals of gas counter-pressure casting, “Prof. Marin Drinov” Academic publishing house, Sofia, 2017.

2. A. Maneva, S. Bushev, Numerical simulation temperature field in solidification, Proceed. Fourth national conference with international participation “Materials science, hydro- and aerodynamics and national security’2014”, 23-24, October, 2014, Sofia, ISSN 1313-8308

3. S. Bushev, Theoretical model of structureformation in die casting, XXII International scientific technical conference “FOUNDRY 2015”, 16-17.04.2015, Pleven, Bulgaria, Year XXIII, ISSUE 3(166), April 2015, p.60-63, ISSN: 1310-3946 (In Bulgarian)

4. S. Bushev, Casting – micro-models, XXIV International scientific technical conference “FOUNDRY 2017”, 5-7.04.2017, Pleven, Bulgaria, Year I, ISSUE 1(1), p.68-70, Publisher: Scientific technical union of mechanical engineering “INDUSTRY-4.0”. ISSN: 2535-017X

5. M. Borisov, K. Marinova, Uvod vav fizikata na tvardoto tialo, I chast, „Nauka i izkustvo”, Sofia, 1977. (In Bulgarian)

6. U. Mizutani, Introduction to the electron theory of metals, Cambridge University Press, 2003, ISBN 0 511 01244 6

7. E. Pavarini, E. Koch, F. Anders, and M. Jarrell (Eds.) Correlated Electrons: From Models to Materials, Autumn School organized by the Forschungszentrum Jülich and the German Research School for Simulation Sciences, 3 – 7 September, 2012. ISBN 978-3-89336-796-2

8. U. Landman, Materials by numbers: Computations as tools of discovery, PNAS, May 10, 2005, vol. 102, no. 19, 6671–6678

9. C. Kisielowski, B. Freitag, M. Bischoff, H. van Lin, S. Lazar, G. Knippels, P. Tiemeijer, M. van der Stam, S. von Harrach, M. Stekelenburg, M. Haider, S. Uhlemann, H. Müller, P. Hartel, B. Kabius, D. Miller, I. Petrov, E. A. Olson, T. Donchev, E.A. Kenik, A.R. Lupini, J. Bentley, S.J. Pennycook, I.M. Anderson, A.M. Minor, A.K. Schmid, T. Duden, V. Radmilovic, Q.M. Ramasse, M. Watanabe, R. Erni, E.A. Stach, P. Denes, U. Dahmen, Detection of Single Atoms and Buried Defects in Three Dimensions by Aberration-Corrected Electron Microscope with 0.5-Å Information Limit, Microscopy and Microanalysis 14, 454–462, 2008. doi: 10.1017/S1431927608080902

10. A. Balevski, Metaloznanie, „Tehnika”, Sofia, 1962. (In Bulgarian)

11. https://en.wikipedia.org/wiki/Quantum_nanoscience

12. https://en.wikipedia.org/wiki/Nanomechanics

13. M. Ohta, Strong instability of standing waves for nonlinear Schrëodinger equations with a harmonic potential, H. Kubo, T. Ozawa, H. Takamura, Organizers of Conference Mathematical Analysis for Stability in Nonlinear Dynamics in honor of Professor Vladimir Georgiev on his 60th birthday, August,2016, Faculty of Science, Hokkaido University August 24 – 26, 2016. Series #167.

http://eprints3.math.sci.hokudai.ac.jp/view/type/techreport.html

14. S. Bushev, Knowledge transfer industry 4, International scientific journal Industry 4.0, Nm 4, p.51-54, 2016, Year I, ISSUE 1/2016, ISSN 2543-8582

15. R. P. Feynman, There’s plenty of the room at the bottom, (1959), http://caltech.library.caltech.edu/47/2/1960Bottom.pdf

ROBUST DESIGN AND MULTIPLE CRITERIA OPTIMIZATION OF ELECTRON BEAM GRAFTING OF CORN STARCH

Assoc. Prof. M.Sc. Eng. Koleva E. PhD.[1,2], M.Sc. Eng. Koleva L. [2], M.Sc. Eng. Nemțanu M.R. PhD.[3], M.Sc. Brașoveanu M. PhD.[3]
Institute of Electronics, Bulgarian Academy of Sciences, Bulgaria [1]
University of Chemical Technology and Metallurgy, Bulgaria [2]
National Institute for Lasers, Plasma and Radiation Physics, Electron Accelerators Laboratory, Romania [3]

eligeorg@abv.bg

Abstract: *Electron beam (EB) irradiation has the ability to modify polymer substrates by process of graft copolymerization to synthesize water-soluble copolymers having flocculating potential. Models - depicting the dependencies of the described quality characteristics (their means and variances) from process parameters - are estimated by implementation of the robust engineering methodology for quality improvement. Multiple criteria optimization based on the desirability function approach, involving requirements for economic efficiency, assurance of low toxicity, high copolymer efficiency in flocculation process, good solubility in water, bias, robustness, quality of prediction and the relative importance of responses, is presented.*

Keywords: GRAFT COPOLYMERIZATION, ELECTRON BEAM IRRADIATION, WATER-SOLUBLE COPOLYMERS, STARCH, ACRYLAMIDE, RESPONSE SURFACE METHODOLOGY

1. Introduction

The model-based robust approach for improving the quality of the process [1, 2] can be successfully applied to different industrial processes. For each of the quality performance characteristics, using their regression models, two other models are estimated - for their mean values and variances. The quality improvement is performed using some overall criterion or simply by the performance characteristics variances minimization, while keeping their mean values close to their target values. The Robust Parameter Design (RPD) is an issue of numerous papers in the literature since 1990 [3, 4], but there are much less of them in the area of application of RPD [1, 5] for multiple responses. Some of these articles consider the multi-response case, when replicated observations are available [6], while others are focused on formulation of appropriate optimization criteria. A systematic procedure implementing response surface methodology and desirability function for optimization of multiple response surface (MRS) problems that accommodates all of bias, robustness and quality of prediction besides relative importance of responses in a single framework is developed in [7] and compared with other multiple response techniques.

Electron beam (EB) grafting is a process of modification of polymer substrates implementing radiation-induced graft copolymerization in order to yield water-soluble copolymers having flocculation abilities [8]. The irradiation was performed with linear electron accelerator of mean energy of 5.5 MeV, and the influence of the variation of the following parameters: acrylamide/starch (AMD/St) weight ratio, electron beam irradiation dose and dose rate was investigated. The characterization of graft copolymers was carried out by monomer conversion coefficient, %; residual monomer concentration, %; intrinsic viscosity, dL/g; and Huggins' constant.

In this paper the robust parameter design methodology is applied for estimation of models, describing the dependencies of the means and the variances of the investigated quality characteristics. Multiple criteria optimization based on the desirability function approach, involving requirements for economic efficiency, assurance of low toxicity, high copolymer efficiency in flocculation process, good solubility in water, bias, robustness, quality of prediction and the relative importance of responses, is presented.

2. Robust parameter design

EB modification of polymer substrates through radiation-induced graft copolymerization is generally used to develop a wide variety of ion exchangers, polymer-ligand exchangers, chelating copolymers, hydrogels, affinity graft copolymers and polymer electrolytes, having various applications in water treatment, chemical industry, biotechnology, biomedicine, etc. [9, 10].

The synthesized graft copolymers were characterized [8] by the following performance quality parameters: y_1 [%] - residual monomer concentration, y_2 [%] - monomer conversion coefficient, y_3 [dL/g] - intrinsic viscosity and y_4 - Huggins' constant. The variation regions [z_{min}-z_{max}] of the process parameters were: EB irradiation dose (z_1) – [0.64 - 1.44 kGy]; the EB irradiation dose rate (z_2) – [0.45 - 1.40 kGy/min] and the (AMD/St) weight ratio (z_3) – [5.00 - 10.02]. The concentration of St for these experiments varies from 2.00% to 6.15% and the concentration of AMD varies from 10.00% to 33.67%.

The conducted experimental design consisted in 20 experimental process parameter sets [8]. For each set of the process parameters three replicated measurements were used for estimation of the means and the variances of the quality characteristics of the graft copolymers. The estimated values of the means $\bar{y}_u$ and the variances s_u^2 can be considered as two responses at the design points and ordinary least squares method can be used to fit regression models for the mean value and for the variance for each quality characteristic [1]:

$$\tilde{\bar{y}}(\vec{x}) = \sum_{i=1}^{k_y} \hat{\theta}_{yi} f_{yi}(\vec{x})$$

$$\ln\left(\tilde{s}^2(\vec{x})\right) = \sum_{i=1}^{k_\sigma} \hat{\theta}_{\sigma i} f_{\sigma i}(\vec{x}),$$

where $\hat{\theta}_{yi}$ and $\hat{\theta}_{\sigma i}$ are estimates of the regression coefficients, and f_{yi} and $f_{\sigma i}$ are known functions of the process parameters x_i. The variance of normally distributed observations has a χ^2-distribution. The use of the logarithm transformation of the variance function makes it approximately normally distributed, which improves the efficiency of the estimates of the regression coefficients.

The response surfaces models for the mean and standard deviation of the quality characteristic are estimated and presented in Table 1 for coded values of the process parameters in the region [-1÷1]. The coding of the process parameter values is done, using the following equation:

$$x_i = (2z_i - z_{i,\max} - z_{i,\min})/(z_{i,\max} - z_{i,\min})$$

where x_i and z_i are the coded and the natural values of the process parameter, correspondingly, $z_{i,min}$ and $z_{i,max}$ are the minimal and the maximal values of the parameter experimental variation region.

Table 1: *Models for the means and variances of the product quality characteristics*

Parameter	Models	R^2	w'
$\tilde{\bar{y}}_1(\vec{x})$	$1.8416958 - 1.4711672x_1 + 0.39465799x_2 + 0.76523861x_1^2 - 1.4618933x_1x_2$	0.8172	0.1652
$\tilde{\bar{y}}_2(\vec{x})$	$89.612983 + 6.1859389x_1 + 2.921934x_3 + 5.2145372x_2^2 - 2.1297402x_1x_3$	0.7415	0.1499
$\tilde{\bar{y}}_3(\vec{x})$	$4.2786392 - 0.95051438x_2 + 2.2118238x_3 + 1.2412826x_2^2 - 7.0991376x_1^2x_2 + 0.721455x_2x_3 - 1.2935142x_1^2x_3$	0.7921	0.1602
$\ln(\tilde{\bar{y}}_4(\vec{x}))$	$0.86268086 + 1.5188592x_2 - 1.6109201x_3 + 0.87526587x_1x_3 - 1.6469938x_2x_3 + 1.4461714x_1^2x_3$	0.6191	0.1252
$\ln(\tilde{s}_1^2(\vec{x}))$	$-3.0237265 - 0.60469566x_2 - 1.0612263x_3 - 4.3482641x_1^2 - 4.2402799x_2^2 + 5.604919x_1x_2 - 2.2657548x_2x_3$	0.7179	0.1451
$\ln(\tilde{s}_2^2(\vec{x}))$	$0.09316988 - 1.0210062x_2 - 1.7785371x_3 - 4.6387008x_1^2 - 4.9999832x_2^2 + 6.047145x_1x_2 - 2.242544x_2x_3$	0.7550	0.1527
$\ln(\tilde{s}_3^2(\vec{x}))$	$-2.5452688 - 0.67825221x_3 - 2.7034767x_1^2 - 2.1048188x_2^2 + 3.2229606x_1x_2 + 0.88934159x_2^2x_3$	0.5028	0.1017

Table 2: *Specification regions and target values for the mean values and the standard deviation of response variables*

Bounds	$\tilde{\bar{y}}_1(\vec{x})$	$\tilde{\bar{y}}_2(\vec{x})$	$\tilde{\bar{y}}_3(\vec{x})$	$\tilde{\bar{y}}_4(\vec{x})$	$\tilde{s}_1^2(\vec{x})$	$\tilde{s}_2^2(\vec{x})$	$\tilde{s}_3^2(\vec{x})$
lb	0	90	6	0.3	0	0	0
ub	5	100	9	1	0.2	1.8	0.6
τ	smaller	larger	larger	0.6	smaller	smaller	smaller

In Table 1 the estimated response model's quality of prediction is measured by the squared multiple correlation coefficient R^2.

3. Desirability function approach

An approach for optimization of multiple responses simultaneously is combining them into a single function. The desirability technique analysis is presented by Derringer and Suich [11]. This approach includes systematic transform of the quality characteristic $\tilde{\bar{y}}_j(\vec{x})$ into individual desirability function $d_j(\vec{x})$, calculated depending on the optimization tasks:

- cases with defined target values:

$$d_j(\vec{x}) = \begin{cases} \dfrac{\tilde{\bar{y}}_j(\vec{x}) - lb_j}{\tau_j - lb_j}; & lb_j \le \tilde{\bar{y}}_j(\vec{x}) \le \tau_j \\ \dfrac{\tilde{\bar{y}}_j(\vec{x}) - ub_j}{\tau_j - ub_j}; & \tau_j < \tilde{\bar{y}}_j(\vec{x}) \le ub_j \\ 0; \quad \tilde{\bar{y}}_j(\vec{x}) < lb_j \ \ or \ \ \tilde{\bar{y}}_j(\vec{x}) > ub_j \end{cases}$$

- cases the larger the better:

$$d_j(\vec{x}) = \begin{cases} 0; & \tilde{\bar{y}}_j(\vec{x}) \le lb_j \\ \dfrac{\tilde{\bar{y}}_j(\vec{x}) - lb_j}{ub_j - lb_j}; & lb_j < \tilde{\bar{y}}_j(\vec{x}) \le ub_j \\ 1; & \tilde{\bar{y}}_j(\vec{x}) \ge ub_j \end{cases}$$

- cases the smaller the better:

$$d_j(\vec{x}) = \begin{cases} 1; & \tilde{\bar{y}}_j(\vec{x}) \le lb_j \\ \dfrac{ub_j - \tilde{\bar{y}}_j(\vec{x})}{ub_j - lb_j}; & lb_j < \tilde{\bar{y}}_j(\vec{x}) < ub_j \\ 0; & \tilde{\bar{y}}_j(\vec{x}) \ge ub_j \end{cases}$$

In this way the individual optimization desirability functions of the mean values of each response (d_{oj}) scaled in the region between 0 and 1 can be calculated, together with the individual robustness desirability functions (d_{rj}) [7]. Here lb_j and ub_j are the minimal and the maximal acceptable levels for the mean responses and the standard deviations, τ_j is the target or the desirable value of the *j*-th quality characteristic (Table 2). The robustness here refers to the low sensitivity of the quality characteristics to the noise factors. This can be achieved by a proper selection of values for the controllable process parameters, and can lead to a reduction for variance of the response in production conditions.

For the consideration of robustness in multiple response optimization problems, the following measures are defined [7]:

- Optimization desirability function D_{opt}, defined as the weighted geometric average of the individual optimization desirability functions:

$$D_{opt}(\vec{x}) = d_{o1}(\vec{x})^{w_{1\mu}} \ d_{o2}(\vec{x})^{w_{2\mu}} \ \dots \ d_{om}(\vec{x})^{w_{m\mu}};$$

- Robustness desirability function D_{rob}, defined as the weighted geometric average of the individual robustness desirability functions:

$$D_{rob}(\vec{x}) = d_{r1}(\vec{x})^{w_{1\sigma}} \ d_{r2}(\vec{x})^{w_{2\sigma}} \ \dots \ d_{rm}(\vec{x})^{w_{m\sigma}};$$

A multi-response optimization problem requires an overall optimization, i.e. simultaneous satisfaction with respect to the mean and standard deviation of all of the quality characteristics by using a combined desirability function between optimization and robustness. The overall desirability function can be defined as follows:

$$D_{overall}(\vec{x}) = D_{opt}(\vec{x})^{w_{opt}} \ D_{rob}(\vec{x})^{w_{rob}}.$$

In order to formulate weights for a given magnitude of predictive capability, a relationship between the weights and a predictive capability index (squared multiple correlation coefficient, R^2) is needed (see Table 1):

$$w'_j = \frac{R_j^2}{\sum R_j^2}.$$

4. Optimization results and discussion

The overall desirability function in the considered EB induced synthesis of graft copolymers is calculated by:

$$D_{overall}(\vec{x}) = d_{o1}(\vec{x})^{w_{1\mu}} \ d_{o2}(\vec{x})^{w_{2\mu}} \ d_{o3}(\vec{x})^{w_{3\mu}} \ d_{o4}(\vec{x})^{w_{4\mu}} \ d_{r1}(\vec{x})^{w_{1\sigma}} \ d_{r2}(\vec{x})^{w_{2\sigma}} \ d_{r3}(\vec{x})^{w_{3\sigma}}$$

The acceptable specification regions and the type of the case for the individual desirability functions (target value, the larger the better, the smaller the better) are presented in Table 2.

Desirability functions are formulated for several cases:

Case 1: Without consideration of the models predictive capabilities, the weights w_j are their optimization and robustness geometric average degrees:

$w_{o1} = w_{o2} = w_{o3} = w_{o4} = 1/4$ and $w_{r1} = w_{r2} = w_{r3} = 1/3$; $w_{opt} = w_{rob} = ½$.

Case 2: With consideration of the models predictive capabilities, the weights w_j' are calculated in Table 1.

Case 3: Without consideration of the models predictive capabilities the weights w_j are calculated, considering the mean and variances as equivalent functions by their geometric average degrees:

$w_{o1} = w_{o2} = w_{o3} = w_{o4} = w_{r1} = w_{r2} = w_{r3} = 1/7$;

Case 4: Without consideration of the models predictive capabilities, the weights w_j are equal [7]:

$w_{o1} = w_{o2} = w_{o3} = w_{o4} = w_{r1} = w_{r2} = w_{r3} = 1$, $w_{opt} = w_{rob} = 1$.

Table 3: *Optimal individual and overall desirability functions*

Case	z_1	z_2	z_3	d_{o1}	d_{o2}	d_{o3}	d_{o4}	d_{r1}	d_{r2}	d_{r3}	$D_{overall}$
1	1.3800	0.45	7.7108	0.6016	1	1	0.9990	0.9964	0.9988	0.9843	0.9351
2	1.3560	0.45	7.7359	0.6165	0.9826	1	0.9980	0.9947	0.9982	0.9802	0.9176
3	1.3760	0.45	7.7108	0.6042	1	1	0.9960	0.9962	0.9988	0.9836	0.9271
4	1.3760	0.45	7.7108	0.6042	1	1	0.9960	0.9962	0.9988	0.9836	0.5889

Table 4: *Optimal values of the means and variances of the product quality characteristics*

Case	$\tilde{\bar{y}}_1(\vec{x})$	$\tilde{\bar{y}}_2(\vec{x})$	$\tilde{\bar{y}}_3(\vec{x})$	$\tilde{\bar{y}}_4(\vec{x})$	$\tilde{s}_1^2(\vec{x})$	$\tilde{s}_2^2(\vec{x})$	$\tilde{s}_3^2(\vec{x})$
1	1.9920	100.00	21.9203	0.6004	0.00072	0.0024	0.0094
2	1.9173	99.83	20.5134	0.6008	0.0011	0.0032	0.0119
3	1.9792	100.00	21.6812	0.5988	0.00077	0.0022	0.0098
4	1.9792	100.00	21.6812	0.5988	0.00077	0.0022	0.0098

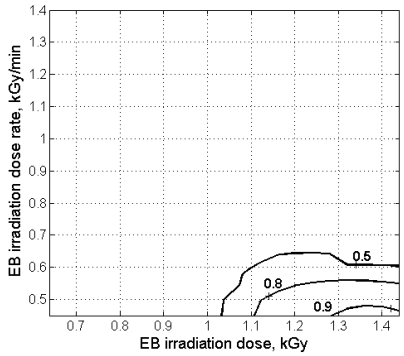

Fig. 1 *Overall desirability function as a function of the process parameters EB irradiation dose (z_1) and the EB irradiation dose rate (z_2) at (AMD/St) weight ratio z_3 = 7.7108 – case 3.*

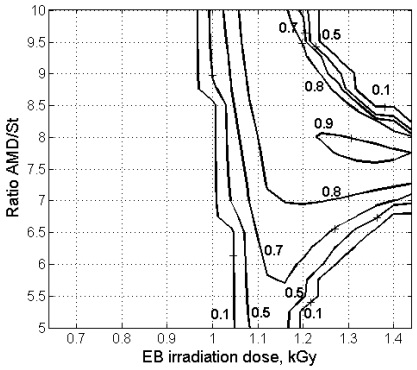

Fig. 2 *Overall desirability functions as a function of the process parameters EB irradiation dose (z_1) and (AMD/St) weight ratio (z_3) at EB irradiation dose rate z_2 = 0.45 kGy/min – case 3.*

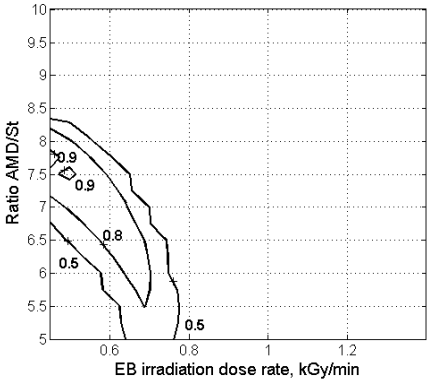

Fig. 3 *Overall desirability functions, as a function of the process parameters EB irradiation dose rate (z_2) and (AMD/St) weight ratio (z_3) at EB irradiation dose z_1 = 1.38 kGy – case 3.*

In Table 3 the individual (d_i) and overall desirability functions $D_{overall}$ are presented for the four considered cases, together with the obtained optimal process parameter values. The corresponding values of the estimated means and variances of the performance characteristics are shown in Table 4. It can be seen that there are no considerable differences in the obtained optimal process parameters and the means and variances of the quality characteristics, despite the differences in the calculated optimal overall desirability function values.

Fig. 1 – Fig. 3 display the contour plots of the overall desirability function as a function of different combinations of the process parameters: EB irradiation dose (z_1), the EB irradiation dose rate (z_2) and (AMD/St) weight ratio (z_3) for case 3.

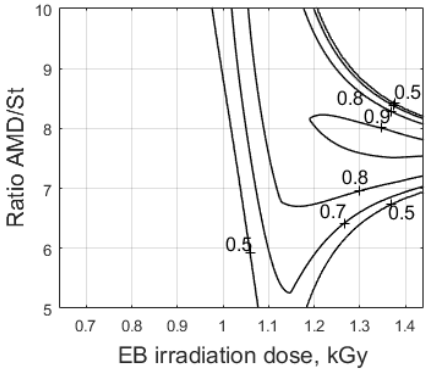

Fig. 4 *Overall desirability functions as a function of the process parameters EB irradiation dose (z_1) and (AMD/St) weight ratio (z_3) at EB irradiation dose rate z_2 = 0.45 kGy/min – case 1.*

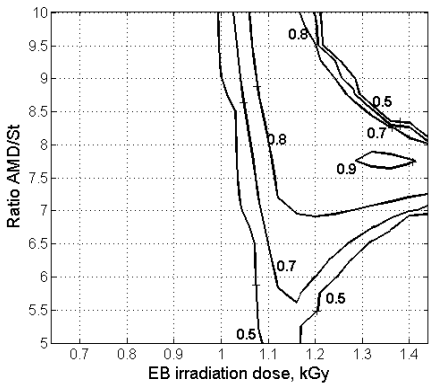

Fig. 5 *Overall desirability functions as a function of the process parameters EB irradiation dose (z_1) and (AMD/St) weight ratio (z_3) at EB irradiation dose rate z_2 = 0.45 kGy/min – case 2.*

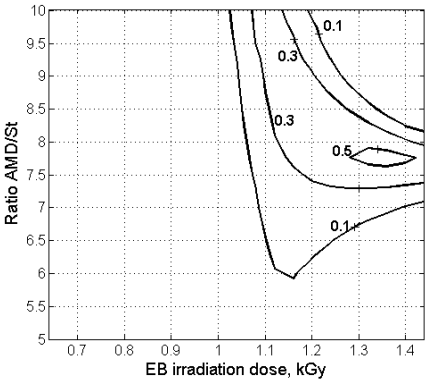

Fig. 6 *Overall desirability functions as a function of the process parameters EB irradiation dose (z_1) and (AMD/St) weight ratio (z_3) at EB irradiation dose rate z_2 = 0.45 kGy/min – case 4.*

Fig. 4 – Fig. 6 represent the contour plots of the overall desirability function as a function of the process parameters EB irradiation dose (z_1) and (AMD/St) weight ratio (z_3) at a constant value of the EB irradiation dose rate z_2 = 0.45 kGy/min for case 1, case 2 and case 4.

5. Conclusions

A multiple response optimization approach, based on overall desirability function, which considers the robustness as well as optimization of the process parameters at production conditions, is considered. Robustness and optimization desirability functions are calculated by evaluation of individual desirability functions of the means and variances of the product quality characteristics. The applied approach gives possibility to use weights for adjustment of the desirability functions according to the quality of model prediction and in favor of robustness or multiple response optimization.

Electron beam induced graft copolymerization used to synthesize water-soluble copolymers having flocculation abilities is investigated. The parameter optimization is performed in direction of fulfilling requirements for economic efficiency, assurance of low toxicity, high copolymer efficiency in flocculation process, good solubility in water, bias, robustness, quality of prediction and the relative importance of the quality characteristics.

Acknowledgements

This research was conducted under bilateral joint project between the Institute of Electronics at Bulgarian Academy of Sciences and the National Institute for Lasers, Plasma and Radiation Physics at the Romanian Academy. This work was also partially supported by a grant of the Romanian National Authority for Scientific Research, CNDI–UEFISCDI, project number 64/2012.

References

[1]. Vuchkov I. N, Boyadjieva L. N. Quality improvement with design of experiments, The Netherlands, Kluwer Academic Publishers, 2001.
[2]. Koleva E., I. Vuchkov, Model-based approach for quality improvement of EBW applications in mass production, Vacuum 77, 2005, pp. 423-428.
[3]. Box G., S. Jones. Designing Products that are robust to the Environment. Quality and Productivity Report 56 Univ. of Wisconsin, CPQI, 1990.
[4]. Vining G. G., R. H. Myers. Combining Taguchi and Response Surface Philosophies; A Dual-Response Approach. Journal of Quality Technology, 22, 1990, pp. 38-45.
[5]. Myers R. H., D. C. Montgomery, G. G. Vining, C. M. Borror, S. M. Kowalski. Response Surface Methodology: A Retrospective and Literature Survey. Journal of Quality Technology, 36,1, 2004, pp. 53-77.
[6]. Chiao C., M. Hamada. Analyzing Experiments with Correlated Multiple Responses. Journal of Quality Technology, 33, 2001, pp.451-465.
[7]. Najafi S., A. Salmasnia, R. B. Kazemzadeh. Optimization of Robust Design for Multiple Response Problem. Australian Journal of Basic and Applied Sciences, 5(9), 2011, pp. 1566-1577
[8]. Koleva E., L. Koleva, V. Tzotchev, M. Nemtanu, M. Brașoveanu, K. Vutova. Robust engineering approach for optimization of electron beam grafting of corn starch. Science, Engineering & Education, v.1(1), 2016, pp. 89-96.
[9]. Stephen C. Lapin, Modification of Polymer Substrates using Electron Beam Induced Graft Copolymerization, UV+EB Technology • Issue 1, 2015, pp. 44-49.
[10]. Nasef M.M., Radiation-grafted copolymers for separation and purification purposes: Status, challenges and future directions, Progress in Polymer Science, 37, 2012, pp. 1597– 1656.
[11]. Derringer, G., R. Suich, Simultaneous optimization of several response variables. Journal of Quality Technology, 12, 1980, pp. 214-219.

ANALYSIS OF A CONTROL ELECTROMETER

M.Sc. Radeva T. PhD.[1]
Department of Electrical Power Engineering – Technical University of Sofia, Bulgaria
tania_rr@abv.bg

Abstract: *The purpose of the study is to test the presented electrometer in a single-pole erect and deformed current. At the same time, it aims at maximizing the functions and capabilities of the test meter. For a certain period of time a current of equal effective value and different shape is supplied. Analytically, the power is calculated. The readings of the power from the electric meter are taken and conclusions are made. A purely active load is used.*

Keywords: STANDARD ELECTROMETER, TESTING, STATIC ELECTRICITY METERS

1. Увод

В зависимост от принципа на действие електромерите могат да бъдат индукционни и статични. Отчитането на показанията на електромера може да се извършва непосредствено или дистанционно. Отчитането на консумираната електроенергия е в киловат часове, означени с"кWh" или в кило вар часове, означени с"кVarh" . Методиката за изпитвания и проверка определя методите и средствата за първоначална и последваща проверка на електромери.

Методиката за изпитвания и проверка се отнася за електромери, предназначени за измерване на консумираната активна и реактивна енергия в еднофазни и трифазни (3 и 4 проводникови) вериги чрез интегриране на активна и реактивна моіцност по отношение на времето.

Метод за проверка:

- Метод на пряко сравняване с еталон:

Методът се изразява в пряко сравняване на стойностите на енергията, измерена от еталон и от проверяван електромер.

За Контролен електромер ще използваме статичен трифазен електромер на компанията ,,AMPY AUTOMATION", които е предназначен да измерва 220/380 Vac — 240/415 Vac за фаза, 50 Hz, 5(10)20 — (100)120 А. Има 3 независими измервателни елемента позволяващи консумираната енергия да бъде измерена в 4 проводна система на свързване. Измерва и регистрират kWh с клас на точност 1.0 u kVArh с клас на точност 2.0. Има 2 червени светло диоди монтирани на лицевия панел, пулсиращи с честота 1,000 импулса за kWh u kVArh измерени от всичките 3 елемента.

2. Изследване на статични електромери

Целта на изследването е да се реализира изпитване на представения електромер при еднополупериодно изправен и при деформиран ток. Едновременно с това се цели максимално използване на функциите и възможностите на изпитвания електромер.

Изпитването се извършва, чрез реализиране на посочените по долу схеми. Деформацията и едноплупериодното изправяне на тока се реализира от диода Д. Напрежението се следи от волтметър. Напреженовите и токовите намотки на електромерите са изобразени съответно с индекси "wu" u wi,,. С PF u PJ са означени отчетените от електромерите мощности. За по-голяма точност изпитанията се правят два пъти. Поради активния товар факторът на мощността не се променя: cos φ = 1.

За определен период от време се подава ток с еднаква ефективна стойност и различна форма. По аналитичен път се изчислява мощността. Снемат се показанията на отчетената от електромера мощност и се правят изводи. Използва се чисто активен товар.

За точно отчитане на времето се използва вътрешният часовник на електромера. Софтуерно се прави настройка за смяна на тарифите през определен интервал. Прави се запис на състоянието на електромера преди и след смяната на активните тарифи и се отчита разликата в показанията преди и след него. Първоначалната настройка на тока става с помощта на амперметър с широк честотен обкват и товарните съпротивления Rт. В края на опита се прави точно отчитане и кармоничен анализ на тока и напрежението чрез осцилограма. Напрежението се подава към осцилоскопа чрез трансформатор Т, който служи за галванично отделяне на осцилоскопа от веригата и разширяване обквата му. Използва се трансформатор с коефициент на трансформация Кт=9,17.

$K_T = U_{1H} / U_{2H}$, където U_{1H} = 220 V, U_{2H} = 24 V

Токът се подава към осцилоскопа посредством Rш << Rт и затова неговото влияние не се отчита. В конкретното упражнение се стремим да поддържаме токът I = 3A = const.

Мощността се изчислява с формулата:

$$P = UI\cos\varphi$$

Тъй като cosφ = 1= const, то израза за мощността добива вида:

$$P= UI$$

Изпитване със синусоидален ток и синусоидално напрежение

Схема на опитната постановка.

Схемата е реализирана както е посочено в описанието на изследването — фиг 1. В нея отсъстват изправителният елемент Д. Предполага се, че сметнатата аналитично и измерена от електромер енергия са равни. Използва се чисто активен това. Токовите намотки на двата електромера са свързани последователно, а напреженовите паралелно.

При измерване на напрежението на веригата за галванично отделяне на осцилоскопа се използва трансформаторът Т. Т се използва и за разширяване обхвата на осцилоскопа. Сигналът след Т се подава на единия канал, а на другия се подава токът през шунта Rш.

Амперметърът за задаване на тока е с широк честотен обхват.

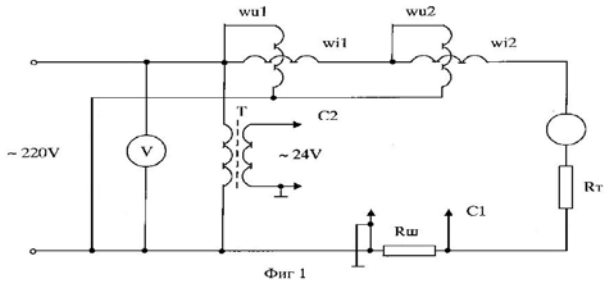

Фиг. 1 *Опитнапостановка на изследването.*

Резултати от измерването за 1 час:

Таблица 1 - Резултати от измерването за 1 час и синусоидален ток

Опит №	I, [A]	U, [V]	P, [W]	Електромер P_J, [W]	Електромер P_J, [W]
1	3	226	678	678	679
2	3	226	678	680	680

Както се вижда от резултатите получени при провеждане на опита електромърът е отчел точно изчислената аналитично мощност.

Осцилограма на тока и напрежението. Хармоничен състав.

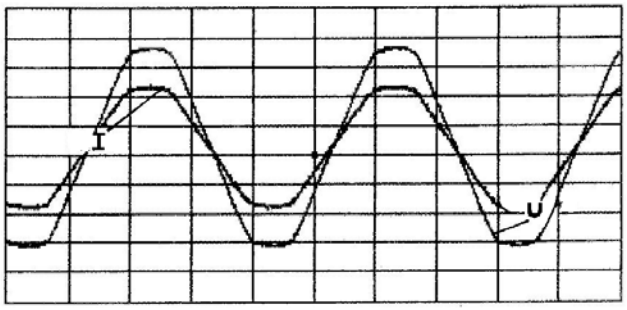

Фиг. 2 *Форма на тока и напрежението. I - ток, U - напрежение*

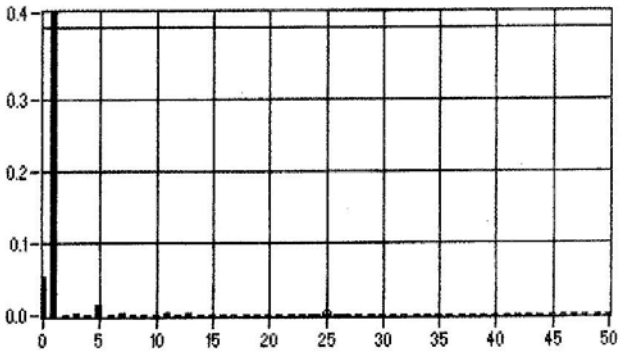

Фиг. 3 *Хармоничен състав на тока*

При синусоидален ток и синусоидално напрежение в хармоничният състав на тока се проявяват нечетните хармоници 1, 3, 5, 7, 11. Нулевият хармоник участва поради ненулирането на осцилоскопа с цел онагледяване на формата на тока и напрежението.

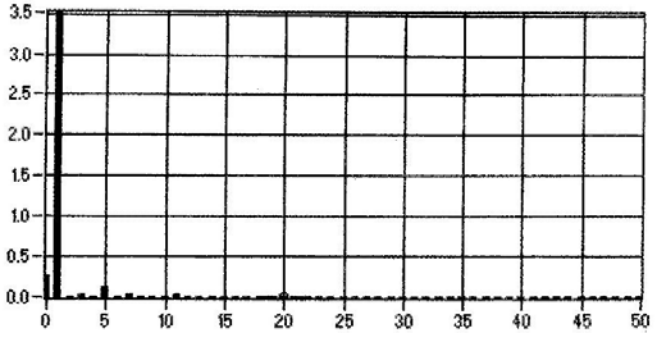

Фиг. 4 *Хармоничен състав на напрежението*

В хармоничният състав на напрежението при. синусоидален ток и синусоидално напрежение също се проявяват нечетните хармоници 1, 3, 5, 7, 11. Нулевият хармоник също участва поради ненулирането на осцилоскопа с цел онагледяване на формата на тока и напрежението.

Изпитване с еднополупериоден изправен ток и синусоидално напрежение.

Схема на опитната постановка.

В схемата вземат участие всички елементи от описанието на опита -фиг 1. Трансформатор за галванично отделяне, шунтов резистор, активен товар, волтмегър, амперметър, диод. Диодът служи за еднополупериодно изправяне на тока.

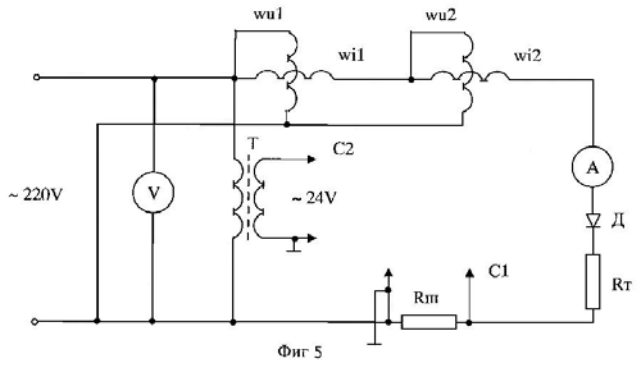

Фиг. 5 *Хармоничен състав на напрежението*

Резултати от измерването за 1 час:

Таблица 2 - Резултати от измерването за 1 час

Опит №2	Хармоник	I, [A]	U, [V]	P, [W]	Електромер P_F, [W]	Електромер P_T, [W]
1	1	2.92	229.6	480.323	-	-
	3	0.015	1.576	0.024	-	-
	5	0.086	7.828	0.673	-	-
	Сума	-	-	481	487	487
2	1	2.071	227.4	741.945	-	-
	3	0.028	1.556	0.044	-	-
	5	0.085	9.293	0.79	-	-
	Сума	-	-	472	476	477
Данни отчетени чрез осцилоскоп KIKUSUI						
1	-	2.935	229.7	674	487	487
2	-	2.903	227.6	660	476	477

*Началните фази на хармониците не се отчитат.

Резултатите от опита показват точността на статичния електромер при подаване на еднополупериоден изправен ток и синусоидално напрежение.

Фиг. 6 *Форма на тока и напрежението. I - ток, U - напрежение*

От осцилограмата се вижда влиянието на диода върху тока и напрежението. При поставянето на диод в токовата веригата токът се изправя еднополупериодно. Напрежението запаза формата си.

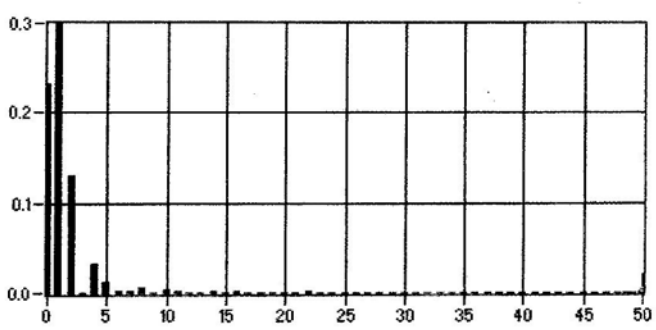

Фиг. 7 *Хармоничен състав на тока*

При еднополупериоден изправен ток и синусоидално напрежение в хармоничният състав на тока освен нечетните вече се проявяват и четните хармоници 2, 4, 8, 10. Силно влияние оказват 2, 4 кармоници. Засилва се вилянието и на нулевият хармоник.

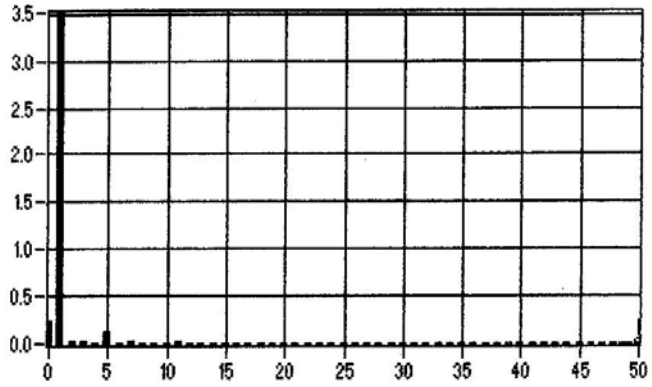

Фиг. 8 *Хармоничен състав на напрежението*

Хармоничният състав на напрежението запазва познатото присъствие на нечетни хармоници.

Изпитване с деформиран ток - Схема на опитната постановка.

В схемата вземат участие всички елементи от описанието на опита фиг 4.9. За деформиране на токът се използва резултантния ток на еднополупериоден изправен и синусоидален ток. За получаванеот на ток с исканата форма се използват товарните съпротивления RT 1, RT2 и диода Д.

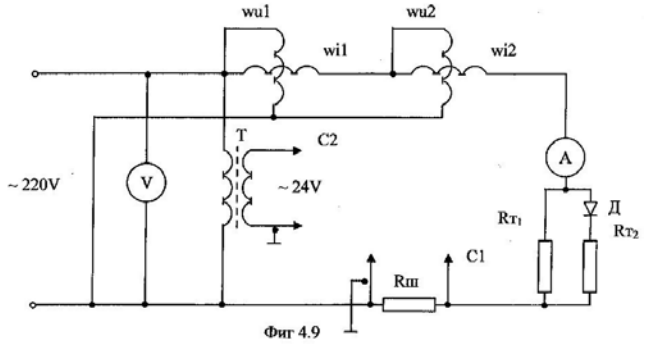

Фиг. 9 *Хармоничен състав на напрежението*

Опит №2	Хармоник	I, [A]	U, [V]	P, [W]	Електромер PF, [W]	Електромер Pт, [W]
1	1	2.87	225.521	647.245	-	-
	3	0.02	1.543	0.031	-	-
	5	0.117	7.678	0.899	-	-
	Сума	-	-	648	656	657
	1	2.885	226.195	652.573	-	-
	3	0.02	1.543	0.0	-	-
	5	0.098	7.698	0.754	-	-
	Сума	-	-	653	661	661
Данни отчетени чрез осцилоскоп KIKUSUI						
	-	2.947	225.7	665	656	657
	-	2.965	226.3	671	661	661

Осцилограма на тока и напрежението. Хармоничен състав.

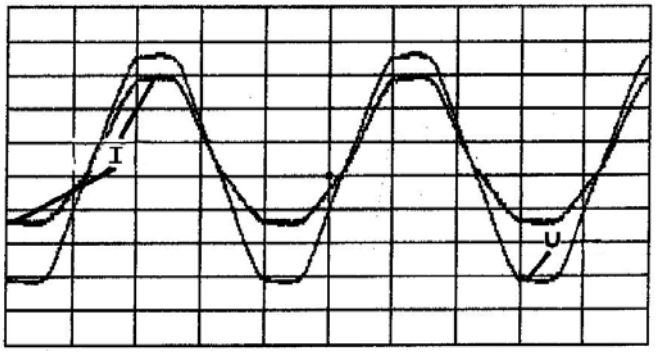

Фиг. 10 *Форма на тока и напрежението. I - ток, U - напрежение*

Вижда се резултантният ток на еднополупериоден изправен и синусоидален ток следствие на използването на диода Д и R_{T1}, R_{T2}.

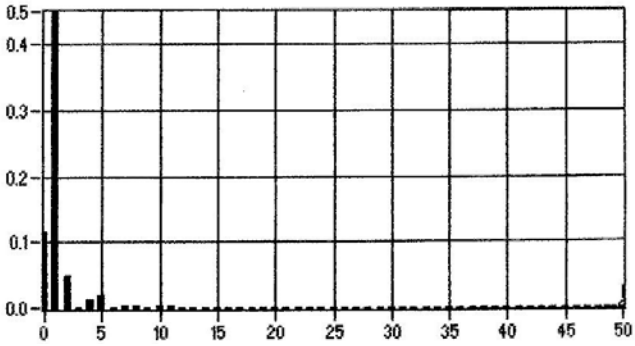

Фиг. 11 *Хармоничен състав на тока*

В хармоничния съста на тока вече влиянието на четните и нечетните хармоници е по-равномерно. Наблюдават се 1, 2, 4, 5, 7, 10, 11 хармоници. Нулевия хармоник отслабва влиянието си.

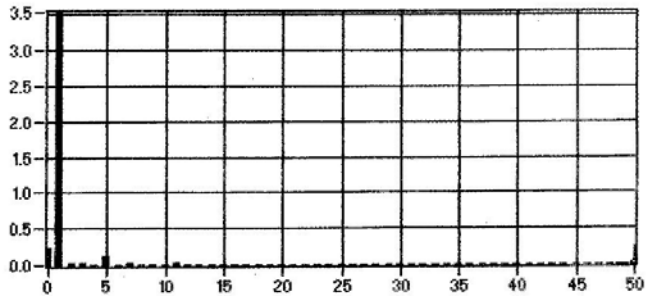

Фиг. 12 *Хармоничен състав на напрежението*

Както и при предишният опит хармоничния състав на напрежението запазва познатото присъствие на нечетни хармоници.

3. Изводи

Статичните електромери трябва да притежават:

- Измерване на електрическа енергия независимо от тарифите;

- По висока точност на измерването на електрическата енергия в сравнение с обикновените електромеханични електромери с 1 клас на точност
- Широк диапазон на измерваните токове (от 5% до 1200% от стойноста на номиналния ток под 0,4% Iб)
- Ниска стойност на стартиращия ток
- Ниска стойност на енергийните загуби в токовия кръг в сравнение с тези при електромеханичните електромери
- Достъпни и лесниза регулиране регулиращи компоненти
- Диапазона на ток и напрежение, свързването на лемите, изпълнението на терминалния блок, възможностите за програмиране
- Надежно и просто свързване към мрежата
- Предпазни мерки срешу външна намеса,защити, пароли
- Измерване и запис на максималните стойности, продължителност и дата на събитието
- Съхраняване на измерената електрическа енергия в дълговременна памет
- Съхраняване на други измерени данни, реално време и дата на програмните стойности
- За работа в широк диапазон на температури от -40ºC до +70ºC
- Подържане на всички измерени данни за енергията и мощността, всички програмни стойности и непрекъсната работа на часовника за реално време при прекъсване на напрежението

4. Нормативни позовавания и Стандарти:

Стандартите за статични електромери трябва да бъдат унифицирани за различните страни. При въвеждането в експлоатация на статичните електромери те задължително преминават процедура по установяване тяхната годност или негодност. Тази процедура за България се базира на, методиката за проверка на статични електромери на "Държавна агенция по стандартизация и метрология", ГД "Национален център по метрология", сектор "Електроенергийни измервания", съобразена с:

Закон за измерванията (ДВ, бр. 46/2002)

Наредба за средствата за измерване, които подлежат на метрологичен контрол (ДВ, бр. 98/2003)

Наредба за единиците за измерване, разрешени за използване в •Република България (ДВ, бр. 115/2002).

БДС 17397-1: 2005. Част 1: Международен речник на основни и общи термини по метрология.

БДС EN 62053-11 Променливотокови електромери класове 0.5, 1 БДС EN 62053-22 Променливотокови статични електромери за активна енергия класове 0.2S и 0.5S

БДС EN 62053-21 Променливотокови статични електромери за активна енергия класове 1 и 2

БДС EN 62053-23 Променливотокови статични електромери за реактивна енергия класове 2 и 3

БДС 8.259-83 Електромери индукционни. Методи за проверка МП 09-09/2001 Методика за проверка на статични електромери

5. Библиография

[1] Техническа документация за статични електромери AMPY

[2] Експлоатационна документация за статични електромери AMPY

[3] Стандарти за статични електромери БДС 17371-95г., БДС IES 1036, БДС 8,259-83г., БДС EN 61036+A1-2001г., БДС EN 60687-2001г.

[4] Стандарти за превключващи часовници, за превключване на тарифи и управление на тарифи БДС EN 61038+A1+A2-2002г.

AN ANALYSIS OF TECHNICAL CHARACTERISTICS FOR MEASURING ELECTRICAL ENERGY

M.Sc. Radeva T. PhD.[1]
Department of Electrical Power Engineering – Technical University of Sofia, Bulgaria
tania_rr@abv.bg

Abstract: *The aim of this paper is to analyse the variety of ways and methods of measuring electrical energy. The need to measure electrical energy in a way to proper distribute and use of electrical energy requires a widespread use of electricity meters. They are integrated devices designed to record the amount of used electrical energy for a certain time interval. The most popular approaches for active power measurement are analyzed and their precision is comparatively estimated.*

Keywords: MEASURMENT, ELECTRICITY METER, STANDARTS

1. Увод

Единицата за измерване на електрическа енергия се нарича джаул (J) u е равна на 1 W x 1 s. В практиката намират приложение извънсистемните единици за електрическа енергия ват час (Wh), киловат час (kWh), мегават час (MWh) u др. Необходимостта от измерване на електрическата енергия с оглед на правилното разпределение и използване налага широко използване на електромерите. Те са интегриращи апарати, предназначени за регистриране на количеството електрическа енергия за определен интервал от време. В зависимост от вида на веригите те биват еднофазни и трифазни. Според принципа на действие те биват индукционни и статични. Електромерите се използват за измерване на активна, реактивна енергия и др.

С напредването на научния прогрес постепено новите разработки в различните области навлизат все по-широко. Подобряването на характеристиките, намаляването на грешките и компактността на новите продукти са неоспорими доводи в тяхна полза. Съвременните разработки постепенно изместват старите. Разнообразието предлагано от производителя също играе важна роля във въвеждането на новите продукти. До момента има разработени най-различни конкурентноспособни продукти, плод на новите технологии:

- статични монофазни и трифазни електромери;
- статични монофазни и трифазни електромери с кредитно плащане;
- статични монофазни и трифазни електромери с предплащане, с карта;
- статични монофазни и трифазни електромери за дистанционно отчитане.

Електромерите, като средства за измерване трябва да притежават някои качества, осигуряващи надеждността и гарантиращи точността на измерването. Те са средство за контрол на произведената и продадена/доставена електроенергия от производителя до потребителя. С тяхна помощ се осъществява възвращаемостта на вложените средства за производство, пренос и експлоатация на съоръженията обезпечаващи тези процеси. Чрез намаляване грешката при измерване на енергията се намаляват съответно и загубите. Това се постига с увеличаване на чувствителността на уредите и повишаване на изискванията за намаляване на влиянието, което оказват различните външни и вътрешни фактори на измервателните уреди за по-точно отчитане на измерваните величини.

Статичните електромери за момента притежават характеристики, много по-добри от индукционните си предшественици. Поради тази причина те постепенно изместват старите електромери. Въпреки по-добрите показатели и високата точност, все още тези измервателни уреди са навлезли частично в експлоатация поради някои икономически фактори.

За България до момента са намерили приложение за масова употреба статични електромери отговарящи на съответните стандарти. Други са в процес на изпитване. Като цяло, тенденцията е за пълно заменяне на индукционни със статични електромери.

Като орган за контрол на Република България които трябва да гарантира стабилна основа за постигане на точност и проследимост на измерванията в страната на всички използвани средства за измерване и да създаде предпоставки за развитие на законовата метрология, акредитацията и сертификацията и за повишаване на конкурентоспособността е Главна Дирекция "Национален център по метрология" (ГД към Държавна агенция по метрология и технически надзор (ДАМТН).

2. Стандарти и методика за изпитване и проверка на статични електромери

Област на приложение:

Методиката за изпитвания и проверка се отнася за електромери, предназначени за измерване на консумираната активна и реактивна енергия в еднофазни и трифазни (3 и 4 проводникови) вериги чрез интегриране на активна и реактивна моіцност по отношение на времето.

В зависимост от принципа на действие електромерите могат да бъдат индукционни и статични. Отчитането на показанията на електромера може да се извършва непосредствено или дистанционно. Отчитането на консумираната електроенергия е в киловат часове, означени с"кWh" или в кило вар часове, означени с"кVarh" . Методиката за изпитвания и проверка определя методите и средствата за първоначална и последваща проверка на електромери.

Нормативни позовавания и Стандарти:

Стандартите за статични електромери трябва да бъдат унифицирани за различните страни. При въвеждането в експлоатация на статичните електромери те задължително преминават процедура по установяване тяхната годност или негодност. Тази процедура за България се базира на, методиката за проверка на статични електромери на "Държавна агенция по стандартизация и метрология", ГД "Национален център по метрология", сектор "Електроенергийни измервания", съобразена с:

Закон за измерванията (ДВ, бр. 46/2002)

Наредба за средствата за измерване, които подлежат на метрологичен контрол (ДВ, бр. 98/2003)

Наредба за единиците за измерване, разрешени за използване в •Република България (ДВ, бр. 115/2002).

БДС 17397-1: 2005. Част 1: Международен речник на основни и общи термини по метрология.

БДС EN 62053-11 Променливотокови електромери класове 0.5, 1 БДС EN 62053-22 Променливотокови статични електромери за активна енергия класове 0.2S и 0.5S

БДС EN 62053-21 Променливотокови статични електромери за активна енергия класове 1 и 2

БДС EN 62053-23 Променливотокови статични електромери за реактивна енергия класове 2 и 3

БДС 8.259-83 Електромери индукционни. Методи за проверка МП 09-09/2001 Методика за проверка на статични електромери

Термини, определения, съкращения, означения:

2.1 Термини:

2.1.1. Базов ток* (Ib) - стойност на тока, в съответствие с която се определя съответната работна характеристика на електромер за директно свързване.

2.1.2. Обявен ток (In) - стойност на тока, в съответствие с която се определя съответната работна характеристика на електромер, който работи с трансформатор.

2.1.3. Максимален ток (Imax) - най-голямата стойност на тока, при която електромерът все още отговаря на изискванията за точност.

2.1.4. Минимален ток (Imin)- минималната стойност на тока, над която грешката е предвиден» да се намира в предписаните граници.

2.1.5. Предписано (номинално) напрежение* (Un) - стойност на напрежението, спрямо която с установени съответните (работни) характеристики на електромера.

2.1.6. Предписана (номинална) честота* (fn) - стойност на честотата, спрямо, която с установени съответните (работни) характеристики на електромера.

2.1.7. Константа - стойност, която изразява отношението между енергията, регистрирана от електромера, и съответната стойност на изхода за проверка. Ако тази стойност е брой импулси,- константата трябва да бъде изразена или в imp/кWh (imp/кVarh) или в Wh/ imp. Ако тази стойност е брой обороти, константата трябва да бъде изразена или в оборот/кWh(оборот/кVarh) или в Wh/оборот (Varh/оборот).

*Забележка: Ако нещо друго не е специфицирано, термините "ток" и"напрежение" означават ефективна (средноквадратична) стойност.

2.2 Съкращения:

БИМ - Български институт по метрология

ГД МИУ - Главна дирекция "Мерки и измервателни уреди"

ЗИ - Закон за измерванията

БДС - български държавен стандарт

МП - методика за проверка

СИ - средство за измерване

3. Метод за проверка

- Метод на пряко сравняване с еталон:

Методът се изразява в пряко сравняване на стойностите на енергията, измерена от еталон и от проверяван електромер.

- Метод за измерване на мощността и времето:

Методът се изразява в задаване на постоянна стойност на електрическа енергия, която едновременно се измерва с ватмегър и с хрономегър.

Препоръчва се методът да бъде използван само при стабилно напрежение.

Проверочни операции и средства за извършване на проверките :

При проверката се извършват операциите, посочени в таблица №1:

№ по ред	Наименование на операциите	Точка от МП	Първ. про-верка	Посл. провер-ка след ремонт	Посл. перио-дична проверка
1	Административно проучване				
1.1	Проверка за съответствие с одобрения тип	5,1	да	да	да
1.2	Проверка за комплектност	5,2	да	не	не
1.3	Наличие на надписи и означения	5.3 .	да	да	да
2	Техническо и функционално изследване				
2.1	Подготовка за извършване на проверка	7,2	да	да	да
2.2	Проверка на техническите изисквания	9,1	да	да	да
2.3	Изпитване на изолационните свой-ства с променливо	9,2	да	да	да
3	Метрологично изследване				
3.1	Изпитване на работа без товар (самоход)	9,3	да	да	да
3.2	Изпитване на пусковите условия (праг на реагиране)	9,4	да	да	да
3.3	Проверка на точността на електромера	9,5	да	да	да
3.4	Проверка на константа на електромера	9,6	да	да	да
3.5	Проверка на работата на показва-щото устройство (показват_ците)	9,7	да	да	да
3.6	Проверка на работата на превключващият електромагнит (реле)	9,8	да	да	да

Проверка в регистъра на одобрените СИ.

Наличие на техническо досие (или техническо описание и инструкция за експлоатация).

Всеки електромер трябва да има фирмена табелка, върху която да са нанесени следните незаличими, лесно четими и видими отвън данни:

- идентификационен знак или търговска марка на производителя и година на производство;
- тип на електромера;
- клас на електромера;
- знак за одобрен тип;
- означение на броя и схемите на електрическата система, към която се включва електромерът в една от формите: еднофазен двупроводен, трифазен четирипроводен и т.н, или чрез символите, съответстващи на национален стандарт;

- стойност на номиналното напрежение;

- стойност на номиналния и максималния ток;

- номинална честота в херцове;

- константа на електромера, изразена във вида: "xWh/оборот" или "x обороти/кWh", или "xWh/импулси", или "x импулси/ kWh;

- знак двоен квадрат за електромери с изолираща кутия с клас на защита II;

- предписана работна температура, ако е различна от 23 °C.

- Електромерът може да носи информация за мястото на производство, информация за собственост, търговско описание, специален сериен номер, знак за съответствие с български стандарт, въвеждащ европейски, и идентификационен номер на схемата за свързване. Всяка друга информация или надпис са забранени освен ако се допуска в удостоверението за одобрен тип.

- Всеки електромер трябва да носи лесно разбираема схема на свързване, която показва съответствието между изводите за свързване, включително изводите на спомагателните устройства и проводниците, които трябва да се свържат. Обозначението на клемите се посочва в схемата.

- При трифазни електромери се посочва последователността на фазите, за която са предназначени.

- Схемите на свързване могат да се заменят от съответен номер, посочён в национален стандарт и отбелязан върху табелката с основни данни.

Използвани еталони и спомагателно оборудване:

При проверката се използват следните еталони:

Еднофазен или трифазен еталонен електромер с обхвати:

- по напрежение от 50 V до 320 V;

- по ток от 0,02 A до 120 A;

- клас на точност:

* при проверка чрез метода на непосредствено сравнение еталонът, с който се извършва проверката, трябва да осигурява определянето на действителната стойност на енергията с грешка по-малка или равна на 1/3 от максимално допустимата основна грешка (по натагък допустима грешка) на проверяваните електромери.

* само при проверка на електромери с клас на точност 0,2S се допуска това отношение да бъде равно на 1/2, но в този случай се отчита грешката на еталона според свидетелството му за калибриране. Изискваните отношения са при съответното натоварване;

* при проверка чрез метода на измерване на мощността и времето еталоните са:

- ватмегър за променлив ток и напрежение с клас на точност не по- нисък от 0,2;

- хрономегър с неопределеност u = + 0,5 s.

4. Анализ на техническите качества на средствата за измерване на електрическа енергия

Електромерът като средство за измерване на електрическа енергия с оглед .,

на нейното правилно разпределение и използване налага широко използването им. Те са една голяма фамилия с различни видове модели. В зависимост от вида на веригите те биват еднофазни и трифазни за директно или индиректно (трансформаторно) включване, измерване на активна и реактивна енергия.

Статичните електромери са разработени на базата на най-съвременните технологии което осигурява точно измерване и възможност за много тарифи. За измервателни елементи в електромерите се използуват две технологии: специални линейни токови трансформатори или сензори с така наречения ефект на Хол и последващо аналого- цифрово преобразуване. За електромери до 140A се прилага директно свързване на измерващият датчик, като се измерва директно консумираната енергия. За консуматори на ток над 140A се използва свързване чрез външни трансформатори, включени преди електромера. Измервателните обхвати на електромерите трябва да се избират съобразно индивидуалните върхови товари и коефициента на едновременност. Електромера трябва да не се претоварва и същевременно да измерва вярно при малки товари. Чувствителността е съществен показател на статичните електромери. Трябва да се има предвид че предшествениците им масово разпространените индукционни електромери с обхват 10/40A и 10/3 OA започват да регистрират енергия при мощност над 11 W npu директно мерене. За точно измерване на енергията при индиректно мерене трябва коефициента на трансформация се избира така че при 25% от мощността на потребителя вторичния ток на токовия трансформатор да не спада под 1 O% от номиналната стойност. При статичните електромерите се използва принципа на редуцирано сканиране (Reduced Scan Principle) т.е. токът и напрежението се измерват последователно и всяко измерване се използва два пъти, докато при обикновените методи токът и напрежението се измерват едновременно в един и същи момент.

Статичните електромери имат часовник за реално време и календар предвиждат всички възможни сложни операции по превключване на тарифи и тарифни зони, базирани на дневни и седмични разписания, както и списък на официални празнични дни. При развитието им те трябва да позволяват натрупване на статистика, която да дава възможности за анализ на натоварването и ефективността на тарифните комбинации.

Данните могат да бъдат снемани от течнокристален LSD дисплей. Те се изобразяват с обозначаване на съответната им мерна единица последователно за някакъв интервал от време, но при други имат опция да бъдат извиквани последователно на дисплея чрез бутон. Всички данни могат да бъдат автоматично прочетени през оптичен интерфейс и ръчен преносим терминал. Сериен интерфейс тип токов кръг позволява електромерът да бъде използван за отдалечено четене. Може да се използва вграден модем за комуникация по електрическите кабели. Всички тези комуникации се определят в зависимост от стандарта IEC61107.

Електромери за търговско отчитане преди да се пуснат в експлоатация трябва да отговарят по БДС на клас на точност за активна и реактивна електрическа енергия. Не маловажна е и проверката за самоход тя се извършва при отсъствие на ток в последователни вериги и при стойност на напрежението 115% Un. На изхода на статичните електромери не трябва да се получава повече от един импулс. Влиянието на околната среда не трябва да пречи на нормалната работа на електромера от — 400C до +700C.

Специфичните за различни приложения функции и режими на работа на статичния електромер могат да бъдат определени чрез персонален компютър преди монтажа му или чрез ръчен преносим терминал по време на експлоатацията. По този начин могат да бъдат заредени следните параметри:

- Брой тарифи

- Тарифни зони и запомняни стойности

- Период за натрупване и измерване на максимални или средни стойности на потребление

- Поляризация на контактите на релетата
- Календарни данни и превключващи таблици
- Потребителски номер
- Експлоатационен номер
- Време и дата и др.

Всички фази се използват за закранване на електромера. Информацията задължително се запомня в енергонезависима памет (EEPROM). Електромерът е с висока степен на защита срещу смущения в мрежата, претоварване по напрежение и токови удари, а също и срещу електромагнитни полета.

Статичните електромери се обслужват от софтуерни продукти различни за всеки вид и марка. Той трябва да е лесен за експлоатация. Софтуерът задължително трябва да бъде защитен от прочитане на показанията и за параметризация на електромерите чрез пароли.

5. Изводи

Многофункционалните статични електромери трябва да отговарят на всички стандарти и БДС

Статичните електромери трябва да притежават:

- Измерване на електрическа енергия независимо от тарифите;
- По висока точност на измерването на електрическата енергия в сравнение с обикновените електромеханични електромери с 1 клас на точност
- Широк диапазон на измерваните токове (от 5% до 1200% от стойноста на номиналния ток под 0,4% Iб)
- Ниска стойност на стартиращия ток
- Ниска стойност на енергийните загуби в токовия кръг в сравнение с тези при електромеханичните електромери
- Достъпни и лесниза регулиране регулиращи компоненти
- Диапазона на ток и напрежение, свързването на лемите, изпълнението на терминалния блок, възможностите за програмиране
- Надежно и просто свързване към мрежата
- Предпазни мерки срешу външна намеса,защити, пароли
- Измерване и запис на максималните стойности, продължителност и дата на събитието
- Съхраняване на измерената електрическа енергия в дълговременна памет
- Съхраняване на други измерени данни, реално време и дата на програмните стойности
- За работа в широк диапазон на температури от -40ºC до +70ºC
- Подържане на всички измерени данни за енергията и мощността, всички програмни стойности и непрекъсната работа на часовника за реално време при прекъсване на напрежението

В лабораторни условия мможе да се направи сравнение на работата на електромера със синусоидален и с деформиран ток

За деформиране на тока е прието еднопътно изправяне и комбинация от синусоидален и деформиран ток

С цифров осцилоскоп се реализира запис на явленията, изчисляване на ефективните стойности на токовете и напреженията, хармоничен анализ

Сранява се енергията за един и същи период от времеконсумирана при синусоидален ток и синусоидално напрежение, и при деформиран ток и синусоидално напрежение

6. Библиография

[1] Техническа документация за статични електромери AMPY

[2] Експлоатационна документация за статични електромери AMPY

[3] Стандарти за статични електромери БДС 17371-95г., БДС IES 1036, БДС 8,259-83г., БДС EN 61036+A1-2001г., БДС EN 60687-2001г.

[4] Стандарти за превключващи часовници, за превключване на тарифи и управление на тарифи БДС EN 61038+A1+A2-2002г.

IMPROVING THE QUALITY OF MEDICAL PRODUCTS THROUGH ROBUST ENGINEERING DESIGN

Assos. Prof. Dr. Eng. Elena Koleva[1], Dipl. Mag. Toni Paneva, PhD student[2]
[1]Institute of Electronics – BAS, 72 Blvg. "Tsarigradsko shosee", 1784 Sofia, Bulgaria
[2] University of Chemical Technology and Metallurgy, 8, Kliment Ohridski, Blvd. Sofia, 1756, Bulgaria

[1]eligeorg@abv.bg
[2]tony_pan@abv.bg

Abstract: *Four quality parameters that are very important for pharmaceutical manufacture of solid dosage forms are studied on the base of experimental data from three batches. The quality parameters Weight (Y_1), Thickness (Y_2), Strength (Y_3) and Diameter (Y_4) are investigated depending on process parameters: Depth (X_1), Major compression force (X_2), Precompression force (X_3) and Major compression height (X_4) under production conditions. Regression analysis, robust engineering design and methods for single criterion and multiple criteria optimization are implemented to meet the stated requirements.*

Keywords: QUALITY, ROBUST ENGINEERING DESIGN, REGRESSION ANALISIS, OPTIMIZATION, PHARMACEUTICAL MANUFACTURE OF SOLID DOSAGE FORMS

1. Introduction

Design of Experiments, Response Surface Methodology (RSM) [1], Robust Engineering Design Methodology [2], combined with methods for parameter optimization; provide opportunities for improving the quality of the drug production, for obtaining cheaper production products through an appropriate choice of components, to save raw materials and energy, to ensure the sustainability of the quality indicators in terms of noise and variation impacts of different nature.

During the development of a medicinal product and the manufacturing process, both input process parameters and output characteristics of the product are studied. The reason is to determine the optimal input parameters and output characteristics of the process, their tolerance limits and how to control them best. Various experimental and analytical techniques can be used to characterize the process. The purpose of this investigation is to understand the process as well as the dependencies of the influence of the input process parameters with the output product quality characteristics in presence of errors in the process parameters during the production of solid dosage forms. The main features of a product and process are: Critical Quality Output Characteristics, Input Process Parameters, Process Capabilities, and Quality Control Techniques.

The model-based robust design approach for improving the quality of the process is successfully applied to different industrial processes [2-4]. For each of the quality performance characteristics, using their regression models, two other models are estimated - for their mean values and variances in production conditions, taking into account the heteroscedasticity of the observations due to errors in the factor levels. The application of the proposed method gives the possibility to reduce the predicted variance of the responses at production conditions and in this way to improve the quality of the obtained product with minimum invested expenses. The quality improvement is performed using some overall criterion or simply by the performance characteristics variances minimization, while keeping their mean values close to their target values. The model of the mean value of the performance characteristic, which is a subject to errors is [2]:

$$\tilde{y}\,(\mathbf{p}) = \mathrm{E}[y(\mathbf{z})] = \eta(\mathbf{p}) + \boldsymbol{\theta}^{\mathrm{T}}\mathrm{E}(\mathbf{g}),$$

where $\eta(\mathbf{p})$ is a model of the quality performance characteristic, for example polynomial regression obtained by the RSM. The second term takes into account the bias caused by the errors transmitted from the process parameters **p** to the performance characteristic $\tilde{y}\,(\mathbf{p})$, where $\boldsymbol{\theta}^{\mathrm{T}}$ is the vector of the coefficients in the regression model $\eta(\mathbf{p})$. $\mathrm{E}(\mathbf{g})$ stands for the mathematical expectation of $\mathbf{g} = \mathbf{h} - \mathbf{f}$, **h** is a vector of the regressors **z** in the regression model, considered as containing errors **e** (for any process parameter – $z_i = p_i + e_i$) and **f** is the regressors vector of the process parameters **p**. The model for the variance is [2]:

$$\tilde{s}^2 = \mathrm{E}(\boldsymbol{\theta}^{\mathrm{T}}\boldsymbol{\psi}\boldsymbol{\psi}^{\mathrm{T}}\boldsymbol{\theta}) + \sigma_{\varepsilon}^2 = \boldsymbol{\theta}^{\mathrm{T}}\boldsymbol{\Psi}\boldsymbol{\theta} + \sigma_{\varepsilon}^2$$

where $\psi = \mathbf{g} - \mathrm{E}(\mathbf{g})$, is defined on the basis of the variances for each process parameters **p**, which can be calculated using the tolerance limits of the process parameters or on the base of replicated observations, $\boldsymbol{\Psi} = \mathrm{E}(\boldsymbol{\psi}\boldsymbol{\psi}^{\mathrm{T}})$ depends on the structure of the regression model and the experimental design, σ_{ε}^2 is the estimate of the random error of the performance characteristic.

The aim of the present work is to study the quality parameters weight (y_1), thickness (y_2), strength (y_3) and diameter (y_4) of the tablet depending on process parameters: depth of filling (p_1), major compression force (p_2), precompression force (p_3), and major compression height (p_4) under production conditions based on experimental data from three batches. Regression analysis, robust engineering design and parameter optimization method are applied.

2. Experiment

Pharmaceutical manufacturing of solid dosage medical product has been investigated. The production scheme is presented in Table 1.The first step is to prepare the granulating solution - the starting material Povidone K and dissolving it into purified water. The second step is the preparation of dried granulate. At this stage the active substance is added and the granulating solution is introduced into the mixer-granulator. The actual granulation (wet calibration) follows. The wet granule is transferred toward the dryer. After the stage of drying follows the preparation of the tablet mixture. The resulting granulate is weighted, sieved, homogenized with lactose monohydrate, wheat starch and talc. Magnesium stearate previously weighed is added, sieved and homogenized with the dried granulate. The obtained tablet mixture goes to a tablet press to produce solid dosage tablet forms (Stage IV, Fig. 1). Table 2 presents the critical process parameters.

Table 1: *Production scheme*

Stage I	Stage II	Stage III	Stage IV	Stage V
Preparation of granulating solution	Preparation of dried granulate	Preparation of tablet mixture	Preparation of solid dosage tablet forms	Packaging

Experimental data from three batches on Stage IV (Preparation of solid dosage tablet forms, Table 1) are obtained. The studied quality parameters are weight (y_1), thickness (y_2), strength (y_3) and diameter of the tablet (y_4). the process parameters influencing this stage of the process and vary during the conducted experiments are:

- depth of filling (p_1),

- major compression force (p_2),
- precompression force (p_3),
- major compression height (p_4).

The data for the four parameters were taken from a tablet press with a built-in multi-check. There are 45 different observations from the three batches. Table 3 presents the process parameters, their dimensions, designations and variation ranges.

Fig. 1 *Tablet press*

Table 2: *Critical process parameters and limits*

Critical process parameters	Limits
Addition of the granulating solution	
Time for addition of the solution, min	3-5
Cycle of large paddle, rpm	20
Granulation	
Cycle of large paddle, rpm	30-40
Cycle of small paddle, rpm	3000
Rotating moment, Nm	800-1000
Wet calibration	
Sieve size, mm	6.0-12.0
Drying	
Temperature of input air, ºC	70-80
Temperature of the product, ºC	38-42
Air flow, m^3/h	800-1500
Dry calibration	
Sieve size, mm	1.5

Table 3: *Natural and coded values of the process parameters*

Process parameter	Dimensions and designations (natural/coded)		Pi,min	Pi,max
Depth of filling	mm	p'_1/p_1	6.4	7.2
Major compression force	kN	p'_2/p_2	24.3	29.1
Precompression force	kN	p'_3/p_3	14.2	19.3
Major compression height	mm	p'_4/p_4	2.21	2.26

3. *Robust engineering design approach*

In order to apply the model-based robust design approach regression models for the mean values and dispersion of weight (y_1), thickness (y_2), strength (y_3) and diameter (y_4) of the tablets are evaluated. The influence of the process parameters affecting the Preparation of solid dosage tablet forms (Stage IV, Table 2) and varied during the experiment - depth of filling (p_1), major compression force (p_2), precompression force (p_3) and major compression height (p_4) is investigated. In Table 4 the obtained regression models for the considered quality characteristics, together with the corresponding multiple correlation coefficients R are shown. It can be seen that the worst result is obtained for the diameter of the tablets. The reason for this can be that other factors, which are not taken into account, also influence this quality characteristic. Further investigations are needed in this direction.

The regression models are presented for coded values (p_i) of the process parameters in the region [-1÷1]. The coding of the process parameter values is done, using the following equation:

$$p_i = (2p'_i - p'_{i,\max} - p'_{i,\min})/(p'_{i,\max} - p'_{i,\min})$$

where x_i and z_i are the coded and the natural values of the process parameter, correspondingly, $z_{i,min}$ and $z_{i,max}$ are the minimal and the maximal values of the parameter experimental variation region (Table 3).

Table 4: Estimated regression models

Parameter	Regression model	R, %
Weight (y_1),	$y_1 = 645.16422-3.2692262p_1-7.5503882p_2 +12'+6.1562681p_1p_2^2-2.9175446p_2p_3+8.581206p_2p_4$	84.5
Thickness (y_2)	$y_2 = 3.9706842-0.06904059p_1-0.04230538p_2 +0.06404791p_3+0.01621124p_4-0.08141767p_2^2p_4 +0.13320574p_3^2p_4$	97.3
Strength (y_3)	$y_4 = 120.19469+3.671664p_1+35.229717p_2- 44.268124p_1^2p_2-12.759921p_2^2p_4-8.4861574p_3p_4^3 +10.865539p_1p_2^2$	77.9
Diameter (y_4)	$y_4 = 2.5645643-0.00255684p_1-0.00199133p_2- 0.00529735p_2^2 +0.0122456p_1^2p3-0.00810537p_2p_4 +0.01528108p_3p_4-0.0159247p_2^2p_4+0.00728304p_3^2p_4$	60.2

Second step for estimation of models for the mean values and dispersion of quality characteristics is to estimate the variances in the factor levels. The variation in the process parameters during the production process can be caused by different reasons and can be estimated through replicated observations or by process parameters tolerance limits (see Table 5).

Table 5: *Tolerance limits of the process parameters*

Process parameter	Dimension	P_{io}'	ω	Coded value	Tolerance limits
Depth of filling	mm	6.8	0.4	p_1	p_1±3% p_1
Major compression force	kN	26.7	2.4	p_2	p_2±2
Precompression force	kN	16.75	2.55	p_3	p_3±2% p_3
Major compression height	mm	2.235	0.025	p_4	p_4±2% p_4

Determination of the variances σ_i^2 of the process parameters from the tolerance limits depends on type of the tolerance limit – tolerance limit, set as percentage of the nominal value of the parameter:

$$\left(p'_i - \frac{\delta_i p'_i}{100}, p'_i + \frac{\delta_i p'_i}{100}\right)$$

or a tolerance limit, set as a constant value, which does not depend on the nominal value of the parameter:

$$(p'_i - \varsigma_i, p'_i + \varsigma_i),$$

The coded variances can be obtained using the following equations correspondingly for the two types of tolerance limits:

$$\sigma_i^2 = \vartheta_{0i} + \vartheta_{1i} p_i + \vartheta_{2i} p_i^2$$

or

$$\sigma_i^2 = \sigma^2(p_i) = \sigma_i^2(p'_i)/\omega_i^2 = \sigma'^2_i/\omega_i^2 = \varsigma_i^2/9\omega_i^2,$$

where $\vartheta_{0i} = \left(\frac{\delta_i p'_{io}}{300\omega_i}\right)^2$, $\vartheta_{1i} = \frac{2\delta_i^2 p'_{io}}{300^2\omega_i}$, $\vartheta_{2i} = \left(\frac{\delta_i}{300}\right)^2$,

$\omega_i = |p'_{i\max} - p'_{i0}|$ and $p'_{i0} = (p_{i\min} - p_{i\max})/2$ (see Table 5).

In Table 6 a presented the calculated coded variances for all the process parameters.

Table 6: *Coded variances*

Factors	Coded variances σ_i^2
p_1	0.0289 + 0.0034 p_1 + 0,0001 p_1^2
p_2	0.0771
p_3	0.0438 + 0.00058 p_3 + 0.000044p_3^2
p_4	0,3552 + 0.00795 p_4 + 0.000044p_4^2

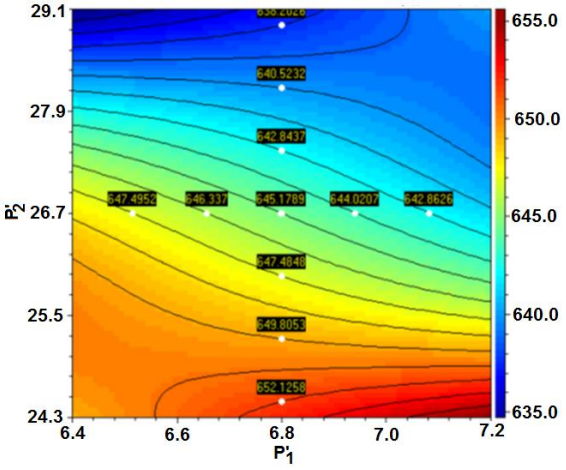

Fig. 2 *Contour plot for the mean value of the weight ($\tilde{y}_1$) depending on the depth of filling (p'_1, mm) and major compression force (p'_2, kN) at precompression force p'_3 = 16.75 kN and major compression height p'_4 = 2.235 mm*

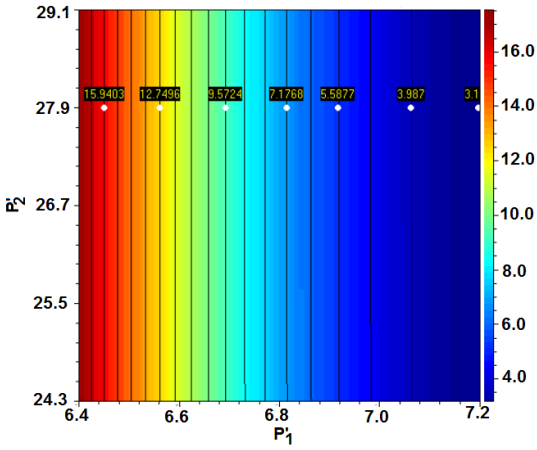

Fig. 3 *Contour plot for the variance of the weight (σ_1^2) depending on the depth of filling (p'_1, mm) and major compression force (p'_2, kN) at precompression force p'_3 = 16.75 kN and major compression height p'_4 = 2.235 mm*

The estimated models for the mean values and the variances for the quality parameters are used to study their dependencies on process parameters. Visualization of these dependencies are presented on Fig. 2 and Fig. 3 by the contour plots of the weignt of the tablet, calculated by the software package QstatLab [5]. On Fig. 2 is shown the contour plot for the mean value of the weight ($\tilde{y}_1$) depending on the depth of filling (p'_1, mm) and major compression force (p'_2, kN) at precompression force p'_3 = 16.75 kN and major compression height p'_4 = 2.235 mm. The contour plot for the variance σ_1^2 of the weight of the tablet at the same conditions is given on Fig. 3. It can be seen, that as major compression force (p'_2) increases, the mean weight value ($\tilde{y}_1$) decreases over the entire range of depth of filling (p'_1, mm), while this increase does not affect the variance of the weight. For the variance decrease more important parameter is the parameter depth of filling (p'_1), which should be increased at the selected levels of the precompression force p'_3 and the major compression height p'_4.

4 Optimization

The estimated models for the mean values and the variances for the quality parameters enable to fulfil different optimization tasks for these quality characteristics under manufacturing conditions.

A requirement is set to minimize the variance of the weight (σ_1^2) under restricted range for the quality characteristics the mean weights ($\tilde{y}_1$) and the mean thickness ($\tilde{y}_2$) values of the tablets under production conditions as follows:

645 mg $\leq \tilde{y}_1 \leq$ 655 mg

3.95 mm $\leq \tilde{y}_2 \leq$ 4.05 mm.

Genetic algorithm is the selected optimization method using QstatLab software with up to 2500 iterations at different points of the factor space. The resulting minimum variance value $\sigma_{1\,\min}^2$ = 3.0317 is determined by the search process. The values of the optimal process parameters, at which the optimal solution is obtained, are as follows:

- $p'_{1,opt}$ = 6,97544 mm,
- $p'_{2,opt}$ = 27,6062 kN,
- $p'_{3,opt}$ = 18,0079 kN,
- $p'_{4,opt}$ = 2,25332 mm.

The restriction conditions for the mean values of weight ($\tilde{y}_1$) and mean thickness ($\tilde{y}_2$) values are met and the following values are obtained:

- $\tilde{y}_1$ = 649.03 mg,
- $\tilde{y}_2$ = 3.97 mm.

In Fig. 4 and Fig. 5 is presented the optimal solution (the yellow point) at which the minimizing variance of the weight (σ_1^2) is obtained. The restriction conditions for the mean values of weight ($\tilde{y}_1$) and mean thickness ($\tilde{y}_2$) values are given by contour lines as follows:

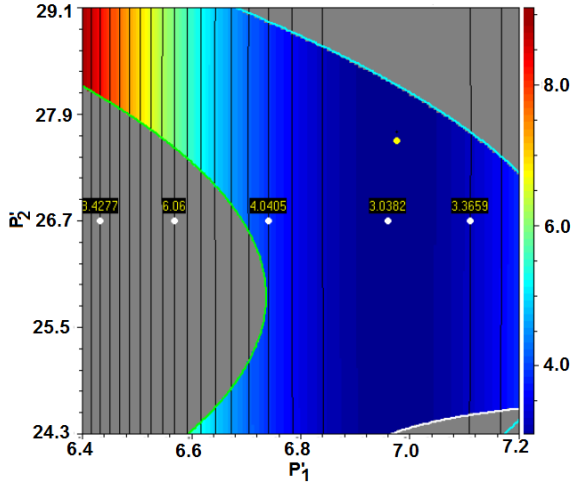

Fig. 4 *Optimal solution – minimal value of the variance of the weight (σ_1^2) depending on the depth of filling (p'_1, mm) and major compression force (p'_2, kN) at precompression force $p'_{3,opt}$ = 18,0079 kN and major compression height $p'_{4,opt}$ = 2,25332 mm*

- The limit of mean value of weight $\tilde{y}_1$=645 mg is marked with pink color;
- The limit of mean value of weight $\tilde{y}_1$=655 mg is marked with white color;
- The limit of mean value of thickness $\tilde{y}_2$=3.95 mm is marked with aqua color;
- The limit of mean value of thickness $\tilde{y}_2$=4.05 mm is marked with light green color.

The colored area marks the regions for the process parameters, where the restrictions for the considered quality characteristics are met. The values of the missing on the figures process parameters are set constant to their optimal levels.

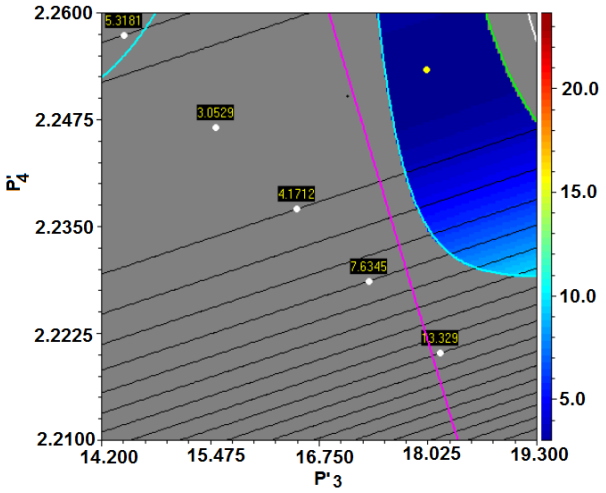

Fig. 5 *Optimal solution – minimal value of the variance of the weight (σ_1^2) depending on the precompression force p'$_3$, kN and the major compression height p'$_4$, mm at constant values of the depth of filling p'$_{1,opt}$ = 6,97544 mm and major compression force p'$_{2,opt}$ = 27,6062 kN.*

5. Conclusions

In the present work the quality parameters weight (y_1), thickness (y_2), strength (y_3) and diameter (y_4) of the tablet depending on process parameters: depth of filling (p_1), major compression force (p_2), precompression force (p_3), and major compression height (p_4) under production conditions based on experimental data from three batches is studied.

For each of the quality performance characteristics, using their regression models, two other models are estimated - for their mean values and variances in production conditions, taking into account the heteroscedasticity of the observations due to errors in the factor levels. The application of the proposed method gives the possibility to reduce the predicted variance of the responses at production conditions and in this way to improve the quality of the obtained product with minimum invested expenses.

Parametric optimization has been performed for specific quality assignment. The estimated models can be applied for numerous other optimization reuirements, aiming imptoving the quality of the tablet form of the considered medical product.

References

[1]. Myers R. H., D. C. Montgomery, G. G. Vining, C. M. Borror, S. M. Kowalski. Response Surface Methodology: A Retrospective and Literature Survey. Journal of Quality Technology, 36,1, 2004, pp. 53-77.

[2]. Vuchkov I. N, Boyadjieva L. N. Quality improvement with design of experiments, The Netherlands, Kluwer Academic Publishers, 2001.

[3]. Koleva E., I. Vuchkov, Model-based approach for quality improvement of EBW applications in mass production, Vacuum 77, 2005, pp. 423-428.

[4]. Koleva E., L. Koleva, V. Tzotchev, M. Nemtanu, M. Braşoveanu, K. Vutova. Robust engineering approach for optimization of electron beam grafting of corn starch. Science, Engineering & Education, v.1(1), 2016, pp. 89-96.

[5]. http://www.qstatlab.co.uk/bg/index.html

MODELING AND SIMULATION OF CONVOLUTIONAL ENCODERS USING LOGISIM FOR TRAINING PURPOSES IN THE UNIVERSITY OF RUSE

Assist. Prof. M.Sc. Borodzhieva A. PhD.[1], M.Sc. Aliev Y.[2], Assoc. Prof. M.Sc. Ivanova G. PhD[2]
Faculty of Electrical Engineering, Electronics and Automation – University of Ruse "Angel Kanchev",
Bulgaria, Department of Telecommunications[1], Department of Computer Systems and Technologies[2]
aborodzhieva@uni-ruse.bg

Abstract: *In telecommunication, a convolutional code is a type of error-correcting code that generates parity symbols via the sliding application of a Boolean polynomial function to a data stream. A general convolutional encoder consists of a k*L-stage shift register and n modulo-2 adders, where L is the constraint length of the encoder. Convolutional codes are used to achieve reliable data transfer in numerous applications, such as digital video, radio, mobile communications and satellite communications. These codes are often implemented in concatenation with a hard-decision code, particularly Reed-Solomon codes. The material presented in the paper is used in the educational process in the University of Ruse. In order to better perception of the material active learning methods are applied. An individual assignment is given to each student and he/she has to solve the task during the practical exercise and present it at the end of the classes to the lecturer. The student should synthesize a convolutional encoder with NAND/XOR gates and flip-flops and to simulate its operation using Logisim, an educational tool for designing and simulating digital logic circuits.*

Keywords: MODELING AND SIMULATION, CONVOLUTIONAL ENCODERS, LOGISIM, ACTIVE LEARNING METHODS

1. Introduction

In telecommunications, a convolutional code is a type of error-correcting code that generates parity symbols via the sliding application of a Boolean polynomial function to a data stream. Convolutional codes were introduced in 1955 by Peter Elias. In 1967 Andrew Viterbi determined that convolutional codes could be maximum-likelihood decoded with reasonable complexity using time invariant trellis based decoders – the Viterbi algorithm [1].

A convolutional code is described by three integers, *n*, *k*, and *L*, where the ratio $r = k/n$ has the same code rate significance that it has for block codes; however, *n* does not define a block or codeword length as it does for block codes. The integer *L* is a parameter known as the *constraint length*. It represents the number of *k*-tuple stages in the encoding shift register. An important characteristic of the convolutional codes is that the encoder has memory – the *n*-tuple emitted by the convolutional encoder is not only a function of an input *k*-tuple, but is also a function of the previous $L - 1$ input *k*-tuples. In practice, *n* and *k* are small integers and *L* is varied to control the capability and complexity of the code [2].

Convolutional codes are used to achieve reliable data transfer in numerous applications, such as digital video, radio, mobile communications and satellite communications. These codes are often implemented in concatenation with a hard-decision code, particularly Reed-Solomon codes. Prior to turbo codes such constructions were the most efficient, coming closest to the Shannon limit. An especially popular Viterbi-decoded convolutional code used since the Voyager program has a constraint length $L = 7$ and a rate $r = ½$. Longer constraint lengths produce more powerful codes, but the complexity of the Viterbi algorithm increases exponentially with constraint lengths, limiting these more powerful codes to deep space missions where the extra performance is easily worth the increased decoder complexity. Mars Pathfinder, Mars Exploration Rover and the Cassini probe to Saturn use *k* of 15 and a rate of 1/6; this code performs about 2 *dB* better than the simpler $L = 7$ code at a cost of 256 times in decoding complexity (compared to Voyager mission codes) [1].

2. Convolutional encoding

A typical block diagram of a digital communication system and a version of this functional diagram, focusing primarily on the convolutional encode/decode and modulate/demodulate portions of the communication link, are presented in [2]. The input message is denoted by the sequence $\mathbf{m} = m_1, m_2, \ldots, m_i, \ldots$, where each m_i represents a binary digit (bit), and *i* is a time index. It is assumed that each m_i is equally likely to be a one or a zero, and independent from bit to bit. Being independent, knowledge about bit m_i gives no information about m_j $(i \neq j)$. The encoder transforms each sequence **m** into a unique codeword sequence $\mathbf{U} = G(\mathbf{m})$. A key feature of convolutional codes is that a given *k*-tuple within **m** does *not* uniquely define its associated *n*-tuple within **U** since the encoding of each *k*-tuple is *not only* a function of that *k*-tuple but is also a function of $L - 1$ input *k*-tuples preceding it. The sequence **U** is partitioned into a sequence of codewords $\mathbf{U} = U_1, U_2, \ldots, U_i, \ldots$. Each codeword U_i consists of binary *code symbols*, often called *channel symbols*, *channel bits* or *code bits*; unlike the input message bits the code symbols are not independent [2].

A general convolutional encoder is shown in Fig. 1. It consists of a *kL*-stage shift register and *n* modulo-2 adders, where *L* is the constraint length.

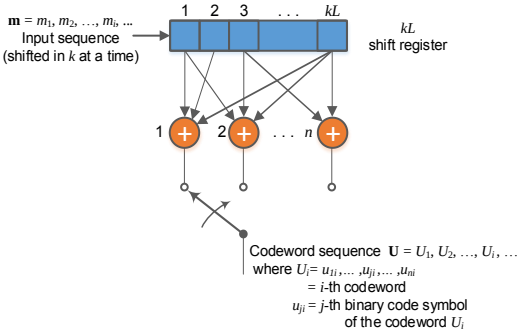

Fig. 1. *Convolutional encoder with constraint length L and rate k/n* [2]

The constraint length represents the number of *k*-bit shifts over which a single information bit can affect on the encoder's output. At each moment of time, *k* bits are shifted into the first *k* stages of the register; all bits in the register are shifted *k* stages to the right, and the outputs of the *n* adders are sequentially sampled to yield the *binary code symbols* or *code bits*. Since there are *n* code bits for each input group of *k* message bits, the code rate is *k/n* message bit per code bit, where $k < n$ [2].

Only the most commonly used binary convolutional encoders for which $k = 1$ are considered in the paper. For the $k = 1$ encoder, at the i^{th} unit of time, message bit m_i is shifted into the first shift register stage, all previous bits in the register are shifted one stage to the right, and the outputs of the *n* adders are sequentially sampled and transmitted. Since there are *n* code bits for each message bit, the code rate is 1/*n*. The *n* code symbols occurring at time t_i comprise the i^{th} codeword $U_i = u_{1i}, u_{2i}, \ldots, u_{ni}$, where u_{ji} $(j = 1,2,\ldots,n)$ is the j^{th} code symbol belonging to the i^{th} codeword. For the rate 1/*n*

encoder, the *kL*-stage shift register can be referred to as a *L*-stage register, and the constraint length *L*, expressed in units of *k*-tuple stages, can be referred to as constraint length in units of bits [2].

For describing a convolutional code, the encoding function $G(\mathbf{m})$ needs to be characterized so that given an input sequence **m**, the output sequence **U** can be readily computed. Several methods are used for representing a convolutional encoder, the most popular being the *connection pictorial*, *connection vectors or polynomials*, the *state diagram*, the *tree diagram*, and the *trellis diagram*. In the paper the connection representation is used and described below.

The convolutional encoder, shown in Fig. 2, is used as a model for discussing convolutional encoders. The figure illustrates a (2, 1) convolutional encoder with constraint length $L = 3$. There are $n = 2$ modulo-2 adders; thus the code rate k/n is ½. At each moment, a bit is shifted into the leftmost stage and the bits in the register are shifted one position to the right. Next, the output switch samples the output of each modulo-2 adder (i.e., first the upper adder, then the lower adder), thus forming the code symbol pair of the codeword associated with the input bit. The sampling is repeated for each input bit. The choice of connections between the adders and the stages of the register gives rise to the characteristics of the code. Any change in the choice of connections results in a different code. The connections are not chosen or changed arbitrarily. The problem of choosing connections to yield good distance properties is complicated and has not been solved in general; however, good codes have been found by computer search for all constraint lengths less than about 20 [2].

Unlike block codes having a fixed codeword length *n*, convolutional codes have no particular block size. However, convolutional codes are often forced into a block structure by *periodic truncation*. This requires a number of zero bits to be appended to the end of the input data sequence, for the purpose of clearing or flushing the encoding shift register of the data bits. Since the added zeros carry no information, the effective code rate falls below *k*/*n*. To keep the code rate close to *k*/*n*, the truncation period is generally made as long as practical.

One way to represent the encoder is to specify a set of *n* *connection vectors*, one for each of the *n* modulo-2 adders. Each vector has dimension *L* and describes the connection of the encoding shift register to that modulo-2 adder. A one in the i^{th} position of the vector indicates that the corresponding stage in the shift register is connected to the modulo-2 adder, and a zero in a given position indicates that no connection exists between the stage and the modulo-2 adder.

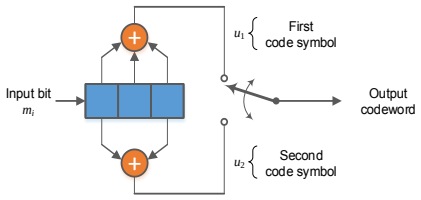

Fig.2. *Convolutional encoder (rate ½, L = 3)* [2]

For the encoder in Fig. 2, the connection vectors for the upper and for the lower connections are as follows $\mathbf{g}_1 = 111$, $\mathbf{g}_2 = 101$.

Let the message vector $\mathbf{m} = 101$ be convolutionally encoded with the encoder shown in Fig. 2. The three message bits are entered, one at a time, at times t_1, t_2, and t_3, as shown in Fig. 3. Subsequently, $(L-1) = 2$ zeros are entered at times t_4 and t_5 to flush the register and thus ensure that the tail end of the message is shifted the full length of the register. The output sequence will be 1110001011, where the leftmost symbol represents the earliest transmission. The entire output sequence, including the code symbols as a result of flushing, are needed to decode the message. Flushing the message from the encoder requires zeros, one less than the number of stages in the register, or $L-1$ flush bits. Another zero input at time t_6 is shown in Fig. 3, for verifying that the flushing is completed at time t_5. Thus, a new message can be entered at time t_6 [2].

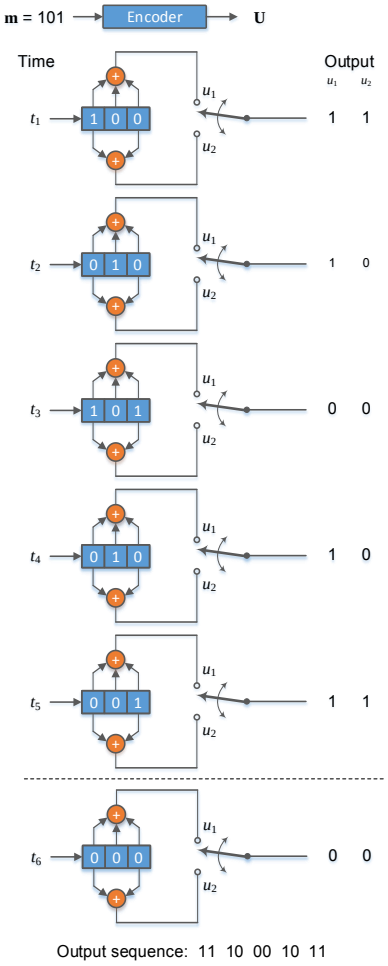

Fig. 3. *Convolutionally encoding a message sequence with a rate ½ and L = 3 encoder* [2]

The convolutional encoder can be presented in terms of its *impulse response* – the response of the encoder to a single "one" bit moving through it. The content of the register in Fig. 2, as a one moves through it, is considered below:

Register content	Codeword	
	u_1	u_2
100	1	1
010	1	0
001	1	1
Input sequences:	**1 0 0**	
Output sequences:	**11 10 11**	

The output sequence for the input "one" is called the *impulse response* of the encoder. Then, for the input sequence $\mathbf{m} = 100$, the output may be found by the *superposition* or the *linear addition* of the time-shifted input "impulses" as follows:

Input **m**	Output				
1	11	10	11		
0		00	00	00	
1			11	10	11
Modulo-2 sum:	**11**	**10**	**00**	**10**	**11**

It seems that the output is the same as that obtained in Fig. 3, demonstrating that *convolutional codes are linear*. It is from this property of generating the output by the linear addition of time-shifted impulses, or the convolution of the input sequence with the impulse response of the encoder, therefore the name *convolutional encoder* is derived.

The *effective code rate* for the example with a 3-bit input sequence and a 10-bit output sequence is $k/n = 3/10$ – quite a bit less than the rate ½ that might have been expected from knowing that each input data bit yields a pair of output channel bits. The reason for the disparity is that the final data bit into the encoder needs to be shifted through the encoder. All output channel bits are needed in the decoding process. If the message had been longer, say 300 bits, the output codeword sequence would contain 604 bits, resulting in a code rate of $300/604$ – much closer to ½ [2].

3. Logisim – an educational tool for designing and simulating digital logic circuits

Logisim is an educational tool for designing and simulating digital logic circuits. With its simple toolbar interface and simulation of circuits as the user builds them, it is simple enough to facilitate learning the most basic concepts related to logic circuits. With the capacity to build larger circuits from smaller subcircuits, and to draw bundles of wires with a single mouse drag, Logisim can be used to design and simulate entire CPUs for educational purposes. Logisim is used by students at colleges and universities around the world in many types of classes, ranging from a brief unit on logic in general-education computer science surveys, to computer organization courses, to full-semester courses on computer architecture. The main features of the product are: 1) It is free; Logisim is open-source (GPL). 2) It runs on any machine supporting Java 5 or later; special versions are released for MacOS X and Windows. 3) The drawing interface is based on an intuitive toolbar. Color-coded wires aid in simulating and debugging a circuit. 4) The wiring tool draws horizontal and vertical wires, automatically connecting to components and to other wires. So it is very easy to draw circuits. 5) Completed circuits can be saved into a file, exported to a GIF file, or printed on a printer. 6) Circuit layouts can be used as "subcircuits" of other circuits, allowing for hierarchical circuit design. 7) Included circuit components include inputs and outputs, gates, multiplexers, arithmetic circuits, flip-flops, and RAM memory. 8) The included "combinational analysis" module allows for conversion between circuits, truth tables, and Boolean expressions [3].

Features of the components used to build the encoder

The XOR, XNOR, Even Parity, and Odd Parity gates compute the respective function of the inputs, and emit the result on the output. By default, any inputs left unconnected are ignored if the input truly has nothing attached to it, not even a wire. In this way, the user can insert a 5-input gate but only attach two inputs, and it will work as a 2-input gate; this relieves the user from having to worry about configuring the number of inputs every time he/she creates a gate. The two-input truth table for the gates is the following [4]:

x	y	XOR	XNOR	Odd	Even
0	0	0	1	0	1
0	1	1	0	1	0
1	0	1	0	1	0
1	1	0	1	0	1

It seems that the Odd Parity gate and the XOR gate behave identically with two inputs; similarly, the Even Parity gate and the XNOR gate behave identically. But if there are more than two specified inputs, the XOR gate will emit 1 only when there is exactly one 1 input, whereas the Odd Parity gate will emit 1 if there is an odd number of 1 inputs. The XNOR gate will emit 1 only when there is *not* exactly one 1 input, while the Even Parity gate will emit 1 if there is an even number of 1 inputs. The XOR and XNOR gates include an attribute titled Multiple-Input Behavior that allow them to be configured to use the Odd Parity and Even Parity behavior. Otherwise, it is necessary to use two 2-input XOR gates to implement a 3-input XOR gate (Fig. 4). Many authorities contend that the shaped XOR gate's behavior should correspond to the odd parity gate, but there is not agreement on this point. Logisim's default behavior for XOR gates is based on the IEEE 91 standard. It is also consistent with the intuitive meaning underlying the term *exclusive or* [4].

Each flip-flop stores a single bit of data, which is emitted through the *Q* output. Normally, the value can be controlled via the inputs. In particular, the value changes when the **clock** input, marked by a triangle on each flip-flop, rises from 0 to 1 (or otherwise as configured); on this rising edge, the value changes according to the table below [4]:

D Flip-Flop		T Flip-Flop		J-K Flip-Flop			S-R Flip-Flop		
D	*Q*	*T*	*Q*	*J*	*K*	*Q*	*S*	*R*	*Q*
0	0	0	*Q*	0	0	*Q*	0	0	*Q*
1	1	1	*Q'*	0	1	0	0	1	0
				1	0	1	1	0	1
				1	1	*Q'*	1	1	?

1) D Flip-Flop: When the clock triggers, the value remembered by the flip-flop becomes the value of the *D* (*Data*) input at that instant. **2) T Flip-Flop:** When the clock triggers, the value remembered by the flip-flop either toggles or remains the same depending on whether the *T* (*Toggle*) input is 1 or 0. **3) J-K Flip-Flop:** When the clock triggers, the value remembered by the flip-flop toggles if the *J* and *K* inputs are both 1 and the value remains the same if both are 0; if they are different, then the value becomes 1 if the *J* (*Jump*) input is 1 and 0 if the *K* (*Kill*) input is 1. **4) S-R Flip-Flop:** When the clock triggers, the value remembered by the flip-flop remains unchanged if *R* and *S* are both 0, becomes 0 if the *R* (*Reset*) input is 1, and becomes 1 if the *S* (*Set*) input is 1. The behavior in unspecified if both inputs are 1. In Logisim, the value in the flip-flop remains unchanged. By default, the clock triggers on a rising edge, i.e. when the clock input changes from 0 to 1. However, the Trigger attribute allows this to be changed to a falling edge (when the clock input changes from 1 to 0), a high level (for the duration that the clock input is 1), or a low level (for the duration that the clock input is 0). The level-trigger options are unavailable for *T* and *J-K* flip-flops, because the flip-flop behaves unpredictably when told to toggle for an indeterminate amount of time [4].

The clock toggles its output value on a regular schedule as long as ticks are enabled. A "tick" is Logisim's unit of time; the speed at which ticks occur can be selected from the Simulate menu's Tick Frequency submenu. The clock's cycle can be configured using its High Duration and Low Duration attributes. Logisim's simulation of clocks is quite unrealistic: In real circuits, multiple clocks will drift from one another and will never move in lockstep. But in Logisim, all clocks experience ticks at the same rate [4.]

The circuit of the convolutional encoder shown in Fig. 3 is drawn and tested in Logisim, to verify its operation. The circuit is built by inserting in the editing area its components – three 2-input XOR gates (XOR Gate) and three D flip-flops (D Flip-Flop) first as a sort of skeleton and then connecting them with wires. To add an input m and two outputs u1 and u2 into the diagram, the Input tool ( ) and the Output tool ( ) are selected and the pins are placed down. Then the Clock component (Clock) is placed down and connected to the flip-flops. The operation of the convolutional encoder in Fig. 3 is shown in Fig. 4. The results in Fig. 4 and its operation in Fig. 3 are identical.

4. Application in the Educational Process

The material is used in the educational process in the courses "Coding in Telecommunication Systems", "Digital Circuits" and "Pulse and Digital Devices" included in the curriculum of the specialties "Internet and Mobile Communications", "Computer Systems and Technologies", "Electronics", "Computer Management

and Automation", and "Information and Communication Technologies" for the students of the Bachelor degree in the University of Ruse.

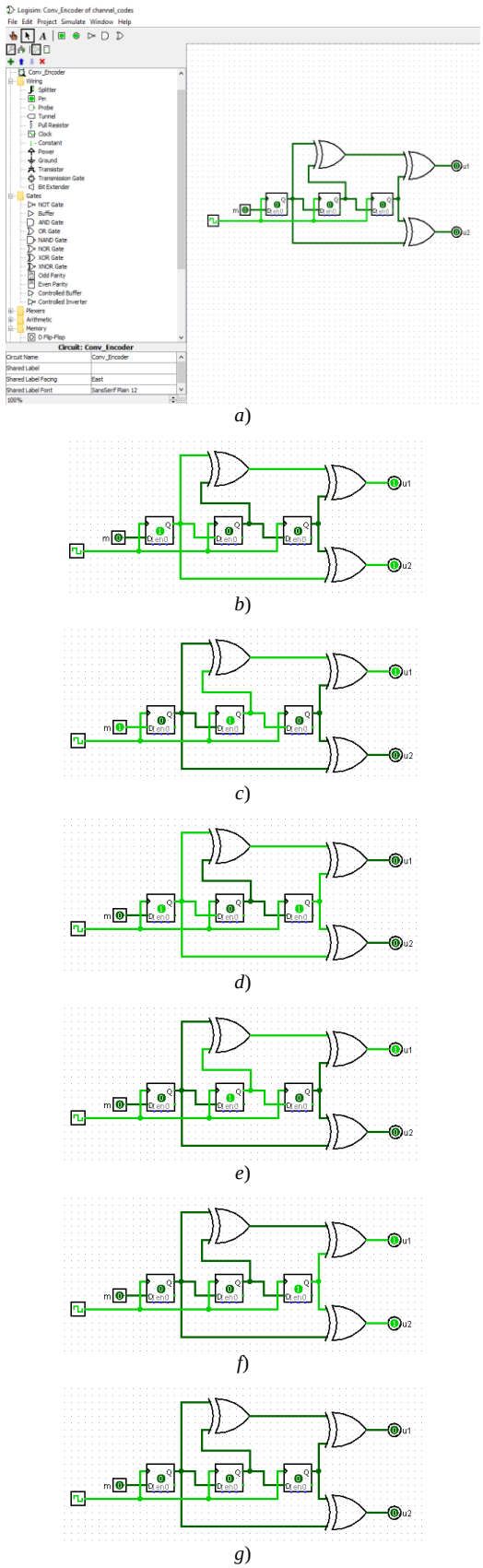

Fig. 4. a) Logisim and its simple toolbar interface + the circuit of the encoder (initial state – all-zeros) and its operations at the instances…; b) t_1; c) t_2; d) t_3; e) t_4; f) t_5; g) t_6

In order to better perception of the material active learning methods are applied in the educational process. An individual assignment is given to each student and he/she has to solve the task during the practical exercise and present it at the end of the classes to the lecturer. The student should synthesize a convolutional encoder with NAND/XOR gates and flip-flops and to simulate its operation using Logisim.

Table 1 presents the results of 10 options applied in the educational process for encoding the 3-bit message **m** = 101 using different convolutional encoders.

Table 1: *Results of 10 options applied in the educational process for encoding the 3-bit message 101 using different convolutional encoders*

№	Connection vectors for the …		Code bits
	upper adder	lower adder	
1	111	011	**10 11 01 11 11**
2	101	110	**11 01 01 01 10**
3	011	101	**01 10 10 10 11**
4	110	111	**11 11 10 11 01**
5	011	110	**01 11 11 11 10**
6	101	011	**10 01 01 01 11**
7	111	110	**11 11 01 11 10**
8	110	101	**11 10 10 10 01**
9	011	111	**01 11 10 11 11**
10	110	011	**10 11 11 11 01**

6. Conclusion

Incorporating active learning into the curriculum transforms the classroom into an exciting, dynamic learning environment. In order to easily assimilation of the material studied by students, active learning is applied. An individual assignment is given to each student. The assignment includes: 1) filling in the blanks for a given convolutional encoder (Fig. 3); 2) synthesizing a convolutional encoder with XOR gates and D flip-flops and simulating its operation using Logisim (Fig. 4); 3) synthesizing a convolutional encoder with NAND gates and D flip-flops and simulating its operation using Logisim; 4) synthesizing a convolutional encoder with XOR gates and J-K flip-flops and simulating its operation using Logisim. During the practical exercises, the student must solve his/her tasks of pre-prepared form published in the e-learning platform of the University of Ruse and submit to the teacher at the end of the classes. The opportunity for extra work is given to the curious students – for example, synthesizing a convolutional encoder with XOR gates and D flip-flops and simulating its operation using Logisim based on 4-bit or 5-bit shift registers with more than two output code bits. The material is used in the educational process in the courses "Coding in Telecommunication Systems", "Digital Circuits" and "Pulse and Digital Devices" included in the curriculum of the specialties "Internet and Mobile Communications", "Computer Systems and Technologies", "Electronics", "Computer Management and Automation", and "Information and Communication Technologies" for the students of the Bachelor degree in the University of Ruse.

The study was supported by contract of University of Ruse "Angel Kanchev", № BG05M2OP001-2.009-0011-C01, "Support for the development of human resources for research and innovation at the University of Ruse "Angel Kanchev"". The project is funded with support from the Operational Program "Science and Education for Smart Growth 2014-2020" financed by the European Social Fund of the European Union.

7. References

1. https://en.wikipedia.org/wiki/Convolutional_code (visited in November 2017).

2. Sklar, B. Digital Communications. Fundamentals and Applications. Second Edition. Communications Engineering Services, Tarzana, California, 2001. http://userspages.uob.edu.bh/-mangoud/mohab/Courses_files/sklar.pdf (visited in November 2017).

3. www.cburch.com/logisim/ (visited in November 2017).

4. Logisim Documentation (11 October 2014).

SIMULATION OF THE PROCESSES OF ENCODING AND DECODING WITH LINEAR BLOCK CODES DETECTING AND CORRECTING ERRORS

Assist. Prof. M.Sc. Borodzhieva A. PhD.[1], M.Sc. Aliev Y.[2], Assoc. Prof. M.Sc. Ivanova G. PhD[2]
Faculty of Electrical Engineering, Electronics and Automation – University of Ruse "Angel Kanchev",
Bulgaria, Department of Telecommunications[1], Department of Computer Systems and Technologies[2]
aborodzhieva@uni-ruse.bg

Abstract: *In coding theory, a linear code is an error-correcting code for which any linear combination of codewords is also a codeword. Linear codes are traditionally divided into block codes and convolutional codes. Linear codes allow more efficient encoding and decoding algorithms than other codes using the syndrome decoding. Linear codes are applied in methods for transmitting symbols on a communication channel so that, if errors occur in the communications, some errors can be corrected or detected by the recipient of a message block. The codewords in a linear block code are blocks of symbols that are encoded using more symbols than the original value to be sent. A (6, 3) linear block code example and its decoder implementation using Logisim, an educational tool for designing and simulating digital logic circuits, are given in the paper. The processes of encoding and decoding when detecting and correcting errors using this (6, 3) linear block code are illustrated. The material presented in the paper is used in the educational process in the University of Ruse.*

Keywords: MODELING AND SIMULATION, LINEAR BLOCK CODES, LOGISIM, ACTIVE LEARNING METHODS

1. Introduction

Channel coding refers to the class of signal transformations designed to improve communications performance by enabling the transmitted signals to better withstand the effects of various channel impairments, such as noise, interference, and fading. These signal-processing techniques can be thought of as vehicles for accomplishing desirable system trade-offs (e.g., error-performance versus bandwidth, power versus bandwidth). The use of large-scale integrated circuits and high-speed digital signal processing techniques have made it possible to provide as much as 10 *dB* performance improvement through these methods, at much less cost than through the use of most other methods such as higher power transmitters or larger antennas [1, 2].

2. Linear block codes

Linear block codes are a class of parity-check codes described by the (n,k) notation. The encoder transforms a block of *k* message digits (a message vector) into a longer block of *n* codeword digits (a code vector) constructed from a given alphabet of elements. When the alphabet consists of two elements (0 and 1), the code is a binary code comprising binary digits (bits) [1].

The *k*-bit messages form 2^k distinct message sequences, referred to as *k*-tuples (sequences of *k* bits). The *n*-bit blocks form 2^n distinct sequences, referred to as *n*-tuples. The encoding process assigns *one* of the 2^n *n*-tuples to each of the 2^k message *k*-tuples. A *block code* represents a one-to-one assignment, whereby the 2^k message *k*-tuples are uniquely mapped into a new set of 2^k codeword *n*-tuples; the mapping can be accomplished via a look-up table. For *linear codes*, the mapping transformation is *linear* [1].

The set of all binary *n*-tuples, V_n, is called a *vector space* over the binary field of two elements (0 and 1). The binary field has two operations, addition and multiplication, such that the results of all operations are in the same set of two elements. The arithmetic operations of addition and multiplication are defined by the conventions of the algebraic field. For example, in a binary field, the rules of addition and multiplication are as follows: 1) $0 \oplus 0 = 0$, $0 \oplus 1 = 1 \oplus 0 = 1$, $1 \oplus 1 = 0$; 2) $0 \cdot 0 = 0$, $0 \cdot 1 = 1 \cdot 0 = 0$, $1 \cdot 1 = 0$. The addition operation, designated with the symbol $\oplus$, is the modulo-2 operation. The summation of binary *n*-tuples always entails modulo-2 addition.

A subset *S* of the vector space V_n is called a *subspace* if the following two conditions are met: 1) The all-zeros vector is in *S*. 2) The sum of any two vectors in *S* is also in *S* (known as the *closure property*). These properties are fundamental for the algebraic characterization of linear block codes. Let $\mathbf{V}_i$ and $\mathbf{V}_j$ be two codewords (or code vectors) in an (n,k) binary block code. The code is said to be *linear* if, and only if $\mathbf{V}_i \oplus \mathbf{V}_j$ is also a code vector. A linear block code, then, is one in which vectors outside the subspace cannot be created by the addition of legitimate codewords (members of the subspace). For example, the vector space V_4 consists of the following 2^4 = sixteen 4-tuples: 0000, 0001, 0010, 0011, 0100, 0101, 0110, 0111, 1000, 1001, 1010, 1011, 1100, 1101, 1110, 1111. An example of a subset of V_4 that forms a subspace is: 0000, 0101, 1010, 1111. It seems that the addition of any two vectors in the subspace can only yield one of the other members of the subspace. A set of 2^k *n*-tuples is called a *linear block code* if, and only if, it is a subspace of the vector space V_n of all *n*-tuples. Fig. 1 illustrates the structure of linear block codes [1].

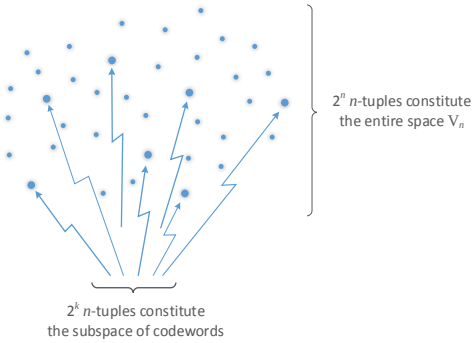

Fig. 1. *Linear block-code structure* [1]

The vector space V_n consists of 2^n *n*-tuples. Within this vector space there exists a subset of 2^k *n*-tuples forming a subspace. These 2^k vectors (points), shown "sprinkled" among the more numerous 2^n points, represent the legitimate (allowable) code-words. A message is encoded into one of the 2^k allowable code vectors and then transmitted. Because of noise in the channel, a corrupted version of the codeword (one of the other 2^n vectors in the *n*-tuple space) may be received. If the corrupted vector is not too distant from the valid codeword, the decoder can decode the message correctly. The basic goals in choosing a particular code can be stated in the context of Fig. 1 as follows: 1) for coding efficiency packing the V_n space with as many codewords as possible, to expend a *small amount of redundancy* (excess bandwidth); 2) the codewords must be as *far apart from one another* as possible, so that even if the vectors are corrupted during transmission, they may still be correctly decoded, with a high probability [1].

3. A (6, 3) linear block code example

The following coding assignment describing a (6, 3) code is examined. There are $2^k = 2^3 = 8$ message vectors, and therefore eight codewords. There are $2^n = 2^6 = 64$ 6-tuples in the V_6 vector space. It seems that the eight codewords in Table 1 form a subspace of V_6 (the all-zeros vector is present, and the sum of any two codewords yields another codeword member of the subspace). Therefore, these codewords represent a *linear block code*. A unique assignment for a particular (n, k) code does not exist; however, there is no complete freedom of choice.

Table 1. *Assignment of codewords to messages*

Message vector	Codeword
000	000000
100	110100
010	011010
110	101110
001	101001
101	011101
011	110011
111	000111

If k is large, a *table look-up* implementation of the encoder becomes prohibitive. For a (127, 92) code there are 2^{92} or approximately 5×10^{27} code vectors. The size of the memory necessary to contain such a large number of codewords is large, but it is possible to reduce the complexity by generating the required codewords as needed, instead of storing them [1].

Since a set of codewords that forms a linear block code is a k-dimensional subspace of the n-dimensional binary vector space ($k < n$), it is always possible to find a set of n-tuples, fewer than 2^k, that can generate all the 2^k codewords of the subspace. Generating the set of vectors is said to *span* the subspace. The smallest *linearly independent* set that spans the subspace is called a *basis* of the subspace, and the number of vectors in this basis set is the dimension of the subspace. Any basis set of k linearly independent n-tuples $\mathbf{V}_1, \mathbf{V}_2, \ldots, \mathbf{V}_k$ can be used to generate the required linear block code vectors, since each code vector is a linear combination of $\mathbf{V}_1, \mathbf{V}_2, \ldots, \mathbf{V}_k$. Each of the set of 2^k codewords $\{\mathbf{U}\}$ can be described by $\mathbf{U} = m_1\mathbf{V}_1 + m_2\mathbf{V}_2 + \ldots + m_k\mathbf{V}_k$, where $m_i = (0 \text{ or } 1)$ are the message bits and $i = 1, \ldots, k$. In general, the generator matrix is defined by the following $k \times n$ array [1]:

$$(1)\quad \mathbf{G} = \begin{bmatrix} \mathbf{V}_1 \\ \mathbf{V}_2 \\ \vdots \\ \mathbf{V}_k \end{bmatrix} = \begin{bmatrix} v_{11} & v_{12} & \cdots & v_{1n} \\ v_{21} & v_{22} & \cdots & v_{2n} \\ \vdots & \vdots & \vdots & \vdots \\ v_{k1} & v_{k2} & \cdots & v_{kn} \end{bmatrix}.$$

Code vectors are usually designated as row vectors. Thus, the message **m**, a sequence of k message bits, is shown below as a row vector ($1\times k$ matrix) $\mathbf{m} = m_1, m_2, \ldots, m_k$.

The generation of the codeword **U** is written in matrix notation as $\mathbf{U} = \mathbf{mG}$, where the matrix multiplication $\mathbf{C} = \mathbf{AB}$ is performed in the usual way by using the rule $c_{ij} = \sum_{k}^{n} a_{ik} b_{kj}$, $i = 1, \ldots, l$, $i = 1, \ldots, m$, where **A** is an $l \times n$ matrix, **B** is an $n \times m$ matrix, and the result **C** is an $l \times m$ matrix. For the example in Table 1, the generator matrix is:

$$(2)\quad \mathbf{G} = \begin{bmatrix} \mathbf{V}_1 \\ \mathbf{V}_2 \\ \mathbf{V}_3 \end{bmatrix} = \begin{bmatrix} 1 & 1 & 0 & 1 & 0 & 0 \\ 0 & 1 & 1 & 0 & 1 & 0 \\ 1 & 0 & 1 & 0 & 0 & 1 \end{bmatrix},$$

where $\mathbf{V}_1$, $\mathbf{V}_2$, and $\mathbf{V}_3$ are three *linearly* independent vectors (a subset of the eight code vectors) that can generate all the code vectors. The sum of any two generating vectors does not yield any of the other generating vectors. Generating the codeword $\mathbf{U}_4$ for the fourth message vector 110 in Table 1, using the generator matrix in Equation (2) is as follows:

$$\mathbf{U}_4 = \begin{bmatrix} 1 & 1 & 0 \end{bmatrix} \begin{bmatrix} \mathbf{V}_1 \\ \mathbf{V}_2 \\ \mathbf{V}_3 \end{bmatrix} = 1\cdot\mathbf{V}_1 + 1\cdot\mathbf{V}_2 + 0\cdot\mathbf{V}_3 =$$

$$(3)\quad = \begin{bmatrix} 1 & 1 & 0 & 1 & 0 & 0 \end{bmatrix} + \begin{bmatrix} 0 & 1 & 1 & 0 & 1 & 0 \end{bmatrix} +$$

$$+ \begin{bmatrix} 0 & 0 & 0 & 0 & 0 & 0 \end{bmatrix} = \begin{bmatrix} 1 & 0 & 1 & 1 & 1 & 0 \end{bmatrix}$$

The code vector corresponding to a message vector is a linear combination of the rows of **G**. Since the code is totally defined by **G**, the encoder needs only store k rows of **G** instead of the total 2^k vectors of the code. For this example, the generator matrix of size 3×6 in Equation (2) replaces the original codeword array of size 8×6 in Table 1, representing a reduction in system complexity [1].

A systematic (n, k) linear block code is a mapping from a k-dimensional message vector to an n-dimensional codeword in such a way that a part of the sequence generated coincides with the k message bits. The remaining $(n-k)$ bits are the parity bits. A systematic linear block code has a generator matrix of the form [1]:

$$(4)\quad \mathbf{G} = \begin{bmatrix} \mathbf{P} \mid \mathbf{I}_k \end{bmatrix} = \begin{bmatrix} p_{11} & p_{12} & \cdots & p_{1,(n-k)} & 1 & 0 & \ldots & 0 \\ p_{21} & p_{22} & \cdots & p_{2,(n-k)} & 0 & 1 & \ldots & 0 \\ \vdots & \vdots & \vdots & \vdots & \vdots & \vdots & \vdots & \vdots \\ p_{k1} & p_{k2} & \cdots & p_{k,(n-k)} & 0 & 0 & \ldots & 1 \end{bmatrix},$$

where **P** is the parity array portion of the generator matrix, $p_{ij} = (0 \text{ or } 1)$, and $\mathbf{I}_k$ is the $k \times k$ identity matrix. With this systematic generator, the encoding complexity is further reduced since it is not necessary to store the identity matrix portion of the array. Each codeword is expressed as [1]:

$$\begin{bmatrix} u_1, u_2, \ldots, u_n \end{bmatrix} = \begin{bmatrix} m_1, m_2, \ldots, m_k \end{bmatrix} \times$$

$$(5)\quad \begin{bmatrix} p_{11} & p_{12} & \cdots & p_{1,(n-k)} & 1 & 0 & \ldots & 0 \\ p_{21} & p_{22} & \cdots & p_{2,(n-k)} & 0 & 1 & \ldots & 0 \\ \vdots & \vdots & \vdots & \vdots & \vdots & \vdots & \vdots & \vdots \\ p_{k1} & p_{k2} & \cdots & p_{k,(n-k)} & 0 & 0 & \ldots & 1 \end{bmatrix},$$

where $u_i = m_1 p_{1i} + m_2 p_{2i} + \ldots + m_k p_{ki}$ for $i = 1, \ldots, (n-k)$ and $u_i = m_{i-n+k}$ for $i = (n-k+1), \ldots, n$.

Given the message k-tuple $\mathbf{m} = m_1, m_2, \ldots, m_k$ and the general code vector n-tuple $\mathbf{U} = u_1, u_2, \ldots, u_n$, the systematic code vector can be expressed as $\mathbf{U} = \underbrace{p_1, p_2, \ldots, p_{n-k}}_{\text{parity bits}}, \underbrace{m_1, m_2, \ldots, m_k}_{\text{message bits}}$, where:

$$p_1 = m_1 p_{11} + m_2 p_{21} + \ldots + m_k p_{k1},$$

$$(6)\quad p_2 = m_1 p_{12} + m_2 p_{22} + \ldots + m_k p_{k2}, \ \ldots,$$

$$p_{n-k} = m_1 p_{1,(n-k)} + m_2 p_{2,(n-k)} + \ldots + m_k p_{k,(n-k)}.$$

Sometimes systematic codewords are written in such a way that the message bits occupy the left-hand part of the codeword and the parity bits occupy the right-hand part. This reordering has no effect on the error detection or error correction properties of the code, and will not be considered further.

For the (6, 3) code example (Table 1), the codewords are described as follows:

(7) $$\mathbf{U}=[m_1,m_2,m_3]\left[\begin{array}{ccc|ccc}1&1&0&1&0&0\\0&1&1&0&1&0\\1&0&1&0&0&1\end{array}\right],$$

(8) $$\mathbf{U}=\underbrace{m_1+m_3}_{u_1},\underbrace{m_1+m_2}_{u_2},\underbrace{m_2+m_3}_{u_3},\underbrace{m_1}_{u_4},\underbrace{m_2}_{u_5},\underbrace{m_3}_{u_6}.$$

Equation (8) provides some insight into the structure of linear block codes. The redundant digits are produced in a variety of ways. The first parity bit is the sum of the first and third message bits; the second parity bit is the sum of the first and second message bits; and the third parity bit is the sum of the second and third message bits. Such structure, compared with single-parity checks or simple digit-repeat procedures, may provide greater ability to detect and correct errors.

A matrix **H**, called the *parity-check matrix*, enables to decode the received vectors. For each $(k\times n)$ generator matrix **G**, there exists an $(n-k)\times k$ matrix **H**, such that the rows of **G** are orthogonal to the rows of **H**, i.e. $\mathbf{GH}^{\mathrm{T}}=\mathbf{0}$, where $\mathbf{H}^{\mathrm{T}}$ is the *transpose* of **H**, and **0** is a $k\times(n-k)$ all-zeros matrix. To fulfill the orthogonality requirements for a systematic code, the components of the **H** matrix and the $\mathbf{H}^{\mathrm{T}}$ matrix are written as [1]:

(9) $$\mathbf{H}=\left[\mathbf{I}_{n-k}\mid\mathbf{P}^{\mathrm{T}}\right],$$

(10) $$\mathbf{H}^{\mathrm{T}}=\left[\frac{\mathbf{I}_{n-k}}{\mathbf{P}}\right]=\begin{bmatrix}1&0&\dots&0\\0&1&\dots&0\\\vdots&\vdots&\vdots&\vdots\\0&0&\dots&1\\p_{11}&p_{12}&\cdots&p_{1,(n-k)}\\p_{21}&p_{22}&\cdots&p_{2,(n-k)}\\\vdots&\vdots&\vdots&\vdots\\p_{k1}&p_{k2}&\cdots&p_{k,(n-k)}\end{bmatrix}$$

It seems that the product $\mathbf{UH}^{\mathrm{T}}$ of each codeword **U**, generated by **G** and the matrix, yields

(11) $$\mathbf{UH}^{\mathrm{T}}=[p_1+p_1,p_2+p_2,\dots,p_{n-k}+p_{n-k}]=\mathbf{0},$$

where $p_1,p_2,\dots,p_{n-k}$ are the parity bits. Once the *parity-check matrix* **H** is constructed to fulfill the orthogonality requirements, it can be used to test whether a received vector is a valid member of the codeword set. **U** is a codeword generated by matrix **G** if, and only if $\mathbf{UH}^{\mathrm{T}}=\mathbf{0}$.

Let $\mathbf{r}=r_1,r_2,\dots,r_n$ be a received vector (one of 2^n *n*-tuples) resulting from the transmission of $\mathbf{U}=u_1,u_2,\dots,u_n$ (one of 2^k *n*-tuples). Therefore **r** can be describe as $\mathbf{r}=\mathbf{U}+\mathbf{e}$, where $\mathbf{e}=e_1,e_2,\dots,e_n$ is an error vector or error pattern introduced by the channel. There are a total of 2^n-1 potential non-zero error patterns in the space of 2^n *n*-tuples. The *syndrome* of **r** is defined as

(12) $$\mathbf{S}=\mathbf{rH}^{\mathrm{T}}.$$

The syndrome is the result of a parity check performed on **r** to determine whether **r** is a valid member of the codeword set. If **r** is a member, the syndrome **S** has a value **0.** If **r** contains detectable errors, the syndrome has some nonzero value. If **r** contains correctable errors, the syndrome has some nonzero value that can earmark the particular error pattern. The syndrome of **r** will be:

(13) $$\mathbf{S}=(\mathbf{U}+\mathbf{e})\mathbf{H}^{\mathrm{T}}=\mathbf{UH}^{\mathrm{T}}+\mathbf{eH}^{\mathrm{T}}.$$

However, $\mathbf{UH}^{\mathrm{T}}=\mathbf{0}$ for all members of the codeword set. Therefore,

(14) $$\mathbf{S}=\mathbf{eH}^{\mathrm{T}}.$$

It is evident that the syndrome test, whether performed on either a corrupted code vector or on the error pattern that caused it, yields the same syndrome. An important property of linear block codes, fundamental to the decoding process, is that the mapping between correctable error patterns and syndromes is one to one.

It is interesting to note the following two required properties of the parity-check matrix: 1) No column of **H** can be all zeros, or else an error in the corresponding code-word position would not affect on the syndrome and would be undetectable. 2) All columns of **H** must be unique. If two columns of **H** were identical, errors in these two corresponding codeword positions would be indistinguishable.

Suppose that codeword $\mathbf{U}=101110$ is transmitted and the vector $\mathbf{r}=001110$ is received, i.e. the leftmost bit is received in error. The syndrome vector value $\mathbf{S}=\mathbf{rH}^{\mathrm{T}}$ is found below and it is verified that it is equal to $\mathbf{eH}^{\mathrm{T}}$**.** The syndrome of the corrupted code vector and the syndrome of the error pattern will be [1]:

(15) $$\mathbf{S}=\mathbf{rH}^{\mathrm{T}}=\begin{bmatrix}0&0&1&1&1&0\end{bmatrix}\begin{bmatrix}1&0&0\\0&1&0\\0&0&1\\1&1&0\\0&1&1\\1&0&1\end{bmatrix}=\begin{bmatrix}1&0&0\end{bmatrix}$$

(16) $$\mathbf{S}=\mathbf{eH}^{\mathrm{T}}=\begin{bmatrix}1&0&0&0&0&0\end{bmatrix}\mathbf{H}^{\mathrm{T}}=\begin{bmatrix}1&0&0\end{bmatrix}$$

A single error is detected and it is shown that the syndrome test performed on either the corrupted codeword, or on the error pattern that caused it, yields the same syndrome. It means that the error not only can be detected, but since there is a one-to-one correspondence between correctable error patterns and syndromes, such error patterns can be corrected. Let arrange the 2^n *n*-tuples that represent possible received vectors in an array, called the *standard array*, such that the first row contains all the codewords, starting with the all-zeros codeword, and the first column contains all the correctable error patterns. From the basic properties of linear codes it is known that the all-zeros vector must be a member of the codeword set. Each row, called a *coset*, consists of an error pattern in the first column, called the *coset leader*, followed by the codewords corrupted by that error pattern. The standard array format for an (n,k) code is as follows:

(17) $$\begin{array}{ccccccc}\mathbf{U}_1&\mathbf{U}_2&\dots&\mathbf{U}_i&\dots&\mathbf{U}_{2^k}\\\mathbf{e}_2&\mathbf{U}_2+\mathbf{e}_2&\dots&\mathbf{U}_i+\mathbf{e}_2&\dots&\mathbf{U}_{2^k}+\mathbf{e}_2\\\mathbf{e}_3&\mathbf{U}_2+\mathbf{e}_3&\dots&\mathbf{U}_i+\mathbf{e}_3&\dots&\mathbf{U}_{2^k}+\mathbf{e}_3\\\vdots&\vdots&\vdots&\vdots&\vdots&\vdots\\\mathbf{e}_j&\mathbf{U}_2+\mathbf{e}_j&\dots&\mathbf{U}_i+\mathbf{e}_j&\dots&\mathbf{U}_{2^k}+\mathbf{e}_j\\\vdots&\vdots&\vdots&\vdots&\vdots&\vdots\\\mathbf{e}_{2^{n-k}}&\mathbf{U}_2+\mathbf{e}_{2^{n-k}}&\dots&\mathbf{U}_i+\mathbf{e}_{2^{n-k}}&\dots&\mathbf{U}_{2^k}+\mathbf{e}_{2^{n-k}}\end{array}$$

The all-zeros codeword $\mathbf{U}_1$ plays two roles. It is one of the codewords and it can also be thought of as the error pattern $\mathbf{e}_1$ – the pattern that represents no error, such that $\mathbf{r}=\mathbf{U}$. The array contains all 2^n *n*-tuples in the space V_n. Each *n*-tuple appears in *only one* location – none is missing, and none is replicated. Each coset consists of 2^k *n*-tuples. Therefore, there are $\left(2^n/2^k\right)=2^{n-k}$ cosets [1].

The decoding algorithm calls for replacing a corrupted vector (any *n*-tuple excluding those in the first row) with a valid codeword from the top of the column containing the corrupted vector. Suppose that a codeword $\mathbf{U}_i$ ($i = 1, \ldots, 2^k$) is transmitted over a noisy channel, resulting in a received corrupted vector $\mathbf{U}_i + \mathbf{e}_j$. If the error pattern $\mathbf{e}_j$ caused by the channel is a coset leader, where the index $j = 1, \ldots, 2^{n-k}$, the received vector will be decoded correctly into the transmitted codeword $\mathbf{U}_i$. If the error pattern is not a coset leader, then the decoding will be erroneous. If $\mathbf{e}_j$ is the coset leader or error pattern of the j^{th} coset, then $\mathbf{U}_i + \mathbf{e}_j$ is an *n*-tuple in this coset. The syndrome of this *n*-tuple can be written $\mathbf{S} = (\mathbf{U}_i + \mathbf{e}_j)\mathbf{H}^{\mathrm{T}} = \mathbf{U}_i\mathbf{H}^{\mathrm{T}} + \mathbf{e}_j\mathbf{H}^{\mathrm{T}}$. Since $\mathbf{U}_i$ is a code vector and $\mathbf{U}_i\mathbf{H}^{\mathrm{T}} = \mathbf{0}$, then $\mathbf{S} = (\mathbf{U}_i + \mathbf{e}_j)\mathbf{H}^{\mathrm{T}} = \mathbf{e}_j\mathbf{H}^{\mathrm{T}}$. The name *coset* is short for "a *set* of numbers having a *common* feature." Each member of a coset has the *same syndrome.* The syndrome for each coset is different from that of any other coset in the code; it is the syndrome used to estimate the error pattern [1].

The procedure for error correction decoding proceeds as follows: 1) Calculating the syndrome of $\mathbf{r}$ using $\mathbf{S} = \mathbf{r}\mathbf{H}^{\mathrm{T}}$. 2) Locating the coset leader (error pattern) $\mathbf{e}_j$, whose syndrome is equal to $\mathbf{r}\mathbf{H}^{\mathrm{T}}$. This error pattern is assumed to be the corruption caused by the channel. The corrected received vector, or codeword, is identified as $\mathbf{U} = \mathbf{r} + \mathbf{e}_j$. The valid codeword is retrieved by subtracting out the identified error; in modulo-2 arithmetic, the operation of subtraction is identical to that of addition.

Returning to the example in Table 1, the 2^6 = sixty-four 6-tuples are arranged in a standard array as shown in Fig. 2. The valid codewords are the eight vectors in the first row, and the *correctable error patterns* are the seven nonzero *coset leaders* in the first column. All 1-bit error patterns are correctable. After exhausting all 1-bit error patterns, there remains some error-correcting capability since all sixty-four 6-tuples have not yet been accounted. There is one unassigned coset leader; therefore, there remains the capability of correcting one additional error pattern. There is the flexibility of choosing this error pattern to be any of the *n*-tuples in the remaining coset. In Fig. 2 this final correctable error pattern is chosen, somewhat arbitrarily, to be the 2-bit error pattern 010001. Decoding will be correct if, and only if, the error pattern caused by the channel is one of the coset leaders.

000000	110100	011010	101110	101001	011101	110011	000111
000001	110101	011011	101111	101000	011100	110010	000110
000010	110110	011000	101100	101011	011111	110001	000101
000100	110000	011110	101010	101101	011001	110111	000011
001000	111100	010010	100110	100001	010101	111011	001111
010000	100100	001010	111110	111001	001101	100011	010111
100000	010100	111010	001110	001001	111101	010011	100111
010001	100101	001011	111111	111000	001100	100010	010110

Fig. 2. *Example of a standard array for a (6, 3) code*

The syndrome corresponding to each of the correctable error sequences is determined by computing $\mathbf{e}_j\mathbf{H}^{\mathrm{T}}$ for each coset leader, as follows:

$$(18)\quad \mathbf{S} = \mathbf{e}_j \begin{bmatrix} 1 & 0 & 0 \\ 0 & 1 & 0 \\ 0 & 0 & 1 \\ 1 & 1 & 0 \\ 0 & 1 & 1 \\ 1 & 0 & 1 \end{bmatrix}.$$

The results are listed in Table 2. Since each syndrome in the table is unique, the decoder can identify the error pattern **e** to which it corresponds.

Table 2. *Syndrome Look-Up Table*

Error pattern	Syndrome
000000	000
000001	101
000010	011
000100	110
001000	001
010000	010
100000	100
010001	111

The vector **r** is received and its syndrome is calculated using $\mathbf{S} = \mathbf{r}\mathbf{H}^{\mathrm{T}}$. Then the syndrome look-up table (Table 2) is used to find the corresponding error pattern. This error pattern is an estimate of the error, and it is denoted as $\hat{\mathbf{e}}$. The decoder then adds $\hat{\mathbf{e}}$ to **r** to obtain an estimate of the transmitted codeword $\hat{\mathbf{U}}$**:**

$$(19)\quad \hat{\mathbf{U}} = \mathbf{r} + \hat{\mathbf{e}} = (\mathbf{U} + \mathbf{e}) + \hat{\mathbf{e}} = \mathbf{U} + (\mathbf{e} + \hat{\mathbf{e}}).$$

If the estimated error pattern is the same as the actual error pattern, i.e. $\hat{\mathbf{e}} = \mathbf{e}$, then the estimate $\hat{\mathbf{U}}$ is equal to the transmitted codeword $\mathbf{U}$**.** If the error estimate is incorrect, the decoder will estimate a codeword that was not transmitted, and there is an *undetectable decoding error.*

Assume that codeword $\mathbf{U} = 101110$ is transmitted, and the vector $\mathbf{r} = 001110$ is received. Show how a decoder, using the Table 2 syndrome look-up table, can correct the error. The syndrome of **r** is computed:

$$(20)\quad \mathbf{S} = [0 \quad 0 \quad 1 \quad 1 \quad 1 \quad 0]\mathbf{H}^{\mathrm{T}} = [1 \quad 0 \quad 0].$$

Using Table 2, the error pattern corresponding to the syndrome above is estimated to be $\hat{\mathbf{e}} = 100000$**.** The corrected vector is then estimated by

$$(21)\quad \hat{\mathbf{U}} = \mathbf{r} + \hat{\mathbf{e}} = 001110 + 100000 = 101110.$$

Since the estimated error pattern is the actual error pattern in this example, the error correction procedure yields $\hat{\mathbf{U}} = \mathbf{U}$.

When the code is short as in the case of the (6, 3) code described here, the decoder can be implemented with simple circuitry. The steps that the decoder must take: (1) calculate the syndrome, (2) locate the error pattern, and (3) perform modulo-2 addition of the error pattern and the received vector (which removes the error). The circuit shown in Fig. 3 is made up of exclusive-OR (XOR) gates and AND gates that can accomplish the same result for any *single-error pattern* in the (6, 3) code. Based on Table 2, an expression for each of the syndrome bits can be written in terms of the received codeword bits as

$$(22)\quad \mathbf{S} = \mathbf{r}\mathbf{H}^{\mathrm{T}} = [r_1 \quad r_2 \quad r_3 \quad r_4 \quad r_5 \quad r_6] \begin{bmatrix} 1 & 0 & 0 \\ 0 & 1 & 0 \\ 0 & 0 & 1 \\ 1 & 1 & 0 \\ 0 & 1 & 1 \\ 1 & 0 & 1 \end{bmatrix} \text{ and}$$

$$(23)\quad s_1 = r_1 + r_4 + r_6,\ s_2 = r_2 + r_4 + r_5,\ s_3 = r_3 + r_5 + r_6.$$

These syndrome expressions are used for wiring up the circuit in Fig. 3. The exclusive-OR gate is the same operation as modulo-2 arithmetic and hence uses the same symbol. A small circle at the termination of any line entering the AND gate indicates the logic COMPLEMENT of the signal [1].

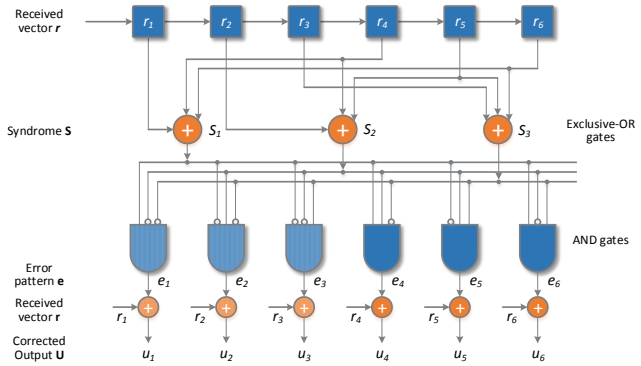

Fig. 3. *Implementation of the (6, 3) decoder* [1]

The corrupted signal enters the decoder at two places simultaneously. At the upper part of the circuit, the syndrome is computed, and at the lower part, that syndrome is transformed to its corresponding error pattern. The error is removed by adding it back to the received vector yielding the corrected codeword. Fig. 3 is drawn to emphasize the algebraic decoding steps – calculation of syndrome, error pattern, and corrected output. In the real world, an (n,k) code is usually configured in systematic form. The decoder would not need to deliver the entire codeword. Its output would consist of the data bits only. Fig. 3 circuitry becomes simplified by eliminating the gates shown with shading. For longer codes, such an implementation is very complex, and the preferred decoding techniques conserve circuitry by using a sequential approach instead of this parallel method. It is also important to emphasize that Fig. 3 has been configured to only detect and correct *single-error patterns* for the (6, 3) code. Error control for a double-error pattern would require additional circuitry.

4. Logisim – an educational tool for designing and simulating digital logic circuits

Logisim is an educational tool for designing and simulating digital logic circuits with simple toolbar interface. With the capacity to build larger circuits from smaller subcircuits, and to draw bundles of wires with a single mouse drag, Logisim can be used to design and simulate entire CPUs for educational purposes. Logisim is used by students at colleges and universities around the world in many types of classes. The main features of the product are: 1) It is free. 2) It runs on any machine supporting Java 5 or later; special versions are released for MacOS X and Windows. 3) The drawing interface is based on an intuitive toolbar. Color-coded wires aid in simulating and debugging a circuit. 4) The wiring tool draws horizontal and vertical wires, automatically connecting to components and to other wires. 5) Completed circuits can be saved into a file, exported to a GIF file, or printed. 6) Circuit layouts can be used as "subcircuits" of other circuits, allowing for hierarchical circuit design. 7) Included circuit components include inputs and outputs, gates, multiplexers, arithmetic circuits, flip-flops, and RAM memory. 8) The included "combinational analysis" module allows for conversion between circuits, truth tables, and Boolean expressions [3].

Features of the components used to build the encoder

The NOT gate emits the complement of the input it receives. The truth table for a NOT gate is the following [4]:

x	out
0	1
1	0

The AND, OR, NAND, and NOR gates compute the respective function of the inputs, and emit the result on the output.

By default, any unconnected inputs are ignored. In this way, a 5-input gate can be inserted but only two inputs are used, and it will work as a 2-input gate; this relieves the user from having to worry about configuring the number of inputs every time a gate is created. The two-input truth table for the gates is the following [4]:

x	y	AND	OR	NAND	NOR
0	0	0	0	1	1
0	1	0	1	1	0
1	0	0	1	1	0
1	1	1	1	0	0

The XOR, XNOR, Even Parity, and Odd Parity gates compute the respective function of the inputs, and emit the result on the output. By default, any inputs left unconnected are ignored. The two-input truth table for the gates is the following [4]:

x	y	XOR	XNOR	Odd	Even
0	0	0	1	0	1
0	1	1	0	1	0
1	0	1	0	1	0
1	1	0	1	0	1

It seems that the Odd Parity gate and the XOR gate behave identically with two inputs; similarly, the Even Parity gate and the XNOR gate behave identically. If there are more than two specified inputs, the XOR gate will emit 1 only when there is exactly one 1 input, whereas the Odd Parity gate will emit 1 if there is an odd number of 1 inputs. The XNOR gate will emit 1 only when there is *not* exactly one 1 input, while the Even Parity gate will emit 1 if there is an even number of 1 inputs. The XOR and XNOR gates include an attribute titled Multiple-Input Behavior that allow them to be configured to use the Odd Parity and Even Parity behavior (Fig. 5). Many authorities contend that the shaped XOR gate's behavior should correspond to the odd parity gate, but there is not agreement on this point. Logisim's default behavior for XOR gates is based on the IEEE 91 standard. It is also consistent with the intuitive meaning underlying the term *exclusive or* [4].

5. Application in the Educational Process

The material is used in the educational process in the courses "Coding in Telecommunication Systems", "Digital Circuits" and "Pulse and Digital Devices" included in the curriculum of the specialties "Internet and Mobile Communications", "Computer Systems and Technologies", "Computer Management and Automation", "Electronics" and "Information and Communication Technologies" for the students of the Bachelor degree in the University of Ruse. In order to better perception of the material active learning methods are applied. An individual assignment is given to each student and he/she has to solve the task during the practical exercise and present it at the end of the classes to the lecturer. The student should synthesize an encoder and a decoder of a linear block code with XOR, NOT and AND gates and to simulate their operation using Logisim.

The circuits of the encoder and the decoder of a (6, 3) linear block code (Table 1, Fig. 3) are drawn and tested in Logisim, to verify their operation. The circuit is built by inserting in the editing area its components – 2-input or 3-input XOR gates (XOR Gate), NOT gates (NOT Gate) and AND (AND Gate) gates first as a sort of skeleton and then connecting them with wires. To add inputs and outputs into the diagram, the Input tool ( ) and the Output tool ( ) are selected and the pins are placed down. The operation of the encoder and the decoder (Table 1, Fig. 3) is illustrated in Fig. 4 and Fig. 6. The results in Fig. 4 and Fig. 6 are identical to Table 1, Fig. 2 (the cells marked) and Fig. 3.

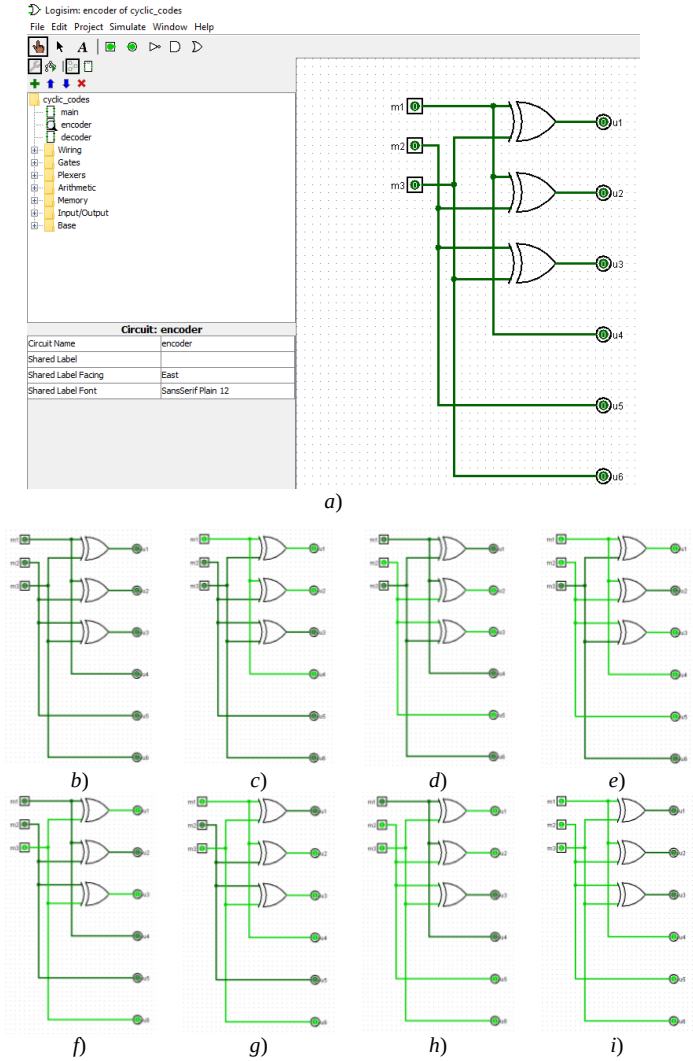

Fig. 4. *a) Logisim and its simple toolbar interface + the circuit of the encoder (initial state – all-zeros) and encoding the message …; b) 000; c) 100; d) 010; e) 110; f) 001; g) 101; h) 011; i) 111*

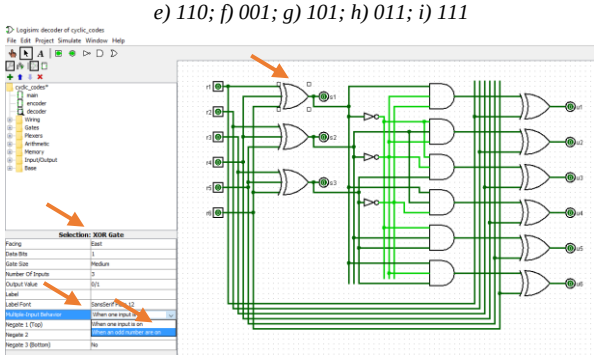

Fig. 5. *Using the attribute Multiple-Input Behavior allowing the XOR gate to be configured to use the Odd Parity behavior*

6. Conclusion

In order to easily assimilation of the material studied by students, active learning methods are applied in the educational process. An individual assignment is given to each student. The assignment includes: 1) filling in the blanks for a given encoder of a (6, 3) linear block code (Table 1, Table 2), after writing down the generator matrix and the parity-check matrix of the code given, implementing the decoder of the code given (Fig. 3); 2) synthesizing the encoder and the decoder of the (6, 3) linear block code with XOR, NOT and AND gates and simulating their operation using Logisim (Fig. 4 and Fig. 6). During the practical exercises, the student must solve his/her tasks of pre-prepared form published in the e-learning platform of the University of Ruse and submit to the teacher at the end of the classes. The opportunity for extra work is given to the curious students – for example, synthesizing the encoder and the decoder of a (8, 4) linear block code using XOR, NOT and AND gates and simulating their operation using Logisim.

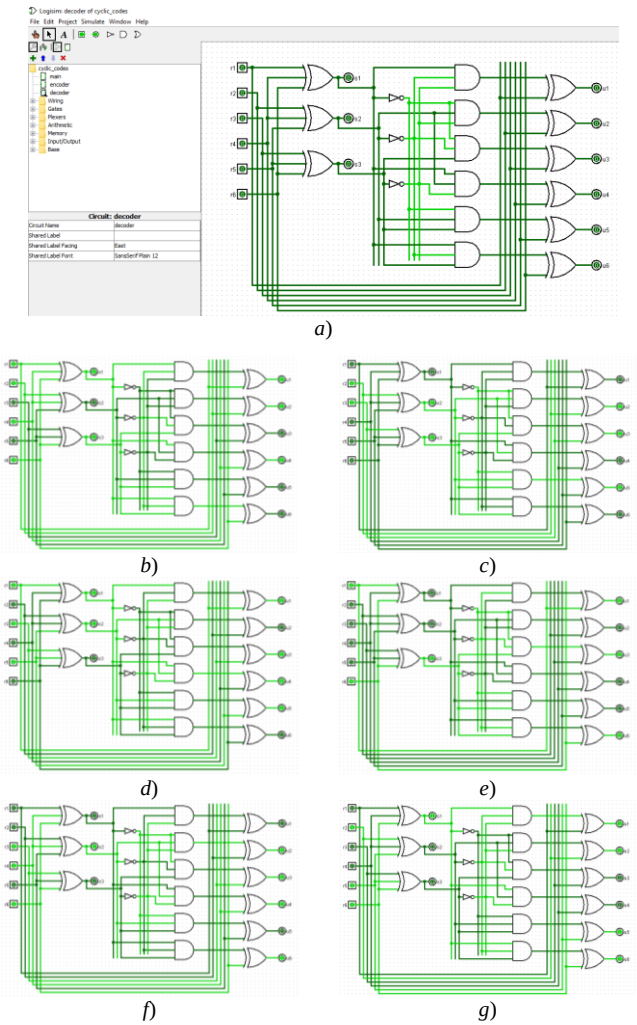

Fig. 6. *a) Logisim and its simple toolbar interface + the circuit of the decoder (initial state – all-zeros); b) 110101; c) 011000; d) 101010; e) 100001; f) 001101; g) 010011*

The study was supported by contract of University of Ruse "Angel Kanchev", № BG05M2OP001-2.009-0011-C01, "Support for the development of human resources for research and innovation at the University of Ruse "Angel Kanchev"". The project is funded with support from the Operational Program "Science and Education for Smart Growth 2014-2020" financed by the European Social Fund of the European Union.

7. References

1. Sklar, B. Digital Communications. Fundamentals and Applications. Second Edition. Communications Engineering Services, Tarzana, California, 2001. http://userspages.uob.edu.bh/mangoud/mohab/Courses_files/sklar.pdf (visited in November 2017).

2. https://en.wikipedia.org/wiki/Linear_code (last visited in November 2017).

3. www.cburch.com/logisim/ (visited in November 2017).

4. Logisim Documentation (11 October 2014).

ПРИЛОЖЕНИЕ НА 3D ИНДУСТРИАЛНА ТОМОГРАФИЯ В ДЕНТАЛНАТА МЕДИЦИНА

APPLICATION OF 3D INDUSTRIAL THOMOGRAPHY IN DENTAL MEDICINE

Казакова С.[1], Каменова Ю.[1], Клочков Л. [2], Стоименов Н.[3], Попов Б.[3], Соколов Б.[3].
e-mail: nikistoimenow@gmail.com
Катедра „Протетична дентална медицина“, Факултет по дентална медицина, Медицински Университет, София [1],
Катедра „Автоматизация на дискретното производство, Машиностроителен Факултет, Технически Университет – София [2],
Институт по Информационни и Комуникационни Технологии, Българска Академия на Науките, София, България [3].

Abstract: *The presented paper examines the possibility of non-destructive testing, investigation and analysis of dental samples by the usage of industrial computer tomography. For the study was used the Nikon XT H 225 3D industrial computer tomography, which provides high accuracy of the internal and external parameters of the samples tested. A test with forty dental samples, pre-treated with Er: Cr / YSGG laser Biolase, Waterlase, MD, USA, in four modes of operation was established. The obtained results are analyzed and discussed. There is a difference in the four modes of operation of the laser.*

Ключови думи: компютърна томография, емайлова повърхност, зъбни образци, Er:Cr/YSGG лазер.

1. Въведение

В съвременната дентална практика минимално инвазивните процедури са широко разпространени. Липсата на необходимост от използването на анестезия се смята за предимство. Осигуряването на адхезивна връзка към емайла представлява процедура, широко застъпена при дентални реставрации, които включват фасети и външно коронкови крепители.

Адхезията към емайла се постига чрез киселинно ецване на този високо минерализиран субстрат. Тази процедура увеличава повърхността за адхезивно свързване. Създават се микро кухини в емайла, композитът прониква в тях и създава повлекла. Адхезивната връзка към емайла представлява основна причина за клиничния успех на редица възстановителни процедури [1].

През последните години в денталната медицина широко приложение намират лазери от типа Er:YAG и Er; Cr:YSGG. Er; Cr:YSGG лазерния лъч селективно навлиза в тъканите и абсорбира от водата (при вода от 3 μm до 10 μm), хидроксилапатита и колагена. Образуват се различни по дълбочина и ширина кратери. Така образуваната повърхност спомага за осигуряване на механична ретенция и увеличава адхезията на композитния цимент към твърдите зъбни тъкани. Тази повърхност може да замести киселинното ецване. През годините са правени редица изследвания с различни режими на лазерно излъчване. Все още литературата не дава яснота за предпочитан режим на работа. Направени са редица експерименти, но най-перспективен съвременен метод е 3D компютърната томография [2-4].

Компютърната томография дава възможност за осъществяване на безразрушителен контрол с висока точност при изследване на вътрешната и външна структура на обекти. Компютърната томография дава допълнителни наблюдения на плътността на материалите и тяхната микроструктура. Приложението на индустриалната 3D компютърна томография се оказва ефективна за получаване на информация относно вътрешната характеристика на изследвания обект.

Целта на настоящата работа е чрез 3D индустриален компютърен томограф да се установят дълбочината и ширината на микро кухини в емайлова зъбна повърхност, образувани след лазерна аблация чрез Er:Cr/YSGG лазер Biolase, Waterlase, MD, USA при различни режими на работа.

2. Експериментално оборудване

За осъществяване на експерименталното изследване са използвани четиридесет зъбни образци, обработени чрез лазерна аблация с помощта на Er:Cr/YSGG лазер Biolase, Waterlase, MD, USA при четири различни режима на работа. След обработването с лазерна аблация е използван 3D индустриален компютърен томограф Nikon XT H 225. Компютърният томограф дава възможност да бъдат определени микро кухините в емайла на зъбните образци.

Biolase, Waterlase, MD, USA представлява водно-енергизиращ YSGG лазер с дължина на вълната 2,780 nm. Патент на този лазер представлява едновременното стимулиране на водните молекули от охлаждащата струя и от тъканта, която е мишена. Така се осъществява биологична, ефективна микроаблация на зъбна структура, кост или мека тъкан.

За анализ на влиянието от лазера при четирите режима на работа върху зъбните образци е използван 3D индустриален компютърен томограф Nikon XT H 225 (фиг. 1).

Компютърната томография (CT) е безразрушителен метод, който осигурява висока точност и има способността да изследва вътрешни и външни размери на предоставените образци (проби, заготовки). Освен това осигурява допълнителен поглед през плътността на материала и микроструктурата му.

Работи на следния принцип: образецът се поставя в хващача на ротационната маса, между рентгеновия източник и детектора; преместването на пробата по-близо до рентгеновия лъч увеличава полученото изображение; генерира се рентгенов лъч, който се предава чрез пробата; цифровият детектор заснема изображение, което се състои от множество нюанси на сивото на базата на сянка, причинени от абсорбцията на рентгенови лъчи при преминаване през сканираната проба; по-дебели или по-плътни материали, като желязо, мед и олово, водят до по-тъмни области, отколкото тънки или леки материали като пластмаси, хартия или въздух [5, 6].

Използването на CT е ефективна технология за получаване на ценна информация от изследваните образци като например подробно заснемане и измерване на вътрешните и външни характеристики, което е от изключителна важност при контрол на качеството. Също така може да се използва за изследване и анализ на материали които са от решаващо значение при различни индустрии като: автомобилна индустрия, космическо инженерство, екструдиране на пластмаси, полимери и др., фармацевтика, медицински изследвания и др. [5, 6].

Фиг. 1. *3D индустриален компютърен томограф Nikon XT H 225.*

Използваният CT притежава рентгенов източник с микро фокус, голям инспекционен обем, висока разделителна способност на изображението (максималната на детектора е 1900x1500 с активна площ 467 cm^2), бърза 3D компютърна реконструкция, петното (сечението) на X-Ray лъча е под 3 μm, разполага с пет-осна система за позициониране. Максимално допустимото тегло, което може да се постави на въртящата маса е 15 kg, а максималните габарити на обекта са 15x15x15 cm.

Получените резултати се представят в 3D обем, който се състои от серии от последователни 2D рентгенови изображения, които се снимат, докато обектът се завърта на 360º. След сканиране, получените изображения се реконструират от софтуера на компютърния томограф, за да се генерира 3D изображение на сканирания обект. Също така реконструирания обект съдържа цялата информация за микроструктурата на повърхностите и на вътрешността. Възможно е наблюдение чрез софтуера на компютърния томограф на всяка една повърхност.

3. Методика за провеждане на изследването.

За осъществяване на изследванията е необходимо да се извършат последователно следните задачи при лазерната аблация и 3D компютърната томография.

За провеждане на лазерната аблация върху зъбните образци е необходимо да се извърши следното: адхезивното свързване на твърди зъбни тъкани с керамични конструкции изисква разграпавяване на зъбната повърхност, с цел пенетрация и микро заключване на композитния цимент. Известна и широко разпространена методика включва ецване на твърдите зъбни тъкани с фосфорна киселина. Целта на настоящето изследване е чрез 3D компютърна томография да се изследва емайлова повърхност след проведена лазерна аблация при различни режими като алтернатива на киселинното ецване. За целта са използвани екстрахирани трети молари, без наличие на кариес или обтурации.

За провеждане на 3D CT сканиране на предоставените зъбни образци след обработката им с Er:Cr/YSGG лазер Biolase е необходимо да се извърши следната последователност от действия:

1. Запознаване с нуждата от 3D CT сканиране на зъбните образци.
2. Поставяне на зъбния образец в подходяща за монтиране в компютърния томограф основа.
3. Определяне позицията на зъбния образец спрямо X-Ray лъча.
4. Задаване необходимата сила на лъча.
5. Определяне необходимия брой прожекции (от 2000 до 8000).
6. Подготовка и избиране на нужни параметри за 3D реконструкция.
7. Анализ на получените изображения.
8. Определяне на микро кухини.
9. Измерване на микро к.
10. Анализ на получените резултати.

Изпълнението и определянето на поставените задачи е персонално за всеки зъбен образец. Горепосочените задачи са ключовите, от които следва разширяване на някои методи и създаване на нови.

4. Провеждане на изследването.

Четиридесет екстрахирани трети молара съхранявани във вода и са използвани до три месеца след екстракцията. Зъбните образци са разделени на четири групи. Букалната емайловата повърхност на зъбните образци е обработена с Er:Cr/YSGG лазер Biolase, Waterlase, MD, USA при четири режима по методиката на проф. Каменова [7]:

1. Мощност на лазера 1 W; 30Hz; 10% вода; 15% въздух.

2. Мощност на лазера 1.25 W; 10 Hz; 30% вода; 30% въздух.

3. Мощност на лазера 1,5 W; 20Hz; 30% вода; 60% въздух.

4. Мощност на лазера 2,5 W; 20Hz; 20% вода; 60% въздух.

Честотата на лазера представя за колко секунди пулса създава вълна. Използваният лазер е с широк спектър на честота [8]. Друго предимство на лазера, който бе използван е, че честотите могат да бъдат задавани. Честотните изменения основно се отнасят до повишена топлина. В други статии се установяват липса на статистическа разлика при стойности от 20Hz до 40Hz [2]. Поради тази причина в това изследване са използвани различните режими, в интервал от 10 Hz до 30 Hz.

При използването на по-мощни лазери от 3 W до 6 W се наблюдават малки повърхностни пукнатини, което според авторите е следствие от мощността на лазера или наличие на термичен стрес от процеса на облъчване [9, 10].

Накрайникът на лазера е разположен на разстояние от 1 mm от емайловата зъбна повърхност. Продължителността на лазерната аблация за всеки зъб е с продължителност от 15s. Лазерният лъч се разполага перпендикулярно на повърхността на всички образци с цел максимална режеща ефективност.

Всички зъби са подложени на 3D рентгеново сканиране с индустриален компютърен томограф. Образците се закрепват в порест материал с по-ниска плътност. По този начин се избягва появата му при сканирането. Порестият материал се закрепва за специална стойка, предназначена за поставяне в зоната на сканиране. Обектите са поставени максимално близо до рентгеновия лъч с цел постигане на по-детайлна картина. Определени са необходимата мощност на лъча и броя проекции. Използван е софтуера на фирмата производител за отчитане на стойностите на повърхностните микро кухини.

5. Анализ на получените резултати

Експерименталните данните получени от 3D рентгеновото сканиране от индустриалния компютърен томограф са анализирани посредством мощен 3D софтуер за анализ и обработка на сканирани изображения.

Дадени са някои примери от проведените сканирания на зъбните образци, които са подбрани от четирите режима на работа на уреда използван при лазерната аблация – Er:Cr/YSGG лазер Biolase, Waterlase, MD, USA.

Направено е и изследване на зъбен образец, третиран по конвенционалните методи в България, чрез ецване с фосфорна киселина.

На фиг. 2 е показан зъбен образец, третиран чрез лазерна аблация, реконструиран от софтуера на компютърния томограф. Третираният зъб е от режим 1 на работа. Ясно се вижда зоната, третирана чрез лазерна аблация от лявата страна на изображението (а), като от дясната страна на изображението е показана не третираната страна (б).

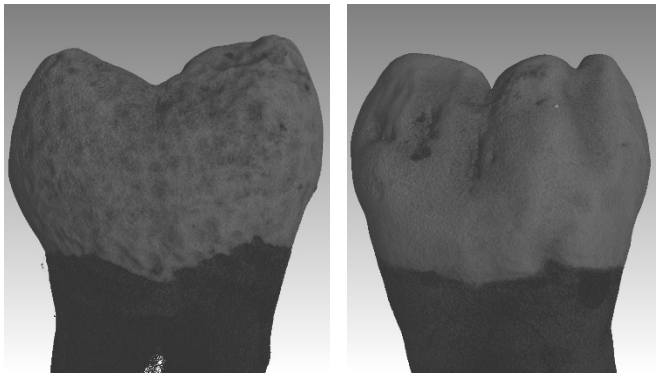

а) *б)*

Фиг. 2. *Сканиран зъбен образец по метод 1 – а) третирана страна, б) не третирана страна.*

На фиг. 3 е показано 3D изображение с отчетени размери на микро кухините в ширина и дълбочина. На всеки зъб са направени по минимум 10 измервания на микро кухини с цел проверка на експерименталните данни. Тъй като лазерът е настроен на определен режим на работа, времето за което работи е фиксирано, както и отстоянието от зъбите би трябвало микро кухините да имат сходни стойности. Това се потвърждава и от резултатите, предоставени от софтуера на компютърния томограф. Средната дълбочина на микро кухините е от порядъка на 0,04 mm, а ширината е 0,19 mm.

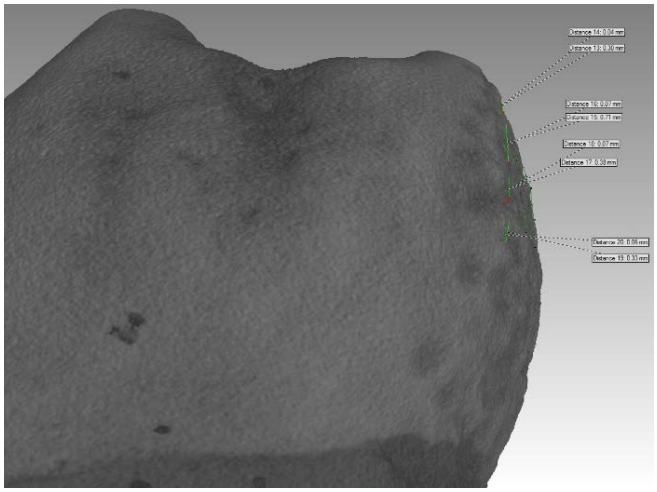

Фиг. 3. *Данни от лазерна аблация, режим 1.*

Фигура 4 показва 2D рентгеново изображение, от което са снети размери от лазерна аблация, извършена чрез режим 2. Отново са направени 10 измервания на ширина и дълбочина. Средната стойност на дълбочините е от порядъка на 0,06 mm, а ширината е 0,43 mm.

На фиг. 5 са представени данни от режим 3 на лазерна аблация. Изображението представлява изглед от горната част на зъба. Отново измерванията са 10 - по ширина и дълбочина на микро кухините. Средната стойност на дълбочините е от порядъка на 0,05 mm, а ширината е 0,33 mm.

Четвъртият режим на работа на лазера Er:Cr/YAG е показан на фиг. 6. Данните за дълбочина на микро кухините е от порядъка на 0,13 mm, а ширината е 0,55 mm.

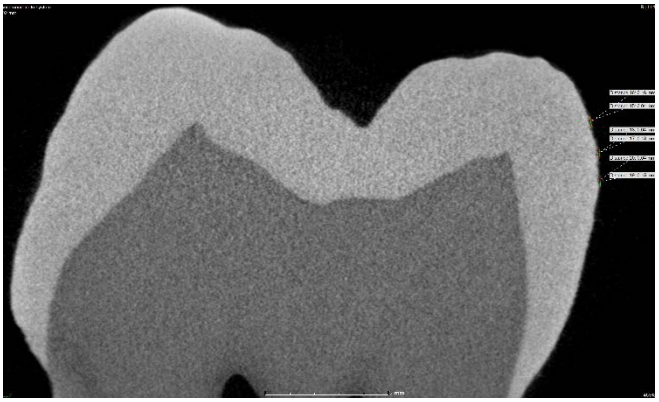

Фиг. 4. *Данни от лазерна аблация, режим 2.*

Фиг. 5. *Данни от лазерна аблация, режим 3.*

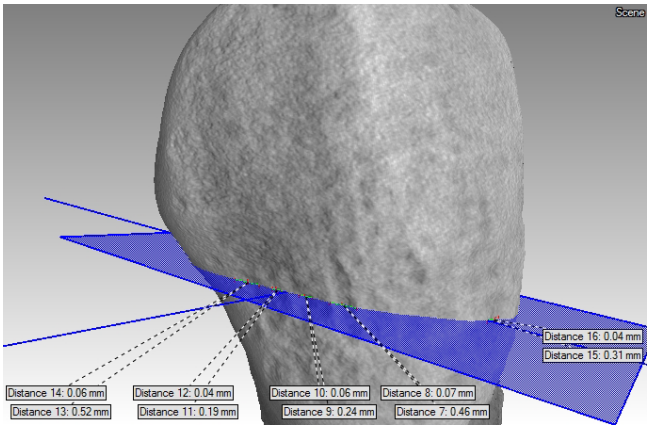

Фиг. 6. *Данни от лазерна аблация, режим 4.*

На фиг. 7 е показана снимка от зъбен образец, третиран чрез киселина. На него не са ясно изразени третираните области и не се установи наличие на микро кухини. Фиг. 7 а) показва чистата част на зъба (не третираната), а на фиг. 7 б) е показана третираната с киселина повърхност.

Получените микро пукнатини следствие на лазерна аблация са подготовка на зъбните образци за композитно циментиране. Микро пукнатините подобряват връзката между композитния цимент и зъба. Следствие на това се образува адхезивна връзка и се избягва нежелано отлепване или наличие на микропропускливост.

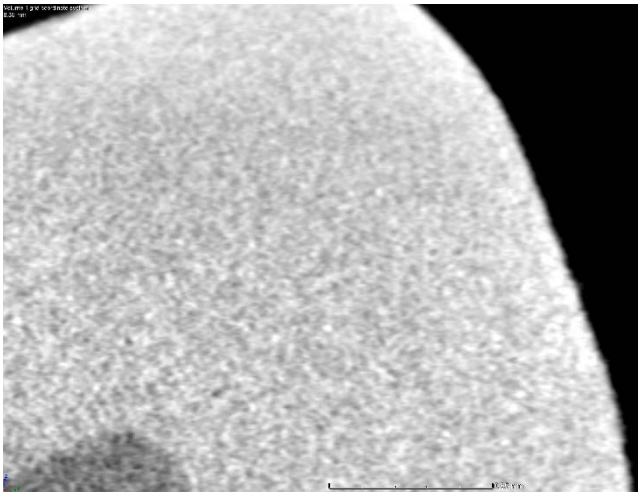

а) Не третирана повърност.

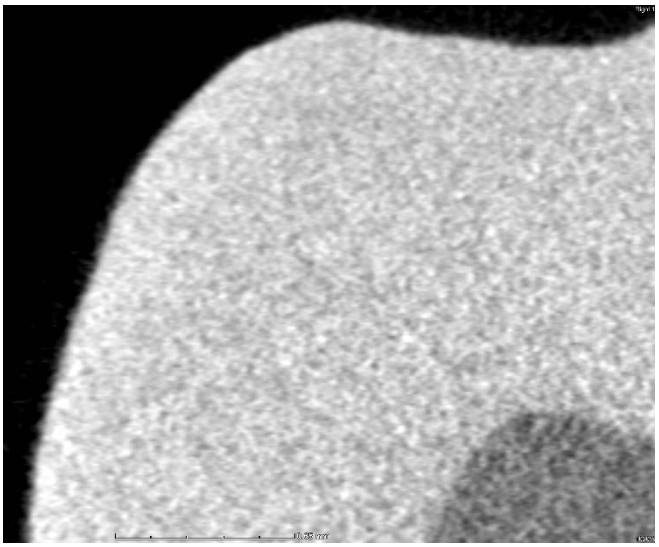

б) Третирана с киселина повърхност.

Фиг. 7. *Третиран образец с киселина.*

6. Заключение

От направените изследвания на четиридесет обработени зъбни образци с Er:Cr/YSGG лазер Biolase, Waterlase, MD, USA при четири режима на работа и с помощта на индустриален 3D компютърен томограф се установи очакваната разлика от режимите на работа по посочената методика.

Избраната мощност на лазера от 1W до 2.5 W позволи наблюдение само наличие на микро кухини и се избегна термичния стрес.

Резултатите от анализа на измерената дълбочина на кухините показват значителна разлика между първите три групи и четвъртата група. Първите три режима са сходни и няма значителна разлика между техните стойности.

При четирите групи зъбни образци, при които са измерени ширината на образуваните кухини, вследствие на различните режими на лазерна аблация, не се наблюдава повторяемост на получените резултатите при анализа. Наблюдават се значителни разлики между първа и втора и между първа и четвърта група от зъбните образци.

Следващ етап от изследванията е да бъде проверена дълбочината на пенетрацията на композитен цимент при адхезивната връзка със зъбния образец.

Литература

1. Silverstone LM, Saxton CA, Dogon IL, Fejerskov O. Variations in the pattern of etching of human dental enamel examined by scanning electron microscopy. Caries Res. 1975;9:373–87.
2. Baygin O, Korkmaz FM, Tuzuner T, Tanriver M. The effect of different techniques of enamel etching on shear bond strengths of fissure sealents. Dentistry 2011;1:109.
3. Lee B, Hsieh T, Lee Y. Bond strengths of orthodontic bracket after acid etched, Er:YAG laser irradiated & combined treatment on enamel surface. The Angle Orthodontist. 2002;73:565–70.
4. von Fraunhofer JA, Allen DJ, Orbell GM. Laser etching of enamel for direct binding. Angle Orthod. 1993;1:73–6
5. Nicon Metrology Brochure (http://www.nikonmetrology.com/en_EU/Products/X-ray-and-CT-Inspection/Computed-Tomography/XT-H-225-ST-Industrial-CT Scanning/).
6. Ruzic J., Stoimenov N., Advanced copper matrix composites, 2016 – Monography in English, „Prof. Marin Drinov“ Publishing House of Bulgarian Academy of Sciences, ISBN 978-954-322-859-1
7. Ю. Каменова. Приложение на диодните лазерни системи в денталната медицина. Иврай. София 2014.
8. Coluzzi DJ. Fundamentals of dental lasers: Science and instruments. Dent Clin North Am 2004;48:751-70, v.
9. Issar R, Masundar D, Ranjan S, Krishna N, Kole R, Singh P. Comparative evaluation of the etching pattern of Er,Cr:YSGG &acid etching on extracted human teeth – a SEM analysis. J Clin Diagn Res. 2016 10:ZC01-ZC05.
10. Oho T, Morioka T. A possible mechanism of acquried acid resistance of human dental enamel by laser irradiation. Caries Res. 1990;24:86–92.

SURFACE MORPHOLOGY AND WETTABILITY OF GRADIENT (Ti,Al,V)N/TiO_2 COATING

Nikolova M. PhD.[1]

Faculty of Mechanical and Manufacturing Engineering – University of Ruse "A. Kanchev", Bulgaria[1]

mpnikolova@uni-ruse.bg

Abstract: *Physical surface properties including surface roughness, topography, morphology, and wettability could influence the implant material behavior, bio-response, bacterial contamination and contact with other bio-active surfaces or fluids. This work investigates micro- and nanoscale roughness parameters and surface morphology of PVD deposited (Ti,Al,V)N/TiO_2 coating using optical microscopy, white light interferometry (WLI), contact profilometer and scanning electron (SEM) microscopy. Results indicated that vacuum oxidized surface possessed medium roughness values, anisotropy in surface texture and irregular morphology. The vacuum oxidation of the nitride maintained the oxide with nano-crystal size and showed pores at the interface between the layers. The effect of prolonged exposure to Ringer-Braun solution droplet on the modified crystalline structure of the oxide was also explained.*

Keywords: VACUUM OXIDIZED PVD (TiAlV)N COATING, SEM, WLI, CONTACT PROFILER, WETTABILITY

1. Introduction

The identification, assessment, and quantification of the implant topographic features are essential for ensuring desirable cellular response and successful performance of the implant. In general, the rougher topography shows increased bone apposition in comparison with smooth surfaces (as-machined) that exhibit poor fixation strength [1]. The roughened implant surface serves as adhesion scaffold for the cell facilitating their localization and immobilization. However, compared to the smooth surface, roughened one enhances the accumulation of infectious bacteria [2]. Therefore, surface roughness and texture will determine the healing rate through enabling the bone cell to colonize the implant surface and will contribute to the strength of bone-to-implant contact as well as the surface morphology will exercise influence on bacterial proliferation.

Titanium alloys are commonly employed to manufacture hard tissue replacement, including dental implants, bone plates and artificial hip joints [3]. Many experiments confirmed the feasibility of using TiO_2 thin films as a biocompatible material [4-6]. A mixture of crystalline and amorphous titanium oxide film with a few nanometers thickness is formed naturally in the air. Titanium oxide layers formed at room temperature (e.g. anodically oxidized, sol-gel produced) are often obtained mainly in amorphous form, which can be converted to anatase (300 – 500 °C) or rutile (> 550 °C) by a thermal treatment [7]. The need for crystallization is because the crystal TiO_2 is demonstrated to improve the bioactivity on biomedical implant surfaces [8]. At the same time, a significant temperature-dependent growth of the crystals takes place. The problem that occurs with titanium adhesive joints is that the transformation of amorphous titanium oxide into titanium oxide crystals leads to failure due to the change of oxide volume at the interphase [9]. The amorphous oxides residues could worsen the bonding strength to the crystal substrate. The biological outcomes of anatase crystal architecture are highly significant for implants [10, 11]. Additionally, the micrometer scale surface topography with dimensions comparable to cells possesses the ability to influence cell adhesion, morphology, and contact guidance.

Commonly used surface characterization tools for quantitative analysis are optical microscopy (OM) analysis, white light interferometry (WLI - non-contact optical technique) and scanning electron microscopy (SEM). In this regard, the work reports on surface characteristics of gradient functional (Ti,Al,V)N/TiO_2 coating describe by complementary analysis (OM, WLI and SEM) in order to investigate its topography and morphology. No additional substrate roughening before the modification is applied so as to determine only the surface characteristics of coating and to facilitate the examinations and interpretation of results. The information about the morphological characteristics is used to explain the observed time-related wettability of the modified surface. The results were post-processed and schematically shown so that they give a more comprehensive set of data.

2. Materials and Methods

Specimens in disk form (Ø20 x 6mm) of commercially pure Ti (cpTi) (Grade 1 in ASTM classification) were prepared by turning and fine-polishing. Thereafter, they were ultrasonically washed with ethanol, acetone, isopropanol and distilled water for 5 min. (TiAlV)N/TiO_2 coatings were deposited on the substrates in a hand-made PVD chamber while the specimens were rotated with a frequency of 0.5 Hz. After loading the specimens, the PVD chamber was evacuated up to a pressure of 1.10^{-4} mbar. A cleaning in glow discharge (substrate bias -400 V) was applied in pure Ar atmosphere at a pressure of $2.5.10^{-2}$ mbar for 60 min. To ensure the coating stress relaxation and necessary adhesion a very thin pure layer from the TiAl5V4 target (at $2.5.10^{-3}$ mbar for 5 min.) was previously applied. Thereafter, the (Ti,Al,V)N film was made by reactive arc deposition in the N_2 atmosphere at 300 °C substrate temperature for a time of 120 min., 120 A arc current (3000 W target power), bias -250 V and $2.5.10^{-3}$ mbar pressure in the working chamber. Directly after deposition, on the (TiAlV)N layer a second TiO_2 film with 0.2-0.3 µm thickness was made by oxidizing, using glow discharge at a negative bias voltage of 400 V in an oxygen atmosphere at a pressure of $2.5.10^{-2}$ mbar for a deposition time of 90 min.

After the PVD patterning and oxidation, the samples were analyzed using an optical microscope (NIKON, Japan) to obtain optical micrographs of the surface of the sample. The images were used to obtain 3D surface plot by Image J software. WLI Photomap 3D (FOGALE Nanotech, France) with sub-nanometer vertical resolution (down to 0.1 nm) at all magnifications, was used to determine roughness parameters for the samples. The two-dimensional surface roughness values of the coatings were measured by MITUTOYO Surftest SJ-201P contact stylus profiler. Scanning electron microscopy (JEOL/EO Version 1.0 JSM-5510) was performed at various magnifications under an acceleration voltage of 10 kV. For wettability studies sessile drop method (CSEM Alpha–Kit CH-2000) was used to measure hydrophilicity by surface contact angle at room temperature after 5 seconds and every 5 minute thereafter with Ringer-Braun solution (8.60 g/L NaCl, 0.30 g/L KCl, 0.33 g/L $CaCl_2.2H_2O$, pH = 5.7±0.02 at 37°C) droplet. CpTi was used as reference material in order to determine the influence of the oxidation in the (Ti,Al,V)N on the surface hydrophilicity of natural titanium oxide layer and vacuum oxidized one. Before the tests, the surfaces were rinsed with distilled water and dried in air. The droplet of 100 µl volume was pipetted onto the surface using a micro-syringe. It was illuminated with diffuse light in order to obtain an image of the drop with sharp borders. The images were recorded with a camera and the angle between the

baseline of the drop and the tangent at the droplet boundary was measured.

3. Results

Figure 1 shows the software obtained 3D image representing surface characteristics determined by OM. The pseudo-colored height map (Fig. 1) gives a relative view of peaks density without actual roughness values. The measured roughness values by the contact stylus profiler and WLI method are shown in Table 1. Taking into account that the multiphase coating reflects light differently because of the micro-roughened surface, small oxide thickness, underlying (Ti,Al,V)N gold color and its roughness, etc., and the contact method sensitivity limitations, the perceived differences in the average roughness values are identifiable. Although the former factors affect the OM image accuracy, the model surface topography establishes a rough picture of the overall surface morphology.

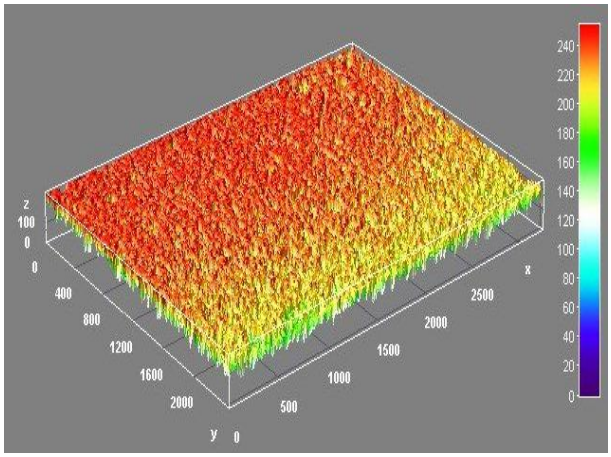

Fig. 1 *Optical microscopy 3D model surface (Image J), objective – Nikon x20.*

Table 1*. Comparison of the average surface roughness values obtained by WLI (x = 847.51 μm, y = 639.78 μm area) and contact stylus profiler (base line 0.25 mm).*

Method	**Roughness parameters**	R_a, [nm]	R_q, [nm]	R_z, [μm]	R_y, [μm]
Contact stylus profiler	Bare cpTi values	90	95	0.87	0.87
	Coating values	270	370	2.21	2.21
WLI	**Roughness parameters**	S_a, [nm]	S_q, [nm]	S_p, [μm]	S_v, [μm]
	Coating values	467.45	583.46	2.81	2.43

The WLI measured S_a roughness value for the scanned area of 847.51 x 639.78 μm is 467.45 nm in contrast to R_a value of 270 nm obtained by the contact profiler. The differences could be attributed to the damageable surface heights during the measurements with the contact profiler. WLI determined that the maximum peak hight S_p was equal to 2.81 μm and the maximum valley depth S_v was 2.43 μm. Using WLI analysis, the surface morphological information on the dimensional scale of lateral resolution is as good as 1 μm while the depth resolution reaches down to 1 nm [12]. Despite the lack of contact with the sample and wear of its surface, the lateral pixel sampling was less than the light wavelength and a part of the peaks and sub-micron features were masked which affected the measurements. It is known that WLI can lead to significant errors when applied to measure or image surfaces that contain features that are less than 3 μm in lateral extent and less than 500 nm in height [1] and in this context, including the (Ti,Al,V)N/TiO_2 coating.

SEM is the gold standard in morphology analysis to obtain qualitative descriptions of the surface over multiple length scale and amplitude. In such case, tilting the sample is a useful imaging technique to explore coating morphology and disclose 3D effect. Typical tilted SEM images providing secondary electron contrast are shown in Fig. 2.

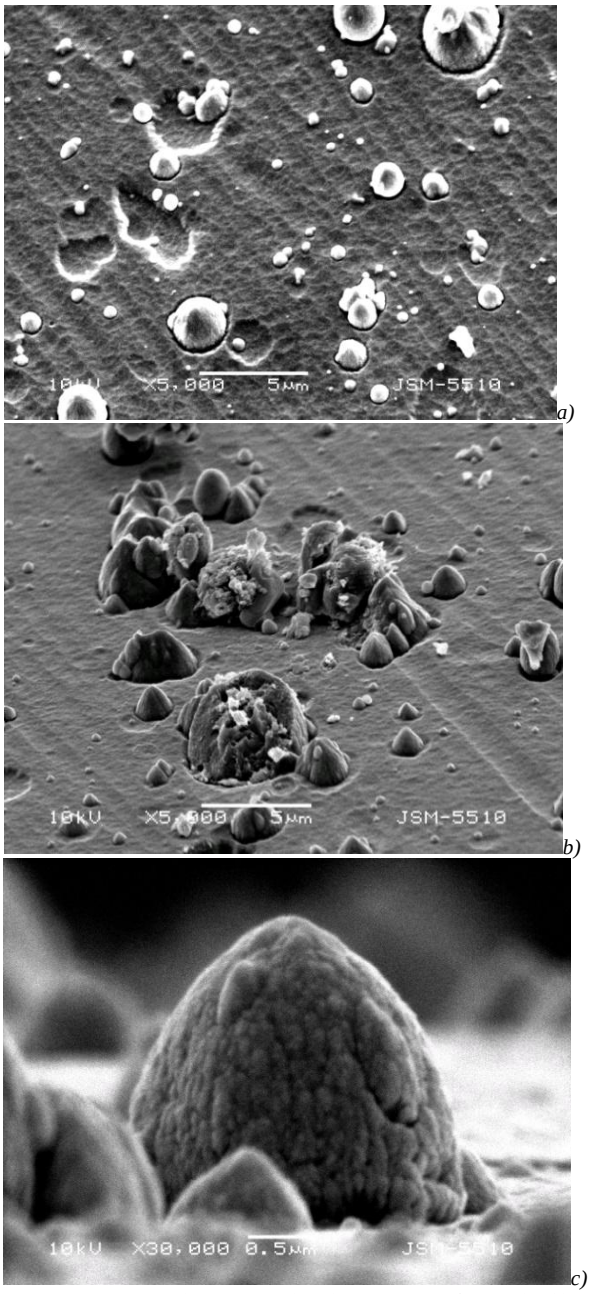

a)

b)

c)

Fig. 2 *SEM images (SE contrast); a) top view (θ =10°); b) tilted topographic image at θ = 45°; c) oxidized droplet of the coating on the surface seen at θ = 90°.*

High-resolution SEM revealed clearly the presence of micro- and nanofeatures on the surface of the coating (Fig. 2a). The surface displayed uneven topography with well-defined peaks with semispherical, "vulcanoes"- like shapes and shallow valleys (Fig. 2b). Both peaks and valleys had random distribution on the surface. The higher peaks produced during the Arc deposition of the nitride layer were spread at a distance of about 1 to 30 μm. The finer texture of the flatter surface contained repetitive microwaved morphology with dimensions from 0.5 to 1 μm that corresponded to step growth of the nitride coating. The crystal architecture of the thin nanostructured uppermost TiO_2 on the droplets' peaks and the flatter nanoscaled surface is demonstrated in Fig. 3c.

The wettability of the surface is important for the adsorption of physiological fluids that take place immediately after the implantation process. The kinetics of contact area evolution of the droplet on the coated surface depending on the interaction time is schematically shown in Fig. 3. It was found out that after 30 min. of emersion, the contact angle value of the coating yielded 18° (Fig.

3a), whereas the smooth titanium surface produced contact angle of 32° (Fig. 3b). Therefore, the Ringer-Braun solution contact angles of the modified substrate showed close to high (but not extremely) hydrophilic properties.

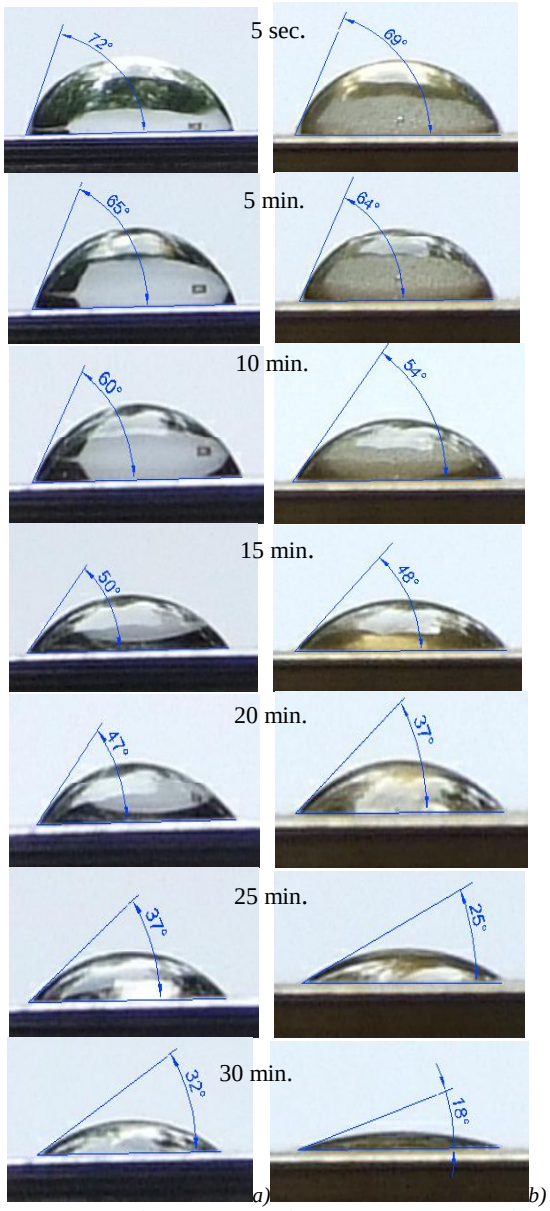

Fig. 3 *Measurements of the evolution of contact angle droplet of Ringer-Braun solution with time: a) pristine Ti substrate; b) (Ti,Al,V)N/TiO_2 coated cpTi.*

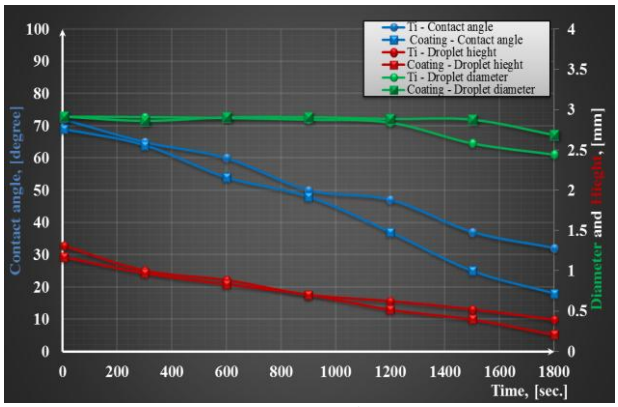

Fig. 4 *Comparative measurements of Ringer-Braun solution droplet contact angles, contact diameters D and droplet heights (in mm) with time.*

The evolution of the contact angle does not provide information on whether the changes in time were caused by surface morphology or chemistry or they were related to the kind and way that the molecules were adsorbed. In order to determine if the observed effect is simply due to the surface differences or due to binding strengths and wetting mechanism, the droplets contact diameters and heights were measured. The lines almost parallel to each other were seen for measured values up to 15 min. (Fig. 4), indicating constant droplet diameters and heights of both surfaces. After that moment, the inconsistencies in the measured values increased. The linear slope of the angle and droplet heights decreases with time (20 and 30 minutes) with insignificant change in the droplet diameter, especially for the coated samples.

4. Discussions

The topographic observations indicate that the (Ti,Al,V)N/TiO_2 coating has an anisotropic morphology. As regards the roughness values, S_a (average height) value of 467.45 is more descriptive parameter than R_a due to the latter takes into account a single line profile while S_a parameter determines the whole area observed. Like R_q value, S_q is making sense when the height points are uniformly distributed according to the normal distribution curve [13]. As randomly placed peaks are present on the oxidized coating, the S_q values are not precisely determined but in comparison with a smooth sample (S_q< 0.1 nm), the topographic parameter S_q (583.46 nm) of the modified surface is enhanced. There is conflicting work in the literature whether an ordered topography or a disordered topography is superior in soliciting a favorable cellular response and effective protein adsorption [14]. Despite having relatively low values, it is commonly accepted that the moderately rough surfaces (500 nm up to 2 μm) have shown better results concerning osseointegration.

The SEM analysis clearly reveals the micro- and nanofeatures on the modified surface. On the (Ti,Al,V)N/TiO_2 coating the larger pits sidewalls are smooth with gradually decreasing curvatures and their bottoms are flattened. On the basis of the shallow valleys with small size and form, it could be suggested that the larger depressions are the result of the droplets initial attack and interference with surface and their movements before condensation. Such valley morphology would less entrap and even impede the bacterial rigid cell wall to adhere. Furthermore, considering the crystalline structure of the oxide, seen in Fig. 2c, its crystal architecture would be more beneficial for the decreased bacterial proliferation because Del Curto B et al. [15] discovered that the amorphous TiO_2 promote bacterial attachment. According to Pokrowiecki R. et al. [16], nano-rough titanium plates were much less colonized by bacterial cells than the conventional machined surface.

The wetting behavior differences upon emersion should be considered in conjunction with the differences in the surface structure of the oxide. After pipetting, the molecules and ions on both samples are physically adsorbed to the surface with no systematic orientation (Fig. 3). The Ti-O bond is generally thought to be ionic with negligible covalence. Even in the presence of small quantity of Al, Ti atoms bond stronger to the O than Al [17]. Increasing the time of emersion, due to the hydrophilic interaction surface monolayer of amphiphilic water molecules orients close to the surface in order to compensate the ionic surface polarization charge. On one hand, the increase of surface energy (decrease of the contact angle) of the modified surface can be related to the increase of surface roughness. In contrast, on polished cpTi the naturally formed compact oxide film is discovered to show predominant flat morphology and thickness of 3.17 nm achieved after 1 day of exposure to air [18]. For the machined cpTi Mendonça G. et al. [19] found no evidence of nanofeatures on the surface. In the particular case, the topographical pattern of the surface modification decreases the contact angle compared to the polished cpTi surface even at 5 sec. time. The nanostructured oxide morphology of the coating unequivocally established a nanoscaled roughness (Fig. 3) with an increased number of atoms and, therefore, charge density on the surface. The considerable vertical surface roughness influences not

only its topography but also increases the coating superficial area. Thus, the superficial activity of the real surface area is increased and the quantities of the H-bonds and ions interactions are substantially greater.

However, the slope of the angle decreases with time (20 and 30 minutes) with insignificant change in the droplet diameter (Fig. 4), indicating an increase in adsorbate-surface interactions. Due to the liquid penetration in the modified surface, the effective area wetted by the solution in case of micro- and nano-rough surfaces is larger than the area of the smooth surface. It is likely the liquid to penetrate deeper in the oxidized coating because of the intrinsic polarity of the material. In the bottom side of the oxide, the fine-grained morphology and its uneven structure that contains pores with different sizes are also seen (Fig. 5 b). The reasons for the presence of larger pores are the smaller droplet phases surrounded by the oxide that remained unstuck at the nitride surface (Fig. 5a).

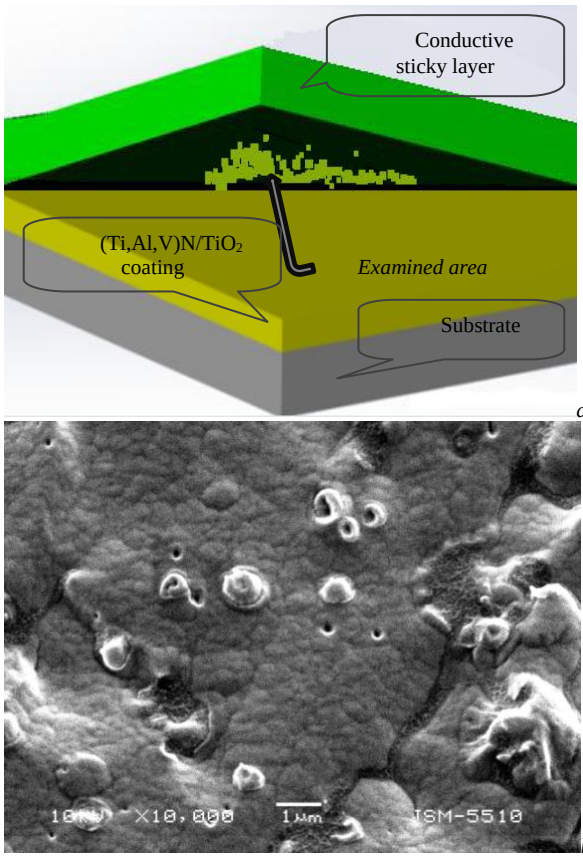

Fig. 5 *Oxide characteristics: a) scheme of the surface sampling for examining the bottom area of the oxide; b) SEM images (SE mode) of surface oxide structure at the bottom side.*

The other reason for the small covered pores presence at the oxide-nitride interference suggests not only the explanation of oxide-solution interaction but the mechanism of (Ti,Al,V)N oxidation. It follows that near to the surface the nitride undergoes complete phase transformation during the oxidation procedure. Underneath the TiO_2 area, the low temperature of the glow discharge during vacuum oxidation does not provide high mobility of oxygen species for complete phase segregation. Then, below the surface oxide, a complex titanium oxy-nitride nanostructure is reasonable to be expected. In addition to the interstitial atom positioning, lateral fluxes of oxygen through already existing voids, defects and/or strained parts in the small grains could be estimated. The highly reactive oxygen atoms are likely to occupy the nitrogen position in the fcc lattice of the nitride. Nitrogen atoms recombination during oxidation process should be considered as the cause for the pore presence at the oxide-nitride interface. The precipitation of molecular nitrogen (N_2) would be favored at grain boundaries of the nitride sublayer. The nitrogen depletion provokes augmented titanium oxidation rate in depth. The residual N atoms occupied O-atoms sides in the TiO_2 to form Ti-N bonds. As the vacancy mechanism is known to be more effective than simply expanding the lattice volume, many processes including adsorption, diffusion, incorporation, chemical reactions etc., impact the kinetic coefficients of the processes. The charge compensation is likely to experience downward-pointing electrical gradient near to the surface and below it (in the pores) because of the potential effect inside the micro- and nanopores. Schematic representation of the process is shown in Fig. 7.

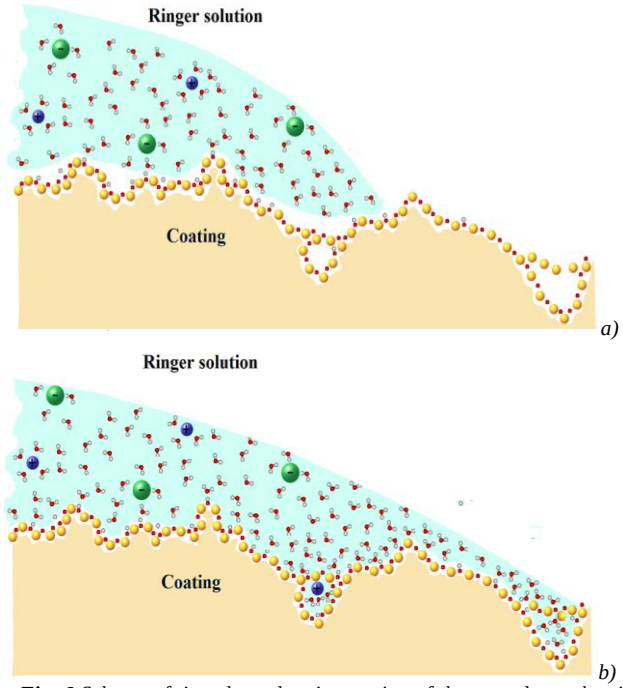

Fig. 6 *Scheme of time-dependent interaction of the coated sample with Ringer-Braun solution droplet: a) initial contact; b) evolution of the adsorbate-surface interactions in time.*

This electrostatic field is also caused by the enhanced compressive strain that follows the nitride-oxide transformation near to the surface. This is because in crystalline TiO_2 the Ti atoms bond with six oxygen atoms that form an octahedral structure and O atoms prefer three titanium atoms as neighbors. As the crystal ionic radii of Ti^{4+} is 74.5 pm and the O^{2-} is 126 pm (in contract to Ti^{3+} - 81 pm and N^{3-} - 134 pm), the lattice parameter of TiO_2 decreases with increasing the oxygen content. Because the oxygen concentration decreases in depth (not shown), the nitride-oxide transformation leads to compressive stress state development near to the surface. The local volume decrease within nitride – oxide phase transformation accompanies strains that contribute to the geometry and strength of adsorbate-surface interactions and capillary phenomenon. For that reason, the relative change in the droplet height with the increase of time substantially decreases for the coated sample (Fig. 7) while the drop diameter stays merely unchanged.

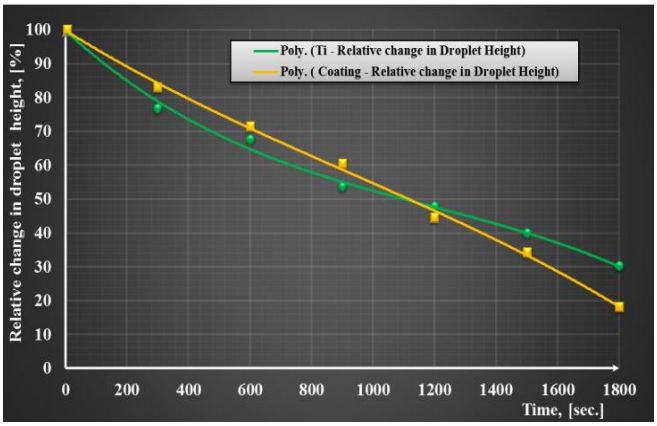

Fig. 7 *Relative change in the Ringer-Broun droplet height in time.*

The Ringer-Braun solution paths for penetration into the interfacial areas via diffusion processes or capillary attraction are tightened at the surface because of the compressive stresses in the coating. The discrepancy in the contact angle values increases with time indicating that the molecules and/or ions from the solution access the coating in depth via pinholes in the TiO_2 layer that are not initially accessible. The porous surface can absorb parts of the solution and because of that, the drop floats in. In this way, the adsorbate-surface interactions increase their strength.

5. Conclusions

In this study biomimetic approach of micro- and nano-metric modification by means of a deposition of a nitride PVD coating and its vacuum oxidizing is used. Complementary topography and morphology analysis in addition to statistical roughness description is performed to obtain a definitive characterization of the (Ti,Al,V)N/TiO_2 surface that is essential to understand different biological effects. The numerous features seen in SEM images show a qualitative difference between OM representation and more comprehensive view at two length scale. The composite film tended to be irregularly rough. The irregular features were random groups of "volcanoes" with different size (from tens of nanometers to several micrometers) and flat valleys with various sizes. The peak-to-peak distance was of the order of about one to five micrometers. The surface morphology was regulated by the physical processes of condensation, crystallographic pre-determined growth, and specific nitride oxidation. The micro- and nano-features of the underlying film and the oxide thickness determine the structure of the overlying oxide. By studying the changes in the drop contact angle it could be seen that the increased wettability compared to the polished cpTi surface was due to a combination of the surface roughness, oxidative treatment, nanocrystal oxide characteristics, coating pattern, and porosity. It is well known that the increased wettability is highly recommended for implant surfaces because the hydrophilic surface has a beneficial impact on the proteins conformation and their folding activity. Simultaneously, the permission of solution along the sidewall down to the substrate could trigger corrosion processes in the implant material. Then the most fundamental question - which surface chemistry or morphology is more important, remains still unanswered.

Acknowledgements

The financial support of this work was provided by the National Science Fund of Ministry of Education and Science, Bulgaria, under Grant project "Gradient functional nano-coatings produced by vacuum technologies for biomedical applications" with number D№ 07/3 (2016).

The author would like to thank D-r Marius Bazu and Phys. Raluca Gavrila from IMT-Bucharest for their assistance with using the institute facilities (WLI) as well as D-r Emil Yankov and Assoc. prof. Danko Tonev for their support in some measurements.

LITERATURE

1. Sosale G., Measurement and Analysis of Surface Topography over Multiple Length Scales: Application to Titanium Bone Implants, Thesis for Master degree of Engineering, McGill University Montreal, Canada 2007;
2. Harris L.G, R.G. Richards, Staphylococci and implant surfaces: a review. Injury 37, 2006, (Suppl. 2);
3. López-Huerta F., B. Cervantes, Biocompatibility and Surface Properties of TiO_2 Thin Films Deposited by DC Magnetron Sputtering Materials 7, 2014, 4105-4117; doi:10.3390/ma7064105;
4. Niinomi, M. Biologically and mechanically biocompatible titanium alloys. Mater. Trans. 49, 2008, 2170–2178;
5. Elias, C. N., J. H. C. Lima, R. Valiev, M. A. Meyers, Biomedical applications of titanium and its alloys. J. Miner. Met. Mater. Soc. 2008, 60, 46–49
6. Okazaki, Y. On the effects of hot forging and hot rolling on the microstructural development and mechanical response of a biocompatible Ti alloy. Materials 2012, 5, 1439–11461
7. Killian M. S., Organic Modification of TiO_2 and other Metal Oxides with SAMs and Proteins - a Surface Analytical Investigation, Dissertation, Friedrich-Alexander-Universität Erlangen-Nürnberg, 2013
8. Lin C.C., H.C. Cheng, C.F. Huang, C.T. Lin, S.Y. Lee, C.S. Chen, K.L. Ou, J. Appl. Phys. 44 (12) (2005) 8590- 8598
9. Shirazi S. N., Wet chemical surface modifications of Titanium and Ti6Al4V alloy and their effect on the hydrothermal aging mechanisms and adhesion properties Dissertation, Bremen, 2010
10. He J., W. Zhou, X. Zhou, X. Zhong, X. Zhang, P,. Wan, B. Zhu, W. Chen, The anatase phase of nanotopography titania plays an important role on osteoblast cell morphology and proliferation. J. Mater. Sci. Mater. Med. 19, 2008, 3465–3472;
11. Sollazzo V., F. Pezzetti, A. Scarano, A. Piattelli, L. Massari, G. Brunelli, F. Carinci, Anatase coating improves implant osseointegration in vivo. J. Craniofac. Surg. 18, 2007, 806–810;
12. Albrektsson T., L. Sennerby, A. Wennerberg, State of the art of oral implants. Periodontology 2000, 2008, 47, pp.15-26;
13. Raposo M., Q. Ferreira, P.A. Ribeiro, A Guide for Atomic Force Microscopy Analysis of Soft Condensed Matter, ©FORMATEX 2007, Modern Research and Educational Topics in Microscopy. A. Méndez-Vilas and J. Díaz (Eds.);
14. Le, X., G.E.J. Poinern, N. Ali, C.M. Berry, D. Fawcett, Engineering a Biocompatible Scaffold with Either Micrometre or Nanometre Scale Surface Topography for Promoting Protein Adsorption and Cellular Response, International Journal of Biomaterials, 2013, pp. 1-16., http://dx.doi.org/10.1155/2013/782549;
15. Del Curto B., M.F. Brunella, C. Giordano, M. P. Pedeferri, V. Valtulina, L., Visai, A. Cigada, Decreased bacterial adhesion to surface-treated titanium. Int J Artif Organs 2005, 28 (7): 718-30;
16. Pokrowiecki R., B. Szaraniec, J. Chłopek, M. Zaleska, Recent trends in surface modification of the titanium biomaterials used for endoosseus dental implants, Engineering of Biomaterials 124 (2014) 2-10;
17. Magnuson M., M. Mattesini, S. Li, C. Höglund, M. Beckers, L. Hultman, O. Eriksson, Bonding mechanism in the nitrides Ti2AlN and TiN: an experimental and theoretical investigation, Physical Review B 76, 2007, 195127
18. Harmankaya N., Titanium Oxide and Bone Anchorage Role of the Complement System, and Delivery of Osteoporosis Drugs from Mesoporous TiO_2, Sahlgrenska Academy at University of Gothenburg, 2013;
19. Mendonça G., D. Baccelli, S. Mendonça, L. Gustavo, P. Simões, A. L. Araújo, E. R. Leite, A. L. Golin, F. J L Aragão, L. F. Cooper, Nanostructured implant surface effect on osteoblast gene expression and bone-to-implant contact in vivo Materials Science and Engineering C 31 (8), 2011, 1809–1818;

МЕТОДИКА ИССЛЕДОВАНИЯ РАБОЧИХ ОРГАНОВ УБОРОЧНЫХ МАШИН

METHODOLOGY FOR THE STUDY OF WORKING BODIES HARVESTING MACHINES

Sadykov ZH. Toilybaev M.S., Sultangaziev T.K., Dosaev K.A.
Kazakh National Agrarian University – Almaty, Kazkhstan

Abstract. The proposed method for determining the rate of leveling biomass coefficient arriving in the threshing-separating device and the device for its implementation makes it possible to solve the technical problem. Provides a technical result as a rapid assessment and determination of the numerical value of the levelling biomass coefficient by the working bodies of harvesting machines with minimal error.

Keywords: *Combine, inclined chamber, threshing of seeds, leveling, biomass, spacer.*

Резюме. Предлагаемый способ определения коэффициента разравнивания биомассы, поступающих в МСУ комбайна и устройство для его осуществления позволяет решить техническую задачу. Обеспечивает технический результат как оперативная оценка и определение численного значения коэффициента разравнивания биомассы рабочими органами уборочных машин с минимальной погрешностью.

Ключевые слова: *Комбайн, наклонная камера, обмолот семян, разравнивания, биомасса, проставка.*

1. Введение

В Республике Казахстан значительный удельный вес имеют площади естественных кормовых угодий, составляющие более 180 млн. га, которые дают дешевый корм и, следовательно, соответствующую животноводческую продукцию. Однако их кормовой запас ограничен из-за низкой продуктивности, которая объясняется аридностью и нерациональным использованием пастбищ, отсутствием должного ухода и улучшения угодий. Основным способом увеличения урожайности аридных пастбищ является коренное улучшение, т.е. создание на их месте сеяных сенокосов и пастбищ путем подсева семян ценных кормовых растений как житняк, приспособленных к местным условиям. В настоящее время продолжаются работы по созданию и совершенствованию машин для уборки семенников пастбищных растений. Однако развития объемов работ по восстановлению кормоемкости пастбищ путем подсева семян пастбищных растений требуют ускорения процесса разработки, освоения и оснащения сельского хозяйства семеуборочными машинами. Анализ существующих отечественных конструкций уборочных машин и темпов оснащения ими сельскохозяйственного производства показывает, что как технический уровень, так и эффективность внедрения уборочных средств не в полной мере соответствуют современным требованиям к сельскохозяйственной технике и процессу потереснижения при уборке [1,2].

В научно-исследовательском центре «Агроинженерных проблем и новые технологии» Казахского национального аграрного университета разработана потереснижающее устройство для уборки семян пастбищных растений. Для оптимизации параметров этого устройства проводятся лабораторно-полевые исследования. С этой целью нами проводится методика исследования рабочих органов зерноуборочного комбайна для уборки семян пастбищных растений.

Предлагаемая методика относится к технике исследования и испытания наклонной камеры нового поколения уборочных машин, в частности к способу определения коэффициента разравнивания биомассы наклонной камерой, связанные с неравномерной загрузкой комбайна по ширине, влиянием неравномерности на показатели обмолота и сепарации, установлением причин, приводящих к такой загрузке при проведении исследовательских работ по уборке пастбищных растений.

2. Предпосылки и решение проблем

Известен способ выявления степени разравнивания биомасс посредством уборочных машин с компоновкой рабочих и транспортирующих органов по Т – образной схеме [3], при которой поток биомассы, поступающий в молотилку, независимо от технологии уборки (прямое или раздельное комбайнирование), сужается до ширины наклонной камеры. Установлено, что валки формируемые валковыми жатками или поток, формирующийся прямым комбайнированием, имеют неравномерное распределение биомассы житняка как в продольном, так и в поперечном направлениях. При обмолоте этих потоков биомассы вследствие недостаточного растаскивающего действия транспортирующих рабочих органов неравномерность увеличивается, обуславливая неравномерную загрузку МСУ (молотильно-сепарирующих органов), что в конечном счете отрицательно сказывается как на производительности, так и на качественных, энергетических и других показателях зернового комбайна. В современных комбайнах коэффициент использования длины барабана составляет 0,6-0,8, то есть 20-40% ширины молотилки в работе не используются. Причем, меньшее значение этого коэффициента относится к более широким молотилкам. Наиболее чувствительным к неравномерной загрузке по ширине сепарирующие органы молотилки (соломотряс и очистка). В свою очередь равномерность загрузки по ширине зависит от параметров и структуры потока биологической массы (валка), подаваемого в молотилку комбайна. Поэтому при исследованиях и испытаниях наклонной камеры нового поколения очень важно точность оценки и определение коэффициента разравнивания биомасс житняка.

Однако известная методика сужения и определения степени разравнивания биомасс житняка допускает значительную погрешность и невозможно определить численное значение коэффициента разравнивания биомасс житняка.

А также известна методика определения степени разравнивания биомасс житняка посредством наклонной камеры зерноуборочного комбайна [4], где равномерную загрузку рабочих органов молотилки, т.е. распределение биомасс по всей ширине наклонной камеры осуществляют колебаниями решетчатого днища наклонной камеры зерноуборочного комбайна. При этом степень разравнивания биомассы оценивается забиваемостью молотилки комбайна биомассой, т.е. частотой вынужденных остановок при обмолоте биологической массы житняка либо производительностью МСУ уборочной машины.

Указанная методика оценки и определения степени разравнивания биомасс житняка наклонной камерой уборочной машины допускает значительные погрешности и не сможет точно определить коэффициент разравнивания биомасс рабочими органами уборочной машины, влияющих на равномерность загрузки МСУ уборочной машины. Кроме того, конструкция устройства для определения степени разравнивания биомасс житняка сложна и имеет низкую работоспособность.

Разработанная методика реализуется посредством устройства [5] показанный на рисунке 1, где приведена схема экспериментальной установки для определения коэффициента разравнивания биомассы житняка, вид сбоку: на рисунке 2 – показана измерительная часть П – образной рамы, вид по А; на

рисунке 3 – П – образная рама и комлевая часть разноцветных стеблей биомассы, вид по Б.

Устройство включает наклонную камеру 1, проставку 2 с питателем 3 и ее транспортер 4, имеющий перемещающуюся П – образную раму 5 с вырезом 6, где закреплен регулируемый по вертикали и перемещающаяся по вырезу фиксатор 7 и метрическая линейка 8. Кроме того за выбросной кромкой наклонной камеры 1 выполнен разгрузочный транспортер 9 с аналогичной перемещающейся рамой 10.

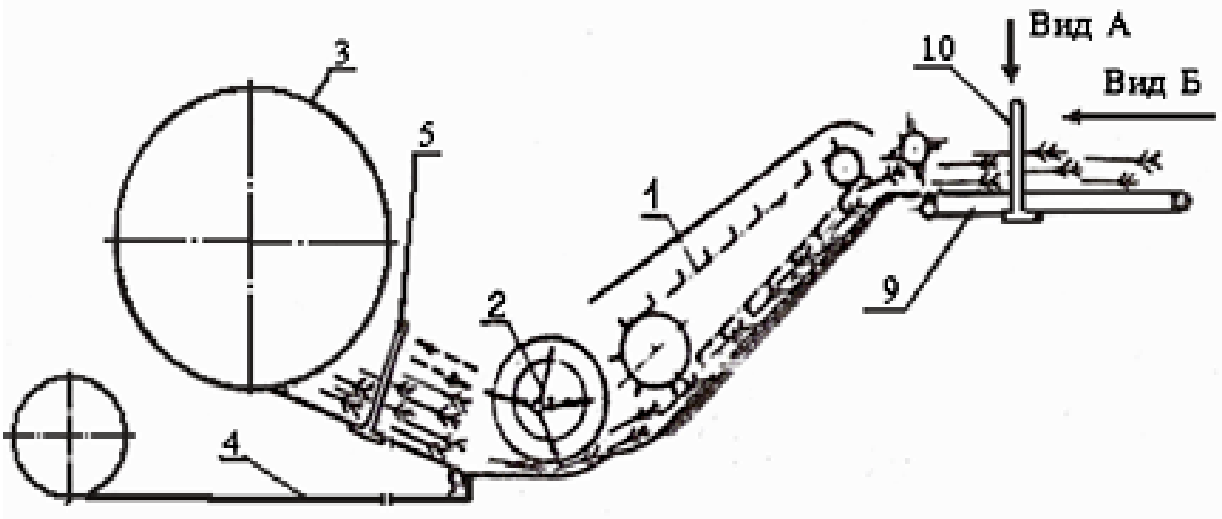

Рисунок 1 - Экспериментальная установка для определения коэффициента разравнивания биомассы житняка:
1-транспортер; 2-шнек; 3-мотовило; 4-транспортер питателя; 5-П-образная змерительная рамка; 9-разгрузочный транспортер; 10-рама.

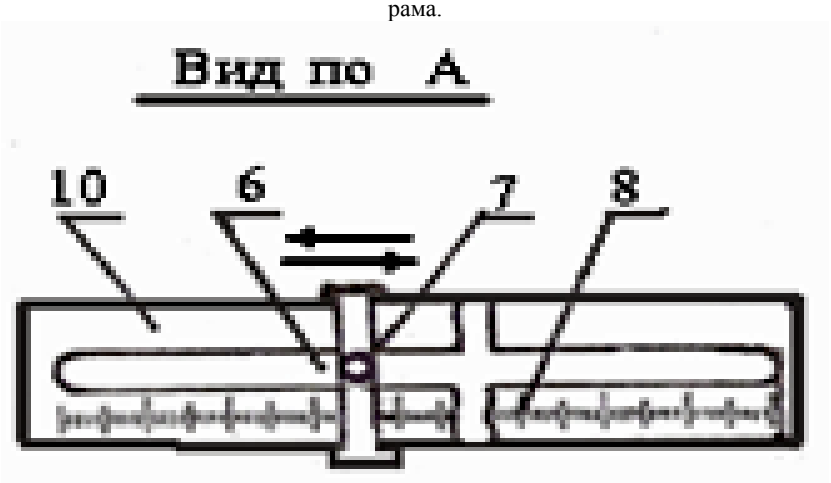

Рисунок 2 - Измерительная часть П - образной рамы вид по А на рисунке 1:
6-прорез рамки; 7-фиксатор; 8-метрическая линейка; 10-рама.

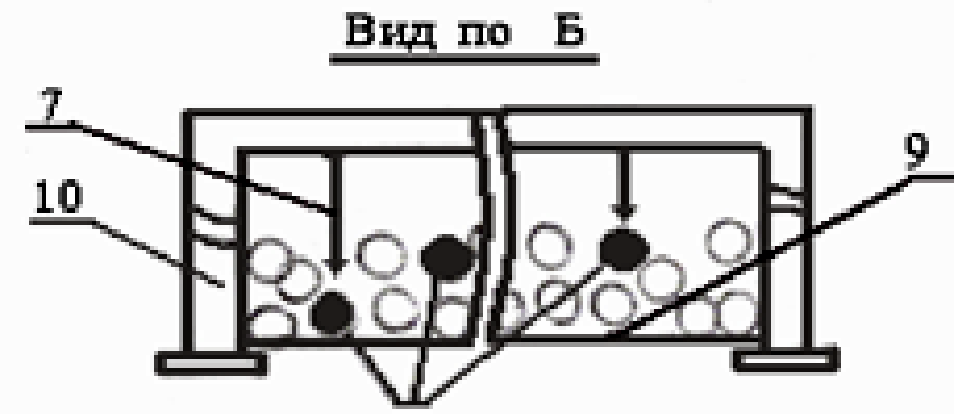

Рисунок 3 - П - образная рама и комлевая часть разноцветных стеблей биомассы житняка, вид по Б на рисунке 1:
7-фиксатор; 9-разгрузочный транспортер; 10-рама.

3. Результаты и обсуждение

Определение коэффициента разравнивания биомассы житняка на этом устройстве осуществляется следующим образом. В отвешенной порции биомассы житняка посредством фиксатора 7 регулируя ее по вертикали и перемещая по вырезу 6 рамы 5 метрической линейкой 8 замеряют исходные координаты комля и колосовой части разноцветно окрашенных стебельков, относительно вдоль центральной оси наклонной камеры. Затем биомасса житняка подается транспортером 4 питателя 3 на проставку 2 и в наклонную камеру 1 нового поколения. Пройдя через исследуемые и оптимизируемые рабочие органы наклонной камеры, они попадают на разгрузочный транспортер 9. Здесь. Также посредством фиксатора 7 регулируя ее по вертикали и перемещая по вырезу 6 рамы 5 метрической линейкой 8 замеряют смещенные координаты комля и колосовой части разноцветно окрашенных стебельков, относительно той же системы отсчета, после чего подсчитывают среднее численное значение разницы наиболее и наименее смещенных координат соответствующих стеблей и оценивают коэффициент разравнивания биомассы житняка по формуле:

$$\mu = \left(\sum X\ \max - \sum X\ \min\right) \Big| \sum X\ \max \qquad (1)$$

где $\sum X\ \max$ - максимальное смещение окрашенных стеблей, мм;

$\sum X\ \min$ - минимальное смещение окрашенных стеблей, мм;

μ - коэффициент разравнивания, подсчитывают численное значение коэффициента разравнивания биомассы житняка.

4. Заключение

Путем демонтажа необходимых узлов наклонной камеры с проставкой экспериментальной установки можно исследовать коэффициент разравнивания биомассы житняка каждым из вышеуказанных подающих органов в отдельности, а при постановке их на место – в комплексе.

Опыты проводятся в трехкратной повторности на сноповой массе житняка. Влажность семян и соломы, длина стеблей определяется по существующей методике.

Применение предлагаемой методики с устройством позволяет наиболее точно, объективно оценить и определить численные значения коэффициента разравнивания рабочими органами уборочных машин, в которых проводятся изменение коэффициента разравнивания биомассы житняка.

4. Conclusion

By dismantling of necessary nodes of the oblique chamber with a spacer of the experimental installation can research coefficient of leveling of biomass of a wheatgrass each of the above-stated giving organs separately, and in case of their setting into place – in a complex.

Experiments are carried out at the triplicates repetition on the sheaf's weight Wheatgrass. Seeds and straw moisture, the length of the stems is determined by existing methodology.

The application of the proposed methodology to the device allows for the most accurate, objective assessment and determination of numerical values of the coefficient of leveling the working bodies of harvesting machines in which the leveling coefficient is being changed biomass.

Литература

1. Садыков Ж.С. Новые технологии и машины для уборки семенных посевов сельскохозяйственных культур. Алма-Ата: КазНИИНКИ, 1992, 88 с.
2. Тойлыбаев М.С. Инновационные технологии и машины для уборки семян пастбищных растений. Монография. Типография «Дулат» Алматы, 2011г. 255с.
3. Комбайн зерноуборочный «Енисей-1200М» и его модификации //ОАО «КЗК», 2002г., ГОСНИТИ СФ. С.22,28, 303.
4. Инновационный патент РК № 20709 «Ускоритель обмолота для уборочных машин» // Садыков Ж.С., Есполов Т.И., Тойлыбаев М.С. и др. 16.05.2011, бюл. №5.
5. Патент РК № 29317 «Способ определения коэффициента разравнивания биомассы, поступающей в МСУ комбайна и устройство для его осуществления» // Садыков Ж.С., Есполов Т.И., Тойлыбаев М.С. и др. от 15.12.2014, бюл №12.
6. Садыков Ж.С., Есполов Т.И. К созданию интеллектуальной наклонной камеры зерноуборочного комбайна. Международн. научно-техническая конференция. «Инновационное развитие АПК России на базе интеллектуальных машинных технологий», ВИМ, Москва, 2014. 17-18.
7. Upgrading the Efficiency of Harvesting Machines by Means of Thrashing Accelerator of a New Type. International Journal of Applied Engineering Research ISSN 0973-4562 Volume 11, Number 16 (2016) pp 8966-8970 (c) Research India Publications, http: //www. Republication. Com// Zharykasyn S. Sadykov, Zhumakul S. Baizakoba, Meyram S. Toylybaev and Tanirnazar K. Sultangaziyev.

ПРИМЕНЕНИЕ МАТЕМАТИЧЕСКИХ МЕТОДОВ ПРИ ОБОСНОВАНИИ ВЫБОРА МОДЕЛИ РИСОУБОРОЧНОГО КОМБАЙНА

APPLICATION OF MATHEMATICAL METHODS IN THE SUBSTANTIATION OF THE SELECTION OF THE MODEL OF RICE-COMBINE

профессор Ж.Садыков, e-mail: sapa_kaz@mail.ru,
докторант Г.Д.Турымбетова
Казахский национальный аграрный университет, Алматы, Казахстан,
e-mail: gulzuhra62@mail.ru

доктор PhD, доцент Караиванов Димитър
Химико-технологического и металлургического университета г. София Болгария

Аннотация. *В статье рассматривается применение метода наименьших квадратов для получения эмпирической формулы, наилучшим образом описывающей экспериментальные данные, полученные на уборке риса раздельным комбайнированием.*

Ключевые слова*: рисоуборочный комбайн, производительность, расходы топлива, метод наименьших квадратов, признаки максимума и минимума функции, аппроксимация.*

Abstract. *The paper considers the application of the least squares method to obtain an empirical formula that best describes the experimental data obtained on rice harvesting by separate combining.*

Key words: *rice harvesting combine, productivity, fuel consumption, least squares method, signs of maximum and minimum functions, approximation.*

Введение. Одной из основных культур, возделываемых в Кызылординской области является рис, на долю которого приходится 79598 га посевных площадей. По заключительным данным текущего года с каждого гектара риса получено по 54,9 центнера урожая, валовый сбор составляет 439,8 тыс. тонн риса.

За последние годы в Кызылординской области интенсивно ведутся работы по обновлению машинно-тракторного парка. В настоящее время рисоводческие хозяйства области предпочитают приобретать современную высокопроизводительную сельскохозяйственную технику иностранного производства. При выборе той или иной техники после выбора ее типажа по производительности очень важно правильно выбрать конструкцию, которая адаптивна к местным особенностям Кызылординской области. Возникает проблема рационального выбора парка рисоуборочных комбайнов с учетом конкретных условий производства. Ранее [1], на основе теории множеств был разработан алгоритм решения задачи выбора оптимального состава МТП.

Решение рассматриваемой проблемы. Цель исследования – установить вид эмпирической зависимости и определить значения неизвестных параметров, наилучшим образом описывающих экспериментальные данные.

В задачи исследования входит: используя метод наименьших квадратов провести аппроксимацию функций полиномом третьей степени, построить линии тренда и провести сравнительный анализ полученныхрезультатов.

Проведенные испытания на уборке риса в Кызылординской области показали, что до 90% и более посевов риса к периоду уборки полегает-степень полеглости очень высокая. Жатки комбайнов не обеспечивают скашивание полеглого риса, поэтому полевые испытания на прямом комбайнировании не проводились. Для этого региона характерны большое число чеков малого размера, повышенная температура воздуха в период уборки и высокая влажность почвенного горизонта. Полевые исследования с нашим участием проводились на подборе и обмолоте валков риса, в рисоводческом хозяйстве Сырдарьинского района Кызылординской области. Уборка осуществлялась на полях со средней урожайностью 58,3 ц/га.

Результаты и дискуссия. Нами получены результаты хронометражных наблюдений рисоуборочных комбайнов на уборке риса раздельным комбайнированием (табл.1).

Таблица 1. Результаты испытаний рисоуборочных комбайнов на уборке риса раздельным комбайнированием

Тип комбайна	Намолот за время испытания, цн	Наработка за время испытания, га	Расходы топлива,л	
			за время испытания	на 1 ц, всего
CASE 2388	7326,7	126	5070	0,7
John Deere STS 9770	15399	265	9840	0,6
TUCANO 580	19712,5	338	8780	0,4
ЕНИСЕЙ-1200РМ	9297,4	160	4650	0,5
LEXION 750	21394,7	367	10250	0,5

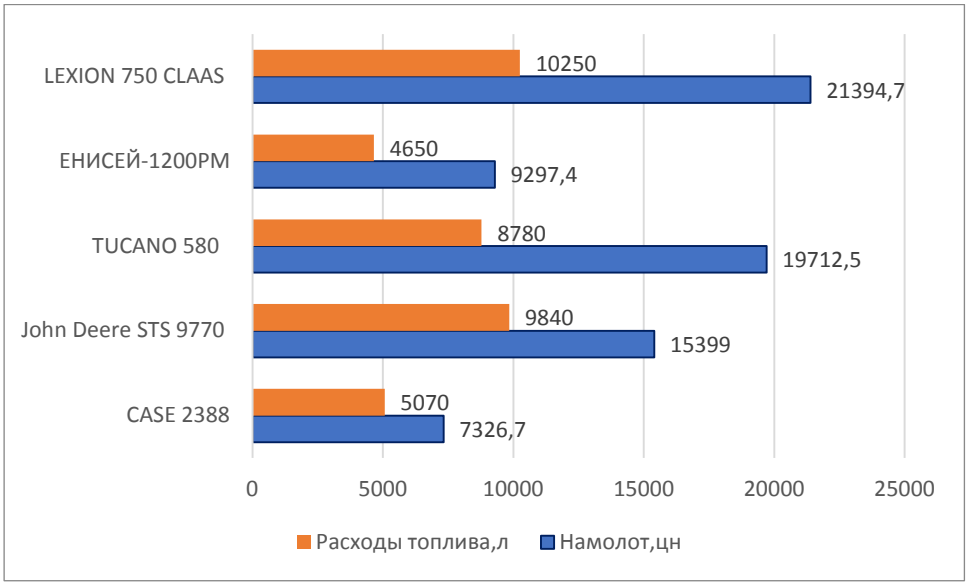

Фиг. 1. Распределение рисоуборочных комбайнов по сезонному намолоту зерна и удельному расходу топлива

Анализ полученных эксплуатационно-технологических показателей работы комбайнов показывает следующее. Согласно результатам испытания комбайны LEXION 750 и TUCANO 580 превзошли других участников сразу по нескольким ключевым параметрам. Прежде всего комбайн LEXION 750 показал лучший результат по сезонному намолоту зерна - 21394,7 цн (суточная производительность 822,87 цн зерна). Это на два процента выше, чем у TUCANO 580 - 19712,5 цн (суточная производительность 788,5 цн зерна) и на семь процентов, чем у John Deere STS 9770 - 15399 цн (суточная производительность 627,16 цн зерна), которые заняли последующие места. Комбайн CASE 2388 отстал от LEXION 750 сразу на 19 процентов, а ЕНИСЕЙ-1200РМ на 16 процентов (рис.1).

Комбайн модели CASE 2388 показал на уборке суточную производительность - 410,38 цн зерна, но функционировал в течение сезона не более 17 рабочих дней, т.е. сезонный намолот не превысил 7326,7 цн; комбайном модели ЕНИСЕЙ-1200РМ намолочено 9297,4 цн зерна за 27 рабочих дней, а его суточная производительность составила 361,3 цн зерна. Таким образом, комбайн CASE 2388 по суточному намолоту выше, а по сезонной производительности - ниже, чем комбайн модели ЕНИСЕЙ-1200РМ.

В условиях растущих цен на топливо комбайн CLAAS TUCANO 580 оказался самым экономичным по расходу горючего – 0,4 литра на один центнер, что значительно ниже, чем у других аналогов (LEXION 750 – 0,5, ЕНИСЕЙ-1200РМ – 0,5). Американские комбайны John Deere STS 9770 и CASE 2388 показали на Кызылординском поле низкие результаты 0,6 и 0,7 литров на один центнер зерна.

По результатам испытании нами получена таблица (данные о расходе топлива в зависимости от сменной производительности рисоуборочных комбайнов) с произвольным расположением аргументов: $(x_i, y_i), i = \overline{1,n}$ (табл.2). Аналитическое выражение табличной функции может быть неизвестным. На основе этой таблицы требуется найти формулу $F = F(x)$, приближённо описывающую зависимость между экспериментальными данными таблицы и исследовать функцию на возрастание, убывание, экстремум и построить ее график. При этом отклонение значений в точках $x_i, i = \overline{1,n}$, вычисленные по формуле $F = F(x)$, от экспериментальных данных y_i должны быть минимальными.

Таблица 2. Точки наблюдения $(x_i, y_i), i = \overline{1,n}$

y	29	40	37	26	28
x	6,4	7,4	10,6	13,5	14,1

Поиск эмпирической формулы $F(x)$ начинается с определения класса функций, которые лучше всего отражают связь между табличными данными. Эффективным методом для этого являются графические изображения. На координатной плоскости отмечаются определяемые данной функцией точки, а затем по характеру их расположения подбирается вид приближения из числа известных элементарных функций.

На основании графического изображения в качестве эмпирической функции выбирается функция:

$$y = ax^3 + bx^2 + cx + d$$

Рассчитаем коэффициенты модели можно стандартным Методом наименьших квадратов (МНК). Сущность метода наименьших квадратов состоит в отыскании параметров модели тренда, минимизирующих ее отклонение от точек исходного временного ряда, т. е. в минимизации суммы квадратических отклонений между наблюдаемыми и расчетными величинами[2]. Для определения параметров функции составляется вспомогательная таблица (табл.3).

i	x_i	y_i	x_i^2	x_i^3	x_i^4	x_i^5	x_i^6	$x_i y_i$	$x_i^2 y_i$	$x_i^3 y_i$
1	6.4	29	40.96	262.144	1677.72	10737.41	68719.47	185.6	1187.84	7602.17
2	7.4	40	54.76	405.224	2998.65	22190.06	164206.49	296	2190.4	16208.96
3	10.6	37	112.3	1191.01	12624.76	133822.55	1418519.11	392.2	4157.32	44067.59
4	13.5	26	182.25	2460.375	33215.06	448403.34	6053445.14	351	4738.5	63969.75
5	14.1	28	198.81	2803.221	39525.41	557308.36	7858047.97	394.8	5566.68	78490.18
$\sum$	52	160	589.14	7121.98	90041.62	1172461.75	15562938.19	1619.6	17840.74	210338.66

Таблица 3. Экспериментальные данные для проведения расчетов

Система уравнений для нахождения коэффициентов a,b,c и d :

$$\begin{cases} a\sum x_i^3 + b\sum x_i^2 + c\sum x_i + nd = \sum y_i \\ a\sum x_i^4 + b\sum x_i^3 + c\sum x_i^2 + d\sum x_i = \sum x_i y_i \\ a\sum x_i^5 + b\sum x_i^4 + c\sum x_i^3 + d\sum x_i^2 = \sum x_i^2 y_i \\ a\sum x_i^6 + b\sum x_i^5 + c\sum x_i^4 + d\sum x_i^3 = \sum x_i^3 y_i \end{cases} \Leftrightarrow$$

$$\begin{cases} 7121.98a + 589.14b + 52c + 5d = 160 \\ 90041.62a + 7121.98b + 589.14c + 52d = 1619.6 \\ 1172461.75a + 90041.62b + 7121.98c + 589.14d = 17840.74 \\ 15562938.19a + 1172461.753.62b + 900.41.62c + 7121.98d = 210338.66 \end{cases}$$

Решая эту систему уравнений методом Крамера, получим:

$$y = 0.3452x^2 - 11.3174x^2 + 117.9427x - 352.8257$$

Для оценки значимости параметров регрессии и корреляции сначала найдем y средний:

$$\overline{y} = \frac{1}{n}\sum y_i = \frac{160}{5} = 32$$

Составим таблицу вспомогательных величин, где $\varepsilon_i = y_i - \hat{y}_i$, $\Delta\varepsilon_i = \varepsilon_i - \varepsilon_{i-1}$, $A_i = \left|\frac{y_i - \hat{y}_i}{y_i}\right|$.

Таблица 4. Вспомогательная таблица

i	x_i	y_i	$\hat{y}_i$	$y_i - \hat{y}$	$(y_i - \hat{y})^2$	ε_i	ε_i^2	A_i	$\Delta\varepsilon_i$	$(\varepsilon_i)^2$
1	6,4	29	28.9432	-3	9	0.0568	0.0032	0.002	-	-
2	7,4	40	40.0997	8	64	-0.0997	0.0099	0.0025	-0.1564	0.0245
3	10,6	37	36.9045	5	25	0.0955	0.0091	0.0026	0.1952	0.0381
4	13,5	26	26.1729	-6	36	-0.1729	0.0299	0.0067	-0.2685	0.0721
5	14,1	28	27.8797	-4	16	0.1203	0.0145	0.0043	0.2933	0.086
$\sum$	-	-	-	-	150	-	0.0667	0.018	-	0.2206

Индекс корреляции

$$R = \sqrt{1 - \frac{\sum (y_i - \hat{y}_i)^2}{\sum (y_i - \hat{y}_i)^2}} = \sqrt{1 - \frac{0.0667}{150}} = 0.9998$$

Индекс детерминации: $R^2 = 0.9998^2 \approx 0.9996$

Средняя ошибка аппроксимации: $\overline{A} = \frac{1}{n} \sum \left| \frac{y_i - \hat{y}_i}{y_i} \right| \cdot 100\,\% = 0.3596\,\%.$

Проверим правильность расчетов с помощью линии тренда в MS Excel. Услуга Мастера диаграмм Построение линии тренда реализует метод наименьших квадратов для поиска коэффициентов эмпирической функции и построения её графика (рис.3).

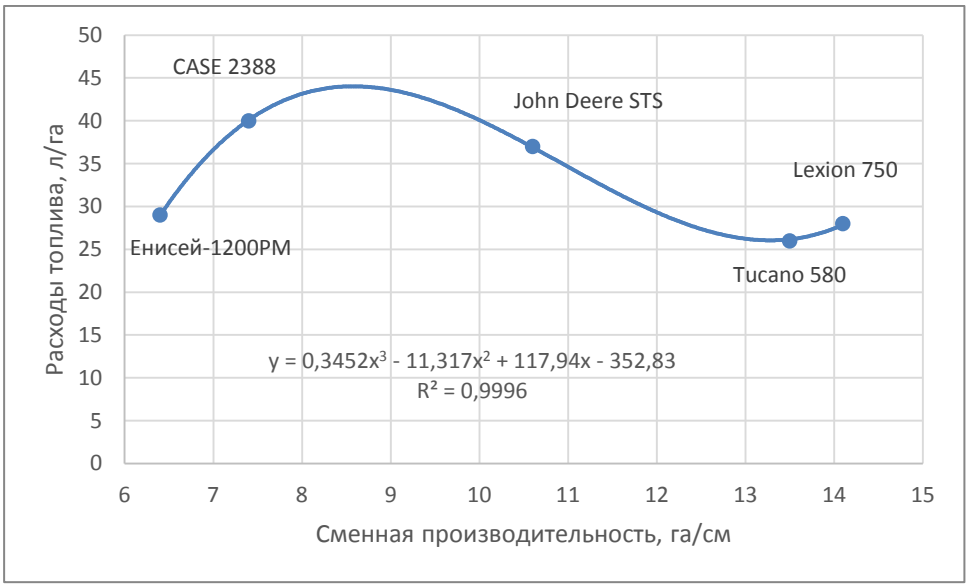

Фиг. 2. Распределение рисоуборочных комбайнов по сменной производительности и удельному расходу топлива

Полученная полиномиальная линия тренда третьей степени (два экстремума) отображает зависимость расхода топлива от сменной производительности рисоуборочного комбайна (рис.1). Близкая к единице величина достоверности аппроксимации (0,9996) свидетельствует о хорошем совпадении кривой с данными.

На основании полученных результатов можно сделать вывод о том, что аппроксимация более точная. Искомая аппроксимирующая функция

$$y = 0{,}3452x^3 - 11{,}317x^2 + 117{,}94x - 352{,}83$$

приближает экспериментальные данные наилучшим образом и позволяет прогнозировать, расходы топлива рисоуборочного комбайна («игрек») при том или ином значении сменной производительности (том или ином значении «икс»). Полученный прогноз будет лишь прогнозом, но во многих случаях он окажется достаточно точным.

Для исследования функции на наибольшее и наименьшее значение на заданном промежутке X используем график функции $y = f(x)$, а также находим производную функции, приравниваем ее к нулю, решаем полученное уравнение и выбираем подходящие корни.

Вычислим частные производные первого порядка и найдем стационарные точки

$$\frac{d}{dx} f(x) = 0$$

и корни этого уравнения будут экстремумами данной функции

$$\frac{d}{dx} f(x) = 1{,}0356x^2 - 22{,}634x^2 + 117{,}94 = 0$$

Корни этого уравнения

$$x_1 = 8{,}575$$

$$x_2 = 13{,}28$$

Точки $x_1 = 8{,}575, x_2 = 13{,}28$ - точки возможного экстремума. Вычисляем значения функции и выберем среди них наибольшее и наименьшее значения. Так как

$$y(8{,}75) = 0{,}3452 \cdot 8{,}75^3 - 11{,}317 \cdot 8{,}75^2 + 117{,}94 \cdot 8{,}75 - 352{,}83 = 44$$

$$y(13{,}28) = 0{,}3452 \cdot 13{,}28^3 - 11{,}317 \cdot 13{,}28^2 + 117{,}94 \cdot 13{,}28 - 352{,}83 = 26$$

Следовательно, $\max y = y(8{,}75) = 44, \min y = y(13{,}28) = 26$.

Найдем точки перегибов, для этого надо решить уравнение

$$\frac{d^2}{dx^2} f(x) = 0$$

Корни полученного уравнения будут точками перегибов для указанного графика функции:

$$\frac{d^2}{dx^2} f(x) = 2{,}0712x - 22{,}634 = 0$$

Корни этого уравнения $x_1 = 10{,}927$

$$y(10{,}927) = 0{,}3452 \cdot 10{,}927^3 - 11{,}317 \cdot 10{,}927^2 + 117{,}94 \cdot 10{,}927 - 352{,}83 = 35$$

Выполненное исследование показало, что целевая функция достигает минимального расхода топлива, при выполнении всего объёма работ в точке (TUCANO 580;13,5;26). Большое практическое значение имеет поиск существующих альтернативных вариантов состава парка рисоуборочных комбайнов с небольшим увеличением значения целевой функции вблизи экстремума. Пример поиска альтернативных вариантов решения по критерию минимального расхода топлива представлен на рис. 3.

Фиг. 3. График функции $y = f(x)$

Заключение

1.Анализ результатов расчетов и построенный график показывает, что аппроксимация функций полиномом наилучшим образом описывает экспериментальные данные. Минимум функции (26 л/га) достигается при значении объясняющей переменной, равном 13,5 га/см.

2. При окончательном выборе оптимального рисоуборочного комбайна большую практическую значимость представляет поиск альтернативных вариантов решения, которые соответствуют или находятся вблизи экстремума целевой функции, что позволяет снизить количество используемых комбайнов.

Литература

1. Браславец М.Е. Экономико-математические методы в организации и планировании сельскохозяйственного производства /М.Е. Браславец. – М.: Экономика, 1971. - 358 с

2. Машунин Ю. К. Разработка управленческого решения. Владивосток. Издательство Дальневосточного университета. 1998г. - 111с.

MATERIALS FOR CORROSION PROTECTION OF MACHINES AND EQUIPMENT IN LIVESTOCK FARMS

Chief Assistant Dr. Ivan Mortev, Dr. Evgenia Aschakanova
Agricultural Academy - Sofia

Sofia 1331, kv. Republica ,Shose Bankia Str. 3
e-mail: ivan_mortev@abv.bg

Abstract: *An analysis was made of the materials used for the anticorrosion protection of machines and equipment in livestock farms. The advantages and disadvantages of individual groups of anticorrosion materials and their applicability are outlined. Techno-economic criteria for choices tailored to the specifics of the work environment are proposed.*
KEY WORDS: *MACHINERY, EQUIPMENT, LIVESTOCK FARMS, ANTI-CORROSION MATERIALS, TECHNOLOGIES, CRITERIA.*

The machines and facilities in agriculture in the process of exploitation are subjected to the intensive impact of various factors causing corrosion [1,2]. The reason for corrosive damage is the lacking, insufficient or inadequate anticorrosion protection, due to errors in planning, poor quality of the materials, improper application of the technologies, poor maintenance preservation and conservation.

The choice of materials and the way of protection must correspond to the aggressiveness of the environment and the specifics of the object of protection- machine, installation or facility [3,4]. As far as buildings are concerned, apart from the choice of materials of considerable importance is the adequate shaping of the external walls with regard to the heat conditions and humidity. This is of major importance with buildings for animal breeding with regard to their microclimate as well as their long life. The external walls often do not provide the necessary coefficient of thermal conductivity, especially at the points where the separate elements are connected, as well as the windows where thermal bridges are formed. The lower effectiveness of the heat isolation of the partition where the thermal bridges are causes condense on the cooler surfaces and leads to faster destruction of the isolation and constructive materials. The insufficient thermal isolation worsens the microclimate of the buildings and has a negative effect on the weight gain of the animals.

The main constructive materials are steel and concrete. They are not resistant to the impact of aggressive factors in agricultural buildings. Therefore they need additional coatings which do not allow direct contact of the construction with the aggressive environment. For steel such covers are:

- metal coatings- zinc, aluminum, cadmium, etc.
- paint, polymer coatings, water wax base coatings, coatings based on inhibited mineral oils, polymer oils, etc.

For concrete:

- varnish and paint coatings
- bituminous coatings
- ceramic coatings

The choice of coating is based on economic calculations and durability. We can choose between more expensive materials which are long lasting and do not require renovation and additional expenses. The analyses of choosing a certain kind of protective coating should be based on a number of major criteria:

- resilience of the aggressive environment
- adhesiveness
- durability
- resistance to cracking
- waterproofness
- biological influence of the technological processes

These factors should be considered in determining the conditions in which the coatings will perform their protective role. Paints and varnishes are widely used for the protection of machines and equipment. Depending on the conditions of exploitation these coatings should provide protection against the atmospheric, biological, thermal and mechanical factors. The effectiveness of their use depends most of all on the choice of the material for coating with regard to the degree of aggressiveness of the environment. The paints used as anticorrosive coating should meet the following requirements:

- they should not contain toxic elements
- chemically stable
- easily applicable
- waterproof

These requirements are met by materials based on chlorine polymers such as vinyl polymers, chlorine rubber and polyethylene. As a blend they are resistant to the impact of chemicals. The pigments are chemically neutral, the fillers and colorants are resistant to light and the atmospheric conditions. The preparation of the surfaces is of major importance in the use of paints as anticorrosive protection. Coatings applied on inadequately prepared surfaces have 30 to 50% lower adhesiveness. Very good protective qualities have materials based on epoxy ester paint, applied through electrophoresis [4].

Research shows [4,5,6] that the preparation of the surface by means of microcrystalline phosphatization increases 2-3 times the life of the anticorrosive coating, especially at atmospheric conditions. Phosphatization allows decreasing the thickness of the coating thus decreasing the cost and increasing the durability of the coating.

In an environment with mineral fertilizers the most resistant are the materials containing polyvinyl minerals with a coating of at least 0.08mm. An increased durability and resistance of the coating is achieved through the application of a middle layer of thixotropic paint, which increases the thickness of the coating to 0.15mm. Coatings of powder epoxy and epoxyester paints can be used to protect materials in contact with mineral fertilizers.

Several types of Paint are suitable for anticorrosive protection of machines and equipment working with fertilizer liquids. The best protective qualities have the coatings based on epoxy electrophoresic paint and phthalic carbamide enamel, and primer diluted with water. Good protection in an environment with fertilizer liquids provide coatings with alkyd primer containing zinc powder in combination with phthalic carbamide enamel.

For the protection of machines subject to the influence of pesticides are suitable mainly epoxy, epoxyester and polyurethane paints. An increase of the durability of the protection can be achieved by phosphating the working surfaces before applying the paint. Research shows that coatings of the widely used paints with thickness of 0.06 to 0.08mm (two, three layers) have similar corrosive resistance. If this thickness is insufficient and the increase of the number of layers is ineffective, other materials with a thicker layer should be used.

One of the prospective directions to provide complex protection against corrosion is the use of wax and polymer multifunctional film. The transition to water based anticorrosive means with temporary or permanent effect is determined by the restrictions in the requirements of reduced emissions of solvents in

the atmosphere, as well as by the increased price of organic solvents.

Microcrystalline waxes are a mixture of solid hydrocarbons, paraffins, cerisins, isoparaffins which have good water-repellent, low gas and vapor permeability. The protective physiochemical properties of microwaxes are enhanced by special additives - inhibitors, hydrophobic substances, polymeric materials, synthetic surfactants, detergents releasing corrosive active electrolytes and water on the surface of the metal. The microplate coatings are a transparent or light brown film, sufficiently rigid, non-stick, and usually not requiring removal from decontamination. The microplate coatings are a transparent or light brown film, sufficiently rigid, non-stick, and usually not requiring removal after deconservation.

Of particular interest are microwax compositions used as a preservative instead of preservative lubricants for temporary protection of articles with a different application. For this purpose, microwax solvent emulsions or water are used. Water-wax emulsions, unlike those in solvents, are non-inflamable and non-toxic. After surface application and drying, a thick plastic coating with good adhesion is formed. Emulsions are applied to metal and non-metallic materials, galvanic and varnish coatings, wood, leather, rubber, textile and synthetic materials, plastics. The film formed by the water-wax emulsion is resistant to atmospheric effects, does not break and is not washed by rain. It has good protective properties from the abrasive action of dust, especially important in the transport of technology.

The improvement of the protective properties of the water-wax compositions is achieved by the introduction of corrosion inhibitors. These are effective means of protection against atmospheric corrosion, corrosion in water-saturated systems, sulfur-hydrogen corrosion and others. For agricultural machinery with regard to storage conditions the most suitable are atmospheric corrosion inhibitors. For machines and farm facilities, a suitable package of inhibitors is selected, tailored to the specifics of the work environment. The essence of protection of the water-wax compositions inhibited by atmospheric corrosion additives is the chemical and physical interaction of the inhibitor with moisture, oxygen and other corrosive agents. As a result, neutral substances with regard to corrosion are formed or passivation of the metal surface , hydrophobization or co-reaction occurs.

The ability of water-soluble corrosion inhibitors to expel water from the surface of the material allows the application of a protective layer on a wet surface. In this way the development of the corrosion process is inhibited and the water absorption of the system is reduced.

The practical application of water-wax compositions is based primarily on the following advantages:

- reliable protection against corrosion for 12-18 months
- have no negative impact on repairs and subsequent exploitation
- do not require complicated application facilities
- do not contain inflammable, explosive and environmentally harmful substances
- do not require complex pre-surface preparation
- Versatility of application on a variety of materials

Studies have shown that the protective action on clean (uncovered) metal surfaces is insufficient due to the fact that the water-emulsion phase acts on the clean metal surface as a corrosion-supporting medium. The wax film formed after drying is relatively thin and partially porous, therefore the barrier effect is insufficient. The corrosive action of the aqueous phase of the wax emulsion is ignored or inhibited by the introduction of inhibitors such as amines, nitrites, benzoates and the like.

The suitability of the water-wax compositions as a temporary corrosion protection agent is mainly determined by:

- Emulsion stability
- good adhesion properties and the ability to achieve a certain coating
- the anticorrosion protective action of the coating

The water-wax emulsion is a complex colloidal system. Addition of inhibitors consisting of polar molecules acting as softeners and emulsifiers can have an effect reducing their stability and leading to the separation of the aqueous phase and the wax components. Inhibitors are usually added as a package of grafts that perform different functions: anticorrosion, congeal regulators, or better lubricating properties. In such a system, the grafts act independently from one another and we can not rely on their interaction. It is considered beneficial if they do not have a negative influence.

Conclusion

There is a wide variety of materials and tools for anticorrosive protection of machines and equipment in livestock farms. The suitability of the choice of materials for corrosion protection to the aggressiveness of the working environment is decisive for the reliability of the machinery and the durability of the equipment.

The choice of materials and technologies for their application should take into account both the main technical criteria and the economic and operational factors.

Literature:

1.Михов М. Надеждност на машините в земеделието, С., 2012 г., стр.130.

2. Михов М., Г.Тасев Техническо обслужване и ремонт на машините, С., 2012 г., стр.149.

3. Михов М. и др. Методически указания за извършване на технически прегледи на стационарна земеделска техника- С., 2001 - с.41.

4.Аврамов Б. Хабилитационен труд, София, 1988г.

5.Severin A.D. Storage of agricultural machinery, Moscow, 1985.

6.Годишен научен отчет на ИММ, София 2003-2005 г.

ANTICORROSIVE PROTECTION OF MACHINES AND EQUIPMENT IN LIVESTOCK BREEDING

Chief Assistant Dr. Ivan Mortev, Dr. Evgenia Aschakanova
Agricultural Academy - Sofia
Chief Assist. Dr. Ivan Mortev
Sofia 1331, kv. Republica ,Shose Bankia Str. 3
e-mail: ivan_mortev@abv.bg

Summary (Abstract) :*The main reasons and prerequisites that cause the destruction of material corrosion and its losses are discussed.*
The process of conducting anticorrosive protection with its basic stages: cleaning of treated surfaces of dirt and corrosion products, surface degreasing, deposition of protective materials and final operations.
A qualitative assessment of the applied technologies was made at the various stages of the corrosion protection of the machines and equipment.
KEYWORDS: *MACHINES, EQUIPMENT, LIVESTOCK FARMS, ANTI-CORROSION MATERIALS, TECHNOLOGIES, EQUIPMENT.*

Agricultural machinery in the process of operation is subject to the intense impact of various factors causing corrosion of materials. Reasons for this may be mechanical, physical, chemical, biological, and a combination of factors [1,2]. A major precondition for excessive and unjustified corrosion damage is human activity in the production and operation of machinery.
Damage caused by corrosion wear is significant, though difficult to calculate. There is a loss of premature decommissioning, additional costs of repair, indirect costs of incomplete use and increased machine failure [3,4]. The prevention of corrosion wear should start from the design stage of the machinery and equipment. Constructions should not favor the formation of corrosion outbreaks and unwarranted rapid breakdown of protective coatings. In summary, the basic constructional requirements from the point of view of the anti-corrosion protection are:
- minimizing the unfolding of the external surfaces of the structural members;
- Providing optimum conditions for draining of liquids and possibility of ventilation of the internal spaces;
- Minimizing the number of joints, gaps and hollow spaces;
- providing the possibility of subsequent application of protective coatings;
- elimination of the inappropriate contact of metals with a significant difference in electrode potentials;
- reducing the impact of mechanical stresses;
- Easy cleaning and drying.
In a technological aspect, the prevention or reduction of the corrosion process intensity is effected by coating the surfaces with protective coatings [3]. Besides the means of long-term protection, these include temporary protection. For its part, it includes the protection of non-ferrous iron alloys and iron alloys, ranging from production, warehousing, transport to commissioning. Depending on the time the machines and equipment are protected from corrosion processes, it considers:
- short-term protection - up to 6 months;
- medium-term protection - up to 18 months;
- long-term protection - over 18 months.
The process of conducting anti-corrosion measures includes [5,6], as a rule, the following operations (steps):
- cleaning the treated surfaces from dirt and corrosion products; degreasing of surfaces;
- application of protective materials;
- final operations.

Cleaning and removal of corrosion products

The cleaning and removal of corrosion products from the surfaces to be protected is an important step in the technological process [2]. Applying protective coatings on poorly cleaned surfaces has no positive effect. It is even possible to get negative results as the coating encapsulates contamination and corrosion products and furthermore creates corrosion conditions.
Pollution is cleaned with hot or cold water jet at stationary washing points or with mobile units. In the preparation for storage of tractors, cars and agricultural machinery, it is appropriate to do so at specially prepared stationary washing stations, while machines and equipment on livestock farms are more suitable for mobile furniture, given the stationary type of machines. Washing is done under high pressure which, in addition to better washing quality, reduces water consumption. In stationary washing installations, water is used repeatedly, after removal of coarse soil contamination, oils, mineral fertilizers and additional filtration. In order to accelerate the water purification process for reuse, the coagulation method is used, i. artificial bonding through appropriate chemicals in conglomerates that, when precipitated, binds the particles of dirt and is exported to sediments.
Removal of corrosion products occurs mainly by mechanical, chemical or mixed methods. The mechanical rust cleaning method provides for the use of electric or pneumatic devices with metal brushes or abrasive disks. For mobile installations, pneumatic devices are not suitable due to high air consumption. For example, a pneumatic grinder has an average air flow rate of 1.6-2.0 m3 / min, at an operating pressure of 0.5 to 0.6 MPa. This determines the pneumatic devices mainly for stationary stations. A good effect is achieved by sandblasting on corroded surfaces, but the operation is considerably more expensive than other mechanical devices. The electrochemical method of cleaning is inappropriate for ground-based machines and equipment due to the large size of the parts. It is suitable for smaller parts and industrial production.
The chemical cleaning method involves mainly passivation and conversion of corrosion processes. It is based on the reaction between acid and iron oxide. Current transducers converting the corrosion products into passive or poorly soluble compounds can be divided into two groups. The first group includes those containing inorganic acids - usually orthophosphoric and nitric, and in the second - non-containing inorganic acids. In the case of chemical cleaning, it is necessary to perform a preliminary degreasing. It can be carried out with organic solvents, either chemically or electrochemically. Practically applicable in the preservation and anti-corrosion protection of agricultural machinery is degreasing with organic solvents - petrol, petrol, turpentine, trichloroethylene and others.

Applying protective coatings

Next step in the anti-corrosion protection is the application of protective coatings [5,6]. It is done through:
- immersing the details;
- with a brush;
- pneumatically;
- airless (hydrodynamic) application.
The first method is applicable to the application of protective coatings on small details and is not of particular interest in the anti-corrosion protection of agricultural machinery. The method of applying a coating by hand with a brush has a limited application and, if necessary, minor corrections.
The pneumatic way of applying protective coatings has been widely used for a number of advantages, such as:
- universality of the method ie. enables use under almost any condition;

- possibility of application for parts, assemblies and aggregates of different sizes and groups of complexity;
- the availability of facilities and services as well as the security of the work process;
- Possibility to work with almost all kinds of protective materials - slow and fast drying, one or two-component, also cold or heated;
- coatings are characterized by high quality.

Pneumatic application [6] involves the release of a large amount of aerosols degrading sanitary and hygienic working conditions and requiring intensive removal of contaminated air. This results in the loss of airflow material reaching up to 55% in complex configuration details. Typical of the process is the increased solvent consumption to obtain the appropriate viscosity of the material. The working pressure is 0.2-0.6 MPa, at a viscosity of 17-60 seconds with B3-4.

Applying pre-heated paint to the pneumatic method makes it possible to significantly increase the efficiency and cost-effectiveness of the process. Upon raising the temperature, the viscosity of the material sharply decreases, allowing high-viscosity materials to be used without further dilution. At the same time, it is possible to reduce the number of layers applied at the expense of the approximately twice the thickness of one layer. This ensures better coverage and high performance. In case of preheating of the material, the working viscosity is reduced to 12s, as a result of which the air pressure may drop to 1.0-1.5 MPa. The heating temperature usually does not exceed 80 ° C.

For the application of lacquer materials are used both stationary installations in industrial conditions, so hand guns. Because of its simplicity, ease of service and versatility, the method is widely applied to articles of different configurations and complexities, although in some cases performance is not high. It is mainly related to the fact that it is operated in individual cases in arbitrary, unprocessed diffusion modes of different air pressure, causing aerosol loss of material. Despite the versatility of the method, it is not recommended to process bars such as bars, screens, pipes with a long diameter, mainly due to the large material losses [6].

The method of airless coating of protective coatings is based on the high hydraulic pressure in the system. Compared to the pneumatic method, the airless way has a number of advantages:
- reduces aerosol loss of material (up to 20%);
- reduces solvent consumption due to the possibility of depositing materials with higher viscosity;
- lower environmental pollution due to the fact that only vapors of the solvent and not of the parent material are released.
- the possibility of applying a layer of greater thickness, which reduces the number of layers.

Spraying of the material by airless application is at the expense of high hydraulic pressure up to 25MPa. The method allows to work with all kinds of paints and enamels. This is done with increased viscosity up to 120s on B3-4, for example:
- pentaphthalenes - 120m;
- melamine salts - 100s;
- nitrocellulose -100s.

The device for inertial application of protective materials is a separate unit, the main unit of which is the high pressure pump. It can be differential type, with double action, with pneumatic or electric drive, valve system and filters, regulating and control-measuring apparatus. The unit may have a self-contained volume for the material or a suction hose for external volume supply. A high-pressure gun and a hose connecting the pistol to the pump are also included in the system.

There are two types of installations that differ from the node assembly. The first type refers to systems with a submersible pump attached to the container with a material. These are compact, portable installations with a volume of 20-60 liters. The second type refers to devices where the pumps are not fitted to the vessels with a material that allows different vessels and volumes to be used. Each of the two types has its advantages. The choice is predominantly determined by the organization and volume of the works. Installations of the first type are preferred for a small volume of work, and the second type is predominantly stationary.

Depending on power, performance and weight, airless systems can be divided into three groups: small portable with output up to 1.0 kg / min and weight up to 20 kg; medium-sized with a capacity of up to 2.0kg / min and weight up to 60kg and large, multipurpose or stationary with a performance above 5.0kg / min and weight over 100kg.

The airless application method allows working with a wide range of materials: pentaftalic, phenolic, nitrocellulose, epoxide, alkyd-styrene, oil-bituminous, perchlorinyl and the like. It is not recommended to use materials with coarse or easily settling pigments and fillers that pollute spray nozzles.

The main technological parameters influencing economical and efficient operation are the spray gun performance, working pressure and viscosity of the material. Depending on the dimensions of the work pieces and the type of protective material, the optimum performance of the gun is determined by selecting a suitable nozzle with such a cost and width of the print to obtain a uniform coating with minimal material losses.

It is recommended to work with high-performance systems to process large-dimensional products with a simple configuration and when working with high-quality materials.

The working pressure is selected depending on the type and viscosity of the material and nozzle performance [6]. When applying a material of a certain type to obtain a good dispersion of dispersion, it is necessary to operate not high but with minimal working pressure. It should be taken into consideration that, when the pressure rises above a certain optimal value, unnecessary fragmentation of the material and an increase in aerosol losses occurs. The viscosity is selected based on the requirement to obtain a single layer of a certain thickness.

Literature

1.Михов М. Надеждност на машините в земеделието, С., 2012 г., стр.130.

2.Михов М., Г.Тасев Техническо обслужване и ремонт на машините, С., 2012 г., стр.149.

3.Михов М. Диагнозиране на машините и съоръженията в животновъдните ферми.- Сп.“Механизация на селското стопанство”, 1987, N6, с 17 - 20.

4.Михов М. и др. Методически указания за извършване на технически прегледи на стационарна земеделска техника- С., 2001 - с.41.

5.Severin A.D. Storage of agricultural machinery, Moscow. 1985.

6.Годишен научен отчет на ИММ, София 2003-2005 г.

DEVELOPMENT OF NEW NANOSIZED SOL GEL COATINGS ON STEEL WITH ENHANCED CORROSION RESISTANCE

Assoc. Prof. dr. Stambolova I. [1], Assoc. Prof. dr. S. Yordanov[2], Prof. dr. Lakov L.[2], Assoc. Prof. dr. Blaskov V.[1], dr. Toncheva K.[2], Assoc. Prof. dr. Jivov B.[2], Ph.D Student Kostova Y.[2]

[1]Institute of General and Inorganic Chemistry – Bulgarian Academy of Sciences, Acad. G. Bonchev St. , bl.11, 1113 Sofia, Bulgaria

[2]Institute of Metal Science, Equipment and Technologies with Hydro- and Aerodynamics Centre "Acad. A. Balevski", Bulgarian Academy of Sciences, Shipchenski Prohod Blvd. 67, 1574 Sofia, Bulgaria

[*]stancho14@abv.bg

Abstract*: The steels have wide application in industry, due to its valuable physicochemical properties, such as mechanical which include strength, hardness etc. However, in specific environments the steel have tendency to corrode in the presence of halide ions. This is the reason to develop and investigate new protective coatings with good barrier properties. It is known, that ceramic nanosized oxide coatings are potential good candidates due their excellent chemical stability.*

Sol gel method gives possibility to deposit coatings with definitely chemical and phase composition at low temperatures using simple a low cost techniques. Here we report an application of sol gel method by dip coating technique to prepare a several type of nanosized coatings: (a) one component coatings such as TiO_2, Nd doped TiO_2 and CeO_2 and (b) bicomponent multilayer, which contain as sublayer CeO_2 or SiO_2 and upper layer ZrO_2, TiO_2 and CeO_2. The coatings were characterized by XRD, SEM, AFM and XPS analyses. The morphological investigations of the coatings revealed that they have relatively dense surface with good adhesion. The studies of their corrosion protection properties were estimated by exposing to the action of salty solution of 3.5% NaCl and was evaluated the weight loss. After the corrosion test the surface roughness not changes significantly. Pin holes, pits and other signs of corrosion are not found according to AFM and SEM analyses. These results proved that the investigated oxide coatings exhibit good corrosion resistance.

KAY WORDS: *SOL GEL METHOD, NANOMATERIALS.*

Acknowledgements

The authors are grateful to the financial support of Bulgarian National Science Fund at the Ministry of Education and Science, Contract No DN07/2 14.12.2016.